

Université de Montréal

Application de l'EEG-SPIRf aux soins intensifs neurologiques : une nouvelle approche multimodale d'enregistrements à long terme de l'activité épileptiforme

vEEG-fNIRS in the neuro-intensive care unit: a new approach for long-term multimodal recording of epileptiform activity

Par
ALI KASSAB

Département de neurosciences, Faculté de médecine

Thèse présentée en vue de l'obtention du grade de Philosophiae Doctor (Ph.D.) en neurosciences

Novembre 2023

© Ali Kassab, 2023

Université de Montréal

Faculté des études supérieures et postdoctorales

Cette thèse intitulée :

Application de l'EEG-SPIRf aux soins intensifs neurologiques : une nouvelle approche multimodale d'enregistrements à long terme de l'activité épileptiforme

Présentée par:

Kassab, Ali

a été évaluée par un jury composé des personnes suivantes :

Pierre Duquette

Président-rapporteur

Dang Khoa Nguyen

Directeur de recherche

Patrick Cossette

Codirecteur de recherche

André Denault

Membre du jury

Christophe Grova

Examineur externe

Guillaume Emeriaud

Représentant du doyen

RÉSUMÉ

La spectroscopie proche infrarouge fonctionnelle (SPIRf) est une technique de neuro-imagerie noninvasive permettant de mesurer les changements de concentration d'hémoglobine oxygénée ($\Delta[\text{HbO}]$) et désoxygénée ($\Delta[\text{HbR}]$). Au cours des deux dernières décennies, notre groupe (et d'autres) ont combiné la SPIRf avec l'électroencéphalographie (EEG) pour effectuer des enregistrements chez des patients avec épilepsie réfractaire afin d'évaluer son potentiel comme 1) technique de cartographie cérébrale noninvasive (par exemple, localisation des aires impliquées dans le langage et localisation du foyer épileptique) et 2) comme approche noninvasive pour étudier le couplage neurovasculaire pendant les pointes épileptiques interictales ainsi que lors des crises épileptiques. Malgré des résultats prometteurs, de nombreux enjeux demeurent avant que la EEG-SPIRf puisse être implantée en pratique clinique. En effet, l'installation de l'équipement prend encore trop de temps, l'obtention de signaux de qualité nécessite encore une surveillance serrée et un certain inconfort apparaît au fur et à mesure que les enregistrements progressent dans le temps. C'est d'ailleurs pourquoi les enregistrements EEG-SPIRf ont, jusqu'à maintenant, été généralement de courte durée (c. à d. rarement plus de deux heures) avec une couverture limitée du cortex cérébral (c. à d. généralement une ou deux aires corticales) et dans un milieu contrôlé de recherche (plutôt qu'au chevet dans un milieu clinique).

Compte tenu de son potentiel clinique, il y a lieu de poursuivre les efforts pour développer la EEG-SPIRf pour usage clinique. Notamment, un grand potentiel est pressenti pour la EEG-SPIRf aux soins intensifs neurologiques. D'une part, les patients qui y sont admis étant souvent comateux et/ou sous sédation, l'inconfort relié au port d'électrodes et d'optodes n'est plus en enjeu. D'autre part, ces patients présentent généralement des pathologies graves souvent associées à des anomalies épileptiformes fréquentes à l'EEG (décharges périodiques, crises subcliniques, état de mal non convulsif) dont l'impact hémodynamique sur cerveau tout comme leur prise en charge demeurent controversés. Les techniques actuellement utilisées aux soins intensifs (moniteur de pression intracrânienne, sonde de saturation veineuse jugulaire en oxygène, doppler transcrânien, EEG seul sans SPIRf) présentant des limitations, l'ajout d'une composante de SPIRf à l'EEG permettrait possiblement d'élucider l'impact de certaines de ces anomalies épileptiformes, guider leur traitement et en améliorer leur surveillance.

Ainsi, cette thèse visait à 1) développer et valider un système d'EEG-SPIRf compact, sans fil et couvrant toute la tête, destinée à une surveillance à long terme de patients souffrant de divers troubles neurologiques; 2) évaluer la faisabilité et le potentiel d'une surveillance vidéo-EEG-SPIRf (vEEG-SPIRf) à long terme auprès de patients comateux admis aux soins intensifs neurologiques présentant des décharges périodiques, des crises ou un patron électrophysiologique de bouffées-suppression; et 3) étudier la dynamique neurovasculaire associée à l'état de mal épileptique non convulsif chez des patients comateux.

La première et la deuxième partie du projet décrivent le développement et la validation d'un système EEG-SPIRf hybride et de "casques" EEG-SPIRf personnalisés destinés à surveiller l'hémodynamique corticale entière chez les patients neurologiques. Nous avons d'abord démontré sa performance globale chez des participants sains effectuant deux tâches cognitives spécifiques (c.-à-d. des tâches linguistiques et visuelles) en position assise (pour la première) et en pédalant sur une bicyclette (pour la seconde). Les mesures électrophysiologiques et hémodynamiques ont été validées à l'aide de deux systèmes commerciaux et ont montré, chez tous les participants, une sensibilité et une spécificité spatiotemporelle élevées. Nous avons ensuite démontré le potentiel clinique de notre système chez quatre patients souffrant de divers troubles neurologiques (par exemple, épilepsie réfractaire et maladies vasculaires cérébrales). Nous avons ainsi réalisé avec succès des enregistrements prolongés vEEG-SPIRf au chevet de tous ces patients et observé des changements hémodynamiques cliniquement pertinents et en concordance avec d'autres modalités de neuro-imagerie fonctionnelle. Une originalité particulière de ce projet réside dans sa capacité à "personnaliser" une technique d'imagerie fonctionnelle prometteuse à un environnement clinique (c.-à-d., à l'étage de neurologie et à l'unité de soins intensifs dans notre cas). Cette étude est la première à rapporter avec succès des changements hémodynamiques sur l'ensemble du cortex chez des patients neurologiques à l'aide d'une surveillance vEEG-SPIRf prolongée au chevet.

Par la suite, nous avons évalué la faisabilité de la surveillance vEEG-SPIRf à long terme dans un environnement plus ardu : les soins intensifs neurologiques. Nous avons réalisé avec succès de multiples sessions de surveillance vEEG-SPIRf de très longue durée auprès de 11 patients comateux présentant différentes anomalies épileptiformes. Une augmentation significative de [HbO] et une diminution de [HbR] était présentes lors des crises. De plus, ces changements étaient

relativement proportionnels à la durée des crises. Bien qu'elles étaient de moins grande amplitude, de similaires $\Delta[\text{HbO}]$ et de $\Delta[\text{HbR}]$ était présents durant les bouffées lors de patrons de bouffées-suppression et lors de décharges périodiques de basses fréquences (i.e., $< 2\text{Hz}$).

Finalement, dans une étude subséquente, nous avons exploré l'hémodynamique corticale chez 11 patients comateux en état de mal épileptique non convulsif. Nous avons observé dans la majorité des cas, une augmentation de $[\text{HbO}]$, du volume sanguin cérébral et du débit sanguin cérébral, mais avec des changements variables de $[\text{HbR}]$ lors de courtes crises (inférieure à 100s). Cependant, lors de longues crises (plus de 100s), une augmentation de $[\text{HbR}]$ était observée. Ces résultats préliminaires suggèrent que les mécanismes de couplage neurovasculaire pendant l'état de mal épileptique peuvent être dysfonctionnels chez certains patients et induire un état hypoxique, notamment lors de crises prolongées.

En conclusion, les observations rapportées dans cette thèse confirment le potentiel clinique de la vEEG-SPIRf chez l'adulte, notamment pour la surveillance des patients admis aux soins intensifs neurologiques à haut risque de décharges épileptiformes. La poursuite de son développement pourrait éventuellement fournir aux neurologues et intensivistes un autre outil de surveillance neurologique.

Mots-clés : spectroscopie proche-infrarouge fonctionnelle, électroencéphalographie, crise épileptique, état de mal épileptique, décharges périodiques, bouffée-suppression, neuro-imagerie fonctionnelle, surveillance cérébrale, soins intensifs neurologiques, couplage neurovasculaire.

ABSTRACT

Functional near-infrared spectroscopy (fNIRS) is a noninvasive neuroimaging technique that measures concentration changes in oxy- and deoxyhemoglobin ($\Delta[\text{HbO}]$ and $\Delta[\text{HbR}]$) associated with brain activity. Over the past two decades, our group (and others) have combined fNIRS with electroencephalography (EEG) to record patients with refractory epilepsy and evaluate its potential as 1) a noninvasive brain mapping technique (e.g., language area localization and localization of epileptic foci) and 2) as a noninvasive approach to study neurovascular coupling during interictal spikes as well as during seizures. Despite promising results, many challenges remain before the EEG-fNIRS can be implemented in clinical practice. Indeed, installing the equipment still takes too much time, obtaining and maintaining good signal quality still requires close monitoring, and the appearance of discomfort as the recordings progress in time. For those reasons, EEG-fNIRS recordings to date have generally been of short duration (i.e., rarely more than two hours) with limited coverage of the cerebral cortex (i.e., typically one or two cortical areas) and in a controlled research setting (rather than at the bedside in a clinical setting).

Given its clinical potential, there is a need for continued efforts to develop fNIRS-EEG for clinical use. In particular, fNIRS-EEG has great potential in neurological intensive care. On the one hand, since patients admitted to the ICU are often comatose and/or sedated, the discomfort of wearing electrodes and optodes is no longer an issue. On the other hand, these patients generally present serious pathologies often associated with frequent epileptiform abnormalities on the EEG (periodic discharges, nonconvulsive seizures and status) whose hemodynamic impact on the brain, as well as their management remain controversial. The techniques currently used in intensive care units (intracranial pressure monitor, jugular venous oxygen saturation probe, transcranial Doppler, EEG alone without fNIRS) have limitations. Adding an fNIRS component to the EEG could perhaps elucidate the impact of some of these epileptiform abnormalities, guide their treatment and improve their monitoring.

Thus, this thesis aimed to 1) develop and validate a compact, wireless, whole-head EEG-fNIRS system for long-term monitoring of patients with various neurological disorders; 2) to evaluate the feasibility and potential of long-term video EEG-fNIRS (vEEG-fNIRS) monitoring of comatose patients admitted to the neurological intensive care unit with periodic discharges, seizures or an

electrophysiological pattern of burst-suppression; and 3) to study the neurovascular dynamics associated with nonconvulsive status epilepticus in comatose patients.

The first and second parts of the project describe the development and validation of a hybrid EEG-fNIRS system and personalized EEG-fNIRS "caps" to monitor whole cortical hemodynamics in neurological patients. We first demonstrated its overall performance in healthy participants performing two specific cognitive tasks (i.e., language and visual tasks) while sitting (for the former) and pedalling a bicycle (for the latter). Electrophysiological and hemodynamic measurements were validated using two commercial systems and showed, in all participants, high sensitivity and spatiotemporal specificity. We then demonstrated the clinical potential of our system in four patients suffering from various neurological disorders (e.g., refractory epilepsy and cerebrovascular diseases). We successfully performed prolonged vEEG-fNIRS recordings at the bedside of all these patients and observed clinically relevant hemodynamic changes* in agreement with other functional neuroimaging modalities. A particular originality of this project is its ability to "customize" a promising functional imaging technique specific clinical settings (i.e., neurology ward, epilepsy monitoring unit, and intensive care unit in our case). This study is the first to successfully report hemodynamic changes across the cortex in neurological patients using extended bedside vEEG-fNIRS monitoring.

Subsequently, we evaluated the feasibility of long-term vEEG-fNIRS monitoring in a more challenging environment: the neurological intensive care unit. We successfully performed multiple sessions of very long-term vEEG-fNIRS monitoring in 11 comatose patients with different epileptiform abnormalities. During seizures, a significant increase in [HbO] and a decrease in [HbR] were present. Moreover, these changes were relatively proportional to the duration of the seizures. Although they were of lesser magnitude, similar changes in [HbO] and [HbR] were present during bursts in burst-suppression patterns and with low-frequency (i.e., < 2Hz) periodic discharges.

Finally, in a subsequent study, we explored cortical hemodynamics in 11 comatose patients in nonconvulsive status epilepticus. We observed in the majority of cases an increase in [HbO], CBV and CBF, but with variable changes in [HbR] during short seizures (less than 100s). However,

* Throughout this thesis, we commonly referred to "cortical" hemodynamic changes simply as "hemodynamic changes". That latter terminology might be confusing clinically, as it might intuitively misguide the reader to "systemic" hemodynamic changes such as blood pressure and heart rate. Therefore, unless the word "systemic" or "cardiovascular" was used, "hemodynamic changes" represent the measurement obtained by fNIRS and correspond to "cortical" hemodynamic changes in the brain.

during prolonged seizures (more than 100s), an increase in [HbR] was seen. These preliminary results suggest that neurovascular coupling mechanisms during status epilepticus may be dysfunctional in some patients and induce a hypoxic state, especially during protracted seizures.

In conclusion, the observations reported in this thesis confirm the clinical potential of vEEG-fNIRS in adults, especially for monitoring patients admitted to neurological intensive care units at high risk of epileptiform discharges. Further development could eventually provide neurologists and intensivists with another tool for neurological monitoring.

Keywords: functional near-infrared spectroscopy, electroencephalography, seizures, status-epilepticus, periodic discharges, burst-suppression, functional neuroimaging, neuromonitoring, neurocritical care, neurovascular coupling.

CONTRIBUTION OF AUTHORS

Manuscript 1: Multichannel wearable fNIRS-EEG system for long-term clinical monitoring.

Published in Hum Brain Mapping (2018) Jan; 39(1): 7–23.

Authors: **Ali Kassab**, Jérôme Le Lan, Julie Tremblay, Phetsamone Vannasing, Mahya Dehbozorgi, Philippe Pouliot, Anne Gallagher, Frédéric Lesage, Mohamad Sawan, and Dang Khoa Nguyen

Ali Kassab contributed to the design of the study. Specifically, he suggested and implemented a unique validation process for healthy participants and patients. In the former, he also implemented a specific task (i.e., a visual task while pedalling on a bicycle) that would fully highlight the performance of the hybrid vEEG-fNIRS system. During the early stages of this study, he also contributed to the hardware and software optimization by 1) performing different acquisitions in patients with epilepsy and 2) suggesting and implementing new ideas that would facilitate the acquisition in clinical settings, including the development of novel EEG-fNIRS caps. He recruited the healthy participants, prepared the acquisition setup environment (fNIRS, EEG, neuronavigation system, tasks/stimulation system), and performed all the acquisitions (i.e., healthy subjects in a controlled laboratory environment and neurological patients at the clinical bedside). He analyzed and interpreted the results and wrote the manuscript. Jérôme Le Lan was the leading hardware developer and wrote the hardware aspects of the prototype in the method section of the manuscript. Julie Tremblay provided the homemade statistical toolbox and contributed to the analysis of fNIRS data. Phetsamone Vannasing contributed to the idea and development of the novel EEG-fNIRS caps and offered instructions on the use of the commercial NIRS (Imagent Tissue Oxymeter, ISS inc., Champlain, Illinois, USA) and EEG (Neuroscan SynAmps2 EEG/EP, Compumedics Ltd.) systems. Mahya Dehbozorgi was the leading software developer and wrote the software aspect of the prototype in the method section of the manuscript. Philippe Pouliot, Anne Gallagher, Frédéric Lesage, Mohamad Sawan, and Dang Khoa Nguyen supervised the project, contributed to the design of the study, interpretation of the results, redaction and revision of the manuscript. Dang Khoa Nguyen also analyzed the EEG and identified abnormal EEG patterns (e.g., seizures).

Manuscript 2: Cerebral hemodynamic changes during limb-shaking TIA: A near-infrared spectroscopy study.

Published in Neurology (2016) March 22;86(12):1166-8

Authors: **Ali Kassab**, Julie Tremblay, Alexandre Y. Poppe, Laurent Létourneau-Guillon, Anne Gallagher, Dang Khoa Nguyen

Ali Kassab prepared the setup environment for the acquisitions and performed the acquisitions at the patient's bedside. He analyzed and interpreted the results and wrote the manuscript. Julie Tremblay provided the homemade statistical toolbox, and contributed to the analysis of fNIRS data. Alexandre Y. Poppe, Laurent Létourneau-Guillon and Anne Gallagher contributed to the interpretation of the results, redaction and revision of the manuscript. Dang Khoa Nguyen supervised the project, contributed to the design of the study, interpretation of the results, redaction and revision of the manuscript.

Manuscript 3: Hemodynamic changes associated with common EEG patterns in critically ill patients: Pilot results from continuous EEG-fNIRS study

Published in Neuroimage Clinical (2021); 32:102880

Authors: **Ali Kassab**, Dènahin Hinnoutondji Toffa, Manon Robert, Frédéric Lesage, Ke Peng, Dang Khoa Nguyen

Ali Kassab had the idea of adding quantitative electrophysiological measurements (i.e., qEEG). For this study, he adopted and customized the Homer2 toolbox to simplify the analysis. He prepared the acquisition setup in the neuroICU and performed all the acquisitions at the patient's bedside. He curated and prepared all the data for the study. He analyzed, interpreted the result, and wrote the manuscript. He also helped in the marking of the EEG. Dènahin Hinnoutondji Toffa analyzed the EEG data, visually identifying all abnormal EEG findings (i.e., spikes, seizures, periodic discharges). Manon Robert contributed to the installation and data acquisition. Frédéric Lesage supervised the project and contributed to the interpretation of the results, redaction and revision of the manuscript. Ke Peng provided expertise in fNIRS data analysis. He developed and

validated the personalized methodological and statistical tools to analyze the fNIRS data. He also contributed to the writing of the methodological section of the manuscript. Dang Khoa Nguyen supervised the project, contributed to the design of the study, interpretation of the results, redaction and revision of the manuscript.

Manuscript 4: Cortical hemodynamics of electrographic status epilepticus in the critically ill
Submitted to Neurology

Authors: **Ali Kassab**, Dènahin Hinnoutondji Toffa, Manon Robert, Frédéric Lesage, Ke Peng, Dang Khoa Nguyen

Following the acquisition of a new commercial fNIRS system by Rogue Inc., Ali Kassab first tested and validated the new system on healthy participants and one patient with refractory epilepsy in the epilepsy monitoring unit before performing bedside recordings in the neuroICU. He had the idea of implementing early during this project the use of collodion for installing the optodes. To simplify the installation of optodes, he developed small, customizable 3D optode holders compatible with collodion. He also had the idea of including continuous systemic physiological measurement. He prepared the acquisition setup in the neuroICU and performed all the acquisitions at the patient's bedside. He curated and prepared all the data for the study. He analyzed, interpreted the result, and wrote the manuscript. He also helped in the marking of the EEG. Finally, he refined the quantitative EEG analysis, customized the Homer2 toolbox and integrated the NIRStorm toolbox. Dènahin Hinnoutondji Toffa analyzed the EEG data, visually identifying all abnormal EEG findings (i.e., spikes, seizures, periodic discharges). Manon Robert contributed to the installation and data acquisition. Frédéric Lesage supervised the project, contributed to the interpretation of the results, redaction and revision of the manuscript. Ke Peng provided expertise in fNIRS data analysis and contributed to the statistical analysis of the data. He also contributed to the redaction and revision of the manuscript. Dang Khoa Nguyen supervised the project, contributed to the design of the study, interpretation of the results, redaction and revision of the manuscript.

STATEMENT OF ORIGINALITY

- In order to facilitate the long-term acquisition of simultaneous electrophysiological and hemodynamic brain activity in the clinical setting, we developed and validated a compact and wearable hybrid EEG-fNIRS system, including customizable EEG-fNIRS caps.
- This fairly unique system (even by today's standards) enabled us to conduct for the first time long-term whole-head bedside vEEG-fNIRS measurements in several neurological patients. Patients' symptoms and electrophysiological disturbances were associated with relatively specific hemodynamic changes.
- Further pushing the limits of conducting long-term vEEG-fNIRS monitoring, we used our hybrid vEEG-fNIRS system to monitor patients in the neuroICU, non-invasively capturing for the first time in adults, continuous hemodynamic changes associated with critical care seizures. Additionally, we also captured cortical hemodynamics during periodic discharges, and burst-suppression patterns highlighting the ability to employ vEEG-fNIRS to assess the neurovascular coupling associated with various abnormal epileptiform patterns in critically ill adult patients.
- We integrated collodion and systemic physiological monitoring into our methodology and performed long-term whole-head vEEG-fNIRS monitoring to assess the cortical hemodynamics of critically ill patients presenting clinically silent recurrent and/or prolonged seizures (i.e., nonconvulsive status epilepticus).
- Finally, we report for the first time continuous hemodynamic changes **over the entire cortex** during electrographic (i.e., nonconvulsive) status epilepticus.

TABLE OF CONTENTS

RÉSUMÉ	1
ABSTRACT.....	4
CONTRIBUTION OF AUTHORS.....	7
STATEMENT OF ORIGINALITY	10
Table of contents.....	11
List of tables.....	16
List of figures.....	17
List of symbols and abbreviations	20
Dedications	30
Acknowledgments.....	31
CHAPTER 1 - INTRODUCTION.....	34
1.1 Background and motivation	34
1.2 Problem statement, hypothesis and objectives.....	38
1.3 Thesis order.....	42
CHAPTER 2 – SEIZURE, EPILEPSY, AND EPILEPTIFORM DISCHARGES.....	43
2.1 Terminology	43
2.1.1 A brief overview on critical care seizures	43
2.1.2 Seizures.....	43
2.1.3 A brief overview on epilepsy.....	45
2.1.4 Interictal epileptiform discharges (IEDs)	45
2.2 Electroencephalography (EEG).....	46
2.3 Clinically challenging EEG patterns in the critically ill	48
2.3.1 Nonconvulsive seizures (NCS) and nonconvulsive status epilepticus (NCSE)	48
2.3.2 Interictal-ictal continuum	51
2.3.3 Burst-suppression EEG pattern	59
CHAPTER 3 – NEUROVASCULAR COUPLING.....	61
3.1 Physiological (“normal”) neurometabolic and neurovascular coupling	61
3.1.1 Brain metabolism and neurometabolic coupling.....	61
3.1.2 Brain circulation and neurovascular coupling	64
3.2 Metabolism during seizures	68

3.3 Hemodynamics and neurovascular coupling during seizures	69
3.4 Metabolism during periodic discharges	70
3.5 Hemodynamics and neurovascular coupling during periodic discharges	71
3.6 Metabolism during burst-suppression	72
3.7 Hemodynamics and neurovascular coupling during burst-suppression	73
CHAPTER 4 – CURRENT TECHNIQUES TO INVESTIGATE AND MONITOR EPILEPTIFORM DISCHARGES IN CRITICALLY ILL PATIENTS	75
4.1 Positron emission tomography (PET)	75
4.2 Single-photon emission computerized tomography (SPECT)	76
4.3 EEG-fMRI	77
4.4 Noninvasive continuous electrophysiological monitoring	78
4.5 Invasive neuromonitoring modalities	79
4.5.1 Invasive continuous EEG monitoring	79
4.5.2 Intracranial pressure monitoring (ICP)	80
4.5.3 Jugular venous bulb oximetry (SjvO ₂)	80
4.5.4 Intraparenchymal cerebral oxygenation monitoring (PbtO ₂)	81
4.5.5 Cerebral microdialysis	82
4.5.6 Laser Doppler Flowmetry and Thermal Diffusion Flowmetry	83
4.7 Additional modalities	83
4.7.1 Pupillometry	83
4.7.2 Transcranial Doppler	84
4.7.3 Brain ultrasound	84
CHAPTER 5 – FUNCTIONAL NEAR-INFRARED SPECTROSCOPY FOR THE STUDY OF EPILEPTIFORM DISCHARGES	86
5.1 Functional near-infrared spectroscopy	86
5.1.1 Terminology	86
5.1.2 Brief historical overview and early application	87
5.1.3 Technological progress	88
5.1.4 Instrumentation type	90
5.1.5 Physical principles and principle of diffuse optical tomography	97
5.2 Brief overview on the current applications of fNIRS in neuroscience	106
5.3 Applications in non-critical care seizures and epilepsy	109

5.4 Investigating seizures, periodic discharges, and burst-suppression in the critically ill with fNIRS: a critical review.....	116
5.5 Current clinical challenges of EEG-fNIRS	125
CHAPTER 6 – METHODOLOGY AND INSTRUMENTATION	128
6.1. Multichannel vEEG-fNIRS system for long-term whole-head monitoring.....	128
6.2 The brain-optode interface for long-term whole-head vEEG-fNIRS monitoring.....	133
6.2.1 “Optode probe”.....	133
6.2.2 “Adhesive techniques”	135
6.2.3 Optode profile.....	137
6.3 Toolboxes for NIRS data: statistical analysis and image reconstruction.....	140
6.3.1 Video-EEG analysis	141
6.3.2 Preprocessing and statistical analysis of fNIRS data.....	141
6.3.3 Cortical reconstruction	149
CHAPTER 7 – MANUSCRIPT #1.....	151
7.1 Abstract	152
7.2 Introduction.....	152
7.3 Material and Methods.....	154
7.3.1 General Description of the Portable fNIRS-EEG Prototype and Headgear.....	154
7.3.2 EEG and NIRS Circuitry	156
7.3.3 Digital Architecture	157
7.3.4 Phantom studies.....	159
7.3.5 Patient Population.....	159
7.3.6 Validation and Performance Studies	159
7.3.7 Data Processing and Signal Analysis	164
7.4 Results.....	166
7.4.1 Phantom validation.....	166
7.4.2 Physiological Validation.....	166
7.4.3 Prototype Validation in Clinical Conditions	172
7.5 Discussion	175
7.5.1 Comparison with other ‘portable’ fNIRS systems:	176
7.5.2 Limitations.....	178
7.5.3 Future perspectives.....	178
7.6 Conclusions	178

7.7 Acknowledgements	179
7.8 Appendix	180
CHAPTER 8 – MANUSCRIPT #2.....	192
8.1 Introduction	193
8.2 Case report.....	193
8.3 Discussion	195
8.4 Appendix	196
CHAPTER 9 – MANUSCRIPT #3.....	197
9.1 Abstract	198
9.2 Introduction	198
9.3 Material and methods	201
9.3.1 Patients.....	201
9.3.2 cEEG-fNIRS data acquisition.....	202
9.3.3 Data processing and analysis	203
9.4 Results	209
9.4.1 Patient clinical information	209
9.4.2 Hemodynamic changes associated with NCS in NCSE	213
9.4.3 Hemodynamic changes associated with BS	217
9.4.4 Hemodynamic changes associated with PDs.....	222
9.4.5 Case studies	223
9.5 Discussion	226
9.5.1 Increased blood oxygenation during seizures in status epilepticus	227
9.5.2 Non-uniform cortical hemodynamic profile during burst-suppression	227
9.5.3 Potential factors associated with hemodynamic response to PDs	229
9.5.4 Feasibility of conducting cEEG-fNIRS in the neuroICU.....	230
9.5.5 Limitations.....	231
9.6 Conclusions	232
9.7 Acknowledgements	233
9.8 Appendix	234
CHAPTER 10 – MANUSCRIPT #4.....	236
10.1 Abstract	237
10.2 Introduction	238

10.3 Materials and methods	239
10.3.1 Study design and clinical data collection	239
10.3.2 EEG interpretation and event marking	240
10.3.3 Long-term whole-head vEEG-fNIRS monitoring protocol.....	240
10.3.4 fNIRS data analysis	241
10.3.5 Systemic physiology and sedation level.....	244
10.4 Results.....	245
10.4.1 Patient clinical and monitoring information.....	245
10.4.2 Temporal changes of cortical hemodynamic.....	249
10.4.3 Group analysis of cortical hemodynamic changes and seizure duration.....	258
10.4.4 Prediction of response directionality based on seizure duration	260
10.4.5 Systemic physiological monitoring and laboratory results.....	261
10.5 Discussion	261
10.5.1 Summary of findings	261
10.5.2 Cortical oxygen dynamics during recurring short and/or prolonged electrographic seizures	262
10.5.3 Potentials of vEEG-fNIRS monitoring in critical care seizures	265
10.5.5 Limitations.....	265
10.6 Conclusions.....	267
10.7 Acknowledgements	267
10.8 Appendix	268
CHAPTER 11 – GENERAL DISCUSSION AND CONCLUSION.....	276
11.1 Summary of main contributions.....	276
11.1.1 Objective 1.....	277
11.1.2 Objective 2.....	279
11.1.3 Objective 3.....	282
11.2 Limitations and future directions	283
11.2.1 Limitations.....	283
11.2.2 Future directions.....	286
11.3 Conclusion.....	287
CHAPTER 12 – PARRALEL AND COLLABORATIVE WORK.....	289
REFERENCES	291

LIST OF TABLES

Table 1	46
Table 2	65
Table 3	90
Table 4	93
Table 5	96
Table 6	108
Table 7	122
Table 7 (continued)	123
Table 7 (continued)	124
Table 8	139
Table 9	144
Table 10	168
Table 11	171
Table 12	174
Table 13	186
Table 14	187
Table 14 (continued)	188
Table 14 (continued)	189
Table 14 (continued)	190
Table 15	191
Table 16	210
Table 17	211
Table 18	246
Table 18 (continued)	247
Table 19	248
Table 20	250
Table 20 (continued)	251

LIST OF FIGURES

Figure 1	41
Figure 2	47
Figure 3	49
Figure 4	52
Figure 5	53
Figure 6	53
Figure 7	54
Figure 8	56
Figure 8 (continued).....	57
Figure 8 (continued).....	58
Figure 9	59
Figure 10	63
Figure 11	65
Figure 12	90
Figure 13	97
Figure 14	101
Figure 15	103
Figure 16	104
Figure 17	110
Figure 18	115
Figure 19	118
Figure 20	125
Figure 21	131
Figure 22	132
Figure 23	136
Figure 24	138
Figure 25	155
Figure 26	156
Figure 27	161
Figure 28	163

Supplementary Figure 1	180
Supplementary Figure 1 (continued)	181
Supplementary Figure 2	182
Supplementary Figure 3	183
Supplementary Figure 4	184
Supplementary Figure 5	185
Figure 29	195
Supplementary Figure 6	196
Figure 30	202
Figure 31	212
Figure 32	215
Figure 33	216
Figure 34	218
Figure 35	219
Figure 36	221
Figure 37	221
Supplementary Figure 7	234
Supplementary Figure 8	235
Figure 38	253
Figure 39	256
Figure 39 (continued)	257
Figure 40	259
Figure 41	260
Figure 42	261
Supplementary Figure 9	268
Supplementary Figure 10	269
Supplementary Figure 11	270
Supplementary Figure 12	271
Supplementary Figure 13	272
Supplementary Figure 14	273
Supplementary Figure 15	274

Supplementary Figure 16.....	275
------------------------------	-----

LIST OF SYMBOLS AND ABBREVIATIONS

2D	Two-dimensional
3D	Three-dimensional
Δ	Relative changes/differences
[X]	Concentration of species X
$\Delta[X]$	Change concentration of species X
#	Number
\bar{x}	Average
\approx	Approximately
\uparrow	Increasing
\downarrow	Decreasing
\updownarrow	Fluctuation
$\mu\alpha$	Absorption coefficient
$\mu\sigma$	Scattering coefficient
φ	Phase delay
α -KGDH	α -ketoglutarate dehydrogenase
a	Absorption (or extinction) coefficient of a specific compound
A	Light intensity or optical density attenuation
A	Amps or ampere
ACNS	American Clinical Neurophysiology Society
ACV	Assisted controlled ventilation
ADC	Analog-to-digital converter
ADC	Apparent diffusion coefficient
AEDs	Antiepileptic drugs
aEEG	Amplitude EEG
Ah	Ampere hour
AI	Adrenal insufficiency
Aka	Also known as
AM	Arachnoid mater
ANT	Adenine nucleotide translocator
AntPFC	Anterior prefrontal cortex

AP	Aspiration pneumonia
APD	Avalanche photodiode
ARF	Acute renal failure
ASL	Arterial spin labeling
ASMs	Antiseizure medications
ATP	Adenosine 5'-triphosphate
B	Bilateral
BFI ^{ICG}	Blood flow index using near-infrared spectroscopy and indocyanine green
Bi	Bilateral
BIPDs	Bilateral independent periodic discharges
BIRDs	Brief potentially ictal rhythmic discharges
B _L	Broca left
BLL	Beer-Lambert law
BMI	Body mass index
BNC	Bayonet Neill–Concelman
BOLD	Blood-oxygenation-level-dependent
B _R	Broca right
BS	Burst-suppression
<i>c</i>	Concentration of the absorbing compound
CBF	Cerebral blood flow
CBV	Cerebral blood volume
CBZ	Carbamazepine
CcO	Cytochrome <i>c</i> oxidase
CLB	Clobazam
cm ²	Square centimeter
CMB	Cerebral microbleed
CMR _{glu}	Cerebral metabolic rate in glucose
CMRO ₂	Cerebral metabolic rate in oxygen
CNS	Central nervous system
CO	Carbon monoxide
Com.	Commercial

COPD	Chronic obstructive pulmonary disorder
CPA	Cardio-pulmonary arrest
CPTO	Centro-parieto-temporo-occipital
CS	Citrate synthase
CSE	Convulsive status epilepticus
CSF	Cerebrospinal fluid
CT	Cortical thickness
CTP	Citalopram
CTscan	Computed tomography scan
CW	Continuous-wave
<i>d</i>	Optical pathlength or thickness of the medium
D	Detectors
DAC	Digital-to-analog converter
DC	Direct current
DCA	Diffuse cerebral atrophy
Decd.	Deceased
DLFC	Dorsolateral frontal cortex
DM	Dura mater
DOT	Diffuse optical tomography
DPF	Differential pathlength factor
DRE	Ddrug-resistant epilepsy
DWI	Diffuse weighted imaging
Dx	Diagnosis
ECoG	Electrocorticography / depth electroencephalography
ECSE	Electroclinical status epilepticus
EEG	Electroencephalography
EKG	Electrocardiogram
EMU	Epilepsy monitoring unit
EROS	Event-related optical signal
ESE	Electrographic status epilepticus
ESES	Electrical status epilepticus of slow-wave sleep

ETC	Electron transport chain
EtCO ₂	Mean end-tidal carbon dioxide
F	Female
F	Frontal
FC	Fronto-central
FCD	Focal cortical dysplasia
FCT	Fronto-centro-temporal
FD	Frequency domain
FLAIR	Fluid attenuated inversion recovery
FM	Frequency multiplexed
fMRI	Functional magnetic resonance imaging
FMSE :	Focal motor status epilepticus
fNIRS	Functional near-infrared spectroscopy
FPL	Fronto-parietal lobe
FTDI	Future Technology Devices International
F _{TOE}	Fractional tissue oxygen extraction
<i>G</i>	Additional factors responsible for light attenuation
GCK	Glucokinase
GCS	Glasgow Coma Scale
GLM	General linear model
GPDs	Generalized periodic discharges
GPDs + S	Generalized rhythmic delta activity + spike
GUI	Graphical user interface
H	Hemisphere
HbD	Hemoglobin difference
HbO	Oxygenated hemoglobin
HbO ₂	Oxygenated hemoglobin
HbR	Deoxygenated (or reduced) hemoglobin
HbT	Total hemoglobin
HE	Hashimoto encephalopathy
HIBI	Hypoxic-ischemic brain injury

HIE	Hypoxic-ischemic encephalopathy
HIT	Heparin-induced thrombocytopenia
HME	Hemimegalencephaly
HTN	Hypertension
HR	Heart rate
HRF	Hemodynamic response function
Hz	Hertz
I_0	Incident light signal
I_x	Transmitted light signal at different distance “x”
$I(t)$	Temporal point spread function of the transmitted light signal
ICA	Independent Component Analysis
ICG	Indocyanine green
ICH	Intracranial hemorrhage
ICG ^{fluo}	Indocyanine Green Fluorescent Imaging
ICU	Intensive care unit
IDH	Isocitrate dehydrogenase
IEDs	Interictal epileptiform discharges
IFG	Inferior frontal gyrus
IHT	Inter-hospital transfer
IIC	Ictal-interictal continuum
iSPECT	Ictal single position emission computed tomography
iiSPECT	Interictal single positron emission computed tomography
I-Sz-I	Inter-seizure-interval
“K”	One thousand (\$)
kHz	Kilo hertz
L	Left
LCM	Lacosamide
LDs	Laser diodes
LEDs	Light-emitting diodes
LEV	Levetiracetam
LF	Left frontal

LGS	Lennox-Gastaut syndrome
LH	Left hemisphere
LI	Laterality index
LPDs	Lateralized periodic discharges
LPDs + F	Lateralized periodic discharges + fast activity
LPDs + R	Lateralized periodic discharges + rhythmic activity
LT	Left temporal
LTG	Lamotrigine
“M”	One million (\$)
m	Milli
M	Male
MAs	Motion artifacts
MABP	Mean arterial blood pressure
MAP	Mean arterial pressure
mBLL	Modified Beer Lambert Law
MCA	Middle cerebral artery
MDZ	Midazolam
MED	Multiple electrolyte disorders
MEG	Magnetoencephalography
MFG	Middle frontal gyrus
MfPDs	Multifocal periodic discharges
min	Minutes
MNT	Monitoring
MPDs	Monolithic photodiodes
MRA	Magnetic resonance angiography
MRI	Magnetic resonance imaging
MSE	Myoclonic status epilepticus
Mu	Multi
Na ⁺ /K ⁺	Sodium/potassium
NADH	Nicotinamide adenine dinucleotide + hydrogen
NeuroICU	Neurointensive care unit

NCS	Nonconvulsive seizure
NCSE	Nonconvulsive status epilepticus
NIRS	Near-infrared spectroscopy
NIRSm	Near-infrared spectroscopy monitoring
NORSE	New-onset refractory status-epilepticus
NR	Not reported
NVC	Neurovascular coupling
NE	Not evaluated
N/R	Not reported
N/A	Not available
OD	Optical density
P	Pedalling
PbTO ₂	Continuous brain tissue oxygen
PCA	Principal component analysis
PCB	Printed circuit board
PDs	Periodic discharges
PDH	Pyruvate dehydrogenase
PET	Positron emission tomography
PFK	Phosphofructokinase
PHT	Phenytoin
PL	Pathlength
PK:	Pyruvate kinase
PM	Pia matter
PNS	Peripheral nervous system
PPF	Partial pathlength factor
PreCG	Precentral gyrus
Prot.	Prototype
PSE	Partial status epilepticus
PTL	Posterior temporal lobe
PVF	Partial volume factor
R	Right

RA	Magnetic resonance angiography
RASS	Mean Richmond Agitation and Sedation Scale value
rCBF	Regional cerebral blood flow
RCSE	Refractory convulsive status epilepticus,
RDA	Rhythmic delta activity
RF	Right frontal
R _H	Right hemisphere
RNCSE	Refractory nonconvulsive status epilepticus
RSE	Refractory status epilepticus
rSO ₂	Regional cerebral oxygen saturation
s	Seconds
S	Sources
SaO ₂	Arterial oxygen saturation (in %)
SE	Status epilepticus
S.E.	Standard error
sec	seconds
S.D.	Standard deviation
SFG	Superior frontal gyrus
SiPD	Silicon photodiode
SIRPIDs	Stimulus-induced rhythmic, periodic, or ictal discharges
SK	Skull thickness
SPECT	Single photon emission computed tomography
SPI	Serial Peripheral Interface
SMG	Supramarginal gyrus
SNR	Signal-to-noise ratio
SR	Sampling rate
SREAT	Steroid-responsive encephalopathy associated with autoimmune thyroiditis
SRS	Spatially resolved spectroscopy
SRSE	Super-refractory status epilepticus
STESS	Status Epilepticus Severity Score
STL	Superior temporal lobe

SpO ₂	Mean peripheral oxygen saturation
Ss	Sitting still
StO ₂	Tissue oxygen saturation (in %)
SvjO ₂	Continuous jugular bulb venous oxygen saturation (in %)
SVT	Sinus venous thrombosis
SW	Spike-and-wave or sharp-and-wave
Sz	Seizure
T2D	Type 2 diabetes
T°	Mean temperature
T	Temporal
TCA	Tricarboxylic acid
TCD	Transcranial doppler
TD	Time-domain
<i>TIA</i>	Transient ischemic attack
TIA	Transimpedance amplifier
TL	Temporal lobe
TME	Toxico-metabolic encephalopathy
TMS	Transcranial magnetic stimulation
TOI	Tissue oxygenation index
TPM	Topiramate
TSC	Tuberous sclerosis complex
TSE	Tonic status epilepticus
TSI	Tissue saturation index
TWs	Triphasic waves
U	Unilateral
UART	Universal asynchronous receiver/transmitter
UIPDs	Unilateral independent periodic discharges
USB	Universal Serial Bus
UTI	Urinary tract infection
V	Voltage / volts
VAC	Volume assisted control

VCSEL	Vertical-cavity surface-emitting laser
vEEG	Video-electroencephalography
VEP	Visually evoked potential
VS	Vegetative state
w B	With batteries
WL	Wavelength
w/o B	Without batteries

DEDICATIONS

*To my beautiful mother who has dedicated her entire life to me.
Despite all the hardship and sacrifice you have been through, you have never shown anything
less than love, affection, and devotion.*

I also dedicate this work to my father, aunts, and uncles; I love you very much.

ACKNOWLEDGMENTS

I firmly believe that a simple expression of my gratitude and appreciation to my research director would be a great understatement. Dr. Dang Khoa Nguyen took me under his supervision at a quite difficult time in my academic path. Despite my interests in neurology and epilepsy, I approached Dr. Dang Khoa Nguyen without any real experience in clinical research, even less in functional neuroimaging and everything related to optical imaging (i.e., acquisition, signal processing/analysis, statistics). However, Dr. Dang Khoa Nguyen believed in me and gave me an opportunity that generally very few would have offered. As one of his students, he was always kind, respectful, and extremely patient. He was a constant source of guidance, nourishing me with suggestions and ideas to achieve the goals of this Ph.D. He also pushed me to strive further in my projects and constantly encouraged me in my personal path. Throughout the years, I have been impressed by his vast and profound knowledge as a researcher and clinician and admired his calm, humane, and professional approach toward his patients. While I learned so much knowledge, I wished I had been able to spend more time by his side learning even more. Personally, Dr. Dang Khoa Nguyen is more than a supervisor, but a great mentor, someone I look up to, hopefully, to follow in his "big" footsteps one day. I will always be highly grateful for all the opportunities he gave me.

I would also like to thank all members I worked with of the Imagine group at the Polytechnique Montreal: Prof. Mohamad Sawan, Prof. Frédéric Lesage, Prof. Philippe Pouliot, Jérôme Le Lan, Mahya Dehbozorgi, Amal Kassab, and our collaborators at the Saint-Justine Hospital: Dr. Anne Gallagher, Phetsamone Vannasing, Julie Tremblay. It was an honour to be part of a multidisciplinary group passionate about optical imaging and its applications in neuroscience. Certainly, it is quite impressive to see what can be achieved when different fields of science come together to share knowledge, ideas and passion.

I want to especially thank Prof. Frédéric Lesage for opening his optical imaging lab and assisting me whenever I faced technical difficulties with our system. His vast knowledge in optical brain imaging and critical inputs at each meeting were precious for the quality of these projects. Similarly, I would like to thank Prof. Philippe Pouliot for his expertise in statistical analysis early in our project involving neuroICU patients.

I would also like to thank Dr. Anne Gallagher, who opened her lab without reluctance, particularly when a second validation of our system was required. I greatly appreciate the time she took for my internal evaluations and the guidance and resources she kindly offered during my Ph.D. I must also especially acknowledge two individuals in her lab: Phetsamone Vannasing and Julie Tremblay, who welcomed me during my master's studies, taught me the basics of fNIRS acquisitions and analysis, and together with Amal Kassab, the foundations of EEG-fNIRS caps development.

I must especially acknowledge my close and very dear colleagues. Dr. Dènahin Hinnoutondji Toffa who shared his expertise in EEG and gave so much of his precious time, day and night, to mark the EEGs. I learned so much about the art of EEG interpretation thanks to him. Dr. Ke Peng, who with his vast expertise in fNIRS analysis, has provided enormous and invaluable help in these projects. He spent considerable time making sure everything was analyzed with the highest standards and was always available at any time to help whenever I faced a particular problem. Manon Robert, who welcomed me in our first lab back at Notre-Dame Hospital and taught me the basic skills for proper EEG setups. She was of great assistance during the numerous and lengthy testing periods and recordings and was the "moral support" of the lab, always ensuring that everyone felt fine. Honestly, I believe that without their help, it would have been nearly impossible to achieve what we have accomplished during this time. Also, thanks to my other colleagues in the lab: Thi Phuoc Yen Tran, Parikshat Sirpal, Eli Bou Assi, and Daphné Citherlet, for being present, exchanging at some times great ideas, and, most importantly, always smiling back.

I am sincerely grateful to Dr. Patrick Cossette for taking the time for my internal evaluations and the guidance he provided, as well. Likewise, I am deeply thankful Dr. Arline Bérubé and Dr. Samuel Lapalme-Remis, who believed in this project and kindly referred some patients. I would also like to thank the entire epilepsy monitoring unit and neuroICU staff at the Centre Hospitalier de l'Université de Montréal for their kindness, patience and assistance during our recordings. Also, special thanks to Micheline Gravel and Veronique Cloutier for their kindness and for taking care of all the administrative paperwork for these projects.

I would also like to deeply recognize all the patients and families who have contributed or considered contributing to these studies. These patients are human beings inflicted with severe conditions that profoundly touch the families and everyone who cares for them.

Finally, thanks to all the financial support provided by the Department of neurosciences of the Université de Montréal and the Fonds de recherche santé du Québec (FRSQ). This project was also supported by the Canadian Institutes of Health Research (CIHR), the Heart and Stroke Foundation of Canada in Partnership with CIHR, the National Sciences and Engineering Research Council in partnership with CIHR, the Engineering Research Council in partnership with CIHR, and the TransMedTech Excellence Scholarship from Canada First Research Excellence Fund.

CHAPTER 1 - INTRODUCTION

1.1 Background and motivation

In healthy individuals, the brain is a highly vascularized organ in which cerebral blood flow (CBF) is tightly regulated to brain activity, ensuring that it constantly receives enough oxygen and glucose. The macroscopic and microscopic regulatory mechanisms that tightly link neuronal activity and changes in CBF are called neurovascular coupling mechanisms (Iadecola, 2017). Under normal physiological condition, neuronal activity, either due to an external or internal stimulus, lead to an increase in neuronal metabolism (i.e., cerebral metabolic rate of oxygen and cerebral metabolic rate of glucose) and, consequently, to an increase in brain hemodynamics (e.g., brain tissue oxygen concentration, oxyhemoglobin – [HbO], total hemoglobin – [HbT], cerebral blood volume – CBV, and CBF). It is by this feed-forward mechanism that our “brain” attempts to perfuse active neurons with “fresh” blood (Iadecola, 2017). At the microscopic level, neuronal activity generates changes at the neurovascular unit comprised of the contractile vasculature’s elements (i.e., smooth muscle cells in the arterioles and pericytes in capillaries), endothelial cells, neurons and glial cells (i.e., astrocytes) (Philips et al., 2016; Iadecola, 2017). The release of glutamate, which acts on both neurons and astrocytes, further releases chemical signals necessary to regulate CBF. In addition to the close temporal link between neuronal activity and cerebral hemodynamics, a spatial relationship also exists, where brain regions with higher activity receive higher blood flow (i.e., functional hyperemia) (Philips et al., 2016; Iadecola, 2017).

Researchers investigating the neurovascular coupling rely on a wide range of techniques in neuroscience to explore the structure and function of the brain in health and disease. While microscopic modalities used in animal studies (e.g., patch-clamp, calcium imaging, two-photon imaging) remain essential to our understanding of brain electrophysiology, metabolism and hemodynamics, other methods enable a more direct investigation of the living human brain. Among those methods are functional brain imaging techniques such as positron emission tomography (PET), single-photon emission computerized tomography (SPECT) and functional magnetic resonance imaging (fMRI). These methods are attractive as surrogates of neuronal

activity (i.e., metabolism and hemodynamics) can be measured directly in *in-vivo* with little (i.e., PET, SPECT) to no (i.e., fMRI) invasiveness.

Seizures are transient clinical manifestations related to abnormal and excessive neuronal discharges. Symptoms and signs vary according to the location, extent, propagation and duration of the ictal discharge. As such, several types of seizures exist, the most commonly known being bilateral tonic-clonic seizures (i.e., convulsions). Seizures are said to be “acute” when occurring in an acute context (acute brain hemorrhage or acute brain infection) or “spontaneous” when occurring outside of an acute context (e.g., six months after an acute brain hemorrhage due to residual brain scarring). While most seizures last less than five minutes, some may be more prolonged (> 5 minutes) or are repetitive without return of consciousness in between, a condition called status epilepticus (SE). In general, patients presenting seizures also have interictal epileptiform discharges (IEDs) (*aka* “spikes”) which are brief (20-200 milliseconds) discharges clearly identifiable on EEG but are not sustained or strong enough to generate symptoms. Furthermore, particularly in patients with acute brain injury, a wide range of abnormal epileptiform patterns have been described based on their appearance on EEG including periodic discharges (*aka* PDs) which are brief discharges recurring every second or more, stimulus-induced rhythmic, periodic, or ictal-like/appearing discharges (*aka* SIRPIDs) which are longer discharges brought about or exacerbated by an alerting stimulus (e.g., sternal rub, nail bed pressure), brief ictal-like rhythmic discharges (*aka* BIRDs) which are epileptiform discharges lasting less than 10 seconds, nonconvulsive seizures (*aka* NCS) which are epileptic discharges lasting more than 10 seconds but without clinical manifestations, and nonconvulsive status epilepticus (*aka* NCSE) which are NCS lasting > 10 minutes or repetitive NCS. Lastly, during the pharmacological management of patients with NCSE, a burst-suppression pattern (*aka* BS) is commonly induced which is characterized by periods of high-voltage brain activity (i.e., burst) alternating with periods of low amplitude activity or isoelectric quiescence (i.e., suppression).

Unlike “normal” (physiological) cortical processing, seizures are abnormal (pathological) brain events characterized by a massive increase in neuronal metabolism, placing cerebral autoregulation in a supranormal state. Whether the mechanisms that govern the neurovascular response during physiological brain activity can adapt to meet the heightened demand of the

“seizing” brain, or not and consequently contribute to neuronal injury is a matter of ongoing research (Schwartz, 2007; Baruah et al., 2020). Over the years, several animal and human studies have reported contradicting results regarding brain hemodynamics during seizures and, indirectly, the integrity of neurovascular coupling mechanism during seizures (Schwartz, 2007). Seizure-induced hyperperfusion has been widely observed by brain perfusion studies (Gibbs, 1933; Penfield, 1933, 1939; Zhao et al., 2009). Meanwhile, PET studies have been less consistent, with some researchers observing ictal hypometabolism, suggesting inadequate perfusion and altered neurovascular coupling (Savic et al., 1997; Lamusuo et al., 2001) and others reporting hypermetabolism suggesting the opposite (Bansal et al., 2016; Schur et al., 2018). As for human studies employing EEG-fMRI, they have favored a preserved neurovascular coupling during IEDs and seizures (i.e., adequate CBF perfusion) (Aghakhani et al., 2004; Salek-Haddadi et al., 2002, 2006) although negative blood-oxygen-level-dependent (BOLD) activations have also been observed during IEDs in up to 40% of patients with epilepsy (Pittau et al., 2013; Jacob et al., 2014). Only a few number of studies have looked at the brain hemodynamics of acute seizures in critically ill patients; the number of studies assessing the hemodynamic impact of other abnormal epileptiform patterns are even fewer. During NCS (including NCSE), heterogeneous changes in brain metabolism (Doherty et al., 2004; Siclari et al., 2013; Vespa et al., 2016) and oxygen levels have been reported (Claassen et al., 2013). Regarding PDs, the hemodynamic changes and potential risk of neuronal injury seem to depend upon their frequency, with higher frequency discharges being possibly associated with hypoxia and a greater risk of neuronal damage (Witsch et al., 2017). As for BS patterns, animal studies using EEG-fMRI (Mäkiranta et al., 2002) and optical imaging (Sutin et al., 2014) have reported an increase in BOLD and CBV, respectively, during burst activity. Clearly, additional studies are required to improve our understanding of the neurovascular coupling during spontaneous/chronic seizures in patients with epilepsy as well as acute seizures and other abnormal epileptiform discharges commonly seen in the critically ill.

While functional neuroimaging techniques such as SPECT, PET, and fMRI can capture whole-brain metabolism and hemodynamics, one major limitation is their low temporal resolution. Seizures are a highly dynamic process that constantly changes over time. Similarly, the various mechanisms involved during neurovascular coupling are also dynamic. Therefore, in order to fully appreciate the neurovascular coupling dynamics involved during seizures, it is crucial to have

continuous electrophysiological, metabolic and hemodynamic measurements, and ideally at different spatial scales (Yang et al., 2021). None of the above-mentioned techniques are suited for prolonged recordings (necessary to capture and study seizures). Moreover, none can be performed at the bedside (a must to study critically ill patients). Functional near-infrared spectroscopy (fNIRS) is a relatively novel noninvasive neuroimaging and neuromonitoring technique. Since its introduction in the late 70s (Jöbsis, 1977), fNIRS have shown great potential in various subfields of neurology including epilepsy (Obrig et al., 2014; Peng et al., 2016). It is currently the only technique that offers the possibility of investigating widespread cortical hemodynamics and metabolism with high temporal and relatively high spatial resolutions (on the cortex). In addition, it can easily be combined with video-EEG (i.e., vEEG-fNIRS), enabling to capture electrophysiological brain activity simultaneously.

Unfortunately, few studies have applied vEEG-fNIRS to investigate seizures in patients with epilepsy, and even fewer to investigate acute seizures and other abnormal epileptiform patterns in the critically ill. These have primarily been performed in a pediatric population, mostly in single patients or small series, with a small number of seizures captured, and with limited spatial coverage. This is primarily due to the numerous challenges researchers face when performing long-term whole-head vEEG-fNIRS monitoring in the clinical setting.

1.2 Problem statement, hypothesis and objectives

The **general objective** of this Ph.D. is:

To perform bedside long-term whole-head vEEG-fNIRS monitoring in order to assess the neurovascular dynamics of seizures and other epileptiform discharges in patients admitted with an acute neurological condition.

Three specific objectives are stated below with corresponding hypotheses.

Objective 1: To develop and validate an integrated high-channel wireless, compact and wearable EEG-fNIRS system intended for neurological clinical settings.

- Hypothesis 1.1: We believe that we can build a system with enough optodes (i.e., at least 50 optodes) to cover the entire head while at the same time be worn comfortably by a patient, and compact enough to facilitate its clinical integration at the bedside.
- Hypothesis 1.2: We believe that it will be able to retrieve relatively similar hemodynamic responses as commercial EEG and fNIRS systems, as well as clinically relevant brain hemodynamic changes in neurological patients.

ARTICLE 1: Ali Kassab, Jérôme Le Lan, Julie Tremblay, Phetsamone Vannasing, Mahya Dehbozorgi, Philippe Pouliot, Anne Gallagher, Frédéric Lesage, Mohamad Sawan, and Dang Khoa Nguyen., *Multichannel wearable fNIRS-EEG system for long-term clinical monitoring.*, Hum Brain Mapping (2018) Jan; 39(1): 7–23.

ARTICLE 2: Ali Kassab, Julie Tremblay, Alexandre Y. Poppe, Laurent Létourneau-Guillon, Anne Gallagher, Dang Khoa Nguyen., *Cerebral hemodynamic changes during limb-shaking TIA: A near-infrared spectroscopy study.*, Neurology (2016) March 22;86(12):1166-8.

Objective 2: To evaluate the feasibility of performing vEEG-fNIRS monitoring in an adult critical care setting.

- Hypothesis 2.1: We expect to be able to record long (i.e., ≥ 4 h) vEEG-fNIRS sessions in the neurointensive care unit (neuroICU).
- Hypothesis 2.2: We believe that these prolonged recordings in the neuroICU will facilitate the capture of various and diverse abnormal EEG patterns (i.e., increase the probability of capturing abnormal electrophysiological patterns, such as seizures).
- Hypothesis 2.3: For EEG patterns reflecting increase in neuronal activity such as seizures, high-frequency periodic discharges and burst patterns, we believe that an increase in [HbO], CBV, and a decrease in [HbR] should be observed; an opposite hemodynamic response should occur during suppression patterns. Also, we expect to find some level of hemodynamic heterogeneity in the time course and spatial distribution of the hemodynamic changes, particularly for burst-suppression patterns.

ARTICLE 3: Ali Kassab, Dènahin Hinnoutondji Toffa, Manon Robert, Frédéric Lesage, Ke Peng, Dang Khoa Nguyen., *Hemodynamic changes associated with common EEG patterns in critically ill patients: Pilot results from continuous EEG-fNIRS study.*, *Neuroimage Clinical* (2021); 32:102880.

Objective 3: To investigate the hemodynamic change associated with recurrent and/or prolonged seizures in the critically ill.

- Hypothesis 3.1: We believe that for the majority of seizures recorded, an increase in cortical hemodynamics will be observed during the ictal period, while a decrease in hemodynamics will be present in the post-ictal period.
- Hypothesis 3.2: We expect to find a positive relationship between seizure duration and amplitude of changes in hemodynamics.
- Hypothesis 3.3. With prolonged seizures, a gradual increase in reduced hemoglobin will be seen (suggesting that the neurovascular response is insufficient to meet the metabolic demand during prolonged seizures).

ARTICLE 4: Ali Kassab, Dènahin Hinnoutondji Toffa, Manon Robert, Frédéric Lesage, Ke Peng, Dang Khoa Nguyen., *Cortical hemodynamics of nonconvulsive status epilepticus in the critically ill.*, submitted to Neurology.

A timeline for this thesis is presented below (**Figure 1**).

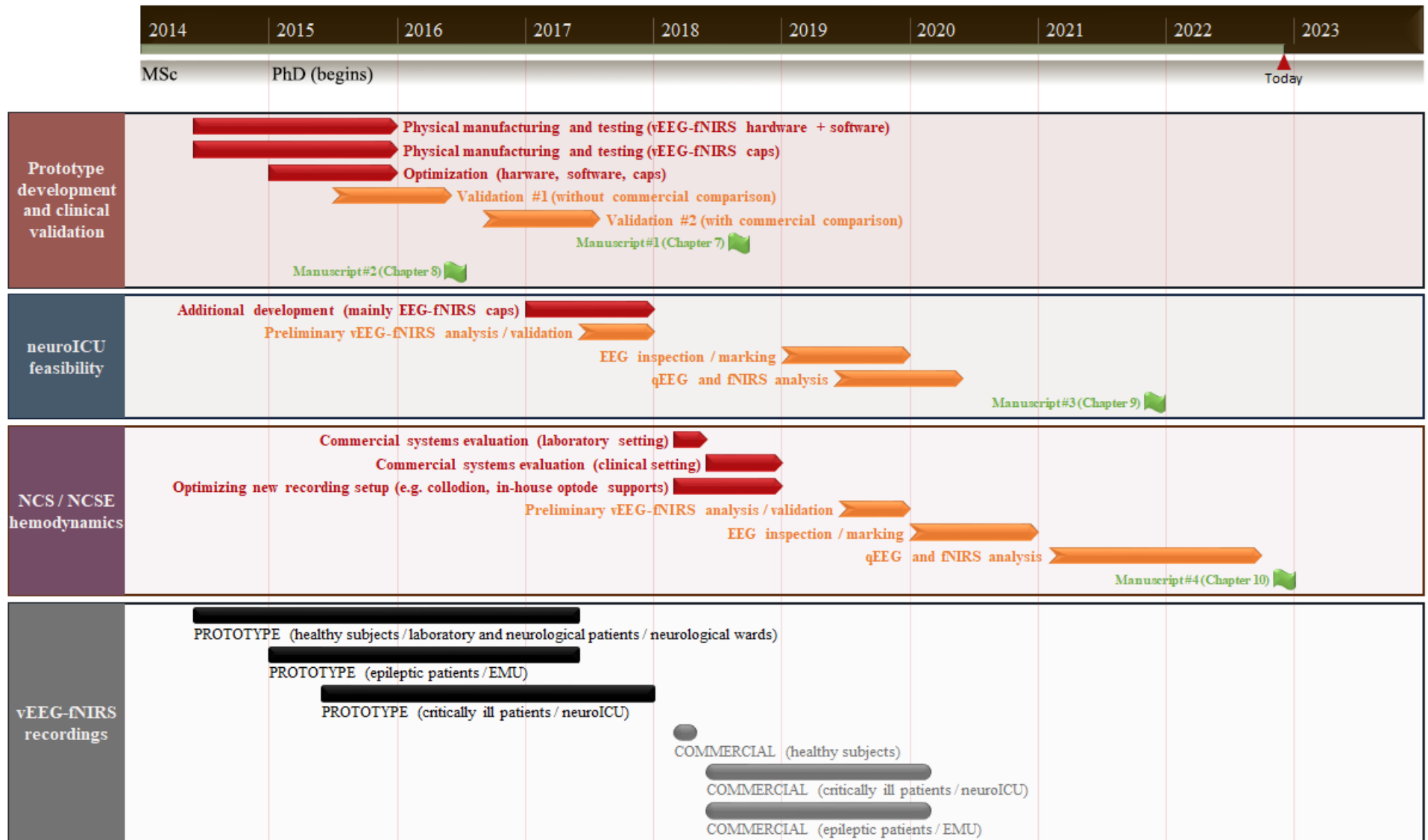


Figure 1 – Thesis timeline.

1.3 Thesis order

This thesis is organized as follows. **Chapter 2** gives an overview of epilepsy, acute seizures, and additional epileptiform patterns commonly encountered in the critically ill. **Chapter 3** will review the neurometabolic and neurovascular coupling mechanisms during “normal” and “abnormal” (i.e., seizures, periodic discharges, burst-suppression patterns) brain activity. **Chapter 4** provides a focused technical and clinical overview of functional neuroimaging and neuromonitoring techniques commonly used to investigate seizures and other abnormal epileptiform patterns. **Chapter 5** will focus on the main modality of this thesis: fNIRS. First, it will provide a brief historical background, early applications, and progress in the field of fNIRS. The theoretical (i.e., biophysical) principles underlying fNIRS and image reconstructions will be discussed. Then, the current application of fNIRS in neuroscience will be described, including a more detailed review of its application in epilepsy, seizures in the critically ill, periodic discharges, and burst-suppression patterns. The challenges imposed by long-term whole-head vEEG-fNIRS monitoring at the patient’s bedside are also discussed. **Chapter 6** describes the methodology of this body of work in detail, including hardware, monitoring setup and data analysis. **Chapters 7 and 8** provide two published manuscripts ([Kassab et al., 2016](#), [Kassab et al., 2018](#)) describing the development, validation and application of a compact and hybrid EEG-fNIRS system for whole-head long-term bedside monitoring in patients presenting with various neurological disorders. **Chapter 9** presents our latest published manuscript ([Kassab et al., 2021](#)). For this body of work, we successfully performed long-term vEEG-fNIRS monitoring in critically ill adults and captured large-scale cortical hemodynamic changes associated with seizures, periodic discharges, and burst-suppression. Then, in the following chapter (i.e., **chapter 10**), we focused on performing long-term whole-head vEEG-fNIRS on several critically ill patients presenting with clinically silent prolonged and/or repetitive refractory seizures to investigate the neurovascular changes associated with NCSE. This body of work will constitute the last article of this thesis, to be submitted before the oral defense ([Kassab et al., in preparation](#)). Finally, **Chapter 11** concludes by discussing the contributions of this work, its limitations, and future directions.

CHAPTER 2 – SEIZURE, EPILEPSY, AND EPILEPTIFORM DISCHARGES

2.1 Terminology

2.1.1 A brief overview on critical care seizures

Seizures in the critically ill are frequent, especially those with acute neurologic injury (Claassen et al., 2004). Indeed, it is estimated that 8-10% of general ICU patients and 34-64% of patients in the neuroICU will have seizures at some point during their hospitalization (Claassen et al., 2004; Oddo et al., 2009). Those seizures can either be the motive for ICU admission (i.e., uncontrolled seizures requiring aggressive treatment) or develop secondarily after the patient has been admitted to the ICU for other reasons. In those settings, seizures can result from numerous etiologies (e.g., acute systemic illness, primary neurologic pathology, medication side effect) and manifest in a wide array of symptoms ranging from a generalized convulsive activity to coma (Towne et al., 2000; Claassen et al., 2004). Nevertheless, they increase the risk of brain damage, prolonged ICU stays, ventilator dependency, and overall ICU-acquired infections (Trieman et al., 1981; Lothman, 1990; Young and Jordan, 1998; Vespa et al., 2010). Untreated, isolated seizures in the critically ill can quickly escalate to recurrent and/or prolonged seizure activity (i.e., SE) that can take the form of generalized convulsive activity (i.e., CSE) or, more frequently, as NCSE, which is associated with high morbidity and mortality (DeLorenzo et al., 1996; Logroscino et al., 2005, 2008). Finally, the clinical management of SE in the ICU can be quite complex, and a portion of SE patients will become refractory (i.e., refractory SE – RSE and super-refractory SE – SRSE), requiring more aggressive treatment with opioids and anesthetics (Dham et al., 2014; Mirski and Varelas, 2008).

2.1.2 Seizures

A **seizure** is a transient abnormal, excessive, and hypersynchronous discharge in a population of cortical neurons due to an imbalance in excitatory and inhibitory brain mechanisms (Bromfield et al., 2006; Badawy et al., 2009; Stafstrom, 2015). This abnormal discharge can be visualized using surface electrodes that can record the brain's electrical activity in the form of a rhythmic electrical

discharge evolving in amplitude, frequency and distribution, typically for 10 seconds to a few minutes (Niedermeyer et al., 2009).

Seizures are usually divided into two main categories, based on the “acuteness” and the underlying etiology. The term “**acute symptomatic seizure**” refers to seizures provoked by an acute brain insult or injury such as a stroke, subarachnoid hemorrhage, trauma, infection or metabolic encephalopathy (e.g., alcohol consumption or withdrawal, drug use). These seizures are generally “isolated” and cease once the underlying cause is treated.

Some individuals with acute seizures will continue to have seizures long after the initial brain insult (e.g., when the brain infection has been treated or intraparenchymal blood has cleared). These seizures are termed: “**unprovoked**” or “**spontaneous**” seizures. When these “unprovoked” or “spontaneous” seizures become recurrent, the term **epilepsy** is generally employed. It describes an individual with a chronic predisposition to epileptic seizures, impacted by its neurobiological, cognitive, psychological and social consequences. While the traditional definition of epilepsy required someone to have at least two unprovoked seizures (to confirm the idea of recurrency), the new practical definition established by the International League Against Epilepsy states that even someone with only one unprovoked seizure can be diagnosed with epilepsy if it is estimated that he has > 60% of having another seizure.

Most seizures are associated with clinical manifestations that will vary according to various factors including the localization of the abnormal excessive discharge, its duration, and how it propagates. Symptoms may range from minor experiential sensations (déjà vu, anxiety, fear, flashing lights, etc.) to more disabling manifestations such as transient impaired awareness and tonic-clonic convulsions. Note that some seizures are said to be only “**electric**” (or “**electrographic**”, or “**nonconvulsive**”) because, while visible on the EEG, there are no obvious clinical manifestations. This can occur either because the discharge is limited to a part of the brain that is relatively ‘silent’ (non-eloquent) or that is no longer able to generate symptoms because it is dysfunctional.






2.1.3 A brief overview on epilepsy

Epilepsy is the second most common neurological disorder affecting nearly 60 million people worldwide (Leonardi and Ustun, 2002; GBD 2016 Epilepsy Collaborators, 2019). According to the Public Health Agency of Canada and the Center for Disease Control and Prevention, it is estimated that ~300 000 Canadians and ~3.5 million Americans live with epilepsy (Gilmour et al., 2016; Zack and Kobau, 2017). Individuals living with epilepsy have a lower quality of life, higher comorbidity (medical and psychological) rates, and higher medication use than the general population (Berto, 2002). Numerous conditions, usually related to the patient's age, can cause epilepsy. For example, childhood epilepsies are usually caused by hypoxia (during conception or birth), congenital lesions, or genetic mutations. In contrast, epilepsies seen in the elderly are usually related to vascular and degenerative disease as well as brain tumours. Therefore, identifying the cause of epilepsy is essential as it is a significant determinant of the clinical course and prognosis (Shorvon, 2011). Regarding the pharmacological treatment of epilepsy, the main goal when treating patients with epilepsy is achieving seizure freedom with minimal side effects (Kubota and Awaya, 2010). While there is no “cure” for epilepsy, clinicians rely on various antiseizure medications, which have various mechanisms of action that all lead to re-establishing the balance between neuronal excitation and inhibition (Kwan et al., 2001). These antiseizure medications are effective in controlling seizures in ~60% of patients with epilepsy (Kwan and Brodie, 2000; Chen et al., 2018). However, around 30% of patients will continue to have seizures despite various combinations of antiseizure medications. A small percentage of these patients with drug-resistant epilepsy are candidates for epilepsy surgery (Rathore and Radhakrishnan, 2015).

2.1.4 Interictal epileptiform discharges (IEDs)

In between seizures (or ‘ictus’), patients with epilepsy often have **IEDs** (also known as “spikes”) that are brief (70-200 msec) sharp/spiky discharges that are not strong/sustained enough to generate symptoms but are visible on the EEG (Tatum et al., 2018). Common types of IEDs are summarized in **Table 1**.

Table 1 – Spikes, sharp waves, spike-and-wave, polyspikes, and polyspike and waves.

IEDs	Morphology	Duration	Example
Spikes	sharply contoured	20-70 msec	
Sharp waves	sharply contoured	70-200 msec	
Spike-and-waves	spike followed by a slow wave (usually spike with larger amplitude)	≥ 90 msec	
Polyspikes	≥ 2 spikes	≥ 40 msec	
Polyspike and waves	≥ 2 spikes associated with ≥ 1 slow waves	≥ 110 msec	

IEDs: interictal epileptiform discharges, msec: milliseconds

Pathophysiologically, they reflect a “paroxysmal depolarizing shift” characterized by a sequence of sustained depolarization resulting in a burst of action potentials, a plateau-like depolarization associated with another action potential, followed by rapid repolarization and finally, hyperpolarization occurring in a group of neurons (Ayala et al., 1973).

2.2 Electroencephalography (EEG)

EEG has been used for over a century and remains the most employed electrophysiological technique to date, allowing to visualize abnormal neuronal activity (e.g., interictal discharge, brief asymptomatic paroxysmal EEG transient, seizures) from background or normal electrophysiological brain activity (*for further information on normal electrophysiological brain*

activity and how the EEG electrodes are positioned on the head, please refer to Britton et al., 2016). As it was previously pointed out, the EEG is essential for identifying seizures and IEDs, especially when the former are “clinically silent”. **Figure 2** shows an example of EEG electrodes positioned according to the international 10-20 system (Jasper, 1958).



Figure 2 – 10-20 system EEG electrode placement. Left two figures shows a healthy subject before placing the EEG electrodes. Right two figures shows the same subject after installing the EEG electrodes.

There are several types of continuous EEG recordings. “Short-term EEG recordings” (i.e., routine, sleep, or ambulatory EEG, with or without video) (~30-60 min) are usually performed to confirm the diagnosis and further manage the seizure condition (Pillai and Sperling, 2006; Adams and Knowles, 2007). Because seizures occur randomly, they are rarely captured by short-term EEG recordings because of their short duration unless seizure frequency is very high. Longer (for days or weeks) EEG recordings are required to record seizures, as it is sometimes required for diagnostic purposes or epilepsy surgery evaluation. In such instances, a patient is generally admitted to an epilepsy monitoring unit and antiseizure medication frequently reduced or weaned. Moreover, longer EEG recordings are required in patients during the management of seizures and SE in the neuroICU. In these settings, continuous EEG monitoring is typically combined with simultaneous video recordings (i.e., vEEG) for electroclinical correlation (i.e. correlating EEG activity with clinical symptomatology to establish the diagnosis of epilepsy, to localize the epileptic focus, to distinguish the different types of seizures etc.). While certain abnormal EEG patterns are well described and recognized by clinicians, others can be clinically challenging.

2.3 Clinically challenging EEG patterns in the critically ill

The introduction of continuous vEEG recordings in the neuroICU has greatly improved the way patients are cared, allowing intensivists to determine if some abnormal movements are epileptic in nature, accurately detect seizures for appropriate treatment, monitor treatment response, gauge the level of sedation, etc. The use of continuous vEEG recordings in this particular population has shown us that subtle or even asymptomatic (*aka* “electrical”, “nonconvulsive”) are common and that NCSE are not rare. While all recognize the need to treat convulsive seizures as they are clinically disabling and lead to brain hypoxia, it is less clear how aggressive we should be in the treatment of NCS as treatment itself may sometimes generate adverse events.

The increasing use of continuous vEEG in this population has also revealed to clinicians the existence of several abnormal EEG patterns distinct from the typical IEDs and seizures. Indeed, while the classical sporadic millisecond brief sharp/spikish wave of IEDs or the sustained (10 s to 5 min) evolving rhythmic activity of seizures can still be found in critically ill patients, other epileptiform-like patterns have been reported that are not clear-cut sporadic spikes nor seizures and are said to be on the interictal-ictal continuum. Because their significance and impact are largely unknown, their management also remains quite controversial ([Ch’ang and Claassen, 2017](#)).

In the following subsections, common clinically challenging EEG patterns are detailed.

2.3.1 Nonconvulsive seizures (NCS) and nonconvulsive status epilepticus (NCSE)

Nonconvulsive seizures (NCS) are electrographic seizures without overt clinical manifestations. Nonconvulsive status epilepticus (NCSE), also referred to as electrographic status epilepticus, is defined by electrographic seizures for ≥ 10 continuous minutes or for a total duration of $\geq 20\%$ of any 60-minute period of recording (**Figure 3**) ([Hirsch et al., 2021](#)).

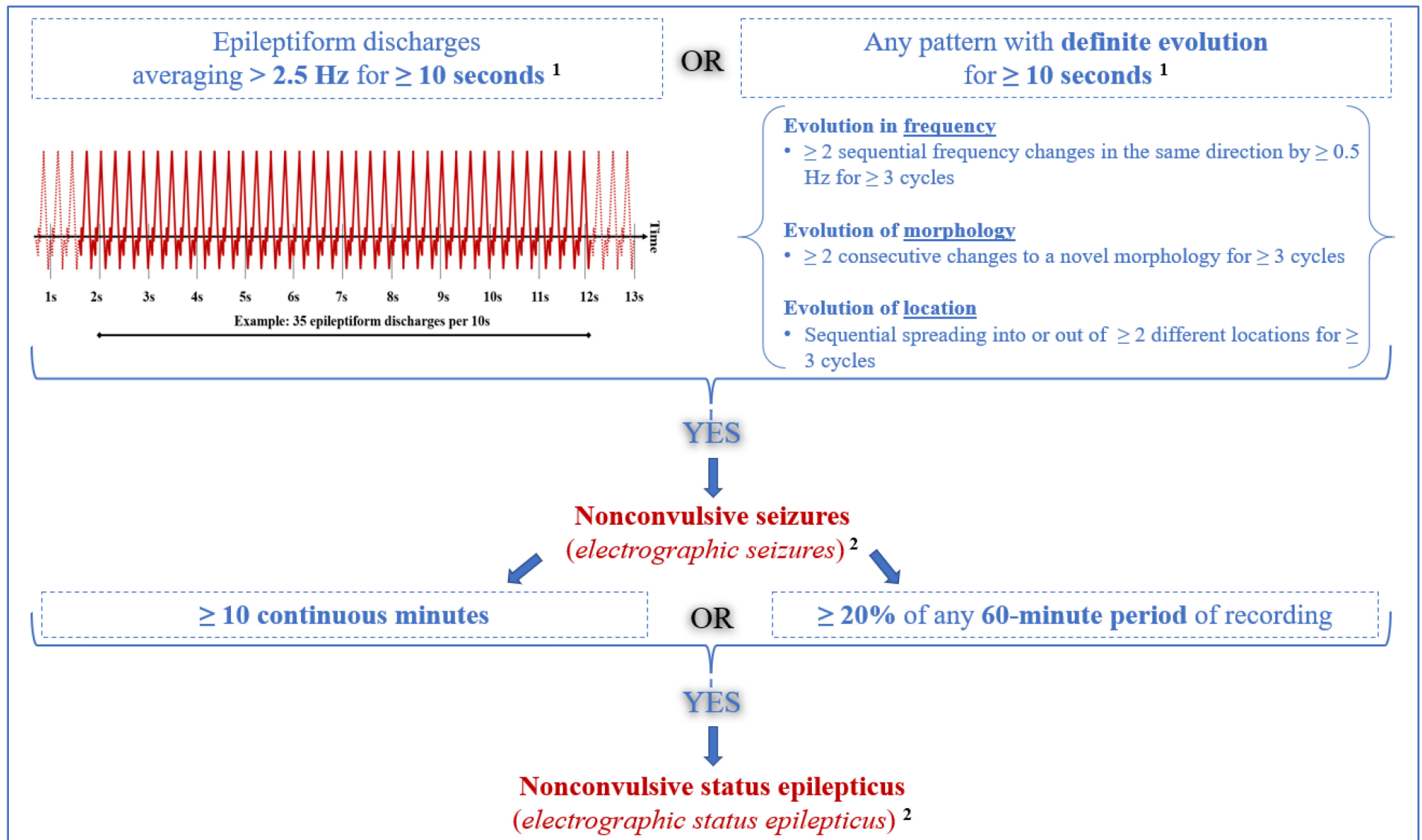


Figure 3 – Criteria for NCS and NCSE (*Inspired by Hirsch et al., 2021*). ¹There is currently no consensus on whether to maintain or eliminate the “10 second rule”. ²NCS (including NCSE) do not have any definite time-locked clinical correlate nor do antiseizure medication improve, both, the EEG and clinical manifestations. s: seconds.

NCS (including NCSE) are the most common type of seizure in comatose ICU patients, accounting for nearly 90% of seizures (Claassen et al., 2004). In comatose patients with NCSE, more than 60% had either hypoxic/anoxic brain injury ($\approx 40\%$) or stroke ($\approx 20\%$), with the remaining cases occurring in a relatively similar proportion (i.e., $\approx 5\%$) in patients with brain tumors, metabolic encephalopathy, infection, head trauma (unknown etiology $\approx 10\%$) (Towne et al., 2000).

As NCS/NCSE do not have overt clinical signs, diagnosis requires continuous EEG monitoring. Another topic of debate, previously pointed out, is regarding the urgency and aggressiveness of treating NCS and NCSE. Currently, the treatment of these conditions follows that of generalized convulsive status epilepticus (i.e., immediate and aggressive treatment). This comes from the fact that many studies have shown that generalized convulsive status epilepticus is associated with a (time-dependent) reduction in cerebral oxygenation, cerebral glucose levels and CBF culminating in neuronal injury, increased morbidity and mortality (Lowenstein and Alldredge, 1998; Treiman et al., 1998; Treiman and Walker, 2006;). However, there is a paucity of data for the treatment of NCS and NCSE (Cascino, 1993). This practice may be leading to over-treatment with intravenous sedating medications and potentially adverse outcomes. Some believe that NCS and NCSE are less damaging to the brain than CSE and, therefore, may not need to be treated similarly. On the other hand, this idea has been challenged, as patients with NCSE have been found to have elevated serum neuron-specific enolase (marker of brain injury) (Robinowicz et al., 1995). Thus, without knowing the degree of ongoing neuronal injury for patients with varying degrees of NCSE (as well as NCS), it is likely that a “one-size fits all” treatment paradigm is not justified and may even be inappropriate/detrimental. With increasing evidence that intravenous antiseizure medications and anesthetics may even be detrimental (i.e., prolonged intubation, delirium, drug-induced hypotension, propofol infusion syndrome) for patients with NCS and NCSE (Jordan and Hirsch, 2006; Hwang et al., 2013; Allen and Vespa, 2019), clinicians must consider “appropriately aggressive therapy” in regards to the electroencephalographic end-point (seizure suppression vs. burst suppression or even complete background suppression) and when to decide if additional medication is futile (Jordan and Hirsch, 2006; Perks et al., 2012). Available studies have shown conflicting results regarding the ideal depth of EEG “suppression”. Most clinicians aim for a burst-suppression pattern in controlling refractory status epilepticus but it is still controversial whether this approach can effectively prevent brain damage.

2.3.2 Interictal-ictal continuum

In addition to NCS, critically ill patients often (i.e., >25% of patient) often present other abnormal EEG patterns that do not meet the criteria for definitive seizures or IEDs, lying along a spectrum referred to as the “ictal-interictal continuum”. First introduced by Pohlmann-Eden and his colleagues in 1996, the ictal-interictal continuum was defined as “an EEG signature of a dynamic pathophysiological state arising from an unstable neurobiological process, with the nature of the underlying neuronal injury, the patient's pre-existing propensity to have seizures, and the coexistence of any acute metabolic derangements all contributing to whether seizure occurs or not” (Pohlmann-Eden et al., 1996; Chong and Hirsch, 2005; Claassen, 2009). In order to standardize their reporting in clinical practice and facilitate research on these abnormal patterns, the American Clinical Neurophysiology Society (ACNS) proposed a ‘Standardized Critical Care EEG Terminology’ for ICU EEG recordings first published in 2012 (Hirsch et al., 2013), and recently updated in 2021 (which are summarized in **Figure 4**). In sum, these abnormal patterns are currently divided into 3 categories: 1) periodic discharges (PDs) (**Figures 5**), 2) rhythmic delta activity (RDA) (**Figures 6**), and 3) spike-and-wave (SW) (**Figures 7**).

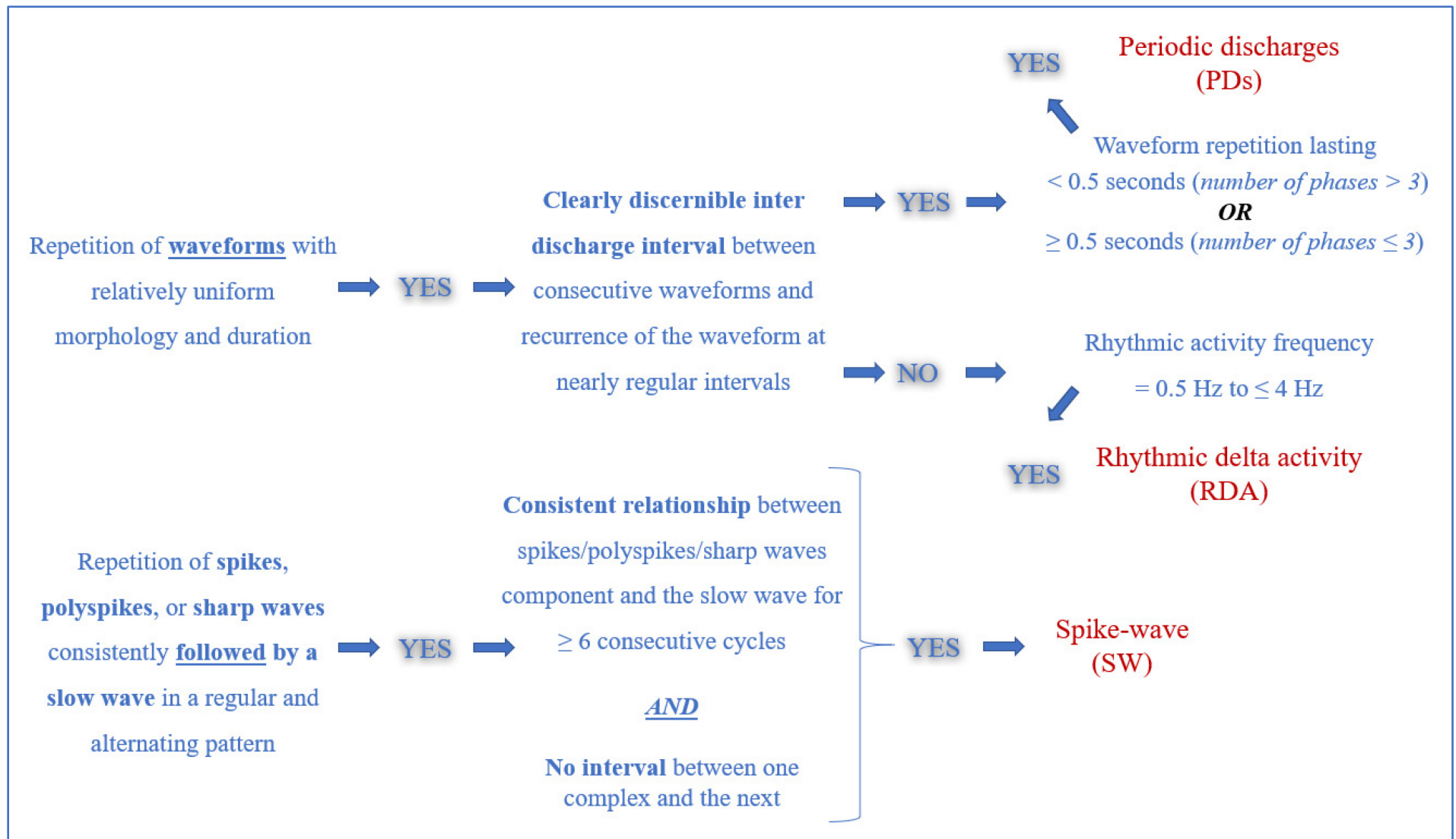


Figure 4 – Criteria for patterns falling in the “ictal-interictal continuum” (Inspired by Hirsch et al., 2021). PDs: periodic discharges, RDA: rhythmic delta activity, SW: spike-and-wave or sharp-and-wave.

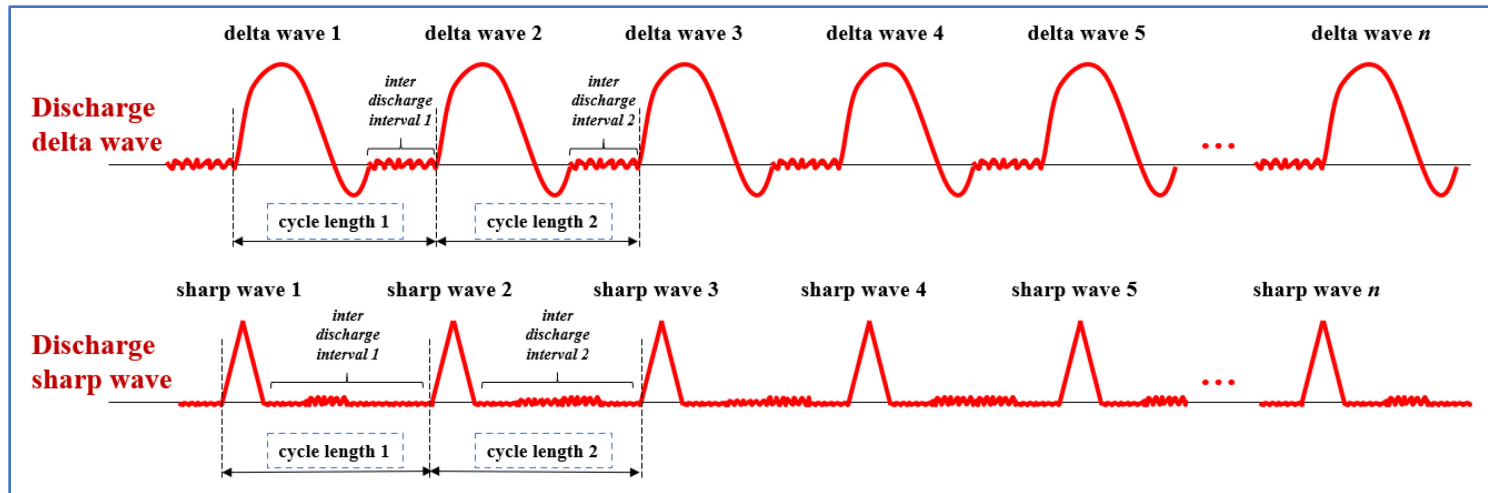


Figure 5 – Electrographic characteristics of periodic discharges (PDs) (*Inspired by Hirsch et al., 2021*).

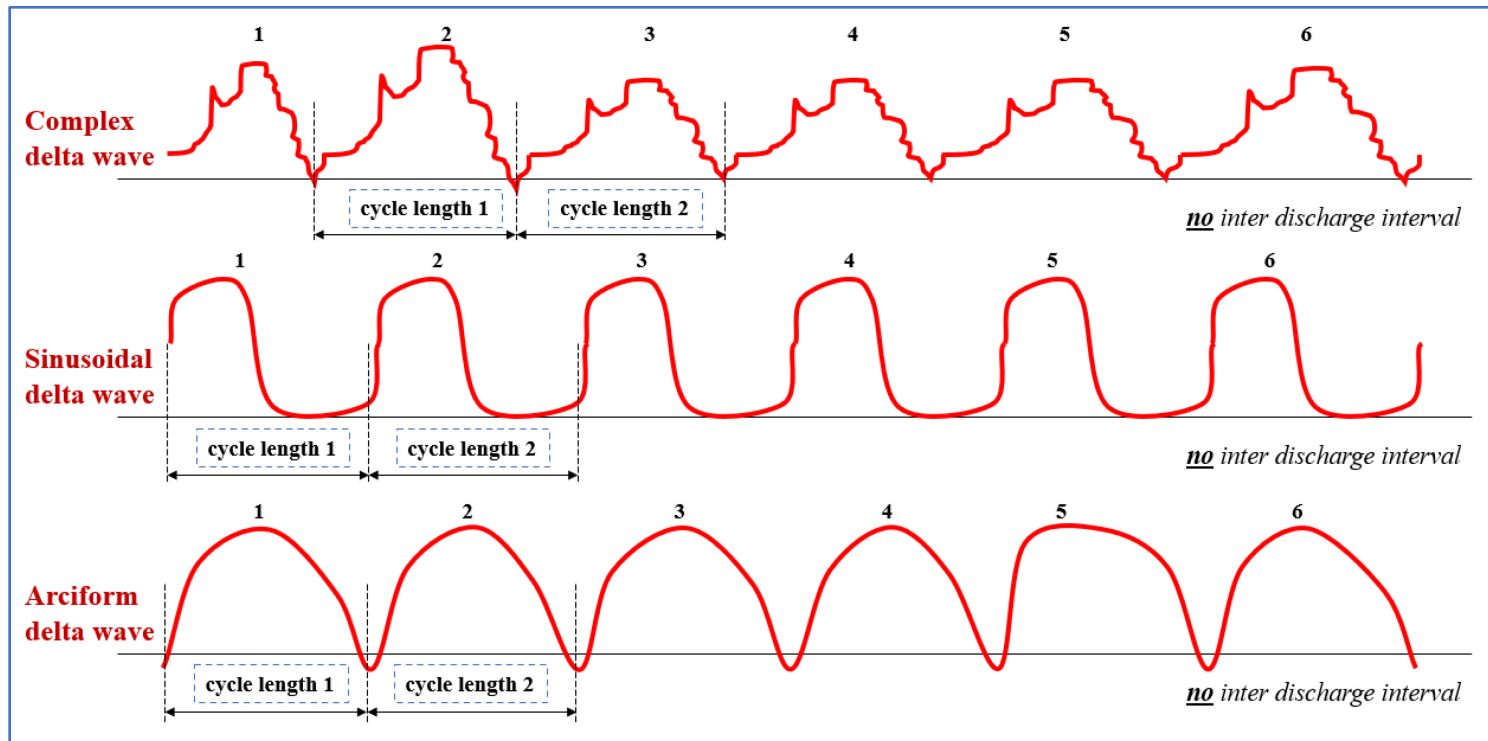


Figure 6 – Electrographic characteristics of rhythmic delta activity (RDA) (*Inspired by Hirsch et al., 2021*).

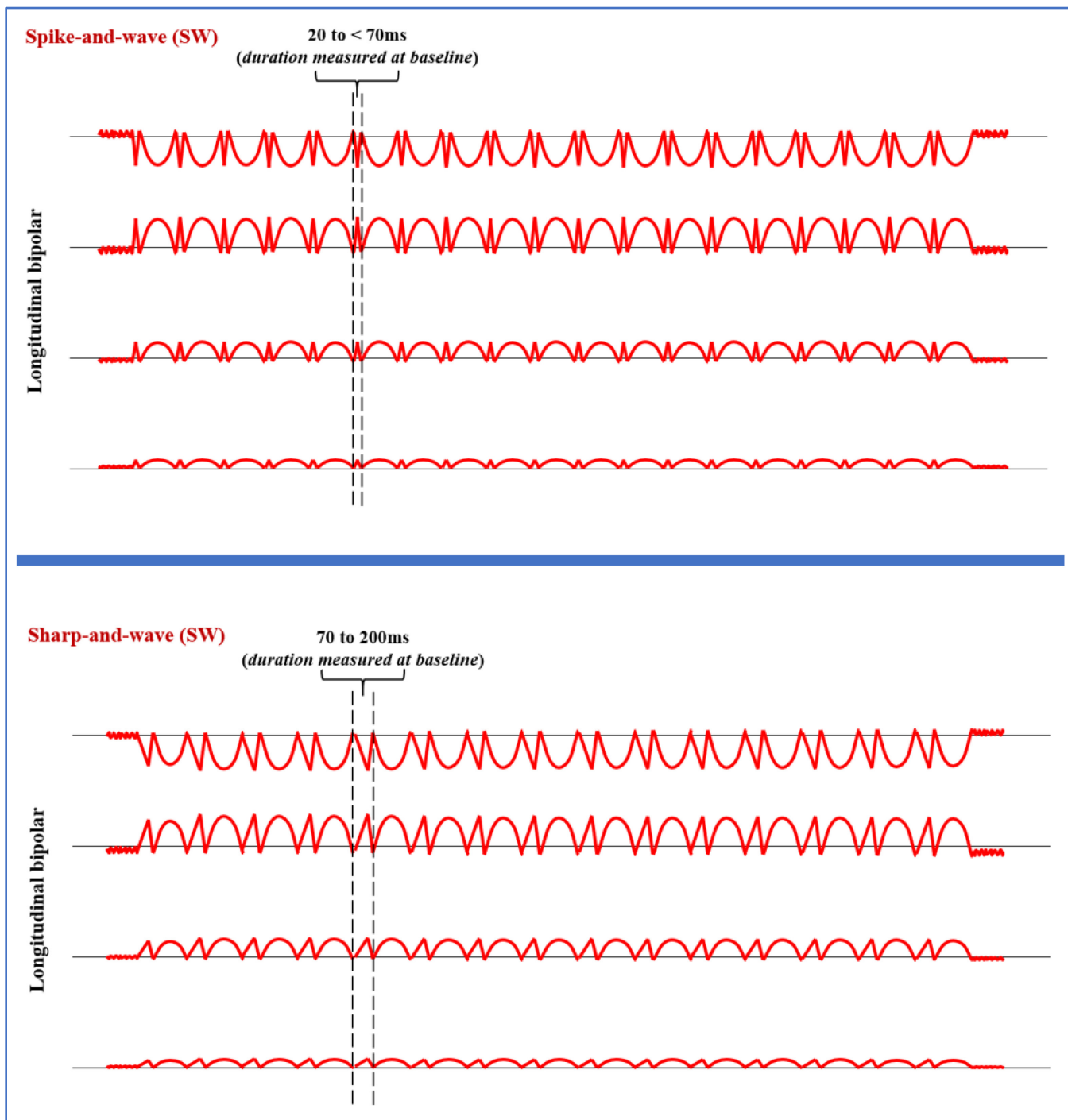


Figure 7 – Electrographic characteristics of spike-and-wave (top) and sharp-and-wave (bottom) (*Inspired by Hirsch et al., 2021*). msec: milliseconds.

PDs, RDAs, and SW can be characterized further. For example, periodic patterns (e.g., PDs) can occur as 1) one single pattern in both brain hemispheres synchronously and symmetrically (i.e., generalized PDs or GPDs) (**Figure 8A**), 2) one single pattern only (or mainly) in one hemisphere (i.e., lateralized PDs or LPDs) (**Figure 8B**), 3) two independent lateralized patterns, each in one hemisphere, and occurring simultaneously (i.e., bilateral independent PDs or BIPDs) (**Figure 8C**), 4) two independent lateralized patterns, in the same hemisphere, and occurring simultaneously (i.e., unilateral independent PDs or UIPDs) (**Figure 8D**), or 5) three or more lateralized independent patterns, in both hemispheres, and occurring simultaneously (i.e., multifocal PDs or MfPDs) (**Figure 8E**). In addition, when periodic or rhythmic patterns are reproducibly induced or exacerbated by an alerting stimulus (e.g., sound, touch, pain), they are referred to as “stimulus-induced” (i.e., stimulus-induced rhythmic or periodic discharges or SIRPDs). Lastly, a “plus” or “+” feature can also be added when periodic or rhythmic patterns occur with a superimposed 1) “fast” activity (i.e., lateralized periodic discharges PLUS F or LPDs + F) (**Figure 8F – top**), 2) rhythmic activity (i.e., lateralized periodic discharges PLUS R or LPDs + R) (**Figure 8F – middle**), or 3) sharp waves or spike (i.e., generalized rhythmic delta activity PLUS S or GRDA + S) (**Figure 8F – bottom**), all features rendering the pattern more ictal-appearing (i.e., more closely resembling an EEG pattern seen during seizures).

The recently proposed terminology is an essential first step in allowing researchers to have a common language to study the underlying pathophysiology, impact and management of the myriads of abnormal EEG patterns seen in the ICU. However, in previous decades, studies trying to understand these patterns have often lumped together many subtypes of EEG patterns whose recognition were not based on universally recognized criteria. Possible mechanisms evoked by these studies to explain such discharges have included: metabolic derangement, hypoxia/ischemia, aberrant synchronization with extensive refractory periods secondary to damage to cortical and/or subcortical networks of neurons, large-scale synchronization secondary to abnormally connected networks of neurons, and spectral condensation of neuronal activity leading to synchronization of neuronal oscillations ([Pohlmann-Eden et al., 1996](#); [Chong and Hirsch, 2005](#); [Claassen, 2009](#)).

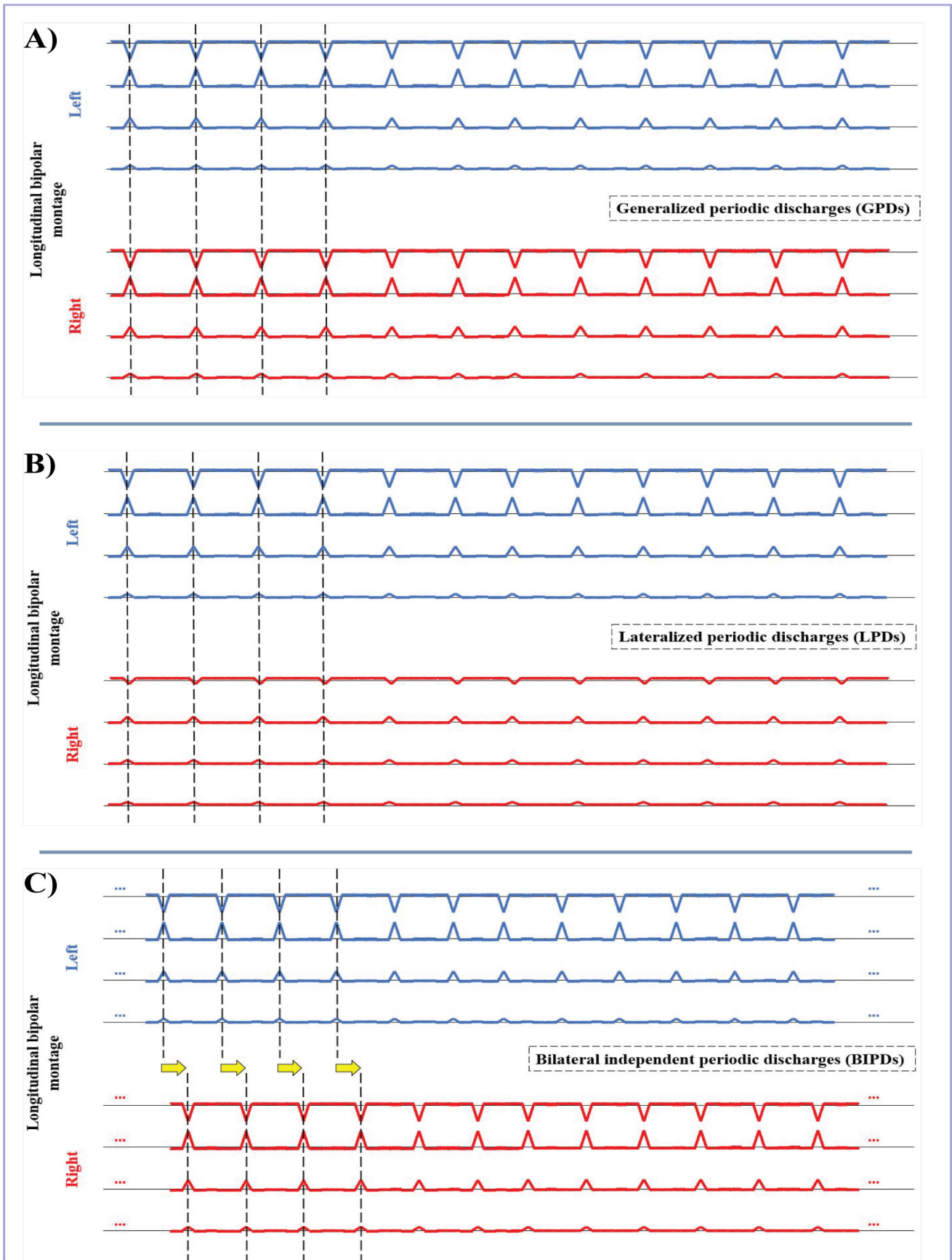


Figure 8 – EEG example illustrating PDs with different characteristics (*Inspired by Hirsch et al., 2021*). A) generalized periodic discharges (GPDs), B) lateralized periodic discharges (LPDs), and C) bilateral independent periodic discharges (BIPDs).

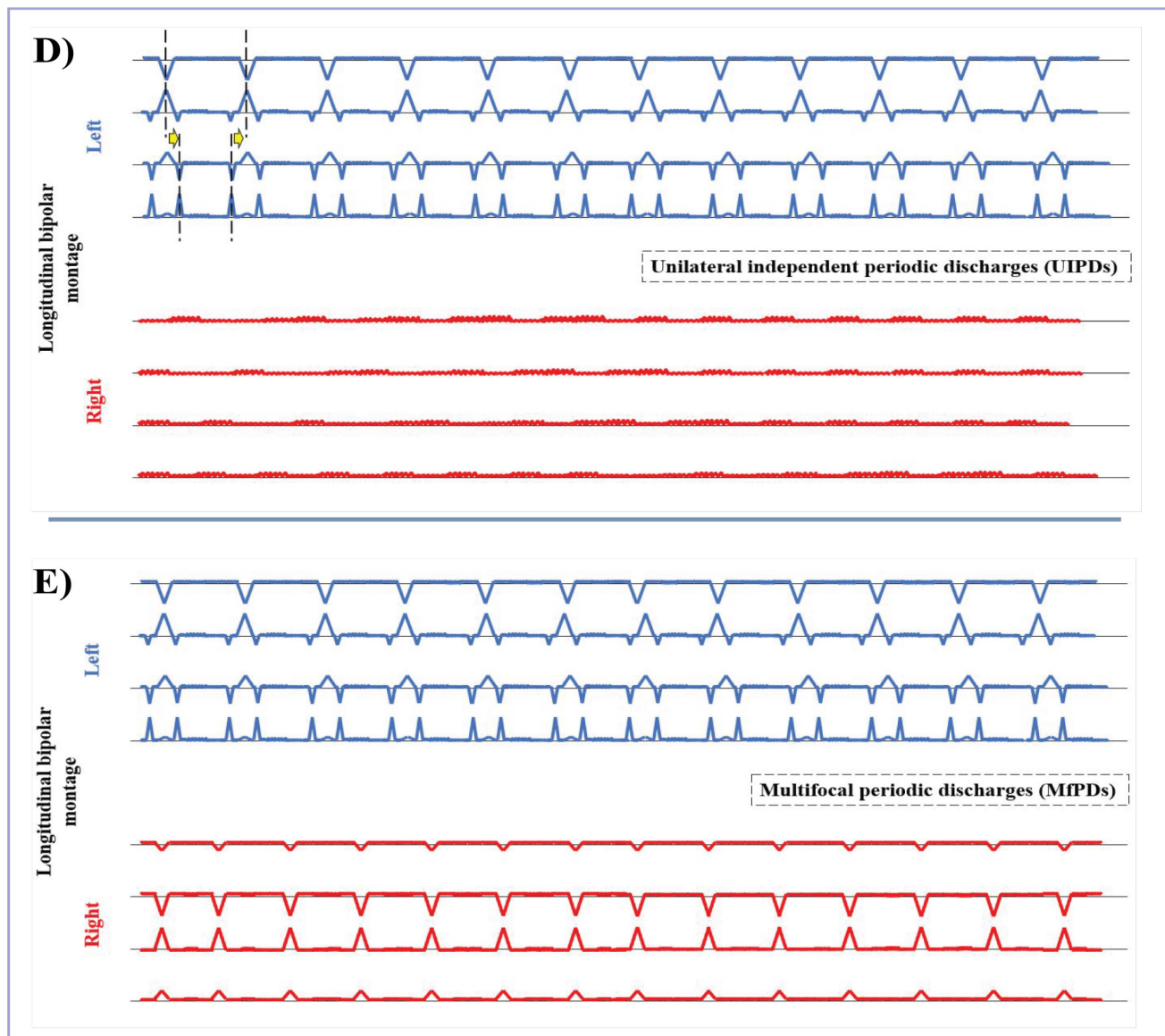


Figure 8 (continued) – EEG example illustrating PDs with different characteristics (*Inspired by Hirsch et al., 2021*). D) unilateral independent periodic discharges (UIPDs), E) multifocal periodic discharges (MfPDs).

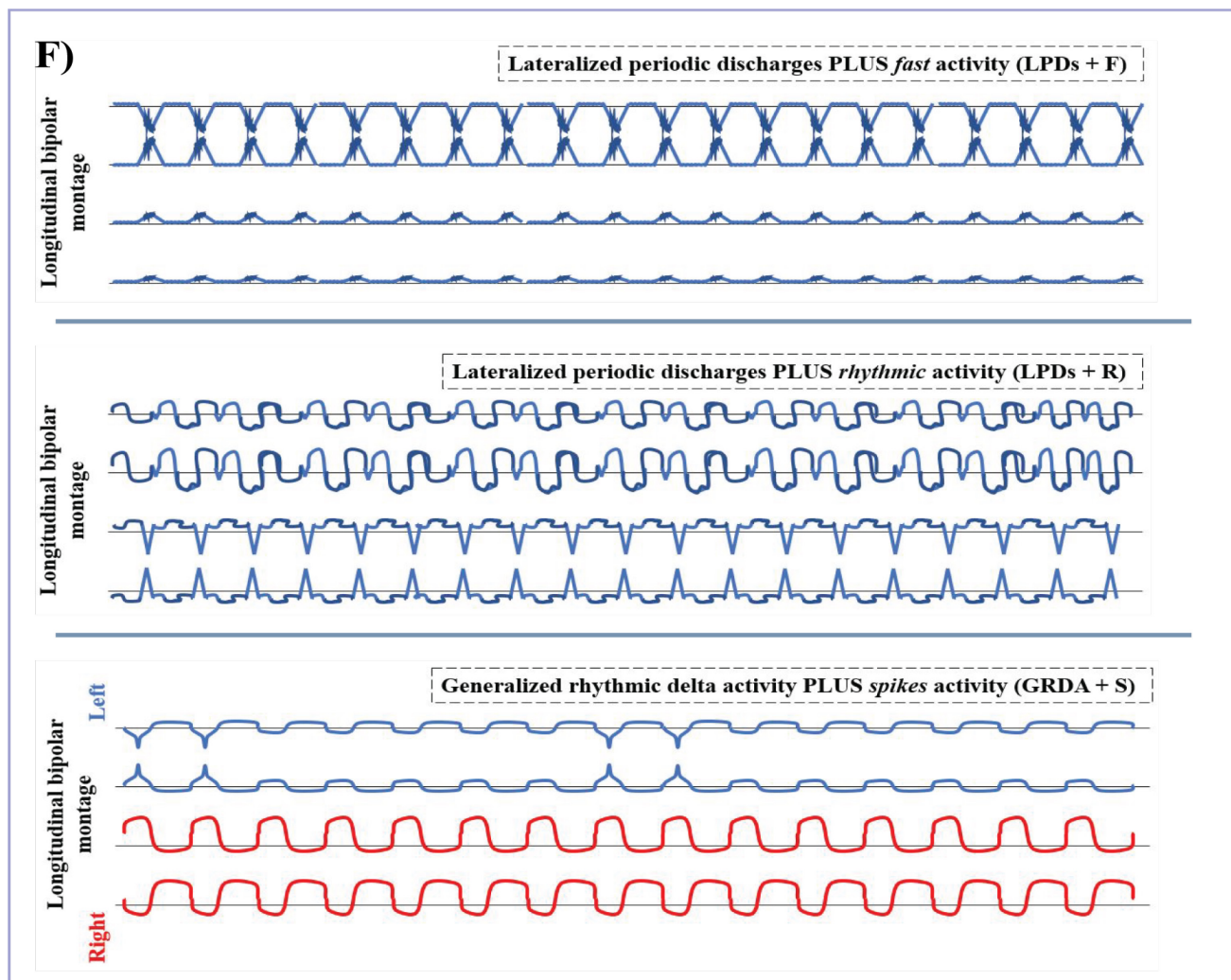


Figure 8 (continued) – EEG example illustrating PDs with different characteristics (*Inspired by Hirsch et al., 2022*). F) (top) lateralized periodic discharges + *fast* activity (yellow arrows) (LPDs + F), (middle) lateralized periodic discharges + *rhythmic* activity (black arrows) (LPDs + R), and (bottom) generalized rhythmic delta activity + *spike* (orange arrows) (GRDA + S).

2.3.3 Burst-suppression EEG pattern

Burst-suppression is an EEG pattern in which periods (or epochs) of high voltage (150–350 μV) brain activity (“burst”) alternate quasi-periodically with periods of low amplitude ($< 25 \mu\text{V}$) activity or isoelectric quiescence (“suppression”) (**Figure 9**). Clinically, burst-suppression is associated generally with a state of unarousable unresponsiveness and is often considered, although disputed, as a global state of profound brain inactivation (Lewis et al., 2013; Amzica, 2015).

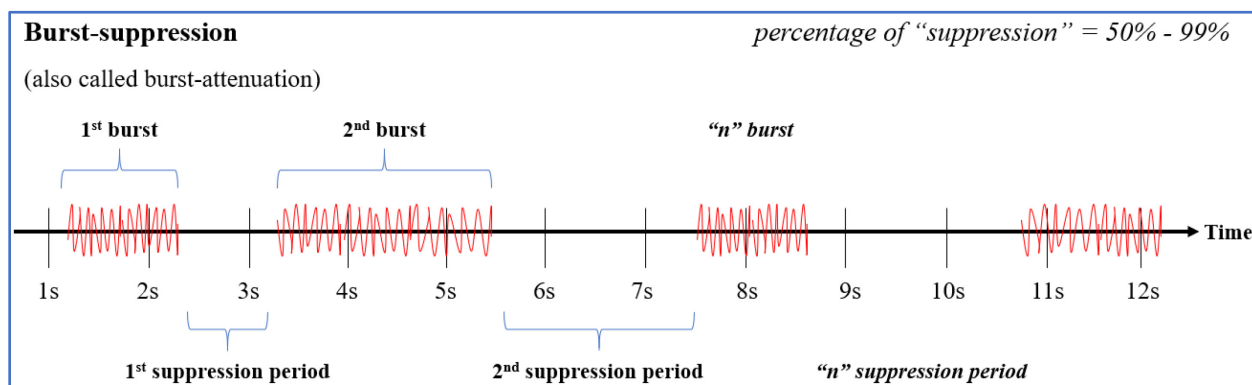


Figure 9 – EEG example illustrating a burst-suppression pattern (*Inspired by Hirsch et al., 2021*). s: seconds.

While burst-suppression patterns are frequently seen in the critically ill, they are not specific to any particular etiology as they can occur in the context of anesthesia (Ma et al. 2022), trauma (Stockard et al., 1975), metabolic encephalopathy (Scher, 2001; Niedermeyer et al., 2007) and hypoxic-ischemic brain injury (Bauer et al., 2013), SE (Treiman et al., 1990) and coma (Young, 2000). Burst-suppression can also be iatrogenic, induced voluntarily using sedative agents to offer transient brain protection by decreasing brain metabolism and CBF (Doyle and Matta, 1999) and/or directly inhibiting seizure activity (Hunter and Young, 2012). Therefore, it is commonly used as an electrophysiological endpoint for critical care and surgical patients. Well-known indications include therapeutic hypothermia after cardiac arrest (Marion et al., 1997; Stecker et al., 2001; Westover et al., 2015), medically-induced coma during surgery (Schwartz et al., 1989; Ravussin et al., 1993; Akrawi et al. 1996; Brown et al. 2010), treatment for refractory intracranial hypertension (Doyle and Matta, 1999) and refractory/super-refractory status epilepticus (Van Ness 1990; Doyle and Matta, 1999; Rossetti et al. 2005; Kalviainen et al., 2007; Hunter and Young, 2012; Phabphal et al. 2018).

Prognosis and outcomes associated with burst-suppression are highly dependent on whether they are 1) associated with an underlying pathology (spontaneous burst-suppression), and 2) generated by treatment (medically-induced burst-suppression) (Sekar et al. 2019). Spontaneous burst-suppression signals a state of agony and is associated with a high mortality and poor outcome (Niedermeyer et al., 2009; Cloostermans et al., 2012; Rossetti et al., 2017). In contrast, medically-induced BS and spontaneous post-treatment burst-suppression are understandably associated with better neurological outcomes (Niedermeyer et al., 2009; Sekar et al., 2019).

Despite clear clinical benefits (e.g., cerebral protection, prognosis improvement), the biophysical mechanisms responsible for burst-suppression genesis and its effects on the brain remains poorly understood (Liley and Walsh, 2013). Possible reasons include the etiological heterogeneity of this pattern, the significant degree of electroencephalographic variations (i.e., morphology, frequency, duration) (Lamblin et al., 2013), and the limited number of studies investigating the neurophysiological foundations of this pattern in the living human brain (Amzica, 2015).

In this chapter, we have defined the concept of seizures and epilepsy, introduced the technique of EEG to investigate patients with seizures and epilepsy, and described the different type of abnormal epileptiform discharges that can be found in patients with seizures in the neuroICU EEG. The next chapter will examine the metabolic and brain hemodynamic changes associated with these clinically challenging EEG patterns.

CHAPTER 3 – NEUROVASCULAR COUPLING

As we briefly mentioned in the first chapter, seizures and other epileptiform discharges induce brain metabolism and hemodynamics changes. However, it is still unclear whether or not the increase in brain hemodynamics can compensate for the excessive neuronal activity seen during seizures. A better understanding of neurovascular coupling mechanisms will allow us to better understand the neurometabolic and neurovascular dynamics associated with abnormal EEG patterns. In time, this could potentially guide us in the management of these abnormal epileptiform discharges found both in critically ill and non-critically ill patients.

Despite its relatively small size, the brain receives approximately 15-20% of total cardiac output (i.e., $CBF \approx 1/5^{\text{th}}$ total cardiac output) and consumes around $1/5^{\text{th}}$ (20%) of the body's total energy production. Unlike other organs (e.g., liver, muscles) that can store macronutrients (e.g., carbohydrates/glycogen), the brain is dependent on a constant input of oxygen and nutrients (mainly glucose) in order to produce adenosine triphosphates (ATP) and function.

The mechanism by which CBF is linked to neuronal activity is known as neurovascular coupling. Indeed, increased neuronal activity increases CBF and, consequently, greater delivery of glucose and oxygen to meet the increased demand for ATP by neurons. This continuous supply of energy substrate is “dynamic” providing a constant basal level to maintain its baseline activity and increase supply at times of higher brain activity (i.e., functional hyperemia).

3.1 Physiological (“normal”) neurometabolic and neurovascular coupling

3.1.1 Brain metabolism and neurometabolic coupling

The primary source of energy in the healthy brain is ATP, which is produced mainly from the fast oxidative (i.e., aerobic) metabolism of glucose which occurs in the mitochondria (Siesjo, 1978). Brain activity is closely coupled with energy metabolism. Indeed, the close relationship between neuronal activity and the main supportive substrates of glucose and lactate defines “neurometabolic coupling” (Li and Freeman, 2015).

Physiological brain activity (e.g., motor processing, somatosensory processing, learning/memory) involves several specific cellular and molecular signalling processes at the level of neurons. Therefore, neuronal activity involves several signal transduction steps, including generating a postsynaptic action potential (excitatory or inhibitory). For simplicity, we will only focus on the action potential in general. However, it is essential to remember that while the postsynaptic action potential is the one consuming most of the energy, other essential steps involved in signal transduction (e.g., maintaining resting potential, reversing ionic fluxes, transmitter release and recycling) are also energy-dependent (Hall et al., 2012; Engl and Attwell, 2015).

Neuronal activity is associated with a transient change in the ionic permeability of the cell membrane resulting in local changes in the transmembrane ion gradient (i.e., intracellular \uparrow $[\text{Na}^+]$ / \downarrow $[\text{K}^+]$ and extracellular \downarrow $[\text{Na}^+]$ / \uparrow $[\text{K}^+]$). These transmembrane flows of ions produce an electrical spike called action potential (Hodgkin and Huxley, 1952). Following an action potential, Na^+/K^+ pumps are responsible for “resetting” intracellular and extracellular ionic concentration back to its pre-action potential levels, enabling neurons to generate future action potential (i.e., physiological or pathological neuronal activity). The Na^+/K^+ pump is an electrogenic transmembrane ATPase, also referred to as $\text{Na}^+-\text{K}^+\text{ATPase}$ (Pivovarov et al., 2018).

As neurons use ATP, the intracellular $[\text{ATP}]$ decrease, and intracellular concentration of adenosine di- and monophosphate increase. These changes in adenylate concentration have immediate consequences on neurons’ energy regulation mechanism, which can be summarized in the figure below (**Figure 10**). Usually, the increase in glycolytic activity exceeds the increase in aerobic metabolism, and the excess pyruvate is exported in the form of lactate (Berndt et al., 2015). More interestingly is the fact that the increase in cerebral metabolic rate of glucose (and cerebral metabolic rate of oxygen) remains lower than the increase in CBF (Fox and Raichle, 1986; Fox, 2012). This disproportional increase in CBF is responsible for the washout/dilution effect (i.e., decrease in oxygen extraction fraction– associated with neuronal activity) (Hoge et al., 1999a,b).

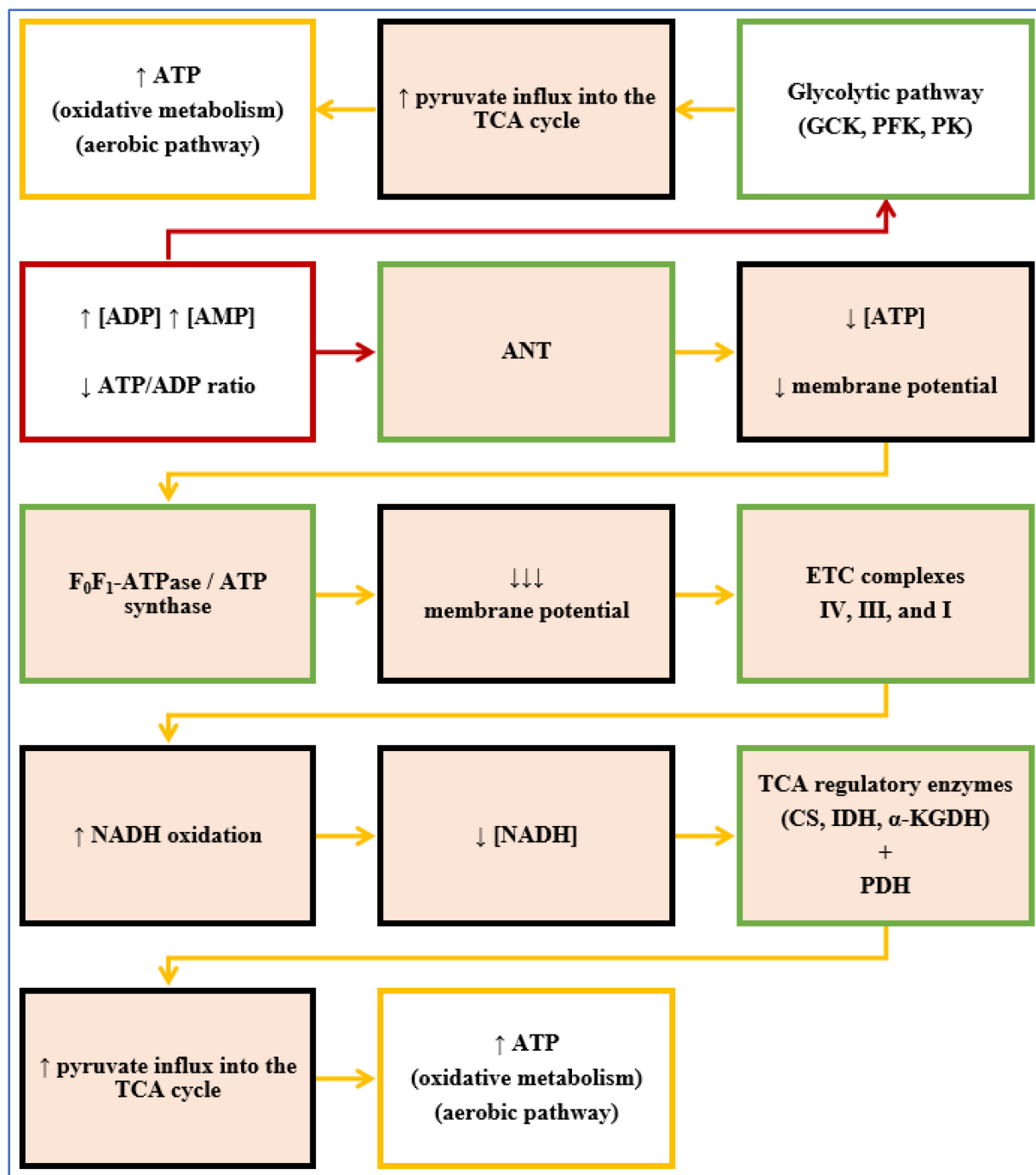


Figure 10 – Physiological metabolism regulation in neurons (*Inspired by Kovac et al., 2018*). White colored: occurring in the cytoplasm; orange colored: occurring in the mitochondria; red frame: initial metabolic changes; green frame: activation; yellow frame: metabolic endpoints following neuronal activation. α -KGDH: α -ketoglutarate dehydrogenase, ANT: adenine nucleotide translocator, CS: citrate synthase, ETC: electron transport chain, GCK: glucokinase, IDH: Isocitrate dehydrogenase, NADH: nicotinamide adenine dinucleotide + hydrogen, PDH: Pyruvate dehydrogenase, PFK: phosphofructokinase, PK: pyruvate kinase, TCA: tricarboxylic acid, []: concentration.

3.1.2 Brain circulation and neurovascular coupling

In order to meet the high metabolic demand of the brain, continuous delivery of oxygen and energy substrates to each neuron is needed (Siesjo, 1978). This delivery is achieved by a collective work of unique, well structured, and physiologically regulated angioarchitecture composed of pial arteries and venules, penetrating arterioles and venules, and the subsurface microvascular network (Zlokovic, 2005).

Oxygen and glucose are transported via the bloodstream to the brain through the arterial system. Oxygen transport is mainly bound to an iron-containing protein hemoglobin in red blood cells (98% vs. 2% dissolved in blood plasma). The vascular system of the brain is composed of the internal carotid arteries (anterior circulation), vertebral arteries (posterior circulation), their anastomotic connection (i.e., circle of Willis), from which large cerebral arteries (MCA) emerge and give rise to pial arterioles, penetrating or intracerebral arterioles, and capillaries. Once hemoglobin reaches the capillaries, oxygen dissociates from hemoglobin and can diffuse toward brain parenchyma (i.e., neurons). This is due to the particular affinity of hemoglobin for oxygen which strongly depends on the difference in partial pressure of oxygen between the vessels and brain tissue. Once hemoglobin is dissociated from oxygen, it becomes deoxyhemoglobin; feeding back into the venous system returning the deoxygenated blood to the heart.

3.1.3 Macrovasculature (cerebral autoregulation)

The large cerebral arteries are responsible for 60% of total vascular resistance. The microvasculature is mainly involved in the process of cerebral autoregulation. When changes in cerebral perfusion pressure occur, generally due to changes in mean arterial blood pressure, neurogenic and myogenic regulation mechanism maintain a stable blood flow (~50 ml/min/100g) by changing the diameter of large blood vessels. However, when the mean arterial blood pressure is too low (<40 mmHg) or too high (>160 mmHg), hypoperfusion (and ischemia) and hyperperfusion (and vasogenic edema) occur respectively (**Figure 11**) (Paulson et al., 1990; Lidington et al., 2021).

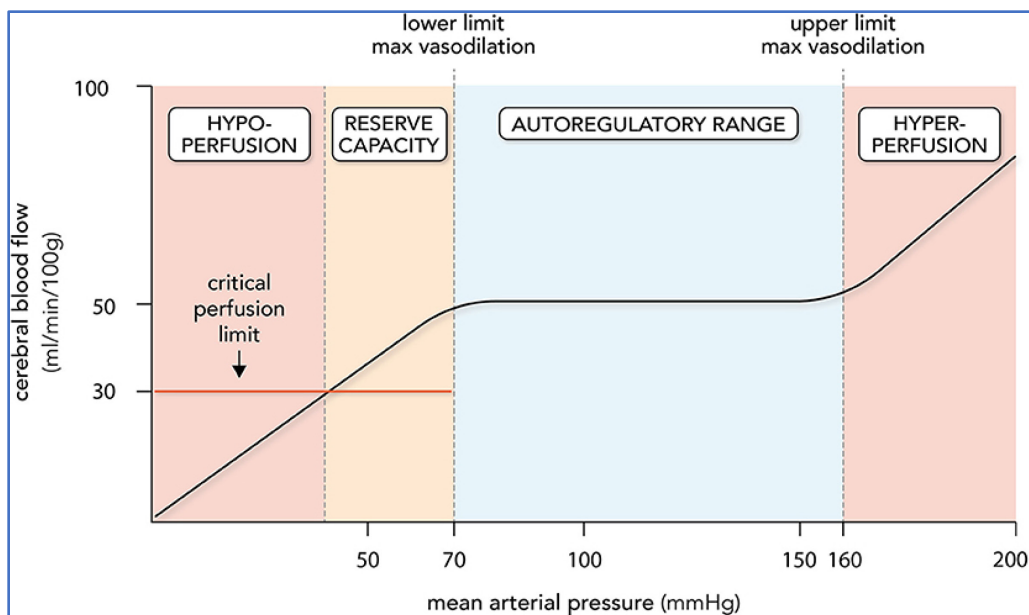


Figure 11 - Cerebral autoregulation (*Adapted from Lidington et al., 2021*).

3.1.4 Microvasculature (neurovascular unit)

On the other hand, pial arteries, penetrating arterioles, capillaries and postcapillary venules are responsible for the remaining vascular resistance (i.e., 40%). The microvasculature is directly involved, although contributing differently, in the neurovascular coupling. The relative uniqueness in the structural composition for each of these vascular segments is what will strongly influence the hemodynamic response (i.e., shape and amplitude of the neurovascular coupling) (**Table 2**).

Table 2 – Structural difference between pial arteries, arterioles and capillaries.

	Pial arteries	Penetrating arterioles	Capillary bed
Anatomy	subarachnoid space	perivascular space	
Smooth muscle cells	Thick layer	Thin layer	No
Innervation	+++ (mainly PNS)	+ (mainly CNS)	
Cell contact	No	Yes (astrocyte > neurons, pericyte)	Yes (astrocyte < neurons, pericyte)

CNS: central nervous system, PNS: peripheral nervous system

The capillaries represent the primary site where oxygen, nutrients, and metabolic waste are exchanged. It is estimated that the total length of capillaries in the human brain is ~400 miles (Begley and Brightman, 2003) and that nearly every neuron in the brain has its “own” capillary (Zlokovic, 2005), demonstrating the critical relationship between the neuronal and vascular compartments. However, the blood flow within the capillaries is highly dependent on the intravascular pressure gradient between precapillary arteriole and postcapillary venule. Capillaries are not composed of smooth muscle cells, unlike pial, penetrating arterioles, and postcapillary venules. Therefore, the regulation of capillary blood flow is mainly dependent on vascular resistance of precapillary arteries and vascular tonus of postcapillaries venules. For example, a decrease in precapillary resistance (i.e., dilatation) will increase precapillary microvascular pressure, increasing the intravascular pressure gradient between the precapillary arteriole postcapillary venule and consequently increase capillary blood flow. It is also important to note that even the flow velocity of red blood cells plays an essential role in the efficiency of oxygen transport, as it is remarkably high (~1mm/sec) and heterogeneous (0.3-3.2 mm/sec) (Wei et al., 1993).

3.1.5 Neurovascular coupling (feed-forward mechanism)

A feed-forward mechanism mainly responsible for the different steps involved during neurovascular coupling as solid evidence suggests that the excessive increase in CBF is directly related to the release of synaptic vasoactive mediators during neural activity (Logothetis, 2001; Attwell et al., 2010; Cauli and Hamel, 2010; Magistretti and Allaman, 2015; Lecrux and Hamel, 2016; Iadecola, 2017).

Neuronal activity is associated with changes in ionic concentration and the synthesis and release of various mediators such as glutamate. Glutamate binds to its postsynaptic receptor and causes an increase in the intracellular concentration of calcium in the postsynaptic neuron. Consequently, the increase in intracellular concentration of calcium activates specific enzymes (e.g., nitric oxide synthase, and cyclooxygenase-2) (Hosford et al., 2019). Activation of those enzymes leads to the production and diffusion of critical potent vasodilators (e.g., nitric oxide), which will lead to smooth muscle cells relaxation and vasodilatation in the precapillary vascular system. Another vasodilatory molecule is lactate which is produced during anaerobic metabolism. Additionally, the

increase in the extracellular concentration of K^+ can also lead to smooth muscle cells relaxation and vasodilatation (Iadecola et al., 2017). Lastly, neurons also release potent vasoconstrictor molecules, such as neuropeptide Y, mainly released by interneurons.

Like neurons, astrocytes can produce vasoactive agents (i.e., vasodilator and vasoconstrictor). Glutamate release by neurons can also activate glutamate receptors on astrocytes. Once activated, these receptors lead to an increased intracellular concentration of calcium (in astrocytes) and activation of phospholipases A2, an enzyme responsible for releasing arachidonic acid and lysophosphatidic acid. Arachidonic acid is further broken down into several potent vasodilators and vasoconstrictors. The increased intracellular calcium concentration also opens smooth muscle cells K^+ channels which favours vasodilatation.

Another important player in the neurovascular coupling is the endothelial cells of capillaries. Endothelial cells can mediate the hemodynamic response through either slow diffusion of vasodilatory molecules (e.g., nitric oxide, proteinoids, endothelin) or cause direct vasodilatation by retrograde electrical propagation through gap junction.

Finally, pericytes are contractile cells surrounding the capillaries and are extremely sensitive to the nitric oxide and prostaglandin E2 concentration. Neuronal activity releases nitric oxide and prostaglandin, which activates and leads to vasodilatation, increasing capillary blood flow.

As we can see neurovascular coupling is complex, involving different molecular and cellular components. In addition, the amplitude or spatial extent of the neurovascular response are also largely influenced by different factors, such as stimulus intensity or amplitude (Devor et al., 2003), cortical depth (e.g., superficial vs. deeper cortical layers) (Uhlirva et al., 2016), and brain state (e.g., sleep/anesthesia vs. wakefulness) (Lecrux et al., 2019).

3.1.6 Neurovascular coupling (feedback mechanism)

A feedback mechanism also contributes to neurovascular coupling to a lesser degree (Powers et al., 1996; Devor et al., 2008; Lindauer et al., 2010). In other words, a decrease in O_2 or glucose is

more likely to play a secondary role by adjusting the CBF delivery to meet the metabolic need of neuronal tissue more closely (Ngai et al., 1988; Drew et al., 2011; Freeman and Li, 2016).

3.2 Metabolism during seizures

Seizures are associated with an increased in metabolism (i.e., cerebral metabolic rate of oxygen) (Chapman et al., 1977, Freund et al., 1989, Ingvar, 1986). However, in contrast to “normal” neuronal activity, seizures reflect a state of “abnormal”, “excessive”, and “hypersynchronous” discharge in pathological neurons (Bromfield et al., 2006). Consequently, neurons are expected to adapt metabolically to sustain the high metabolic rate associated with seizures (Plum et al., 1974; Yang et al., 2013).

Several studies have suggested a shift in the primary pathway involved in energy production during seizures (Sacktor et al., 1966; Acharya et al., 2005; Folbergrova et al., 2007; Yang et al., 2013). A decrease in aerobic enzymes (i.e., aconitase, malate dehydrogenases, and succinate dehydrogenases) (Acharya et al., 2005; Folbergrova et al., 2007) and an increase in anaerobic kinases (i.e., phosphofructokinase and glucose kinase) (Sacktor et al., 1966) have been reported in neurons involved in seizure activity. This shift from primary aerobic metabolism to anaerobic metabolism is responsible for the increase in lactic acid concentration (Kuhr et al., 1988a,b; During et al., 1994; Fornai et al., 2000; Nepl et al., 2001; Darbin et al., 2005). The increased production of lactic acid from the anaerobic pathway, as well as from other sources (e.g., astrocytic glycogen reserve, astrocyte-neuron lactate shuttle, inter-astrocytic gap junction) (Dalsgaard et al., 2007; Pellerin et al., 2007; Rouach et al., 2008) is thought to compensate for the increase in energy demand by providing brain cells with an alternative supply of energy further sustain the exaggerated firing observed during seizures (Schurr et al., 1988; Schurr et al., 1997, Schurr et al., 1999; Solaini et al., 2010; Farrell et al., 2016). Additionally, the relative hypoxic state sometimes seen during seizures also contributes to the metabolic pathway shift through the pro-anaerobic and anti-aerobic effects of “hypoxia-inducible factors”, which are usually produced by “hypoxic” neurons (Solaini et al., 2010; Farrell et al., 2016). Finally, more recently, it was also reported that seizures can also be associated with an enhanced oxidative metabolism (i.e., enhanced aerobic

metabolism) maintaining the primary source of energy production oxygen dependent (Foster et al., 2005; Ivanov et al., 2015; Schoknecht et al., 2017).

Similarly, a state of hypermetabolism can also be observed in neurons involved in recurrent seizures (i.e., SE) (Ingvar et al., 1983; Ingvar et al., 1986; Pereira de Vasconcelos et al., 2002). In humans, PET studies can indeed show hypermetabolism in brain regions involved during recurrent seizures (Doherty et al., 2004). More recently, Vespa et al. (2016) showed, using cerebral microdialysis, elevated cerebral lactate/pyruvate ratio during seizure activity in patients with SE suggesting a state of “metabolic crisis” during which oxygen delivery could not meet the abnormally high demand of neuronal activity, and consequently, shifting neuronal metabolism toward the anaerobic pathway.

While hypermetabolism is seen during seizures, the period after seizures usually shows a decrease in metabolism (Meyer, 1994; Foldvary et al., 1999; Kim and Mountz, 2011; Burneo et al., 2015). Similarly, hypometabolism is also usually seen in chronic epileptic brains. Several hypotheses have been proposed to explain the hypometabolic state during the interictal period in chronic epileptic brain such as depressed functionality and/or tissue/neuronal loss (Hong et al., 2002; Koutroumanidis et al., 2000)

3.3 Hemodynamics and neurovascular coupling during seizures

It is well established that a seizure usually induces a reversible regional vasodilation and, subsequently, a disproportional and transient increase in CBF and CBV (Penfield et al., 1939; Zhao et al., 2009, 2011), which is responsible for the overshooting supply of oxygenated hemoglobin (Raichle, 2001) (Tyvaert et al., 2009; Thornton et al., 2010). This observed increase in hemodynamics (i.e., CBF, CBV, and local oxygen levels) seem to result from a “restorative process” (i.e., increasing blood supply to underperfused areas) (Doman and Pelligra, 2003,2004; Kovács et al., 2018). In vivo studies in anesthetized mice have found that seizures can lead to vasodilatation of cortical penetrating arterioles at the epileptic focus (Gómez-Gonzalo et al., 2011; Zhang et al., 2019) and vasoconstriction in areas remote from the epileptic focus (Girouard et al., 2010; Zhang et al., 2019). This increase in hemodynamics (i.e., CBF, CBV, and local oxygen

levels) can sometimes be preceded by a very brief period of decreased CBF and hypoxia (*aka* as the initial pO₂ “dip”), suggesting a brief period of uncompensated increase in metabolic activity or delayed oxygen extraction pending a sufficient neurovascular response. More preoccupying is the demonstration of relative hypoxia observed in some seizures (Zhao et al., 2009, 2011; Bahar et al., 2006; Suh et al., 2006; Ma et al., 2013; Harris et al., 2014) which can be long in some cases of SE (Claassen et al., 2013). Following seizure offset, a sustained period of hypoxia has been reported using continuous oxygen detection in rodents (Farrell et al., 2016).

These findings have been supported by recent observations indicating the presence of altered blood-brain barrier resulting in a disturbed neurovascular unit, especially during SE (Gorter et al., 2015; Bar-Klein et al., 2017). This disturbance in neurovascular coupling mechanisms appears to be spatially heterogeneous (Fabene et al., 2007; Harris et al., 2018). For example, following pilocarpine-induced SE, Fabene and his colleagues observed an expected and normal neurovascular coupling (i.e., CBF increase) in superficial arteries and veins (e.g., pial arterial and proximal portion penetrating arterioles). In contrast, deeper arterioles (e.g., the distal portion of penetrating arterioles and capillaries) showed vasoconstriction, resulting in ischemia (Fabene et al., 2007). Another possible cause of neurovascular coupling dysfunction is pericytic injuries. Significant redistribution of pericytes has been shown after SE (Milesi et al., 2014), and more recently, pericyte-mediated capillary vasospasm following seizure onset was observed in a genetic and kainic acid model of epilepsy (Leal-Campanario et al., 2017). Several studies have shown the vulnerability of pericytes in several conditions associated with the formation of oxygen and nitrogen-derived free radicals (Yemisci et al., 2009; Hall et al., 2014). Similarly, both in vivo (Folbergrová et al., 2012) and in vitro studies (Kovács et al., 2002, 2009) are also associated with an increase in those same free radicals, particularly during SE. Finally, vascular remodeling during SE might also occur, as observed during lasting epileptiform activity (Morin-Brureau et al., 2011).

3.4 Metabolism during periodic discharges

PET hypermetabolism and hypometabolism have been reported with periodic discharges and may change over time owing to treatment/resolution of periodic discharges, recent seizure activity, and surrounding brain injury. In a study by Franck and his colleagues, 3 (12%) out of 25 patients with

seizures had lateralized periodic discharges. Interictal PET hypometabolism was found in 20 patients (80%), while PET hypermetabolism and an increase in CBF were found, both during seizures and lateralized periodic discharges (Franck et al., 1986). More recently, Struck and his colleagues analyzed 18 patients with patterns falling on the ictal-interictal continuum. Fourteen patients (78%) had periodic discharges (74% lateralized periodic discharges, 36% generalized periodic discharges), and four patients (22%) had rhythmic delta activity (all generalized). In patients with lateralized periodic discharges (10 patients), focal hypermetabolism was observed in 7 (71%) and hypometabolism in 3 (29%). As for patients with generalized periodic discharges (5 patients), hypermetabolism was observed in 80% (3 patients). In addition, patients with generalized rhythmic delta activity were divided into those with a frequency > 3Hz (1 patient) and those with a frequency < 3Hz (3 patients). Only generalized rhythmic delta activity with a frequency >3Hz was associated with focal PET hypermetabolism (Struck et al., 2016). Similarly, resolution of PET hypermetabolism and clinical improvement after cessation of lateralized periodic discharges were observed by others (Handforth et al., 1994; Kim et al., 2012; Sakakibara et al., 2014).

Using cerebral microdialysis and electrocorticography in patients with traumatic brain injury Vespa et al. (2007; 2016) suggested that periodic discharges could also be associated with signs of metabolic crisis (i.e., lactate/pyruvate ratio increase, decrease in extracellular glucose, glutamate increase, brain tissue hypoxia) same as during seizures and SE. Authors suggested that in patients with traumatic brain injury, periodic discharges should be managed similarly (as aggressively) as seizures (Vespa et al., 2016). Similar findings (i.e., a state of metabolic crisis) were also reported by Harting et al. (2011) in traumatic brain injury patients with prolonged cortical spreading depression associated with periodic discharges (Harting et al., 2011).

3.5 Hemodynamics and neurovascular coupling during periodic discharges

Periodic discharges associated with hyperperfusion on SPECT (Lee et al., 1988; Assal et al., 2001; Ali et al., 2001; Bozkurt et al., 2002; Ergun et al., 2006; Claassen et al., 2009) and MR perfusion (Venkatraman et al., 2017) was observed by several authors. In one study of 18 patients, SPECT hyperperfusion was associated and co-localized with lateralized periodic discharges (Assal et al.,

2001). Resolution of lateralized periodic discharges resulted in SPECT hypoperfusion (Assal et al., 2001), suggesting that the increase in CBF probably resulted from abnormal vasodilation secondary to a decrease in oxygen extraction fraction. Other studies have reported similar findings with SPECT (Lee et al., 1988; Ali et al., 2001; Bozkurt et al., 2002; Ergun et al., 2006). Conversely, cases of SPECT hypoperfusion during periodic discharges have also been reported (Kan et al., 1992; Hisada et al., 2000; Aye et al., 2013; Fushimi et al., 2003). Similarly, no changes in blood flow during SIRPIDs have been reported (Zeiler et al., 2011; Smith et al., 2014).

More recently, a retrospective study employed invasive methods capable of continuously monitoring brain hemodynamics, such as partial brain tissue oxygenation (PbtO₂), thermal-diffusion flowmetry (to measure regional CBF), and depth EEG (i.e., electrocorticography) in 90 comatose patients with high-grade subarachnoid hemorrhage, in order to determine whether distinct periodic discharges patterns can cause, similar to electrographic seizures, brain tissue hypoxia. In their study, Witsch and his colleagues observed an association between high-frequency periodic discharges (i.e., ≥ 2 Hz), increase regional CBF and reduced PbtO₂ suggesting that higher-frequency periodic discharges may reflect inadequacies in brain compensatory mechanisms and might lead to additional damage after acute brain injury (Witsch et al., 2017).

3.6 Metabolism during burst-suppression

Metabolism during burst-suppression has mainly been studied in anesthesia-induced burst-suppression and very little in burst-suppression induced by acute brain injury.

It has been proposed that burst-suppression results from the interaction of two distinct (but interrelated) processes operating at different time scales (Ching et al., 2012). First, a fast (millisecond timescale) dynamic process is responsible for the fast-neuronal oscillations seen in the EEG background activity (i.e., “resting” EEG activity present before the onset of burst suppression) and reappearing during bursts. Second, a slow (seconds-to-minutes timescale) dynamic process linked to neuronal metabolism serves as a gating (or modulating) mechanism for the first process. According to this model, each period of burst-suppression is associated with a cyclic change in cerebral metabolic rate of oxygen and ATP depletion/recovery in cortical and

subcortical networks. Fast neuronal activity is responsible for the increase in ATP consumption. Consequently, ATP concentration depletion reduces ATP-gated K^+ channels function, which is required for membrane depolarization and burst termination (i.e., suppression initiation). During suppression, slow ATP regeneration begins, leading to a recovery of function of ATP-gated K^+ channels and consequently fast neuronal activity or burst activity (i.e., suppression termination). Differences in metabolic state and energetic demand in local circuits might explain the spatially inhomogeneous pattern observed during medically-induced burst-suppression (Ching et al., 2012; Lewis et al., 2013; Westover et al., 2015). Indeed, in the study performed by Lewis and his colleagues, they reasoned that local variation in cerebral metabolism (i.e., different regions of the brain with different cerebral metabolic rate of oxygen rates) might be responsible for different probability periods of burst or suppression in distinct networks of neurons which could recruit the heterogeneous population of neurons into going into burst or suppression.

3.7 Hemodynamics and neurovascular coupling during burst-suppression

Unfortunately, few studies have investigated the neurovascular dynamics during burst-suppression patterns. Animal studies using EEG-fMRI (Mäikiranta et al. 2002, Liu et al. 2011) and optical imaging (Sutin et al., 2014) have observed a strong presence of neurovascular coupling during spontaneous EEG burst activity, which was characterized by the presence of a BOLD response, increase in CBF and [HbO]. In humans, only one study reported direct hemodynamic changes occurring during burst-suppression (Chalia et al., 2016). In this study, heterogeneous spatial changes in [HbO] and [HbR] were present during burst activity. More specifically, burst activity was associated with characterized by an initial decrease in [HbO], followed by a pronounced increase in [HbO] that reaches a peak 10-12s after the burst onset (Chalia et al., 2016). These observations are concordant with previous a report of intracranial pressure changes (i.e., increase) seen during bursts in two critically ill patients, most likely suggesting an increase in CBV secondary to an increase of CBF associated with burst (Connolly et al., 2015).

In summary, this chapter described what is know about neurovascular and metabolic changes associated with seizures, periodic discharges and burst-suppression. Better characterizing the spatial and temporal hemodynamic changes during these EEG events, especially in pathological

contexts, could better help determine if (or when) these patterns lead (or could lead) to neuronal injury ([Lewis et al., 2013](#)), which is the topic of the following chapter.

CHAPTER 4 – CURRENT TECHNIQUES TO INVESTIGATE AND MONITOR EPILEPTIFORM DISCHARGES IN CRITICALLY ILL PATIENTS

Critically ill patients have a high risk of secondary brain injuries such as (or caused by) seizures and brain ischemia. In order to determine brain function, clinicians have long relied on serial bedside neurologic examination and neuroimaging exams. However, neurological or imaging exam changes reflecting cerebral ischemia may occur long after catastrophic and irreversible brain damage is clinically or radiographically apparent (Korbakis and Vespa, 2017; Yang et al., 2020). Thus, while these serial bedside approaches are still performed in the critical care setting, clinicians now rely on different functional neuroimaging and neuromonitoring modalities to understand brain physiology and guide therapeutic interventions to prevent secondary brain injury (LeRoux et al., 2014). This chapter reviews the most common functional neuroimaging and neuromonitoring techniques used to detect (i.e., monitor), as well as investigate (i.e., assess the neurophysiological impact) of epileptiform discharges in critically ill patients.

4.1 Positron emission tomography (PET)

PET is a semi-invasive functional neuroimaging technique that indirectly measures neuronal activity by measuring its metabolism (i.e., cerebral glucose metabolism) (Fougère et al., 2009; Lee et al., 2001). After a radioactive glucose analogue (i.e., tracer) such as ^{18}F fluorodeoxyglucose (i.e., ^{18}F FDG-PET) is injected, it travels through the vascular system and is taken up by cells. This uptake-fixation period can take anywhere from >30 min (Fougère et al., 2009). In the brain, ^{18}F FDG is captured by active neurons and phosphorylated into FDG-6-phosphate. FDG-6-phosphate cannot be metabolized further in the glycolytic pathway and remains within neurons for a significant amount of time (i.e., 15-30 min) to perform the scan. During this period, fluorine decays emit positrons, which releases high energy photons (i.e., gamma rays) detected and reconstructed in 3D by the tomograph (Bailey et al., 2005). In patients with chronic epilepsy, ^{18}F FDG-PET usually captures the interictal period due to its long uptake-fixation period (Kim et al., 2011; Sager et al.,

2011); the epileptogenic zone usually shows interictal hypometabolism (Engel, 1991; Savic et al., 1997).

Limitations include its low temporal resolution i.e., it can only provide a single snapshot of brain metabolism and cannot be used for continuous monitoring (Duncan et al., 2016). Moreover, PET is costly, relies on radioactive substances, requires specialized facilities and cannot be performed at the bedside continuously.

4.2 Single-photon emission computerized tomography (SPECT)

Similar to PET, SPECT is a semi-invasive functional neuroimaging imaging that also uses a gamma-emitting radiotracer to measure dynamic perfusion changes (i.e., regional CBF) in 3D (Groch and Erwin, 2000). ^{99m}Tc -hexamethyl-propyleneamine oxime (^{99m}Tc -HMPAO) is commonly used as the radiolabeled tracer. ^{99m}Tc -HMPAO crosses the blood-brain barrier and becomes trapped in tissue within the first passage of blood for a few hours. This very short uptake-fixation time allows the tomograph (Anger gamma camera) to measure and reconstruct in 3D the distribution of regional CBF, which is proportional to its distribution (Fougère et al., 2009; Kim et al., 2011). The very short uptake-fixation time and long retention (i.e., few hours) of the tracers offer the ability to measure regional CBF associated with seizures (ictal SPECT) even after they have ceased. However, the timing of the injection is critical and, ideally, must be short prior to seizure offset. Furthermore, SPECT sensitivity can be further improved by more advanced subtraction and coregistration methods (i.e., subtraction ictal SPECT coregistered to MRI) (Foiadelli et al., 2020). During a seizure, the epileptic focus usually shows the maximal site of increase in regional CBF from the baseline (i.e., hyperperfusion), while the interictal period shows a decrease in regional CBF (i.e., hypoperfusion) (Van Paesschen, 2004, 2007; Goffin et al., 2008;).

Limitations are similar to PET i.e., low temporal resolution, high cost, semi-invasiveness, and not possibly for continuous measurements at the bedside.

4.3 EEG-fMRI

EEG-fMRI provides the opportunity to study hemodynamic changes (i.e., BOLD response) associated with transient epileptiform activity captured on the scalp EEG (e.g., IEDs) (Faro and Mohamed, 2006; Goebel, 2009) with a great spatial (3-5mm) and relatively good temporal resolution (1s) (Cunningham et al., 2008; Moeller et al., 2013; van Graan et al., 2015). The principles of BOLD-fMRI are founded on the different magnetic properties of the HbR and HbO molecules and the basis of neurovascular coupling (i.e., \uparrow neuronal activity \rightarrow \uparrow CBF \rightarrow \uparrow [HbO] + \downarrow [HbR] = \uparrow BOLD signal – activation, and vice versa, although the physiological interpretation of deactivation remains debated) (Cohen and Bookheimer, 1994; Gaillard et al., 2000; Stefanovic et al., 2004; Berman et al., 2006). Despite several reports demonstrating that the shape of the hemodynamic response during IEDs and seizures might defer from the predicted canonical response, time-series EEG-fMRI data still relies on linear regression employing a canonical general linear model (GLM) (Benar et al., 2002; Bagshaw et al., 2004,2005,2006; Lu et al., 2006; Lemieux et al., 2007; Masterton et al., 2010; Grouiller et al., 2010, 2016; Beers et al., 2015; Salek-Haddadi et al., 2006). In patients with refractory epilepsy, EEG-fMRI shows great sensitivity in localizing the epileptogenic zone based on IEDs (Gotman et al., 2006; Moeller et al., 2009a,b; Lemieux et al., 2011; Pittau et al., 2012), and predicting surgical outcome (Thornton et al., 2010; van Houdt et al., 2013; An et al., 2013; Coan et al., 2016). Additionally, EEG-fMRI has also been used in patients with epilepsy to investigate epileptic networks and map seizure-related hemodynamic changes (Gotman, 2008; Kobayashi et al., 2009; Leite et al., 2013).

Unfortunately, EEG-fMRI has several limitations, including short scanning time (generally less than two hours) and immobility constraints since motion can profoundly impact data quality. While few studies involving electrographic seizures or seizures with minimal motion have been reported (Kobayashi et al., 2009; Tyvaert et al., 2009; Chaudhary et al., 2013), investigating seizures or any other abnormal EEG pattern with EEG-fMRI is impractical, especially in challenging patient populations (e.g., children with epilepsy, patients with intellectual disabilities, critically ill patients). Similar to PET and SPECT, EEG-fMRI requires specialized facilities, cannot be performed at the bedside and cannot be used for continuous monitoring.

4.4 Noninvasive continuous electrophysiological monitoring

EEG is the most widely used monitoring tool and represents the gold standard in seizure monitoring (Korbakis and Vespa, 2017). Thus, the main indication for continuous EEG monitoring in the ICU is detecting and managing seizures (Vespa et al. 1999, Jette et al., 2006; Claassen et al. 2006, 2007). In the critical care setting, up to 92% of these seizures are nonconvulsive (Claassen et al., 2004). Therefore, a rapid diagnosis is vital to start treatment quickly. In patients with NCS or NCSE, continuous EEG recordings has proven to be a crucial monitoring technique, successfully allowing clinicians to properly manage critical care patients presenting with seizures.

Other indications for continuous EEG monitoring in the ICU include 1) clarifying the nature of abnormal movements (e.g., myoclonus, posturing, eye deviation), 2) grading the severity of encephalopathy (Young et al., 1992a,b; Vespa et al., 2016), 3) medication titration (Mecarelli et al. 2001; Bewernitz et al., 2012; Kasab et al., 2016), 4) for prognostication purposes, especially in patients with anoxic-ischemic encephalopathy (Young, 2009; Perera et al., 2022), subarachnoid hemorrhage (Claassen et al., 2007) and stroke (Tzvetanov et al., 2005; Claassen et al., 2006; Zandbergen et al., 2006), and 5) for ischemia detection (Friedman et al., 2009).

In regards to brain ischemia, this is due to the close association between relatively specific electrophysiological (i.e. EEG) patterns and CBF levels (Sharbrough et al., 1973). Indeed, as CBF decrease, a decrease in oxygen and glucose leads to changes in cortical neuron metabolism (Nagata et al., 1989; Powers, 1991) and electrophysiological activity (i.e., oscillation frequency) (Evans, 1976; Jordan, 1999,2004). When CBF reaches the infarction threshold (~10-12 ml/100g/min), irreversible neuronal damage becomes inevitable. Thus, clinicians rely on a narrow window before irreversible damage occurs to act and restore perfusion as quickly as possible. Continuous EEG monitoring in the setting of brain ischemia has been employed to prevent primary (e.g., clamping/cardiovascular surgery, refractory hypotension, sepsis-associated encephalopathy) (Herrschaft, 1977) or secondary ischemic brain injury (i.e., ischemic stroke) (Sharbrough et al., 1973).

Over the years, advances in computational methods have made it possible to transform extended periods of raw EEG into a numerical value (i.e., quantitative EEG, qEEG). Like continuous EEG monitoring, qEEG is becoming more utilized in critical care seizures, mainly for seizure detection (Haider et al., 2016). qEEG is also capable of reflecting changes in blood flow and metabolism (Laman et al., 2001) and has been used in stroke patients (i.e., correlating with stroke severity, radiographic findings, and response to treatment (van Putten MJ et al., 2004a,b), prognostication (Hebb et al., 2007; Rossetti et al., 2010a,b) and, more recently, in the early detection of delayed cerebral ischemia (Vespa et al., 1997; Gollwitzer et al., 2015). For similar reasons as continuous EEG, qEEG is currently not used for ischemia detection in critical care seizures.

Despite its importance, continuous EEG monitoring remains a laborious monitoring method, requiring a certified electrophysiology technician to apply and maintain electrodes on the head and an expert physician capable of interpreting the EEG in a timely fashion (Gavvala et al., 2014; Trinkka et al., 2015,2022). EEG is also prone to motion and other sources of artifacts in the ICU (e.g., electronic equipment, ventilator). Finally, in critical care seizures, EEG does not provide any information on cerebral hemodynamic status (e.g., oxygenation, metabolism, CBF).

4.5 Invasive neuromonitoring modalities

4.5.1 Invasive continuous EEG monitoring

Intracortical seizures are frequent in patients with acute brain injury, and very often, these seizures have no corresponding ictal activity on scalp EEG (Waziri et al., 2009; Claassen et al., 2013; Vespa et al., 2016). Subdural strip electrodes or intracortical depth electrodes have been used for detecting seizures that are not visible by traditional noninvasive continuous EEG monitoring (Claassen and Vespa, 2014). While intracranial EEG monitoring may provide higher sensitivity for detecting seizures and improve the signal-to-noise ratio compared to surface electrical activity, this technique comes with non-negligible risks (hemorrhage, infection) and provide only limited spatiotemporal sampling, which explains why it is used only in rare instances (Blount et al., 2008; Parvizi et al., 2018).

4.5.2 Intracranial pressure monitoring (ICP)

ICP measurements may be achieved via pressure sensors located within the fluid-filled ventricles (i.e., external ventricular drain), the brain parenchyma (i.e., intraparenchymal intracranial pressure monitor), subarachnoid (i.e., subarachnoid intracranial pressure monitor), or epidural (i.e., epidural intracranial pressure monitor) space. ICP monitoring can also estimate cerebral perfusion pressure which can be calculated by subtracting the intracranial pressure from the mean arterial blood pressure, and cerebral autoregulation, better known as the pressure-reactivity index.

The most accurate ICP monitoring is through external ventricular drain. Clinical indications include 1) cerebral edema with suspicion of elevated ICP (e.g., traumatic brain injury, subarachnoid hemorrhage, ischemic stroke), 2) hydrocephalus, 3) surgery (e.g., subarachnoid hemorrhage, resection of Chiari malformation, brain tumour), and 4) direct pharmacological administration in the ventricular system of the brain (e.g., ventriculitis, brain tumour) (Czosnyka et al., 2017). Concerns with intracranial pressure monitoring devices include deep venous thrombosis (including catheter-related septic thrombophlebitis), bleeding (especially in patients on antiplatelet or anticoagulant therapy), and technical difficulties and malfunctioning and the need for frequent calibration (for intraparenchymal ICP monitors). Moreover, ICP dressing (or dressing change) requires an experienced user.

4.5.3 Jugular venous bulb oximetry (SjvO₂)

Jugular venous bulb oximetry or cerebral venous oxygen saturation is a continuous global measure of cerebral oxygenation. After inserting a specialized catheter into the dominant internal jugular vein, jugular venous saturation (SjvO₂), which reflects the balance between cerebral oxygen supply and cerebral metabolic demand, can be measured (Chieregato et al., 2003). An oxygen extracting ratio can also be calculated by comparing SjvO₂ with systemic oxygen delivery (i.e., arterial blood oxygenation, SaO₂).

Indications for SjvO₂ monitoring include traumatic brain injury (most common), subarachnoid hemorrhage, and hyperventilation therapy in patients with high ICP (Coles et al., 2002). Normal jugular venous oxygen saturation (SjvO₂) ranges from 55 to 75 %. Values below and above this range reflect cerebral ischemia and hyperemia, respectively. Low SjvO₂ is associated with poor

outcomes in neurologically injured patients (Gupta et al., 1999). In patients with traumatic brain injury, an elevation of S_{ijv}O₂ is thought to reflect either reduced cerebral metabolic rate or hyperemia with impaired autoregulation (Fortune et al., 1994) and has been associated with poor outcomes (Cormio et al., 1999). On the other hand, low S_{ijv}O₂ may indicate cerebral ischemia (Cormio et al., 2001).

Limitations include 1) the need for a lateral skull scan (to confirm catheter placement), 2) infection and non-occlusive jugular vein thrombosis (Coplin et al., 1997), 3) the underestimation of the degree of regional brain ischemia (especially when S_{ijv}O₂ values are below 60%), and 4) the need to regular (every 8h-12h) calibration. In addition, several potential confounding sources of low (low cardiac output, anemia, severe vasoconstriction, systemic hypoxia, increased oxygen utilization) and high (hyperemia, significant sedation, neuronal hypometabolism, and cell death and high cardiac output, caudal displacement of the catheter) S_{ijv}O₂ values must be considered.

4.5.4 Intraparenchymal cerebral oxygenation monitoring (PbtO₂)

Intraparenchymal cerebral oxygen monitoring or PbtO₂ is the partial pressure of oxygen in the extra-cellular fluid of the brain and reflects the availability of oxygen for oxidative metabolism. In comparison to S_{ijv}O₂, PbtO₂ monitors local cerebral changes in oxygen concentration. It requires the insertion of a probe into the brain parenchyma. It allows for continuous monitoring of absolute brain oxygen concentration. Index of tissue oxygen reactivity and cerebral autoregulation can also be assessed with intraparenchymal cerebral oxygen monitoring (Jaeger et al., 2007). Normal values for PbtO₂ are still a topic of debate. However, strong clinical evidence shows a clear correlation between low PbtO₂ values and poor outcomes in traumatic brain injury and subarachnoid hemorrhage patients (Ramakrishna et al., 2008; Narotam et al., 2009; Spiotta et al., 2010; Oddo et al., 2014; Eriksson et al., 2012).

Limitations of this monitoring include 1) the necessity to place the probe in a normal-appearing brain region, which is technically demanding and needs an experienced operator, 2) the effect of contusions or perilesional edema on PbtO₂ values, 3) the need for CT-scan to confirm probe positioning, 4) the long calibration time (up to 1h), 4) the risk of bleeding and infection, and 5) the ability to only measure a limited and small region of the brain (Ponce et al., 2012).

4.5.5 Cerebral microdialysis

Cerebral microdialysis is an invasive monitoring technique that allows for continuous quantification of brain metabolism at the bedside. A thin catheter with a semipermeable membrane tip is placed into the white matter of the brain parenchyma through a borehole or a bolt system. Molecules within the brain interstitial system diffuse across the semipermeable membrane and are collected into a portable analyzer that determines analytes concentrations. The concentration of molecules in the dialysate is proportional to the interstitial molecule concentration in the brain (Tisdall and Smith, 2006).

Standard molecules of interest include glucose, lactate, pyruvate, and markers of excitotoxicity or cell damage (e.g., glutamate and glycerol) (Tisdall and Smith, 2006). They provide essential information regarding neuronal integrity and signs of metabolic distress. Other measurements include the lactate-pyruvate ratio, which reflects the intracellular redox state, and mitochondrial function. Compared to lactate or pyruvate concentration alone, lactate-pyruvate ratio is a more specific marker of cerebral ischemia (Enblad et al., 1996). Isolate increases in lactate-pyruvate ratio reflect an increase in brain metabolism. However, it does not suggest the presence or absence of neuronal damage (Tisdall and Smith, 2006; Zeiler et al., 2017). An elevated lactate-pyruvate ratio and low interstitial brain glucose can be indicative of hypoxia or ischemia and has been shown to correlate with poor outcome in patients with traumatic brain injury (Timofeev et al., 2011) and subarachnoid hemorrhage (Kett-White et al., 2002a,b; Sarrafzadeh et al., 2004). Inversely, patients with subarachnoid hemorrhage (Oddo et al., 2008, 2018) or spontaneous intracerebral hemorrhage (Nikaina et al., 2012) who present with a decrease in lactate-pyruvate ratio have better outcomes.

Glycerol and glutamate are potential markers of cell loss and metabolic distress, respectively. Although normal concentration ranges for glycerol and glutamate are not well established, elevated concentration of glycerol has been associated with ischemia and poor outcome in patients with traumatic brain injury (Paraforou et al., 2011). Similarly, a high glutamate concentration can indicate delayed cerebral ischemia in patients with subarachnoid hemorrhage (Nilsson et al., 1999) and ischemic and non-ischemic secondary brain injury in traumatic brain injury and subarachnoid hemorrhage patients (Zauner et al., 1996; Chamoun et al., 2010).

While the insertion of the probe is considered safe (Tisdall and Smith, 2006; Hutchinson et al., 2000), cerebral microdialysis remains an invasive technique (i.e., risk of infection and hemorrhage) with limitations. First, fluid analysis is generally (at most institutions) performed every hour (i.e., semi-continuous measurements), which may be a limitation when cerebral microdialysis parameters have to be compared to other monitoring modalities with higher time resolution or when monitoring or investigating dynamic processes such as seizures. Second, probe calibration takes time, and analyte concentration collected within the first two hours after catheter placement may demonstrate abnormalities and thus are usually discarded. Third, a CT scan is required to confirm the correct probe placement. Finally, before cerebral microdialysis monitoring, antibiotic prophylaxis is commonly used, and cerebral microdialysis is generally not performed in critically ill patients with significant platelet deficiency and/or coagulation problems.

4.5.6 Laser Doppler Flowmetry and Thermal Diffusion Flowmetry

Laser Doppler and thermal diffusion flowmetry are two continuous and invasive techniques capable of measuring very local (i.e., $\sim 3 \text{ cm}^3$) changes in CBF (i.e., regional CBF), by utilizing the Doppler shift of laser light for the first (Tamura, 2014) or by using a temperature gradient, as the tracer for the later (Carter, 1996). Both techniques have been used for in patients with traumatic brain injury or subarachnoid hemorrhage for early detection of vasospasm or ischemia, and prognostication (Zeiler et al., 2018; Mauritzon et al., 2022).

4.7 Additional modalities

4.7.1 Pupillometry

Light can be used to stimulate the retina in critically ill patients and assess brainstem function. A standard measurement of the diameters of the eyes' pupils using a penlight is simple and inexpensive but qualitative (i.e., prone to subjectivity) (Olson et al., 2015). To overcome such limitation, the use of automatic pupillometry has been favoured over standard pupillometry in recent years (Sandroni et al., 2022) to detect intracranial hypertension (Papangelou et al., 2018) and as a prognostic tool in patients with acute brain injury (Sandroni et al., 2021). Limitations include the need for an intact mechanism of vision and afferent/efferent visual pathways, a

decreased sedation drug measurement sensitivity, and interindividual variability in pupil size and reactivity (Sandroni et al., 2022).

4.7.2 Transcranial Doppler

TCD ultrasound is a non-invasive technique that allows the assessment of cerebral hemodynamics at the bedside. A probe insonates the major cerebral arteries and measures the peak systolic, end-diastolic, and mean flow velocities, pulsatility index, hemispheric index, and TCD flow velocity (Naqvi et al., 2013). TCD ultrasound is a reliable technique and is strongly recommended by the International Multidisciplinary Consensus Conference of Multimodality Monitoring in Neurocritical Care for predicting, detecting and monitoring angiographic vasospasm and delayed cerebral ischemia in patients with aneurysmal and traumatic subarachnoid hemorrhage (SAH) (LeRoux et al., 2014). Calculated resistive and pulsatility index by TCD ultrasound can also be used as a non-invasive surrogate of ICP in patients with severe TBI (Naqvi et al., 2013). Although less common, TCD ultrasound can detect microemboli during acute ischemic stroke. Progress in TCD ultrasound technology (i.e., Power M-Mode TCD, TC colour-coded duplex, contrast agent-TCD) has extended its application in the ICU to monitor arterial occlusion in acute ischemic stroke and detection of microembolic signals in carotid stenosis and cardioembolic disease (Naqvi et al., 2013).

TCD monitoring also has limitations (Naqvi et al., 2013). First, it is operator-dependent. An experienced physician is required to perform the exam at the bedside and interpret the results. In addition, only semi-continuous data can be acquired (i.e., continuous monitoring is currently not possible). Second, TCD cannot be performed in 5-20% of patients due to the absence of a temporal window (essential to obtaining a reliable Doppler signal). TCD is also insensitive to detecting distal vasospasm.

4.7.3 Brain ultrasound

Brain ultrasound or ultrasonography can be employed in critical care patients to evaluate brain anatomy and pathology (e.g., hemorrhage, hydrocephalus) (Robba et al., 2019). However, it can also be used to non-invasively assess cerebral circulation (i.e., cerebral blood flow velocity) at the bedside. It shares similar limitations as TCD (Robba et al., 2019).

In summary, there are techniques which can be used to monitor patients at risk of secondary brain injury such as seizures, study the associated hemodynamic responses, and assess the impact of such events on the brain. As pointed out throughout this chapter, each have significant limitations when applied in hospital and critical care settings. In the following chapter, we present a relatively novel functional neuroimaging and neuromonitoring technique, fNIRS, which has the potential to be useful in the monitor at the bedside patients at high risk of epileptiform activity, study the neurovascular response to such activity, and determine its impact on the brain. The next chapter will first cover essential background aspects of this modality such as its origin and physical principles, before focusing on the applications of fNIRS in neuroscience, particularly in epilepsy and critical care seizures, as well as the numerous clinical challenges currently facing this community.

CHAPTER 5 – FUNCTIONAL NEAR-INFRARED SPECTROSCOPY FOR THE STUDY OF EPILEPTIFORM DISCHARGES

5.1 Functional near-infrared spectroscopy

5.1.1 Terminology

The term “**biophotonics**” can be defined as integrating the field of biology and photonics (Popp et al., 2011). It is a large body in science where scientific and technological methods are applied in biomedicine to generate, manipulate, and detect photons. In other words, biophotonics is the "development and application of optical techniques, particularly imaging, to the study of biological molecules, cells and tissue" (Goda et al., 2019). Over the years, there has been a growing interest in applying optical techniques for studying different biological systems. When the organ investigated by optical methods is the brain, a more specific term can be used: “**neurophotonics**”. The field of neurophotonics is constantly growing. It applies a range of optical methods to probe the structure and function of the healthy and diseased brain at a multi-scale level.

Spectroscopy refers to the interaction between matter and radiated energy. On the other hand, **spectrophotometry** is “a branch of spectroscopy concerned with the quantitative measurement of the reflection or transmission properties of a material as a function of wavelength”. In neuroscience, **fNIRS** is when “NIRS” is applied to measure cortical hemodynamics in response to normal or abnormal neuronal activity.

Finally, the terms **diffuse optical topography and tomography (DOT)** refer to, respectively, the projection (2D) or reconstruction (3D) of hemodynamic changes onto the cortex. Other acronyms commonly used for DOT are: **diffuse optical spectroscopy (DOS)**, **near-infrared imaging (NIRI)**, **diffuse optical imaging (DOI)**, **near-infrared optical tomography (NIROT)**, and **high-density tomography (HD-tomography)**.

5.1.2 Brief historical overview and early application

The idea that continuous light could be used to investigate human tissue noninvasively dates back as early as the 19th century (Bright, 1831; Curling, 1856; Cutler, 1931). Later, in Germany, Hoppe-Seyler (1862) described the spectrum of oxyhemoglobin (HbO) and, two years later, a British named Stokes (1864) described the spectrum of deoxyhemoglobin (HbR) and stressed the importance of hemoglobin for the transport of oxygen (Perutz, 1979, 1980, 1995). In 1876, Karl von Vierordt (1876) was the first to measure the spectral changes of light penetrating tissues (von Vierordt, 1876; Severinghaus, 1986, 2007), and two decades later, *in vitro* determination of the absolute and relative [HbO] and [HbR] was achieved by Hüfner (Gorelov, 2008).

Following these early works, no significant report in that field was published. It was not until the 1930s that Kramer (1934) and Nicolai (1932) successfully reproduced von Vierordt work in animal and human tissues, respectively (Kramer, 1934; Nicolai, 1932). During the same period, two Germans by the name of Matthes and Gross used two separate wavelengths in the near-infrared spectrum to determine the spectroscopic properties of HbO and HbR in human tissues (Matthes and Gross, 1939a,b,c).

Those studies subsequently led to the development of the first muscle and peripheral oxygen saturation monitors (Matthes, 1935; Squire, 1940; Millikan, 1941; Wood and Geraci, 1949), and later in 1951, the development of the first brain oximeter (Zijlstra, 1953). Unfortunately, these monitors never made it into the clinical setting due to the relative hardware bulkiness and the complex calibration it required. It was not until 1972 that enough progress was made, leading to a breakthrough in clinical monitoring as Aoyagi invented the first pulse oximeter (Miyasaka et al., 2021).

However, applying optical methods to the living brain had to wait until 1977, when F. Jöbsis, a Professor of Physiology at Duke University (USA) and regarded today as the founding father of cerebral oximetry, demonstrated for the first time the possibility to measure tissue oxygenation and metabolism directly through the skin and skull *in vivo* in animals (i.e., rats' heart, and cats' brain) and humans (Jöbsis, 1977). During a hyperventilation experiment in healthy participants, he was able to continuously and noninvasively monitor brain oxygenation simply by

transillumination and measuring the attenuation of light in the NIR (Jöbsis, 1977) (for a detailed historical review on this topic, please refer to Bale et al.2016 and Piantadosi, 2007).

From there on, it was possible to monitor noninvasively and in real time the concentrations of different chromophores due to 1) the presence of an “optical window” in the brain (i.e., 650–900 nm NIR range), and 2) the relative specificity in the absorption spectra of each chromophore (Delpy and Cope, 1997). Soon after, several groups, including Jöbsis and his colleagues, used this technique in the clinical setting to monitor cerebral oxygenation in specific populations (i.e., sick neonates and adults) (Brazi et al., 1985; Ferrari et al., 1986; Wyatt et al., 1986), which eventually led to name this technique as “medical NIRS”. This breakthrough incited further research and development, leading by 1995 to nine companies manufacturing different systems. Early applications of medical NIRS was to monitor brain oxygenation in critical ill neonates and during cardiovascular surgery in adults (Madsen and Secher, 1999; Murkin and Arango, 2009; Green et al., 2017). As of today, there are five manufacturers of medical NIRS system in the US alone (Tosh and Patteril, 2016).

5.1.3 Technological progress

Since the first commercial continuous wave (CW) “NIRS” instrument was developed in 1989, numerous technological achievements in this field have been made (for a complete review on these developments, please refer to Ferrari and Quaresima, 2012 and Quaresima and Ferrari, 2019).

Over the years, “NIRS” systems have evolved from **single-channel** systems (Chance 1993, Villringer 1993, Hoshi 1993, and Kato 1993) to **multi-channel** topographic imaging systems (Watanabe et al., 1996; Maki and Koizumi, 1999; Miyai et al., 2001), thanks to the progress in high dynamical range and low inter-channel crosstalk systems. Today, several commercial and in-house systems allow **whole-head and high-density fNIRS** measurements (White and Culver, 2010; Eggebrecht et al., 2014). At the same time, **advances in image reconstruction** allowed the transition from topographic brain activity imaging to 3D tomographic imaging (Hoshi et al., 2016; Lee et al., 2017; Fantini et al., 2018; Zhao et al., 2021).

Another significant progress was the development of **hybrid EEG-fNIRS systems** due to the growing interest in simultaneous EEG and fNIRS acquisitions for multimodal assessment of brain function in neuroscience and clinical neurology (Obrig et al., 2014; Chiarelli et al., 2017).

Over the years, our group has developed several hybrid EEG-fNIRS systems (Chénier and Sawan, 2007; Lareau et al., 2011; Sawan et al., 2013; Kassab et al., 2018). Technological refinements in hardware size and weight, including optical fibre and optodes technology, battery-powered and wireless capability, were achieved, enabling the “integration” of each multimodal circuitry into one physical system (Safaie et al., 2013; Sawan et al., 2013; von Luhmann et al. 2015,2017; Kassab et al. 2018; Lee et al. 2019). More recently, the implementation of microchip-based technology (i.e., Complementary Metal Oxide Semiconductor - CMOS, integrated circuits and system on a chip - SoC) enabled “fusing” the circuitry of both modalities into a single microchip, further reducing the size and weight of hybrid EEG-fNIRS system (Chua et al., 2011; Ha et al., 2016) (for a detailed review of commercial and in-house development of hybrid EEG-fNIRS systems, please refer to Chapter 7). In addition to EEG, simultaneous use of functional MR (fMRI)-fNIRS (Huppert et al., 2017; Scarapicchia et al., 2017), magnetoencephalography (MEG)-fNIRS (Huppert et al., 2017), and more recently with transcranial Doppler (TCD)-fNIRS (Cho and Jang et al., 2017) and transcranial magnetic stimulation (TMS)-fNIRS (Curtin 2018, 2019; Cai et al., 2022) have also been reported.

Other active areas in fNIRS research includes **probe development** (Kassab et al., 2015), and **data analysis** (Tak et al., 2014; Yucel et al., 2016; Tachtsidis et al., 2016, Pinti et al., 2019). More recently, further hardware development and clinical integration of time-domain fNIRS were also reported (Torricelli et al., 2014; Yamada et al. 2019; Lange et al., 2018,2019; Sudakou et al., 2021; Ortega-Martinez et al., 2022). Probe development and data analysis are further discussed in Chapter 6.

5.1.4 Instrumentation type

Pulse oximetry vs. “NIRS” vs. “fNIRS”

“Pulse oximetry” and “NIRS” are often mistakenly used interchangeably. Despite a close historical and fundamental proximities, they greatly differ in **1)** the number of spectroscopic wavelengths, **2)** tissue penetration depth, and **3)** vascular compartment specificity (**Table 3, Figure 12**) (Al-Rawi, 2006; Samraj and Nicolas, 2015). Briefly, pulse oximetry uses light in the infrared and red regions to measure hemoglobin derived arterial oxygen saturation. In contrast, NIRS uses light in the near-infrared region (NIR) to measure hemoglobin-derived oxygen saturation from all microvascular compartments (arterioles, capillaries and venules).

Table 3 – Comparison between pulse oximetry and NIRS.

	Pulse oximetry	“NIRS”
# wavelength	≤ 2	≥ 2
Tissue penetration depth	Low	High
Vascular compartments discrimination	Yes (arterial compartment only)	No (all vascular compartments)

NIRS: near-infrared spectroscopy

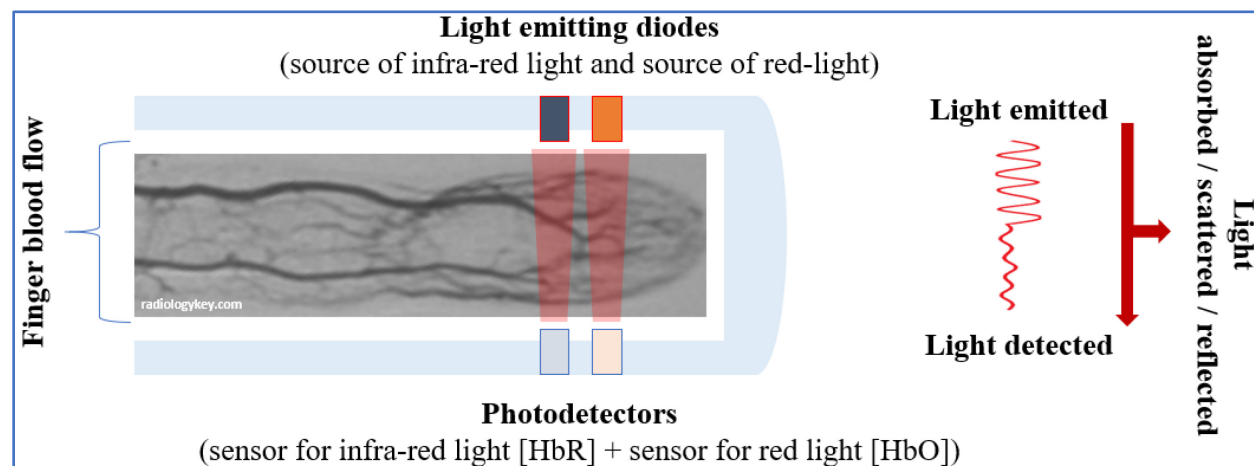


Figure 12 – Principles of pulse oximetry. [HbO]: oxyhemoglobin concentration, [HbR]: deoxyhemoglobin concentration.

Another important distinction is between “**cerebral oximetry**” and “**fNIRS**”, as both have been used in the field of neurology (including epilepsy) and critical care (**Table 4**).

As previously mentioned, “**medical NIRS**” systems are essentially cerebral oximeters. Cerebral oximeters are all CW-type instruments that essentially monitor regional tissue oxygen saturation (rSO_2 , %) which is derived from the $[HbO]/[HbT]$ ratio, and reflects the index of changes in tissue O_2 saturation relative to “rest” (or baseline). In other words, cerebral oximeters essentially measure the balance between O_2 delivery and tissue O_2 consumption. Depending on the position of the light source and detector, cerebral oximeters can measure rSO_2 by transmission (light detectors positioned contralateral to light sources – transmission mode) or reflectance (i.e., light detectors positioned ipsilateral to light sources – reflectance mode). In addition to rSO_2 , the Masimo system (e.g., Masimo O3™ Regional Oximetry System) can measure and display relative changes in $[HbO]$, $[HbR]$, and $[HbT]$ ([Shaaban-Ali et al., 2021](#); [Calderone et al., 2022](#)). Among all available commercial cerebral oximeter, the NIRO system (e.g., NIRO 300 SRS Hamamatsu Photonics) is the only cerebral oximeter that is capable to measure absolute the tissue oxygenation index (TOI) by spatially resolved spectroscopy (SRS) technique to estimate photon pathlength. TOI provides a similar measurement as blood arterial gas. More specifically, it represents the average $[HbT]$ saturation in small vessels within the photon path, accounting for changes proportional to the volume of $[HbO]$ and $[HbT]$ in a small region of tissue.

Cerebral oximetry is used both in **research** and **clinically**, where it has become a common neuromonitoring tool in pediatric ICUs ([Hoffman et al., 2017](#); [Hansen et al., 2022](#)) and, in adults, during cardiovascular and general surgery ([Green and Kunst, 2017](#); [Hansen et al., 2022](#)).

On the other hand, **fNIRS** focuses on capturing several hemodynamic parameters (e.g., $\Delta[HbO]$, $\Delta[HbR]$, $\Delta[CcO]$, rSO_2 , TOI). In addition, when multiple channels are used, it is possible to apply a complex image reconstruction algorithm to convert these hemodynamic changes into 2D and 3D images, mapping hemodynamic changes onto the brain with relatively high temporal resolution. However, due to some limitations such as its relative complexity (i.e., to operate), higher cost (i.e., fNIRS: > 40,000\$ vs. cerebral oximeter: < 20,000\$), and lack of medical accreditation (e.g., Food

and Drug Administration, Canadian Food Inspection Agency), fNIRS remains only a research modality in the field of neuroscience. Nonetheless, the unique advantages of fNIRS over cerebral oximetry have led, similarly to the early days of medical NIRS systems, to the emergence of several companies manufacturing various commercial fNIRS systems to meet the increasing demands of fNIRS users.

Table 4 – Comparison between cerebral oximetry and fNIRS.

	Cerebral oximetry	fNIRS
# channels	Low (usually < 8)	Variable (usually ~ 8-16 to >100)
Hemodynamic parameters (relative or absolute)	rSO ₂ * (mainly relative) *	Δ[HbO], Δ[HbR] Δ[HbT] or CBV Δ[HbD] or CBF Δ[CcO], rSO ₂ , TOI BFI ^{ICG} , ICG ^{fluo} , EROS (relative <i>or</i> absolute)
Light detector position (mode)	Contralateral (transmission mode) <i>or</i> Ipsilateral (reflectance mode)	Ipsilateral (reflectance mode)
Hemodynamic brain mapping	No	Yes
Research applications	+++	++++
Clinical applications (available clinical guidelines)	Yes (Yes**)	No (No)

*With the exception for the NIRO-300TM system (Hamamatsu, Japan) and O3TM Regional Oxymetry system (Masimo, USA) which allow additional measurements. **Yoshitani et al., 2019. BFI^{ICG}: blood flow index using near-infrared spectroscopy and indocyanine green, CBF: cerebral blood flow, CBV: cerebral blood volume, [CcO]: cytochrome c oxidase concentration, EROS: event-related optical signal, [HbD]: difference in hemoglobin concentration, [HbO]: oxyhemoglobin concentration, [HbR]: deoxyhemoglobin concentration, [HbT]: total hemoglobin concentration, ICG^{fluo}: indocyanine green fluorescent imaging, rSO₂: regional oxygen saturation, TOI: tissue oxygen index.

NIRS spectrophotometry devices can be divided into three main categories depending on their level of sophistication, ease of application, algorithms used and number of wavelengths employed (Ferrari et al., 2004, 2011) (**Table 5**).

Continuous-wave NIRS (CW-NIRS systems)

The first NIRS systems functioned on CW technology. CW technology measures the attenuation of light emitted at a constant intensity from an arbitrary start (i.e., rest/baseline). In other words, CW systems measure the relative change in light intensity passing through tissues. Therefore, they provide only semiquantitative changes in oxygenated and deoxygenated hemoglobin within small blood vessels. This largely explains why they are currently only suitable as trend oxygen monitors in the clinical setting (Brazy et al., 1985; Ferrari et al., 1986). However, measurements of absolute changes in [HbO] and [HbR] are also possible using CW technology when second derivative (Wray et al., 1988; Matcher et al., 1994; Delpy and Cope, 1997) and thought SRS (Valipour et al., 2002; Ali et al., 2001; Murkin et al., 2007; Owen-Reece et al., 1994,1999; Al-Rawi et al., 2005) strategies are applied. Compared to other NIRS instruments, CW systems are less expensive, have a higher temporal resolution (i.e., faster sampling rate), and are the most versatile, as they can easily be combined with other modalities (e.g., EEG), as well as miniaturized, enabling portability, wearability and deployment outside the laboratory environment. Because of all these advantages, most manufactured spectrometer systems today (i.e., cerebral oximeters and fNIRS) are CW-type instruments.

Frequency-domain NIRS (FD-NIRS systems)

Frequency-domain are also called frequency-resolved or intensity-modulated NIRS systems. FD-NIRS system emits a modulated light intensity (~100-200 MHz) and measures the attenuation, phase delay (or phase shift), and light modulation depth. Light emitters rely on laser diodes or modulated white light technologies, while light detectors usually rely on photon-counting or gain-modulated technologies (Delpy and Cope, 1997). FD technology can compute the optical properties of tissues (i.e., light scattering and absorption coefficients) from frequency and phase shifts (Duncan et al., 1996; Madsen et al., 1999) and, therefore, can measure absolute estimates for [HbO] and [HbR]. Several configurations exist (e.g., single wavelength and fixed interoptode

distance, multiple wavelengths and fixed interoptode distance, single wavelength and multiple interoptode distances) (Davies et al., 2017).

Time-domain NIRS (TD-NIRS systems)

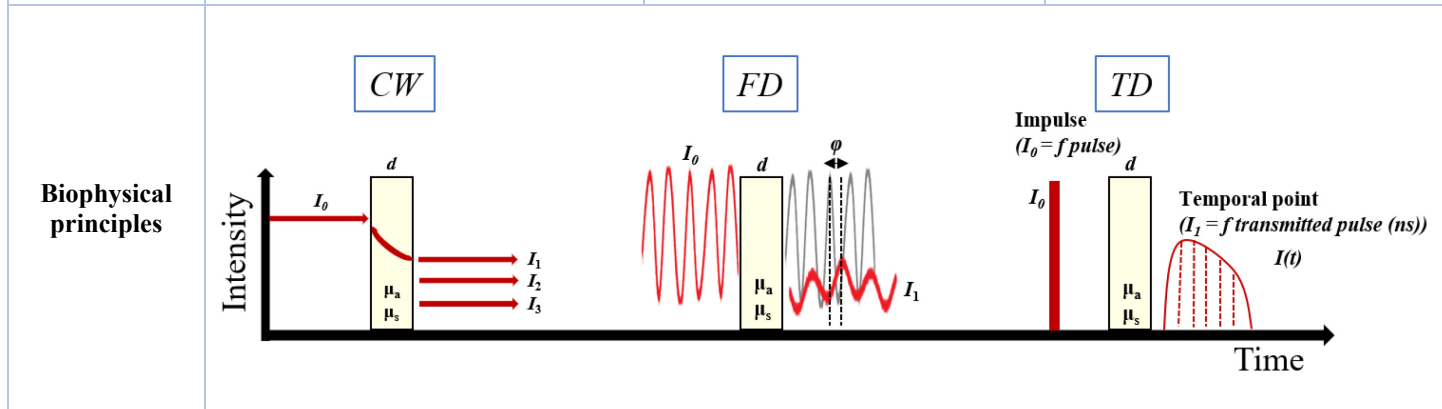
Time-domain NIRS systems are also called time-of-flight or time-resolved NIRS systems. TD-systems emit very short pulses of light (at the picoseconds time scale) through the tissue and measure the arrival times of detected photons using either a synchroscan streak camera or a time-correlated single-photon counting detector (Torricelli et al., 2014; Delpy and Cope, 1997; Wray et al., 1988). TD systems generally rely on semiconductors or solid-state lasers for light sources. Similar to FD-NIRS systems, TD technology can also distinguish between light absorption and scattering effect and estimates absolute [HbO] and [HbR] (Lange et al., 2018, 2020; Kovacsova et al., 2021). While TD technology yields the highest and most accurate amount of information, it is also the most expensive and most complex type of NIRS instrument. Few commercial TD-NIRS systems are currently available and they are not used routinely in NIRS research due to additional limitations: low sampling rate, bulky, and lack of stabilization.

Other systems

It is also possible to measure quantitative changes in CBF by combining NIRS with a light-absorbing tracer (e.g., indocyanine green, ICG) (Boushel et al., 2000). This technology relies on the Fick principle, where a ratio between tissues and arterial ICG is calculated using NIRS (i.e., photodensitometry). This method is invasive, but less invasive alternatives exist (Guennette et al., 2011). Finally, diffuse correlation spectroscopy, another noninvasive optical imaging modality close to NIRS, can also estimate CBF by measuring the intensity fluctuations in blood cells within vessels (for further information on this topic, please refer to Buckley et al., 2014).

Table 5 – fNIRS techniques comparison.

	CW	FD	TD
[HbO / HbR / HbT]	Relative	Absolute*	Absolute
rSO ₂	Yes*	Yes*	Yes
Cortical reconstruction	Yes	Yes	Yes
# channels	Variable (typically 16-1000)	Variable (typically 8-500)	Low (usually 1-30)
Sampling rate	Up to 100 Hz	Up to 50 Hz	Up to 10 Hz
Depth sensitivity	Low**	Deep**	Deep
Commercially	Yes (>15 compagnies)	Yes (1-2 compagnies)	Yes (1-2 compagnies)
Instrument size	Variable (can be portable/wearable)	Bulky (can be transportable)	Bulky (can be transportable)
Cost	Variable***	High	Very high



*requires multi-distance measurements. **depends on source-detector position. *** Low channels (low cost) vs. high-density multichannel channels systems (high cost). CW: continuous-wave, d : thickness of the medium, FD: frequency-domain, [HbO]: oxyhemoglobin concentration, [HbR]: deoxyhemoglobin concentration, [HbT]: total hemoglobin concentration, I_0 : incident light signal, I_x : transmitted light signal at different distance “x”, $I(t)$: temporal point spread function of the transmitted light signal, rSO₂: regional cerebral oxygen saturation, TD: time-domain, μ_a : absorption coefficient, μ_s : scattering coefficient, ϕ : phase delay. Yellow vertical rectangle: biological tissue.

5.1.5 Physical principles and principle of diffuse optical tomography

Theoretical basis

It is essential to understand how light, at a given wavelength, interacts with biological tissues (e.g., the brain) as it forms the underlying physical principles of all CW-NIRS measurements. These principles are described below and summarized in **Figure 13** (for all equations, wavelength dependence was ignored for clarity purposes).

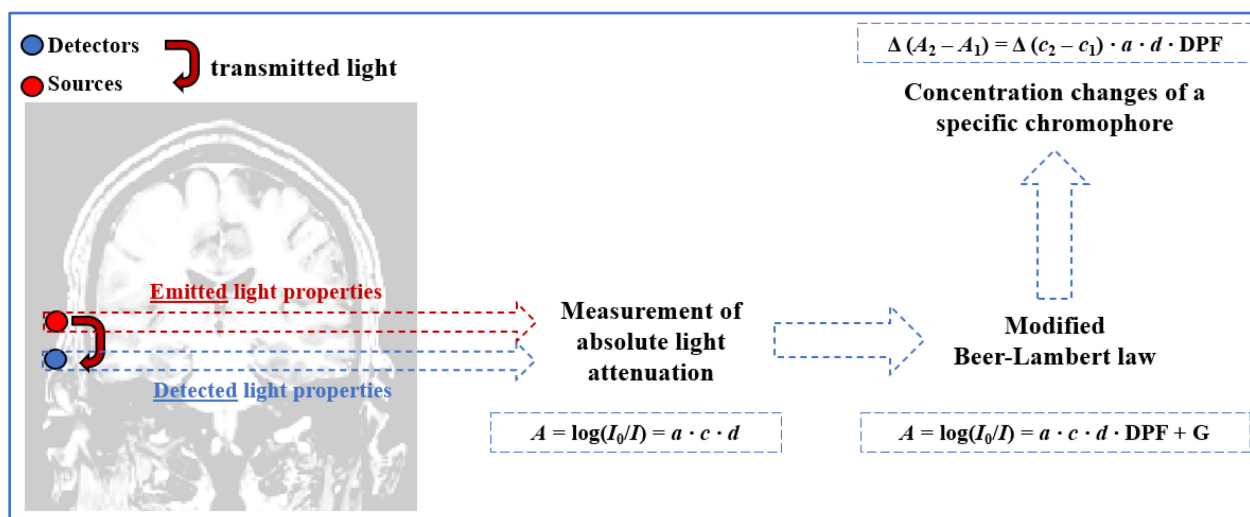


Figure 13 – Theoretical principles of fNIRS measurements. A : light intensity or optical density attenuation, a : extinction or absorption coefficient of a specific compound, c : concentration of the absorbing compound, d : optical pathlength, DPF: differential pathlength factor, G : additional factors responsible for light attenuation, I_0 : incident light intensity, I : transmitted light intensity, Δ : relative changes/differences.

In a clear, non-scattering or purely absorbing medium, attenuation of light intensity is determined by the optical path length (i.e., the average distance travelled by the beam of light through the medium), the concentration of chromophores (which is usually assumed homogeneous in the medium), and the absorption coefficient (i.e., “absorption potential”) of chromophores. This relationship between “light absorption” and “chromophore concentration” is a simple exponential relationship stated by the Beer-Lambert law (BLL) (**Equation 1**) (Boas et al., 2001; Kocsis et al., 2006).

Equation 1:
$$A = \log(I_0/I) = a \cdot c \cdot d$$

Where A is the attenuation of light intensity or optical density (OD); I_0 is the incident light intensity; I is transmitted light intensity; a is the specific extinction or absorption coefficient of the compound ($\mu\text{mol}^{-1} \text{cm}^{-1}$); c is the concentration of the absorbing compound, and d is the optical pathlength (i.e., the distance travelled by the light beam in tissue) (cm).

Biological tissues usually contain several chromophores, which contribute to OD total attenuation. In the brain, these chromophores are water, lipids, melanin, myoglobin, HbO, HbR, and cytochrome c oxidase (CcO). The absorption contribution of each chromophore can be linearly summed to calculate the total attenuation of OD in the tissue (**Equation 2**).

Equation 2:
$$[a_1c_1 + a_2c_2 + a_3c_3 + \dots a_nc_n] \cdot d$$

As we mentioned earlier, these principles can be applied to non-scattering mediums (i.e., non-biological tissue). However, the **brain** is a **high scattering** biological tissue. Indeed, approximately 80% of the total light attenuation in the brain is due to scattering (compared to only 20% due to absorption). The scattering effect of the brain is greatly responsible for increasing the distance travelled by photons and consequently increase the absorption of light in the tissue.

Hence, in the brain, attenuation of light is not purely due to absorption but a mixture of absorption, scattering, and reflection. Moreover, additional factors, such as the angle at which the beam of light is emitted, brain structure/geometry, and the selected wavelength, can also influence OD pathlength trajectory and attenuation. To account for the scattering properties of the brain and the loss due to other factors responsible for light attenuation, we must modify the Beer-Lambert law (mBLL) by adding two additional variables: 1) a differential pathlength factor (DPF) and 2) a G factor (**Equation 3**).

Equation 3:
$$A = \log(I_0/I) = a \cdot c \cdot d \cdot \text{DPF} + G$$

The differential path-length factor may be calculated using FD- and TD-NIRS technology ([Delpy et al., 1988](#)). Over the years, several studies have measured the differential path-length factor

taking into consideration the type of biological tissue (i.e., muscle vs. brain), age (i.e., children vs. adults), wavelength specificity (Scholkmann and Wolf, 2013) and the geometrical head shape (Zhao et al., 2005; Strangman et al., 2013). The differential path-length factor measurements are publicly available and used by CW-type instruments. However, it is essential to accurately select a DPF (or directly estimate it when possible), as a wrong value can strongly affect the quantitative accuracy of fNIRS measurements and give rise to crosstalk errors between $\Delta[\text{HbO}]$ and $\Delta[\text{HbR}]$ measurements.

Another variable is the partial volume factor which is often added to the modify the Beer-Lambert law to consider the partial volume effect commonly encountered in various neuroimaging techniques. In fNIRS, the partial volume effect is caused by the non-uniform distribution of hemoglobin changes along the illuminated tissue, which are spatially more sensitive in the cortical region of the brain, as well as the areas involved in the hemodynamic response to given stimuli. Like the differential path-length factor, the partial volume effect can have severe implications in estimating hemoglobin concentration changes (Boas et al., 2001; Strangman et al., 2003). While it is possible to add a partial volume factor to adjust for the effective pathlength of light through the region where absorption changes occur, the partial volume effect remains an important issue in fNIRS, limiting comparisons between studies and, consequently, the clinical validity of fNIRS measurements when compared with other functional neuroimaging techniques (e.g., fMRI).

It is essential to highlight that the BLL and mBLL only reflect changes occurring in small blood vessels (i.e., arterioles, capillaries, venules) since minimal light absorption and multiple complete passages of photons occur in those vessels, as opposed to large vessels (e.g., arteries and veins), where the molar quantity of blood is too high resulting in near-total light absorption (i.e., light is completely absorbed).

Assuming that all the chromophores in the brain have the same G factor and that I_0 , d , and DPF all remain constant (i.e., are time-invariant, which is generally true when small physiological changes occur), we can eliminate the unknown variable from the modify the Beer-Lambert law and calculate the relative changes in chromophore concentration by subtracting the continuous changes

in OD (at a specific wavelength or for a specific chromophore) at two different time points (i.e., baseline state vs. non-baseline state) (**Equation 4**).

Equation 4:

$$\Delta (A_2 - A_1) = \Delta (c_2 - c_1) \cdot a \cdot d \cdot DPF$$

As depicted in **Figure 14**, the brain has an optical window in the NIR region (650-900 nm) where photons can penetrate the different layers of head tissues to reach the cerebral cortex.

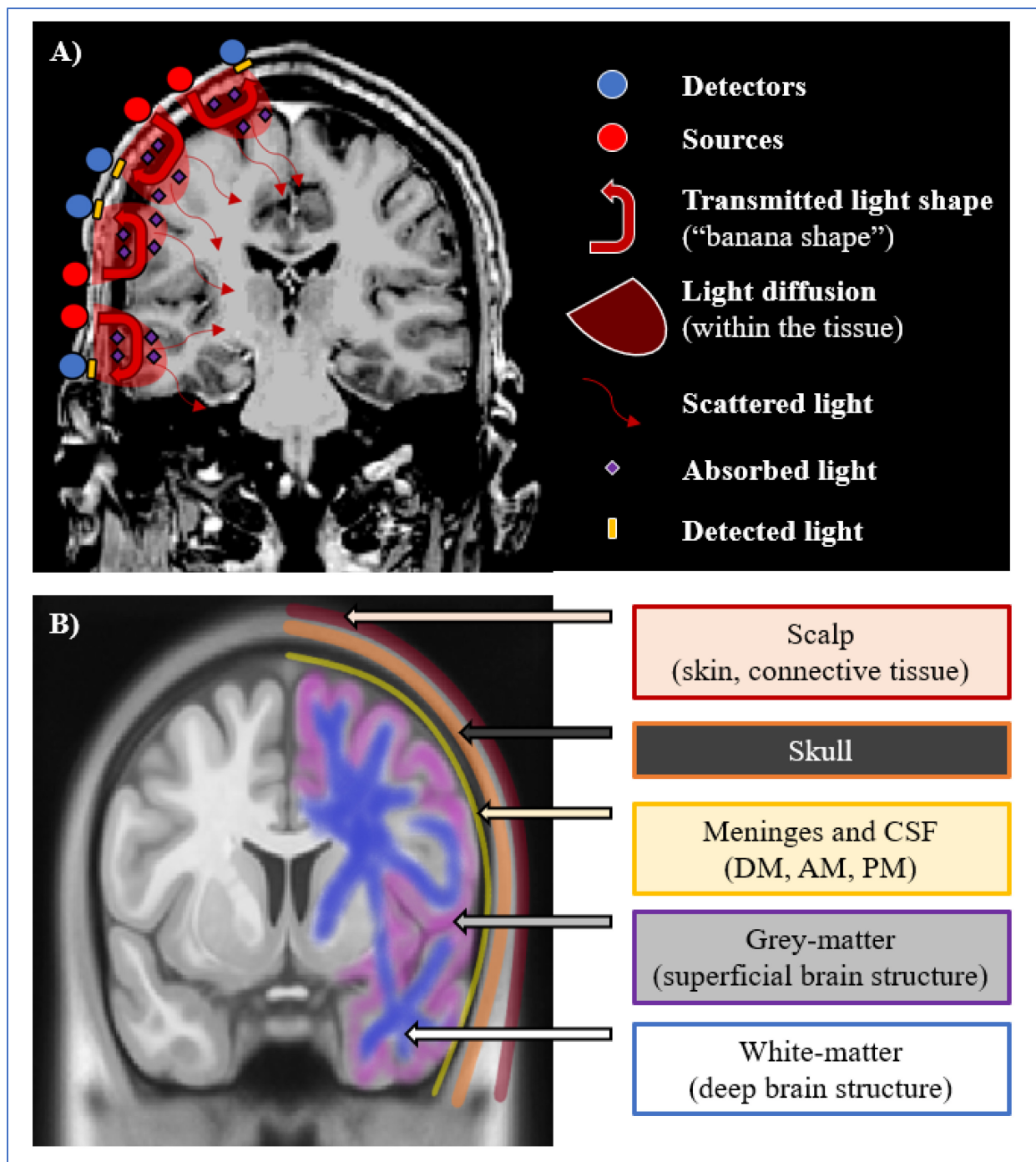


Figure 14 – Schematic arrangement of light sources and light detectors. A) light absorption, scattering, and diffusion (visualized on a patient MRI). B) different layers of the human head (visualized on the Colin27 template). AM: arachnoid mater, CSF: cerebrospinal fluid, DM: dura mater, FPL: fronto-parietal lobe, PM: pia matter, TL: temporal lobe.

Within the optical window, the most significant absorbers are water, lipids, melanin found in integuments, myoglobin mainly found in the frontalis and temporalis muscles, HbO, HbR, and CcO. Regarding fNIRS, chromophores of interest are HbO, HbR, and CcO, as the other chromophore normally do not vary between different brain states. HbO, HbR, and CcO have a spectrum range of absorption, which allows us to distinguish them, and, consequently, measure each ΔOD (or concentration Δ) by using at least two wavelengths (within a specific spectrum range) for HbO and HbR, and at least three for CcO.

Ideally, when measuring $\Delta[HbO]$ and $\Delta[HbR]$, one wavelength should be ~ 830 nm while the other < 760 nm, as several studies have shown that this combination reduces the influence of measurement noise drastically (Uludag et al., 2004; Sato et al., 2004). As for $\Delta[CcO]$, > 3 wavelengths are generally needed (i.e., broadband NIRS systems) due to their low concentration in tissue (Uludag et al., 2004). Additional wavelengths can also be considered in order to provide more robust estimates of $\Delta[HbO]$, $\Delta[HbR]$, and $\Delta[CcO]$ (Arifler et al., 2015).

Once $\Delta[HbO]$ and $\Delta[HbR]$ are measured, it is possible to calculate $\Delta[HbT]$ and $\Delta[HbD]$ by, respectively, adding $\Delta[HbR]$ or subtracting $\Delta[HbR]$ from $\Delta[HbO]$. Assuming that the hematocrit in small vessels remains constant, $\Delta[HbT]$ is directly proportional to ΔCBV (Wyatt et al., 1985,1990). As for $\Delta[HbD]$, it represents a biomarker of cerebral oxygen delivery (Mitra et al., 2016, 2020), although few studies have shown that it was correlated with CBF, assuming oxygen consumption does not change (Tsuji et al., 1998; Soul et al., 2000). However, its pure sensitivity to CBF remains debated and, therefore, less often reported than $\Delta[HbT]$ in fNIRS studies (Pham et al., 2019).

Image reconstruction: Diffuse Optical Tomography (DOT)

Measurements from multichannel fNIRS can yield meaningful spatial information (5-10 mm) and allow mapping of changes in optical properties or, by proxy, changes in hemoglobin concentration. The process of image reconstruction can be divided into three steps which are detailed below (Figure 15) (for an in-depth detailed mathematical description of each step, please refer to Deghani et al., 2009).

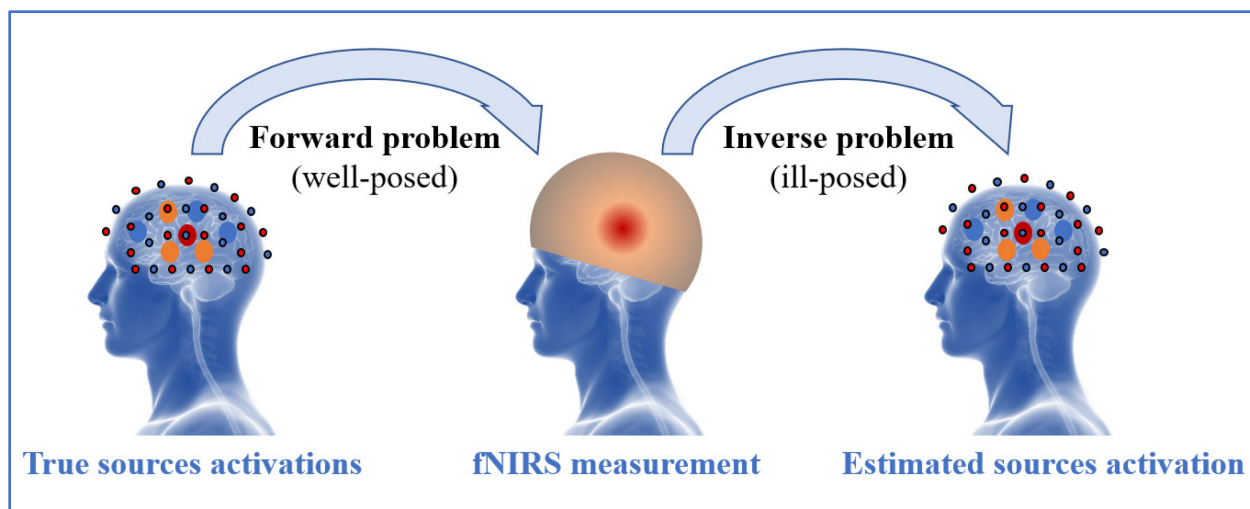


Figure 15 – Functional near-infrared spectroscopy (fNIRS) forward and inverse problems. In the forward problem, a well-posed model maps the true sources activation to the fNIRS measurement vector. In the inverse (and ill-posed) problem, an inverse operator maps the measurement vector to the estimated sources activation.

1st step – solving the forward problem

The first step requires modelling light propagation throughout the different head structures (i.e., solving the "well-posed" forward problem) (Arridge, 1999). This can be performed by 1) calculating the photon density at every point in a 3D volume or 2) simulating the photon trajectory within the tissue (Boas et al., 2002). While the first method (i.e., calculating the photon density at every point in a 3D volume) is computationally expensive, two alternative strategies can be used.

The first strategy utilizes a diffusion equation (or diffusion approximation) and solves the equation by exploiting the Green's method (Culver et al., 2003), the finite element method (FEM) (Arridge et al., 1993), or the boundary element method (Elisee et al., 2011).

The second strategy uses advanced statistical methods to solve the forward model. The Monte Carlo method (**Figure 16**) is a widely used approach for simulating photons trajectories (Fang et al., 2010).

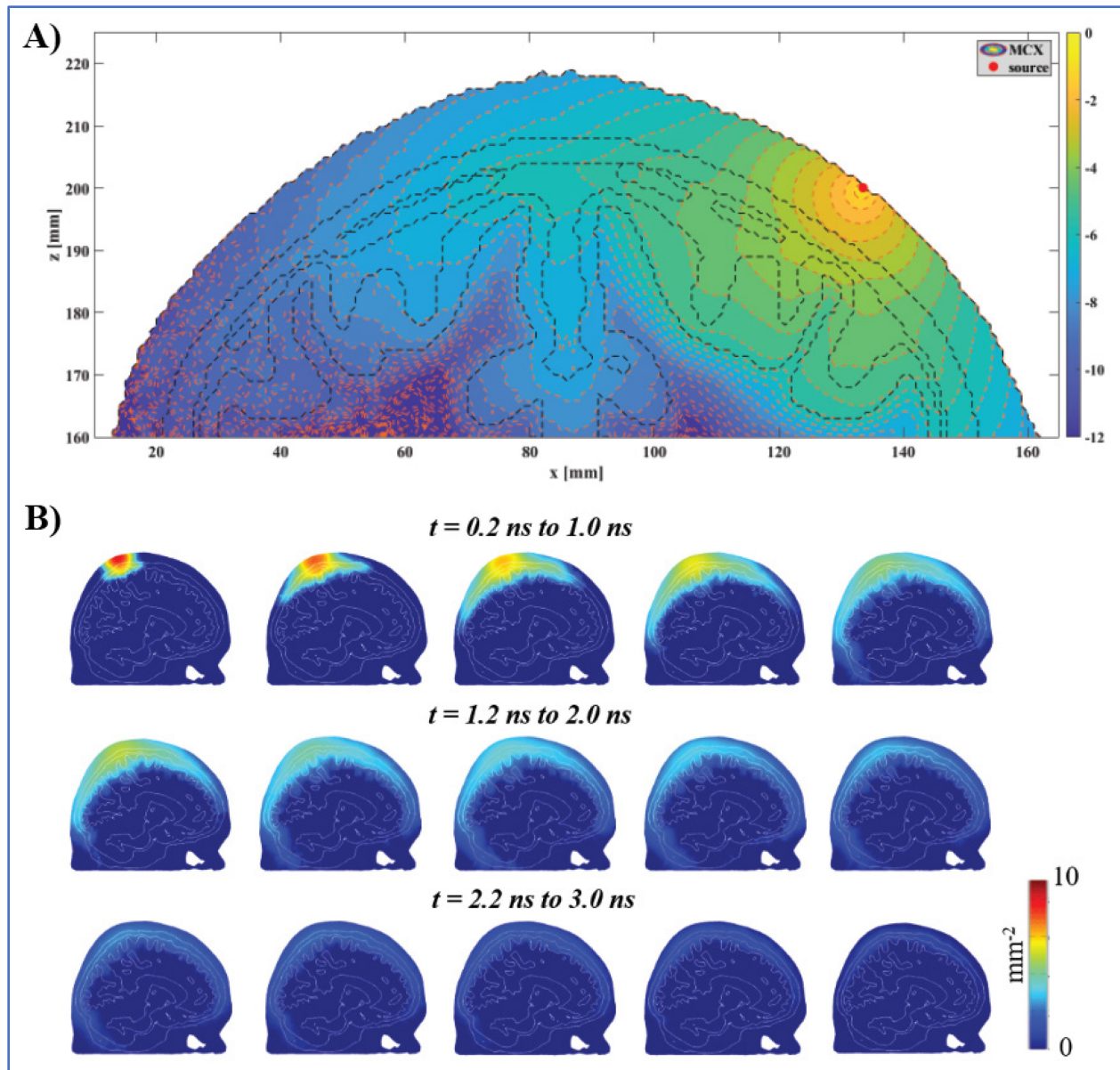


Figure 16 – Monte Carlo photon propagation simulation (*Estimated in MATLAB using MCXLAB – Fang and Boas, 2009*). A) Light transport in a in a full-head atlas template (USCBrain Atlas), B) Time-resolved simulation (Colin 27 Average Brain).

In terms of photon trajectory modelling, it is considered the gold standard as it is not dependent on the assumption of light diffusivity and therefore tends to be more accurate than other methods (Fang and Boas, 2009; Fang et al., 2010). However, this statistical approach is computationally demanding (Fang and Boas, 2009; Fang et al., 2010).

An important prerequisite for solving the forward model requires accurate modelling of the object (under investigation) (Gibson et al., 2005; Brigadoi et al., 2015). Concerning the human head, two approaches are commonly employed (i.e., generic homogenous model vs. specific heterogeneous head model). The latter (i.e., head model based on the subject-specific structural image) is considered, at the current moment, the most accurate method in fNIRS image reconstruction. While attributing a specific attenuation or scattering baseline value for each tissue remains an issue, several softwares can segment the structural anatomy into accurate subject-specific and multi-layered head meshes. Additionally, photogrammetric, electromagnetic, and 3D digitization techniques can accurately determine sensors and detectors' location on the scalp.

Using these light propagation modelling methods, several studies demonstrated a “banana-shaped” flux density profile (i.e., absorption change over the volume) with a maximal value near sources and detectors, as well as toward the superficial layers of the head (Gibson et al., 2005; Brigadoi et al., 2015). The distance between sources and detectors affects the cortical sensitivity of fNIRS measurements. In adults, sources and detectors are typically spaced 3-4cm.

2nd step – calculating the sensitivity matrices

The sensitivity matrix defines how the optical intensity for each channel will be affected by a change in chromophore concentration at a specific location. The sensitivity matrix can be estimated by combining several methods (i.e., the Monte Carlo method and linearization methods such as the Rytov approximation) (Boas et al., 2004; Madsen, 2000; Gibson et al., 2005; Brigadoi et al., 2015). Sensitivity matrices are not uniform but vary substantially around the head, with the occipital pole and central regions exhibiting the highest sensitivity (Strangman et al., 2013,2014). Sensor placement can also influence sensitivity matrices. Additionally, anatomical factors such as skull and cerebrospinal fluid (CSF) thickness, distortion caused by the arachnoid trabeculae, and the presence of large extracerebral blood vessels can all affect sensitivity measurement.

3rd step – solving the inverse problem

Compared to the forward problem, the inverse problem is ill-posed for two main reasons. First, there are significantly more unknowns than there are measurements. Secondly, the errors in the reconstructed image are disproportionately sensitive to small changes in the data, systemic errors

caused by motion (for example), surface effects such as sweating, and skin hemodynamics. Therefore, inverting the sensitivity matrix perfectly to obtain our image is nearly impossible. A standard method to solve the inverse problem is regularization, such as the Markov random field method (Doerschuk et al., 1994), the most common form of regularization used in medical imaging, or by Tikhonov (Nguyen et al., 2001). Since the scale of the reconstructed image is strongly influenced by regularization methods, careful and consistent selection of the regularization parameters is essential to obtain accurate and comparable reconstructions. Selection of the regularization parameters can be done subjectively or objectively (e.g., discrepancy principle, L-curve approach) (Correia et al., 2009). Due to the limited depth sensitivity of near-infrared light, image reconstruction with fNIRS is limited to the superficial structures of the brain (i.e., cortices), although the use of non-linear methods can significantly improve spatial resolution (Cai et al., 2021, 2022). Finally, it is essential to mention that spatial overlap between measurements is crucial to promote accurate DOT and overcome simple cortical image projection.

5.2 Brief overview on the current applications of fNIRS in neuroscience

Ever since the early application of NIRS in the '90s, the use of fNIRS in neuroscience has been on an exponential rise (Chen et al., 2020). Even more fascinating is the pace at which various subfields in neuroscience have adopted this functional neuroimaging technique, which can be attributed to the numerous advantages offered by fNIRS compared to more common functional neuroimaging (fMRI, PET, SPECT) and electrophysiological (MEG, EEG) techniques (**Table 6**).

In neuroscience today, fNIRS is used in several fields of applications (including psychology/linguistics (e.g., cognition, neurodevelopment, emotion), economics (i.e., neuroeconomics), neuroergonomics, basic research (e.g., brain–computer interface, walking, driving, hyperscanning) and medicine (e.g., neurology, psychiatry) *(for a recent and detailed review on the current application in each field mentioned above, please refer to Quaresima and Ferrari, 2019)*

While fNIRS remains a research modality in neuroscience, progress in real-time analysis, spatial resolution (e.g., high-density montages, 3D optodes digitization, anatomical co-

registration), neurovascular sensitivity/specificity (i.e., short-channel, multi-dimensional signal), and integration with other modalities will undoubtedly increase its use as a wide-spread clinical tool similar to its older cousin (i.e., cerebral oximetry) ([Quaresima and Ferrari, 2019](#); [Chen et al., 2020](#)).

Table 6 – Comparison of fNIRS with other functional neuroimaging modalities.

	fNIRS	fMRI	PET/SPECT	MEG	EEG
Signal measured	[HbO], [HbR] *	[HbR] / BOLD	CMR _{glu} , CBF	Electrophysiology	Electrophysiology
Penetration depth (brain structure)	Low (superficial)	High (whole brain measurement)	High (whole brain measurement)	High (whole brain measurement)	Close to MEG (superficial)
Spatial resolution	High (2-3 cm)	Very high (1-2 mm)	Very high (4 mm)	Very high (2-6 mm)	Low (7-10 cm)
Temporal resolution	High (up to 10 Hz)	Low (1-3 Hz)	Very low (0.1 Hz)	Very high (> 1000 Hz)	Very high (> 1000 Hz)
Robustness to motion	Yes (very good)	No (very poor)	No (very poor)	No (very poor)	No (better than MEG)
Potential for naturalistic recording	Very high (almost any settings)	No (specialized environment)	No (specialized environment)	No (specialized environment)	Very high (almost any settings)
Potential in various populations and groups	Very high (almost anyone) No contraindication	Limited (challenging in children, and in any individual with special needs, e.g., claustrophobic, intellectual disability) Several contraindications (e.g., metallic implants)	Limited (challenging in children, and in any individual with special needs, e.g., claustrophobic, intellectual disability) Several contraindications (e.g., contrast allergy)	Limited (challenging in children, and in any individual with special needs, e.g., claustrophobic, intellectual disability) Several contraindications (e.g., metallic implants)	Very high for EEG (almost anyone) No contraindication
Potential for portability/wearability	Very high	None	None	None	Very high
Potential for simultaneous multimodal recording (require compatible device)	Yes ** EEG/fMRI/TCD/TMS (no)	Limited mainly EEG (yes)	Limited mainly EEG (yes)	Limited mainly EEG (yes)	Yes ** EEG/fMRI/TCD/TMS (no)
Systemic physiological contamination	Yes	Yes	Yes	No	No
Comfortability	Very high	Low (physical constraints/supine position, noisy environment)	Low (physical constraints/supine position, semi-invasive)	Low (physical constraints/sitting downs, noisy environment)	Very high
Cost	10K-100K	> 2M	> 2M	> 2M	10K-100K

CBF: cerebral blood flow, CMR_{glu}: cerebral metabolic rate of glucose, EEG: electroencephalography, fMRI: functional magnetic resonance imaging, fNIRS: functional near-infrared spectroscopy, [HbO]: oxyhemoglobin concentration, [HbR]: deoxyhemoglobin concentration, K: one thousand dollars, M: one million dollars, MEG: magnetoencephalography, PET: positron emission tomography, TCD: transcranial Doppler, TMS: transcranial magnetic stimulation, SPECT: single-photon emission computerized tomography

5.3 Applications in non-critical care seizures and epilepsy

EEG-“NIRS” has slowly but increasingly been used to assess the neurovascular coupling associated with seizures in patients with epilepsy (a visualization of the typical hemodynamic response measured in fNIRS is depicted in **Figure 17**). Indeed, with the notable exception of EEG, fNIRS is the only other modality that is suited for long-term recording ([Peng et al., 2016](#)).

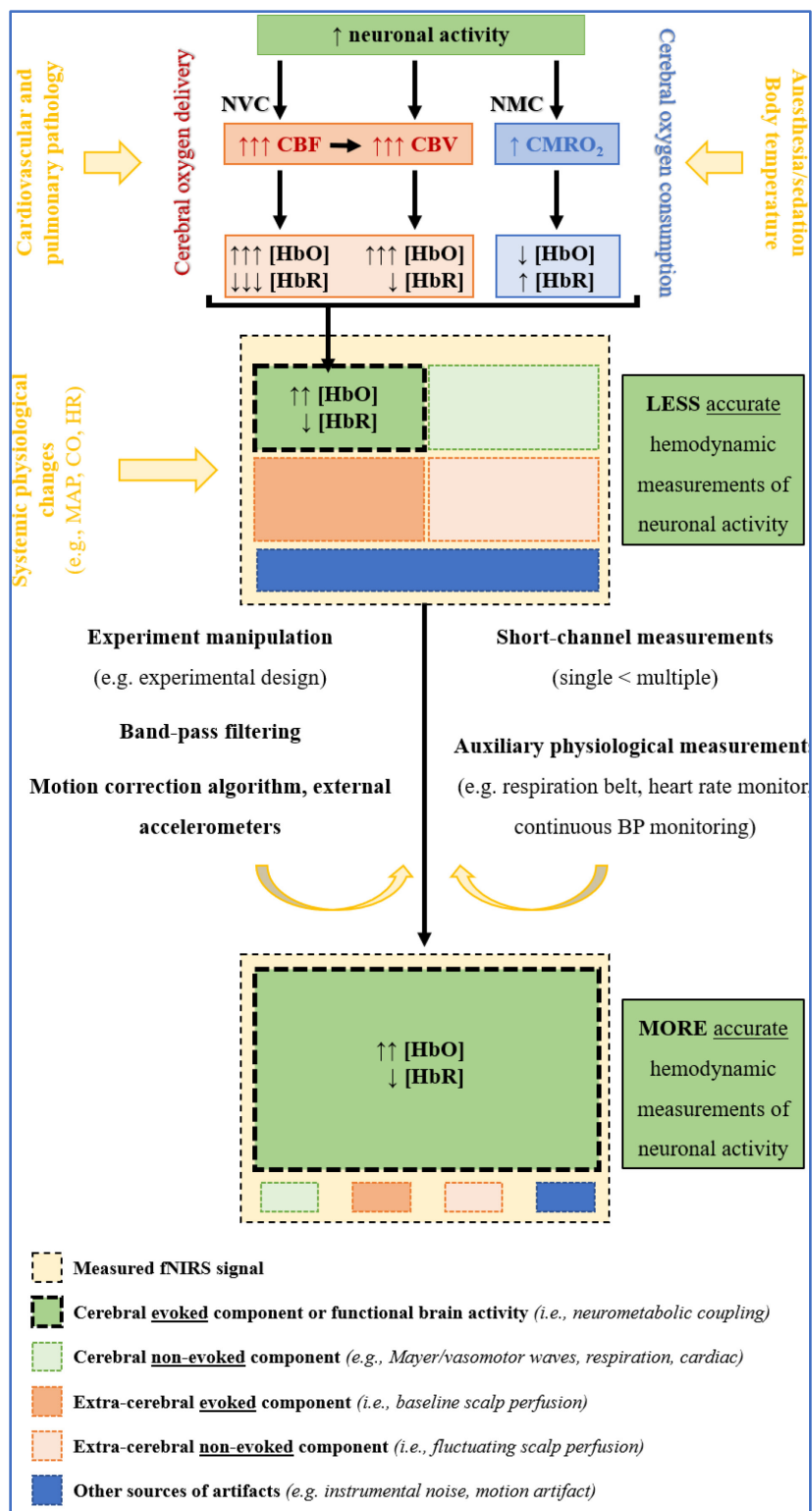


Figure 17 – Signals contributing to the measured fNIRS signal during increased neuronal activity (e.g., seizure). CBF: cerebral blood flow, CBV: cerebral blood volume, CMRO₂: cerebral metabolic rate of oxygen, CO: carbon monoxide, [HbO]: oxyhemoglobin concentration, [HbR]: deoxyhemoglobin concentration, HR: heart rate, MABP: mean arterial blood pressure.

In the early 90s, Arno Villringer, one of the first pioneers in the applications of medical NIRS, assessed for the first time the utility of combined EEG and cerebral oximetry to investigate the brain hemodynamics and oxygenation during spontaneous epileptic seizures in three patients with focal epilepsy (with presumably extratemporal epilepsy). In his study, he observed, in two patients, a significant increase in [HbO] and CBV during complex partial seizures with mixed distribution (ipsilaterally only in the first, bilaterally in the second). However, in the third patient, he observed a large drop in [CcO] without significant changes in [HbO] and [HbR] (Villringer et al., 1993). However, opposing results were observed three years later in a study by Steinhoff and his colleagues. The authors investigated brain oxygenation changes over the frontal areas in two patients with intractable epilepsy of mesial temporal origin. They observed an ipsilateral desaturation (i.e., a decrease in rSO₂) during the seizures reaching a peak during the postictal phase (Steinhoff et al., 1996). Later, it was revealed that the increase or decrease in brain oxygenation might have been related to the type of seizures (Sokol et al., 2000). Indeed, assessing the utility of EEG-“NIRS” in distinguishing between different types of seizures, Sokol and his colleagues observed a frontal increase in brain oxygenation in patients with complex partial seizures, while secondarily generalized complex partial seizures were associated with frontal lobe deoxygenation (Sokol et al., 2000).

Similar to the observations made by Sokol et al. (2000), generalized epileptic activity induced by electroconvulsive therapy resulted in a significant pattern of deoxygenation (\downarrow [HbO], \downarrow [HbT], \uparrow [HbR], \downarrow [CcO]) in 90 patients with drug-resistant depression (Saito et al., 1995). Similar observations were also reported in three adults with absence seizures (i.e., deoxygenation during seizures) (Buchheim et al., 2004), while a frontal hyperoxygenation was observed during generalized spike-and-wave discharges in six children with absence epilepsy (hyperoxygenation in the preictal phase, deoxygenation just prior seizure onset, hyperoxygenation during seizure) (Roche-Labarbe et al., 2008). However, the deoxygenation reported by only few studies was often associated (even possibly caused by) with important systemic deoxygenation, often associated with generalized tonico-clonic seizures (Saito et al., 1995; Sokol et al., 2000), stressing the importance of controlling the impact of systemic factors when interpreting brain hemodynamics.

Similarly, different changes in brain hemodynamics associated with different seizure types were observed in a study performed on children with various types of epilepsy (Haginoya et al., 2002).

Early studies laid down the potential fundamental value of fNIRS in investigating the neurovascular coupling during various seizures. However, these studies generally relied on a small number of patients, single or low number of channels and coverage was generally limited to hairless regions (e.g., forehead).

Therefore, later studies decided to apply multichannel and image projection EEG-fNIRS. This not only allowed to investigate hemodynamic changes associated with seizures and IEDs over a large portion of the head but also assess the clinical potential for fNIRS as a seizure focus lateralization/localization technique during presurgical planning of patients with drug-resistant epilepsy.

Watanabe and his colleagues were the first to measure hemodynamic changes bilaterally over a larger region by using multichannel (i.e., 8 and 24 channels) fNIRS system in patients with drug-resistant epilepsy (Watanabe et al., 2000; Watanabe et al., 2002). After inducing the seizures (with bemegride injection), they observed in all patients (n=12) a rapid increase in regional CBV at seizure onset, which lasted ~ 1 min (Watanabe et al., 2000). Similar observations (i.e., significant hyperperfusion) associated with unprovoked seizures were also observed in a later study in 29 patients (out of 32) with pharmacologically intractable epilepsy (Watanabe et al., 2002). More interestingly was the ability of multichannel fNIRS to facilitate the identification of seizure focus by the observation of a localized increase in hemodynamics (increases in [HbO] and [HbR], increase in CBV) in some channels only (Watanabe et al., 2000), and the higher sensitivity (i.e., 96%) of focus lateralization compared to other functional neuroimaging methods, such as SPECT (Watanabe et al., 2002).

Later in a series of studies, our group has also applied multichannel (> 100 channels) whole-head vEEG-fNIRS monitoring and reconstructed 2-dimensional (2D) topography in a large number of patients suffering from nonlesional temporal (n=9) (Nguyen et al., 2012), frontal (n=18) (Nguyen et al., 2013), and occipital (n=9) lobe epilepsy (Pouliot et al., 2014) whose focus was defined by

separate intracranial EEG recordings. Temporal lobe seizures were associated with an increase in [HbO], CBV and triphasic changes in [HbR] (initial decrease followed by an increase, and then prolonged decrease). Spatially, these hemodynamic changes were bilateral, and heterogeneous hemodynamic changes also occurred in frontal and/or parietal areas. Frontal lobe seizures were associated increase in [HbO], CBV and a less consistent decrease in [HbR] (i.e., usually decreased, but sometimes unchanged or increased). While these hemodynamic changes occurred locally (i.e., over the seizure focus), a spread of activation to homologous areas in the contralateral hemisphere was also noted. Similar observations were also observed for posterior seizures showing relatively good sensitivity (i.e., ~78%) in localizing the epileptic focus. More recently, EEG-fNIRS have also been used to investigate blood volume and neurovascular coupling in infantile spasms (Bourel-Ponchel et al., 2017).

Our group and others have also investigated the hemodynamic response to IEDs (Machado et al., 2011; Pouliot et al., 2014; Peng et al., 2014; Peng et al., 2016; Pelligrino et al., 2016). Using more sophisticated analysis (i.e., canonical GLM based approach) to improve the detection of hemodynamic changes associated with epileptic activity using fNIRS, early studies observed a focal significant increase in [HbO] and decrease in [HbR] associated with IED concordant with the seizure focus in one child with frontal epilepsy (Machado et al., 2011) and three adults with occipital epilepsy (Pouliot et al., 2014). Later the same methodology was applied to a larger cohort of adults (n=18) with neocortical epilepsies (Peng et al., 2014). However, in the latter study, significant changes in hemoglobin concentration change were not observed in 11 patients and only showed changes in the epileptic focus in 28% (for \uparrow [HbO]) and 21% (for \downarrow [HbR]). The limited sensitivity and specificity to localize the epileptic focus during fNIRS presurgical evaluation of IEDs have brought several studies to reconsider the non-specific modelling hemodynamic response function (HRF) of IEDs to a more patient-specific approach (Peng et al., 2016; Pelligrino et al., 2016) which have shown an increase in the number of hemodynamic response detected by fNIRS during IEDs (compared to other methods, e.g., EEG-fMRI), as well as in the sensitivity and specificity in focus localization based on the hemodynamic response of IEDs (Peng et al., 2016; Pelligrino et al., 2016).

EEG-fNIRS has also been widely used during presurgical evaluation to map higher brain functions, such as areas involved in language production (Watanabe et al., 1998; Watson et al., 2004; Gallagher et al., 2007; Gallagher et al., 2008a, b, Gallagher et al., 2012) and comprehension (Gallagher et al., 2007; Gallagher et al., 2008, Gallagher et al., 2012). Additionally, fNIRS has been used for other purposes such as the study of functional connectivity (Sato et al., 2012; Sirpal et al., 2019), in the context of rehabilitation (Honda et al., 2009; Visani et al., 2014), and, more recently, for seizure detection (Sirpal et al., 2019) and prediction (Sirpal et al., 2021). Methodological improvements have also been achieved, particularly with the use of collodion to reduce motion artifacts during seizures and recover the hemodynamic response (Yücel et al., 2014), data-based filtering techniques in the analysis of prolonged fNIRS data (Vinette et al., 2015), the development of an algorithm for automatic generation of an optimal montage to maximize the spatial sensitivity over a specific epileptic focus region (Machado et al., 2014, 2018) and more recently the use of deconvolution based approach on DOT for accurately estimating the hemodynamic response during abnormal epileptic activity (Machado et al., 2021).

In summary, ~ 50 studies conducted over the past three decades have demonstrated the clinical potential of “EEG-NIRS” as a multimodal functional neuroimaging technique to investigate seizures in the non-critically ill patients (i.e., patients with epilepsy). These studies have shown how complex the hemodynamic changes can be during epileptic events (i.e., IEDs, seizures) and highlighted limitations encountered during focus localization.

Unfortunately, several important drawbacks have limited its widespread application, especially in the clinical setting. These limitations are summarized in **Figure 18** and further discussed in the following sections, as some are shared by the use of fNIRS in critical care seizures.

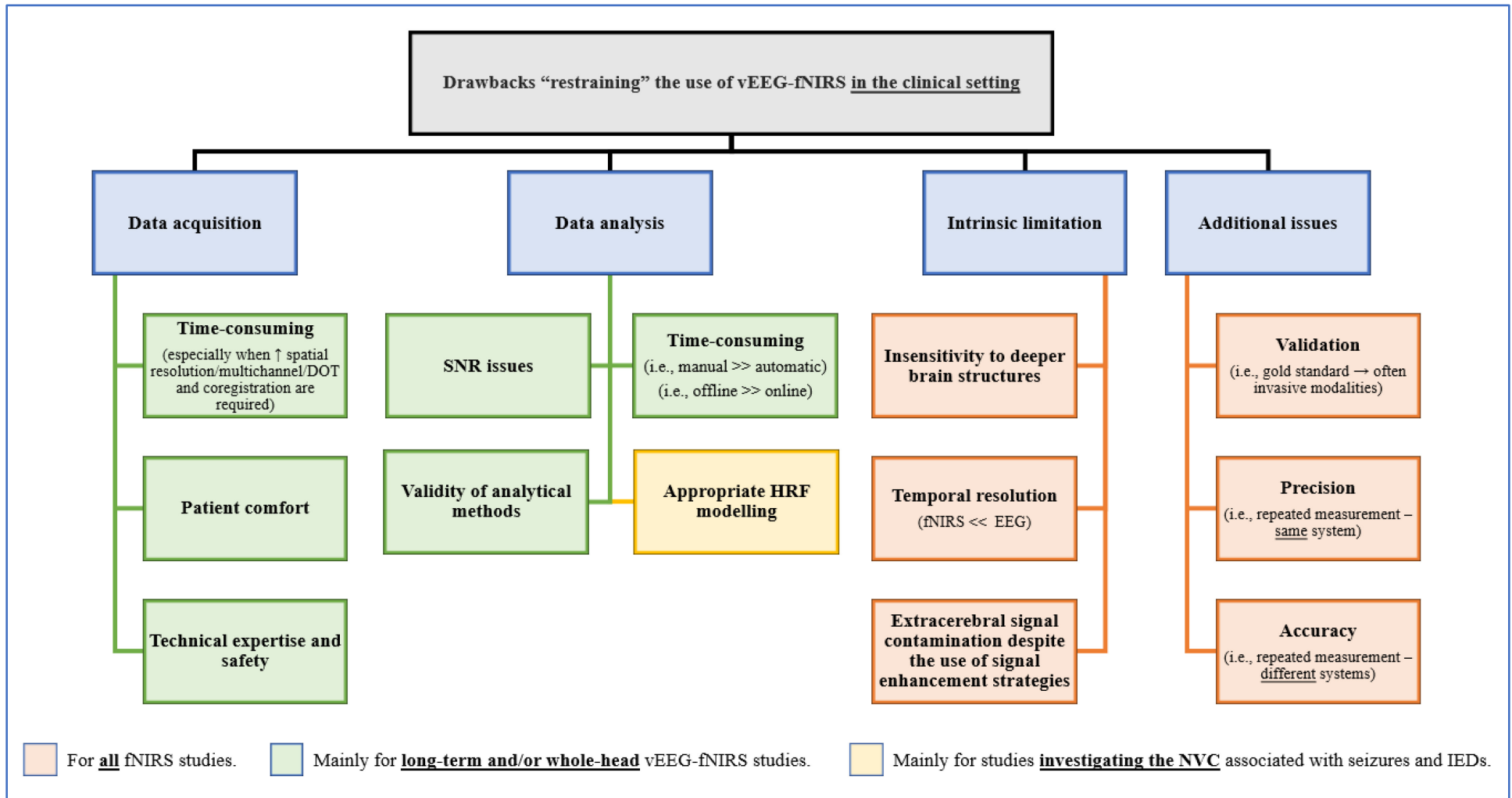


Figure 18 – Main drawbacks of vEEG-fNIRS in clinical neurology. DOT: diffuse optical tomography, fNIRS: functional near-infrared spectroscopy, IEDs: interictal epileptiform discharges, NVC: neurovascular coupling, vEEG-fNIRS: simultaneous video-electroencephalography and functional near-infrared spectroscopy acquisition, ↑: increase.

5.4 Investigating seizures, periodic discharges, and burst-suppression in the critically ill with fNIRS: a critical review

Functional neuroimaging techniques such as SPECT, PET and fMRI are not frequently performed in critically ill patients due to technical, logistic or ethical reasons. Therefore, over the years, few groups have employed “NIRS”-based neuroimaging to investigate hemodynamic changes associated with critical care seizures (Wallois et al., 2009; Cooper et al., 2011; Singh et al., 2014; Sokoloff et al., 2015), SE (Adelson et al., 1999; Haginoya et al., 2002; Arca Diaz et al., 2006; Giorni et al., 2009; Monrad et al., 2015; Mitra et al., 2016a,b; Martini et al., 2019) (**Table 7, Figure 19**), BS patterns (Roche-Labarbe et al., 2007; Chalia et al., 2016) (**Figure 19**), and more recently periodic discharges (Winslow et al., 2021) (**Figure 19**).

Over the past two decades, nine case reports (Adelson et al., 1999; Haginoya et al., 2002; Arca Diaz et al., 2006; Giorni et al., 2009; Wallois et al., 2009; Singh et al., 2014; Monrad et al., 2015; Mitra et al., 2016a,b; Martini et al., 2019), one case series (Cooper et al., 2011), and one correlation study (Sokoloff et al., 2015) have used “NIRS” to investigate seizures in the critically ill. Among those study, seven case reports (Adelson et al., 1999; Haginoya et al., 2002; Arca Diaz et al., 2006; Giorni et al., 2009; Monrad et al., 2015; Mitra et al., 2016a,b; Martini et al., 2019) have focused on SE. In all of these studies, the population investigated ranged from neonates to teenagers (youngest patient: 38 weeks; oldest patient: 13 years of age) with various forms of acute seizures and SE. Despite some variability between studies in the hemodynamic results obtained, an increase in hemodynamic (\uparrow rSO₂, \uparrow [HbO], \uparrow CBV) was mainly observed during acute seizures in the critically ill.

Regarding burst-suppression, a biphasic change in HbO (i.e., a decrease followed by an increase) was observed during spontaneous bursts in premature neonates presenting with neurological distress (Roche-Labarbe et al., 2007). Later, using simultaneous EEG-DOT, various hemodynamic changes was reported during hypothermia-induced burst-suppression in critically ill neonates with hypoxic-ischemic encephalopathy (Chalia et al., 2016). Two years later, an extended cohort study in 16 patients with cardiac arrest investigated the relationship between real-time changes in cerebral oxygenation (rSO₂) and various EEG patterns, including voltage suppression (78% of

patients), theta (8%) and delta (5%) background activity, bilateral periodic discharges (4%), burst-suppression (2%), and spike and wave EEG activity (1%) (Reagan et al., 2018). Burst-suppression patterns were associated with a $rSO_2 > 20\%$ (over the forehead). Similarly, an $rSO_2 > 20\%$ was also present during bilateral periodic discharges. In contrast, rSO_2 values $\leq 19\%$ and $> 40\%$ were associated with voltage suppression and theta and delta background activity, respectively, suggesting that distinct EEG patterns may correlate with the quality of cerebral resuscitation and oxygen delivery (Reagan et al., 2018; Maciel and Hirsch, 2018). More recently, cerebral oximetry was used to investigate hemodynamic changes associated with lateralized periodic discharges (Winslow et al., 2021). In their study, Winslow and his colleagues reported an ipsilateral (to the lateralized periodic discharges) increase and contralateral decrease in rSO_2 in most patients. In addition, the % changes in rSO_2 were also dependent on the frequency of lateralized periodic discharges, with higher frequencies exhibiting lower rSO_2 values ipsilaterally (Winslow et al., 2021).

While these studies have been among the first to use optical imaging technique to investigate seizures, periodic discharges and burst-suppression patterns in the critically ill, important limitations found in those studies have to be highlighted. While these studies are among the first to apply NIRS for investigating seizures in the critically ill, they nevertheless had several methodological limitations.

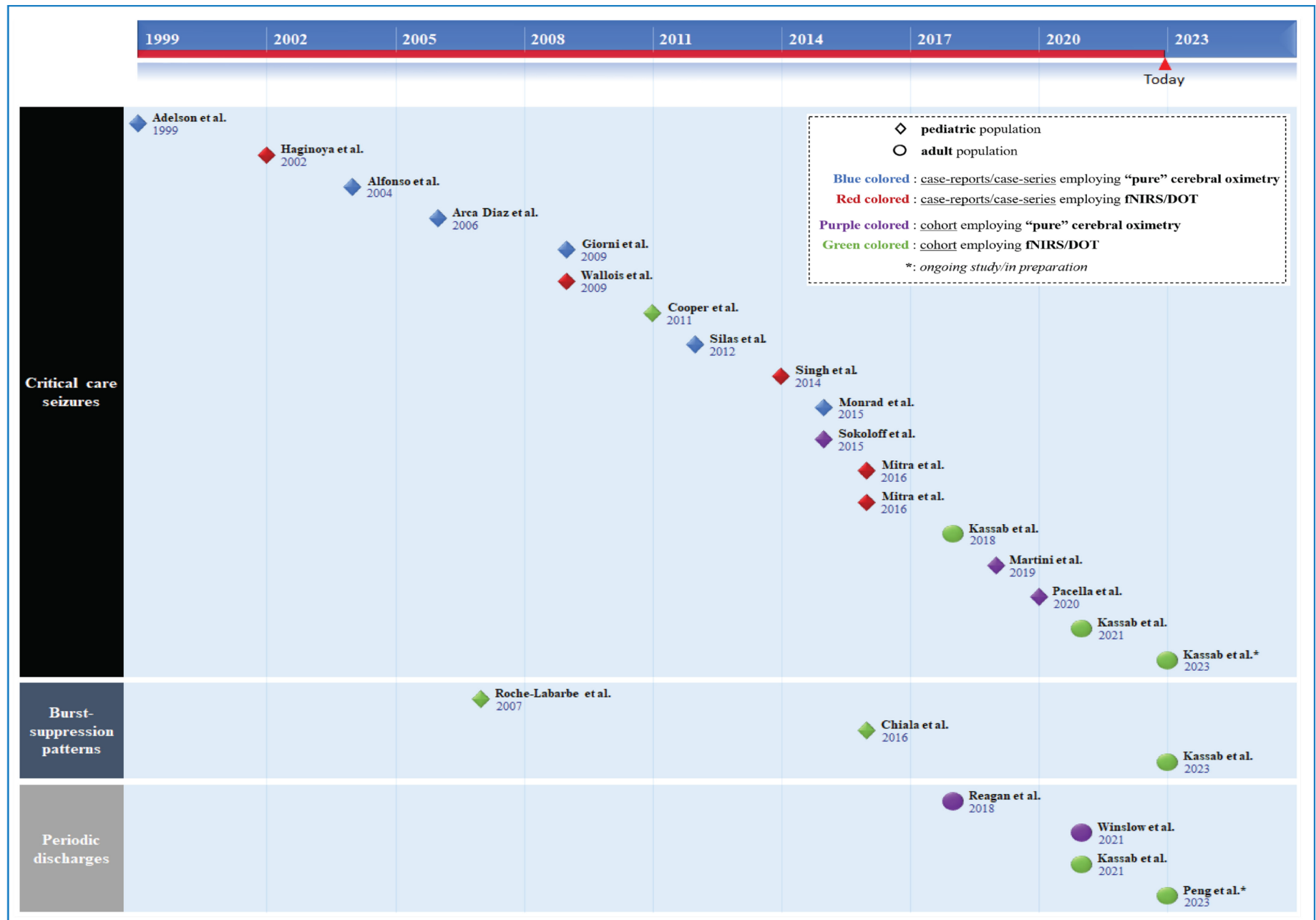


Figure 19 – Historical timeline of “NIRS” studies investigating abnormal EEG pattern in the critically ill. DOT: diffuse optical tomography, fNIRS: functional near-infrared spectroscopy

Drawback #1: NIRS as pure cerebral oximeters and extracerebral signal contamination

With the notable exception of the NIRO300 systems (Hamamatsu Photonics, Hamamatsu City, Japan), most commercial NIRS systems, including the INVOS series (Somanetics/Covidien/Medtronic, Inc., Boulder, USA), function solely as a cerebral oximeter, focusing on monitoring regional tissue oxygen saturation (i.e., rSO₂). While rSO₂ is a sensitive index of tissue hypoxia or ischemia, pure cerebral oximeters do not offer a more detailed quantitative assessment (i.e., $\Delta[\text{HbO}]$, $\Delta[\text{HbR}]$, $\Delta[\text{CcO}]$, CBV, TOI) of cortical hemodynamics during seizures and SE. In addition, while most commercial oximeters can reduce signal components originating from the extracerebral layer by employing multidistance measurements (Scholkmann et al., 2014), it has been shown that changes in scalp tissue oxygenation can still affect the accuracy of commercial cerebral oximeters (Sørensen et al., 2015; Davie and Grocott, 2012).

Drawback #2: NIRS systems variability (validation, precision, accuracy)

While most NIRS systems used in those studies share a similar technology (i.e., CW-type instruments), they are different in several ways, such as the 1) computational algorithm, 2) wavelengths values and numbers, 3) optode (i.e., light sources and detectors) technology, and 4) distance between optodes. These methodological differences can cause substantial measurement inaccuracy. Indeed, numerous adult and neonate studies have compared several commercial cerebral oximeters to establish clinical guidelines for cerebral oximetry in various clinical settings. Significant differences were observed between systems for both relative and absolute measurements in human studies (Dix et al., 2017) and even in phantom studies (Kleiser et al., 2018). In addition, the lack of absolute rSO₂ value and inaccuracies in estimating the optical path length of light within biological tissues are additional factors that can further contribute to measurement inaccuracy. Therefore, caution must be taken when comparing hemodynamic changes obtained with different NIRS systems. Another common issue is the validation of cerebral oximeters (i.e., the ability to detect valid tissue oxygen alteration), usually achieved by comparing measurements obtained with the cerebral oximeter with a gold standard or via ICG. While the use of invasive oxygen measuring modalities can be complex (i.e., impossible to correctly quantify how each vascular compartment contributes to the overall light attenuation), it is also unethical

(not feasible) in healthy and vulnerable populations (e.g., neonatal patients) due to the risk associated with it. Alternatively, optical phantoms can be used, or well-known tasks on healthy can be used but have limitations. Studies employing “NIRS” to investigate seizures in the critically ill do not always clearly state how the in-house or commercial system was validated. Finally, the precision of commercial oximeters can largely vary (Dullenkopf et al., 2003; Sorensen and Greisen, 2006; Hyttel-Sorensen et al., 2011), in addition to the need to control for potential extracranial sources of brain desaturation (Denault et al., 2007), which can be unsuitable for clinical use.

Drawback/limitation #3: Small head coverage

Cerebral oximeters usually have one or two optical patches. Most studies install these optical probes over the hairless forehead. While the forehead provides an easy installation method to monitor brain oxygenation in patients rapidly, hemodynamic changes measured over the frontal cortices do not necessarily reflect changes in other cortical areas. Indeed, seizures, including focal seizures, are known to induce changes in oxygenation and blood flow ipsilaterally and contralaterally (Chaudhary et al., 2012; Harris et al., 2014). The case report by Singh et al. (2014) clearly illustrates the importance of whole-scalp coverage when investigating seizures with noninvasive optical monitoring (Singh et al., 2014). In their study, they captured several seizures in a neonate. Spatial variability in the hemodynamic changes was observed despite not having a focal onset. In addition, they were able first to report DOT images of the cortical hemodynamic response in neonatal seizures since multiple channels were used (Singh et al., 2014).

Drawback/limitation #4: No simultaneous EEG

The use of EEG (or brain electrophysiology) in epilepsy and seizure research is crucial. Simultaneous EEG is important not only to precisely determine seizure onset and offset and characteristics (e.g., duration, spatial distribution), which is essential when investigating the neurovascular dynamics associated with seizures, but also to confirm if a clinical manifestation is indeed related to a seizure. Furthermore, it is essential to electrographic (nonconvulsive) seizures.

Drawback/limitation #5: Short recordings and a small number of seizures recorded

Similar to fNIRS in epilepsy, the duration for most "NIRS" recordings performed to investigate the hemodynamic changes associated with seizures and SE in the critically ill is generally ~1h. This is dramatically less than the typical duration using continuous EEG monitoring in the same population. While longer recordings have important challenges to consider, especially in the adult population, long-term whole-head monitoring in neonates is generally easier to perform. In addition, more extended monitoring techniques (e.g., continuous EEG monitoring, PbtO₂) generally yield more seizures being studied. To understand the neurovascular changes and compare hemodynamic changes between modalities, a large number of recorded seizures is warranted.

Despite these drawbacks, these studies are remarkable by providing the first evidence that NIRS could be applied to investigate and monitor SE in the neonatal intensive care unit. In addition to showing that the shape of the hemodynamic response in neonates/children experiencing seizures might be different than what can be observed during normal somatosensory stimuli in the same age group (or even adults), they provided clinically relevant observations for understanding some pathophysiological mechanisms associated with acute seizures and SE (e.g., neuronal damage) and the potential for "NIRS" to become a brain monitoring technique in the critically ill presenting with seizures (i.e., seizure diagnostic, cerebral ischemia detection, pharmacological management).

Table 7 – Studies employing NIRS to investigate seizure in the critically ill (*Kassab et al., in preparation*).

	Adelson et al. (1999)	Haginoya et al. (2002)	Alfonso et al. (2004)	Arca Diaz et al. (2006)	Giorni et al. (2009)
Study purpose	Pathophysiology	Pathophysiology	Pathophysiology	Treatment	Diagnosis
Study design	Case-series (n = 3)	Cohort / prospective (n = 15)	Case-report (n = 1)	Case-report (n = 1)	Case-report (n = 1)
# critically ill / SE (sex, age)	n = 1 (M, 4 months)	n = 1 (F, 13 year-old)	n = 1 (M, 3 week-old)	n = 1 (M, 2.5 months)	n = 1 (F, 2.5 months)
Clear seizures (#)	Yes (NR)	Yes (15)	Yes (7)	Yes (15)	Yes (NR)
Clear SE diagnosis (SE category)	Yes (CSE)	Yes (TSE)	Yes (MSE, NCSE/coma)	Yes (FMSE)	Yes (NCSE/coma)
Clinical manifestations	Yes	Yes	Yes	Yes	No
\bar{x} seizures duration	NR	< 1min	32-45min	1-2min	“several minutes”
\bar{x} inter-seizure-interval	180s to 60min	2-3min	NR	30s to 1.5min	NR
Management	Multiple ASMs	Multiple ASMs	Multiple ASMs	Multiple ASMs	Multiple ASMs
Underlying pathology	TBI	LGS	HME, TSC	FCD	HIBI
NIRS device (technology / SR / #WL)	INVOS3100A (CW / NA / 2)	NIRO300 (CW-SRS / NR / 4)	INVOS5100 (CW / NA / 2)	INVOS300 (CW / NA / 2)	INVOS300 (CW / NA / 2)
NIRS biomarkers (absolute)	rSO ₂ (no)	[HbT/HbO/HbR] (no)	rSO ₂ (no)	rSO ₂ (no)	rSO ₂ (no)
# channels (cortical coverage)	4 (forehead U)	12 (forehead B)	4 (forehead U)	4 (forehead B)	4 (forehead B)
NIRSm duration (simultaneous EEG / systemic monitoring)	≈ 30h (Yes / No)	< 1h (Yes / No)	24h (Yes / No)	< 1h (Yes / No)	“several days” (Yes / Yes)
Results/analysis	Continuous measurements	Continuous measurements	Continuous measurements	Continuous measurements	Continuous measurements
Pre-ictal changes	↑ rSO ₂	↓ [all]	NR	NR	NR
Ictal changes	↑ < ↓ rSO ₂	↑ [HbO] > [HbT] > [HbR] ↓ amplitude [all] (over Sz course) ↑ [HbR], ↓ ↓ [HbO] and [HbT] (as Sz repeated)	↓ rSO ₂	↑ ↓ rSO ₂ (correlating with 69% of Sz)	↑ ↓ rSO ₂
Post-ictal changes	NR	NR	↑ ↓ rSO ₂ , delayed baseline return	↓ rSO ₂	rSO ₂ normalization
Anatomical MRI collected (findings)	No	Yes (cerebral atrophy)	Yes (Right HME)	Yes (B frontoparietal FCD)	No

aEEG: amplitude EEG, ASMs : antiseizure medications, B: bilateral, [CcO]: cytochrome c-oxidase concentration, CSE: convulsive SE, CW: continuous-wave, DRE : drug-resistant epilepsy, ESES: electrical status epilepticus of slow-wave sleep, F: female, FM: frequency multiplexed, FCD: focal cortical dysplasia, FMSE : focal motor SE, FTOE: fractional tissue oxygen extraction, HME : hemimegalencephaly, HIBI: hypoxic-ischemic brain injury, HIE: hypoxic-ischemic encephalopathy, [HbO]: oxyhemoglobin concentration, [HbR]: deoxyhemoglobin concentration, [HbT]: total hemoglobin concentration, [HbD]: difference between oxy- and deoxyhemoglobin concentration, ICH: intracranial hemorrhage, LGS: Lennox-Gastaut syndrome, M: male, NCSE : nonconvulsive SE, NIRSm: NIRS monitoring, NR: not reported, MSE: myoclonic SE, rSO₂: regional cerebral oxygen saturation, SE : status-epilepticus, SR : sampling rate, SRS: spatially-resolved spectroscopy, SVT: sinus venous thrombosis, Sz: seizure, TOI: tissue oxygen index, TSC : tuberous sclerosis complex, TSE : tonic SE, U: unilateral, WL : wavelength, # : number, \bar{x} : average, ≈: approximately, ↑ ↓ : fluctuation.

Table 7 (continued) – Studies employing NIRS to investigate seizure in the critically ill (*Kassab et al., in preparation*).

	Wallois et al. (2009)	Cooper et al. (2011)	Silas et al. (2012)	Singh et al. (2014)	Monrad et al. (2015)
Study purpose	Pathophysiology	Pathophysiology	Pathophysiology	Pathophysiology	Pathophysiology
Study design	Case-report (n = 1)	Cohort / prospective (n = 4)	Case-report (n = 1)	Case-report (n = 1)	Case-series (n =)
# critically ill / SE (sex, age)	n = 1 (M, 10 day-old)	n = 4 (NR, 8 day-old)	n = 1 (M, < 4 day-old)	n = 1 (F, 10 day-old)	n = 1 (M, 10 year-old)
Clear seizures (#)	No (12)	No (NR)	Yes (13)	Yes (7)	Yes ()
Clear SE diagnosis (SE category)	No	No	Yes (NCSE/coma)	No	Yes (ESES)
Clinical manifestations	No	No	No	No	NR
\bar{x} seizures duration	\approx 28s	NR	\approx 8min	54.3s	NR
\bar{x} inter-seizure-interval	407s	393.6s	15min-20h	441.3s	NR
Management	Phenobarbital	Multiple ASMs	Therapeutic hypothermia and phenobarbital or phenytoin or midazolam	Multiple ASMs	NR
Underlying pathology	Acute fetal distress	Stroke, sepsis, hypoglycemia	HIE	HIE	NR
NIRS device (technology / SR / #WL)	Imagent (CW-FM / NR / 2)	UCL OT System™ (CW-FM / 10Hz / 2)	NIRO200 (CW-SRS / NR / 4)	UCL OT System™ (CW-FM / 10Hz / 2)	INVOS (CW / NA / 2)
NIRS biomarkers (absolute)	[HbT/HbO/HbR] TOI, FTOE (no)	[HbT/HbO/HbR] (no)	TOI (yes)	[HbT/HbO/HbR] (no)	rSO ₂ (no)
# channels (cortical coverage)	8 (parietal B)	60 (whole-head)	NR (frontoparietal U)	58 (whole-head)	2 (forehead U)
NIRSm duration (simultaneous EEG / systemic monitoring)	1.5h (Yes / Yes)	1.5h (Yes / No)	20-24h (Yes / Yes)	1h (Yes / No)	< 1h (Yes / No)
Results/analysis	Continuous measurements and mean changes	Continuous measurements	Continuous measurements	Continuous measurements	Continuous measurements
Pre-ictal changes	NR	NR	NR	↑ [HbO] + ↑ [HbR] + ↑ [HbT]	NR
Ictal changes	↑ [HbR] → ↓ [HbR] + ↑ [HbO] + ↑ [HbT] ↓ TOI (slightly) ↑ FTOE Some variability between events	↑ [HbO] + ↑ [HbR] + ↑ [HbT] → ↓ [HbO] + ↓ [HbR] + ↓ [HbT] [HbR] not significant [HbO] and [HbR] out of phase	8 Sz (62%): ↑ TOI in 5 Sz, decrease in 3 Sz – ↑ MABP in 7 Sz, ↓ MABP in 1 Sz 5 Sz (38%): no change in TOI – ↑ MABP in 1 Sz	↑ [HbO] + ↑ [HbR] + ↑ [HbT] (until max, then) ↓ [HbO] + ↓ [HbR] + ↓ [HbT] Significant spatial variability	↑ rSO ₂
Post-ictal changes	NR	NR	NR	↓ [HbO] + ↓ [HbR] + ↓ [HbT] (prolonged)	NR
Anatomical MRI collected (findings)	No	No	Yes (acute hypoxic-ischemic changes)	No	Yes (normal)

Table 7 (continued) – Studies employing NIRS to investigate seizure in the critically ill (*Kassab et al., in preparation*).

	Sokoloff et al. (2015)	Mitra et al. (2016)	Mitra et al. (2016)	Martini et al. (2019)	Parcella et al. (2020)
Study purpose	Treatment	Pathophysiology	Pathophysiology	Pathophysiology	Prognostic
Study design	Cohort / prospective (n = 20)	Case-report (n = 1)	Case-report (n = 1)	Case-report (n = 1)	Cohort / retrospective (n = 62)
# critically ill / SE (sex, age)	n = 11 (10M, “fully term neonates”)	n = 1 (NR, 9.5 day-old)	n = 1 (NR, 10 day-old)	n = 1 (NR, 9 day-old)	38 (18M, < 3 day-old)
Clear seizures (#)	Yes (40)	Yes (4)	Yes (16)	Yes (10)	23/38 patients (NR)
Clear SE diagnosis (SE category)	No	Yes (NCSE/coma)	No	Yes (TSE)	No
Clinical manifestations	NR	No	No	Yes	NR
\bar{x} seizures duration	\approx 120s	\approx 5min	\approx 90s	\approx 10min	NR
\bar{x} inter-seizure-interval	NR	3-8min	NR	15-30min	NR
Management	Phenobarbital	Therapeutic hypothermia	Multiple ASMs	Therapeutic hypothermia and multiple ASMs	Therapeutic hypothermia
Underlying pathology	HIE, neonatal epilepsy, stroke, sepsis, ICH, SVT	HIE	Stroke	HIE	HIE
NIRS device (technology / SR / #WL)	INVO5100 (CW / 0.2Hz / 2)	Homemade system (CW / NR / NR)	Homemade system (CW / NR / NR)	NR (NR)	INVOS (CW / NA / 2)
NIRS biomarkers (absolute)	rSO ₂ , FTO ₂ (no)	[HbO/HbR /HbT/HbD/CcO]	[HbO/HbR /HbT/HbD/CcO]	rSO ₂ (no)	rSO ₂ (no)
# channels (cortical coverage)	4 (parietal B)	6 (forehead B)	6 (forehead B)	NR (NR)	2 (forehead U)
NIRSm duration (simultaneous EEG / systemic monitoring)	1h (Yes / Yes)	1.5h (Yes-quantitative / Yes)	3h (Yes-quantitative / Yes)	6h (Yes-quantitative / Yes)	72h (Yes / Yes)
Results/analysis	Continuous measurements and mean changes	Continuous measurements	Continuous measurements and mean changes	Continuous measurements	Continuous measurements and mean changes
Pre-ictal changes	\bar{x} rSO ₂ \approx 79.4 %	NR	NR	NR	NR
Ictal changes	\downarrow rSO ₂ , \uparrow FTOE (within physiological range) (\uparrow with \uparrow phenobarbital dose) Independent from systemic changes	\uparrow [CcO] \rightarrow \downarrow [CcO] \rightarrow \uparrow [CcO] (after aEEG peak) \downarrow [HbT] + \downarrow [HbD] \rightarrow \uparrow [HbT] + \uparrow [HbD] (after aEEG peak)** No systemic changes	Asymmetric \downarrow [HbO], [HbR], and [CcO] (\downarrow stroke hemisphere > non-stroke hemisphere) No systemic changes	\uparrow \downarrow rSO ₂ \rightarrow delayed \downarrow rSO ₂ \rightarrow \uparrow rSO ₂ close to the end (correlating with \uparrow Sz amplitude) rSO ₂ baseline increased with each subsequent Sz	rSO ₂ was higher in severe group (i.e., patients with seizures)
Post-ictal changes	rSO ₂ normalization	NR	\downarrow [HbO] + \downarrow [HbR] + \downarrow [CcO] \rightarrow slow \uparrow [HbO] + \uparrow [HbR] + \uparrow [CcO]	rSO ₂ normalization	NR
Anatomical MRI collected (findings)	No	Yes (abnormal + \downarrow signal intensity)	Yes (\downarrow signal intensity + restriction diffusion)	No	Yes (all abnormal)

5.5 Current clinical challenges of EEG-fNIRS

The last two subsections highlighted the potential for EEG-fNIRS in epilepsy and the investigation of acute seizures and SE in the pediatric population. Similarly, recently, researchers have used optical methods for investigating periodic discharges and burst-suppression patterns unlocking a new methodological approach for investigating those EEG patterns in patients. Unfortunately, and despite the numerous advantages of fNIRS, no study in any field of clinical medicine (i.e., stroke, epilepsy, headaches) has yet combined fNIRS and EEG as a continuous whole-head bedside long-term monitoring technique. This has been mainly due to several important challenges still imposed by performing such complex patient monitoring. These difficulties can be divided into three broad categories.

Clinical factor # 1: Installation time

With the exception of using a cerebral oximeter, or low-channel fNIRS systems, the time required to prepare a proper EEG-fNIRS setup at the bedside, and install the electrodes and optodes on the patient's head is considerable and affected by several factors (**Figure 20**).

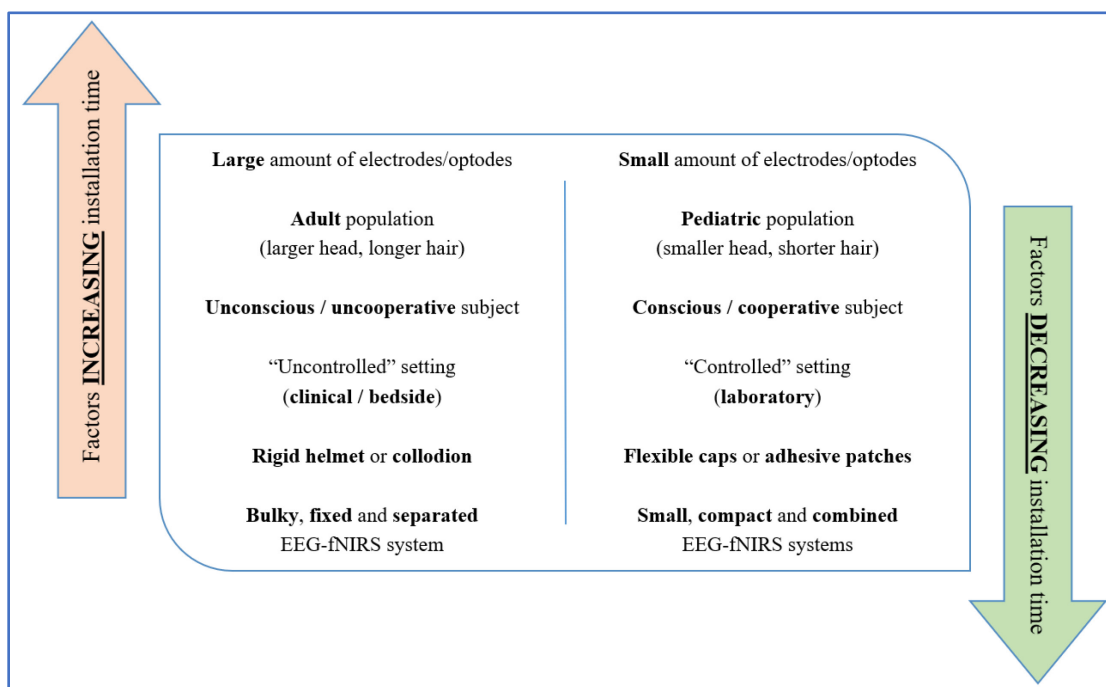


Figure 20 – Main factors affecting the installation time. EEG-fNIRS: simultaneous electroencephalography combined with functional near-infrared spectroscopy.

While whole-head EEG-fNIRS recording has been performed previously in neonates (Cooper et al., 2011; Singh et al., 2014; Chalia et al., 2016), whole-head EEG-fNIRS recordings in adults have only been reported by our group (Nguyen et al., 2012, Nguyen et al., 2013). From past experiences, the installation time for whole-head vEEG-fNIRS recording in a patient with epilepsy is ~1 hour. For these recordings, patients were generally transferred to a dedicated optical imaging room (i.e., laboratory setting), where the monitoring modalities were already set up (i.e., positioned, connected and running). After positioning the patient in a conformable chair, electrodes and optodes are installed using a rigid helmet. Afterwards, registration and system calibration were performed, usually taken ~30-45 min, before vEEG-fNIRS monitoring began, typically lasting for ~1-2 hours. In contrast, in our recent experiments (Kassab et al., 2016; Kassab et al., 2018; Kassab et al., 2021; Chapter 10), bringing the vEEG-fNIRS set-up to the patient's bedside and modifying our methodology to enable long-term monitoring significantly increased the installation time anywhere from 4-5 hours (whole-head bedside vEEG-fNIRS monitoring in the epilepsy monitoring unit using a personalized cap) to 8-10 hours (whole-head bedside vEEG-fNIRS monitoring in the neuroICU using a collodion). However, this methodology enables long-term whole-head monitoring lasting >24 hours. Nevertheless, as we can see, the current installation time for typical vEEG-fNIRS monitoring in the clinical setting is still longer than a typical EEG installation (e.g., 30-60 minutes).

Clinical factor # 2: Patient comfort

Another critical factor stalling the clinical integration of vEEG-fNIRS is patient comfort. Usually, as the number of optodes increases, so does the weight and the amount of pressure. While comfort is subjective and varies from one individual to another, healthy subjects and patients can tolerate whole-head coverage generally up to ~1-2 hours (i.e., average duration usually found in the literature when a large head coverage is performed). Beyond that time, patients generally start to experience pain, which increases as time goes on. At some point, the pain becomes unbearable, and the recording needs to stop. Additional factors that can potentially increase patients' discomfort are 1) long installation time, 2) optodes geometry (e.g., flat optodes with a large surface area vs. straight optodes with small surface area, 3) headgear characteristics (e.g., rigid helmet vs. soft cap).

Once again, this contrasts with long-term continuous EEG monitoring, where it rarely causes any discomfort or pain, at least for the first few days.

Clinical factor # 3: Technician expertise and safety consideration

Cerebral oximeters are user-friendly and usually do not require an expert user. In contrast, a typical whole-head EEG-fNIRS study usually **requires someone with experience**. In addition, the **user** is also required to **remain at the patient's bedside** throughout the monitoring period. While fNIRS is considered a safe modality and usually does not require constant surveillance, such as during brain oxygenation monitoring using a cerebral oximeter in a patient undergoing cardiovascular surgery, the situation is different in patients experiencing seizures in the epilepsy monitoring unit or the ICU. During complex partial or generalized (convulsive) seizures, the patient might move uncontrollably. This might lead to significant tension on the patient's head and neck, which might potentially cause injuries and damage the delicate equipment (e.g., optical fibres, electrical cable). Moreover, when performing vEEG-fNIRS monitoring in the ICU, constant care is provided by the medical personnel, which might require the user to make essential adjustments in order to maintain or improve the quality of the signal (e.g., turning off the lights, readjust the cap). Medical complications might occur requiring urgent care (e.g., resuscitation) or an exam (e.g., CT scan) to be performed quickly. In those situations, it is necessary that vEEG-fNIRS monitoring be stopped promptly to reduce any interference with proper care or allow the patient to be transported for further evaluation. These challenges will need to be addressed in the near future, as they can limit the number of studies applying long-term whole-head vEEG-fNIRS monitoring in the clinical setting and, consequently, the clinical integration of this cost-effective multimodal monitoring modality not only in patients with epilepsy or in the critically ill, but for neurological patients in general.

CHAPTER 6 – METHODOLOGY AND INSTRUMENTATION

6.1. Multichannel vEEG-fNIRS system for long-term whole-head monitoring

As we have also pointed out previously, multimodal EEG-fNIRS recordings are achieved by integrating each modality into one system (i.e., hybrid EEG-fNIRS system) or recording each modality simultaneously and separately (from each other). While hybrid systems can collect data simultaneously and synchronously without requiring external synchronization, the latter requires external synchronization to align both signals temporally (i.e., vEEG and fNIRS).

In this thesis, **two separate fNIRS systems (both CW-type instruments) have been used**. While they differ in several aspects (technology, portability/wearability, hybrid EEG integration), they are composed of a main hardware platform from which optic fibres or electric wires project to light sources (i.e., emitting optodes or emitters) and light detectors (i.e., receiving optodes, receivers) which are mounted on the scalp. The sources emit light into the head at a known intensity (at two or more wavelengths), and the detectors capture the light (after it has traveled through the human head), transferring it back to the main hardware. A software integrated into the main hardware (i.e., all in one system) or independent (i.e., installed on a separate computer) saves the optical signal data. Additionally, some software also offers the possibility to preprocess and analyze the optical signal in real-time.

The **first system** has been detailed extensively in **Chapter 7**. Briefly, it is a homemade hybrid EEG-fNIRS system. It comprises 32 light sources, 32 light detectors, and 32 EEG channels, allowing up to 128 NIRS channels and 32 EEG to be sampled simultaneously. It is compact ($12 \times 9 \times 7 \text{ cm}^3$) and lightweight ($< 700 \text{ g}$), allowing it to be worn during recordings. Additionally, it is battery powered ($\sim 24 \text{ h}$ autonomy) and can transmit the signal wirelessly (up to 10 m) through Bluetooth® Wireless Technology, enabling higher portability and motion freedom during long monitoring sessions at the bedside.

The **second system** is the **Brainsight[®] CW NIRS system** from Rogue Research (Rogue Research Inc., Canada) (**Figure 21, Figure 22**).

The technology used in this system is laser diodes for light sources, avalanche photodetectors (APDs) for “high-sensitivity” detectors, and standard photodiodes for “proximity” detectors. Laser diodes allow for coherent light emission with a narrower bandwidth and have a higher-power emission (10 mW) (compared to more traditional light-emitting diodes, < 10 mW). Avalanche photodiodes have a high sensitivity (< 0.5 pW for high-sensitivity” detectors and < 1 pW for “proximity” detectors). In addition, they have moderate to high gains in the order of 100 and a dynamic range of ~ 60 (i.e., > 100 dB for the Brainsight[®] CW NIRS system). These characteristics are essential for acquiring signals from sources positioned at different distances (i.e., overlapping measurements). In addition, compared to other types of detectors, they are more robust to ambient light and faster, allowing them to be modulated with frequencies exceeding 100 MHz. Taking advantage of this feature, the Brainsight[®] CW NIRS system can minimize the demodulation crosstalk and distinguish the origin of each source detected; light emitters are modulated at different frequencies using a Frequency Division Multiple Access (FDMA) method.

Light is conveyed from or to the main hardware using lightweight and long (3 m) optical fibres (single core optic fibres for light sources and bundles of tiny glass fibres for light detectors). The distal extremity of each optic fibre is composed of a low profile optode (optode height ~7 mm), ideal for gluing the optodes on the scalp with collodion. This low-profile optode configuration is obtained by fusing the distal portion of the optic fibres to a 90° coated prism sitting on a plano-convex lens.

The main hardware consists of 4 bays, each containing one optical module and totaling four optical modules. Each module allows up to 4 dual-wavelength (685 nm, 830 nm) light sources, 4 “proximity” detectors, and 8 “high-sensitivity” detectors for a total of 16 light sources and 48 light detectors. The hardware is mounted on a mobile trolley and has a telescopic 180° rotating arm providing stable optical fibre support and easy maneuverability of the system at the patient's bedside. Optical data collected from the main hardware is transmitted to the Brainsight[®] computer

using an ethernet connection. A user-friendly proprietary software manages data acquisition setup and collection from the Brainsight® system. The sampling rate is adjustable (1-100 Hz).

To digitize the optodes, the Brainsight® CW NIRS system uses its integrated Brainsight® neuronavigation software to communicate with an optical position sensor (Polaris Vicra®, NDI, Canada). Digitalization of each optode and common registration points (nose tip, nasion, inion, left periauricular, right periauricular) is performed using a subject tracker and a pointer affixed with retro-reflective spheres. Mapping the optode coordinates back to an MRI template or the subject-specific MRI space is done by calculating the spatial transformation from the subject's head to his or her MRI image ([Insight Toolkit software – https://itk.org/ITKSoftwareGuide/html/Book2/ITKSoftwareGuide-Book2.html](https://itk.org/ITKSoftwareGuide/html/Book2/ITKSoftwareGuide-Book2.html) – Yoo et al., 2002).

In order to capture both optical and electrophysiological signals, we combined the Brainsight® CW NIRS system with a commercial EEG system from BrainProducts® (Brain Products GmbH, Gilching, Germany). The main parts of the EEG system are the amplifiers (BrainAmp Standard, Brain Products GmbH, Gilching, Germany) and its proprietary EEG software for data collection (BrainVision Recorder, Brain Products GmbH, Gilching, Germany). We used traditional wet gold cup EEG electrodes (Grass® Reusable Gold Cup EEG Electrodes, Natus Medical Incorporated, USA).

Between 25 and 29 electrodes were usually employed. In case where 29 electrodes were employed, 25 were dedicated to the scalp according to the 10-20 (reference FCz) (Jasper, 1958) and 10-10 (F9, T9, P9, F10, T10, P10) systems (Acharya et al., 2016), two for the electrocardiography and two for electrooculography. Systemic hemodynamic monitoring, such as heart rate, SpO₂, and blood pressure, were acquired using the Finapres® NOVA SpO₂ system (Finapres Medical Systems, Enschede, the Netherlands).

Physiological data was fed directly into the BrainVision Recorder, allowing synchronized EEG and systemic physiological data collection. Synchronization of vEEG and fNIRS data was performed using E-Prime® 2.0 software (Psychology Software Tools, Pittsburgh, PA).

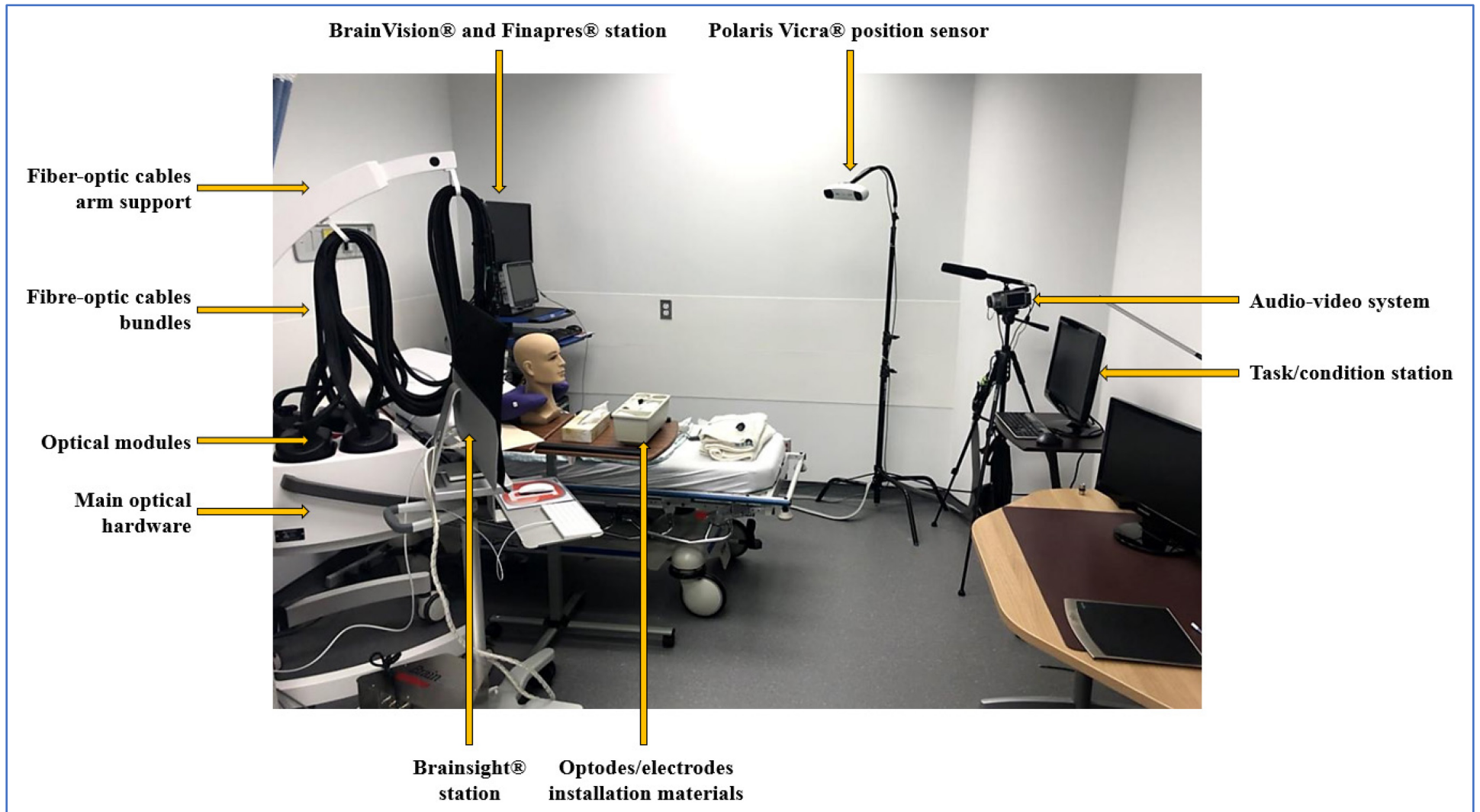


Figure 21 – Simultaneous video electroencephalography and functional near-infrared spectroscopy (vEEG-fNIRS) setup in the lab.

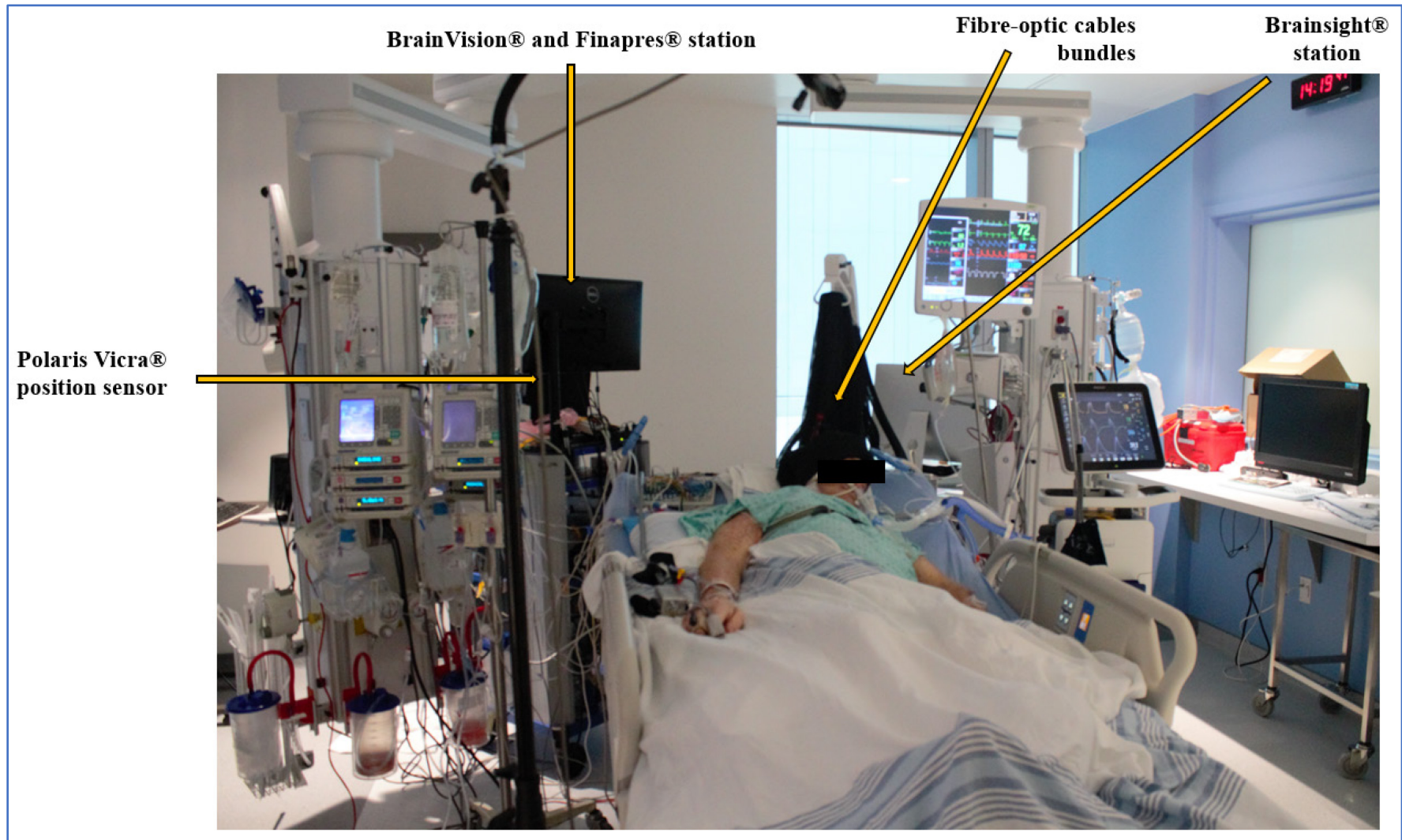


Figure 22 – Simultaneous video electroencephalography and functional near-infrared spectroscopy (vEEG-fNIRS) setup in the neuroICU at the CHUM.

6.2 The brain-optode interface for long-term whole-head vEEG-fNIRS monitoring

The “coupling” between the scalp and the optodes strongly influences the quality of the NIRS signal. While fNIRS is less susceptible to movement artifacts than other neuroimaging techniques, poor stability between the optodes and the scalp will lead to displaced optodes and motion artifacts. Therefore, carefully “securing” the optodes on the head is a crucial step for any fNIRS experiment. Indeed, over the years, several private companies and research groups, including us, have worked on developing several methods that can secure the optodes on the scalp.

These methods can be divided into two broad categories ([for a detailed review on this topic, please refer to Kassab et al., 2015](#)).

6.2.1 “Optode probe”

“Optode probes”, or simply “probe”, is a general term that refers to any non-adhesive headgear or headwear used to secure the optodes on the head through the use of sockets (optode holder). Probes can take various shapes and sizes. The most common include straps, patches, helmets, headbands and caps.

Straps, patches and helmets are usually made from rigid or semi-rigid polymer (i.e., plastic) material (e.g., polyethylene or polystyrene), with or without semi-rigid Velcro[®] straps. In contrast, headbands and caps are usually made of soft elastic fabric. Therefore, soft caps are usually lighter, more comfortable, and convenient (i.e., easier to transport, install, and wash). However, as these caps are lighter and more flexible, they tend to move over time, especially when motion is required (e.g., during a walking task) or unavoidable (e.g., during seizures)

Displacement of the optodes from their original position can lead to data misinterpretation, especially when multichannel fNIRS is used for localization purposes. Some companies and groups have relied on adding additional strapping support (e.g., chin or chest strap) to reduce the likelihood of optode moving. However, these stabilizing alternatives increase pressure, cause discomfort, and limit recording time. Finally, and except when a premanufactured standard cap is used (e.g., Easycap[®] EEG recording caps), the manufacturing process of personalized soft caps is

long, as these require careful stitching in order to precisely “mould” the cap into the shape and size of a specific population or age group.

A trade-off is usually made between 1) comfort, 2) optode stability, 3) usability/convenience, 4) head coverage and 5) signal quality. Over the years, several sophisticated commercial fNIRS optode probes have been developed, trying to meet all of the essential goals of an “ideal” fNIRS caps (i.e., comfortable, stable, usability, whole-head coverage, signal quality). However, these caps have been developed mainly for cognitive studies (i.e., typically short duration (~20-30 min) experiments that do not require whole-head coverage). In those settings, comfort and signal quality become less of an issue but become problematic when recording time increases and more optodes are added. Therefore, in the context of long periods of recordings exceeding two hours in the clinical setting (such as in long-term vEEG-fNIRS monitoring), these commercial solutions are not ideal. Moreover, very few commercial fNIRS caps integrate EEG in their design, leading to additional issues for multimodal EEG-fNIRS studies.

In order to tackle some of these limitations, several groups, including us, have been developing in-house probes (Ishikawa et al., 2011; Giacometti and Diamond, 2013; Kassab, 2014; Nguyen et al., 2016; Kassab, 2018). In our latest development of EEG-fNIRS cap described in Chapter 8, we used a combination of breathable elastic fabric and specialized comfort “pads” of various shapes and sizes to create personalized caps. Our caps were easy to install and operate, and provided comfort while maintaining good signal quality and relatively adequate stability. This individualized approach enabled us to perform long-term whole-head vEEG-fNIRS monitoring in the clinical setting (Kassab, 2016; Kassab, 2018; Kassab, 2021). However, our caps still have some limitation related to the issue of optode stability, which is why regular surveillance is necessary with adjustments required every couple of hours to ensure that the optode positioning remained constant throughout the monitoring period.

As we can see, the development of probes remains a challenge. While we are currently addressing this issue by developing a new generation of more stable EEG-fNIRS caps, another solution, in the meantime, is the use of **collodion**.

6.2.2 “Adhesive techniques”

The use of adhesives is not new. Indeed, commercial cerebral oximeters have been using self-adhesive optode pads/patches ever since they were commercially available. Using self-adhesive pads allows easy installation by any user without experience. However, it limits their positioning (and therefore the cortical coverage) to hairless regions (e.g., forehead) since hair can strongly impact adhesion, uncouples the optodes and affects the optical signal.

More recently, the use of collodion (e.g., Collodion, Mavidon, FL), a clinical adhesive commonly used to apply EEG electrodes for long-term vEEG monitoring, has shown to be extremely useful in providing comfort, optode stability and signal quality during long periods of recordings (~6 h in one patient and ~18 h in another patient) (Yücel et al., 2014). In their study, the authors compared this method to a standard Velcro-based probe array of optical fibres and reported 1) an increase in the signal-to-noise ratio by six and three-fold at 690 and 830 nm wavelengths, respectively, 2) a 90% reduction in signal change due to movement artifacts, and 3) statistically lower $\Delta[\text{HbO}]$ and $\Delta[\text{HbR}]$ during motion artifacts. These advantages, provided by collodion, allowed the authors to capture three epileptic seizures with good quality and despite excessive motion in two patients with epilepsy. Indeed, this method was also used in a later study investigating the hemodynamic response to IEDs in 9 patients with epilepsy (Pellegrino et al., 2016).

Thus, we decided to consider this approach in our latest study. After carefully covering the patient shoulder (to protect their clothing or any medical equipment nearby from collodion), we gently move away the hair using a cotton-tipped stick, apply the optode or electrode on the scalp, and cover it with a square (~3 cm²) of collodion impregnated gauze before drying it using compressed air. Once dried, the gauze forms a tight seal around the optode or electrode, preventing any possible displacement (**Figure 23**). Our own experience (Chapter 10) confirms the benefits of collodion for long-term EEG-fNIRS monitoring reported previously by Yücel and her colleagues regardless of head shape variation we had in our population. However, this approach has two significant limitations.



Figure 23 – Multiple optodes installed using gauzes impregnated with collodion on a subject in our lab.

First, the optodes must be compatible with collodion (and the solvents used to remove it, e.g., acetone or collodion remover). Optode must be of low-profile and composed of materials resistant to collodion and at least one of its solvents. In our case, the optodes manufactured by Brainsight® are low-profile and are resistant to collodion and collodion remover. Second, and probably the most crucial aspect for the long-term whole-head monitoring at the bedside (and the eventual integration of multichannel fNIRS in the clinical setting), is the long installation time. In the study performed by Yücel and her colleagues, there were no details regarding the time it took to install six optodes with collodion. However, from our experience, installing numerous optodes takes a considerable amount of time.

While installing the first optodes is relatively quick (~1 min max each), it usually gets tougher and longer to apply the next optodes, with the last ones taking as much as 5 min each. This is mainly because the head becomes “crowded” with optodes, electrodes, gauzes, and even fibre-optic cables that can obstruct the view, further extending the installation of an optode. Additional factors (e.g., unresponsive patients, patients with long and curly hair) can also significantly increase the installation time. From our experience with whole-head coverage, the time required to install, with collodion, 48 optodes and at least 19 electrodes can take anywhere from 4 hours (e.g., bald/very short hair patient in the epilepsy monitoring unit) to 6 hours (i.e., long or very curly hair patient in the neuroICU). For this main reason, we focused on a whole-head sparse and double-density montage (i.e., optode distribution) in our studies instead of more high-density montages, which are currently not realistic for long-term whole-head bedside monitoring in the clinical setting.

6.2.3 Optode profile

In addition to the method used to install the optodes, the design of the optode itself (i.e., optode geometry or optode profile) also contributes directly and indirectly to the overall performance and quality of fNIRS experiments.

Several types of optode profiles exist analogous to NIRS instruments and caps. The most common are high-profile optodes, including “still” or straight vertical optodes and “recoilable” or spring-loaded optodes. More recently, several companies have developed low-profile optodes. In contrast to high-profile optodes, low-profile optodes are lighter, less prone to motion (and sliding), and improve the optode holder's overall stability. In addition, they are generally faster to install and induce less discomfort during fNIRS experiments (**Table 8**).

In conclusion, there is currently no “universal” brain-optode interface solution that can be applied to all types of fNIRS experiments. For now, the study characteristics will strongly impact or dictate which brain-optode interface technique would be more suited (**Figure 24**).

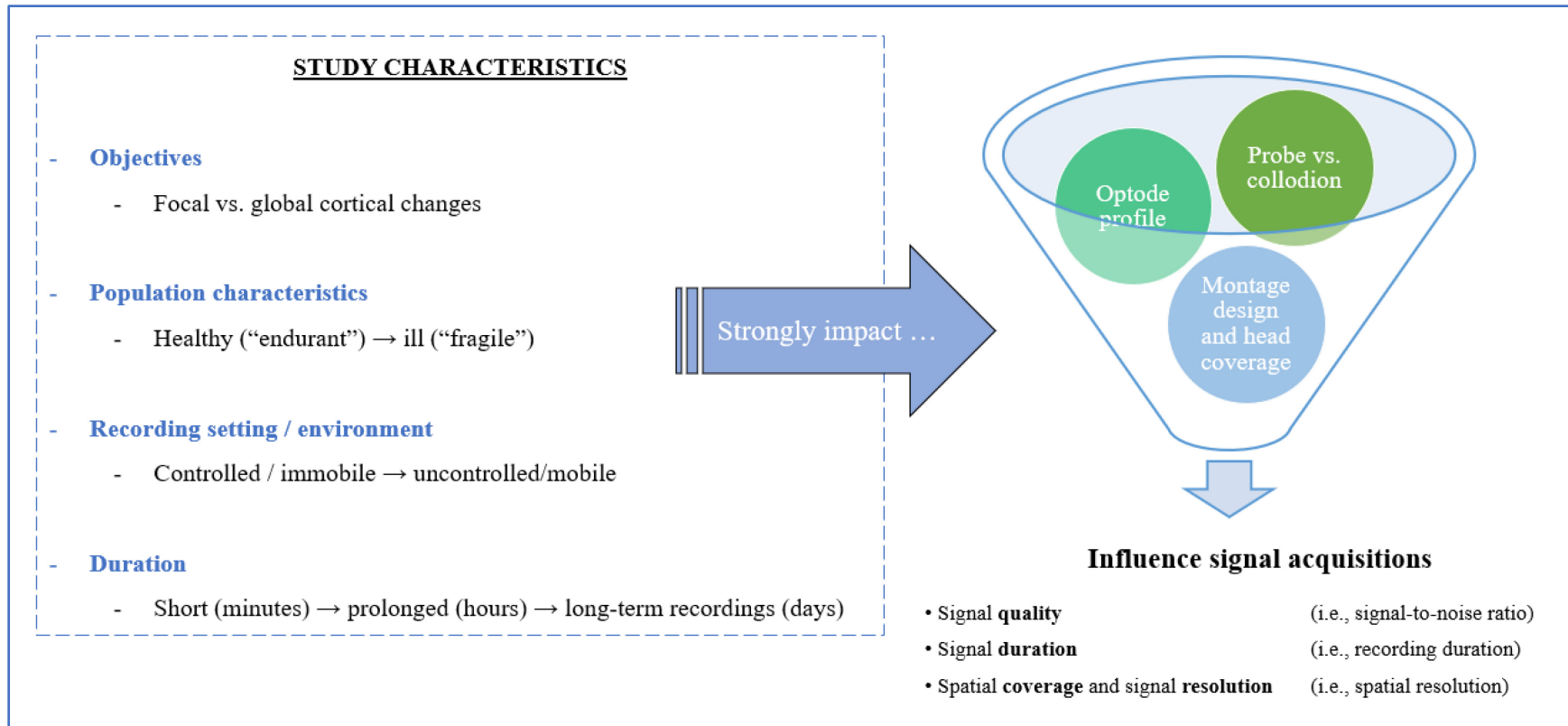


Figure 24 – Factors impacting the different features of the brain-optode interface.

Table 8 – Summary of the advantages and limitation of high- and low- profile optodes.

	High-profile	Low-profile
Usability*	+ (still) / ++ (recoilable)	+++
Comfortability*	+ (still) / ++ (recoilable)	+ (pointy tip) / +++ (flat tip)
Probe stability*	+ (still) / ++ (recoilable)	+++ (pointy tip < flat tip)
Signal quality*	variable	variable
Multimodal compatibility (i.e., EEG, fMRI, MEG)	+	+++
Commercial examples	 <p>© NIRx</p>  <p>© Artinis</p>	 <p>© Rogue Research</p>  <p>© Lumo/Gower Labs</p>

*are also affected by the type of optode holder, and optodes sockets (when used). EEG: electroencephalography, fMRI: functional magnetic resonance imaging, MEG: magnetoencephalography.

6.3 Toolboxes for fNIRS data: statistical analysis and image reconstruction

Currently, there is no gold standard preprocessing pipeline for the analysis of fNIRS data. However, some analytical methods (i.e., preprocessing, processing, statistical test) are usually recommended and applied within the fNIRS community (Yücel et al., 2021). This thesis's main preprocessing steps followed as much as possible the best practices for conducting fNIRS studies (Yücel et al., 2021).

In addition, **several open-source softwares are available** for analyzing and projecting fNIRS data. In Chapter 7 (Manuscripts 1) and Chapter 8 (Manuscript 2), an earlier version of the LIONirs toolbox was used. In Chapter 9 (Manuscript 3), we adopted an in-house version of Homer2/AtlasViewer toolboxes for the analysis. Finally, in Chapter 10 (Manuscripts 4), an in-house version of NIRStorm was also added to our analysis. For any additional information about each toolbox, please refer to:

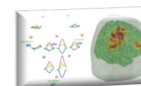
<https://github.com/JulieTremblay3/LIONirs>

(LIONirs toolbox)



<https://github.com/BUNPC/Homer3>

(Homer toolbox)



<https://github.com/BUNPC/AtlasViewer>

(AtlasViewer toolbox)



<https://github.com/Nirstorm/nirstorm>

(NIRSTORM toolbox)



This section presents an overview of the main steps, most of which have been applied in this thesis, involved in fNIRS analysis and image reconstruction. For a more detailed description of the analysis and statistical methods used in this thesis, we kindly refer the reader to the methodology section of each Manuscript (Chapters 7 to 10) as well as a review by Tak and Ye (2014).

6.3.1 Video-EEG analysis

As in most signal analysis pipelines, the first step in EEG analysis obtains a “clean” signal in order to reduce the probability of identifying false events. Cleaning the EEG usually involves preprocessing the EEG signal by applying a band-pass filter (high-pass filter: 0.5-1Hz, low-pass filter: 35-70Hz), re-referencing (optional), and manual and/or automatic artifact removal using specialized algorithms such as Infomax Independent Component Analysis (i.e., infomax ICA) (Bell & Sejnowski, 1995; Makeig et al., 1995). Once cleaned, a simultaneous inspection of the video-EEG, electrocardiogram (EKG) and electrooculogram (EOG) is done to identify abnormal EEG events accurately (e.g., spikes or seizures).

In this thesis, these steps were performed using BrainVision Analyzer (BrainVision Analyzer, Version 2.2.0, Brain Products GmbH, Gilching, Germany) or Brainstorm (Tadel et al. 2011).

6.3.2 Preprocessing and statistical analysis of fNIRS data

Analysis of fNIRS data can be divided into six steps described below. These steps are essential in order to extract accurate hemodynamic changes in response to a specific stimulus (e.g., visual stimulation) or event (e.g., seizures).

Step 1 – channel pruning

The raw signal is checked to identify channels containing instrumental noise (i.e., channels contaminated by non-physiological noise, such as external light, electrical interference, instrumental degradation or instability) (Huppert et al., 2009), channels containing confounding noise (i.e., channels contaminated by systemic physiological artifacts, such as respiration or non-physiological artifacts such as head or body motion), including channels displaying a negative signals (Scholkmann et al., 2014; Tachtsidis and Scholkmann, 2016; Janani and Sasikala, 2017).

Channels containing significant and non-filterable instrumental noise are removed (pruned) since they contain insufficient data quality (Sappia et al., 2020). The pruning can be performed subjectively by visual inspection (channel intensity and presence of heartbeats) or objectively by measuring a signal-to-noise ratio, a scalp coupling index, a coefficient of variation, or the power spectral density (and visualizing “cardiac peak” around 0.1 Hz) (Eggebrecht et al., 2012; Piper et

al., 2014). While the latter is usually more favoured, the former can be as good when employed by experienced users. As for channels containing systemic physiology and/or motion artifacts, additional steps (described below) can remove or reduce their contribution.

In this thesis, we used visual inspection and automatic channel pruning.

Step 2 – motion artefact rejection or correction

Several sources of motion (e.g., head, body, fibre-optic tension, slow shifting of cap) can occur during fNIRS recordings. These motion sources eventually lead to optode displacement, which can cause motion artifacts in the form of spikes or baseline shifts. These artifacts can seriously affect the functional hemodynamic responses and distort any statistical inferences.

While motion artifacts can be expected when performing a language or walking task, it can also occur unexpectedly in specialized populations (e.g., children, patients with epilepsy, patients with Parkinson's disease). Additionally, the shape, frequency (i.e., components) and duration of these artifacts can vary depending on the studied population (e.g., neonates vs. adults, noncompliant vs. compliant subject).

Similar to channel pruning, motion artifact identification can be performed subjectively or using different motion artifact detection algorithms that take advantage of several characteristics within the fNIRS signal (e.g., amplitude, frequency, and time).

Several strategies are possible once motion artefacts are identified (Brigadoi et al., 2014). They include: **1**) removing the whole channel from the rest of the analysis, **2**) discarding the period where the motion artifacts occur from the rest of the analysis, or **3**) attempting to correct the motion period using common motion artifacts correction methods (**Table 9**). The selection of one particular method over another will largely depend on the type of fNIRS experiment and population (Cooper et al., 2012). In recent years, additional algorithms have been developed, such as autoregressive prewhitening filtering (Barker et al., 2013), empirical mode decomposition (Gu et al., 2016), hybrid combination of spline interpolation method and Savitzky–Golay filtering (Jahani et al., 2018), and the use of temporal derivative (Fishburn et al., 2019).

These motion artifact correction methods rely on fNIRS signals for motion artifacts removal. Alternatively, it is also possible to take advantage of an input signal highly correlated with the motion artifacts (but not with the functional NIRS response) and remove motion artifacts using linear regression, adaptive and Wiener filtering approaches (Izzetoglu et al., 2005; Zhang et al., 2009; Robertson et al., 2010), and more recently regression within a GLM framework (von Lüthmann et al., 2019). Such signal can be obtained via an **external motion detector** (e.g., an accelerometer) (Blasi et al., 2010; Izzetoglu et al., 2010; Virtanen et al., 2011) or using an **additional “reference” NIRS channel** (Robertson et al., 2010).

This thesis used visual inspection and automatic motion detection algorithms (in Homer2). We mainly applied principal component analysis (Zhang et al., 2005) and spline interpolation (Scholkmann et al., 2010) methods for motion correction. Other methods were also evaluated but did not significantly improve the motionlessness quality in our data.

Step 3 – conversion (intensity → OD → concentration)

Usually, the conversion of raw signal from intensity to optical density is performed after channel pruning (i.e., after step 1), while the conversion from OD into changes in hemoglobin species is done after motion artifacts have been dealt with (i.e., after step 2). Changes in hemoglobin are obtained by applying the modified Beer-Lambert law (Delpy et al., 1988). When multiple separations are used during an fNIRS experiment, especially when comparing information from channels of different separations, it is recommended to also include a differential path-length factor during this step-in order to take into account the wavelength and source-detector distance effects on the pathlengths of light through the tissues.

In this thesis, we converted the raw signal after channel pruning. Optical density to hemoglobin concentration was calculated, with a differential path-length factor (Duncan et al., 1995), just before the step 6 was usually applied.

Table 9 – Examples of motion artefact correction methods used in fNIRS processing.

Method	References	Advantages	Limitations
Principal Component Analysis	<i>Zhang et al. (2005)</i>	<ul style="list-style-type: none"> • Very efficient in infants (where motion is the main source of variance) 	<ul style="list-style-type: none"> • Requires multiple channels • Assumes that motion is the dominant source of variance • Tends to remove too much activation in adults
Targeted, recursive PCA	<i>Yücel et al. (2014)</i>	<ul style="list-style-type: none"> • Avoid over-correction (applies principal component analysis only to pre-identified MAs segments) • Performs well in studies where MAs are temporally <u>independent</u> from stimuli 	<ul style="list-style-type: none"> • Requires multiple channels
Correlation-Based Signal Improvement	<i>Xu et al. (2010)</i>	<ul style="list-style-type: none"> • Simple • On-line correction possible • Performs well in studies where MAs are temporally <u>dependant</u> from stimuli (e.g., speech studies) 	<ul style="list-style-type: none"> • Relies on the assumption of a normal HRF • Can introduce artifacts in the HRF
Spline interpolation	<i>Scholkmann et al. (2010)</i>	<ul style="list-style-type: none"> • Simple/fast • Corrects signal offset • Correct only MA segment • Performs well in studies where MAs are temporally <u>independent</u> from stimuli 	<ul style="list-style-type: none"> • Require a reliable technique to identify MAs segment • Fixed parameters may not be optimal for all MAs segments • Overfitting replaces MAs segment with constant values (resulting in lost information)
Kalman filtering	<i>Izzetoglu et al. (2010)</i>	<ul style="list-style-type: none"> • Simple (↑ signal-to-noise ratio) • On-line correction possible 	<ul style="list-style-type: none"> • Accumulation of error over time
Wavelet transformation or filtering	<i>Molavi and Dumont (2012)</i>	<ul style="list-style-type: none"> • Better at maintaining the frequency content (keeps cardiac and respiration fluctuations) 	<ul style="list-style-type: none"> • Very slow • Does not correct signal offsets • Outlier parameter varies for each population

fNIRS: functional near-infrared spectroscopy, HRF: hemodynamic response function, MAs: motion artifacts, PCA: principal component analysis.

Step 4 – removing confounding systemic physiological signals

Extracerebral tissues, particularly the scalp, is vascularized and innervated. Therefore, changes in partial pressure of CO₂ (PaCO₂), systemic blood pressure, heart rate, respiration rate and vascular tone/scalp blood flow systemically can be reflected within extracerebral layers and lead to overestimating or underestimating the actual hemodynamic response (i.e., a hemodynamic response associated with neuronal activity, and not systemic changes) (Scholkmann et al., 2013; Kirilina et al., 2013). Additionally, systemic changes can also impact the vascularization of neurons, which can also lead to misinterpretation of the fNIRS signal (Scholkmann et al., 2013, 2020; Kirilina et al., 2013; Tachtsidis and Scholkmann, 2016; Caldwell et al., 2016). Finally, any head movement, including speaking or raising the eyebrows, can also lead to changes in CBF and brain oxygenation since the brain itself initiates them and, therefore, can induce unwanted hemodynamic changes in the fNIRS signal (Schecklmann et al., 2017; Novi et al., 2020).

Several strategies are usually employed for separating and removing these confounding signals, including digital filtering (Liu et al., 2015; Pinti et al., 2019), and prewhitening/precoloring (Barker et al., 2013). Additional methods such as principal component analysis and short-separation channel within a GLM framework are discussed in the next step.

Prefiltering the data. It is usually recommended to use a low-pass filter (e.g., Butterworth filter or Chebyshev filter or 0.2 Hz, 0.5 Hz or higher) (Scholkmann et al., 2013), which can quickly reduce or remove unwanted components in the signal such as high-frequency instrumental noise and heart activity (~0.5 to 2 Hz) (Huppert et al., 2009). A high-pass filter of 0.01 Hz can also be added to remove lower unwanted frequency components in the signal (Huppert et al., 2009). However, it must be added with caution as it can remove the actual desired brain signal, especially when the duration of the task is comparable to the frequency threshold of the filter. As for respiration and blood pressure fluctuations (0.08 to 0.12 Hz) (i.e., Mayer wave oscillations), these confounders cannot simply be removed by bandpass filtering, as their frequencies fall into the same frequency range of the hemodynamic response (Huppert et al., 2009). Additionally, it is worth mentioning that even the resting state heart rate can, in some cases, overlap with the hemodynamic response (Huppert, 2016).

A finite impulse response filter may be used (instead of an infinite impulse response such as the Butterworth filter). Selection between the two types of filters will largely depend on the type of data. Finite impulse response and infinite impulse response filters can safely be applied to online and offline data. In contrast, online data can only be processed with FIR filters. It is also important to distinguish digital filtering from adaptive filtering, which uses a system of linear functions within either an open or closed-loop control model to reduce the amount of physiological noise present in fNIRS (Pinti et al., 2019). Finally, an alternative approach to digital filtering is to add a drift factor into the GLM as a regressor to model the low-frequency oscillations in the data (e.g., third-order polynomial drift).

In this thesis, we used a Butterworth low-pass filter of 0.5Hz. A high-pass filter 0.01 was also added mainly for the first study with healthy participants.

Noise prewhitening and precoloring. Another alternative to digital filtering is through prewhitening and precoloring. Prewhitening and precoloring remove temporally autocorrelated signals, such as heart rate, by decorrelating physiologic signals not associated with the task. This is achieved in the prewhitening method using an iterative autoregressive approach (Barker et al., 2013; Blanco et al., 2018). In contrast, precoloring methods use a temporal filter (smoothing) matrix to estimate the temporal correlation of fNIRS data (Huppert et al., 2016). In both cases, careful inspection and removal/correction of motion artifact is required as they can strongly affect the accuracy or prewhitening / precoloring algorithms (Blanco et al., 2018). These methods were not used in our studies.

Step 5 – enhancing the reliability of brain activity signals

It is possible to reduce further the possibility of confounding systemic physiological change in the detected fNIRS signal using three additional strategies.

Short-separation regression. The first strategy is to include the parallel usage of short- (ideally ~8 mm in adults and ~ 5 mm in infants) and long- (ideally ~3-5 cm in adults and ~ 2-3 cm in infants) separation channels (Brigadoi et al., 2015). This approach enables “short-separation regression” (i.e., regresses out the signal changes in the extracerebral layer from the long-

separation channel) and maximizes sensitivity to the cerebral cortex while minimizing the sensitivity to the extracerebral layers, therefore improving the recovery of the estimated hemodynamic response (Saager and Berger, 2005; Gagnon et al., 2012a,b; Saager and Berger, 2011; Gagnon et al., 2014; Funane et al., 2014,2015). Several methods have been developed to perform the regression (e.g., least-squares algorithms, Kalman filtering, a combination of the GLM approach with temporally embedded canonical correlation analysis) (Scholkmann et al., 2014; von Lüthmann et al., 2020a,b).

The strongest advantage of using short-separation strategies over the following two approaches is the lower risk of removing brain activity or failing to properly remove systemic physiological components due to the heterogeneity of the vasculature within the scalp. However, this method requires a specially designed optode holder capable of source-detector arrangement with multiple separations. Such optode holder designs are often heavier and more expensive to manufacture. These drawbacks can limit the use of short-channel separations in the clinical setting.

Alternatively, other approaches that take into consideration the depth sensitivity of the optical signal when measuring cortical hemodynamic changes include 1) multidistance measurement methods (i.e., diffusion theory) (Franceschini et al., 2006), 2) image reconstruction (i.e., DOT) (Hoshi et al., 2016), and 3) the use of TD-fNIRS systems (Wabnitz et al., 2010; Torricelli et al., 2014).

Data-driven approaches. Principle Component Analysis (PCA), and Independent Component Analysis (ICA) can decompose fNIRS into brain activity and physiological confounds. By analyzing the fNIRS components in the spatial and time domain, respectively, these approaches have been shown to separate confound components (e.g., global blood flow in the scalp) from components containing the signal of interest (functional hemodynamic response in neurons) (Kohno et al., 2007; Hu et al., 2011; Santosa et al., 2013; Zhang et al., 2016). These methods require multiple fNIRS channels (Zhang et al., 2016).

Systemic physiological augmented fNIRS. Systemic physiological augmented fNIRS refers to the simultaneous measurement and analysis of fNIRS and system physiological signals (Pfeifer et

al. 2018). Measuring peripheral physiological measurements such as heart rate, respiration rate, respiration volume, arterial (CO₂) concentration, SpO₂, blood pressure, and skin conductance enables researchers to account for the systemic components and regress them from fNIRS signals (Ferrari et al., 2014; Meester et al., 2014; Caliandro et al., 2015; Undina et al., 2019). Additionally, it allows to investigate in detail the relationships of these signals with the fNIRS signals (i.e., heart rate variability and autonomic nervous status, mean arterial pressure and origin of oxygenation changes, the influence of electrodermal activity and respiration on fNIRS data) (Hautala et al., 2009; Tachtsidis and Scholkmann, 2016; Quaresima and Ferrari, 2016).

In this thesis, we used several strategies (i.e., short-separation, global PCA, DOT) enhance the reliability of fNIRS signal.

Step 6 – extraction of the hemodynamic response and statistical analysis

In fNIRS, one of the most common methods for extracting the HRF is the GLM (Tak and Ye, 2014). Borrowed from the field of fMRI, the GLM consists of fitting the recorded optical signal with a linear combination of regressors (i.e., explanatory variables) that reflect the events of a particular stimulus during a specific task (e.g., visual task) (or in our case, events captured on vEEG such as seizures).

Regarding fNIRS, it assumes a linear relationship between changes in hemoglobin concentration changes (i.e., symmetrical or opposite changes in hemoglobin) and each block of a specific task. In addition, the time interval between each block must be sufficiently long (i.e., > 2 s) for this assumption to hold (Dale and Buckner, 1997; Pouliot et al., 2012). Modelling the unknown HRF with the GLM can be performed using a model-strict strategy (i.e., canonical HRF or convolution) (Friston et al., 1998; Glover, 1999) or a model-free strategy (e.g., linear estimation models such as Gaussian basis functions, or using a deconvolution approach such as modelling using consecutive impulse function) (Henson and Friston, 2007; Monti et al., 2011; Santosa et al., 2019). While the first approach is the more accessible and most popular, it is less flexible, as it does not take into account inter and intrasubject variability (Aguirre et al., 1998; Handwerker et al., 2012) or any difference in shape and timing (i.e., duration) of [HbO] and [HbR]. In comparison, more flexible approaches allow for to extract of a more realistic HRF, especially in conditions where the

neurovascular coupling is believed to be altered (e.g., epilepsy) (Glover et al., 1999; Pouliot et al., 2012; Lin et al., 2014; Machado et al., 2021). A significant advantage of the GLM is its strong statistical power (i.e., considers the entire high temporal resolution of the whole fNIRS signal).

Other approaches commonly used to extract the HRF are simple block averaging or, when more statistical power is needed, PCA (Strangman et al., 2003; Zhang et al., 2005, 2021), and independent component analysis (Leung et al., 2005; Kohno et al., 2007).

Once the HRF is extracted, additional statistical tests can be performed (i.e., first-level and second-level analysis). For example, a simple t-statistics (for single contrast) or F-statistics (for multiple contrasts) can be calculated (i.e., first-level analysis). As for the second-level analysis, the choice of analysis (i.e., fixed-effects, random-effects, or mixed-effects analysis) will depend on whether inferences on the study population are made (Çiftçi et al., 2008; Tak et al., 2016). Finally, statistical tests should be applied when assessing channel-specific effects. When only a few channels are employed, statistical inference can be made based on an uncorrected p-value (i.e., Z scores calculated using t- or F-statistic). On the hand, when multichannel fNIRS is used, statistical inference should be adjusted to reduce the risk of the type I error by correcting for multiple comparisons (i.e., Bonferroni correction, Holm correction, false discovery rate control, effective multiplicity correction, random field theory, or permutation tests) (Plichta et al., 2006; Singh et al., 2006; Tak et al., 2016; Uga et al., 2015).

In this thesis, extraction of the hemodynamic response was performed by trial-averaging method (mainly in the first study on healthy participants) and model-free GLM analysis. Additionally, changes in hemodynamics were also assessed directly (i.e., direct analysis of the time course). Due to the imposed heterogeneous nature of our clinical studies, only first-level statistical analysis was performed, which is considered appropriate in our clinical context (Yücel et al., 2021).

6.3.3 Cortical reconstruction

Cortical reconstruction of changes in hemoglobin concentration can be performed on an MRI template, such as the Colin 27 average brain (Holmes et al., 1998) or the patient-specific MRI, and these changes are usually constrained along the cortical surface (Huppert et al., 2017). This thesis,

a structural MRI was obtained, when possible, for each patient. Once an MRI is selected, it must be further processed. The first step is head segmentation, which allows segmenting it into five or six layers (i.e., air, skin, skull, cerebrospinal fluid, grey matter, white matter). Once segmented, a co-registration between the optodes coordinates and the MRI is performed, positioning the optodes precisely on the patient MRI. Therefore, this step requires accurate optode digitization. At this stage, some minor corrections can be applied to the segmentation and/or co-registration if needed.

These preprocessing steps on the MRI are essential to obtain a sensitivity matrix (i.e., solving the forward problem) and inverse the sensitivity matrix (i.e., solving the inverse problem). The sensitivity profiles for each source-detector measurement can be estimated by modelling the light transport in tissue using Monte Carlo simulations offered by different packages or by diffusion approximation. Then, the inverse problem can be solved by regularization methods such as Tikhonov (e.g., depth weighted minimum Norm Estimate) ([Hämäläinen & Ilmoniemi, 1994](#)).

Several software support image reconstructions ([Schweiger and Arridge, 2003](#); [Gibson and Dehghani, 2009](#); [Aasted et al., 2015](#); [Cai et al., 2021](#)).

This thesis used the image reconstruction pipelines offered in AtlasViewer and NIRSTORM.

CHAPTER 7 – MANUSCRIPT #1

Multichannel Wearable fNIRS-EEG System for Long-Term Clinical Monitoring

Ali Kassab^a, Jérôme Le Lan^b, Julie Tremblay^c, Phetsamone Vannasing^c, Mahya Dehbozorgi^b, Philippe Pouliot^{b,e}, Anne Gallagher^c, Frédéric Lesage^b, Mohamad Sawan^b, Dang Khoa Nguyen^{a,d}

^aResearch Center, Centre Hospitalier Universitaire de Montréal, Université de Montréal, Montréal, Québec, Canada, H2X 0A9; ^bDepartment of Electrical Engineering, École Polytechnique de Montréal, Montréal, Québec, Canada, H3T 1J4; ^cResearch Center, Hôpital Sainte Justine, Université de Montréal, Montréal, Québec, Canada, H3T 1C4; ^dDepartment of Neurology, Hôpital Notre-Dame (Centre Hospitalier de l'Université de Montréal), Montréal, Québec, Canada, H2L 4M1; ^eResearch Center, Montreal Heart Institute, Montréal, Québec, Canada, H1T 1C8

This article addresses the first objective of this thesis, which was to develop and validate a hybrid whole-head compact and portable EEG-fNIRS system for long-term monitoring in the neurological clinical setting. This article was published in *Human Brain Mapping* in 2018 ([Kassab et al., 2018](#)).

7.1 Abstract

Continuous brain imaging techniques can be beneficial for the monitoring of neurological pathologies (such as epilepsy or stroke) as well as neuroimaging protocols involving movement. Among existing ones, functional near infrared spectroscopy (fNIRS) and electroencephalography (EEG) have the advantage of being non-invasive, non-obstructive, inexpensive, yield portable solutions and offer complementary monitoring of electrical and local hemodynamic activities. This paper presents a novel system with 128 fNIRS channels and 32 EEG channels with the potential to cover a larger fraction of the adult superficial cortex than earlier works, is integrated with 32 EEG channels, is light and battery-powered to improve portability, and can transmit data wirelessly to an interface for real-time display of electrical and hemodynamic activities. A novel fNIRS-EEG stretchable cap, two analog channels for auxiliary data (e.g., electrocardiogram), eight digital triggers for event-related protocols and an internal accelerometer for movement artifacts removal contribute to improve data acquisition quality. The system can run continuously for 24h. Following instrumentation validation and reliability on a solid phantom, performance was evaluated on 1) 12 healthy participants during either a) a visual (checkerboard) task at rest or while pedalling on a stationary bicycle; or b) a cognitive (language) task; and 2) 4 patients admitted either to the epilepsy (n=3) or stroke (n=1) units. Data analysis confirmed expected hemodynamic variations during validation recordings and useful clinical information during in-hospital testing. To the best of our knowledge, this is the first demonstration of a wearable wireless multichannel fNIRS-EEG monitoring system in patients with neurological conditions.

7.2 Introduction

Functional neuroimaging techniques such as positron emission tomography (PET), single-photon emission computed tomography (SPECT) and functional magnetic resonance imaging (fMRI) have allowed significant advances in our understanding of the brain and its disorders. Each has its methodological strengths and limitations. Limitations include their bulkiness, high cost, exposure to radiation (PET, SPECT), high sensitivity to movement, complex statistical analysis (fMRI), need for the participant to lie down in a confined area and inability for continuous monitoring. Functional near-infrared spectroscopy (fNIRS) is an emerging non-invasive, non-ionizing and

relatively low-cost neuroimaging technique that uses the ability of light in the near-infrared spectrum (700-1000 nm) to penetrate biological tissue to assess changes in oxyhemoglobin (HbO_2), deoxyhemoglobin (Hb), blood volume, and tissue oxygen availability with high temporal resolution [Jöbsis et al., 1977; Ferrari et al., 1985; Villringer and Chance, 1994]. Technical and methodological advances have allowed fNIRS to become a relevant research tool in neuroscience [Wolf et al., 2007; Leff et al., 2011; Ferrari and Quaresima, 2012; Torricelli et al. 2014; Ehlis et al., 2014; Boas et al., 2014; Kopton and Kenning, 2014; Naseer and Hong, 2015; Mihara and Muiyai, 2016] and as a clinical tool in the evaluation and monitoring of critically ill neonates and infants notably during cardiac surgeries [Edmonds et al., 2004; Denault et al., 2007; Murkin and Arango, 2009; Cerbo et al. 2012].

Briefly, near-infrared light is projected onto the scalp by optical fibers (sources) and transmitted through the skull [Lloyd-Fox et al., 2010; Scholkmann et al., 2014]. Photons penetrate and propagate diffusely into superficial brain tissue. While some photons are absorbed by chromophores (mainly hemoglobin), others are reflected back and captured by sensor probes (detectors) placed at a certain distance from transmitting optical fibers [Gratton et al., 1994]. By using one wavelength more sensitive to Hb (e.g. 735 nm) and another more sensitive to HbO_2 (e.g. 830 nm), variations in amplitude of backscattered light can be used to infer on local changes in blood oxygenation [Delpy et al., 1988; Cooper et al., 1996]. Furthermore, assuming a constant hematocrit, changes in total hemoglobin ($\text{HbT} = \text{HbO}_2 + \text{Hb}$) can be used as a proxy of cerebral blood volume (CBV) variations [Madsen and Secher, 1999]. In essence, fNIRS is a neuroimaging technique based on the same fundamental principles underlying the pulse oximeter. However, while the latter is a tool now widely used in hospitals to monitor peripheral blood oxygenation, brain fNIRS has had only timid penetration in clinical research and practice [Obrig, 2014]. This is partly explained by certain limitations of current fNIRS systems: a) many have a small number of channels that limits spatial sampling; b) some restrict optodes to the forehead to avoid hair contamination due to the low acquisition chain sensitivity ; c) the majority are neither truly compact (wearable), nor wireless, hampering its use at the bedside or in fields requiring mobility (e.g. rehabilitation); d) all do not seamlessly integrate simultaneous electroencephalography (EEG) monitoring (the only other technique that can monitor brain activity for long duration at the bedside) when required.

The current paper presents a safe and robust high-channel-count combined fNIRS-EEG prototype composed of 32 infrared light sources, 32 photodetectors, and up to 32 EEG channels. Each source can be coupled to four detectors, offering a total of 128 fNIRS channels. In addition to standard measurements on a tissue-equivalent phantom, we present the validation and performance of our prototype through a series of mobile and stationary tasks on healthy subjects as well as preliminary experience with the prototype in diverse clinical settings.

7.3 Material and Methods

7.3.1 General Description of the Portable fNIRS-EEG Prototype and Headgear

Our system is composed of a full head cap with optodes and a control module, linked together with light electrical wires. Three lightweight (~ 200 g) NIRS-EEG caps were designed to accommodate different head sizes to allow the sensor elements to maintain an orthogonal orientation to the scalp: small (head circumference ~ 53 cm), medium (53-58 cm) and large (~ 58 cm). These full-head caps were made of elastic bands and integrated 3D-printed round plastic sockets (separated ~ 3 cm) designed to maintain probes and electrodes in place in close contact with the skin. A hole within sockets allowed users free access to move hair aside from the light path before fastening the optodes. A dark woolen fabric worn over the optical probes served to improve probe-tissue-contact and shield ambient light. A questionnaire was used to assess subject comfort during installation and recording.

NIRS emitter and detector circuits fit on 0.95 cm^2 round printed-circuit boards (PCB) that are packaged in a 3D-printed plastic housing to plug into cap connectors. Inside the housing, a smooth spring pushes the sensor towards the head, providing improved light coupling between scalp and optode, limiting infrared light scattering between the cap and the scalp, while connector design prevents ambient light pollution. Furthermore, we developed a separate connector and socket that can combine both emitter and detector for short distance (1 cm) channels. This optode is meant to measure extracortical hemodynamics.

The prototype can retrieve information from the 128 fNIRS channels and 32 EEG channels (Figure 25).

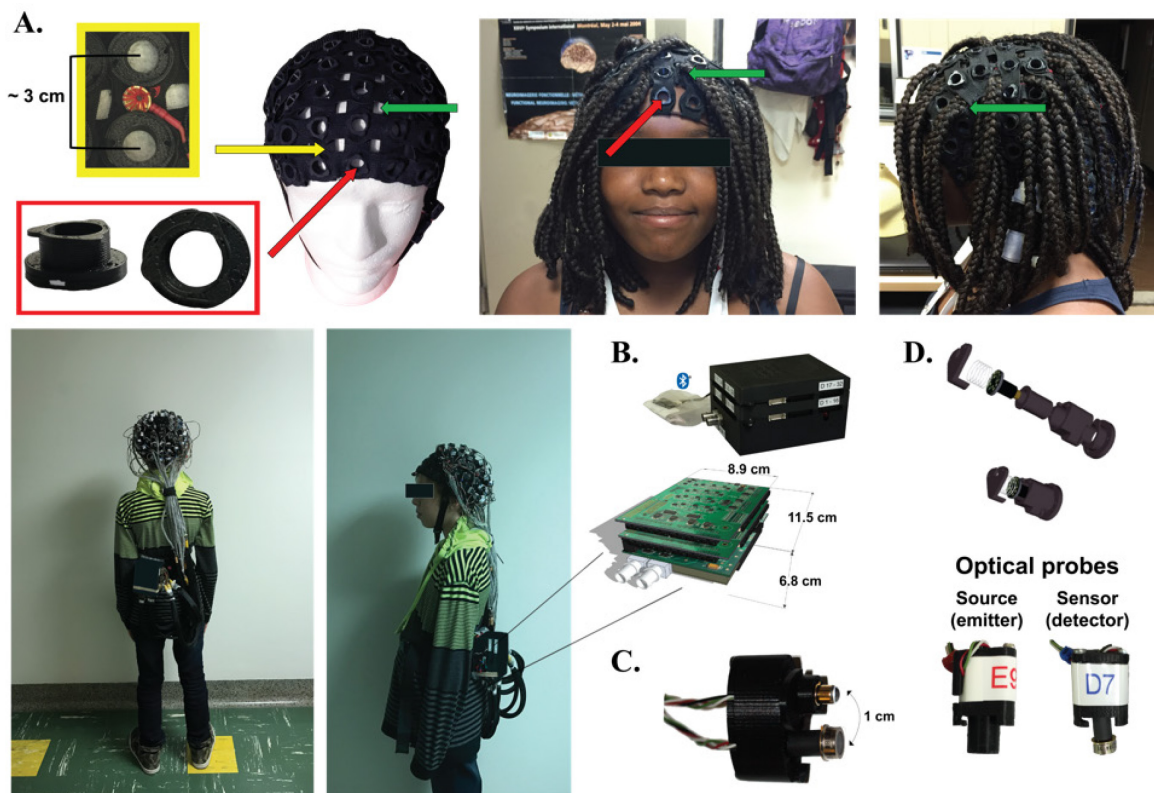


Figure 25 – NIRS-EEG prototype parts including fNIRS-EEG caps. (A), control module (B), double optodes to gather signal from superficial layers (C) and optode design (D). Yellow arrow shows the integration of EEG electrodes between NIRS sockets (red arrows). Opening (wholes) in the cap (green arrows) allow better removal of dense long hair.

During an acquisition, the control module gathers 8 EEG and 4 NIRS data samples at a time, then proceeds with data packing and sends them on a serial port towards a computer through a universal serial bus (USB) cable or a Bluetooth bridge device. A graphical user interface (GUI) developed with LabVIEW retrieves data packets for real-time processing. The GUI can display a total of 294 curves (256 NIRS curves for 128 channels times 2 wavelengths, 32 EEG curves, one curve for the digital triggers, 3 accelerometer curves and 2 auxiliary analog curves) and record them for post-processing. The power consumption during an acquisition using 32 emitters and 32 detectors at full illumination is 2.4 W when a USB cable is used, and 2.6 W with the Bluetooth link. In the

worst-case scenario, with the 7.4 V, 10 Ah battery, the prototype can run an acquisition uninterrupted over a period of 24 hours (**Figure 26**).

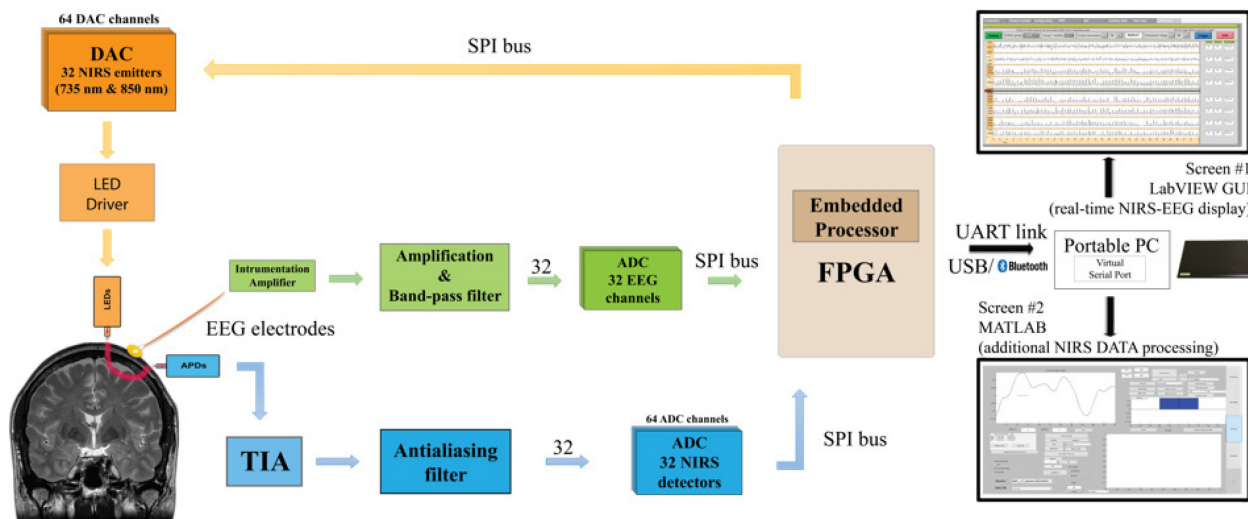


Figure 26 – Global architecture of NIRS-EEG prototype.

7.3.2 EEG and NIRS Circuitry

The EEG acquisition chain consists of amplification and filtering of the difference between measurement and reference electrodes. An instrumentation amplifier at the front-end cuts the common mode interference and noise while amplifying the signal by 100, then a bandpass filter is applied between 0.1 and 100 Hz, and the signal is once again amplified by 100. A reference circuit places the head at a potential of 2.5 V which contains feedback signals from two electrodes placed on the left and right mastoids for common mode interference rejection. The EEG acquisition chain is separated as much as possible from the NIRS chain for crosstalk elimination and parallelism implementation. Located in the control module, the four 8-channel analog-to-digital converter (ADCs) dedicated to EEG signals digitize data in parallel with the NIRS signals through their own serial peripheral interface (SPI) bus, recording 320 samples per second for each channel with a resolution of 16 bits.

The NIRS emitter is a small size two-wavelength (735 & 850 nm) light-emitting diode (LED) from Epitex, and the detector is an avalanche photodiode (APD) S2384 from Hamamatsu coupled with a transimpedance amplifier (TIA) circuit, embedded on the round PCB; the current-voltage gain is

set at 10 MV/A, with a measured 3 dB frequency cut-off of 28 kHz. A negative high voltage (around -150V), generated on the control module by a high-voltage direct current (DC)-to-DC converter regulator (EMCO, CA02-5N), biases all the APDs to provide enough sensitivity to detect diffused infrared light and is current-limited for patient protection.

On the control module, eight 8-channel digital-to-analog converters (DAC) set the illumination intensity for both wavelengths of each emitter, while four 8-channel ADCs, preceded by anti-aliasing filters, digitized amplified TIA measurements with a resolution of 16 bits. As the light sources are not modulated, but only time-multiplexed to decrease power consumption and increase safety, the duration of light emission and detection has to be as short as possible to allow sampling from all 128 channels in 1/20th of a second (20 Hz). This was made possible by maximizing the frequency cut-off value of the TIA. For each wavelength of every emitter, a stabilizing period of time precedes the sampling of the four coupled detectors. For each detector, 8 samples are averaged, and 8 other samples taken in the dark are subtracted to reject ambient lighting and interchannel crosstalk, improving SNR.

LED power consumption is drastically decreased by time-multiplexing: the pulse duration is equal to 390 μ s. At maximal LED illumination, the equivalent total illumination power is 140 μ W for each wavelength, reducing the risks of tissue heating. The duty cycle of the gathered emitters is 0.5, meaning that the light emission is equivalent to one LED emitting 50 % of the time. Sensitivity was, furthermore, improved by maximizing the gain of APDs: the bias voltage is set separately for each APD through potential dividers adapting the unique high voltage signal coming from the regulator.

7.3.3 Digital Architecture

The embedded circuitry consists of three stacked PCBs and battery for a total size of 12 x 9 x 7 cm³ and a weight of 650 g. The first PCB contains an Altera Cyclone III low-power Field-Programmable Gate Array, flash memory and random-access memory to control through SPI buses the acquisition chains of different modules. It also contains the high-voltage regulator and its controlling circuitry, several regulators for different voltage supplies (5 V for analog parts and 3.3 V for digital parts), and the protection and low-power-detection circuits for a rechargeable Li-Ion

7.4 V, 10 Ah battery. An accelerometer is included on this same PCB, providing movement information along the three axes at a rate of 50 Hz for each axis. Two additional external 3D accelerometers can be added on the subject's head if necessary. This data can be used to quantify movement during a task (e.g. gait), and help distinguish, after an acquisition, artifact movement from hemodynamic variations. Also, two Bayonet Neill–Concelman (BNC) connectors can be used to plug an external analog signal for simultaneous digitalization at 340 Hz with 12-bit resolution, for example, electrocardiogram or analog trigger. An optical isolation on SPI lines prevents the prototype from being possibly connected to the power grid, protecting the patient from leakage path. Eight digital triggers complete the additional features; these help identify and synchronize with data 256 different events during event-related potential protocols. The two other PCBs are identical and contain the 32 EEG acquisition chains (16 on each board), and the DACs and ADCs for infrared light illumination and detection, the anti-aliasing filters, and the connectors towards the sensors and electrodes.

The link between the control module and the computer is either a UART RS-232 serial port emulated on a USB cable by a FTDI chip, or a Bluetooth serial port module (OBS421 from connectBlue), able to transmit the required 328 kbps bit rate during an acquisition. The developed communication protocol includes transfer error detection and allows ulterior interpolation of data if packets are lost during their transmission. Through USB cable, the number of lost data is negligible, contrary to Bluetooth communication, where interferences and set-up modifications can alter signal quality; in this case, the protocol can support signal loss for three seconds without the need to start over an acquisition. The data is sent to a LabVIEW-based interface which provides a user-friendly GUI for interaction with the hardware allowing easy configuration of important system parameters and data acquisition. Prior to an acquisition, the user is invited to configure specific parameters: for each emitter, its illumination power, and its four associated detectors, and the APD common bias voltage. These parameters and comments are recorded in a configuration file along with data, and can be imported from a previous acquisition. A calibration window helps detect if one curve is saturating or does not receive enough light, indicating a need to change a parameter or verify optode installation. In addition to manual calibration, the software has an auto-calibration function that can increase or reduce the emitted light in order to obtain adequate SNR.

The curves are recorded in real-time in a LabVIEW format. A Matlab script imports data towards HomER format [Huppert et al., 2009] for further in-depth data processing.

7.3.4 Phantom studies

For phantom validation studies, we used a solid optical phantom made of polyester resin, to which India ink was added as an attenuation agent and TiO₂ as a diffusive agent (coefficient at a wavelength of $\lambda = 758 \text{ nm} = 0.017 \text{ mm}^{-1}$ and diffusion coefficient = 0.7 mm^{-1}). After coupling one single detector to one single light source at 4 cm of distance, we first applied different light intensities and avalanche gains to study the influence of these factors on baseline value and noise amplitude to DC level ratio. Then a 1 Hz sinusoidal light signal similar to in vivo signals was injected in the phantom to compute the SNR with different avalanche gains.

7.3.5 Patient Population

We then conducted signal validation experiments on 12 healthy (6 males, age: 13-27 years) adults and children using either a visual task or two standard language paradigms. The prototype was subsequently tested in four distinct clinical scenarios on patients: a) a patient with limb-shaking transient ischemic attacks admitted to the stroke unit; b) a patient admitted at the epilepsy monitoring unit (EMU); c) a patient admitted to the intensive care unit for status epilepticus; d) a patient undergoing language lateralization assessment in the neuropsychology department. Experiments were approved by our ethics committee and informed consent was obtained from all participants.

7.3.6 Validation and Performance Studies

Preferential coverage allowing higher spatial sampling of certain areas of interest was privileged for these experiments: bilateral occipito-parieto-precentral regions for visual experiments (**Figure 27A**) and bilateral fronto-temporo-parietal regions for language experiments (**Figure 28A**). To ensure that the same brain areas were measured in each subject, optodes localization was determined in relation to the 10-20 system. We further measured the distance from three fiducial points (nasion, left and right pre-auricular) to the horizontal level at Fp1/Fp2, T3 and T4 respectively, and took front and side pictures before and after to verify if any shifting had occurred. To account for installation time and constant probe installation across participants, all installations

were done by the same individuals (AK, PV). Visual and language stimuli were presented electronically using E-Prime 2.0 software (Psychology Software Tools, Pittsburgh, PA) and a BNC digital output cable was used to send trigger signals directly to our prototype.

To evaluate the mobility of our system, a modified version of the experiment performed in Piper et al. (2004) was done during the first validation protocol (**Figure 27A**). It consisted of a visual pattern reversal task (subject B1 to B8) while participants were sitting on a training bicycle that was installed in an acoustically shielded and dimmed room. The task was performed twice: 1) a first time while the participants were sitting still on the bicycle and 2) a second time while the participants were pedalling at an average pace of 15 km/h (10-20 km/h). To evaluate the quality of our EEG (and ERPs), we used stackable jumper/linker cables to simultaneous recording electrophysiological signals with a commercial EEG system (Neuroscan SynAmps2 EEG/EP, Compumedics Ltd.). The signals were amplified by Neuroscan Synamp amplifiers (Compumedics, Charlotte, NC, USA), digitized at a rate of 500 Hz and recorded by Neuroscan Scan 4 Acquire Software (Compumedics, Charlotte, NC, USA).

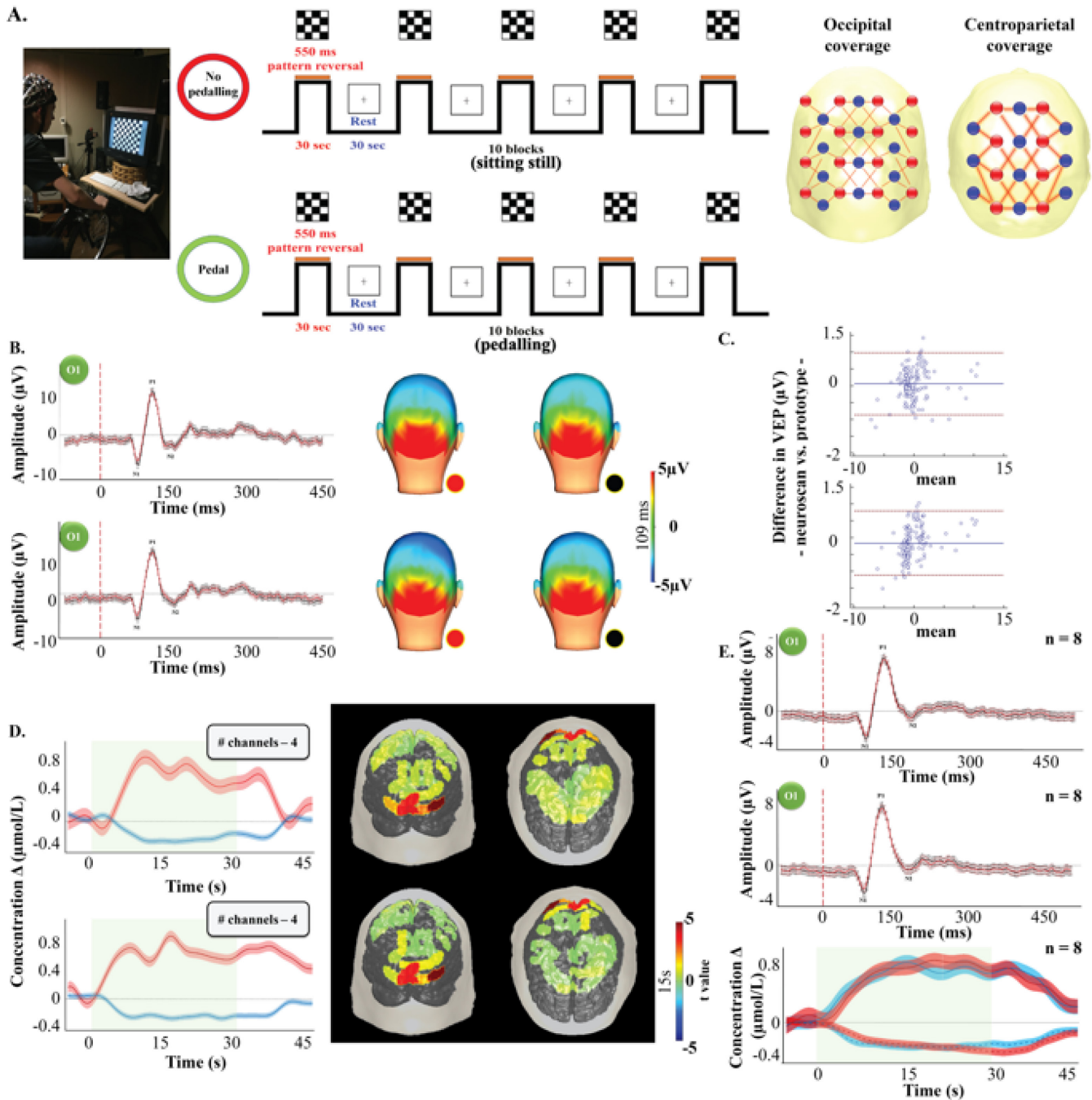


Figure 27 – Channel layout and description of the visual paradigm. (A). P₁₀₀ time course and topography over the visual cortex averaged along every stimulation blocks while sitting still (upper row) and pedalling (bottom row) for participant B4. Black line/dot: Neuroscan system. Red line/dot: fNIRS-EEG prototype (B). Results from the Bland–Altman analysis for the P₁₀₀ amplitude changes at rest (left) and while pedalling (right) between our prototype and Neuroscan. Dotted red line: limits of agreement. Solid blue line: bias (C). Δ[HbO₂] (red line) / Δ[Hb] (blue line) time courses over the visual cortex and Δ[HbO₂] topography (15 sec), with color-coded t-value after Bonferroni-Correction for multiple comparison ($p < 0.0004$), averaged over 8 visual stimulation periods in subject B4 obtained from 5 channels over the visual cortex while sitting still (upper row) and pedalling (bottom row). Red and blue shaded area: standard error of the mean for Δ[HbO₂] and Δ[Hb] respectively. Green shaded area: stimulation period (D). Average P₁₀₀ time course from all 8 participants obtained with our system (solid red line) and the Neuroscan system (solid black line) while sitting still (first row) and pedalling (second row) (E).

The second validation protocol consisted of a language study (**Figure 28A**). The handedness of all participants was assessed using the Edinburgh Inventory [Oldfield, 1971]. Four French-speaking participants (subjects L1 to L4) underwent one session of fNIRS recording. The language experimentation included expressive (verbal fluency) and receptive (passive story listening) language tasks in a block design paradigm [Gallagher et al. 2007]. To evaluate the quality of the fNIRS component, we performed for each participant a second recording within 4-6 weeks using a well-established multi-channel frequency-domain device spectrometer (Imagent Tissue Oxymeter, ISS Inc., Champlain, Illinois, USA) composed of 50 laser diodes (690 nm and 830 nm) modulated at 110.0 MHz and 16 photomultiplier tube detectors. Optical intensity (DC), modulation amplitude (AC), and phase data were acquired with a sampling rate of 15 Hz by its own software (ISS Corporations ‘‘Boxy’’).

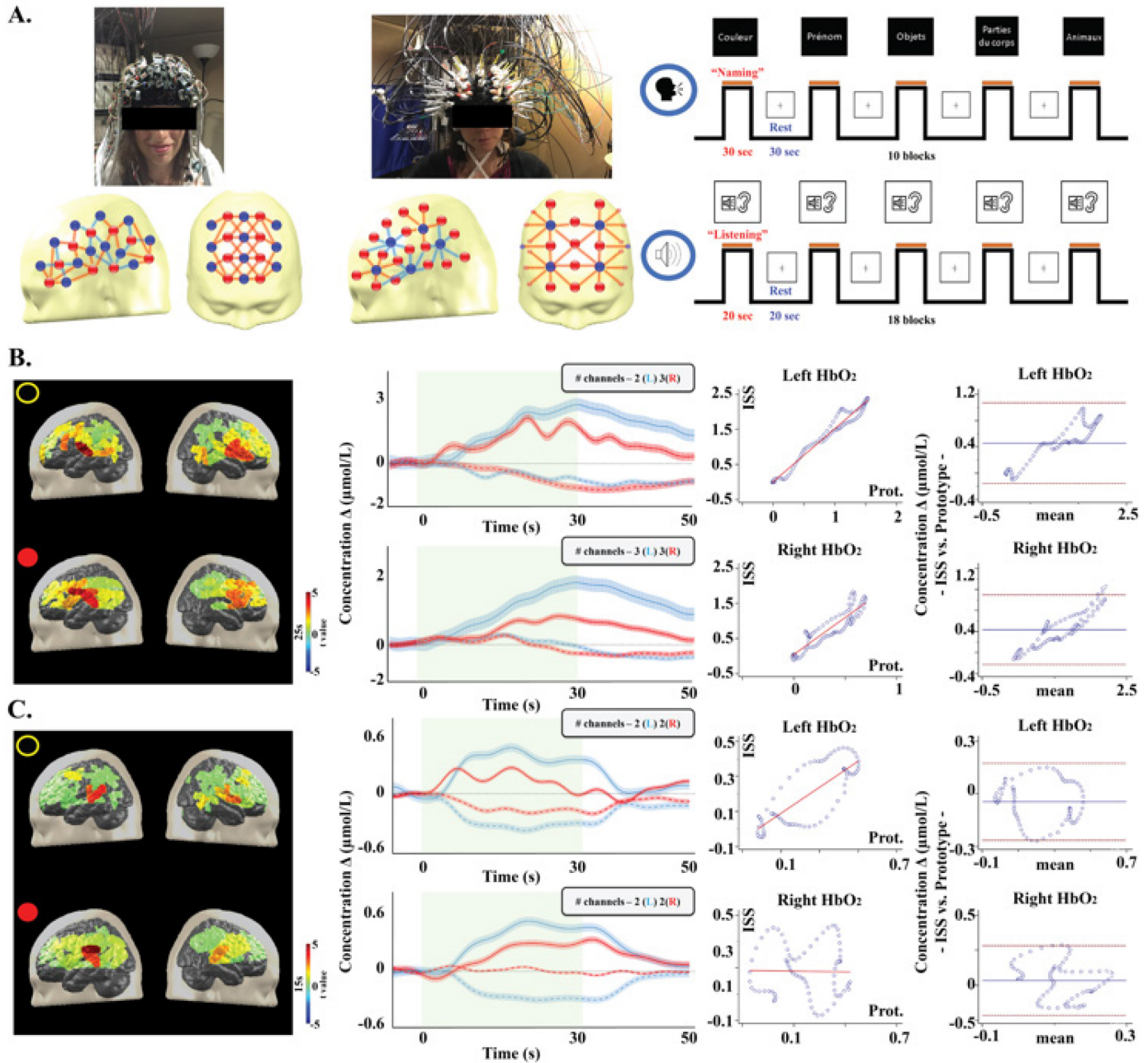


Figure 28 – Channel layout and description of the language paradigm. (A). Δ [HbO₂] topography (15 sec), with color-coded t-value after Bonferroni-Correction, and Δ [HbO₂] (straight line) / Δ [Hb] (dotted line) time courses over the Broca area along all stimulation blocks during the listening task in subject L3 and results from the linear regression and Bland–Altman analysis for Δ [HbO₂] (B). Δ [HbO₂] topography (15 sec), with color-coded t-value after Bonferroni-Correction, and Δ [HbO₂] (straight line) / Δ [Hb] (dotted line) traces over the Wernicke area averaged along all stimulation blocks during the naming task in the same subject and results from the linear regression and Bland–Altman analysis for Δ [HbO₂] (C). Black dot / 1st row: ISS system. Red dot / 2nd row: fNIRS-EEG prototype. Left side: blue line. Right side: red line. Dotted red line: limits of agreement. Solid blue line: bias.

An anatomically specific montage was created based on a normalized structural template from the Montreal Neurological Institute or the patient's own MRI to ensure that optical fibres were placed over the region(s) of interest (ROI). This was done using a stereotaxic system (Brainsight TM Frameless39, Rogue Research, Canada), which enables the transfer of ROI, determined by MRI, onto the cap. This procedure allowed us to obtain the best possible montage in terms of source-detector number and locations of the targeted regions for each participant.

7.3.7 Data Processing and Signal Analysis

Processing of the EEG signal: Offline analysis of the raw EEG data was done using with Brain Vision Analyzer 2.0 (Brain Products GmbH, Munich). The pre-processing of the EEG data obtained from the visual task was done in five steps. First, we re-referenced to both linked mastoids and down-sampling to 256 Hz. Then, the data was filtered (1-50 Hz) to remove high- and low-frequency waves and was visually inspected to check for artifacts. We performed an independent component analysis to correct for eye movement artifacts, before segmenting starting at -100 ms before the stimulus onset and ending at 500 ms after the stimulus onset, resulting in 600 ms segments. In a next step, we used the semiautomatic artifact rejection tool to exclude segments having a minimum and maximum amplitude difference of more than 100 μ V. Visually evoked potentials (VEPs) were obtained by averaging times series from -200 to 500 ms of pattern reversal presentations. As for the clinical EEG, a careful examination for interictal spikes and seizures was performed by an expert electroencephalographer (DKN).

Comparison of EEG signals between systems: To quantitatively assess the EEG data obtained from our prototype, an unpaired t-test ($p < 0.05$) was performed against the EEG data acquired by the commercial EEG system (i.e. Neuroscan SynAmps2) after averaging all VEPs obtained while a) sitting still or b) pedalling. Furthermore, to visualize the agreement between the VEPs (fNIRS-EEG prototype vs. Neuroscan), we used the Bland-Altman method with 95% limits of agreement ($SD \pm 1.96$) [Bland and Altman, 1986, 1996].

Processing of the fNIRS signal: All NIRS data were first processed with the toolbox HomER [Huppert et al., 2009]. Every channel was bandpass-filtered between 0.05 and 0.1 Hz to retrieve the slow hemodynamic variations while eliminating slower drifts. Channels with a raw DC

intensity at the level of the equipment noise or with a standard deviation higher than 20 % were considered as artefactual and excluded from the analysis. Relative changes in HbO₂ and Hb for each measurement position were calculated from the raw light intensity by applying the modified Beer-Lambert law [Kocsis et al., 2006]. For each healthy participant, concentration changes in HbO₂ and Hb were averaged across the blocks. A differential path length factor correction was also applied to generate concentration values. All concentrations represent a variation during activation relative to baseline values, thus are expressed as delta concentrations. Significant activation (i.e., delta concentration amplitude > baseline noise) in the regions of interest (ROIs) for visual (i.e. visual cortex) and language (i.e. Broca's area, Wernicke's areas, and contralateral homologous regions) tasks, as well as for clinical monitoring (e.g. epileptic focus) were identified by computing a two-tailed paired t-test and were further used to qualitatively assess the results. To account for multiple comparisons, p-values were Bonferroni-corrected, setting the significance level after correction to $p = 0.05$. The t-values of the significant ΔHbO_2 channels were color-coded and partially projected onto the gray matter surface of the MNI standard brain model or own MRI scan.

Comparison of fNIRS signals between systems: For the visual task, we used an unpaired (student's) t-test ($p < 0.05$) to test for differences in the mean value of HbO₂ and Hb between 10 s and 30 s after activation onset between the two conditions (i.e. sitting vs. pedalling) during visual stimulation. Group averages for each condition were also calculated. Time course of ΔHbO_2 and ΔHb are displayed with their standard error of mean (SEM). The Dice similarity coefficient (DSC) was used to compare visual mapping obtained with each condition [Dice LR, 1945]. Based on the literature [Zijdenbos et al., 1994; Fleiss JL, 1982] a $\text{DSC} \geq 0.80$ was deemed to reflect very good concordance between maps, a $\text{DSC} \geq 0.70$ was deemed to reflect good concordance between maps, and a $\text{DSC} < 0.70$ was associated with poor concordance. Finally, a one-way ANOVA on DSC values was performed to compare fNIRS visual mapping concordance between the two conditions. For the language tasks, we performed an unpaired (student's) t-test ($p < 0.05$) to compare mean values of HbO₂ and Hb (10 s to 30 s and 5 s to 20 s after activation onset for the fluency and listening task respectively) between our prototype and ISS. Group averages for each language task and for each system were also calculated. We also calculated a language lateralization index (LI) in the left (LH) and right (RH) hemisphere ROIs [Pujol et al., 1999; Seghier, 2008]: $(\text{LH} - \text{RH}) /$

(LH + RH)), where L is the maximal increase in HbO₂ associated with the naming or semantic language task, obtained from an averaged curve of all channels covering left Broca's and Wernicke's areas and R is the HbO₂ value obtained from an average curve of all channels covering the right mirror regions of left Broca's and Wernicke's areas measured at the same time as the maximal left increase in HbO₂. A value < - 0.10 indicates right hemisphere language dominance, a value > 0.10 indicates left hemisphere language lateralization and a value close to zero ($- 0.10 \leq LI \leq 0.10$) reveals a bilateral language distribution. Concordance between individual language lateralization (or LI) results was computed from both systems using unweighted kappa statistics, which consists of comparing the results of HbO₂ LIs from our prototype and HbO₂ LIs from ISS. Quantitative comparison of hemodynamic changes between our system and ISS was done using the same Blant-Altman method previously described. Under the assumption of independence of measurements, we took every 25th measurement of ΔHbO_2 and ΔHb [Chandrasekeran B. 1971; Cox and Wermuth, 1996]. Qualitative comparison of maps of language activations between the two systems was performed qualitatively.

7.4 Results

7.4.1 Phantom validation

We first carried out some long acquisitions on polyester resin phantom mimicking tissue to confirm software and prototype capability to maintain signal quality over time. Beyond slow drifts associated with LED heating that can be filtered out in post-processing, the system was able to record low level signal without significant change in SNR over time. Over 24 continuous hours, the software was able to record every curve with no data loss. The standard deviation of the signal on phantom (calculated on periods of 60 seconds) was constant and equal to 1.2 mV (for a 5 V ADC input range) from the beginning to the end of the recording.

7.4.2 Physiological Validation

Table 10 shows the demographic characteristics, recording information, comfort scores and results for each participant. Five adults (2M) and three children (3M) were recorded using simultaneously our prototype and the commercial EEG system. As expected, the checkerboard protocol showed a clear and significant ($p < 0.05$) VEP and fNIRS activations over the visual areas in all participants

during both conditions (i.e., sitting still and pedalling). No significant electrophysiological (VEP) or hemodynamical (fNIRS) responses were seen over the precentral and parietal regions.

During the non-pedalling condition, our system recorded a mean P₁₀₀ peak amplitude of $5.80 \pm 0.44 \mu\text{V}$ (time = 109 ms) while a peak amplitude of $5.96 \pm 0.43 \mu\text{V}$ (time = 109 ms) was recorded with Neuroscan. During the pedalling condition, mean P₁₀₀ peak amplitudes of $6.49 \pm 0.48 \mu\text{V}$ (time = 109 ms) and $6.74 \pm 0.49 \mu\text{V}$ (time = 109 ms) were recorded with our system and the Neuroscan, respectively. Individual and group comparison showed no statistical differences for both P₁₀₀ peak amplitudes and latencies measured by the two systems. Linear regression comparing our device to the commercial one showed a group average correlation coefficient of $r = 0.99$ ($p < 0.0001$) during the non-pedalling condition and $r = 0.99$ ($p < 0.0001$) during the pedalling condition. Bland-Altman plot showed a group average difference of $-0.01 \mu\text{V}$ (limits of agreement were -0.34 to $0.31 \mu\text{V}$) during the non-pedalling condition and $-0.02 \mu\text{V}$ (limits of agreement were -0.38 to $0.33 \mu\text{V}$) during the pedalling conditions (**Figure 27B-E**). On an individual basis, statistical comparison of the time course between the two conditions (i.e. sitting vs. pedalling) while performing the visual-task showed, for both systems, a statistically significant difference in three participants (B01, B02, B08) (**Supplementary Figure 1**).

Both sitting still and pedalling generated a positive HbO₂ and negative Hb response over visual areas (V1 and V2) during visual stimulation. In the absence of pedalling, we observed a mean peak hemodynamic response average across all participants of $0.71 \pm 0.08 \mu\text{mol/L}$ for HbO₂ and $-0.34 \pm 0.04 \mu\text{mol/L}$ for Hb. During pedalling, a mean HbO₂ increase of $0.69 \pm 0.08 \mu\text{mol/L}$ and a Hb decrease of $-0.28 \pm 0.04 \mu\text{mol/L}$ was observed. For the channels reaching a significant level of activation, individual-level analysis between the two conditions showed a significant difference for the mean ΔHbO_2 time courses in all participants, while the mean Hb time courses showed a significant difference in 50 % of participants. Activation maps comparison between the two conditions showed very good concordance ($\text{DSC} \geq 0.80$) for cortical visual mapping in seven out of eight (88%) participants (mean $\text{DSC} = 0.89 \pm 0.04$). The one-way ANOVA results showed no statistical differences between groups for DSC ($p = 0.074$).

Table 10 – Average electrophysiological and hemodynamic changes during the visual task.

Participant (sex, age, profession)	Screen distance (cm)	Hair description	Installation time (min)	Comfort scale	VEP ^{Prot.} (μ V)		VEP ^{Neuroscan} (μ V)		Δ HbO ₂ Δ Hb (μ mol)		# rejected trials		Dice (HbO ₂)
					Ss	P	Ss	P	Ss	P	Ss	P	
B1 (F, 21, student)	155	Straight, redheaded, medium	48	9	4.31	4.83	4.53	5.2	0.95 -0.34	0.95 -0.45	1	1	0.87
B2 (M, 24, engineer)	138	Straight, black, short	40	6	3.27	5.48	3.74	6.35	0.64 -0.39	1.12 -0.17	1	2	1.00
B3 (M, 28, engineer)	142	Curly, black, short	51	8	4.63	5.99	5.16	6.24	0.32 -0.17	0.31 -0.14	2	2	1.00
B4 (F, 22, student)	155	Dreads, black, long	77	10	9.89	9.89	10.54	10.39	0.86 -0.32	0.84 -0.32	1	0	0.82
B5 (M, 17, student)	153	Straight, blond, medium	53	9	8.06	8.3	7.51	9.03	0.65 -0.40	0.82 -0.31	0	0	0.72
B6 (M, 13, student)	150	Straight, black, medium	61	7	5.92	5.58	5.86	5.4	1.04 -0.39	1.21 -0.34	2	2	0.90
B7 (M, 15, student)	150	Straight, black, short	47	8	4.59	4.53	4.99	4.55	0.77 -0.37	0.86 -0.20	2	3	0.82
B8 (F, 26, student)	134	Curly, black, long	63	9	6.03	6.63	5.91	6.46	0.73 -0.09	1.06 -0.22	0	1	0.82

F: female, Hb: deoxy-hemoglobin, HbO₂: oxy-hemoglobin, M: male, Neuroscan: commercial EEG system, P: pedalling, Prot.: prototype, Ss: sitting still, VEP: visually evoked potential.

For language tasks, all participants were right-handed and spoke French as their first language. Participant demographics, setup time and comfort scale are presented in **Table 11**. During the passive listening task, our prototype recorded over posterior temporal regions a significant [HbO₂] increase and [Hb] decrease, larger on the left (Wernicke) ($x \Delta[\text{HbO}_2]\text{L} = 0.85 \pm 0.07 \mu\text{mol/L}$, $x \Delta[\text{Hb}]\text{L} = -0.45 \pm 0.04 \mu\text{mol/L}$) than the right ($\Delta[\text{HbO}_2]\text{R} = 0.41 \pm 0.04 \mu\text{mol/L}$, $\Delta[\text{Hb}]\text{R} = -0.25 \pm 0.03 \mu\text{mol/L}$) in three participants (L1, L3, L4). Subject L2 exhibited a larger [HbO₂] increase ($\Delta[\text{HbO}_2]\text{L} = 0.10 \pm 0.02 \mu\text{mol/L}$ vs. $\Delta[\text{HbO}_2]\text{R} = 0.72 \pm 0.02 \mu\text{mol/L}$) and [Hb] decrease ($[\text{Hb}]\text{L} = -0.18 \pm 0.06$ vs. $\Delta[\text{Hb}]\text{R} = -0.45 \pm 0.04$) over the right posterior temporal region. In comparison, the ISS also recorded a significantly larger [HbO₂] increase ($x \Delta[\text{HbO}_2]\text{L} = 0.84 \pm 0.07 \mu\text{mol/L}$ vs. $x \Delta[\text{HbO}_2]\text{R} = 0.51 \pm 0.03 \mu\text{mol/L}$) and [Hb] decrease ($x \Delta[\text{Hb}]\text{L} = -0.34 \pm 0.04 \mu\text{mol/L}$ vs. $x \Delta[\text{Hb}]\text{R} = -0.25 \pm 0.03 \mu\text{mol/L}$) over the left posterior temporal area in L1, L3, L4 and a larger [HbO₂] increase ($\Delta[\text{HbO}_2]\text{L} = 0.85 \pm 0.06 \mu\text{mol/L}$ vs. $\Delta[\text{HbO}_2]\text{R} = 1.72 \pm 0.02 \mu\text{mol/L}$) and [Hb] decrease ($[\text{Hb}]\text{L} = -0.21 \pm 0.04$ vs. $\Delta[\text{Hb}]\text{R} = -0.69 \pm 0.06$) over the right posterior temporal area in L2. For both systems, laterality index (LI) computed from the maximum [HbO₂] peak over Wernicke's area and the contralateral homologous region showed left hemisphere dominance for receptive language in participant L1, L3 and L4 and right dominance for participant L2 ($\kappa = 1.0$, $p < 0.0001$). Mean time to peak for HbO₂ was 16 ± 3 s with our system and 15 ± 3 s with ISS ($p > 0.05$).

During the naming task, our system recorded a significantly larger [HbO₂] increase ($x \Delta[\text{HbO}_2]\text{L} = 1.53 \pm 0.15 \mu\text{mol/L}$ vs. $x \Delta[\text{HbO}_2]\text{R} = 0.69 \pm 0.08 \mu\text{mol/L}$) and [Hb] decrease ($x \Delta[\text{Hb}]\text{L} = -0.24 \pm 0.07 \mu\text{mol/L}$ vs. $x \Delta[\text{Hb}]\text{R} = -0.28 \pm 0.06 \mu\text{mol/L}$) over the left inferior frontal area (Broca) in all four participants. A significantly larger [HbO₂] increase ($x \Delta[\text{HbO}_2]\text{L} = 2.67 \pm 0.26 \mu\text{mol/L}$ vs. $x \Delta[\text{HbO}_2]\text{R} = 1.74 \pm 0.13 \mu\text{mol/L}$) and [Hb] decrease ($x \Delta[\text{Hb}]\text{L} = -0.32 \pm 0.15 \mu\text{mol/L}$ vs. $x \Delta[\text{Hb}]\text{R} = -0.28 \pm 0.09 \mu\text{mol/L}$) over the left Broca area in all participants was also observed with ISS. Calculated LIs for both systems showed left hemisphere dominance for expressive language for all participants ($\kappa = 1.0$, $p < 0.0001$). Mean time to peak for HbO₂ was 22 ± 3 s (vs. 26 ± 2 s for ISS) ($p > 0.05$).

A strong correlation ($0.7 < r \leq 1.0$) for left $\Delta[\text{HbO}_2]$ between the two systems was obtained during the passive listening task for L1, L3 and L4. Right $\Delta[\text{HbO}_2]$ showed a strong correlation for L1,

L2 and L4 and a weak correlation ($0.2 < r < 0.4$) for L3. A strong or moderate ($0.4 < r < 0.7$) correlation was found for left or right $\Delta[\text{Hb}]$ for L1, L2 and L4, while a weak correlation was found for right Hb in L3 (data not shown). For the naming task, a strong correlation for left and right $\Delta[\text{HbO}_2]$ was obtained for all participants, except for L4 in which a weak correlation was observed for left $\Delta[\text{HbO}_2]$. A strong correlation for left or right $\Delta[\text{Hb}]$ was found in three participants (L2, L3, L4) and a weak one for L1 (data not shown). Bland-Altman analysis of left and right $\Delta[\text{HbO}_2]$ for each participant can be found in **Table 11**. For the listening task, an overall mean difference of $0.19 \pm 0.17 \mu\text{mol/L}$ (limits of agreement: -0.38 to $0.75 \mu\text{mol/L}$) was calculated for left $\Delta[\text{HbO}_2]$ and $0.32 \pm 0.14 \mu\text{mol/L}$ (limits of agreement: -0.21 to $0.85 \mu\text{mol/L}$) for its right counterpart. For the naming task, an overall mean difference of $0.81 \pm 0.21 \mu\text{mol/L}$ (limits of agreement: -0.26 to $1.87 \mu\text{mol/L}$) was calculated for left $\Delta[\text{HbO}_2]$ and $0.69 \pm 0.16 \mu\text{mol/L}$ (limits of agreement: -0.30 to $1.68 \mu\text{mol/L}$) for right $\Delta[\text{HbO}_2]$. **Figure 28** shows the hemodynamic curves and language maps during language tasks, as well as the linear regression analysis and Bland-Altman analysis for a representative participant (L3).

Table 11 – Average hemodynamic changes during the language task.

Participant (sex, age, profession)		L1 (F, 26, student)	L2 (M, 22, musician)	L3 (F, 18, student)	L4 (F, 30, student)		
Screen distance (cm)	Prot. / ISS	150	142	147	147		
Hair description	Prot. / ISS	straight, black, long	straight, black, medium	straight, brown, long	straight, black, long		
Installation time (min)	Prot. / ISS	55 / 86	49 / 92	53 / 87	50 / 85		
Comfort scale	Prot. / ISS	5 / 2	9 / 2	8 / 4	8 / 4		
Naming task	L – ΔHbO₂ / ΔHb (μmol)	Prot.	0.75 ± 0.08 -0.42 ± 0.04	2.28 ± 0.24 -0.48 ± 0.09	1.53 ± 0.12 -0.05 ± 0.07	1.54 ± 0.15 -0.55 ± 0.07	
		ISS	1.67 ± 0.15 0.26 ± 0.03	3.57 ± 0.35 0.33 ± 0.23	2.40 ± 0.25 -1.04 ± 0.16	3.06 ± 0.28 -0.85 ± 0.19	
	R – ΔHbO₂ / ΔHb (μmol)	Prot.	0.32 ± 0.05 -0.34 ± 0.03	0.91 ± 0.05 -0.01 ± 0.05	0.63 ± 0.03 -0.23 ± 0.05	0.89 ± 0.08 -0.55 ± 0.06	
		ISS	1.08 ± 0.12 0.05 ± 0.02	2.20 ± 0.18 0.09 ± 0.16	1.51 ± 0.13 -0.68 ± 0.09	2.17 ± 0.10 -0.61 ± 0.09	
	# words	Prot. / ISS	16 / 20	13 / 16	20 / 23	16 / 21	
	# rejected trials	Prot. / ISS	1 / 3	2 / 3	3 / 2	3 / 3	
	Correlation coefficient	L HbO ₂	$r = 0.93 (p < 0.001)$	$r = 0.98 (p < 0.001)$	$r = 0.99 (p < 0.001)$	$r = 0.11 (p < 0.001)$	
		R HbO ₂	$r = 0.76 (p < 0.001)$	$r = 0.73 (p < 0.001)$	$r = 0.92 (p < 0.001)$	$r = 0.70 (p < 0.001)$	
	Differences (μmol): mean ± SD	L HbO ₂	0.59 ± 0.13 (0.02-1.15)	1.05 ± 0.31 (0.04-2.01)	0.46 ± 0.22 (-0.27-1.19)	1.14 ± 0.19 (-0.81 - 3.10)	
		R HbO ₂	0.56 ± 0.16 (-0.13 – 1.25)	0.82 ± 0.14 (-0.39 – 2.03)	0.57 ± 0.22 (-0.15 – 1.30)	0.80 ± 0.13 (-0.53 – 2.13)	
	HbO₂ LI (dominance)	Prot. / ISS	0.39 (L) / 0.21 (L)	0.43 (L) / 0.24 (L)	0.41 (L) / 0.23 (L)	0.27 (L) / 0.17 (L)	
	Passive listening task	L – ΔHbO₂ / ΔHb (μmol)	Prot.	1.28 ± 0.10 -0.62 ± 0.05	0.01 ± 0.02 -0.18 ± 0.06	0.50 ± 0.04 -0.28 ± 0.03	0.76 ± 0.07 -0.47 ± 0.05
			ISS	0.83 ± 0.06 -0.25 ± 0.04	0.85 ± 0.06 -0.21 ± 0.04	0.46 ± 0.04 -0.33 ± 0.02	1.23 ± 0.10 -0.45 ± 0.07
		R – ΔHbO₂ / ΔHb (μmol)	Prot.	0.59 ± 0.05 -0.47 ± 0.04	0.72 ± 0.02 -0.45 ± 0.04	0.28 ± 0.03 0.04 ± 0.01	0.37 ± 0.05 -0.32 ± 0.05
ISS			0.55 ± 0.02 -0.25 ± 0.02	1.72 ± 0.02 -0.69 ± 0.06	0.26 ± 0.03 -0.15 ± 0.02	0.71 ± 0.04 -0.36 ± 0.04	
# rejected trials		Prot. / ISS	4 / 4	5 / 5	4 / 4	5 / 5	
Correlation coefficient		L HbO ₂	$r = 0.80 (p < 0.001)$	$r = 0.17 (p < 0.001)$	$r = 0.80 (p < 0.001)$	$r = 0.88 (p < 0.001)$	
		R HbO ₂	$r = 0.66 (p < 0.001)$	$r = 0.94 (p < 0.001)$	$r = 0.02 (p < 0.001)$	$r = 0.96 (p < 0.001)$	
Differences (μmol): mean ± SD		L HbO ₂	-0.22 ± 0.17 (-0.76 – 0.31)	0.31 ± 0.17 (-0.23 – 0.85)	0.46 ± 0.22 (-0.27 – 1.19)	0.21 ± 0.14 (-0.25 - 0.66)	
		R HbO ₂	-0.05 ± 0.04 (-0.54 – 0.43)	0.60 ± 0.22 (-0.12 – 1.33)	0.57 ± 0.22 (-0.14 – 1.30)	0.17 ± 0.05 (-0.01 – 0.34)	
HbO₂ LI (dominance)		Prot. / ISS	0.37 (L) / 0.20 (L)	-0.98 (R) / -0.34 (R)	0.28 (L) / 0.28 (L)	0.35 (L) / 0.26 (L)	

F: female, Hb: deoxy-hemoglobin, HbO₂: oxy-hemoglobin, ISS: Commercial fNIRS system, L: left, M: male, Prot.: prototype, R: right.

7.4.3 *Prototype Validation in Clinical Conditions*

fNIRS-EEG testing in the stroke unit: The prototype was used to investigate a 61 year-old patient admitted to the stroke unit for daily brief episodes of right upper limb shaking and leg weakness, more often while standing up for a prolonged period [Kassab et al., 2016]. Recording was started as the patient was in supine position then in a sitting position. As the patient stood up, his blood pressure decreased gradually from 134/70 to 90/54 after 10 minutes at which point he experienced tremor of the right forearm and hand as well as weakness of both legs and mild dysarthria. fNIRS showed a progressive bilateral decrease in CBV, [HbO₂] and an increase in [Hb] over a one-minute period prior the beginning of the limb-shaking (**Table 12, Supplementary Figure 4 left**). These changes rapidly normalized 15 seconds after the patient sat down and ceased to have any symptoms. Averaging the first 10s of symptom onset, hemodynamic changes were found to be most profound in bilateral right more than left dorsolateral prefrontal cortex and motor area. Similar findings were found in three other episodes of limb shaking triggered by orthostatic hypotension. In all recordings, peripheral oxygen saturation (pulse oximetry) was carefully monitored and remained above 95 %. Simultaneous EEG monitoring showed no epileptiform abnormalities, and only brief diffuse slow (i.e. 6-7 Hz) theta activity more predominantly over the left parasagittal regions at the moment of limb shaking. **Supplementary Figure 4 left** shows blood pressure, hemoglobin concentration curves and EEG while the patient was sitting down and standing up of two episodes during the first monitoring session.

fNIRS-EEG testing in the epilepsy monitoring unit: A 23-year-old female with refractory epilepsy was admitted to the EMU to better assess her condition. During her stay, fNIRS-EEG monitoring was performed at the bedside for several hours over 2 days. A 2 minute-long subtle dyscognitive seizure was recorded starting in the right temporal region with subsequent propagation to the left temporal region based on surface EEG. Hemodynamically, fNIRS revealed an initial brief dip in HbO₂ at seizure onset followed by a larger increase over the middle and posterior portions of the right temporal area (**Table 12, Supplementary Figure 4 right**). A smaller HbO₂ increase in the anterior part of the left temporal region was also seen. A slight decrease in Hb was observed in the right temporal region but more evident over the left temporal region as the seizure evolved (approximately 40 s after the beginning of the seizure). A normalization of HbO₂ and Hb to approximately pre-seizure values occurred 80 s after seizure offset. Peripheral oximetry was above

98% throughout the event. No significant hemodynamic changes were seen elsewhere. SPECT images following the injection of Tc-99m ethyl cysteinate dimer 34 seconds after seizure onset revealed increased cerebral blood flow maximal over the middle and posterior portions of the right temporal lobe as well.

fNIRS-EEG testing in the intensive care unit: A 30-year-old patient with pharmacoresistant right fronto-insular epilepsy was admitted in status epilepticus manifesting as multiple brief (~10s) asymmetrical tonic seizures. Treatment included intravenous lorazepam and phenytoin load, intubation and admission to the intensive care unit. fNIRS-EEG performed at the bedside for 24h recorded 15 brief seizures (without clinical manifestations as the patient was curarized). During these electrical seizures, fNIRS revealed fluctuations in hemoglobin concentration characterized by an increase in $[HbO_2]$ in over both dorsolateral frontal (right more than left) and right lateral temporal regions (**Table 12, Supplementary Figure 5 left**). These changes were associated with a small bilateral increase in $[Hb]$ over the dorsolateral frontal cortices. In the posterior part of the lateral temporal lobe, $[Hb]$ increased on the right, but decrease on the left. Blood pressure and systemic oxygen saturation were stable throughout the monitoring.

fNIRS-EEG testing during neuropsychological evaluation: The prototype was used to assess language hemispheric lateralization in a 51-year-old left-handed patient as part of the neuropsychological work-up done prior to epilepsy surgery. The patient had a past history of hemiconvulsion-hemiplegia-epilepsy (HHE) at the age of 9 months that left her with right spastic hemiparesis and refractory epilepsy. Brain MRI revealed left hippocampal sclerosis and left periventricular gliosis. Neuropsychological evaluation showed significant visuospatial memory impairment compatible with non-dominant hemisphere impairment. Bedside fNIRS performed during expressive language tasks showed right greater than left hemodynamic activations over both Broca and Wernicke's areas (LI over Broca's areas of -0.36) (**Table 12, Supplementary Figure 5 right**). For validation, language fMRI was also obtained, confirming right hemisphere dominance. The patient subsequently underwent a left temporo-insular resection with no language complications.

Table 12 – Clinical data and average changes in HbO₂ concentration during the clinical recordings.

Patient	Age (sex)	Handiness (profession)	Recording duration (# blocs)	Technical issues	Diagnosis	Additional neuroimaging modalities	Δ [HbO ₂] (μ mol/l)
C1	63 (M)	R (retired)	2 x 1 h	None	LS-TIA	MRA: L occlusion of M1, R severe supraclinoid ICA stenosis ASL: decrease rCBF within the L MCA territory	L _H * = -1.50 R _H * = -1.50
C2	23 (F)	R (educator)	10 h	None	Bi-temporal lobe epilepsy	iSPECT: increase CBF over the middle and posterior portions of the right TL	LT = 29.75 RT = 71.09
C3	30 (F)	R (student)	24 h	Helmet not ICU-friendly	Refractory SE	iiSPECT: R posterior temporal seizure focus MEG: temporal spikes from the posterior portion of the insula and R temporal opercula	LF** = 0.49 RF** = 1.63 RT** = 0.51
C4	51 (F)	Right (retired)	8 h (N= 7)	None	Stroke, refractory epilepsy	fMRI: R language dominance	B _L = 0.40 B _R = 0.85 (LI _N = - 0.36)

ASL: arterial spin labeling, B_L: Broca left, B_R: Broca right, F: female, HbO₂: Oxyhemoglobin, ICU: intensive care unit, iSPECT: ictal single position emission computed tomography, iiSPECT: Interictal single positron emission computed tomography, L: left, LF: left frontal, fMRI: functional magnetic resonance imaging, L_H: left hemisphere, LI: laterality index, LT: left temporal, M: male, MEG: magnetoencephalography, MRA: magnetic resonance angiography, rCBF: regional cerebral blood flow, R: right, RF: right frontal, R_H: right hemisphere, RT: right temporal, TL: temporal lobe, *: one session of recording, **: one burst of seizure.

7.5 Discussion

In this paper, we describe a portable multichannel wireless fNIRS-EEG system (32 EEG channels; 32 NIR emitters and 32 detectors, for a total of 128 channels) that allows rapid installation and prolonged simultaneous monitoring of superficial brain electrical and hemodynamic activities at the bedside in various settings. After a first validation on an optical phantom, we successfully demonstrated the performance of our wearable high-channel diffuse optical NIRS-EEG system in both static and mobile conditions using visual and language tasks on healthy individuals.

In regard to the EEG component, expected VEPs were identified in all participants with both the prototype and the commercial EEG system, at rest or during motion, with a good level of agreement and no substantial difference in P_{100} latencies and amplitudes. Interestingly, with both systems, a significant change in P_{100} amplitude was observed in 3 participants during motion versus rest. The effect of exercise on the VEP is beyond the scope of this paper, but prior studies have noted as well that acute and regular exercise can affect the amplitude and/or latency of the different components of VEPs [Delpont et al., 1991; Ozkaya et al., 2003; Ozmerdivenli et al., 2005; Zhao et al., 2009]. In regard to the fNIRS, visual stimulation elicited in all participants the expected activation in visual areas during both non-peddalling and pedalling conditions [Kleinschmidt et al., 1996; Strangman et al., 2002; Hoge et al., 2005; Huppert et al., 2006]. Measured $\Delta[\text{HbO}_2]$ and $\Delta[\text{Hb}]$ was significantly different in terms of amplitude between the resting and pedalling periods at the individual level in all eight participants for $\Delta[\text{HbO}_2]$ and in four subjects for $\Delta[\text{Hb}]$. The heterogeneous response in Hb between both conditions may be due to the fact that HbO_2 is more prone to be influenced by changes in global hemodynamics (e.g. heart rate) than Hb [Obrig et al., 2000; Boas et al., 2004; Huppert et al., 2009; Leff et al., 2011; Kirilina et al., 2012]. In a recent publication, motor-task associated $\Delta[\text{HbO}_2]$ were also found to be affected more than $\Delta[\text{Hb}]$ by pedalling [Piper et al., 2014].

Naming and passive listening tasks elicited an expected increase in $[\text{HbO}_2]$ and decrease in $[\text{Hb}]$ respectively over the inferior frontal and posterior temporal regions predominantly in the left hemisphere [Pujol et al., 1999; Springer et al. 1999] except for one subject with an atypical response [Knecht et al. 2003] during the listening task seen with both our prototype and the

commercial system. In comparison to the latter, our system performed relatively well by showing similar activation maps, no significant difference in the time to peak for [HbO₂] and [Hb] and a good kappa agreement for language dominance. Although heterogeneity in amplitude changes were noted (amplitude differences > 10 %), there was a strong correlation between for left and right Δ [HbO₂] and Δ [Hb] [13/16 (81%) pairs of measurements in each language task]. It must be noted that a range of acceptable concentration variations for cognitive tasks, such as language paradigms, have not yet been reported and concentration values may significantly differ from one system to another [Colier et al.1995; McKeating et al., 1997; Gomersall et al., 1998; Grubhofer et al., 1999; Cho et al., 2000; Yoshitani et al., 2002; Thavasothy et al., 2002; Fellahi et al., 2013; Luengo et al., 2013; Dix et al., 2013; Gunadi et al., 2014; Schneider et al., 2014; Hessel et al., 2014]. Such variability in concentration values between systems have been attributed to device technology (e.g. light source type, quantification method, level of sensitivity to superficial layer, sampling rate) [Wahr et al., 1996; Lloyd-Fox et al., 2010; Gunadi et al., 2014], exact location of optodes, cap differences, as well as performance of each participant.

In regard to in-hospital utilization, initial tests confirmed the feasibility of bedside recordings on patients and revealed potential clinical usefulness. In the neurovascular unit, fNIRS-EEG was able to demonstrate progressive decline in regional cerebral blood volume during postural hypotension in a patient with steno-occlusive disorder leading to transient ischemic attacks. In the epilepsy unit, fNIRS-EEG was able to visualize regional hemodynamic changes throughout a temporal lobe seizure while SPECT could only provide a single snapshot of hemodynamic changes during this seizure. In the intensive care unit, fNIRS-EEG was capable of monitoring seizures in a patient with non-convulsive status. During neuropsychological assessment, adequate language lateralization could be achieved at the bedside with the system in a left-handed patient.

7.5.1 Comparison with other 'portable' fNIRS systems:

To our knowledge, this is the only compact wireless high-channel count EEG-fNIRS device which has undergone such diverse in-lab and in-hospital testing. The growing need to study cortical function outside a tightly controlled laboratory environment without the restrictions of tabletop instruments has led in recent years to the development of wearable and/or wireless fNIRS homemade systems (**Tables 14**). Vaithianathan et al. (2004) were the first to design a semi-

portable fNIRS system for imaging the neonatal brain. However, it was Bozkurt et al. (2005) who performed the first fNIRS recording on an infant with a portable device. Later, a series of motion resistant and multimodal (i.e. ECG, respiration, accelerometers, pulse oximetry, actigraphy) fNIRS devices was developed by the Neural System Group at Harvard [Zhang et al. 2009; Zhang et al., 2011; Zhang et al., 2014]. More recently, the mobility of the prototype version of what is now the NIRSport device was evaluated by Piper et al. (2014) with eight healthy participants performing a hand-gripping task at rest and during pedalling. Moreover, for many years, simultaneous fNIRS and EEG recordings have been done by combining two independent and non-portable systems [Leamy et al., 2011; Flazi et al., 2012, Kaiser et al, 2014, Khan et al., 2013, Putze et al., 2014; Mutalib et al., 2014; Khan and Hong 2017]. Apart from our group (Lareau et al., 2011a,b; Sawan et al., 2012, 2013), only two other groups have designed a true hybrid fNIRS-EEG system albeit testing was limited to only a few healthy participants and with fewer channels (Safaie et al., 2013; von Luhmann et al., 2016).

Parallel progress on homemade fNIRS systems, improvements have been made on commercially available wearable fNIRS systems with now the possibility to measure brain activity on two or more people simultaneously (e.g. fNIR100AW), outdoors or during physical activity (e.g. PortaLite, LIGHTNIRS, NIRSport), with very high spatial sampling (e.g. WOT-100), and/or with cytochrome c oxidase values (e.g. B&W Tek, Avantes, Ocean Optics) (**Table 15**). In comparison to these devices, our system can support a higher number of NIRS optodes that allow sampling of a large portion of the superficial cortex. Furthermore, while several of these companies have made their system compatible with other instruments (ex. EEG), these additional physiological signals come with longer setup time, decrease wearability/mobility and require complex synchronization.

While not the focus of this work, an important feature of our system was the design of an fNIRS-EEG cap. The challenge here was threefold, 1) to provide a stable optical contact with the scalp, 2) to ensure comfort during long-term monitoring and 3) to allow simultaneous fNIRS-EEG signal acquisition. After testing several prototypes using different stretchable material and different form of sockets and optodes housing, we were able to build an easy to use, motion-resistant and comfortable cap (**Table 10-15**). The large socket opening and the space between holes allow pushing hair aside to improve signal quality (Idelson et al., 2015).

7.5.2 Limitations

Some limitations in our study need to be pointed out. First, the portable system was tested on a small number of hospitalized patients and larger clinical studies are obviously required. Second, although a small number of short distance optodes were planned in our original design to assess the contribution of extracerebral superficial layers to the signal, they were not yet available in our first-generation caps. Future recordings will include this component. Third, our prototype only allowed each source to be coupled to a maximum of four detectors. Albeit this allowed for quasi-full head coverage, raising the number of detected per source could provide denser coverage. Fourth, the current optode design do not allow for occipital recording while the participant is in supine position.

7.5.3 Future perspectives

Case studies provided in this paper represent only a few potential applications of a portable multichannel fNIRS-EEG system for long-term monitoring in a hospital environment. Other areas that may benefit from such neuroimaging technology include the operating room (ex. cardiac and vascular surgeries) [Maldonado et al. 2014; Kato et al. 2015], the neurosurgical critical care unit (ex. monitoring of seizures or vasospasm) [Yokose et al., 2010; Keller et al., 2015; Seule et al., 2015; Tanaka et al., 2015] and rehabilitation centers (ex. study of brain plasticity after injury) [Strangman et al., 2006; Arenth et al., 2007; Mihara et al., 2007, 2010; Yoshino et al., 2013; Khan et al., 2013]. These clinical avenues will obviously need to be explored in larger series.

In terms of technical development, incorporating other improvements made by other groups can be explored such as probe miniaturization [Kanayama and Niwayama, 2014], computer-free systems [Si et al., 2015], broadband devices [Chitnis et al., 2016], wireless fNIRS probes [Abtahi et al., 2016], portable diffuse optical topography [Atsumori et al., 2007; Kiguchi et al. 2012; Flexman et al., 2012], and integration of smartphone technology [Yurtsever et al., 2006; Bunce et al., 2006; Sharieh et al., 2014; Watanabe et al., 2016a].

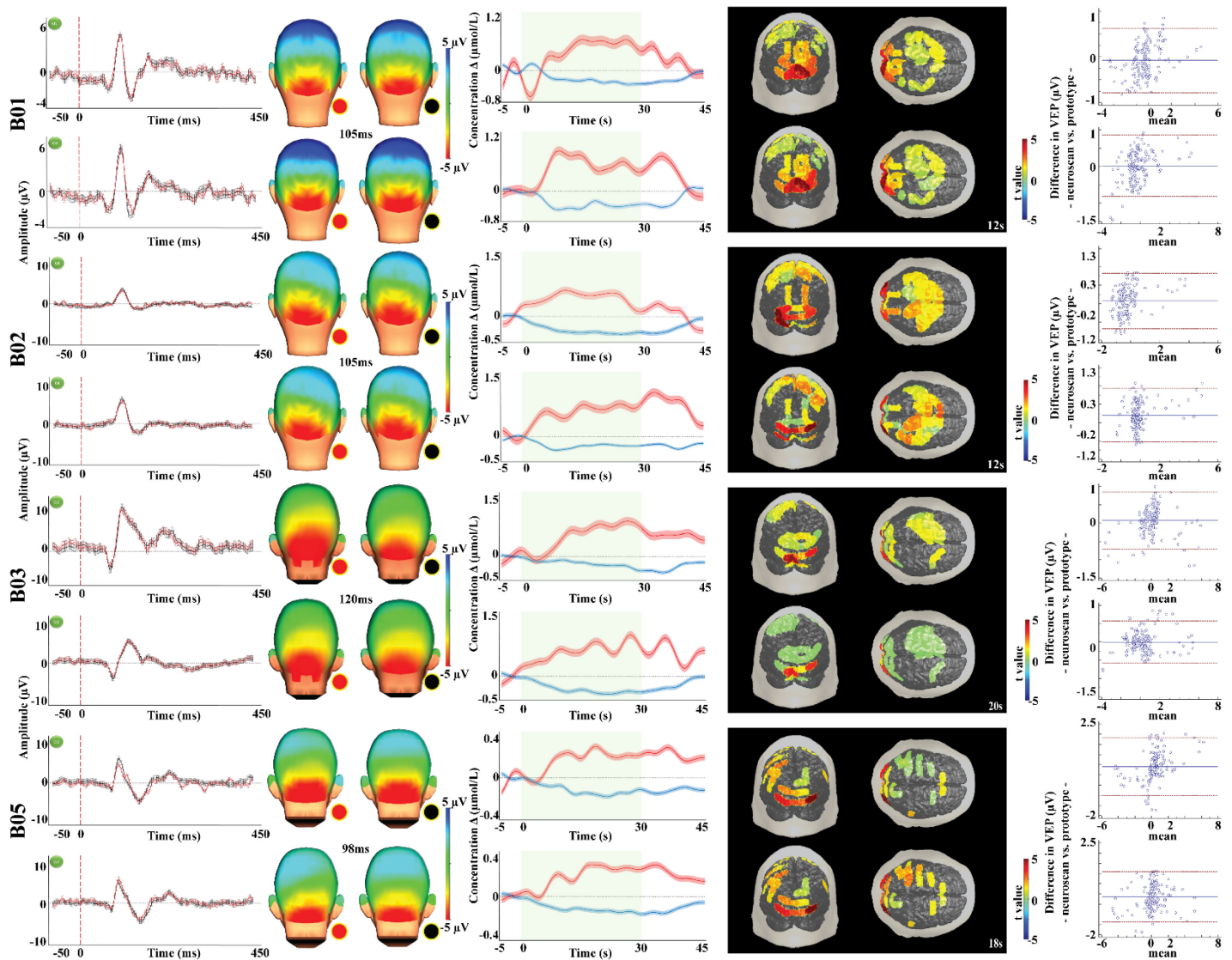
7.6 Conclusions

To answer the need of portability to monitor electrical and hemodynamic brain activities in clinical settings, we developed a novel high channel (128 NIRS and 32 EEG) count and lightweight instrument that can display real-time changes in HbO₂, Hb, HbT and EEG on a portable personal computer through a wireless wearable module. Using visual and language tasks, we established that haemodynamic activations can be retrieved. In-hospital testing on patients with various neurological conditions demonstrated the portability of the device and the potential to provide useful clinical information.

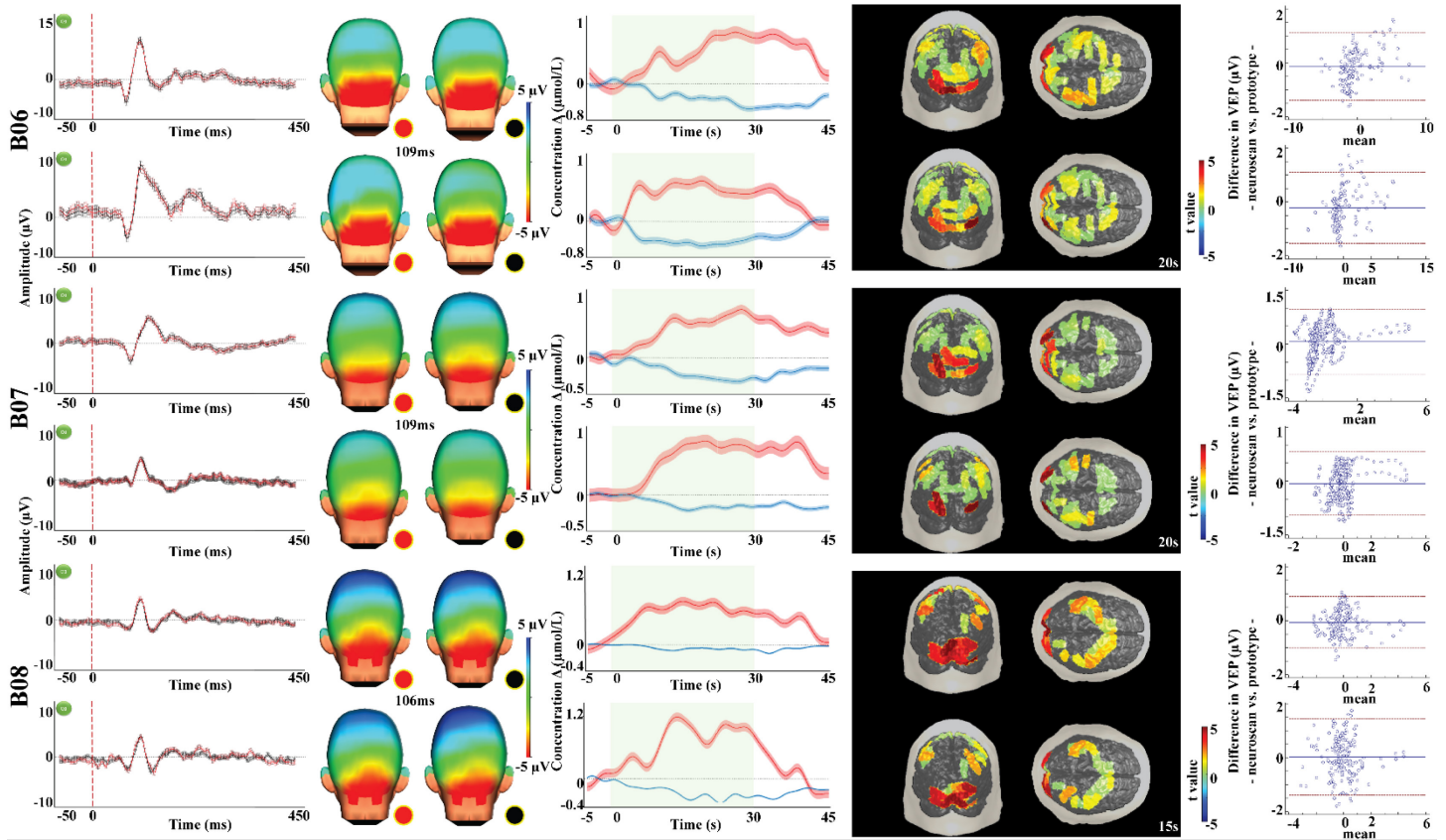
7.7 Acknowledgements

This work was supported by the Canadian Institutes of Health Research (CIHR) (MOP 133643), the Heart and Stroke Foundation of Canada in Partnership with CIHR (01001-000, 01006-000), and the National Sciences and Engineering Research Council in partnership with CIHR (CPG-127774). The authors declare no conflict of interest and have nothing to disclose.

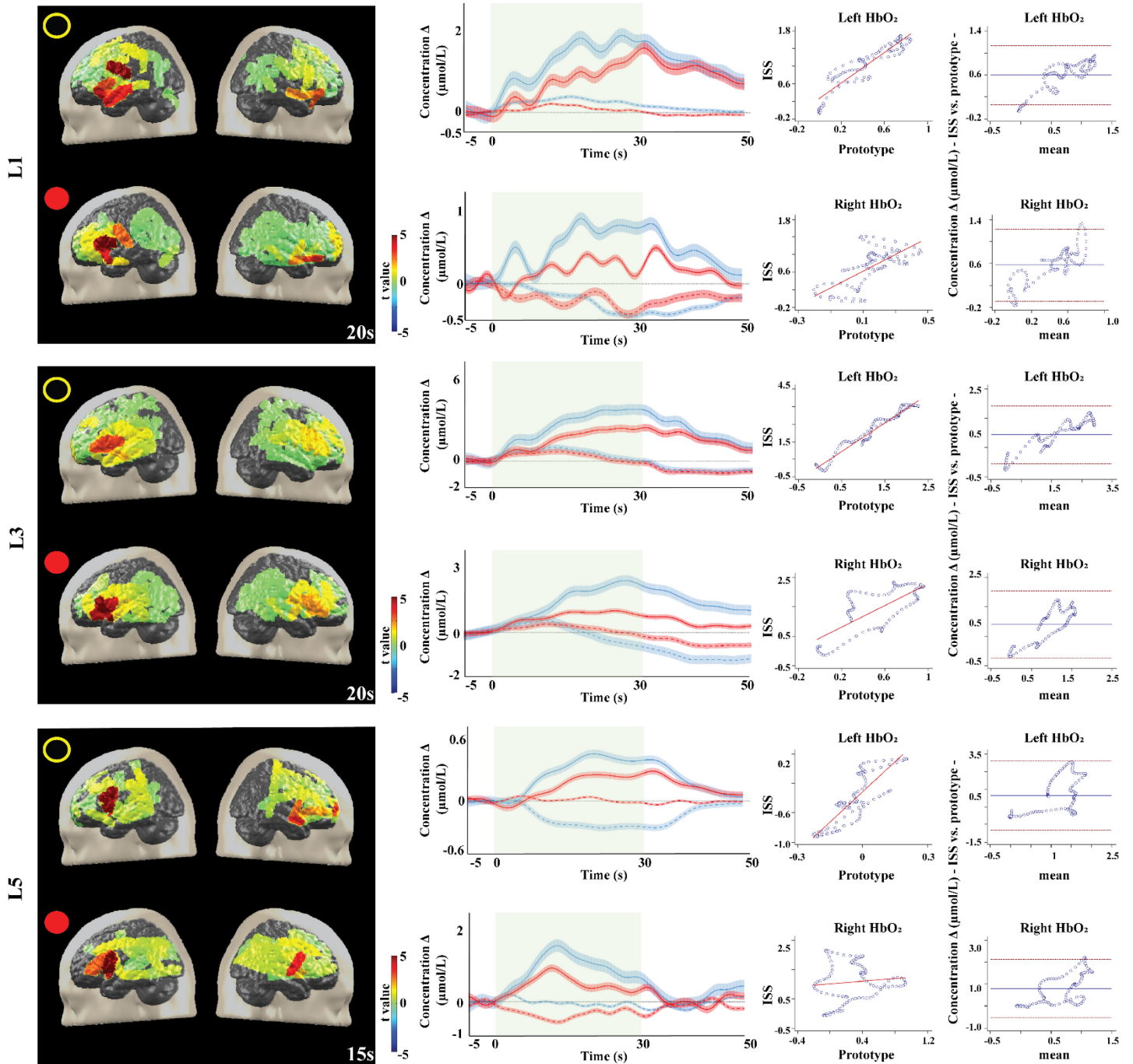
7.8 Appendix



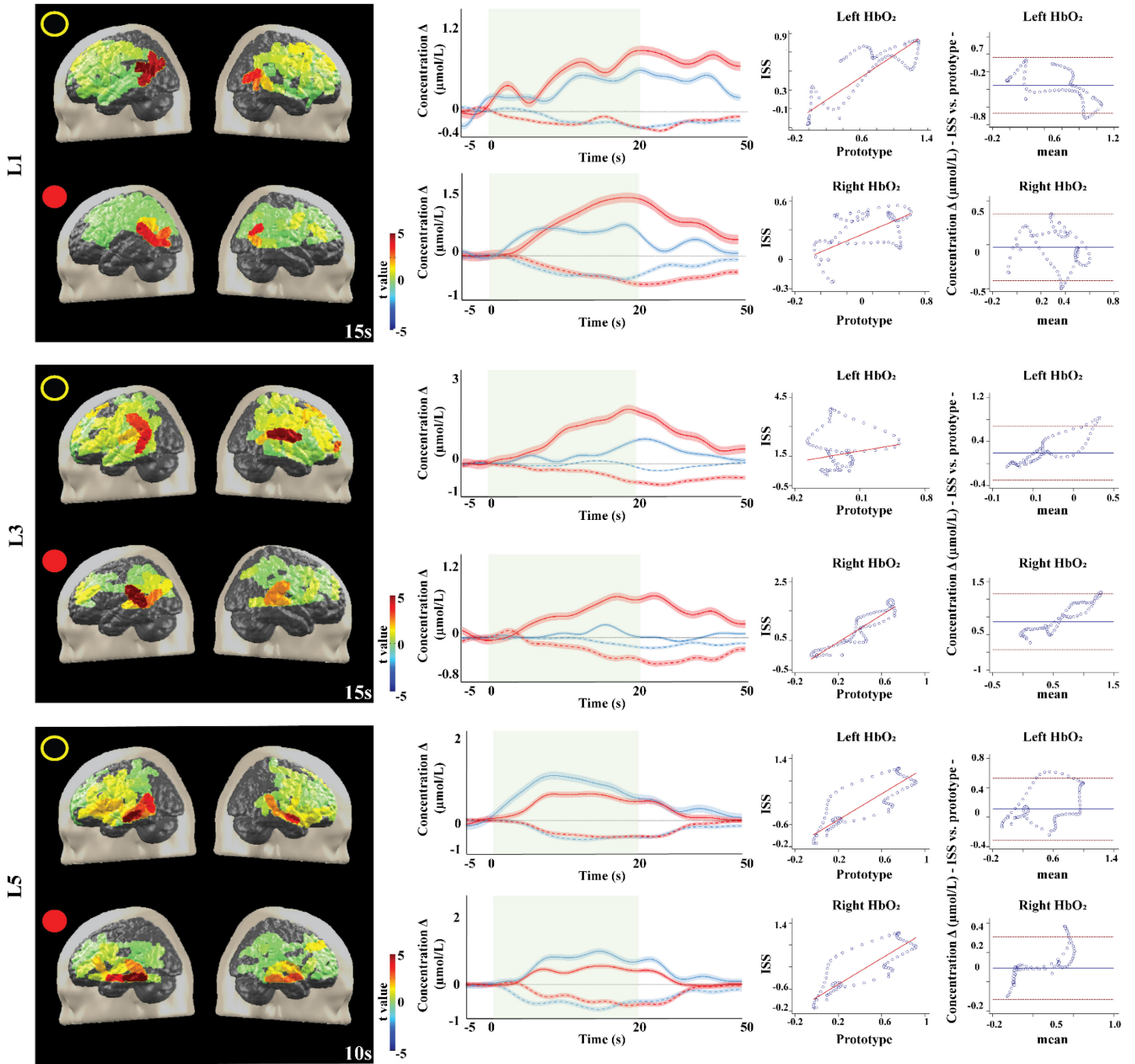
Supplementary Figure 1 – 1st and 2nd row: P100 time course and topography over the visual cortex averaged along every stimulation blocks while sitting still (upper row) and pedalling (bottom row) for each participant. Black line/dot: Neuroscan system. Red line/dot: fNIRS-EEG prototype. 3rd and 4th row: Time course of $\Delta[\text{HbO}_2]$ (red line) and $\Delta[\text{Hb}]$ (blue line) over the visual cortex and $\Delta[\text{HbO}_2]$ topography, averaged over 6 to 8 visual stimulation periods for each participant obtained from 2-6 channels over the visual cortex while sitting still (upper row) and pedalling (bottom row). Red and blue shaded area: standard error of the mean for $\Delta[\text{HbO}_2]$ and $\Delta[\text{Hb}]$ respectively. Green shaded area: stimulation period. 5th row: Results from the Bland–Altman analysis for the P₁₀₀ amplitude changes at rest (left) and while pedalling (right) between our prototype and Neuroscan. Dotted red line: limits of agreement. Solid blue line: bias.



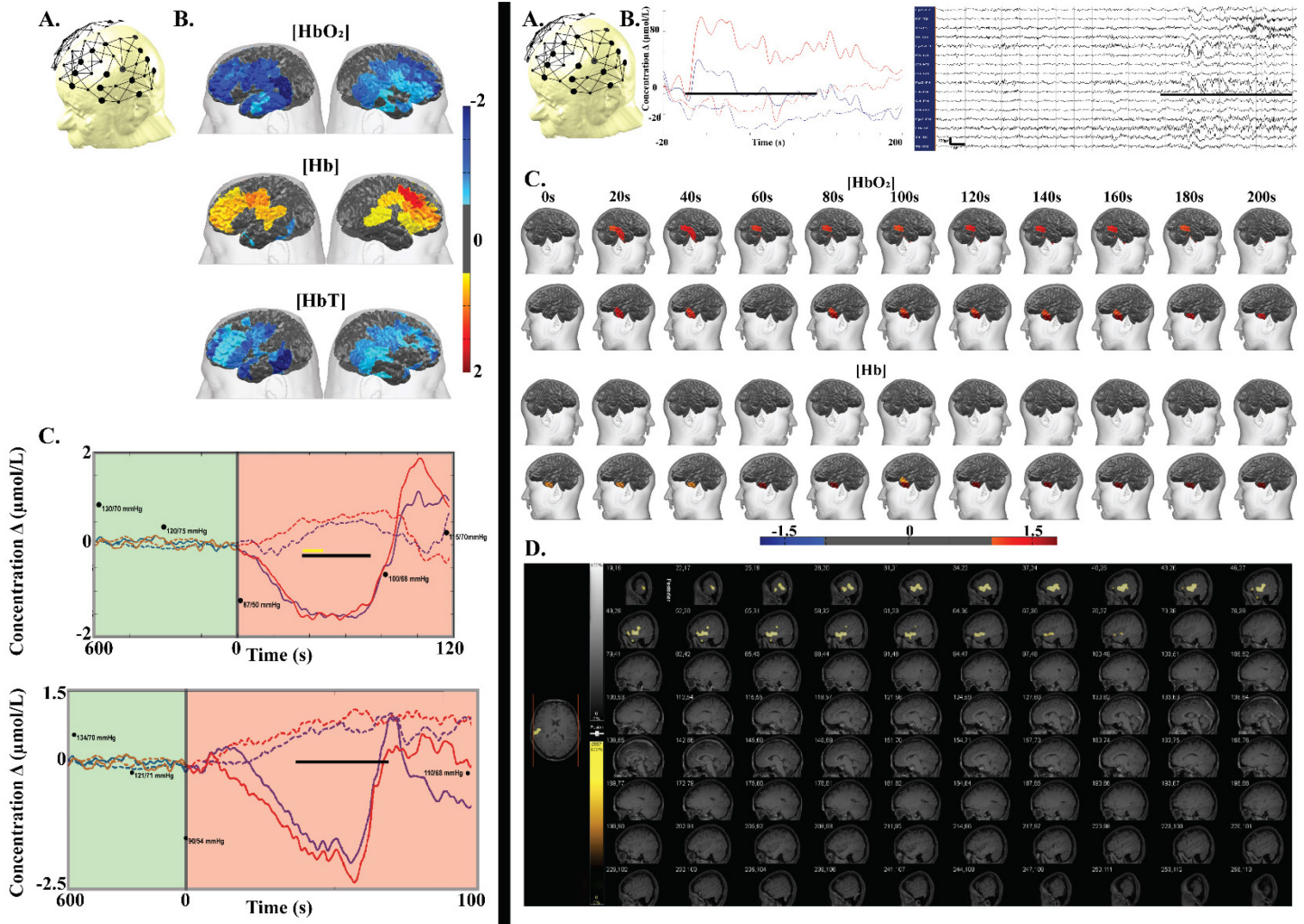
Supplementary Figure 1 (continued) – 1st and 2nd row: P100 time course and topography over the visual cortex averaged along every stimulation blocks while sitting still (upper row) and pedalling (bottom row) for each participant. Black line/dot: Neuroscan system. Red line/dot: fNIRS-EEG prototype. 3rd and 4th row: Time course of $\Delta[\text{HbO}_2]$ (red line) and $\Delta[\text{Hb}]$ (blue line) over the visual cortex and $\Delta[\text{HbO}_2]$ topography, averaged over 6 to 8 visual stimulation periods for each participant obtained from 2-6 channels over the visual cortex while sitting still (upper row) and pedalling (bottom row). Red and blue shaded area: standard error of the mean for $\Delta[\text{HbO}_2]$ and $\Delta[\text{Hb}]$ respectively. Green shaded area: stimulation period. 5th row: Results from the Bland–Altman analysis for the P100 amplitude changes at rest (left) and while pedalling (right) between our prototype and Neuroscan. Dotted red line: limits of agreement. Solid blue line: bias.



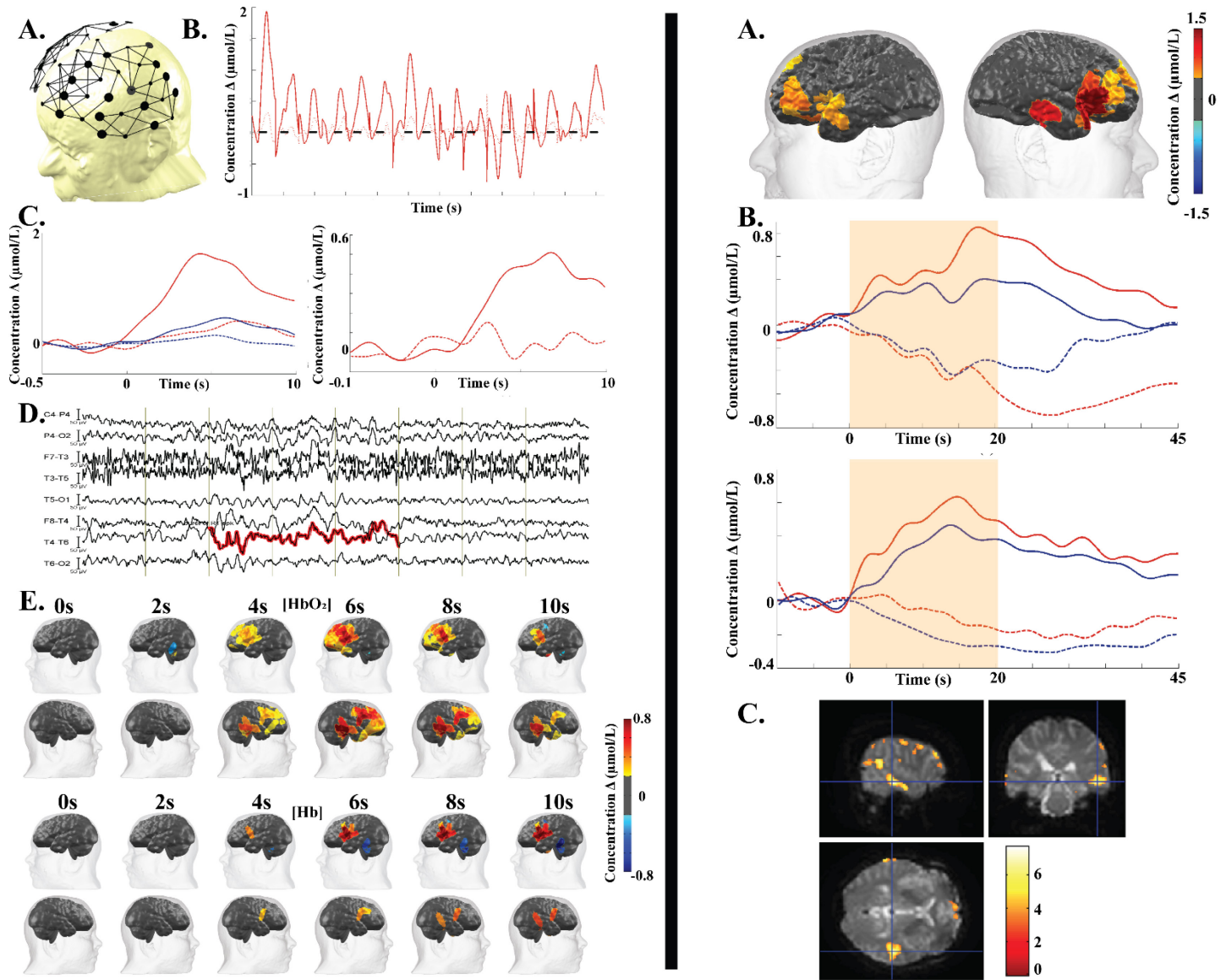
Supplementary Figure 2 – 1st and 2nd column: Δ [HbO₂] topography and time course of Δ [HbO₂] (straight line) and Δ [Hb] (dotted line) over the Broca area along all stimulation blocks during the listening task in the other three participants. 3rd and 4th column: results from the linear regression and Bland–Altman analysis for Δ [HbO₂]. Dotted red line: limits of agreement. Solid blue line: bias.



Supplementary Figure 3 – 1st and 2nd column: Δ [HbO₂] topography and time course of Δ [HbO₂] (straight line) and Δ [Hb] (dotted line) over the Wernicke area along all stimulation blocks during the passive listening task in the other three participants. 3rd and 4th column: results from the linear regression and Bland–Altman analysis for Δ [HbO₂]. Dotted red line: limits of agreement. Solid blue line: bias.



Supplementary Figure 4 – Left - patient C1. Montage configuration (A). Topographic uncorrected T-stats views of $[HbO_2]$, $[Hb]$ and CBV averaged between time 40s to 50s during the first recording session (B). Hemodynamic variations over the DLFC and motor areas during two recording sessions. The first part (green) of these hemodynamic changes are representative of the first 10 minutes while the patient was sitting and the second part (red) represent the hemodynamic changes when the patient was standing up prior to limb shaking. The black line indicates the period during which the patient experienced limb shaking and lower limb weakness. The yellow line indicates the period during which we averaged hemodynamic changes over the frontal, temporal and parietal cortices for topographic representation (C). Dotted line: $[Hb]$. Solid line: $[HbO_2]$. Red: Right hemisphere activations. Blue: Left hemisphere activations. Right - patient C2. Montage configuration (A). Hemodynamic variations (left) over the temporal regions before, during and after the seizure and EEG time course (right) showing the beginning of the seizure in the right temporal lobe and further propagation to the left contralateral side. (B). Topographic uncorrected T-stats views of $[HbO_2]$, and $[Hb]$ during the course of the seizure (C). ictal SPECT 34s after seizure onset showing an increase in CBF most importantly over the middle and posterior portion of the right temporal lobe (D). Dotted line: $[Hb]$. Solid line: $[HbO_2]$. Blue: Left hemisphere activations. Red: Right hemisphere activations.



Supplementary Figure 5 – Left - patient C3. Montage configuration (A). Hemodynamic variations over the right lateral temporal region (epileptogenic region) during each brief seizures (short black line) (B). Averaged hemodynamic variations over the dorsolateral frontal region (left) and right lateral temporal region (right) (C). Blow-out of EEG showing a representative brief seizure over the temporal area (D). Topographic uncorrected T-stats views of $[HbO_2]$, and $[Hb]$ during the course of one brief seizure (E). Dotted line: $[Hb]$. Solid line: $[HbO_2]$. Red: Right hemisphere activations. Blue: Left hemisphere activations.

Right - patient C4. Left and right NIRS activations in a female patient with probable language reorganization (A). Haemodynamic response in region of interest averaged along every stimulation blocks during the naming task showing a clear activation ($\uparrow HbO_2$ & $\downarrow Hb$) in the Broca and Wernicke's area in the right hemisphere (B). fMRI was also obtained, confirming right hemisphere dominance (C). Dotted line: $[Hb]$. Solid line: $[HbO_2]$. Blue: Left hemisphere activations. Red: Right hemisphere activations.

Table 13 – Headgear comfort questionnaire

	Discomfort (yes, no)		Headache (yes, no)		Neck pain (yes, no)		Tolerance (< 1h, 1-2h, > 2h)		Overall appreciation (0-5)		Total	
	NIRS-EEG	ISS	NIRS-EEG	ISS	NIRS-EEG	ISS	NIRS-EEG	ISS	NIRS-EEG	ISS	NIRS-EEG	ISS
B1	No	-	No	-	No	-	> 2h	-	4	-	9	-
B2	Yes	-	No	-	No	-	1-2h	-	3	-	6	-
B3	No	-	No	-	No	-	1-2h	-	4	-	8	-
B4	No	-	No	-	No	-	> 2h	-	5	-	10	-
B5	No	-	No	-	No	-	1-2h	-	5	-	9	-
B6	Yes	-	Yes	-	No	-	> 2h	-	4	-	7	-
B7	No	-	No	-	No	-	> 2h	-	3	-	8	-
B8	No	-	No	-	No	-	> 2h	-	4	-	9	-
L1	Yes	Yes	Yes	Yes	No	Yes	> 2h	< 1h	3	2	5	2
L2	No	Yes	No	No	No	Yes	> 2h	< 1h	4	1	9	2
L3	No	Yes	No	Yes	No	Yes	1-2h	1-2h	4	3	8	4
L4	Yes	No	No	Yes	No	No	> 2h	1-2h	4	1	8	4
C1	-	-	-	-	-	-	-	-	-	-	-	-
C2	No	-	No	-	No	-	> 2h	-	4	-	9	-
C3	No	-	No	-	No	-	1-2h	-	4	-	8	-
C4	No	-	No	-	No	-	> 2h	-	5	-	10	-
Average											7.6	3

0 (very uncomfortable) ←————→ 10 (very comfortable)

Table 14 – Main in-house compact portable NIRS system for brain studies.

Authors (year)	Goal	Validation [# subjects]	Technique [S, D type]	# channels [# S, # D]	Wavelengths (nm)	SR (Hz) / SNR (dB)	Degree of wearability	Mobility	Battery powered [h]	Simultaneous multimodality	Commercial comparison
Yurtsever et al. (2003, 2006) ⁴	Design a miniaturized, wearable system for cognitive activity monitoring.	Phantom	Single distance CW [LEDs, MPDs]	16 [4, 10]	730, 850	3.3 / N/R	High ²	NE	Yes [N/R]	No	No
Vaithianathan et al. (2004)	Design a portable topographic system to image brain activity in preterm and term babies.	Phantom Pressure cuff measurements [6M, 6F]	Single distance CW [LEDs, SiPDs]	56 [24, 14]	780, 880	3 / 3	Low	NE	No	No	No
Bozkurt et al. (2005) Rosen et al. (2005) ¹	Design a portable system to monitor newborn brain metabolism.	Phantom Hearing screening test [1 newborn male]	Single distance CW [LEDs, MPDs]	2 [1, 2]	730, 850	10 / 67	Low	Yes	Yes [30]	No	No
Bunce et al. (2006)	Design a portable and wireless neuroimaging system.	Target categorization and deception detection task [32M, 4F]	Single distance CW [LEDs, MPDs]	16 [4, 10]	730, 805, 850	2 / N/R	High ²	NE	Yes [N/R]	EEG	No
Chénier and Sawan (2007)	Design a portable brain imaging system.	Phantom Measurements of signal physiology [2M, 1F]	Single distance CW [LEDs, SiPDs]	1 [1, 1]	730, 805, 850	23 / 47	Low	NE	Yes [N/R]	No	No
Atsumori et al. (2007, 2009) ⁶	Design a multi-channel, portable and fibreless optical topography-NIRS based system.	Word fluency task [1M]	Single distance CW [VCSELs, SiPDs]	22 [8, 8]	790, 850	12.5 / 65.3	High ²	NE	Yes [2-3]	No	No
Muchlemann et al. (2008) Holper et al. (2010, 2014a) ¹	Design a palm-size wireless system.	Phantom Pressure cuff measurements and motor task [1M]	Single distance CW [LEDs, SiPDs]	12 [4, 4]	760, 870	100 / 32-37	High ²	NE	Yes [3]	No	No
Zhang et al. (2009)	Design of a portable system for tissue oxygenation measurement.	Pressure cuff measurements [1M]	Single distance CW [LED, MPD]	2 [2, 1]	760, 850	40 / N/R	Low	NE	Yes [N/R]	No	No
Lareau et al. (2011a,b)	Design a system that can operate for 24 h on a single battery charge.	Phantom Visual task [5M]	Single distance CW [LD, APD]	32 [8, 8]	735, 850	20 / 19	Low	NE	Yes [24]	EEG ³ (8 channels)	No

Table 14 (continued) – Main in-house compact portable NIRS system for brain studies.

Authors (year)	Goal(s)	Validation [# subjects]	Technique [S, D type]	# channels [# S, # D]	Wavelengths (nm)	SR (Hz) / SNR (dB)	Degree of wearability	Mobility	Battery powered [h]	Simultaneous multimodality	Commercial comparison
Zhang et al. (2011) ⁵	Developing wearable ambulatory neuromonitoring system.	Phantom Valsalva test and parabolic flight test [1M]	Multi distance CW [LEDs, MPDs]	4 [1, 2]	660, 905	250 / 55	Very high ²	Yes	Yes [14]	3ECG ³ , respiration ³ , accelerometers ³	No
Hemmati et al. (2012)	Design a miniaturized system for real-time monitoring in the prefrontal cortex.	Phantom	Single distance CW [LEDs, MPDs]	16 [10, 4]	730, 850	N/R / N/R	Low	NE	Yes [N/R]	No	No
Kiguchi et al. (2012) ⁶	Design a wearable optical topography-NIRS based system for brain region covered by hair.	Finger tapping task [6M]	Single distance CW [VCSELs, SiPDs]	22 [8, 8]	790, 850	12.5 / 65.3	High ²	NE	Yes [2-3]	No	No
Flexman et al. (2012)	Design a wireless system that perform DOT measurements.	Phantom	Multi distance CW [LDs, SiPDs]	8 [4, 2]	780, 808, 850, 904	2.3 / 50	High ²	NE	Yes [N/R]	No	No
Sharieh et al. (2012) ⁴	Design a fully mobile smartphone controllable system.	Breathing [N/R]	Single distance CW [LEDs, SiPDs]	4 [4, 4]	730, 830	100 / N/R	High ²	NE	Yes [3-6]	No	No
Sawan et al. (2012, 2013)	Design of a system for monitoring epileptic and stroke patients.	Finger tapping and visual task [1M]	Single distance CW [LEDs, APDs]	32 [8, 8]	735, 850	20 / 112	High ²	NE	Yes [24]	EEG ³ (8 channels)	No
Ayaz et al. (2013) ^{4,6} McKendrick et al. (2015) ¹	Design a system capable of measurements in brain hemodynamics during air traffic control.	Phantom	Single distance CW [LEDs, MPDs]	16 [4, 10]	730, 850	2 / 75	High ²	NE	Yes [3]	No	No
Safaie et al. (2013) ⁵	Design an integrated wireless and wearable NIRS-EEG system to study the neuro-hemodynamic interaction.	Phantom Pressure cuff measurements and somatosensory test [3M]	Single distance CW [LEDs, MPDs]	64 * [32, 4] *	760, 850	8 / 46	High ²	NE	Yes [5]	EEG ³ (16 channels) *	Yes
Piper et al. (2014) ⁶	Design of a portable system capable of measurements in brain hemodynamics in freely moving subjects.	Hand gripping task at rest and during indoor and outdoor pedalling [6M, 2F]	Single distance CW [LEDs, SiPDs]	20 [8, 8]	760, 850	6.25 / N/R	Very high ²	Yes	Yes [8]	No	No

Table 14 (continued) – Main in-house compact portable NIRS system for brain studies.

Authors (year)	Goal(s)	Validation [# subjects]	Technique [S, D type]	# channels [# S, # D]	Wavelengths (nm)	SR (Hz) / SNR (dB)	Degree of wearability	Mobility	Battery powered [h]	Simultaneous multimodality	Commercial comparison
Kotozaki et al. (2014)	Design a system capable of investigating the anatomical correlated of biofeedback effect.	Biofeedback experiment [30]	Multi distance CW [N/R]	1 [1, 2]	810	10 / N/R	High ²	NE	N/R	No	No
Kanayama and Niwayama (2014)⁶	Design a finger-mounted fetal tissue oximeter.	Neonatal and fetal cerebral oxygen saturation during labor [3 newborns]	Single channel SRS [LEDs, N/R]	1 [1, 1]	770, 810	NA	N/R	NE	Yes [N/R]	No	No
Zhang et al. (2014)	Evaluate of a wearable ambulatory neuromonitoring system for long-term recording.	24-h normal daily activities [1M]	Multi distance CW [LDs, MPDs]	4 [1, 2]	660, 905	250 / 55	Very high	Yes	Yes [24]	ECG ³ , pulse oximetry ³ , actigraphy ³ , respiration ³ , accelerometers ³	No
Agrò et al. (2014, 2016)	Design of a portable multichannel system.	Breath-holding measurements [1M]	Single distance CW [LEDs, SiPMs]	> 128* [64, 128]	735, 850	NA / 45	High	No	Yes [N/R]	No	No
von Lüthmann et al. (2015)	Design an open source multichannel stand-alone system.	Mental arithmetic BCI experiment [12M]	Single distance CW [LEDs, SiPDs]	4 [4, 1]	750, 850	Variable / 28	High	Yes	Yes [N/R]	No	No
Si et al. (2015)⁴	Design a self-contained, computer-free system.	Phantom Finger tapping task [5M, 2F]	Single channel CW [LEDs, APDs]	8 [4, 4]	690, 830	NA / NA	High	NE	Yes [N/R]	No	No
Hallacoglu et al. (2016)	Design a compact high-density DOT system for cerebral oxygenation and perfusion imaging on the bedside.	Phantom	Multi distance CW [LEDs, N/R]	180 [10/18]	690 to 850 (5 wavelengths)	N/A	High ²	NE	No	No	No
Liang et al. (2016)	Design of a multichannel system for measuring frontal hemodynamics during anesthesia.	Valsalva maneuver task and anesthesia monitoring [7M, 4F]	Single distance CW [LEDs, SiPDs]	12 [3, 8]	760, 850	100 / NA	Low	NE	No	No	No
Watanabe et al. (2016)	Design a portable tissue oxygenation monitoring system.	Phantom Pressure cuff and breath-holding measurements [1M]	Single distance CW [LEDs, SiPDs]	2 [3, 1]	735, 810, 850	60 / 60	High ²	NE	Yes [N/R]	No	No

Table 14 (continued) – Main in-house compact portable NIRS system for brain studies.

Authors (year)	Goal(s)	Validation [# subjects]	Technique [S, D type]	# channels [# S, # D]	Wavelengths (nm)	SR (Hz) / SNR (dB)	Degree of wearability	Mobility	Battery powered [h]	Simultaneous multimodality	Commercial comparison
Chitnis et al. (2016)	Design of a wearable device for simultaneous NIRS and EEG monitoring of neurovascular and metabolic physiology.	Phantom Visual task [1M]	Multi distance CW [LEDs, SiPDs]	16 [8, 4]	778, 808, 814, 841, 847, 879, 888, 898	5.56 / > 40	Low	NE	No	No	No
von Lüthmann et al. (2016)	Design a hybrid wireless bio-optical and bio-electrical instrument for BCI application	Phantom Deep breathing measurements [1M]	Single distance CW [LEDs, SiPDs]	8-10 * [5, 5]	750, 850	16.66 / 40-66	High ²	NE	Yes [N/R]	EEG ³ , ECG ³ , EMG ³ , accelerometers ₃	No
Abtahi et al. (2016)	Design a low-cost, wearable and wireless fNIRS path	Phantom Pressure cuff measurements [1M]	Single distance CW [LEDs, MPDs]	10 [4, 4]	770, 930	5 /NA	High ^{2,4}	NE	Yes [6-11]	No	No
Wyser et al. (2017)	Design a fibreless system to reliably and accurately capturing brain hemodynamics.	Phantom Pressure cuff and finger tapping measurements [1M]	Multi distance CW [LEDs, SiPM]	4 [4, 1]	770, 810, 850, 885	100 / 31-64	High ²	NE	Yes [NA]	No	No
Funane et al. (2017)	Design of a system-on-chip fiberless wearable fNIRS system.	Language measurements [1M]	[LEDs, APDs]	N/R [12, 23]	730, 855	10 / NA	High ²	NE	No [NA]	No	No

¹Same prototype used, ²Wireless system, ³Integrated modality, ⁴Smartphone or PocketPC controllable system, ⁶Early prototype of a commercial system, * Number of potential channels, APD: avalanche photodiode, CW: continuous wave, LDs: laser diodes, LEDs: light-emitting diode, MPD: monolithic photodiode, NE: not evaluated, N/R: not reported, SiPD: silicon photodiode, VCSEL: vertical-cavity surface-emitting laser.

Table 15 – Main commercial compact portable NIRS system for brain studies.

Product, [software]	HEO-100/200 [built-in]	fNIR100AW/200-W [fNIRSoft, COBI]	WOT-100 [POTATo]	OEG-16H [NIRS-SPM]	LIGHTNIRS [fNIRS]	NIRSport [NIRStar, nirLAB, NAVI]	PortaLite / OctaMon [Oxysoft]	NIRSIT [built-in mobile app]	Toccare KN-15 [built-in]	NA [NIRS-SPM]
Company [country]	Omron Ltd. Inc. [Japan]	fNIR Devices [USA]	Hitachi [Japan]	Spectratech Inc. [Japan]	Shimadzu [Japan]	NIRx [Germany]	Artinis [The Netherlands]	OBELAB Inc. [South Korea]	Astem Co. Ltd. [Japan]	BioExplorer [USA]
Technology [tS, tD]	CW [LEDs, N/A]	CW [LEDs, SiPDs]	CW [LDs, SiPDs]	CW [LEDs, SiPDs]	CW [LDs, APDs]	CW [LEDs, SiPDs]	CW [LEDs, SiPDs]	CW [LDs, N/A]	SRS [LEDs, N/A]	CW [LEDs]
Number of channels [#S, #D]	2 [2S, 1D]	2-4 [2-4S, 1-2D]	16 [8S, 8D]	16 [6S, 6D]	22 [8S, 8D]	64*** [8S, 8D]	3 (PortaLite) – 8 (OctaMon) [3-8S, 1-2D]	204 [24S, 32D]	1 [NA]	1 [1S, 1D]
Wavelengths (nm)	760, 840	730, 850	750, 830	770, 840	780, 805, 830	760, 850	760, 850	780, 850	770, 830	660, 850
Time resolution (Hz)	0.5-120	2	5	0.76-6.1	13.3	2.5-62.5	50	8.13-16.27	0.5	100
Range (m)	10-30 [handheld]	10-50 [fanny pack belt]	50 [fanny pack belt]	not wireless [backpack]	4 [messenger bag]	30 [backpack]	80-120 [fanny pack belt]	NA [headheld]	not wireless [handheld]	N/A
Battery life (h)	6	3	2	1	2-4	6	6-16	8	15	N/A
Hyperscanning	No	Yes (up to 3)	Yes (up to 4)	Yes (up to 5)	Yes (up to 4)	Yes (up to 2)	Yes (up to 7)	Yes (N/A)	no	N/A
Real-time (online) display	Yes	Yes	Yes	No	Yes	Yes	Yes	Yes	Yes	N/A
Measurable hemodynamic parameters [forehead limited]	$\Delta\text{HbO}_2/\text{Hb}/\text{HbT}$ [yes]	$\Delta\text{HbO}_2/\text{Hb}/\text{HbT}$ [yes]	$\Delta\text{HbO}_2/\text{Hb}/\text{HbT}$ [yes]	$\Delta\text{HbO}_2/\text{Hb}$ [yes]	$\Delta\text{HbO}_2/\text{Hb}/\text{HbT}$ [no]	$\Delta\text{HbO}_2/\text{Hb}/\text{HbT}$ [no]	$\Delta\text{HbO}_2/\text{Hb}/\text{HbT}$ TSI [yes]	$\Delta\text{HbO}_2/\text{Hb}/\text{HbT}$ [yes]	rSO ₂ , TSI [no]	N/A [yes]
System weight (g) [Size] (cm)	340 g (w/o B) [8.5 x 4.2 x 16]	200 g (w B) [83 x 2 x 10.5]	1 300 g (w B) [15 x 11.5 x 6.2]	1 000 g (w/o B) [18 x 17 x 40]	1600 g (w/o B) [25.3 x 22.2 x 6.8]	660 (w B) [10.5 x 17 x 4]	88-230 (w B) [8.4 x 5.4 x 2]	550 (w B) [21.5 x 19.5 x 7.5]	100 [6 x 2.6 x 8.2]	N/A [N/A]
Publications (year)	<i>Shiga et al. (1995)</i> *	<i>Ayaz et al. (2013)</i> **	<i>Pinti et al. (2015)</i> *	<i>Oboshi et al. (2014)</i> *	<i>Yoshino et al. (2013a, b)</i> **	<i>Piper et al. (2014)</i> **	<i>Burtscher and Koch (2015)</i> *	<i>Trakoolwilaiwan, et al. (2016)</i>	<i>Watanabe et al. (2017)</i>	<i>Holper et al. (2014b)</i>
Average price (US \$)	1000 (LED based, single-channel) – 100 000 (Laser based, multi-channel)									

*Many publications, **Studies done on an earlier version or commercial prototype, ***Up to 128 channels (16S and 16D) in a tandem configuration, APDs: avalanche photodiodes, CW: continuous-wave, Hb: deoxyhemoglobin, HbO₂: oxyhemoglobin, HbT: total hemoglobin, LEDs: light emitting diodes, LDs: laser diodes, N/A: not available, rSO₂: regional oxygen saturation, S: sources, D: detectors, SiPDs: silicon photodiodes, TSI: tissue saturation index, w/o B: without batteries, w B: with batteries.

CHAPTER 8 – MANUSCRIPT #2

Cerebral hemodynamic changes during limb-shaking TIA: a near-infrared spectroscopy study

Ali Kassab^{1,2}, Julie Tremblay³, Alexandre Y. Poppe^{1,4}, Laurent Létourneau-Guillon⁵, Anne Gallagher^{3,6}, Dang Khoa Nguyen^{1,2,4}

¹Département de neurosciences, Université de Montréal, Montréal, Québec, Canada, H3T 1J4; ²Centre de Recherche du CHUM, Université de Montréal, Montréal, Québec, Canada; ³Centre de Recherche de l'Hôpital Sainte-Justine, Université de Montréal, Montréal, Québec, Canada, H3T 1C4; ⁴Service de Neurologie, Hôpital Notre-Dame du CHUM, Université de Montréal, Montréal, Québec, Canada, H2L 4M1; ⁵Département de Radiologie, Hôpital Notre-Dame du CHUM, Université de Montréal, Montréal, Québec, Canada, H2L 4M1; ⁶Centre de Recherche en Neuropsychologie et Cognition, Université de Montréal, Montréal, Québec, Canada, H3C 3J7

This article also addresses the first objective of this thesis, further focusing on assessing brain hemodynamics in the clinical setting by monitoring a patient with limb-shaking transient ischemic attacks. This article was published in *Neurology* in 2016 ([Kassab et al., 2016](#)).

8.1 Introduction

Limb-shaking TIA (LS-TIA) is a rare form of TIA manifesting as involuntary movements involving one or more limb(s). Cerebral ischemia in the context of hemodynamic failure has been incriminated [1]. Indeed, LS-TIAs are associated with severe carotid steno-occlusive disease and often precipitated by a decrease in blood pressure [1]. A limited number of studies using transcranial Doppler [2], 133xenon SPECT [3] or ^{15}O -H $_2$ O-PET [4] have shown reduced regional cerebral blood flow (CBF) and diminished vasomotor reactivity. The latter techniques can only provide a single snapshot of regional CBF and do not allow for continuous assessment of cerebral hemodynamic changes during an actual LS-TIA. Functional near-infrared spectroscopy (fNIRS) is a neuroimaging technique that can non-invasively monitor at the bedside cortical changes in oxyhemoglobin ([HbO $_2$]), deoxyhemoglobin ([HbR]) and total hemoglobin ([HbT], as a proxy to cerebral blood volume, CBV) [5]. We report the hemodynamic changes observed throughout the course of LS-TIAs using a simultaneous multichannel fNIRS-EEG system.

8.2 Case report

A 61-year-old man was admitted for daily episodes of right upper limb shaking (LS) and leg weakness for the last three weeks, more often while standing up. The patient had previously been hospitalized 12 years ago for a left hemispheric stroke in association with a 60% stenosis of the M1 segment of the left middle cerebral artery (MCA), which subsequently became occluded later that same year. He recovered well until two months prior to admission at which time he experienced right-sided amaurosis fugax. CT angiography at that time showed a 30% stenosis of the supraclinoid right internal carotid artery (ICA) without any significant stenosis of the external carotid artery. On admission, neurological examination was normal. MRI disclosed no acute lesions. Magnetic resonance angiogram revealed interval progression of the right supraclinoid ICA narrowing to a severe stenosis of more than 70% (**Supplementary Figure 6A**). Dynamic susceptibility contrast T2*-weighted perfusion (**Supplementary Figure 6B**) and arterial spin labeling perfusion (**Supplementary Figure 6C**) both confirmed decreased relative CBF to the left MCA territory while relative CBF within the right carotid artery territory appeared maintained despite the aforementioned stenosis. A homemade portable fNIRS-EEG system was used to record

in real-time [HbO₂], [HbR] and [HbT] over the fronto-temporo-parietal regions bilaterally. This system has been described previously in details [7]. Briefly, our system includes 32 light sources and 32 photodetectors offering a total of 128 NIRS channels with an average interoptode distance of 3 cm. As the patient stood up, blood pressure gradually decreased from 134/70mmHg to 90/54 after 10 minutes at which point he experienced tremor of the right forearm and hand associated with weakness of both legs and mild dysarthria (video e-1). fNIRS showed over bilateral (left more than right) dorsolateral frontal cortices a progressive decrease in [HbO₂] and [HbT] as well as an increase in [HbR] over a one-minute period prior to the onset of LS (**Figure 29**). These changes normalized within 15 seconds after the patient sat down, and LS subsided. Three additional LS episodes were recorded which revealed similar hemodynamic changes starting 20-60 seconds prior LS and weakness. Simultaneous EEG monitoring showed diffuse slow (3-50 μ V, 4-6Hz theta) activity (more predominantly over the left parasagittal regions) at the moment of LS.

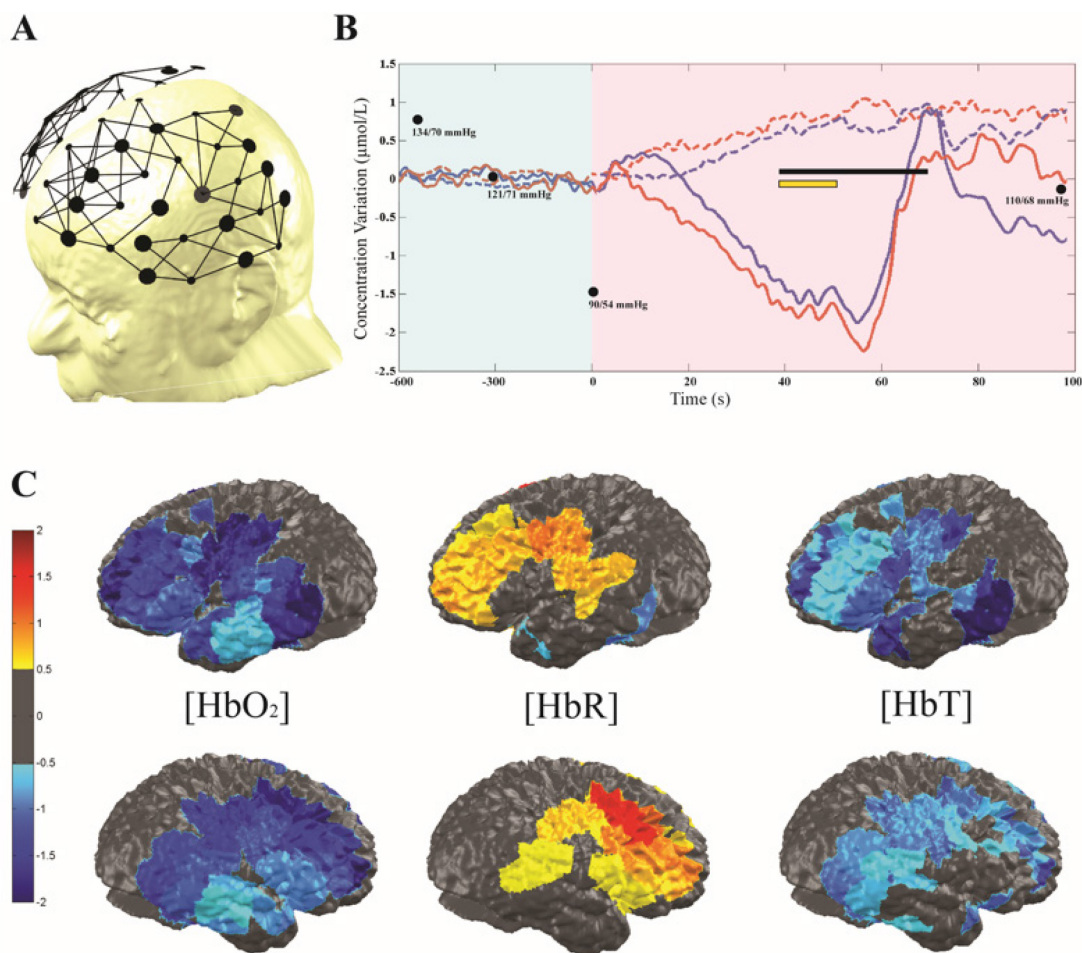


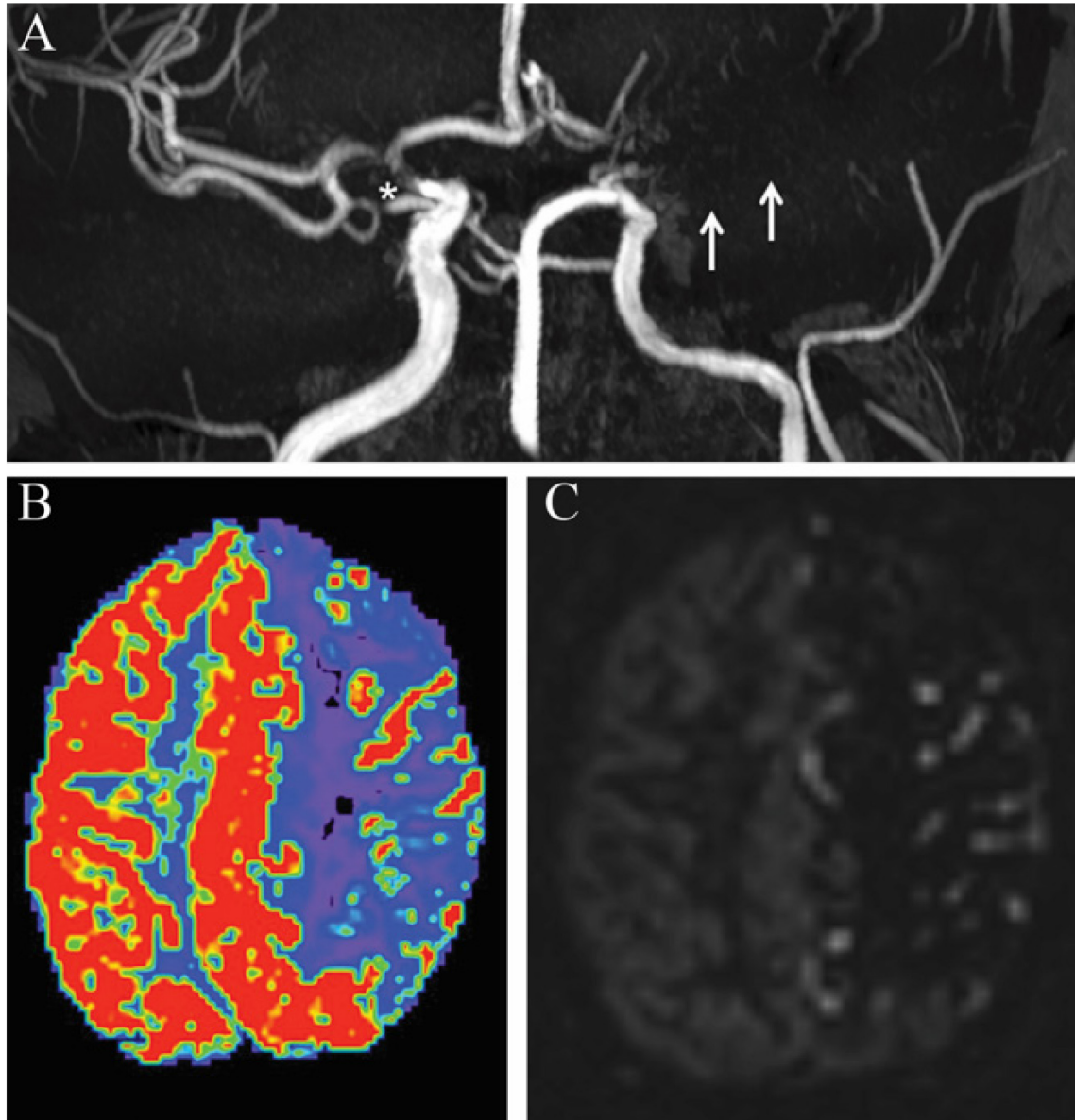
Figure 29 – fNIRS findings during the second episode of LS-TIA. (A) Channel configuration. (B) Hemodynamic variations over the DLFC and motor areas: no significant variations in [HbT], [HbO₂] and [HbR] are found during a period of 10 minutes after standing up (condensed in light-shaded blue); progressive decrease in [HbT] and [HbO₂] and rise in [HbR] at $t = 0s$ (light-shaded purple). The black line indicates the period during which the patient experienced LS and lower limb weakness. The yellow line indicates the period during which we averaged hemodynamic changes over the frontal, temporal and parietal cortices for topographic representation. Solid color line: [HbO₂]. Red: Right. Blue: Left. Black dots: Blood pressure. (C) Topographic views of [HbO₂], [HbR] and [HbT] averaged from all ipsilateral channels between time 40s to 50s.

8.3 Discussion

In this patient with baseline decreased relative CBF in the left MCA territory from carotid stenosis, fNIRS recording showed during postural hypotension gradual brain hypoperfusion (as reflected by the [HbT] decrease) and hypoxia (as suggested by the increase in [HbR]) predominantly over the dorsolateral frontal cortex and motor areas prior to LS. While the relative decrease in [HbT] and [HbO₂] were quasi-similar bilaterally, these changes may have had more impact over the left hemisphere as the baseline CBF was much lower there. Overall, our findings are in line with the prevalent “hypoperfusion theory” [1]. The presence of late diffuse EEG slow waves is not unexpected since the EEG becomes abnormal only when CBF declines to 20-30 ml/100g/min [7]. Although our observations stem from a single patient, the fact that we observed similar hemodynamic changes in four different spells is compelling. One potential point of criticism is the unknown influence of the skin and extracerebral tissue on cerebral fNIRS signal. Because our patient had no significant stenosis of the external carotid artery, the contribution from superficial layers in the observed hemodynamic changes was most likely minimal. Another important limitation that must be reminded is that fNIRS is unable to assess hemodynamic changes in deeper brain structures such as the basal ganglia, which might also be implicated in the genesis of LS.

In conclusion, this fNIRS case study provides further evidence that LS-TIAs are associated with dynamic cerebral cortical hypoperfusion with resulting hypoxia in dorsolateral frontal and motor cortices.

8.4 Appendix



Supplementary Figure 6 – MRI, angiogram and ASL findings associated with LS-TIA. (A) Maximum intensity projection of a time-of-flight MR angiography demonstrating an occlusion of the left M1 segment (arrows) and severe stenosis of the right supraclinoid ICA (asterisks). (B) Dynamic contrast-enhanced T2* perfusion revealing decreased relative CBF to the left middle cerebral artery territory (and anterior aspect of the anterior cerebral territory). (C) Arterial spin labeling showing similar decreased relative CBF mainly within the left middle cerebral artery territory as well as arterial transit artifacts at the periphery.

CHAPTER 9 – MANUSCRIPT #3

Hemodynamic changes associated with common EEG patterns in critically ill patients: pilot results from continuous EEG-fNIRS study

Ali Kassab^{a,b}, Dènahin Hinnoutondji Toffa^b, Manon Robert^{cb}, Frédéric Lesage^{c,d}, Ke Peng^{a,b}, Dang Khoa Nguyen^{a,b,e}

^aDepartment of Neurological Sciences, Université de Montréal, C.P. 6128, succ. Centre-ville, Montreal, Quebec, (H3C 3J7), Canada; ^bCentre de Recherche du Centre Hospitalier de l'Université de Montréal, Université de Montréal, 900 Saint Denis St., Montreal, Quebec (H2X 0A9), Canada; ^cBiomedical Engineering Institute, École Polytechnique de Montréal, 2500 Chemin de Polytechnique, Montréal, Quebec (H3T 1J4), Canada; ^dResearch Center, Montreal Heart Institute, 5000 Rue Bélanger, Montreal, Quebec (H1T 1C8), Canada; ^eDivision of Neurology, Centre Hospitalier de l'Université de Montréal, Université de Montréal, 1000 Saint Denis St. Montreal, Quebec (H2X OC1), Canada

This article addresses the second objective of this thesis, which was to evaluate the feasibility and potential of long-term vEEG-fNIRS monitoring in the adult critical care setting. This article was published in *NeuroImage: Clinical* in 2021 ([Kassab et al., 2021](#)).

9.1 Abstract

Functional near-infrared spectroscopy (fNIRS) is currently the only non-invasive method allowing for continuous long-term assessment of cerebral hemodynamic. We evaluate the feasibility of using cEEG-fNIRS to study the cortical hemodynamic associated with status epilepticus (SE), burst suppression (BS) and periodic discharges (PDs). Eleven adult comatose patients admitted to the neuroICU for SE were recruited, and cEEG-fNIRS monitoring was performed to measure concentration changes in oxygenated (HbO) and deoxygenated hemoglobin (HbR). Seizures were associated with a large increase HbO and a decrease in HbR whose durations were positively correlated with the seizures' length. Similar observations were made for hemodynamic changes associated with bursts, showing overall increases in HbO and decreases in HbR relative to the suppression periods. PDs were seen to induce widespread HbO increases and HbR decreases. These results suggest that normal neurovascular coupling is partially retained with the hemodynamic response to the detected EEG patterns in these patients. However, the shape and distribution of the response were highly variable. This work highlighted the feasibility of conducting long-term cEEG-fNIRS to monitor hemodynamic changes over a large cortical area in critically ill patients, opening new routes for better understanding and management of abnormal EEG patterns in neuroICU.

9.2 Introduction

Continuous scalp electroencephalography (cEEG) monitoring is routinely used in the neurological intensive care unit (neuroICU) for diagnostic purposes, especially when suspecting nonconvulsive seizures (NCS) or nonconvulsive status epilepticus (NCSE) (Young and Mantia, 2017). The addition of functional neuroimaging techniques in clinical monitoring can further aid the diagnosis of NCSE (Hauf et al., 2009; Kutluay et al., 2005), as well as improving the understanding of the underlying pathophysiology (Siclari et al., 2013; Shimogawa et al., 2017). For example, animal studies of SE have reported increases in cerebral blood flow (CBF), oxygen pressure and metabolism (Lee et al., 2018; Wolff et al., 2020), which showed that epilepsy or SE is not just an electrical disorder but also a vascular disorder. Unfortunately, in humans, only few reports have reported relative increase in cerebral blood flow (CBF) and cerebral blood volume (CBV) during

SE using computer tomography perfusion (CTP) (Hauf et al., 2009), arterial spin labelling (Shimogawa et al., 2017), and single photon emission computed tomography (SPECT) (Kutluay et al., 2005). ¹⁸Fluorodeoxyglucose positron emission tomography (¹⁸FDG-PET) have shown both hypermetabolism (Siclari et al., 2013) and hypometabolism during SE (Strohm et al., 2019). Severe metabolic crisis has been described during SE (Vespa et al., 2007), and more recently, in new-onset refractory NCSE (Hurth et al., 2020).

In patients with refractory status epilepticus (RSE), EEG is also used to evaluate seizure control and anesthesia-induced background suppression (i.e. isoelectric or burst-suppression patterns) (Brophy et al., 2012). Achieving such patterns is commonly sought as an electrophysiological endpoint in RSE (Brophy et al., 2012) and intracranial hypertension (Marshall et al., 2010). However, the neuroprotective role of pharmacologically induced BS in the setting of acute brain injury remains debated. Some studies have suggested that BS lowers brain metabolism, which could be beneficial in situations where CBF and oxygen delivery are compromised such as during prolonged seizures (Ching et al., 2012; Doyle and Matta, 1999). Conversely, other studies have found that the brain is in a state of relative hyperexcitability during BS because inhibitory post-synaptic potentials are completely suppressed while excitatory potentials are only partially diminished. In this state of relative cortical excitability, even subliminal stimuli can elicit bursts of whole-brain activity in animal studies, a phenomenon closely resembling SIRPIDS (stimulus-induced rhythmic, periodic, or ictal discharges), a common EEG phenomenon in the critically ill (Ferron et al., 2009). Whichever the case may be, there is little doubt that functional neuroimaging techniques provide valuable information regarding the neurophysiological dynamics of medically induced BS patterns. The study of vascular changes and neurovascular coupling during BS reveals the ability of the brain in responding to spontaneous or externally stimuli, which may help further delineate the putative neuroprotective role in critically ill patients (Berndt et al., 2021).

The increased use of cEEG in the neuroICU has also led clinicians to recognize EEG patterns belonging to the ictal-interictal continuum (IIC) (Pohlmann-Eden et al., 1996), including generalized periodic discharges (GPDs) and lateralized periodic discharges (LPDs). While both GPDs and LPDs are commonly observed in the neuroICU, their clinical significance remains controversial as to whether they truly represent an ictal phenomenon or not (Cormier et al., 2017).

Specifically, LPDs were reported to be usually associated with hypermetabolism (Struck et al., 2016), however, both hypo- and hypermetabolism have been observed during GPDs (Bansal et al., 2016). Clinical functional neuroimaging monitoring of the hemodynamic changes during IIC patterns may serve as an adjunct modality for clinicians to identify potential oxygen undersupply and neuronal damage, which necessitate more aggressive treatment to the patients (Herlopian et al., 2018).

Despite these potentials, conventional non-invasive neuroimaging approaches (e.g., PET, SPECT) are limited by practical aspects in this context and by their temporal resolution whereas invasive methods (e.g., invasive brain tissue oximetry, invasive monitoring of cerebral perfusion pressure) carry risks of medical complications and provide a limited spatial view. Functional near-infrared spectroscopy (fNIRS) is a non-invasive optical neuroimaging technique that reconstructs cortical hemodynamic conditions (in terms of concentration changes of oxyhemoglobin, HbO and deoxyhemoglobin, HbR) from attenuation of near-infrared light during its propagation within the cortex (Scholkmann et al., 2014). Compared with other functional neuroimaging modalities, fNIRS provides long-term continuous measurement of cortical oxygenation at a relatively high temporal resolution (up to the order of 0.01s), making it suitable as a low-cost portable neuromonitoring technique in the neuroICU (Pisano et al., 2020). The use of fNIRS to investigate SE (Haginoya et al., 2002; Diaz et al., 2006; Giorni et al., 2009; Martini et al., 2019; Monrad et al., 2015) has been limited to a few cases reports conducted in young children with thin skull. Moreover, most of those studies have only employed a couple of optodes covering the forehead. Simultaneous EEG was not always present, and recording sessions were typically short in duration (< 1h). To date, investigation of BS with fNIRS has only been performed in neonates (Chalia et al., 2016; Connolly et al., 2015; Roche-Labarbe et al., 2007) and no study has yet investigated PDs using fNIRS or other optical imaging methods.

In this work, we conducted for the first time prolonged cEEG-fNIRS recordings over a large cortical area in critically ill patients admitted to the neuroICU. We extracted the cortical hemodynamic response to each type of the recorded EEG events, which included NCSE, PDs and pharmacologically induced BS patterns. The goals of this study were twofold: we aimed to 1- assess the feasibility of performing long-term cEEG-fNIRS in comatose patients in neuroICU; and

2- to provide first evaluation of the hemodynamic responses associated with each electroclinical condition, relating the characteristics of those changes to the type or duration of the events.

9.3 Material and methods

9.3.1 Patients

This study was approved by the Institutional Review Board at the University of Montreal Hospital Center (CHUM). Eleven neuroICU patients (seven males, age range: 31 to 61 years) with seizures or SE were recruited. At admission, the patients were diagnosed with SE (n=7) or acute encephalopathy (n=4). Written informed consent was obtained from legally authorized representatives. An overview of our study procedures is depicted in **Figure 30**.

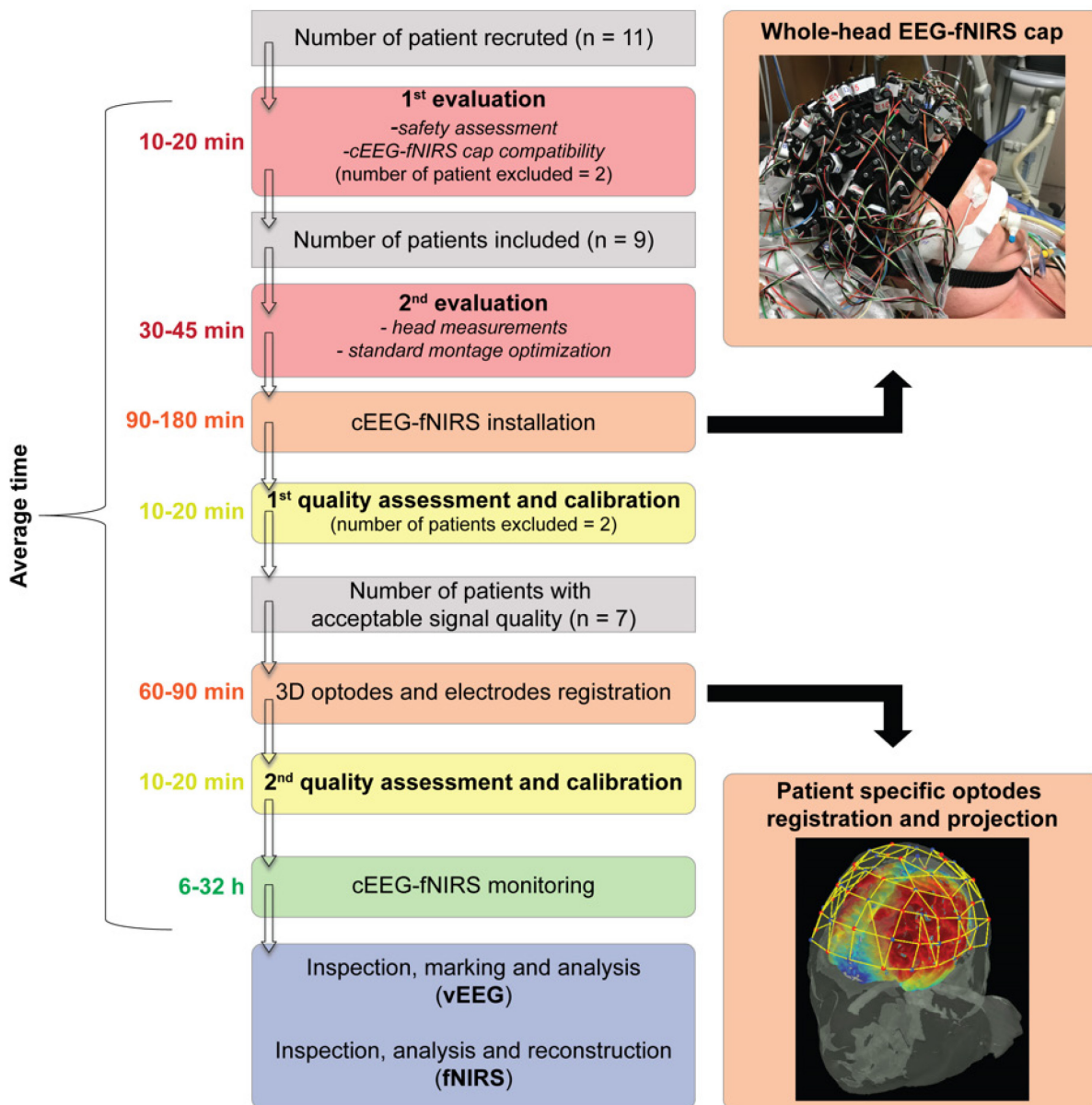


Figure 30 – Sketch plot of the patient evaluation, continuous encephalography and functional near-infrared spectroscopy data acquisition, and data analysis procedures.

9.3.2 cEEG-fNIRS data acquisition

A portable EEG-fNIRS system previously developed and validated by our group (Kassab et al., 2018) was used in this study. 19 EEG electrodes were mounted following the International 10-20 layout. For the fNIRS part, the system allows the installation of up to 32 light emitters and 32 detectors, which form a maximum of 128 fNIRS channels operating at 735 nm and 850 nm. Three previously validated full-head EEG-fNIRS caps (small, medium and large) (Kassab et al. 2018)

were utilized in this study to fit different sizes of patient's head. A base optode montage consisting of rows of sources alternating with rows of detectors was designed for neuroICU patients kept in a supine position which covered most of the frontal lobe, the central areas, the bilateral temporal lobe and the anterior portion of posterior regions. Depending on the actual head shape, size, the presence of skin lesions on the scalp and the location of observed epileptiform activities, the optode layout for each patient was modified from the base montage to maintain an optimal coverage. The distance between an fNIRS light emitter and a light detector that formed a channel was kept within 2.5 cm to 5 cm. If needed, a dark elastic woolen fabric was placed over the cap to improve probe-tissue contact and to reduce ambient light. The acquired EEG data and fNIRS data were sampled at 500 Hz and 20 Hz respectively.

9.3.3 Data processing and analysis

EEG identification of seizures, PDs and BS and EEG data analysis

EEG data were independently reviewed by two epileptologists (DHT and DKN) to label and confirm interictal epileptiform discharges, PDs, as well as electrical onsets and offsets of seizures, bursts and suppression periods. The American Clinical Neurophysiology Society's (ACNS) diagnostic criteria were used for the diagnosis of electrographic and electroclinical seizures (Hirsch et al., 2013). The diagnosis of NCSE was based on both EEG and clinical data following the modified Salzburg Consensus Criteria (mSCNC) (Leitinger et al., 2019). Quantitative EEG analysis was performed offline for the whole EEG recording using Persyst 13 EEG software (Persyst Systems, Arizona, USA), including rhythmicity spectrogram, fast Fourier transform (FFT) spectrogram, asymmetry relative spectrogram, and amplitude EEG spectrogram (for parameters, see **Table 16**).

fNIRS data pre-processing

For each patient, an analysis period representative of the whole recording was selected based on the type and number of presented events, number of valid channels and noise levels. The selected fNIRS data were processed with open-source toolbox Homer2 (Huppert et al., 2009) and in-house developed scripts. fNIRS channels with an intensity of less than 100 (AU) or a signal-to-noise ratio of less than 2 were excluded from further analysis. For the remaining channels, raw optical data were first converted into optical density changes. A principal component analysis (PCA) filter that

removed 90% of the global variance across channels was applied to mitigate motion artifacts and the interferences from superficial layers (e.g., scalp, skin and skull) (Zhang et al., 2005; Virtanen et al. (2009). For comatose patients in the neuroICU, motion artifacts may come from mattress air pressure fluctuations and routine care procedures performed by medical staff. A Homer2 automatic algorithm based on signal standard deviation and amplitude change was then used to further check for remaining motion artifacts. Any EEG event within the time period from 30s prior to a motion artifact to 30s after the artifact was rejected. The remaining EEG events were then manually inspected to ensure no event mislabeling. The fNIRS optical density time courses were passed to a 3rd order Butterworth bandpass filter with cutoff frequencies at 0.01 Hz and 0.20 Hz, and were then transformed into concentration changes in HbO and HbR using the modified Beer-Lambert Law with a partial pathlength factor of 6. The concentration changes in HbT were calculated by a direct sum of HbO and HbR changes.

Extraction of hemodynamic response functions

The estimation of hemodynamic response function (HRF) to each type of EEG patterns/event was conducted through an event-related general linear model (GLM) analysis. We employed a bin approach similar to that used by Chalia et al. (Chalia et al., 2016), which was to group each type of EEG event into 5-second width bins of different durations. For instance, seizures lasted less than 20 seconds were divided into four bins: [0 to 5s], [5s to 10s], [10s to 15s] and [15s to 20s]. These bins were treated as distinct conditions in the following GLM analysis, allowing their associated responses to vary freely from the others. Considering the intrinsic delay of hemodynamic changes relative to the underlying electrical activity, we modeled the hemodynamic response to a particular bin of events from 5 seconds before the EEG onset to 15 seconds after the EEG offset of the longest possible event within the bin (e.g., the response to the bin of seizures from 15 to 20s was modeled from 5 seconds before the seizure onset shown on EEG to 35 seconds after the EEG onset, i.e., 15 seconds after the offset of the longest 20-sec seizure). The functions used in the GLM were consecutive Gaussian functions with a standard deviation of 1 second and a step size of 1 second as well. After the extraction, each HRF was normalized using the mean amplitude from 2 seconds before the event EEG onset to the event onset as the baseline level.

To enable comparisons between conditions, we generated a representative HRF corresponding to each bin and each event type of each patient. This was conducted by performing a PCA on the HRFs of all available channels, reconstructing the HRFs with the components that accounted for at least 80% of global variance, and averaging new HRFs across channels. Including only the principal components allows us to focus on the hemodynamic changes that were most prominent across brain regions, as well as to reduce the possibility of including spurious local signals in the representative HRF. A similar PCA-based extraction method was used by (Chalia et al., 2016). More specifically, the original HRFs were first pre-centered to zero-mean, and were aligned as an $t \times p$ HRF matrix H where t is the number of time points in the HRF and p is the number of available channels. PCA was conducted by performing an eigen decomposition on the covariance matrix $C = H^T H / (t-1)$, i.e.

$$C = VLV^T$$

where V is a matrix of eigenvectors with each column being one eigenvector, L is a diagonal matrix with eigenvalues $\lambda_i, i = 1, 2, \dots, p$, on the diagonal in descending order. The principal components R of matrix H were given by:

$$R = HV$$

In this study, we only kept the principal components that accounted for $\geq 80\%$ of the variance, i.e. we created a new R' :

$$\begin{cases} R'_{j,k} = 0, & \text{for } j = 1, 2, \dots, t \text{ and } k = s, s + 1, \dots, p \\ R'_{j,k} = R_{j,k}, & \text{otherwise} \end{cases}$$

where s was determined by

$$\frac{\sum_{i=s}^p \lambda_i}{\sum_{i=1}^p \lambda_i} \leq 0.2 \quad \text{and} \quad \frac{\sum_{i=s-1}^p \lambda_i}{\sum_{i=1}^p \lambda_i} > 0.2$$

A new HRF matrix H' was then generated by:

$$H' = R'V^T$$

Finally, we added each channel's DC component that was removed in data pre-centering back to the new channel HRF (i.e., each column of H'). The representative HRF was then obtained by a simple averaging of the new HRFs (with DC) across available channels.

To ensure that the extracted representative HRFs were synchronized with the EEG events and to assess the strength of the responses, we presented a confidence level for each representative HRF by employing a surrogate timecourse approach (Peng et al., 2016). Briefly, we took the hemoglobin concentration change time courses of all available fNIRS channels of a patient, performed a fast Fourier Transform on each channel time course, and randomized the phases of the frequency components. Specifically, the same set of randomized phases for frequency components was applied to all the channels. The frequency components with randomized phases of a channel were then re-transferred to the time domain to generate a surrogate time course. Note that by using the phase randomization method (Maiwald et al., 2008), we aimed to maintain the same signal autocorrelation of a channel as in the original timecourse, and by applying the same set of randomized phase set to all the channels, we intended to keep similar covariance structure among different channels. The surrogate timecourses of all channels were then passed to the GLM model and the PCA procedures to produce a spurious representative HRF. The same randomization and extraction process was repeated 100 times for each true representative HRF. The peak amplitude (PA) of the true representative HRF was then compared to the amplitude values during the same time period of all 100 spurious representative HRFs to evaluate the possibility of the peak being generated by chance or noise. More specifically, we approximated the 100 amplitude values of the spurious representative HRFs with a normal distribution, and reported the confidence level of the true representative HRF by calculating the ratio of the tail area marked by the PA of the true representative HRF on the normal distribution relative to the entire area of the distribution. Therefore, the ratio is a scalar value between 0 and 1, and a smaller ratio indicated higher response strength and a less chance of the true representative HRF being generated by pure noise or other artifacts in data processing. For a representative HRF of a bin, the PA was defined as the mean value averaged from 1s before the maximum value of a main peak following the EEG onset of the event (or the minimum value if a nadir was detected) to 1s after the maximum value.

Cortical projection of hemoglobin concentration changes

The projection of hemoglobin concentration changes back onto the cortical surface was carried out using the toolbox AtlasViewer (Aasted et al., 2015) integrated in Homer2. For each patient, the included optical sources and detectors were first co-registered onto the Colin27 five-layer brain atlas. A forward model was computed using the Monte-Carlo algorithm that simulated the migration of 100 million photons at each optical source and detector. The produced sensitivity matrix was used to solve the regularized inverse problem and to generate voxel-wise concentration changes (Custo et al., 2010). For each bin of events, the time period of concentration changes to be displayed on the cortex was selected to be the PA of the HbO representative HRF. We chose HbO over HbR in this study as previous work has generally reported a much higher signal-to-noise ratio in HbO responses than HbR responses (Obrig et al., 2000; Yennu et al., 2016). A threshold of extent was imposed to the generated spatial concentration change images to only keep the cortical areas where the detection sensitivity was high than -2dB. It should be noted that the projections of fNIRS-measured hemoglobin concentration changes were limited by the imaging depth, cortical coverage and the detection sensitivity. Therefore, our interpretation of the hemodynamic response spatial features was only based on the brain areas where a relatively high sensitivity was obtained (see **Supplementary Figure 8** for examples of sensitivity map).

Statistical analysis

To further explore the relationship between detected EEG events and the characteristics of the corresponding hemodynamic responses, we established a linear mixed-effect regression model modeling event duration with fixed effect for response peak amplitude (PA) or response full-width-at-half-maximum (FWHM) and uncorrelated random effect for intercept (grouped by patients) and residual:

$$y = \beta_0 + \beta_1 * d + z * u + \varepsilon$$

where y is an N by 1 vector containing the PAs or FWHM extracted from bin representative HRFs of a certain type of EEG event across all M patients where the type of event was detected; d is an N by 1 vector of the maximum event duration of the bins, z is an N by M random effect design matrix where

$$\begin{cases} z_{n,m} = 1, & \text{if } y_n \text{ is from patient } m; \\ z_{n,m} = 0, & \text{otherwise} \end{cases}$$

u is the corresponding M by 1 random effect variable vector, and ε is the uncorrelated N by 1 model residual vector. We assume $u_m \sim N(0, \sigma_u^2)$ and $\varepsilon_n \sim N(0, \sigma_\varepsilon^2)$. For a representative HRF of a bin, the PA was defined as mentioned in the above section, and the FWHM was defined as the length of the time during which the response was larger than half of the PA (or during which the response was smaller than half of the nadir amplitude). In this study, PA was used to assess the hemodynamic response intensity and the FWHM was chosen to assess the duration of the response.

The goodness of fit of the regression models was evaluated through the calculation of the p -value of an F-test on the fixed effect regression coefficients, as well as the R-squared and the adjusted R-squared values. Specifically,

$$R^2 = \frac{SSR}{SST} = 1 - \frac{SSE}{SST}, \text{ and}$$

$$\text{adjusted } R^2 = 1 - \frac{SSE/(N - l - 1)}{SST/(N - 1)}$$

where SST is the total sum of squares $SST = \sum_{m=1}^M \sum_{n_m=1}^{N_m} (y_{n_m} - \bar{y}_m)^2$, SSR is the regression sum of squares $SSR = \sum_{m=1}^M \sum_{n_m=1}^{N_m} (\hat{y}_{n_m} - \bar{\hat{y}}_m)^2$, and SSE is the error sum of squares $SSE = SST - SSR$. \hat{y} contains the predicted conditional PA or FWHM values using both fixed and random effects of the model. $l = 1$ is the number of fixed effect variable in the model.

9.4 Results

9.4.1 Patient clinical information

Four patients were excluded at the initial quality assessment stage due to the use of intracranial probes (n=1), a recent craniotomy/cranioplasty (n=1), and poor optical signal quality (n=2). The clinical information of the remaining seven patients (five men, age = 44 ± 10 years) is included in **Table 16**. **Figure 31** presents structural and electrophysiological findings with structure image slices and representative EEG clips selected from each patient. **Table 17** summarizes the main electrophysiological and optical findings. The details of the neuroICU care and the collected vital sign signals are shown in **Supplementary Figure 7**.

Table 16 – Study characteristics and clinical details for each patient

Patient (sex, age, BMI)	Admission Dx (cEEG-fNIRS MNT start)	# cEEG-fNIRS MNT sessions (analyzed time)	Neurologic status	Cardio-respiratory status	Vital signs MNT (mean ± SD)	AEDs, anesthetics	Anatomical neuroimaging	Outcome
P1 (F, 31, 40.7)	PSE (5 days)	4 sessions, 31.5 h (68 min)	Comatose	ACV (on inotropes)	MAP: 92 ± 15 mmHg T°: 37 ± 1°C SpO ₂ : 100 ± 0 % EtCO ₂ : 34 ± 1 mmHg Glycemia: 7.0 ± 0.7 mmol/L RASS: -2 ± 1	Propofol, MDZ, TP, CTP, CBZ, PHT	Surgical cavity	Discharged at 15 days Mild clinical improvement (refractory epilepsy)
P2 (M, 50, 23.7)	Pneumonia, CPA, RCSE (same day)	2 sessions, 5.5 h (49 min)	Comatose	ACV (on inotropes)	MAP: 82 ± 5 mmHg T°: 37.6 ± 0.2°C SpO ₂ : 99 ± 0 % EtCO ₂ : 44 ± 2 mmHg Glycemia: 13.4 ± 1 mmol/L RASS: -5 ± 0	Propofol, MDZ, LEV	T2/FLAIR hyperintensities	Discharged at 9 days IHT
P3 (F, 52, 33.4)	NCSE (4 days)	1 session, 4.5 h (99 min)	Comatose	ACV (no inotropes)	MAP: 103 ± 6 mmHg T°: 36.8 ± 0.2°C SpO ₂ : 98 ± 2 % EtCO ₂ : 34 ± 2 mmHg Glycemia: 5.0 ± 0.3 mmol/L RASS: -5 ± 0	Propofol, MDZ, LSM, LEV, PHT	Surgical cavity, hypodensity	Discharged at 4 days IHT
P4 (M, 57, 35.5)	GI bleeding, TME, CSE, NCSE (7 days)	2 sessions, 7 h (97 min)	Comatose	ACV (on inotropes)	MAP: 88 ± 9 mmHg T°: 36.7 ± 0.3°C SpO ₂ : 100 ± 0 % EtCO ₂ : 34 ± 1 mmHg Glycemia: 7.0 ± 0.7 mmol/L	Propofol, LEV, LSM	Restricted diffusion, T2/FLAIR hyperintensities	Deed at 22 days
P5 (M, 40, 23.1)	SE, HE/SREAT (26 days)	3 sessions, 8 h (197 min)	Comatose	ACV (no inotropes)	MAP: 76 ± 4 mmHg T°: 37.5 ± 0.1°C SpO ₂ : 99 ± 1 % EtCO ₂ : 35 ± 2 mmHg Glycemia: 5.4 ± 0.6 mmol/L RASS: -5 ± 0	Propofol, MDZ, LEV, PHT	Normal	Discharged at 155 days VS
P6 (M, 45, 17.6)	CSE, RNCSE (2 days)	5 sessions, 10.5 h (261 min)	Comatose	ACV (on inotropes)	MAP: 70 ± 4 mmHg T°: 37.5 ± 0.2°C SpO ₂ : 97 ± 3 % EtCO ₂ : 37 ± 3 mmHg Glycemia: 7.7 ± 1.2 mmol/L RASS: -5 ± 0	Propofol, MDZ, LSM, LEV, TP, CBZ, CLB	Cortical and sub- cortical thickening, T2/FLAIR hyperintensities	Discharged at 87 days Mild clinical improvement (persistence of short seizures)
P7 (M, 34, 21.3)	R hemiparesis, global aphasia, NCSE (3 days)	3 sessions, 8.5 h (140 min)	Comatose	ACV (on inotropes)	MAP: 75 ± 7 mmHg T°: 37.5 ± 0.2°C SpO ₂ : 100 ± 0 % EtCO ₂ : 41 ± 3 mmHg Glycemia: 4.7 ± 0.5 mmol/L RASS: -5 ± 0	Propofol, MDZ, LSM, LTG, LEV, PHT	Surgical cavity, restricted diffusion, T2/FLAIR hyperintensities	Discharged at 50 days Significant clinical improvement (strength and speech)

Abbreviations. ACV: assisted controlled ventilation, AEDs: antiepileptic drugs, BMI: body mass index, CBZ: carbamazepine, CLB: clobazam, CMB: cerebral microbleed, CPA: cardio-pulmonary arrest, CT: cortical thickness, CSE: convulsive status epilepticus, CTP: citalopram, DCA: diffuse cerebral atrophy, Deed: deceased, EtCO₂: mean end-tidal carbon dioxide, F: female, HE: Hashimoto encephalopathy, IHT: inter-hospital transfer, LCM: lacosamide, LEV: levetiracetam, LTG: lamotrigine, M: male, MAP: mean arterial pressure, MDZ: midazolam, MNT: monitoring, N/A: not available, NCSE: nonconvulsive status epilepticus, PHT: phenytoin, PSE: partial status epilepticus, R: right, RASS: mean Richmond Agitation and Sedation Scale value, RCSE: refractory convulsive status epilepticus, RNCSE: refractory nonconvulsive status epilepticus, SD: standard deviation, SE: standard error, SK: skull thickness, SpO₂: mean oxygen saturation, SREAT: steroid-responsive encephalopathy associated with autoimmune thyroiditis, T°: mean temperature, TME: toxicometabolic encephalopathy, TPM: topiramate, VS: vegetative state.

Table 17 – Summary of electrophysiological and optical findings for each of the seven neuroICU patients

Patient ID	Events on cEEG			Events on qEEG			Events on fNIRS	
	Main events (number)	Duration (Inter-event-interval)	Localization	Rhythmicity	FFT	Amplitude EEG	Representative HRF	Cortical Areas (HbO changes)*
P1	Burst of spikes/ Burst of fast activities (82)	1.5 ± 0.6 s (45.5 ± 58.4 s)	Bi FCT (R > L)	Bi ↑ / 1-16 Hz	Bi ↑ / 1-9 Hz (R > L)	Bi ↑ (R > L)	↑ HbO ↑ HbT ↔ ↓ HbR	Bi MFG, SFG
P2	NCSE seizure (102)	24.3 ± 25.9 s (4.6 ± 3.8 s)	Bi FC (L > R)	Bi ↑ / 1-25 Hz	Bi ↑ / 1-25 Hz (L > R)	Bi ↑ (L > R)	↑ HbO ↑ HbT ↓ HbR	Bi AntPFC, SFG, PreCG, L STL
P3	BS burst (693)	5.9 ± 8.2 s (2.7 ± 1.3 s)	Generalized	Bi ↑ / 1-16 Hz	Bi ↑ / 1-4 Hz (R > L)	Bi ↑ (R > L)	↑ HbO ↑ HbT ↓ HbR	L IFG, TL Bi AntPFC, SFG, MFG, PreCG (diffuse)
	BS suppression (693)	2.7 ± 1.3 s (5.9 ± 8.2 s)	Generalized	Bi ↓	Bi ↓	Bi ↓	↓ HbO ↓ ↑ HbT ↑ HbR	L IFG, Bi PTL
	LPD (1573)	(1.7 ± 4.3 s)	Bi FCT (R > L)	Bi ↑ / 1-9 Hz (R > L)	Bi ↑ / 1-4 Hz (R > L)	Bi ↑ (R > L)	↑ HbO ↑ HbT ↓ HbR	Bi AntPFC, PreCG, MFG, IFG, L TL (diffuse, R > L)
P4	NCSE seizure (64)	10.3 ± 4.4 s (77.1 ± 148.6 s)	Bi CPTO (R > L)	Bi ↑ / 1-9 Hz	Bi ↑ / 1-4 Hz (R > L)	Bi ↑	↑ HbO ↑ HbT ↓ HbR	R PreCG, SMG, AntPFC **
	GPD (4649)	(1.2 ± 0.9 s)	Generalized	Bi ↑ / 1-9 Hz	Bi ↑ / 1-4 Hz (R > L)	Bi ↑	↓ HbO ↓ HbT ↓ HbR	R PreCG, SMG, AntPFC, IFG, MFG, SFG **
P5	BS burst (206)	55.5 ± 55.9 s (2.2 ± 0.7 s)	Generalized	Bi ↑ / 1-16 Hz	Bi ↑ / 1-4 Hz	Bi ↑	↑ HbO ↑ HbT ↓ HbR	Bi AntPFC, IFG, SFG, TL (diffuse)
	BS suppression (205)	2.2 ± 0.7 s (55.5 ± 55.9 s)	Generalized	Bi ↓	Bi ↓	Bi ↓	↓ HbO ↓ HbT ↑ HbR	Bi AntPFC, IFG, SFG, TL (diffuse)
P6	NCSE seizure (33)	5.1 ± 2.3 s (370.7 ± 489.2 s)	Bi FC (L > R)	Bi ↑ / 1-25 Hz	Bi ↑ / 1-16 Hz	Bi ↑	↑ HbO ↑ HbT ↓ HbR	L SFG, IFG, R MFG, Bi PreCG, SMG (L > R)
	BS burst (3333)	2.2 ± 1.3 s (2.5 ± 1.6 s)	Generalized	Bi ↑ / 1-25 Hz	Bi ↑ / 1-9 Hz	Bi ↑	↑ HbO ↑ HbT ↓ HbR	Bi diffuse FL, L SMG, R PTL
	BS suppression (3330)	2.5 ± 1.6 s (2.2 ± 1.3 s)	Generalized	Bi ↓	Bi ↓	Bi ↓	↓ HbO ↓ HbT ↑ HbR	Bi diffuse FL, L SMG, R PTL
	GPD (1970)	(3.9 ± 3.7 s)	Generalized	Bi ↑ / 4-16 Hz	Bi ↑ / 1-16 Hz	Bi ↑	↑ HbO ↑ HbT ↓ HbR	Bi AntPFC, MFG, IFG, SMG, PTL
P7	BS burst (845)	4.6 ± 1.8 s (5.2 ± 2.3 s)	Generalized (R > L)	Bi ↑ / 1-4 Hz (R > L)	Bi ↑ / 1-4 Hz (R > L)	Bi ↑ (R > L)	↑ HbO ↑ HbT ↓ HbR	Bi AntPFC, PreCG, R MFG, PTL (R > L)
	BS suppression (844)	5.2 ± 2.3 s (4.6 ± 1.8 s)	Generalized	Bi ↓	Bi ↓	Bi ↓	↓ HbO ↓ HbT ↑ HbR	Bi AntPFC, PreCG, R MFG, PTL

*Approximate locations based on the main HbO response. HbR responses were seen to be more heterogeneous. **Only right hemisphere signal was obtained. Abbreviations. AntPFC: anterior prefrontal cortex, Bi: bilateral, CPTO: centro-parieto-temporo-occipital, FC: fronto-central, FCT: fronto-centro-temporal, IFG: inferior frontal gyrus, L: left, MFG: middle frontal gyrus, PreCG: precentral gyrus, PTL: posterior temporal lobe, R: right, SFG: superior frontal gyrus, SMG: supramarginal gyrus, STL: superior temporal lobe, TL: temporal lobe.



Figure 31 – Qualitative EEG findings for each neuroICU patient included in the analysis (quantitative EEG, qEEG, results are not show, but representative qEEG results for each patient is described below). For each patient, a selected EEG clips demonstrating the detected abnormal events is presented. EEG clip legend: In patients identified with non-convulsive seizures, the seizure period was shown with red shadowed blocks; in patients with burst-suppression patterns, green vertical bars indicated the onsets of bursts and red vertical bars indicated offsets of bursts; in patients presenting periodic discharges, the timing of the discharges was marked with yellow vertical bars. Patient P1: qEEG analysis during each seizure revealed bilateral increase in rhythmicity, frequency and amplitude ($R > L$). Patient P2:

qEEG analysis during seizures revealed a bilateral increase ($L > R$) in rhythmicity, frequency and amplitude. Patient P3: qEEG analysis revealed an increase in rhythmicity, frequency and amplitude during bursts with a strong tendency toward the right hemisphere. Patient P4: qEEG analysis during non-convulsive seizures revealed an increase in rhythmicity, frequency and amplitude ($R > L$). Patient P5: qEEG analysis during bursts revealed a bilateral increase in rhythmicity, frequency and amplitude. Patient P6: qEEG analysis during seizures (above figure) and bursts (bottom figure) reveal a bilateral increase in rhythmicity, frequency and amplitude. Patient P7: qEEG analysis revealed increases in rhythmicity, frequency and amplitude ($R > L$) during burst.

9.4.2 Hemodynamic changes associated with NCS in NCSE

NCSE was identified from EEG in three patients (P2, P4 and P6). In addition, Patient P1 showed seizure-like activities including bursts of spikes and bursts of fast activities. The representative HRFs to bursts of spikes, bursts of spikes plus and bursts of fast activities all showed large increases in HbO and HbT, and a delayed HbR increase (**Figure 32A**). The associated HbO/HbT increases and HbR decreases were seen to be relatively short which was as expected considering the briefness of the bursts (mostly $< 2s$). In Patients P2, P4 and P6, a total of 199 seizures with a mean duration of 16.6s and a standard deviation of 20.4s were recorded and analyzed. Among them, over 88% of the seizures lasted less than 25s. These seizures formed bins that contained at least three samples in our event-related analysis. In this section, we present the representative HRFs and the cortical projections of hemoglobin concentration changes from bins of seizures less than 25s. On the other hand, bins of seizures with durations $> 25s$ usually did not contain many samples for analysis (i.e. < 3) and were not always present across patients. These bins of longer seizures were treated as events of non-interest in each patient's GLM to control their potential confounding effect in the estimation of the hemodynamic response to other events that were temporally overlapped or adjacent. The results of long seizures are therefore not shown here. In all of the three patients, the representative HRFs showed an overall increase in HbO concentration with mean PA of $0.067 \pm 0.026\mu M$ averaged across patients, an increase in HbT (mean PA = $0.061 \pm 0.029\mu M$) and a decrease in HbR (mean nadir amplitude = $-0.028 \pm 0.021\mu M$) following the onset of an NCS (**Figure 32B, 32C, 32D**). These changes returned to baseline at around 10 seconds after the offset of the NCS. Linear mixed-effects models modelling seizure duration with fixed effects for response PA failed to report significant correlation for any of the hemoglobin types at $\alpha = 0.05$ (**Figure 33A**). However, the relation between seizure duration and response FWHM was statistically significant for HbO with $p = 0.021$ and adjusted R-squared value = 0.569 and for HbT

with $p = 0.034$ and adjusted R-squared value = 0.403 (**Figure 33B**), showing a positive correlation between the lengths of EEG evidence of seizures and the durations of associated hemodynamic changes. An initial dip characterized mainly by a large decrease in HbO at the beginning of the response was observed in Patients P4 (**Figure 32C**, see orange arrows on the representative HRF plots) and P6 (**Figure 32D**, see black arrows).

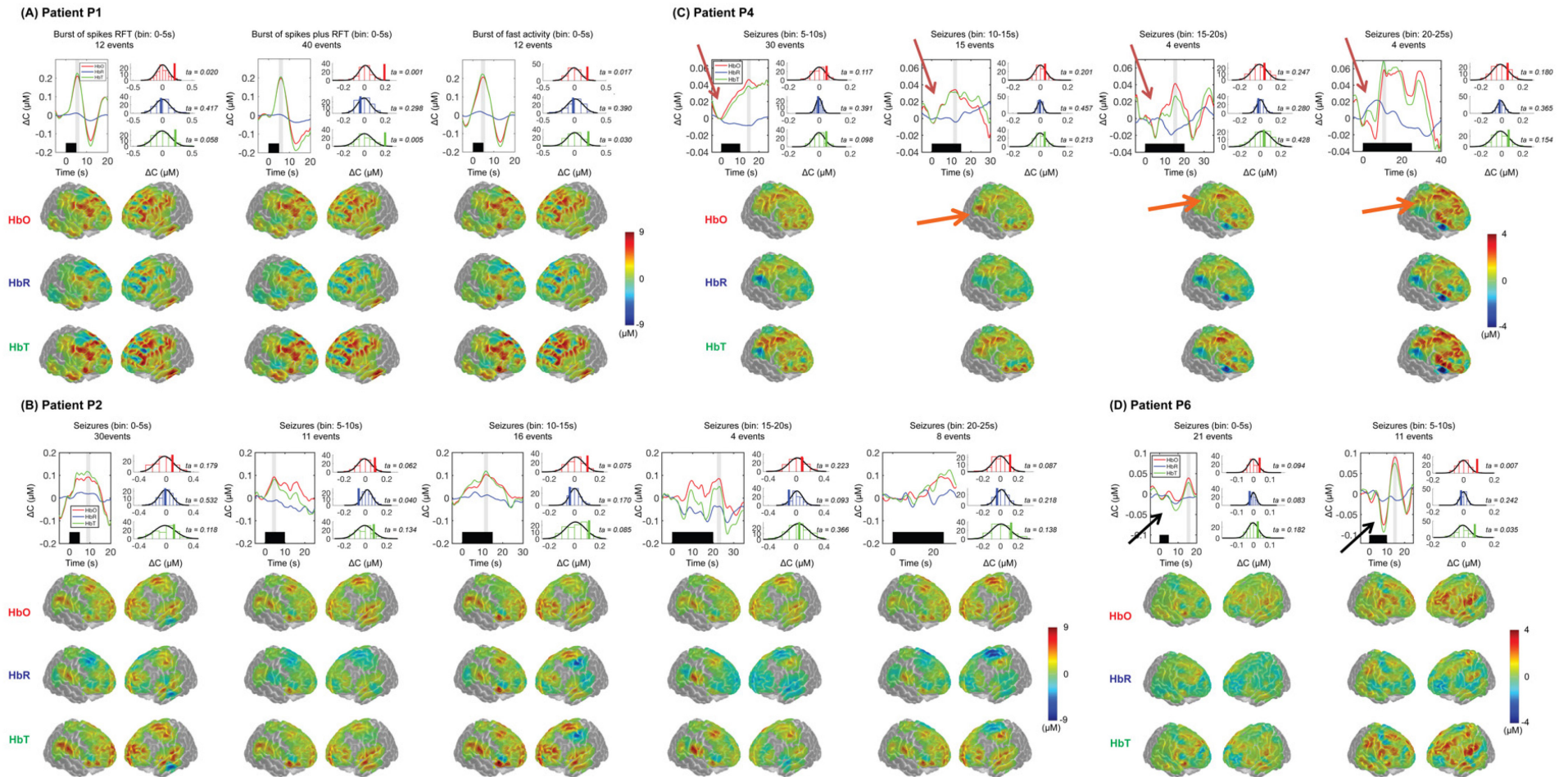


Figure 32 – Hemodynamic changes associated with NCS: (A) Patient P1; (B) Patient P2; (C) Patient P4; (D) Patient P6. Please refer to Figure S2 for optodes distribution montage and cortical sensitivity profile. The top right panel shows the extracted representative HRFs of HbO, HbR and HbT for each of the seizure bins. Note that no error bar was given as the representative HRF was generated from a PCA analysis of the HRFs of individual channels. Instead, a confidence level represented by the ratio of tail area divided by the PA of the representative HRF relative to the entire distribution area of the amplitudes of spurious HRFs generated from surrogate timecourses was shown. The black horizontal bars indicate the timing of seizures observed on EEG. The bottom right panel depicts the cortical projections of PA (averaged within a 2-sec window around the maximum value, or the minimum value if a nadir was detected). The PA time periods averaged are also highlighted with gray shaded bars directly on the representative HRF plots. For Patient P4, only the right-side projections are shown, as cortical coverage was limited on the left side due to the patient's position during the scan.

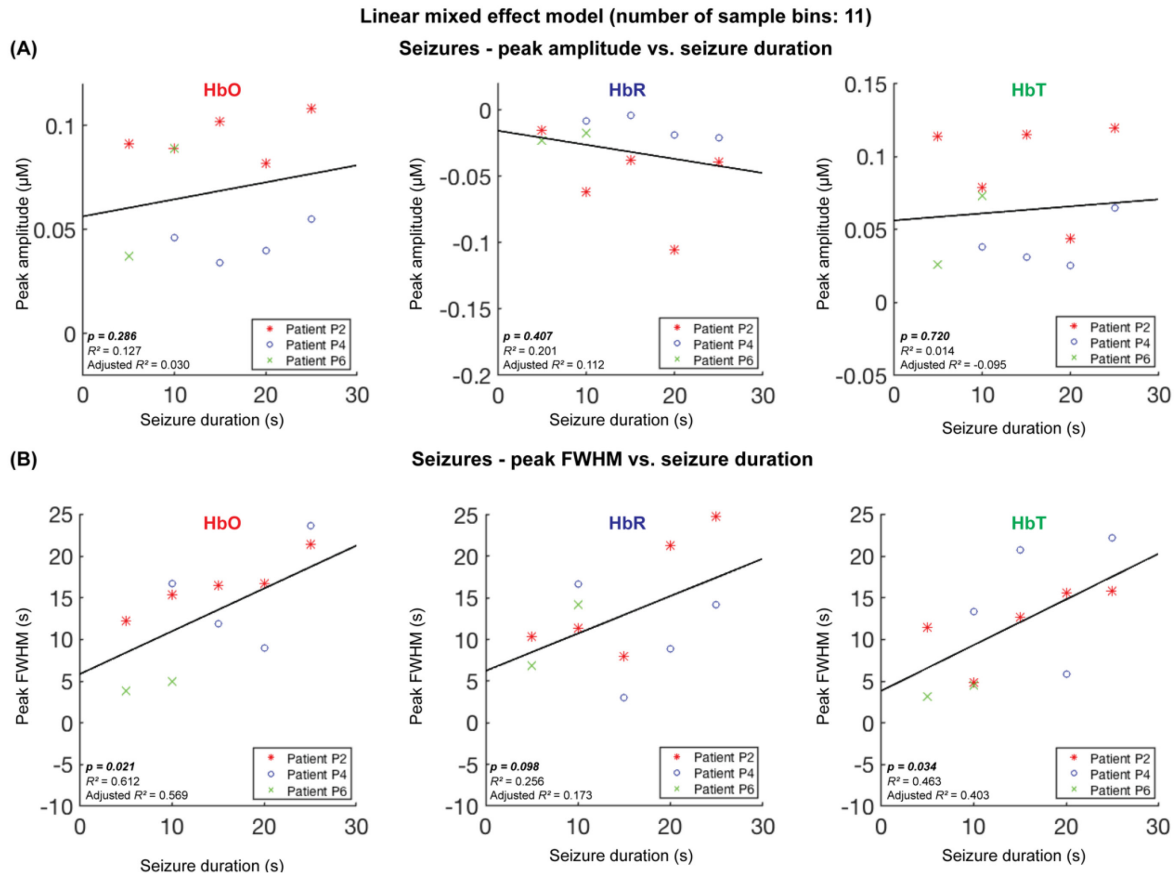


Figure 33 – Regression plots of linear mixed effect regression models relating (A) PA and (B) peak FWHM of representative HRFs to seizures to the duration of seizures identified on EEG. Statistically significant results were obtained for HbO Peak FWHM vs. Seizure duration ($p = 0.021$) and HbT Peak FWHM vs. Seizure duration ($p = 0.034$). The black lines depicted the predicted values using only the fixed effect regression coefficients for demonstration purposes.

For each patient, cortical projection of the hemoglobin concentration changes revealed brain regions that showed a highest level of magnitude in the HbO response to NCS. These regions were in most cases concordant with structural findings and electrophysiological results (**Table 17**, comparison of electrophysiological and optical findings). Moreover, hemodynamic activity in the contralateral region was also noticed in our patients. Examples included Patient P1 whose burst of spikes and fast activities were mostly identified in the right fronto-centro-temporal area on scalp EEG but showed large HbO increases in the left frontal, central and temporal regions together with right side activations (**Figure 32A - Cortical Projections**), as well as Patients P2 and P6 on whom seizures affected more the EEG signals over the left frontocentral area but were seen to be

associated with hemodynamic activations with nearly symmetrical spatial profiles in the corresponding regions of both hemispheres (**Figure 32B and Figure 32D - Cortical Projections**).

9.4.3 Hemodynamic changes associated with BS

BS patterns were observed in four patients (Patients P3, P5, P6, P7). Using the hemoglobin concentration during suppression periods as baseline, we observed increases in HbO (mean PA = $0.079 \pm 0.058\mu\text{M}$) and HbT (mean PA = $0.067 \pm 0.046\mu\text{M}$) and decreases in HbR levels (mean nadir amplitude = $-0.027 \pm 0.019\mu\text{M}$) following the onset of bursts in the representative HRFs of all those patients, see **Figure 34**. Similar to NCS-related responses, the duration and amplitudes of these changes were positively correlated with the lengths of the bursts (**Figure 35**), with $p = 0.000078$ and $p = 0.0096$ and for the HbO PA and FWHM, $p = 0.00017$ and $p = 0.000089$ for HbR nadir amplitude and FWHM, and $p = 0.00023$ and $p = 0.00024$ for HbT PA and FWHM. FWHM, and $p = 0.018$ for a negative correlation between HbR nadir amplitude and burst duration. An HbO decrease prior to the main HbO increase, with its nadir at around 10 seconds after the burst onset time, was observed in Patients P3 (**Figure 34A** purple arrows) and P5 (**Figure 34B** pink arrows).

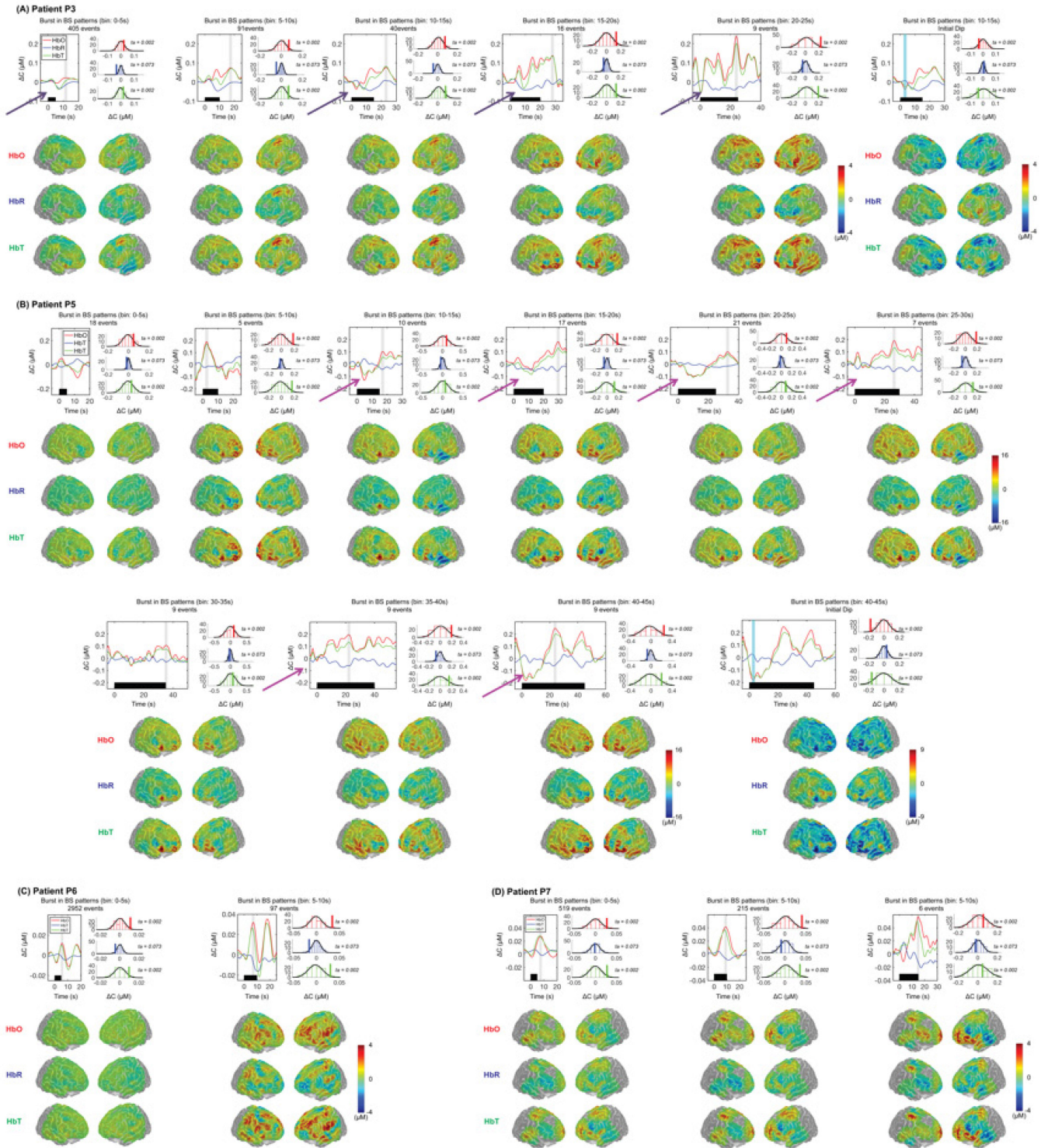
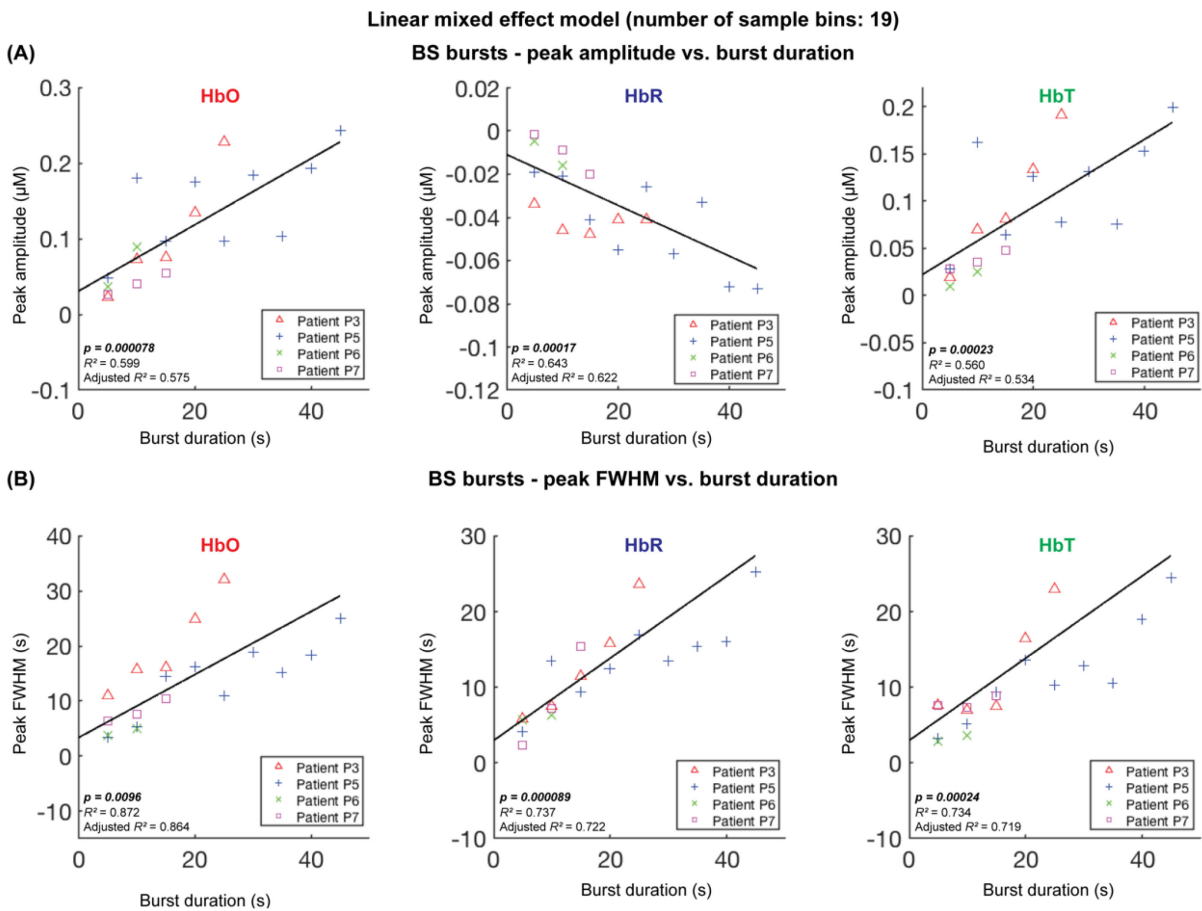


Figure 34 – Hemodynamic changes associated with BS bursts: (A) Patient P3; (B) Patient P5; (C) Patient P6; (D) Patient P7. Please refer to Figure S2 for optodes distribution montage and cortical sensitivity profile. The top right panel shows the extracted representative HRFs of HbO, HbR and HbT for each of the burst bins. A confidence level represented by the ratio of tail area divided by the PA of the representative HRF relative to the entire distribution area of the amplitudes of spurious HRFs generated from surrogate timecourses was shown for each representative HRF. The black horizontal bars indicate the timing of bursts observed on EEG. The bottom right panel depicts the cortical projections of PA. The PA time periods averaged are also highlighted with gray shaded bars directly on the representative HRF plots. For Patient P3 and P5, the last set of projections showed the spatial profile of hemodynamic changes around the initial HbO “dipping” period (highlighted in cyan on the HRF plots).



When using the burst period as the comparison baseline, suppression periods were seen to be associated with a large HbO decrease (mean nadir amplitude = $0.019 \pm 0.014\mu\text{M}$) and HbR increase (mean PA = $-0.050 \pm 0.039\mu\text{M}$) in all four patients (**Figure 36**), indicating a global reduction in oxygen supply during suppression. Unlike the bursts, the main nadir time of the hemodynamic response to suppression periods seemed to be always around 10 seconds after the suppression onset regardless of how long the suppression lasted on EEG (with only one exception in Patient 3, bin of 5s suppression, see **Figure 36A** blue arrow).

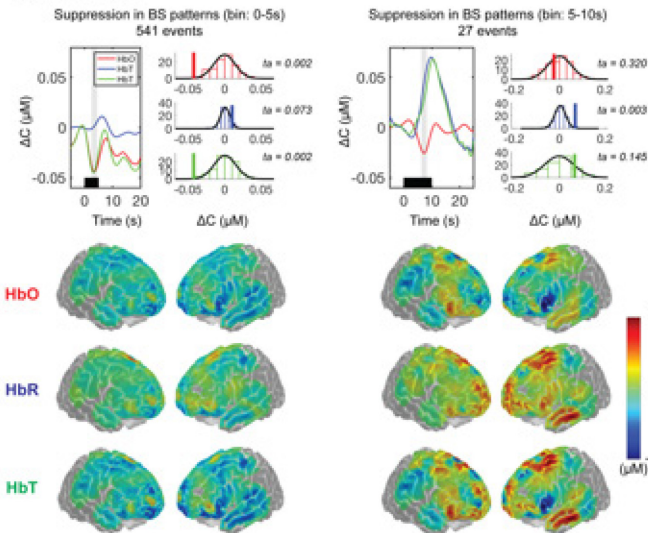
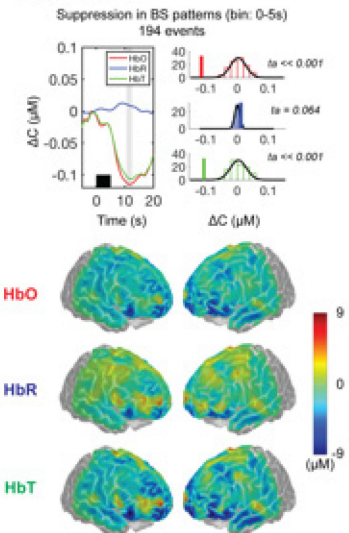
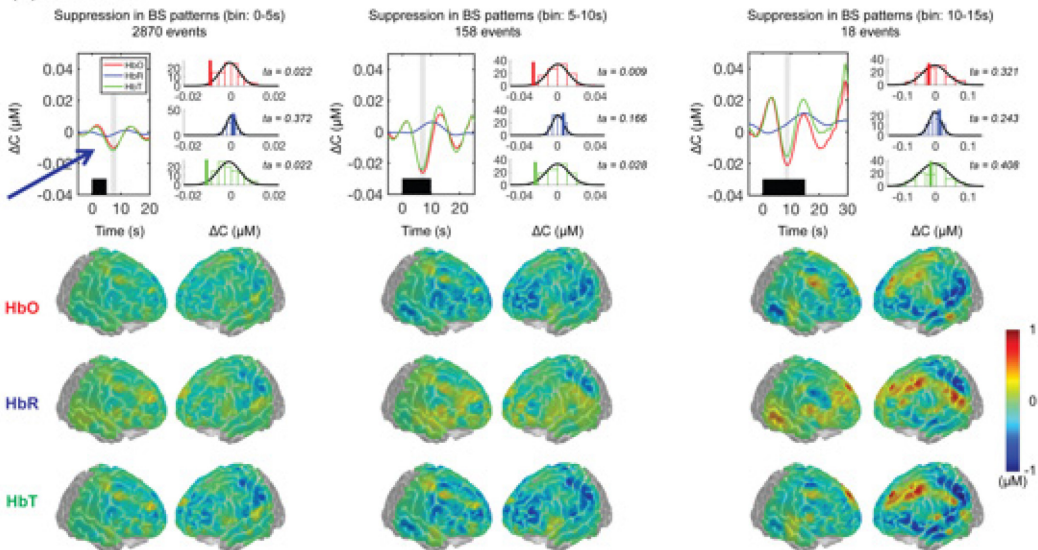
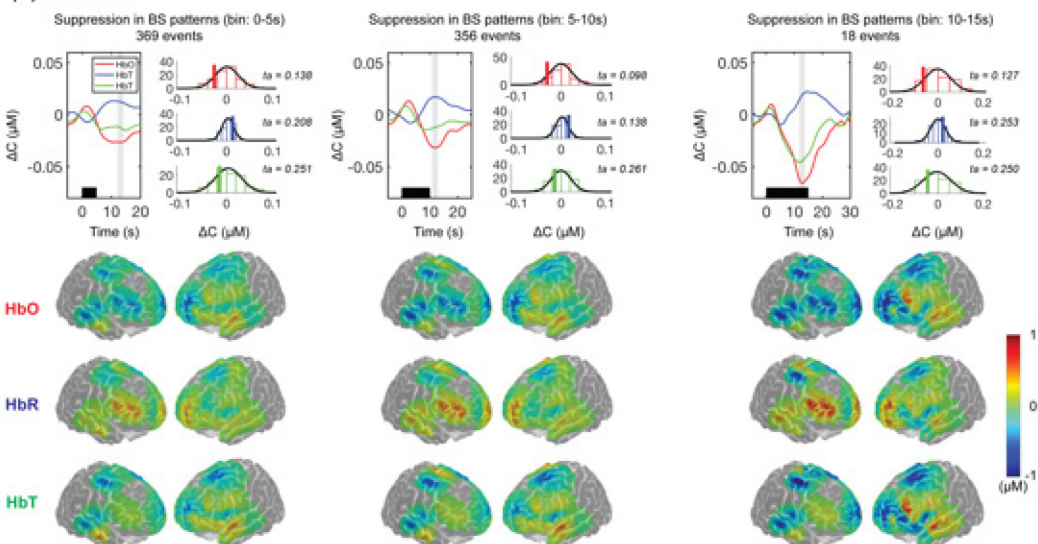
(A) Patient P3**(B) Patient P5****(C) Patient P6****(D) Patient P7**

Figure 36 – Hemodynamic changes associated with BS suppressions: (A) Patient P3; (B) Patient P5; (C) Patient P6; (D) Patient P7. Please refer to Figure S2 for optodes distribution montage and cortical sensitivity profile. The top panel shows the extracted representative HRFs of HbO, HbR and HbT for each of the suppression bins. A confidence level represented by the ratio of tail area divided by the PA of the representative HRF relative to the entire distribution area of the amplitudes of spurious HRFs generated from surrogate timecourses was shown for each representative HRF. The black horizontal bars indicate the timing of suppression observed on EEG. The bottom panel depicts the cortical projections of PA. The PA time periods averaged are also highlighted with gray shaded bars directly on the representative HRF plots.

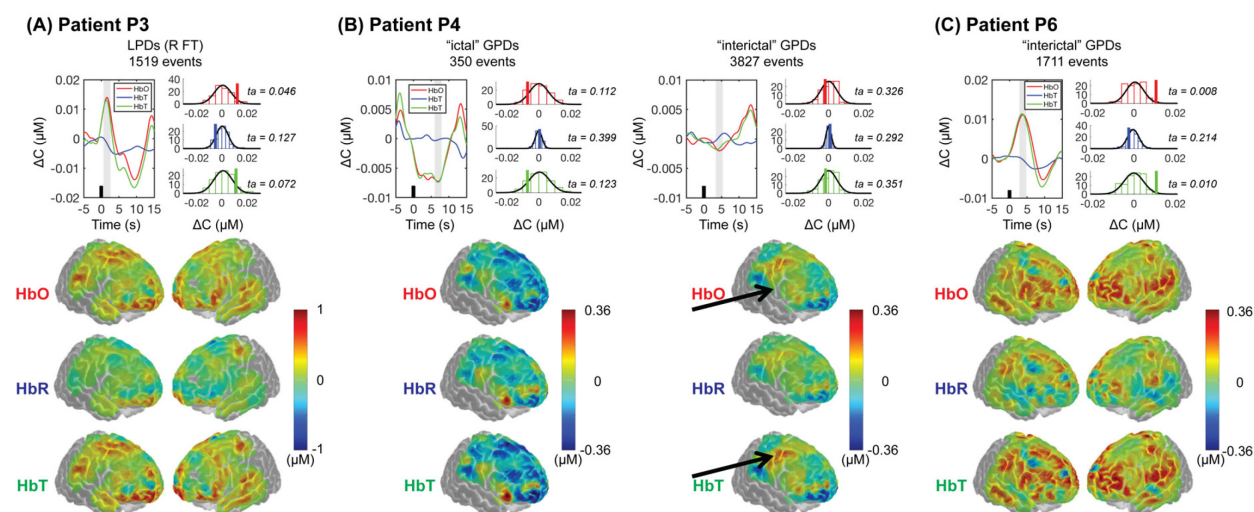


Figure 37 – Hemodynamic changes associated with PDs: (A) Patient P3; (B) Patient P4; (C) Patient P6; (D) Patient P7. Please refer to Figure S2 for optodes distribution montage and cortical sensitivity profile. The top panel shows the extracted representative HRFs of HbO, HbR and HbT for PD bins. A confidence level represented by the ratio of tail area divided by the PA of the representative HRF relative to the entire distribution area of the amplitudes of spurious HRFs generated from surrogate timecourses was shown for each representative HRF. The black vertical bars indicate the timing of PDs observed on EEG. The bottom panel depicts the cortical projections of PA. The PA time periods averaged are also highlighted with gray shaded bars directly on the representative HRF plots. For Patient P4, note that the highlighted window for “interictal” GPDs was selected to be around 4.4s (minimum value of the initial HbO decrease) instead of 13.35s. The main HbO response of “interictal” GPDs, similar to that of “ictal” GPDs, was identified to be the first nadir. The HbO increase peaking at 13s was likely part of the overshoot following the initial HbO decrease.

Cortical projections of the hemodynamic response to bursts confirmed that the increase in HbO and the decrease in HbR were bilateral, and usually affected a large portion of the cortex. However, regions such as the anterior frontal and the central areas were seen to respond more significantly than the others, exhibiting the largest changes in HbO in all of our four patients (e.g., see **Figure**

35A, 35B, 35C Cortical projections). Moreover, decreases in HbO were also noticed, especially in the left temporal lobe (e.g., see Patients P3, **Figure 35A**, P5, **Figure 35B**, P7, **Figure 35D**). Short suppression periods (< 5s) were associated with a general HbO decrease across the cortex (**Figure 36**, bins of suppression less than 5s). Interestingly, as suppressions went longer, some hemodynamic “re-activities” were seen, commonly in areas such as temporal and medial prefrontal regions (e.g., see **Figure 36A** bin of suppression 5-10s, **Figure 36C** bin of suppression 10-15s, **Figure 36D** bin of suppression 10-15s).

9.4.4 Hemodynamic changes associated with PDs

Three patients presented PDs in our cEEG-fNIRS scan. In Patient P3, 1573 right LPDs were identified during bursts of ongoing BS patterns. For Patient P4, we identified 4649 GPDs, including 363 GPDs occurring during NCS (denoted as “ictal PDs”), and 4286 GPDs during interictal periods (i.e. “interictal PDs”). Patient P6 presented patterns of NCSE, continued BS and GPDs throughout the recording. The detected 1970 GPDs only occurred during interictal bursts and not during seizures.

The representative HRFs to PDs showed hemodynamic response with an expected shape in Patients P3 (**Figure 37A**) and P6 (**Figure 37C**), characterized by a major increase in HbO (mean PA = 0.012 μ M) and HbT (mean PA = 0.011 μ M) as well as a decrease in HbR (mean nadir amplitude = -0.004 μ M), followed by an undershoot. The peaking time of HbO **response** was around 1.6s and 3.8s for Patient P3 and P6 respectively, which was earlier than that seen in adult canonical HRFs (peaking around 5-6 s). The representative HRF to PDs showed an inverted shape in Patient P4 with a notable decrease in HbO (PA = -0.007 μ M) and in HbT (PA = -0.007 μ M) for ictal PDs (**Figure 37B**). These decreases were much less significant with interictal PDs, showing a lower nadir amplitude (-0.002 μ M for HbO and HbT) and a lower nadir FWHM, e.g., 3.5s for HbO compared with 8.6s associated with ictal PDs.

Cortical projection of hemoglobin concentration changes showed bilateral and widespread HbO and HbR responses in Patients P3 (**Figure 37A**) and P6 (**Figure 37C**). Furthermore, in those two patients, the cortical areas that exhibited the strongest changes were seen to highly overlap the regions responding to bursts or seizures in the previous analysis (e.g., for Patient P3, see **Figure**

36A Cortical Projections of Burst bins 15-20s and 20-25s). For Patient P3, we observed more significant HbO increase (with regards to response magnitude) in the right side relative to the left side (**Figure 37A**), which was concordant with the EEG finding of LPDs lateralized to the right hemisphere. For Patient P4, simultaneous decreases in HbO and HbR were identified in the frontal regions. However, the central areas showed distinct responses to GPDs, with an HbO decrease following ictal GPDs but a more canonical HbO increase following interictal PDs (see the projected regions marked with black arrows in **Figure 37B**).

9.4.5 Case studies

Below, we provide two case studies to illustrate our study procedures and results in details.

Illustrative case 1, patient P3

A 52-year-old woman with right frontal lobe glioblastoma multiforme (partially resected and treated with radiation four years prior) was admitted for clinical seizures followed by NCSE successfully treated with antiseizure medications and anesthetics towards a burst-suppression pattern. Brain CT showed mild right frontal vasogenic edema (**Supplementary Figure 8C, right**). cEEG-fNIRS monitoring was conducted for a total of 4.5 hours, from which 100 minutes of recording were selected for analysis. During that time period, she presented 693 episodes of burst and suppression (average duration: 5.9 ± 8.1 s, average frequency: 0.1 Hz) and 1573 right frontal LPDs spreading to the left frontal region (average frequency: 0.6 Hz). While BS patterns were generalized, they were observed to be more predominant over the left hemisphere (**Supplementary Figure 8C**).

Fifty-five valid fNIRS channels covered the bilateral anterior prefrontal cortex, medial prefrontal and central regions, and part of the temporal regions (**Supplementary Figure 8C, left**). In the bin analysis, the 693 bursts were grouped into 12 bins. **Figure 34A** depicts the representative HRFs to bursts for bins from [0 to 5 s] to [20 s to 25 s], which contained a total of 670 bursts ($\approx 97\%$). These HRFs of the five bins showed that, relative to the suppression periods, bursts were generally associated with an increase in HbO and HbT as well as a decrease in HbR. Moreover, the durations of the hemodynamic responses were seen to be longer and the magnitudes of the main peak were larger for bursts that lasted longer (**Figure 34A**). Early decreases, or reductions in the increases

for some bins, of HbO and HbT were also observed, which reached the nadir at around 10 s after the onset of the bursts. However, such “inverted” changes were not observed for HbR. For this patient, cortical projections revealed inhomogeneous pattern of hemoglobin concentration changes in different parts of the brain (**Figure 34A - Cortical Projections**). With shorter bursts, the area with the highest level of responsivity was seen to be within the left inferior frontal gyrus. With longer bursts, the increases in HbO were found to be larger across the fNIRS-covered cortex. Consistent with EEG findings, the amplitude of the response was larger for channels located in the left hemisphere than those in the right hemisphere. For example, for the bin of bursts between 20 s and 25 s, the mean PA of HbO response (averaged across a 2-sec window centered at 23.85s) was $0.232\mu\text{M}$ for left hemisphere channels and $0.216\mu\text{M}$ for right hemisphere channels. The HRF analysis of suppression periods relative to bursts showed a decrease in HbO and an increase in HbR for both the [0 to 5s] bin (containing 541 suppression periods) and the [5 s to 10s] bin (27 suppression periods). Unlike the bursts, longer suppression periods (> 5 s) seemed to elicit a much higher HbR increase but an overall weaker HbO decrease for this patient (**Figure 36A**). Consistent with the representative HRFs, cortical projection maps revealed several brain regions that elicited a HbO increase with long suppression periods (while short suppression was associated with a more or less global HbO decrease), including the left anterior temporal lobe and the bilateral precentral areas (**Figure 36A - Cortical Projections**). These results suggested that, despite continued suppression of neuronal activity, rapid changes in the level of oxygen consumption blood supply might still take place in some brain regions towards the end of long suppression periods.

Due to the briefness of the LPDs, the 1519 right frontotemporal LPDs were grouped into a single bin of [0 to 5 s]. These LPDs were present only within the bursts, with an overall mean IPDI of 1.7 s (frequency = 0.6 Hz). The representative HRFs showed an expected increase in HbO and HbT as well as a decrease in HbR following the LPDs (**Figure 37A**). The HbO and HbT increases were seen to peak at around 1.6 s, followed by an undershoot with its nadir at around 9.45s after the LPD. The decrease in HbR reached the minimum value 2.6s after the HbO peak, at around 4.2s post-LPD. Cortical projections revealed bilateral HbO increases in most of the cortical areas covered by fNIRS, showing widespread hemodynamic response to LPDs (**Figure 37A - Cortical Projections**). The mean HbO PA across channels was seen to be larger in the right hemisphere ($0.013\mu\text{M}$) than in the left hemisphere ($0.011\mu\text{M}$). These observations potentially implied a

retained neurovascular coupling process for the generation of LPDs in this patient, albeit of a shorter hemodynamic response time.

Illustrative case 2, patient P4

A 57-year-old male patient with hepatic cirrhosis was admitted to the neuroICU for gastrointestinal bleeding, melena and metabolic encephalopathy. On admission day 1 the patient presented myoclonus, which later evolved, from day 2 and 3 to generalized tonico-clonic seizures, convulsive SE and eventually NCSE on day 4. Two sessions of cEEG-fNIRS was performed 7 days after admission (total duration: 7h), of which a period of 97 minutes was selected for analysis. MRI revealed T2/FLAIR hypersignal and restriction diffusion bilaterally in parietal, temporal, insular and cingulate, and thalami regions (**Supplementary Figure 8D, right**). Sixty-four bilateral seizures (maximum over the right centro-parieto-temporo-occipital regions) with an average duration of 10.3 ± 4.4 s and an averaged interictal period of 77.1 ± 148.6 s, as well as 4649 GPDs (mean IPDI = 1.2 s and mean frequency = 0.8 Hz) were identified from the EEG data (**Supplementary Figure 8D**).

Forty-one valid fNIRS channels were distributed over the bilateral anterior prefrontal cortex, the right medial prefrontal cortex and the right precentral areas (**Supplementary Figure 8D, left**). Unfortunately, due to the patient's position during the scan, fNIRS channels covering the left medial prefrontal and central areas yielded a low SNR and had to be excluded. Based on their durations, 53 NCS were grouped into four different bins with ranges from [5s to 10s] to [20s to 25s], for which the representative HRFs are shown in **Figure 32C**. From the HRFs, we identified an increase in HbO and HbT, and a decrease in HbR (relative to the interictal period) that were associated with the seizures in all of the four bins. Similar to the bursts observed in the previous case study, seizures with longer durations seemed to elicit hemodynamic responses that were also longer in duration and higher in peak magnitude. The initial decrease in HbO and HbT and the increase in HbR prior to the main response (i.e. the "initial dip") were also noticed, especially for seizures that lasted longer. Cortical projections of the concentration changes in the right hemisphere highlighted distinct regions that showed the largest HbO response magnitude within the right central and the right frontocentral areas (**Figure 32C - Cortical Projections**, Orange arrows).

Among the 4177 included GPDs, 3827 GPDs were recorded during the interictal periods (denoted as the “interictal GPDs” in this section) while the rest 350 GPDs were captured during seizures (denoted as the “ictal GPDs”). These two types of GPDs were treated as separate conditions in our HRF analysis to further explore the potential differences in the mechanism. Unlike the other two patients who also presented PDs (Patients F3 and F6), the representative HRFs to the ictal GPDs in this patient were characterized mainly by a large decrease in HbO and HbT along with a small decrease in HbR concentration (**Figure 37B**). The HbO decrease reached its nadir at around 6.95s after the GPD onset. Cortical projection of the HbO concentration revealed that the negative response was seen over a large portion of the covered right hemisphere, including the right anterior prefrontal, the medial prefrontal and the central areas (**Figure 37B Cortical Projections**). On the other hand, representative HRFs to interictal GPDs showed overall much lower HbO and HbT decreases, while the HbR level stayed almost unchanged. In fact, interictal GPDs were observed to elicit a similar HbO decrease in the right anterior prefrontal cortex. However, in the right central area where the large magnitude of hemodynamic response to seizures was located in the previous NCSE analysis, we observed an HbO increase and an HbT increase following interictal GPDs with an expected shape (**Figure 37B** black arrows). These results suggested that the neurovascular coupling for GPDs might be disrupted in some cases. For this particular patient, potential risk factors included the co-presence of seizures and a higher PD frequency (0.8 Hz as opposed to 0.6 Hz in Patient F3 and 0.3 Hz in Patient F6). The hemodynamic response with an expected shape, i.e. increases in HbO and decreases in HbR, to interictal GPDs in the right central area indicated less stress on local oxygen supply for GPDs when seizure activities were not continued.

9.5 Discussion

To the best of our knowledge, this study is the first to report simultaneous electrophysiological and hemodynamic changes observed in critically ill adults patients presenting with SE, PDs and pharmacologically induced BS patterns using cEEG-fNIRS. Through the analysis of seven patients, we assessed the feasibility and the clinical value of cEEG-fNIRS for long-term monitoring in the neuroICU.

9.5.1 Increased blood oxygenation during seizures in status epilepticus

SE represents an extreme ictal phenomenon, in which “normal” mechanisms responsible for seizure termination fail. Among those mechanisms, hypoxia has been proposed (Zubler et al., 2014). Animal models of SE generally showed an increase in cortical blood oxygenation due to higher metabolism of the ictal state (Lee et al., 2018). In humans, both states of hyper and hypometabolism have been reported in patient with NCSE (Siclari et al., 2013). For example, EEG-fMRI acquisition in focal motor status epilepticus cases (*epilepsia partialis continua*) shows a BOLD signal increase in the focus combined with a widespread BOLD signal deactivation (Lazeyras et al., 2000). This dynamic reflects the redistribution of CBF and extreme focal modulation of oxygen extraction in the benefit of the hyperactive ictal focus. Indeed, despite the increase in CBF, anaerobic metabolic distress (increase in lactate/pyruvate ratio) and glutamate excitotoxicity have been documented during focal NCSE in patients with TBI (Vespa et al., 2007). Our findings are in line with previous studies in which ictal metabolism level during SE is associated with an increase in CBF and brain oxygenation. In all three patients, an increase in HbO, generally of larger amplitude, and a decrease in HbR, generally of lower amplitude were observed during seizures. These changes most likely suggested an increase in CBF and CBV that overcompensated the ictal increase in neuronal oxygen needed. In addition, these changes were proportional to seizure duration with shorter seizures manifesting with lower relative HbO increase and HbR decrease, showing potentially sufficient oxygen supply even towards the end of the seizures. Overall, our data do not seem to support the hypothesis that hypoxia is the main cause of seizure termination in SE.

Another important finding is that the fNIRS-measured hemodynamic responses were generally the largest in the focal cortical areas involved in seizures. This is clinically important as fNIRS have the potential to not only help in the diagnosis of NCS and NCSE, but also in improving seizure localization.

9.5.2 Non-uniform cortical hemodynamic profile during burst-suppression

The traditional perception of BS, as a uniform and global state of brain activity, has been challenged over the last decade (Ferron et al., 2009; Lewis et al., 2013). In vivo studies in the

anesthetized cat have shown that neuronal activity in subcortical structures can be increased during suppression, which may elicit bursts sequences in the hyperexcitable cortex (Amzica, 2009). More recently, intracranial EEG recordings performed in anesthetized patients undergoing epilepsy surgery revealed the asynchronous nature of burst-suppression patterns across the cortex (i.e. burst and suppression not occurring at the exact same time and in all regions alike) (Lewis et al., 2013). Neurovascular dynamics and cerebral metabolism seem to be among critical processes underlying the genesis of BS patterns (Ching et al., 2012; Lewis et al., 2013). Using fMRI, spontaneous multifocal fluctuation in CBF and BOLD signals during BS has been observed in anesthetized swine and rats (Liu et al., 2011; MÄkiranta et al., 2002). Optical imaging (NIRS and diffuse correlation spectroscopy) with simultaneous scalp-EEG have also been used in anesthetized rats and showed an increase in metabolism and CBF associated with each burst (Sutin et al., 2014). In humans, transient stereotypic changes characterized by an initial HbO decrease followed by a pronounced HbO increase during spontaneous bursts was reported in premature neonates presenting with neurological distress (Roche-Labarbe et al., 2007), and during hypothermia-induced BS in infants with hypoxic-ischemic encephalopathy (Chalia et al., 2016). The shape of the response was seen to be highly variable across different brain regions and different patients.

This pilot study is the first to assess hemodynamic features of BS in comatose adults. Our results were largely consistent with these previous reports, showing an overall but spatially inhomogeneous increase in HbO and a less significant overall decrease in HbR during bursts relative to the suppression period in all of the four patients in whom BS patterns were identified. The relationship between the amplitude and the duration of the HbO increase and burst length seen on EEG suggested that the neuronal metabolism was adequately compensated. The initial decrease in HbO as noted in previous studies (Chalia et al., 2016; Roche-Labarbe et al., 2007), or an initial reduction in HbO increase, was also noticed in most of our patients. On the other hand, short suppression periods were followed by a more global (but also spatially inhomogeneous) reduction in HbO, suggesting an acute drop in neuronal activity and oxygen supply. Interestingly, the spatial profile of the HbO decrease in the HRF to suppression periods was seen to highly overlap with the spatial profile of the initial HbO decrease in the HRF to bursts (e.g., see the similarity between the spatial profiles of projected hemoglobin concentration changes between **Figure 34A Projection of initial dip** and **Figure 36A** bin of 0-5s, as well as between **Figure 34B Projection of initial**

dip and **Figure 36B**). This suggest that the initial HbO decrease seen in the response to bursts, which usually reached its nadir at around 5-10 sec after the burst onset, could possibly be part of a delayed hemodynamic effect of the suppression periods preceding the bursts. An alternative interpretation is that the initial mismatch between oxygen demand and blood supply at the beginning of bursts occurs at cortical sites that have been mostly suppressed in the suppression periods. Nevertheless, our results provide further evidence for non-uniform hemodynamic changes during BS patterns, and highlight the potential of using fNIRS to study the spatial distribution of this response.

9.5.3 Potential factors associated with hemodynamic response to PDs

Clinical management of critically ill patients presenting with EEG patterns falling within the IIC still poses a significant challenge to physicians. In addition to considering clinical factors (e.g., response to treatment), researchers have resorted to multimodal neuroimaging techniques to better understand the “ictal vs. interictal nature” of these patterns, their impact on the brain and improve the management of the critically ill presenting with IIC patterns (Claassen, 2009). Both FDG-PET hypermetabolism and hypometabolism have been observed in patients with PDs patterns (Sakakibara et al., 2014; Struck et al., 2016). In another study by Vespa et al., PDs displayed a metabolic crisis similar to what has been previously seen during seizures by the same authors (Vespa et al., 2016). More recently, Witsch et al. used invasive EEG recordings, brain tissue oxygen tension (PbTO₂), and rCBF in patients presenting with subarachnoid haemorrhage (SAH) (Witsch et al., 2017). In their study, PDs (GPDs and LPDs) > 2 Hz were associated with a decrease in PbTO₂, while an increase in PbTO₂ was observed for 0.5 < PDs < 2 Hz. Based on these observations, the authors suggested a metabolic decompensation was most likely to occur when PDs > 2 Hz, and, therefore, would require more aggressive treatment.

In our study, two of the three patients with PDs presented an overall increase in HbO and HbT as well as a decrease in HbR (one with GPD and one with LPD), potentially suggesting a normal neurovascular coupling process and sufficient compensation of oxygen following the PDs. These findings are in line with the features reported by Witsch et al. (Witsch et al., 2017) in PDs ≤ 2Hz. The hemodynamic mapping of these changes was widely spread in patients with GPDs, and more focalized in LPDs. However, in the other patient (Patient P4), we observed an inverted shape of

HbO and HbT responses to GPDs. This might be due to a higher PD frequency detected in the patient (0.8 Hz compared with 0.6 Hz in Patient P3 and 0.3 Hz in Patient P6) or the co-presence of seizures. In particular, the GPDs occurring during the seizures (ictal GPDs) showed a prominent HbO decrease over a large portion of the right hemisphere, while the GPDs within the interictal periods were associated with similar HbO decreases in the prefrontal cortex but a weak HbO increase around the presumed epileptic focus area. These observations implied a possible change CBF and blood oxygenation from the other portion of the cortex towards the focus area during PDs. Moreover, the hemisphere-wise HbO and HbT decrease following ictal PDs revealed inadequate oxygen reserve for PDs during seizures, leading to a potential hypoxic-ischemic state. While further confirmation of our results is needed, these data showcase the advantages of cEEG-fNIRS in delineating the full dynamic profile of the hemodynamic response associated with PDs and its potential to be used to assist in the process of clinical management.

9.5.4 Feasibility of conducting cEEG-fNIRS in the neuroICU

The current work represents the first study of using combined cEEG-fNIRS in the adult neuroICU to monitor hemodynamic changes associated with abnormal EEG events, including SE, medically-induced BS and PDs. We were able to place a large number of fNIRS optodes (> 50) to enable coverage of nearly the full head (except occipital and posterior temporal/parietal areas), and performed long-term EEG-fNIRS recordings in 11 comatose patients (for up to 32h). These progresses are important in showing the feasibility of conducting continuous hemodynamic monitoring in the neuroICU. The results revealed specific and dynamic patterns associated with brief and ongoing EEG events over a long period of time. However, special arrangements in both the data acquisition and analysis had to be made to accommodate the complex data collection environment of the neuroICU. While the patients are comatose, their bodies are normally kept in a supine position and their heads tilted towards a certain direction by a pillow. This can complicate the process of installing optodes and maintaining good skin contact in the back and left posterior side of the head. In addition, the presence of stitches, invasive probes and edema may also complicate optode installation. The continuity of fNIRS measurements can be affected by routine clinical care (e.g., examination, blood sampling, suctioning, clapping), imaging needs (e.g., CT, MRI), and some forms of medical interventions (e.g., bronchoscopy). Moreover, examination and care provided by the medical staff and nurses, as well as the use of low air loss beds in the critically

ill, for pressure wounds prevention, can affect the quality of fNIRS measurement by creating significant motion artifacts during the monitoring. In our pilot study, many fNIRS channels had to be excluded due to loss of contact, low SNR or excessive motion artifacts. The exclusion of channels led to reduced coverage of brain areas and inhomogeneous sensitivity in cortical detection, which limited our ability in delineating the spatial features of the hemodynamic responses. One possible way to reduce motion artifacts and prevent optode from sliding during the monitoring would be to glue optodes with collodion (Yücel et al., 2014) directly on the scalp in the same way EEG electrodes are glued for long-term monitoring in epilepsy units. Finally, performing long-term continuous cEEG-fNIRS recording provides huge amount of recorded data. Rather than the offline GLM analysis employed in this study, clinical monitoring using cEEG-fNIRS will almost certainly require online data processing. Recent advances in real-time analysis methods such as those developed for brain-computer interfaces (Lührs and Goebel, 2017) may be considered for a faster feedback of the patient's brain electrophysiological and hemodynamic condition. Nevertheless, the review of EEG/fNIRS data, the identification of abnormal EEG events of interest and their alignment under an offline GLM or online data processing may pose significant practical challenges.

9.5.5 Limitations

This study has several limitations. First is the small sample size for each type of EEG patterns (despite a larger number of patients compared to previous studies). The results presented in this paper mostly involve short-duration events e.g., < 25s for SE seizures and < 35s for bursts in BS patterns. Our findings will have to be validated in a larger cohort of patients. Second, substantial heterogeneity (e.g., regarding age, sex, anatomical differences, type of brain injury, co-morbidities, treatment) exist in our population, which can potentially impact brain hemodynamic signals. Third, systemic physiological factors can also affect cerebral blood flow (Lührs and Goebel, 2017). While we used clinical records of different systemic physiological measurements to “grossly” exclude periods characterized by abnormal or fluctuating vital signs, it was not possible to use these measurements as covariates in our analysis due to their low temporal resolution. Fourth, short-distance optodes were not used to quantify and subtract the contribution of superficial layers (e.g., scalp, skin and skull) to the fNIRS signal. While there are currently no guidelines or gold standard for removing physiological contamination from the fNIRS signal, we decided in this study to use

a PCA filter removing 90% of the global variance. However, some residuals may remain. Finally, while our previous studies revealed significant nonlinear suppression effect in the hemodynamic response to epileptic events that might happen in rapid succession (Pouliot et al., 2012; Peng et al., 2016) (which was the case in many of our patients included in this study, e.g., patients who had PDs with a high frequency), nonlinearity was not specifically modeled in the GLM for the sake of model simplicity and data processing time. The neglect of the nonlinear component in the model may partially account for the relatively low amplitudes of representative HRFs seen in this study compared with previous work (e.g., see **Figure 37** where the amplitudes of HRF to PDs were of the order of $0.01\mu\text{M}$). Other factors that may affect the representative HRF amplitudes include the averaging of HRFs across all channels instead of targeting at a particular activated region, the empirical choice of the partial pathlength factor, the relatively low low-pass filter cutoff frequency (0.2Hz), and the loss of elasticity of cortical tissue in eliciting hemodynamic responses after repetitive, excessive neuronal firing (Arango-Lievano et al., 2018). Future studies further delineating the effects of these physiological or analytical factors may be needed to develop an analysis method that is a more suitable for this type of long and complex neuroICU data.

9.6 Conclusions

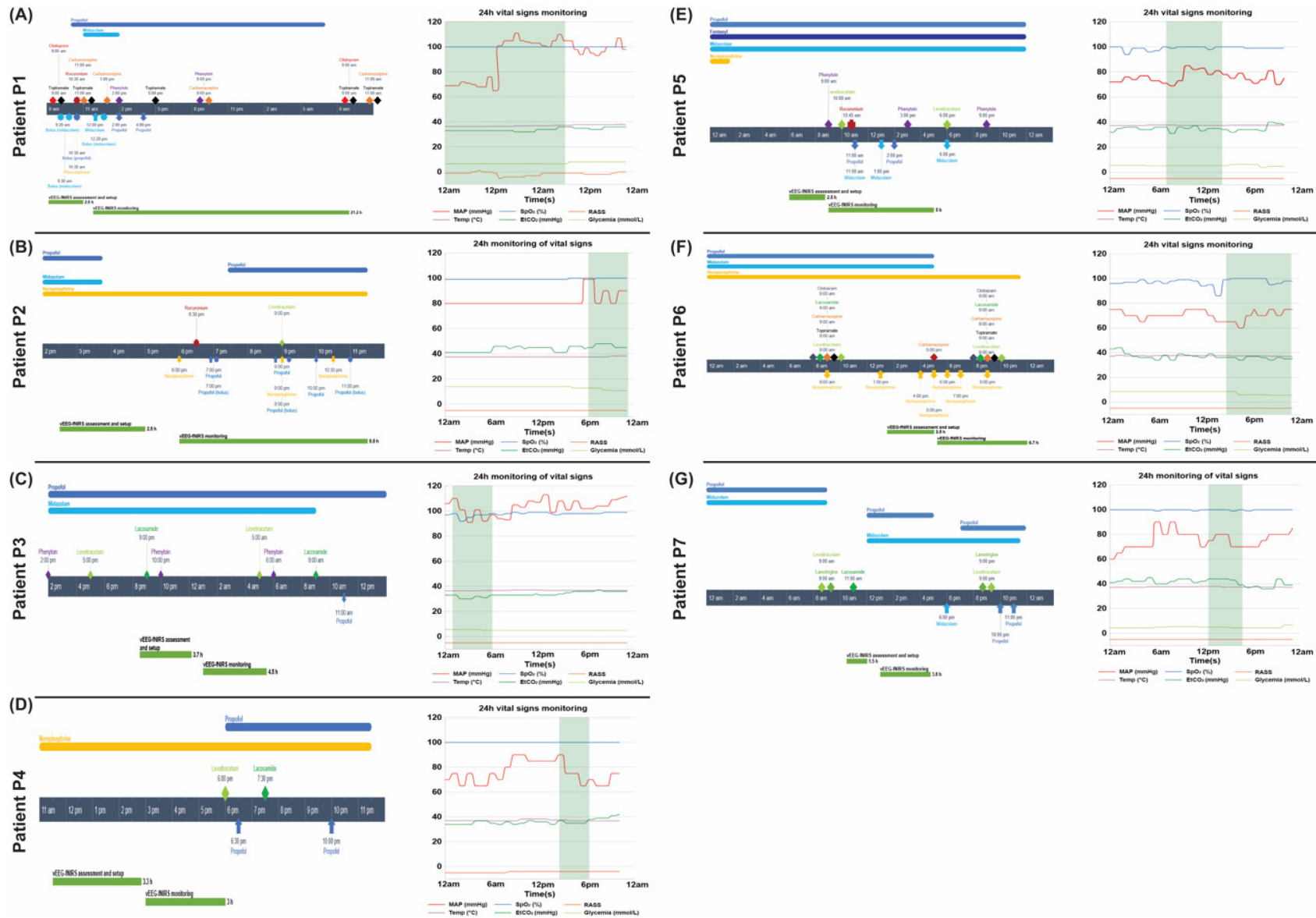
In conclusion, we conducted long-term cEEG-fNIRS recordings in the neuroICU, and analyzed the hemodynamic response to abnormal EEG patterns identified from seven comatose patients. In most cases, the electrical activity in seizures, bursts and PDs was associated with an overall increase in HbO and a decrease in HbR, with the amplitudes and durations of the hemodynamic changes positively correlated to the EEG length of the events. These responses were seen to be spatially inhomogeneous and specific to patients. Our results suggested that normal neurovascular coupling might be partially retained during these abnormal EEG patterns, while highlighting the highly varying nature of these changes across conditions and patients. This pilot work shows the feasibility of conducting cEEG-fNIRS in the neuroICU, however more extensive studies with a larger patient cohort and more advanced data collection and analysis methods (e.g., to further enlarge cortical coverage, reduce motion artifacts, and establish real-time online assessment of cortical responses) are needed to straighten our conclusions, as well as to encourage clinical

hemodynamic and electrophysiological monitoring which may help rethink strategies for patient care and treatment in the neuroICU.

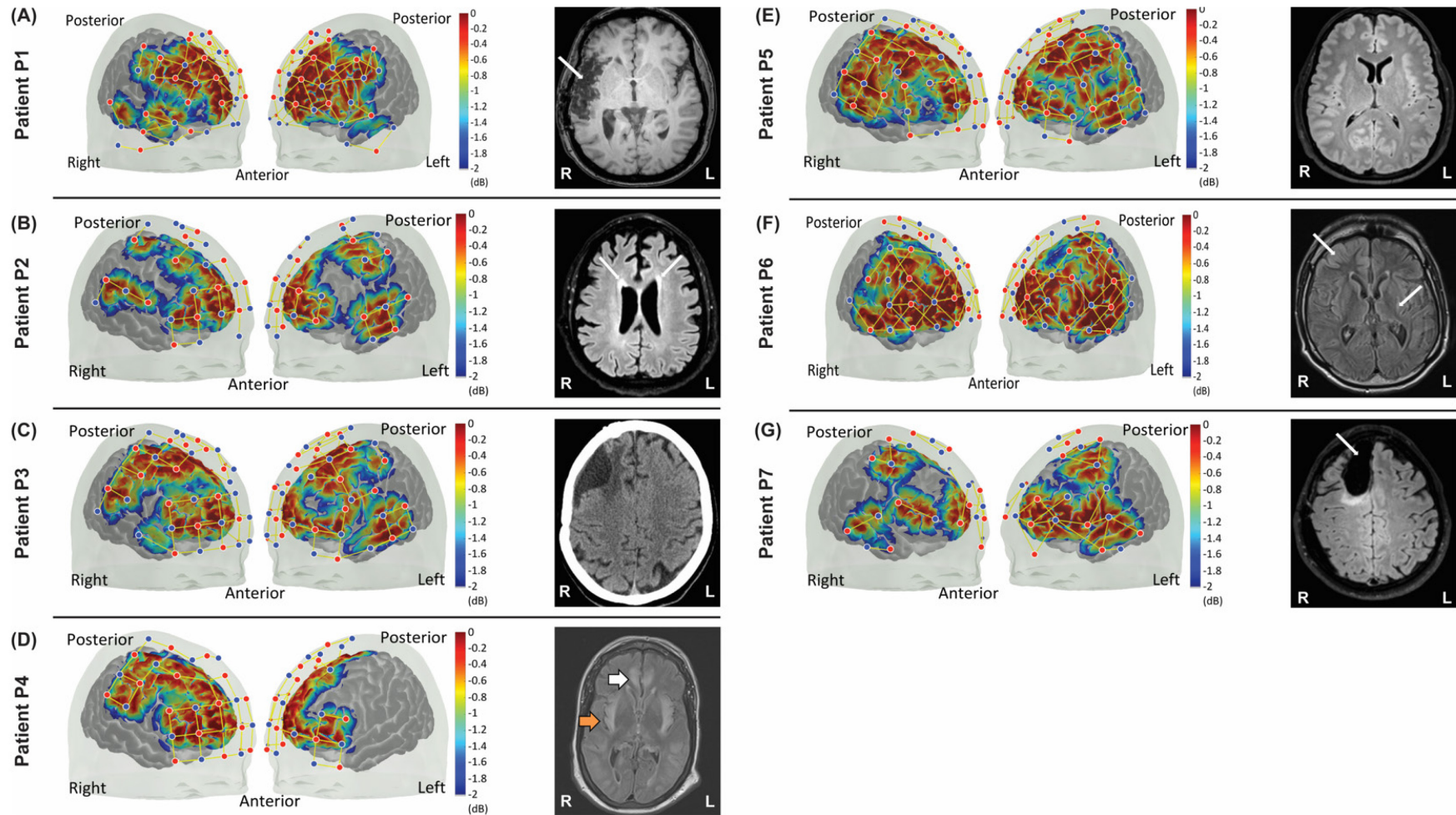
9.7 Acknowledgements

We thank all study subjects and family for their valuable participation. We also thank the ICU nurses and physicians for their support and patience during our study.

9.8 Appendix



Supplementary Figure 7 – Left Panel: Detail procedures of neuroICU care during cEEG-fNIRS recordings. Right Panel: Vital signals collected from patient's hospital records during cEEG-fNIRS recording. (A) Patient P1; (B) Patient P2; (C) Patient P3; (D) Patient P4; (E) Patient P5; (F) Patient P6; (G) Patient P7.



Supplementary Figure 8 – Optical montage (i.e., probe layout) and structural neuroimaging for each neuroICU patients included in the analysis. For each patient, left panel: selected brain slices from MRI imaging; right panel: distribution of optical emitters (red dots), optical detectors (blue dots) and channels (yellow lines) included in the analysis and the corresponding cortical sensitivity profile. Patient P1: MRI image showed surgical cavity (white arrow) from right post-temporal lobectomy. Patient P2: Diffuse cerebral atrophy and peri-ventricular white matter T2/FLAIR hyperintensity (white arrows) suggested microhemorrhage changes. Patient P3: Positron emission tomography image showed right frontal surgical cavity (white arrow). Patient P4: T2/FLAIR MRI showed multifocal and bilateral white matter (white arrow) and cortical hyperintensity lesions (orange arrow). Patient P5: MRI was normal. Patient P6: MRI scan showed cortico-subcortical change in the frontal lobe ($R > L$) (white arrow) associated with oedema and T2/FLAIR hypersignal in the thalamus ($R > L$). Patient P7: MRI image showed surgical cavity (white arrow) following oligodendroglioma resection in the right frontal lobe.

CHAPTER 10 – MANUSCRIPT #4

Cortical hemodynamics of electrographic status epilepticus in the critically ill

Ali Kassab^{a,b}, Dènahin Hinnoutondji Toffa^b, Manon Robert^{cb}, Frédéric Lesage^{c,d}, Ke Peng^{a,b}, Dang Khoa Nguyen^{a,b,e}

^aDepartment of Neurological Sciences, Université de Montréal, C.P. 6128, succ. Centre-ville, Montreal, Quebec, (H3C 3J7), Canada; ^bCentre de Recherche du Centre Hospitalier de l'Université de Montréal, Université de Montréal, 900 Saint Denis St., Montreal, Quebec (H2X 0A9), Canada; ^cBiomedical Engineering Institute, École Polytechnique de Montréal, 2500 Chemin de Polytechnique, Montréal, Quebec (H3T 1J4), Canada; ^dResearch Center, Montreal Heart Institute, 5000 Rue Bélanger, Montreal, Quebec (H1T 1C8), Canada; ^eDivision of Neurology, Centre Hospitalier de l'Université de Montréal, Université de Montréal, 1000 Saint Denis St. Montreal, Quebec (H2X 0C1), Canada

This article addresses the third objective of this thesis, which was to investigate the hemodynamic change associated with recurrent and/or prolonged electrographic seizures (i.e., NCSE) in the critically ill. This article has been submitted to *Epilepsia*.

10.1 Abstract

Status epilepticus (SE) can result in neuronal damage. While the pathophysiological mechanisms leading to brain damage are presumably multifactorial, it remains unclear whether cerebral and systemic hemodynamics are able to match neuronal activity during recurring and/or prolonged seizures, as observations from animal and human studies have been conflictual. fNIRS is currently the only modality that can continuously and safely monitor brain hemodynamics in terms of the variations of oxyhemoglobin (HbO) and deoxyhemoglobin concentrations (HbR) concentrations, which can be used to infer changes in cerebral blood volume (e.g., with the sum of the two hemoglobin concentrations -HbT) and cerebral oxygenation (e.g., with the difference of the two concentrations -HbD). For over two decades, fNIRS has been combined with simultaneous video electroencephalography (i.e., vEEG-fNIRS) in epilepsy research. However, its use in exploring critical care seizures (including SE) has been limited to only a few case studies in the pediatric setting. Moreover, there are no reports of long-term vEEG-fNIRS monitoring in critically ill patients with a large cortical coverage, in part due to the fact that recordings remain a considerable clinical and technical challenge. In order to overcome this issue and to clarify the neurovascular coupling and cerebrovascular changes occurring during recurrent and/or prolonged electrographic SE, we performed whole-head long-term vEEG-fNIRS recordings in the intensive care unit in eleven adult patients. A total of > 200h of monitoring and > 1000 seizures were recorded (seizure duration ranged from ~ 10s to ~2h, and inter-ictal interval ranged from ~1s to ~45 min). For most of the patients, we observed an increase in HbO, HbT, and HbD and a decrease in HbR associated with short-duration seizures (e.g., seizures < 100s). While a similar response could also be seen initially for long-duration seizures (e.g., > 100s), such hemodynamic change was often followed by a progressive decline in HbO, HbT, and HbD concentration and an increase in HbR, suggesting an insufficient oxygen supply and a hypoxic brain state during prolonged seizures, but also for some recurrent short duration seizures. At the systemic level, no significant changes in peripheral oxygenation occurred during seizures and only small changes in mean arterial blood pressure ($\Delta_{\max} = +4$ mmHg, $\Delta_{\min} = -3$ mmHg) and heart rate ($\Delta_{\max} = +3$ bpm, $\Delta_{\min} = -2$ bpm) occurred in 57% and 29% of patients, respectively.

10.2 Introduction

Status epilepticus (SE) is “a condition resulting either from the failure of the mechanisms responsible for seizure termination or from the initiation of mechanisms which lead to abnormally prolonged seizures” (Trinka et al., 2015). In the critically ill, SE can be the reason for admission to the intensive care unit (ICU) or develop, secondarily, in patients already admitted for other critical conditions such as an encephalitis or a brain hemorrhage. These recurrent and/or prolonged seizures can manifest with overt jerking movements (i.e., electroclinical status epilepticus, ECSE) or without any prominent motor activity (i.e., electrographic status epilepticus, ESE). ESE represents the form of SE most frequently seen (i.e., $\approx 90\%$ of cases) and can only be identified using electroencephalography (EEG) (Claassen et al., 2004).

It is well established that ECSE can cause wide-scale acute neuronal injury and death (Covolan et al., 2000; McKhann et al., 2003; Sloviter et al., 2003) even in the absence of systemic complications (Meldrum and Horton, 1973; Meldrum and Brierley, 1973; Meldrum et al., 1973a,b; Fernández et al., 2019). Key mechanisms of ECSE-induced neuronal injury (and death) are multifactorial (Walker et al., 2018), including hypoxia, overproduction of reactive oxygen species caused by excessive activation of N-methyl D-aspartate receptors (Abele et al., 1990; Deshpande et al., 2008; Kovac et al., 2012) and overaccumulation of calcium intracellularly (Camello-Almaraz et al., 2006). In contrast, fewer studies have focused on cerebral hemodynamics and systemic changes during ESE (Vespa et al., 2007; Claassen et al., 2013; Ferlini et al., 2021). Notably, it remains unclear how “clinically silent” recurrent and/or prolonged seizures influence cerebral perfusion, oxygen delivery, and cardiovascular stability.

Functional near-infrared spectroscopy (fNIRS) noninvasive imaging technique that uses near-infrared light to assess cortical hemodynamics. Compared to more commonly used functional neuroimaging techniques in patients with SE (i.e., single-photon emission computed tomography – SPECT, and positron emission tomography – PET), fNIRS has a higher temporal resolution and is currently the only modality capable of continuously monitoring cerebral hemodynamics over a large cortical surface (Scholkmann et al., 2014). Like EEG-fMRI, the simultaneous fusion of EEG and fNIRS allows capturing both sides of the neurovascular response, giving EEG-fNIRS the unique opportunity to investigate neurovascular coupling mechanism safely during interictal

epileptiform discharges (Peng et al., 2014, 2016) and seizures in patients with refractory epilepsy (Nguyen et al., 2012; Nguyen et al., 2013). However, using simultaneous video-EEG and fNIRS (i.e., vEEG-fNIRS) is challenging, especially when long recordings over the entire head are performed at the patient's bedside (Kassab et al., 2018; Kassab et al., 2021). Indeed, only a few pediatric cases have documented cerebral hemodynamics during seizures (including SE) in the critically ill using fNIRS (Adelson et al., 1999; Arca Diaz et al., 2006; Martini et al., 2019).

Over the past decade, our group has been focusing on using vEEG-fNIRS for long-term bedside monitoring in various clinical settings (Kassab et al., 2016; Kassab et al., 2018; Kassab et al., 2021). In our latest study, we demonstrated the feasibility of performing long-term vEEG-fNIRS recordings in critically ill adults presenting with diverse electrographic patterns (i.e., seizures, periodic discharges, and burst-suppression). However, we could not fully explore the neurovascular dynamics associated with ESE as only two patients had a limited number of recurrent seizures during the monitoring period. In this study, we document more extensively the systemic and cortical hemodynamic changes associated with ESE by performing long-term whole-head vEEG-fNIRS recordings while simultaneously monitoring systemic physiology in a larger cohort of critically ill comatose patients.

10.3 Materials and methods

10.3.1 Study design and clinical data collection

We recruited 11 patients (nine men, two women, 30-75 years) admitted to the ICU of the University of Montreal Hospital Center (CHUM). Inclusion criteria were: 1) patients admitted with a confirmed or suspected diagnosis of ESE, or 2) any patients in the ICU with at least one confirmed “electrical” seizure on scalp EEG. All included patients underwent continuous long-term whole-head vEEG-fNIRS monitoring. Patients who were clinically suspected of having ESE but whose subsequent EEG did not demonstrate any ictal findings were excluded. We recorded demographic data (sex, age, body mass index), medical history (epilepsy, neurological and non-neurological comorbidities), and clinical characteristics (SE classification, duration and etiology, use of mechanical ventilation, length of hospitalization, discharge disposition). Additionally, all anesthetics, anti-seizure medications, catecholamines, and neuromuscular blocking agents were

documented. Brain MRIs (Phillips, 3 Tesla) were performed during the management of these patients at the discretion of the attending physicians. This study was approved by the ethics committee of the research center of the CHUM; written informed consent was obtained from legally authorized representatives before starting any research study procedure.

10.3.2 EEG interpretation and event marking

Two board-certified neurologists with epilepsy expertise (DHT, DKN) independently reviewed the vEEG recording. Abnormal patterns or discharges were identified and subcategorized using the standardized critical care EEG terminology of the American Clinical Neurophysiology Society (Hirsch et al., 2021). The 10s-period prior to seizure onset and after seizure offset were selected as the pre- and postictal periods.

10.3.3 Long-term whole-head vEEG-fNIRS monitoring protocol

Patient head inspection and whole-head probe coverage estimation

Before any vEEG-fNIRS recording, a careful inspection of the patient's head was performed for any signs of skin changes lesions that could limit recordings. Different head measurements and photographic images were taken in order to design a preliminary whole-head montage based on the international 10–20 EEG system.

vEEG-fNIRS data collection and synchronization

EEG data were recorded using the BrainAmp EEG amplifier and BrainVision Recorder software (BrainVision Recorder, Version 1.2.2.0 Brain Products GmbH, Gilching, Germany). The BrainVision system was used to capture video simultaneously. Video data was transferred into BrainVision Recorder software using a firewire cable. Twenty-one gold cup EEG electrodes (Grass, Natus Medical Incorporated, USA) were positioned following the International 10–20 layout (Jasper, 1958) and 10-10 (FT9/FT10) systems (Acharya et al., 2016). Two additional electrodes were used for EKG, and two for EOG. Electrodes on the scalp were glued using collodion (Collodion, Mavidon, FL). EEG data were sampled at 500Hz.

fNIRS data were recorded using the Brainsight CW-NIRS system (Rogue Research Inc., Montreal, Canada). A total of 48 optodes, 16 laser diode emitters (wavelength: 685nm and 830nm; average power: ~20mW), 16 standard photodiodes for short-distance detectors, and 32 avalanche photodetectors for long-distance detectors, were used in all patients. The 48 optodes provided a minimum of 100 channels covering the whole-head (**Supplementary Figure 9**). The optodes were glued using collodion in order to minimize sensitivity to motion artifacts and to improve fNIRS signal to noise ratio (Yücel et al., 2014; Machado et al., 2018; Cai et al., 2022) The average distance between the sources and long-distance detectors and sources and short-distance detectors was ~3-4 cm and ~0.8-1.0 cm, respectively. fNIRS data were sampled at 20Hz. In order to synchronize vEEG and fNIRS data, we used E-Prime 2.0 software (Psychology Software Tools, Pittsburgh, PA) to design and run a custom written script.

Electrodes and optodes digitization

Digitization was performed using an optical position sensor (Polaris Vicra®, NDI, Canada) communicating with the integrated Brainsight neuronavigation software through a BNC to USB cable. Each optode and electrode was carefully digitized. In addition, common fiducials (i.e., nose tip, nasion,inion, left periauricular, right periauricular) and an additional 50-100 random points throughout the head were also digitized in order to increase the location sensitivity for each optode.

Preparation time and recording duration

On average, the preparation and installation time for one vEEG-fNIRS monitoring session was ~8h (range: 6h-10h). Except on rare occasions (e.g., medical emergency), each monitoring session consisted of at least one continuous (i.e., non-stop) run of 4h. An experienced fNIRS operator (AK) was present at the patient's bedside during the entire monitoring session, ensuring the patient's safety in case of emergency and signal quality dropout.

10.3.4 fNIRS data analysis

fNIRS data pre-processing

The recorded fNIRS data were pre-processed with the open-source MATLAB toolbox Homer2 (Huppert et al., 2009) and in-house developed scripts. A first visual inspection was performed on

each dataset to remove any non-short distance fNIRS channels without clear cerebral origin (i.e., negative raw amplitude channels, saturating channels, channels without clear heartbeats) (Huppert et al., 2009; Piper et al., 2014). Additionally, fNIRS channels with an intensity of < 1000 photon counts or a signal-to-noise ratio of < 2 were classified as low-quality and excluded from further analysis. Motion artifacts were identified with both visual identification and a Homer2 automatic motion detection algorithm based on signal standard deviation and amplitude changes (Scholkmann et al., 2010). For comatose patients in the ICU, motion artifacts may come from several sources (i.e., mattress air pressure fluctuations, routine care procedures performed by medical personnel, and movements associated with clinical seizures). Once all motion artifacts were marked, they were reassessed by visual inspection simultaneously to the video feed to confirm (i.e., clear or probable motion artifact) or reject (i.e., not motion artifact) motion artefacts. Recording segmentation was performed to remove time periods affected by significant motion artifacts (e.g. artifacts that were long or affected a large number of channels). Any EEG event within the period from 30s prior to a motion artifact to 30s after the artifact was not studied. The remaining EEG events were then manually inspected to avoid event mislabelling.

For each channel, the fNIRS optical data were first transformed into optical density changes (i.e., ΔOD) by taking the logarithm of the time course. A third-order Butterworth low pass filter with the cutoff frequency at 0.20Hz were then applied to remove high frequency signal components (Zhang et al., 2015; Yücel et al., 2016). The filtered optical density time courses were transformed into concentration changes in HbO and HbR using the modified Beer-Lambert Law (Matcher et al., 1995) with a partial pathlength factor of 6 for both wavelengths (Cope et al., 1991; Duncan et al., 1995). Systemic physiological changes in the extracerebral layers (Kirilina et al., 2013) were then regressed out from all fNIRS channels within a general linear regression model framework (Zeff et al., 2007; Gagnon et al. 2012; Tak and Ye, 2014) by using short-separation channel data that had the highest correlation as a regressor (Saager and Berger, 2005). Signal detrending was conducted by adding polynomial regressors up to the 3rd order to the model. In addition, concentration changes in total hemoglobin (HbT, calculated as HbO + HbR), and hemoglobin difference (HbD, calculated as HbO - HbR) were calculated and serve as representative markers of cerebral blood volume (CBV) (Wyatt et al., 1990; Villringer and Chance, 1997) and cerebral oxygenation respectively (Mitra et al., 2016a,b, Bale et al., 2020).

Extraction of hemodynamic response functions

Due to the large number of seizures and duration variability in our recordings, the estimation of the hemodynamic response function (HRF) was performed using a bin analysis approach that is based on the duration of the seizures. For each patient, seizures of comparable durations were grouped into a same bin. We selected the width of each bin to be 10s due to the large range of seizure durations in this study. For instance, seizures lasting < 20 seconds were divided into two bins (i.e., [0 to 10s] and [10 to 20s]), and seizures lasting < 80 seconds were divided into 8 bins: (i.e., [0 to 10s], [10 to 20s], [20 to 30s], ..., [60 to 70s], and [70 to 80s]). For each seizure, we estimated the hemodynamic response (HbO, HbR, HbT and HbD) to each seizure of a patient from 10s before the onset of the seizure to 10s after its offset. We applied a spatial principal component analysis (PCA) to the extracted hemodynamic response functions of all remaining fNIRS channels (after exclusion for motion artifacts and low signal-to-noise ratio, see above) to generate a representative HRF for each bin using principal components that accounted for 80% of global variance. Lastly, biphasic changes in the direction of the HRF were defined as a change in amplitude of relative hemoglobin concentration of $\geq 20\%$ for at least half the duration of the corresponding seizure.

To enable comparisons of the representative HRFs between different bins, we extracted two HRF characteristics for each bin: the Full-Width-at-Half-Maximum (FWHM) that assesses response duration and the normalized Area-Under-the-Curve (AUC) that evaluates response intensity. The FWHM was defined as the length of the time during which the response was larger than half of the peak amplitude (or during which the response was smaller than half of the nadir amplitude), while the normalized AUC was defined as the integral of the HRF with respect to time divided by the total HRF duration. We established a linear mixed-effects model to model seizure duration with fixed effects for response FWHM or normalized AUC and uncorrelated random effect for intercept (grouped by patients) and residual. The goodness-of-fit was evaluated by examining the p -values from F -tests on the fixed-effect regression coefficients, as well as the adjusted R-squared values of the fit.

Prediction of response directionality based on seizure duration

While the bin analysis focused on the relationship between response characteristics and seizure bins of fixed durations, we further made attempts to explore the directionality of the hemodynamic response at any time point during a seizure (i.e., the possibility of getting a positive/negative response at a particular time during a seizure of any length) with a logistic regression model. More specifically, the representative HRFs of recorded seizures of all patients were pulled together as the training set of the model. Considering that the typical response time of a canonical HRF is around 5 seconds, we first downsampled all HRFs of individual seizures to 0.2Hz (one data point every 5 seconds with a random start point) to mitigate the serial correlation in the signal (Upham, 2012). We assumed that, with a time gap of 5s, the value of the HRF at a certain time point is free to vary from its value at the previous time point, and therefore these values could be considered as being independent from each other.

The logistic function is of the form:

$$D(t) = \frac{1}{1 + e^{-(\beta_0 + \beta_1 t)}}$$

where t is the time, and $D(t)$ is the response direction at time point t :

$$D(t) = \begin{cases} 1, & \text{if } HRF(t) \geq 0 \\ -1, & \text{if } HRF(t) < 0 \end{cases}$$

After estimating the regression coefficients β_0 and β_1 , we predicted the probability of getting a positive hemodynamic response at any time point from 0s to 4500s during an ongoing seizure.

10.3.5 Systemic physiology and sedation level

Semi-continuous collection of vital signs, including mean arterial blood pressure ($_{sc}MABP$, mmHg), oxygen saturation ($_{sc}SpO_2$, %), heart rate ($_{sc}HR$, bpm), end-tidal carbon dioxide ($_{sc}EtCO_2$, mmHg), temperature ($_{sc}T$, °C) and Richmond Agitation-Sedation score (RASS) were taken every 15-30 min. Additionally, continuous noninvasive systemic hemodynamic monitoring was collected using the Finapres® NOVA system (Finometer MIDI, TNO Biomedical Instrumentation, Amsterdam, Netherlands). Measured parameters included 1) mean arterial blood pressure (MABP, mmHg) obtained by finger photoplethysmography (set at heart level); 2) peripheral arterial oxygen saturation (SpO_2 , %) and heart rate (HR, bpm) via finger pulse oximetry; and 3) respiration rate

(RR) through a respiration monitoring belt. For continuous measurements, two periods were selected: 1) the preictal period (i.e., 30s before each seizure), and 2) the ictal period (i.e., period starting from seizure onset and ending with its respective offset). If the interval between two consecutive seizures was < 60 s, both seizures were discarded (Ferlini et al., 2021). Finally, arterial blood gas, hemoglobin, lactic acid, sodium, and glucose concentrations were retrospectively collected from medical records.

We compared systemic physiological changes using a paired-t-test. A p -value < 0.05 was considered statistically significant. Data are presented as median \pm median absolute deviation or median [range, min/max]. Statistical analysis was performed using GraphPad Prism version 9.0 (GraphPad Software, Inc., San Diego, CA).

10.4 Results

10.4.1 Patient clinical and monitoring information

Among the 11 patients recruited and monitored, four were excluded from the analysis due to the absence of seizures during the monitoring period ($n = 1$) and low signal quality ($n = 3$). The clinical and vEEG-fNIRS monitoring profile for the remaining patients ($n = 7$, two women, age = 50 ± 13) are summarized in **Table 18** and **Table 19** respectively. Three patients eventually succumbed to their illnesses.

Table 18 – Patient demographics.

Patient	Sex, age (BMI)	SE classification (etiology)	Admission			Complications	Co-morbidities	Mechanical ventilation (mode)
			Dx	STESS	GCS			
P01	M, 63 (26.7)	ECSE → SRSE/NORSE (cryptogenic)	Graft- versus-host disease	6	3	Yes (hypotension, HIT, MED)	Yes (hepatic surgery/cirrhosis, HTN, anemia)	Yes (VAC)
P02	M, 34 (22.7)	ECSE → ESE with impaired consciousness (cryptogenic)	Altered mental status	1	6	Yes (postictal behavioral changes)	Yes (epilepsy, behavior disorder)	Yes (VAC)
P03	M, 33 (23.0)	SRSE/NORSE (cryptogenic)	Seizure	3	3	Yes (AP)	No (no)	Yes (VAC)
P04	M, 40 (28.5)	ESE with impaired consciousness (postanoxic/hypoxia)	Altered mental status	3	3	Yes (AP, UTI)	Yes (epilepsy, HTN, hypothyroidism, asthma)	Yes (VAC)
P05	M, 56 (34.5)	RSE with impaired consciousness (hepatic encephalopathy)	Altered mental status	3	3	Yes (anemia, metabolic acidosis)	Yes (HTN, T2D, DLP, cirrhosis)	Yes (VAC)
P06	M, 48 (24.7)	RSE with impaired consciousness (postanoxic/hypoxia)	Cardiac arrest	2	3	Yes (AP)	Yes (T2D, COPD)	Yes (VAC)
P07	M, 68 (24.9)	RSE with impaired consciousness (drug toxicity)	Altered mental status	0	6	Yes (rhabdomyolysis, ARF)	Yes (brain tumor, epilepsy, hypothyroidism)	Yes (VAC)

AI: adrenal insufficiency, AP: aspiration pneumonia, ARF: acute renal failure, BMI: body mass index, COPD: chronic obstructive pulmonary disorder, Dx: diagnosis, ECSE: electroclinical status epilepticus, ESE: electrographic status epilepticus, F: female, GCS: Glasgow Coma Scale, HIT: heparin-induced thrombocytopenia, HTN: hypertension, M: male, MED: multiple electrolyte disorders, NORSE: new-onset refractory status-epilepticus, RSE: refractory status epilepticus, SRSE: super-refractory status epilepticus, STESS: Status Epilepticus Severity Score, T2D: type 2 diabetes, UTI: urinary tract infection, VAC: volume assisted control.

Table 18 (continued) – Patient demographics.

Patient	# ASMs	# Anesthetics	Vasopressors	MRI abnormalities	Outcome (mortality)
P01	3	2	yes	leukoaraiosis	yes
P02	3	2	no	multiple siderosis foci	no
P03	4	3	yes	↑ DWI / ↓ ADC, ↑ T2 / FLAIR	yes
P04	2	3	no	no	no
P05	2	1	yes	encephalomalacia ↑ DWI / ↓ ADC, ↑ T2 FLAIR	yes
P06	1	1	yes	diffuse atrophy ↑ T2 / FLAIR, ↓ T2	no
P07	3	2	yes	↑ DWI / ↓ ADC, ↑ T2 / FLAIR	no

ADC: apparent diffusion coefficient, ASMs: antiseizure medications, DWI: diffuse weighted imaging, FLAIR: fluid attenuated inversion recovery, GSC: Glasgow Coma Scale, IHT: inter-hospital transfer, NA: not available.

Table 19 – Patient monitoring profile.

Patient	vEEG-fNIRS monitoring time (days after ICU admission)	vEEG-fNIRS monitoring duration	# vEEG-fNIRS monitoring session	# Sz (% included)	Avg duration (min – max)	Avg I-Sz-I (min – max)	Localization	Additional EEG patterns
P01	21	144 hours	11	973 (94%)	48.9s (5.9s – 82.1s)	193.1s (7.4s – 2109.3s)	Generalized	Yes (PDs)
P02	2	5 hours	1	60 (98%)	68.5 (9.6s – 429.0s)	81.8s (5.5s – 3616.3s)	Focal	Yes (TWs)
P03	14	36 hours	4	73 (90%)	1311.7s (52.0s – 8189.3s)	414.0s (5.2s – 5555.0s)	Generalized	No
P04	2	4 hours	1	16 (100%)	112.5s (19.9s – 732.0)	112.9s (7.3s – 236.6s)	Focal	No
P05	6	8 hours	1	19 (95%)	13.1s (5.5s – 29.9s)	844.8s (12.3s – 6396.7s)	Generalized	Yes (PDs)
P06	10	10 hours	1	278 (95%)	23.5s (4.8s – 263.1s)	30.3s (4.0s – 3260.6s)	Generalized	Yes (PDs)
P07	7	8 hours	1	19 (90%)	13.9s (5.6s – 27.6s)	784.5s (5.1s – 3689.3s)	Generalized	Yes (PDs)

F: frontal, I-Sz-I: inter-seizure-interval, L: left, Mu: multi, PDs: periodic discharges, R: right, Sz: seizure, TWs: triphasic waves.

10.4.2 Temporal changes of cortical hemodynamic

Table 20 presents an overview of the bins of seizures for each patient and qualitative assessments of the representative HRFs for each bin in terms of increases (↑) or decreases (↓) of HbO, HbR, HbT and HbD changes.

From most of the HRFs, an **overall** increase in HbO (~83% of the bin HRFs) and HbT (~71%) and a decrease in HbR (~70%) and HbD (~68%) occurred during seizures. In patients where an initial increase in HbO, HbT, and HbD was observed, a second decreasing phase in HbO, HbT, and HbD was observed in 34%, 37%, and 35% among all bin HRFs, respectively. Similarly, for patients exhibiting an initial decrease in HbR, a second phase of HbR increase was observed in approximately one-third of all bins, especially with seizures of longer durations. For example, bins longer than 60s included a significantly higher proportion of seizures exhibiting the second phase of HbO decrease and HbR increase than seizures shorter than 60s (64% vs. 28%, $p = 0.027$) under a two-sample z -test of population proportions.

In the following sections, we present two case studies (i.e., patients P01 and P03) who showed typical uniphasic and biphasic hemodynamic responses to seizures. As for the other patients monitored (i.e., P02, P04, P05, P06 and P07), the HRFs for each bin can be visualized in **Supplementary Figure 10** to **Supplementary Figure 14**. Quantitative concentration changes for each hemoglobin biomarker are detailed in **Table 20** and summarized in **Supplementary Figure 15**.

Table 20 – Changes in directions for HbO, HbR, HbT and HbD (for each seizure duration bins).

		0-10s	10-20s	20-30s	30-40s	40-50s	50-60s	60-70s	70-80s	90-100s	100-200s	200-300s	1000-2000s	2000-3000s	3000-4000s	4000-5000s
P01	<i>HbO</i>	↑	↑	↑	↑	↑↓	↑↓	-	-	-	-	-	-	-	-	-
P02	<i>HbO</i>	-	↓	↑	↑	↑↓	↑	-	↑	-	-	-	-	-	-	-
P03	<i>HbO</i>	-	-	-	-	-	↑	↑	↑↓	↑↓	↑↓	↑↓	↑↓	↑↓	↑↓	↑↓
P04	<i>HbO</i>	-	-	-	↑	↑↓	-	↑	-	↓	-	-	-	-	-	-
P05	<i>HbO</i>	↑	↑↓	↓	-	-	-	-	-	-	-	-	-	-	-	-
P06	<i>HbO</i>	↑	↑	↑	↓	↑↓	↑↓	↓	-	↓	-	-	-	-	-	-
P07	<i>HbO</i>	↑↓	-	↑↓	-	-	-	-	-	-	-	-	-	-	-	-

		0-10s	10-20s	20-30s	30-40s	40-50s	50-60s	60-70s	70-80s	90-100s	100-200s	200-300s	1000-2000s	2000-3000s	3000-4000s	4000-5000s
P01	<i>HbR</i>	↓	↓	↓	↓	↑↓	↑↓	-	-	-	-	-	-	-	-	-
P02	<i>HbR</i>	-	↑	↑	↑	↑↓	↓	-	↓	-	-	-	-	-	-	-
P03	<i>HbR</i>	-	-	-	-	-	↓	↓	↑↓	↑↓	↑↓	↑↓	↑	↑	↑	↑
P04	<i>HbR</i>	-	-	-	↑	↑↓	-	↓	-	↑	-	-	-	-	-	-
P05	<i>HbR</i>	↓	↑↓	↑	-	-	-	-	-	-	-	-	-	-	-	-
P06	<i>HbR</i>	↓	↓	↓	↑	↑↓	↑↓	↓	-	↓	-	-	-	-	-	-
P07	<i>HbR</i>	↑↓	-	↑↓	-	-	-	-	-	-	-	-	-	-	-	-

Graphical table depicting the direction of changes for each Hb biomarkers. A single arrow signifies a uniphasic increase (↑) or decrease (↓), while double arrows (↑↓) refer to bi-phasic changes (i.e., an initial increase, followed by a decrease or an initial decrease followed by an increase). **Green colour** refers to an overall positive change relative to the baseline (i.e., overall increase in HbO for example), while a **red colour** refers to an overall negative change relative to the baseline (i.e., overall decrease in HbO for example).

Table 20 (continued) – Changes in directions for HbO, HbR, HbT and HbD (for each seizure duration bins).

		0-10s	10-20s	20-30s	30-40s	40-50s	50-60s	60-70s	70-80s	90-100s	100-200s	200-300s	1000-2000s	2000-3000s	3000-4000s	4000-5000s
P01	<i>HbT</i>	↑	↑	↑	↑	↑↓	↑↓	-	-	-	-	-	-	-	-	-
P02	<i>HbT</i>	-	↓	↑	↑	↑↓	↑	-	↑	-	-	-	-	-	-	-
P03	<i>HbT</i>	-	↓	↑	↑	↑↓	↑	-	↑	-	-	-	-	-	-	-
P04	<i>HbT</i>	-	-	-	↑↓	↑↓	-	↑↓	-	↓	-	-	-	-	-	-
P05	<i>HbT</i>	↑	↑↓	↓	-	-	-	-	-	-	-	-	-	-	-	-
P06	<i>HbT</i>	↑	↑	↑	↑	↓	↑↓	↓	-	↓	-	-	-	-	-	-
P07	<i>HbT</i>	↑	-	↑↓	-	-	-	-	-	-	-	-	-	-	-	-

		0-10s	10-20s	20-30s	30-40s	40-50s	50-60s	60-70s	70-80s	90-100s	100-200s	200-300s	1000-2000s	2000-3000s	3000-4000s	4000-5000s
P01	<i>HbD</i>	↑	↑	↑	↑	↑↓	↑↓	-	-	-	-	-	-	-	-	-
P02	<i>HbD</i>	-	↓	↑	↓	↑↓	↑	-	↑	-	-	-	-	-	-	-
P03	<i>HbD</i>	-	-	-	-	-	↑	↑	↑↓	↑↓	↑↓	↑↓	↑↓	↑↓	↑↓	↑↓
P04	<i>HbD</i>	-	-	-	↑↓	↑↓	-	↑↓	-	↓	-	-	-	-	-	-
P05	<i>HbD</i>	↑	↑↓	↓	-	-	-	-	-	-	-	-	-	-	-	-
P06	<i>HbD</i>	↑	↑	↑	↓	↓	↑↓	↑↓	-	↑↓	-	-	-	-	-	-
P07	<i>HbD</i>	↓	-	↑↓	-	-	-	-	-	-	-	-	-	-	-	-

Graphical table depicting the direction of changes for each Hb biomarkers. A single arrow signifies a uniphasic increase (↑) or decrease (↓), while double arrows (↑↓) refer to bi-phasic changes (i.e., an initial increase, followed by a decrease or an initial decrease followed by an increase). **Green colour** refers to an overall positive change relative to the baseline (i.e., overall increase in HbO for example), while a **red colour** refers to an overall negative change relative to the baseline (i.e., overall decrease in HbO for example).

Case study 1

A 63-year-old male patient with a long-term history of hypertension and severe cirrhosis was admitted to our institution for a scheduled surgery (i.e., liver transplant). Following the transplant, the patient developed a graft-versus host syndrome associated with refractory seizures. He was diagnosed with new-onset refractory ECSE evolving into ESE with a STESS of 3. In the ICU, the patient remained under three antiseizure medications, two anesthetics, and mechanical ventilation (**Supplementary Figure 16A**). Despite all clinical efforts, his overall medical condition deteriorated and he died 52 days later.

A total of 21 vEEG-fNIRS sessions were performed for two weeks (total duration ~144h). During the first sessions (duration ~4h), we were able to record 181 seizures with an average duration of 85.2s [34.1s – 136.3s] and an average interictal interval of 60.4s [17.1s – 103.7s]. Seizures were mainly characterized by diffuse rhythmic activity with slight left-hemispheric predominance. Additional EEG patterns observed during the vEEG-fNIRS monitoring were periodic discharges with an average frequency of ~1.5Hz.

In the fNIRS data analysis, all 181 seizures were grouped into six different bins with durations ranging from [0-10s] to [50s-60s] (**Figure 38**). However, the majority of recorded seizures were short, lasting between 10s and 30s (170 seizures, 95%). We observed a uniphasic HbO increase and an HbR decrease associated with the seizures of all the six bins. Such HbO and HbR concentration changes were consistent from the onset of the seizure until a few seconds after the seizure offset before gradually returning to baseline. Specifically, the comparison of HRFs between bins showed an increment in the FWHM of both HbO and HbR response with the increase of seizure durations ([0-10s]: 11.4s/15.2s for HbO/HbR; [10s-20s]: 18.0s/17.0s; [20s-30s]: 20.6s/21.4s; [30s-40s]: 31.4s/32.5s; [40s-50s]: 41.6s/33.2s; [50s-60s]: 57.1s/57.8s), as well as increased normalized AUC for HbO and decreased normalized AUC for HbR ([0-10s]: 0.0075 μ M/-0.0033 μ M for HbO/HbR; [10s-20s]: 0.010 μ M/-0.0055 μ M; [20s-30s]: 0.0111 μ M/-0.0060 μ M; [30s-40s]: 0.0178 μ M/-0.0092 μ M; [40s-50s]: 0.0118 μ M/-0.0061 μ M; [50s-60s]: 0.0207 μ M/-0.0126 μ M). Similarly, as seizure duration increased, we observed an increment in the FWHM and the AUC (positive increase) for HbT and HbD (**Table 20**).

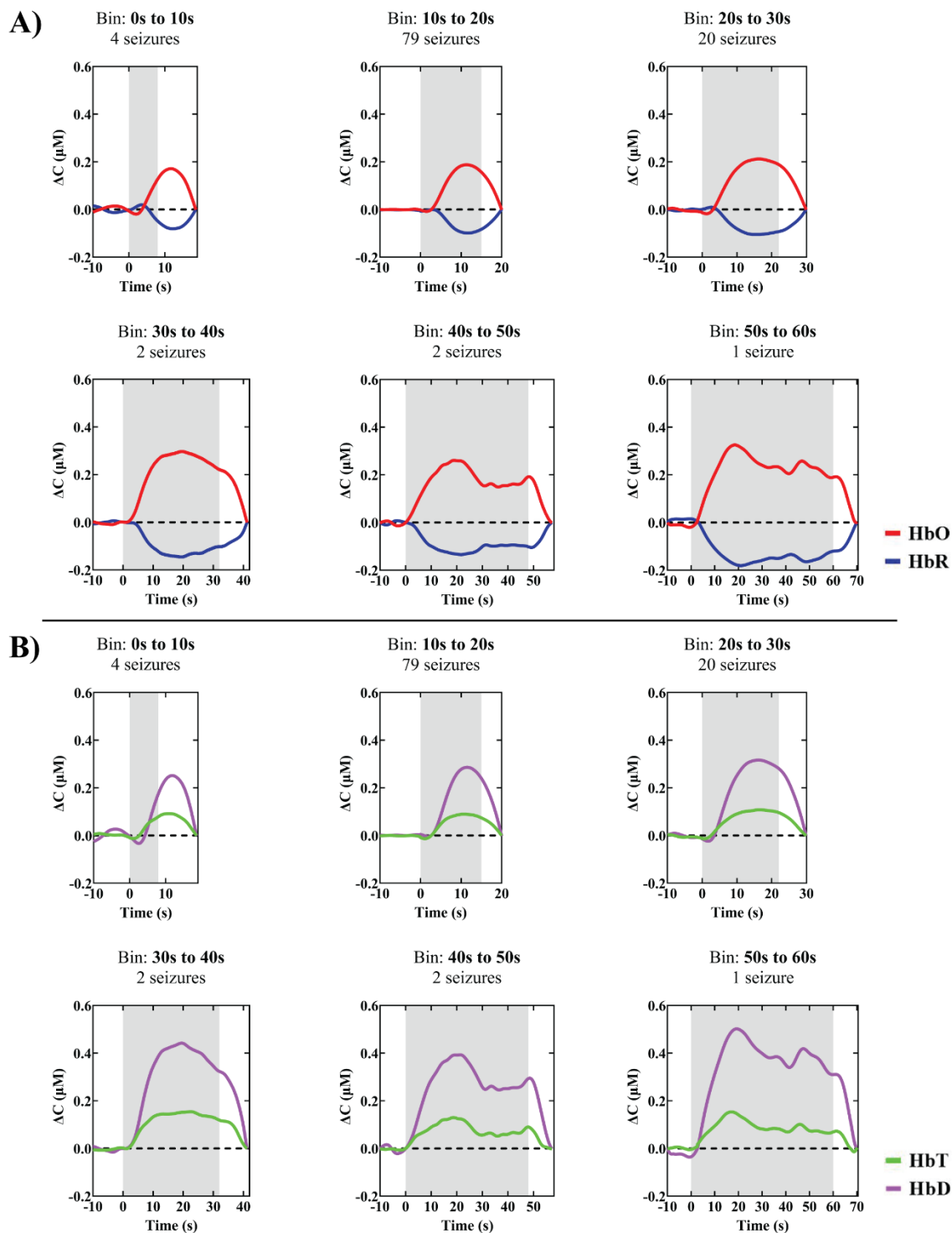


Figure 38 – fNIRS results, patient P01: bin analysis of 181 seizures. Each subplot of the figure shows the hemodynamic response functions (HRFs) of oxy- (HbO), deoxy- (HbR) (A), total (HbT) hemoglobin concentration and difference between HbO and HbR (HbD) (B) associated with the seizures. Shaded area indicates the average (mean) length of the seizures within a bin.

Case study 2

A 33-year-old man without any significant past medical history was admitted to the ICU for recurrent seizures in the context of fever, which started from a recent upper respiratory tract infection and later evolved into SRSE. On admission, GCS and STESS were both measured at 3. He later had aspiration pneumonia which was treated with antibiotics. He was kept on mechanical ventilation, a minimum of four antiseizures medications, three anesthetics, and one vasopressor throughout his entire ICU stay (**Supplementary Figure 16B**). Despite extensive investigations, a specific cause for the seizures could not be found. The patient's global condition did not improve, and in spite of all treatments, he eventually passed away 28 days later.

Four sessions of vEEG-fNIRS were performed over ten days in the ICU (total duration ~36 h). During the first two sessions, which lasted ~ 17h, 30 seizures were recorded. Four seizures were excluded in the preprocessing step. The 26 remaining seizures had an average duration of 841.6s [57.2s – 4283.3s] and an average interictal interval of 813.7s [101.3s – 5555.0s]. Seizure distribution was mainly widespread, with an abrupt onset and offset. No pattern falling in the ictal-inter-ictal continuum was identified during the same period.

A total of 228 channels were used to cover the entire head. Unfortunately, only 159 channels (70%) yielded high SNR throughout the monitoring session and were kept for further analysis. The 26 "full" seizures recorded during the session were divided into 10 categories ("bins") based on their duration from [50s-60s] to [4000s-5000s] (**Figure 39**). The hemodynamic responses were twofold. For relatively short-duration seizures from 50s to 130s, we observed a uniphasic HbO increase along with an HbR decrease during the entire duration of the seizures. Specifically, the FWHM and the normalized AUC seemed to increase with the increasing duration of seizures within this range (FWHM of [50s-60s]: 55.6s/52.0s for HbO/HbR; [60s-70s]: 63.6s/52.5s; [70s-80s]: 51.8s/50.5s; [90s-100s]: 87.8s/73.4s; [120s-130s]: 120.4s/127s. Normalized AUC of [50s-60s]: 0.0266 μ M/-0.0107 μ M; [60s-70s]: 0.0205 μ M/-0.0083 μ M; [70s-80s]: 0.0108 μ M/-0.0045 μ M; [90s-100s]:0.0240 μ M/-0.0104 μ M; [120s-130s]:0.0251 μ M/-0.0099 μ M).

On the other hand, HRFs to more prolonged seizures from 240s to 5000s of this patient showed a more complicated biphasic shape. While the first phase of HbO increase and HbR decrease could

still be seen after seizure onset, these changes were followed by a second phase of response, most notably shown as a long reduction in HbO concentration and a long augmentation of HbR concentration, which persisted until the end of the seizures. Interestingly, the responses to long seizures showed an opposite trend to responses to short seizures, whose FWHM or normalized AUC seemed to decrease with the increase of seizure durations (FWHM of HbO increase/HbR decrease for [240s-250s]: 95.2s/117.9s; [1000s-2000s]: 45.1s/42.4s; [2000s-3000s]: 33.1s/93.3s; [3000s-4000s]:59.2s/27.2s; [4000s-5000s]:0s/85.8s. Normalized AUC of HbO/HbR response for [240s-250s]: 0.0133 μ M/-0.0060 μ M; [1000s-2000s]: -0.0218 μ M/0.0086 μ M; [2000s-3000s]: -0.0105 μ M/0.0070 μ M; [3000s-4000s]: -0.0110 μ M/0.0139 μ M; [4000s-5000s]: -0.0419 μ M/0.0123 μ M). Similarly, we observed an increment in the FWHM, and the AUC (positive increase) for HbT and HbD as seizure duration increased until 240s; after that, a decrease in both HbT and HbD was observed (**Table 20**).

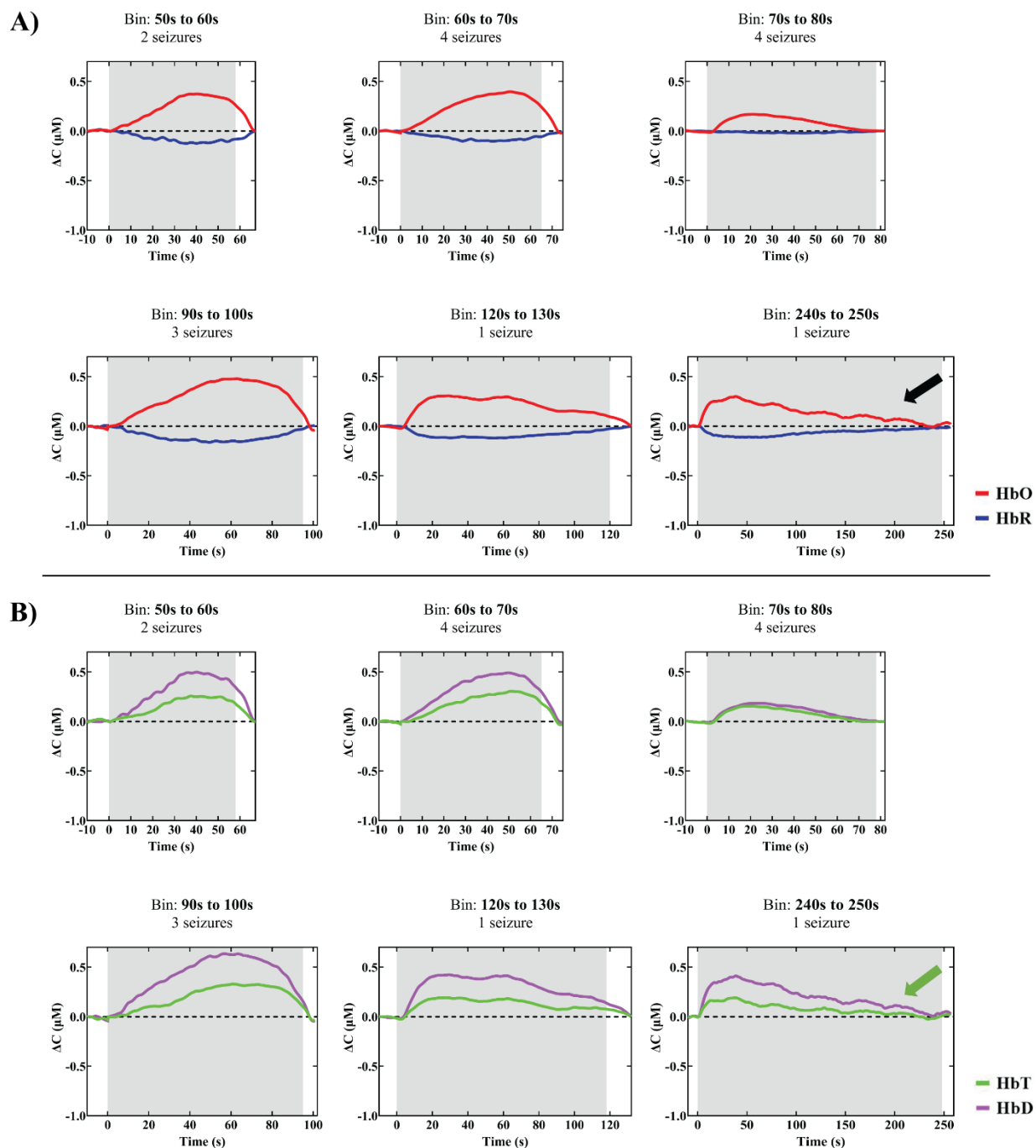


Figure 39 – fNIRS results, patient 5: bin analysis of 26 seizures. Each subplot of the figure shows the hemodynamic response functions (HRFs) of oxy- (HbO), deoxy- (HbR) (A), total (HbT) hemoglobin concentration and difference between HbO and HbR (HbD) (B) associated with the seizures. Shaded area indicates the average (mean) length of the seizures within a bin. The black arrows indicate the second phase of the response characterized by a long decline of HbO concentration and a long increase of HbR concentration.

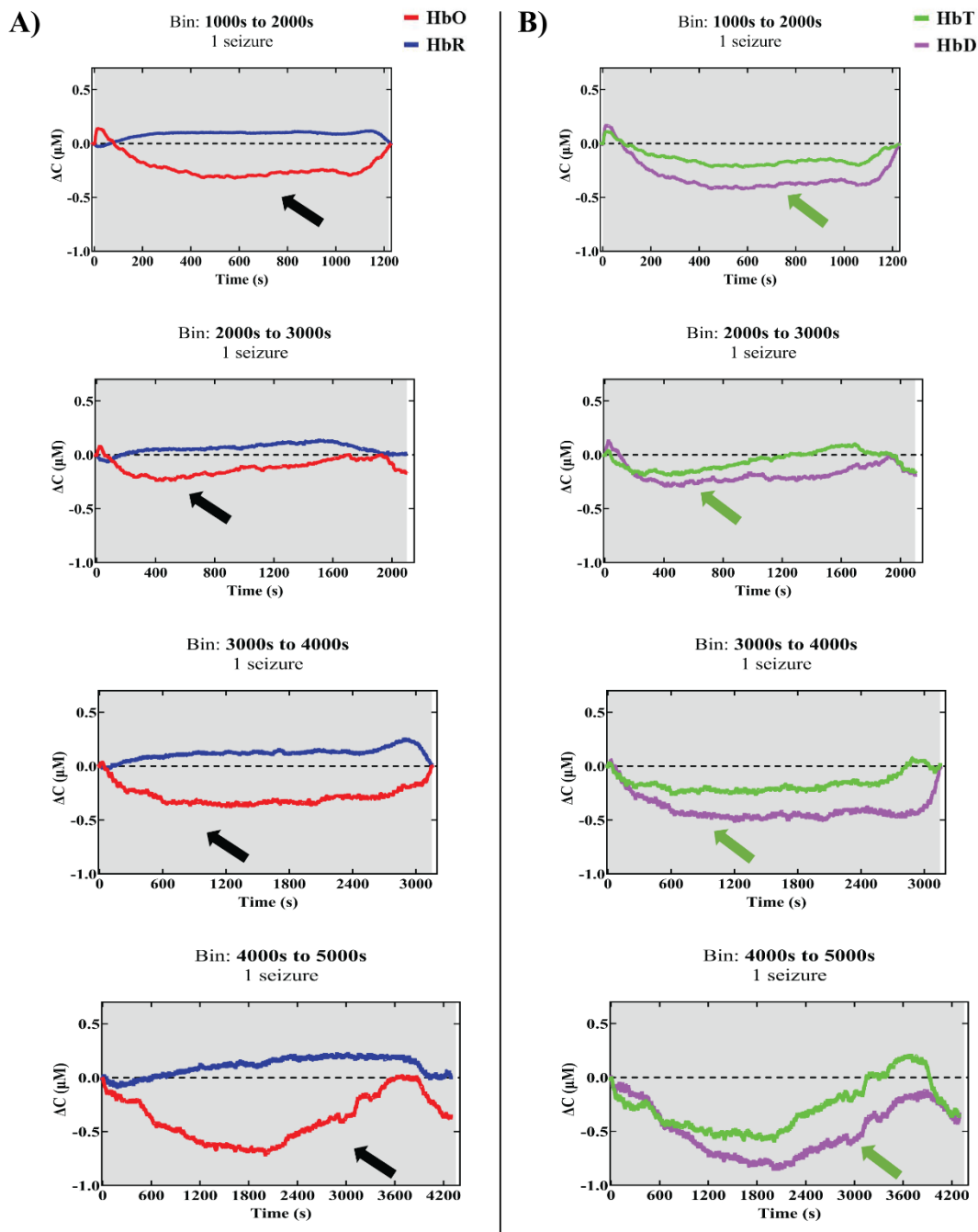


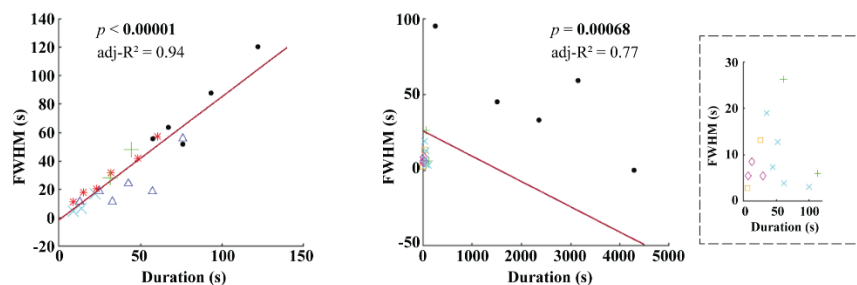
Figure 39 (continued) – fNIRS results, patient 5: bin analysis of 26 seizures. Each subplot of the figure shows the hemodynamic response functions (HRFs) of oxy- (HbO), deoxy- (HbR) (A), total (HbT) hemoglobin concentration and difference between HbO and HbR (HbD) (B) associated with the seizures. Shaded area indicates the average (mean) length of the seizures within a bin. The black arrows indicate the second phase of the response characterized by a long decline of HbO concentration and a long increase of HbR concentration.

10.4.3 Group analysis of cortical hemodynamic changes and seizure duration

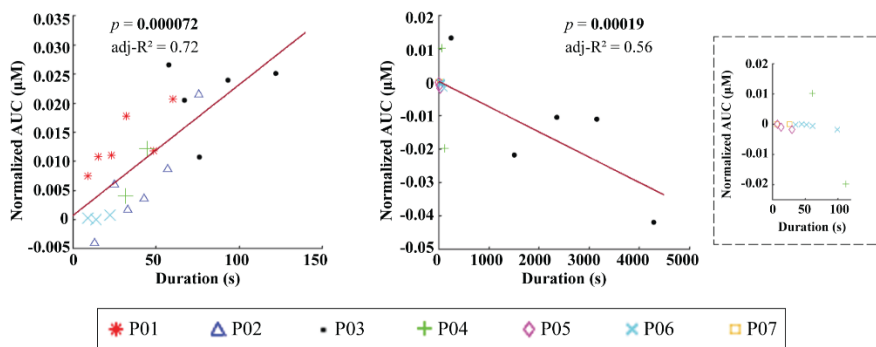
We established a linear mixed-effect model to further explore the relationship between seizure duration and response characteristics. All 39 bins from the seven patients were first divided into two bin groups, with the shorter seizure group containing the bins of the short-length seizures of the patients who had a uniphasic response (i.e., HbO \uparrow and HbR \downarrow) and the longer seizure group consisting of the bins of long-duration seizures of the patients which had a biphasic response (i.e., HbO \uparrow - \downarrow and HbR \uparrow - \downarrow). The results were consistent with the case studies, showing a positive correlation of seizure length with response duration (assessed with the FWHM) in the *shorter seizures* of each patient for both HbO increase ($p < 0.00001$, adjusted R-squared = 0.94) and HbR decrease ($p = 0.00073$, adjusted R-squared = 0.95) (**Figure 40A, Figure 40C**). A positive correlation was also obtained between seizure length and response intensity, showing a higher normalized AUC for HbO ($p = 0.000072$, adjusted R-squared = 0.72) and a more significant negative AUC for HbR ($p = 0.0062$, adjusted R-squared = 0.83) with the increase of seizure length (**Figure 40B, Figure 40D**).

However, such correlations were found to be inverted in the *longer seizure* group that had a biphasic response. We observed a negative correlation between the FWHM of the initial HbO increase ($p = 0.00068$, adjusted R-squared = 0.77) and the normalized AUC ($p = 0.00019$, adjusted R-squared = 0.56 for HbO and $p = 0.0016$, adjusted R-squared = 0.43 for HbR) of the HRF and the seizure duration, which revealed a shorter HbO increase period (phase 1) followed by a more prolonged and more significant HbO decrease and HbR increase period (phase 2) with the further increase of seizure duration in this *longer seizure* group (**Figure 40**).

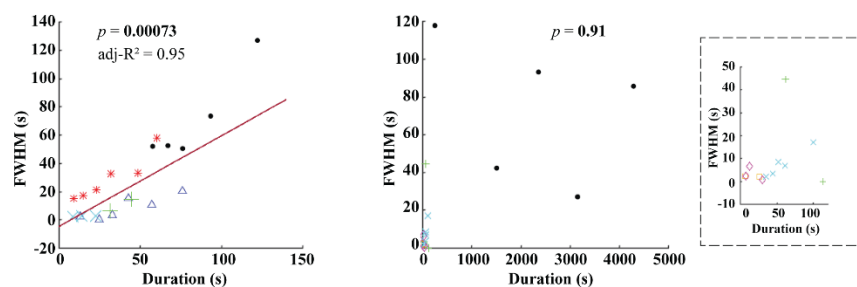
A) Seizure Duration vs. HbO Response Full-Width-at-Half-Maximum (FWHM)



B) Seizure Duration vs. HbO Response Area-Under-Curve (AUC)



C) Seizure Duration vs. HbR Response Full-Width-at-Half-Maximum (FWHM)



D) Seizure Duration vs. HbR Response Area-Under-Curve (AUC)

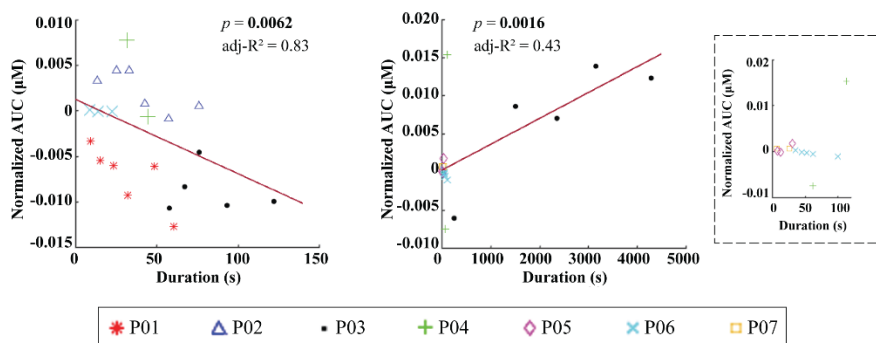


Figure 40 – Group analysis: correlation of seizure duration with (A) bin oxyhemoglobin concentration (HbO) response duration (FWHM of HbO increase), (B) bin HbO response intensity (normalized AUC), (C) bin deoxyhemoglobin concentration (HbR) response duration (FWHM of HbR decrease) and (D) bin HbR response intensity (normalized AUC). Left panel: shorter-duration seizures; Right panel: longer-duration seizures.

10.4.4 Prediction of response directionality based on seizure duration

Extending from the above bin analysis, we set up a logistic regression model on the recorded 243 individual seizures to predict the hemodynamic response directionality using the seizure duration at a particular time point. From the regression, we obtained a significant negative correlation between the binary response directionality (i.e. +1/-1) and seizure time for HbO as well as a significant positive correlation between response directionality and seizure time for HbR ($p < 0.00001$ for both models) (**Figure 41**). For HbO, the prediction results showed a 55% probability of getting an HbO increase at 10s after the seizure onset; a 50% probability at 75s after the onset; a 25% probability at 462s after onset and a less than 5% possibility for seizures longer than 1113s. For HbR, the prediction results indicated a 65% probability of getting an HbR decrease at 10s after seizure onset, a 50% probability at 91s after onset, a 25% probability at 235s after onset (i.e. a 75% probability of getting an HbR increase at $t = 235$ s) and a less than 5% probability for seizures longer than 477s (i.e. more than 95% probability of getting an HbR increase at $t = 477$ s).

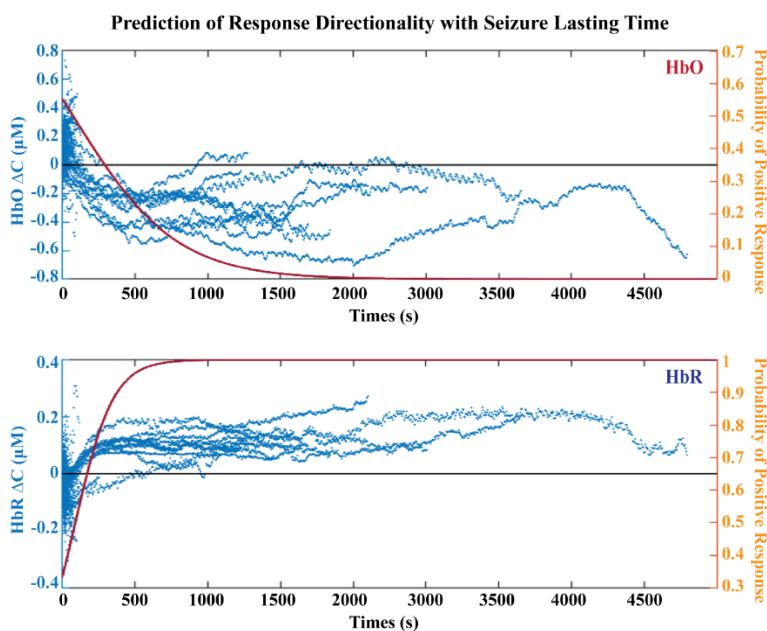


Figure 41 – Prediction of hemoglobin concentration change directionality with a logistic regression model. Top: Prediction of the possibility of getting an oxyhemoglobin concentration (HbO) increase at a particular time point during a seizure. Bottom: Prediction of the possibility of getting a deoxyhemoglobin concentration (HbR) increase at a particular time point during a seizure. The dotted curves show the (downsampled) hemodynamic response functions (HRFs) of all recorded individual seizures used in model training.

10.4.5 Systemic physiological monitoring and laboratory results

Following seizure onset, mild significant changes in MABP and HR occurred in four (57%) and two (29%) patients, respectively (**Figure 42A and 42B**). However, no significant SpO₂ changes occurred during seizures for all patients (**Figure 42C**). Sedation level, semi-continuous systemic and laboratory monitoring were obtained in all seven patients and did not reveal any significant desaturation, anemia, acidosis, hyper/hyponatremia, nor any significant differences between patients.

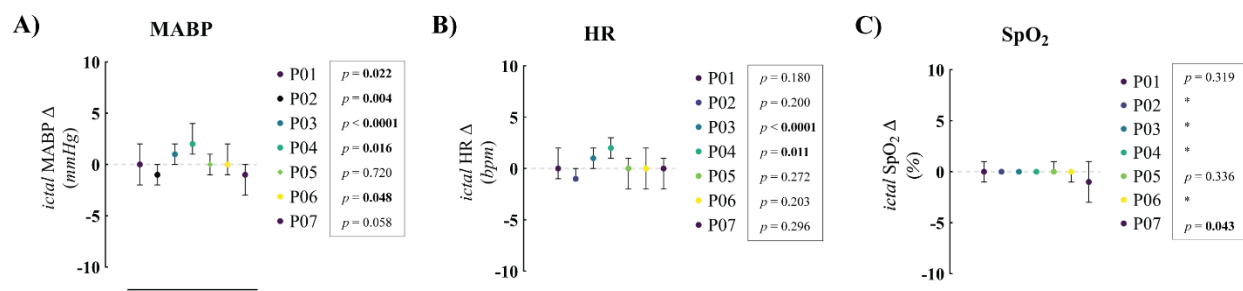


Figure 42 – Ictal changes in systemic parameters (i.e., MABP – mean arterial blood pressure, HR – heart rate, and SpO₂ - peripheral oxygen saturation) for each patient. Data are presented as median ± minimum and maximum values. * Standard error of the difference between the preictal and ictal SpO₂ values was “0”. The most considerable significant positive change in MABP occurred in patient P04 (+4 mmHg). A non-significant decrease (-3 mmHg) and increase (+3 mmHg) in MABP occurred in patient P07 and P04, respectively. In three patients (P05, P06, and P07), a non-significant decrease of 2 bpm occurred with seizure. A tendency of SpO₂ changes following seizure onset occurred in patient P07 (highest increase by 1 % and lowest decrease by -3%).

10.5 Discussion

10.5.1 Summary of findings

This study reports for the first time large-scale electrophysiological and hemodynamic (cortical) brain activity and systemic physiological changes during ESE in critically ill adult patients using long-term multimodal vEEG-fNIRS monitoring in the ICU. Overall, recurrent short (i.e., < 100s) electrographic seizures were associated with a sustained increase in HbO, HbT, and HbD and a decrease in HbR. These changes contrasted with recurrent longer (i.e., ≥ 100s) electrographic seizures which were frequently associated with an HbR increase, while other Hb biomarkers decreased. These cerebral hemodynamic changes could not be attributed to systemic hemodynamic changes as no significant or only mild changes in MABP, HR and SpO₂ were found in all patients.

These observations suggest that neurovascular coupling mechanisms can provide sufficient compensation of oxygen consumption with short seizures but appear insufficient with longer seizures.

10.5.2 Cortical oxygen dynamics during recurring short and/or prolonged electrographic seizures

Previous studies employing diverse neuromonitoring (e.g., oxygen sensing probes, intrinsic optical imaging) and neuroimaging techniques (e.g. SPECT, PET), in animals and humans, have shown, using wide range of functional neuroimaging and neuromonitoring technique, that the heightened metabolic demand and oxygen consumption usually associated with self-limiting (i.e., non-recurring, non-prolonged) seizures, including electrographic seizures, leads to an overall increase in CBF and brain oxygen levels, owing to a relatively well-preserved neurovascular coupling mechanism (Schwartz, 2007; Patel et al., 2013; Kovács et al., 2018). In contrast, fewer studies have employed high temporal resolution neuroimaging methods to investigate brain hemodynamics during ESE, despite *in vivo* signs of metabolic impairment (Duffy et al., 1975; Kovács et al., 2002; Malinska et al., 2010; Zsurka and Kunz, 2015) and *in vitro* evidence of blood-brain barrier (BBB) dysfunction following recurrent and/or prolonged seizures (Abbott and Friedman, 2012; Heinemann et al., 2012; Gorter et al., 2015; Bar-Klein et al., 2017; Prager et al., 2019).

An important finding our study was the influence of seizure duration on the hemodynamic response. While a “classical” cortical hemodynamic response (i.e., decrease in HbR, and increases in HbO, CBV and cerebral oxygenation) was associated with recurrent *short* duration seizures, *prolonged* seizures exhibited an opposite hemodynamic response (i.e., HbR increase, and decreases in HbO, CBV and cerebral oxygenation). Moreover, we also observed the presence of a biphasic hemodynamic response (i.e., initial increase or decrease followed by a decrease or increase, respectively, before seizure offset) for a significant number of seizures recorded. However, the biphasic response remained overall positive (i.e., initial amplitude and duration of increase > final decrease) for the majority of short duration recurrent seizures, while prolonged seizures mainly displayed an overall negative biphasic response (i.e., initial amplitude and duration of increase < final decrease).

Our findings for short-duration recurrent seizures align with previous experimental studies performed in rodents (Choy et al., 2010; Hayward et al., 2010; Lee et al., 2018; Harris et al., 2018; Farrell et al., 2018; Wolff et al., 2020). In a recent study, an increase in partial brain tissue oxygenation was reported in sheep during recurring electrographic seizures lasting between 17.5s and 59.6s (average duration = 36.5s) (Ferlini et al., 2021). In contrast, the cortical hemodynamic changes we observed for prolonged seizures diverge from early *in vivo* animal studies on status-epilepticus (Meldrum et al., 1973; Blennow et al., 1979; Kreisman et al., 1983). For example, an increase in CBF and brain oxygenation was reported during spontaneous long-duration ictal episodes in anesthetized rats (Kreisman et al. 1983). Although no information or definitions was specified for the duration, the authors, nevertheless, did highlight how the increase in brain hemodynamics contrasted the negative response (i.e. a decrease in CBF and brain oxygenation) seen with short-duration seizures (Kreisman et al. 1983).

In humans, multimodal invasive brain monitoring during ESE was performed in patients with TBI (Vespa et al., 2007) and SAH (Ko et al., 2011; Claassen et al., 2013; Fernández-Torre et al., 2022). Claassen et al. (2013) used intracortical electroencephalographic (EEG) and multimodality physiological recordings in 48 comatose subarachnoid hemorrhage patients to better characterize the physiological response to seizures after acute brain injury. While very few details regarding seizure duration or even the number of seizures recorded were provided in that study employing invasive techniques, a characteristic bi-phasic hemodynamic response characterized by a brief rise in PbtO₂ followed by a pronounced and persistent drop in brain oxygenation was observed in 27 patients with prolonged electrographic seizures (i.e., >10 min) (Claassen et al., 2013).

A more detailed account regarding the impact of seizure duration on brain hemodynamics has been provided by non-invasive optical neuromonitoring studies in neonates during ESE (Alfonso et al., 2004; Giorni et al., 2009; Silas et al., 2012; Mitra et al., 2016a). Alfonso et al., (2004) was the first to capture rSO₂ changes during seven electrographic seizures in a 3-week-old newborn with tuberous sclerosis complex and found a decrease in rSO₂ during (or shortly) after seizures that lasted more than 100s, contrasting with seizures < 63s which exhibited an rSO₂ increase (Alfonso et al., 2004). Silas et al. (2012) showed a similar decrease in brain oxygenation during four

seizures; all lasting more than 7 min in a newborn boy (\approx 4 day-old) with hypoxic ischemic encephalopathy (Silas et al., 2012). A decrease in CBV and cerebral oxygenation was reported in all four seizures recorded (all lasting 6-7 minutes) in another newborn (\approx 10 day-old) with hypoxic-ischemic injury (Mitra et al., 2016a). These observations are in contrast with optical neuromonitoring studies performed in neonates with short-lasting seizures without status epilepticus (i.e., not recurrent) reporting an increase in brain hemodynamic (Wallois et al., 2009; Cooper et al., 2011; Singh et al., 2014; Sokoloff et al., 2015; Mitra et al., 2016b; Parcella et al., 2020). Similarly, in adults, our group has previously shown using fNIRS that patients with pharmaco-resistant epilepsy also revealed a dichotomic hemodynamic response, with isolated focal electroclinical seizures lasting 1-2 minutes typically displaying (after an initial decrease in HbR) a relative increase in HbR as seizures progressed in time, as opposed to seizures lasting less than a minute (Nguyen et al., 2012;2013).

Overall, our findings combined with previous work appear to suggest that NVC mechanisms function properly or at least partially, as reflected, respectively, by the “positive” uniphasic or biphasic changes during recurring short-duration seizures. With longer seizures, the partially preserved mechanisms involved in NVC endures until it seems it reaches a certain “critical duration”, after which it decompensates (i.e., neurovascular decoupling) and leads to tissue hypoxia.

Alternatively, or, most likely concurrently in critically ill cases, a rise in intracranial pressure resulting from the increase in CBF, as seen during recurrent electrographic seizures (Vespa et al., 2007; Ko et al., 2011; Claassen et al., 2013), might also alter NVC mechanism leading to brain hypoxia during recurrent electrographic seizures (Moir et al., 2021). Similarly, SE-associated BBB dysfunction and vascular leakage (Bar-Klein et al., 2017; Prager et al., 2019) can also lead to an intracranial pressure or have a direct effect of NVC mechanisms (Bankstahl et al., 2018). Certain brain pathology such as subarachnoid hemorrhage are known to alter NVC mechanisms (Balbi et al., 2017) which can lead to insufficient/impaired vascular response during recurrent seizures (Ko et al., 2011; Claassen et al., 2013).

10.5.3 Potentials of vEEG-fNIRS monitoring in critical care seizures

This study provides some lessons for future clinical applications, as we were able demonstrate the ability to replicate in the clinical setting findings previously made in highly controlled laboratory experiments or using invasive monitoring technique. We reported significant cortical hemodynamic changes associated with recurrent and/or prolonged seizures. While a relative state of brain hypoxia occurred mainly during prolonged seizures, a decrease in cortical oxygenation was also seen with shorter recurrent seizures and vice versa (i.e., increase in cortical hemodynamics with prolonged seizures). These observations, as well as humans reports from previous studies using invasive (Vespa et al., 2007; Ko et al., 2011; Claassen et al., 2013; Fernández-Torre et al., 2021) and noninvasive (Adelson et al., 1999; Alfonso et al., 2004; Arca Diaz et al., 2006;Giorni et al., 2009; Silas et al., 2012; Mitra et al., 2016; Martini et al., 2019; Kassab et al., 2021) monitoring techniques highlight the importance of 1) favoring continuous EEG (cEEG) monitoring (as opposed to discontinuous or routine EEG recordings) during status-epilepticus, and 2) complementing cEEG with another modality capable of measuring, ideally in real-time, brain metabolism and/or hemodynamics. In contrast to invasive neuromonitoring and functional neuroimaging modalities, fNIRS can safely capture brain metabolism and hemodynamics during seizure (both electroclinical and electrographic) at the bedside (cotside) and over the entire cortex (Peng et al., 2016). Moreover, it can easily be combined with vEEG enabling long-term neurovascular brain monitoring (Nguyen et al., 2012, 2013; Kassab et al., 2018, 2021). We are aware that more development is needed to enable faster and easier, and more reliable personalized long-term whole-head recording. Technological and methodological advancement in vEEG-fNIRS will certainly allow easier use of this modality in the critical care patient presenting with seizure which could allow in a nearby future a “real-time” window on brain neurometabolic and neurovascular changes, allowing to perform outcome studies and extract/determine a cutoff level that could be clinically important and help in the management of those patients (Peacock et al., 2018; Alkhachroum et al., 2022).

10.5.5 Limitations

While this study was conducted and reported according to the best practice for fNIRS publications (Yücel et al., 2021), it has some limitations. First, while this study includes more patients and seizures than any previously published work, it still represents a small sample study (7 patients)

with regards to the critically ill and SE population. Specifically, the 11 seizures longer than 1000s came from one single patient (patient P03). Therefore, the estimation of the correlation and the prediction of response directionality of seizures might be biased. Second, most of the analyses carried out in this study were still based on a bin approach that applied averaging to the hemodynamic response to multiple seizures within a certain range of durations. This reduced the temporal resolution of our study to investigate the effect of seizure duration on the brain response. While the choice of using a linear model and short-separation regression to filter out systemic physiological interferences (as applied in this study) is essential (Tak and Ye, 2014), this method has been primarily validated in short NIRS recording (e.g., 10 min) (Chalia et al., 2016; Kassab et al., 2021) and its effectiveness has not been evaluated in datasets with the lengths comparable to our study (i.e. > 6 hours or even several days of continuous recording). Third, we did not directly quantify brain temperature, metabolism, cerebral blood flow or intracranial pressure (Vespa et al., 2007; Ko et al., 2011; Claassen et al., 2013; Fernández-Torre et al., 2021). Fourth, while most seizures are usually <100-120s, we decide to use the 100s cut-off to define short (< 100s) and long (≥ 100 s) seizures in our study. Despite the lack of a clear definition to determine short versus long seizures, we are aware that our cut-off is somehow "arbitrary", and our results should be carefully interpreted, especially when compared with previous experimental animal studies or human reports. Fifth, we did observe significant changes in MABP and HR during seizures in some patients. Cardiovascular changes are known to influence brain hemodynamics potentially (Tachtsidis et al., 2009; Lucas et al., 2010) and, consequently, seizure-induced cortical oxygenation changes (Silas et al., 2012). However, we did not have continuous measurement of cardiac output which are more reliable than MABP and HR to estimate cerebral perfusion. In addition, the effect of central venous pressure on the brain such as during right heart dysfunction was not assessed (Jarry et al., 2023). Nevertheless, we believe changes observed in our population are unlikely to have a significant influence on the direction of the hemodynamic response function, as changes observed in our population were closer to values commonly seen during cognitive tasks in healthy individuals (i.e., ~ 2 to 5 mmHg) (Tachtsidis et al., 2008; Minati et al., 2009), and far less than what has been reported in neonates (range Δ MABP: -3 to 4 mmHg vs. 8-17 mmHg) (Silas et al., 2012). A final limitation was the heterogeneity of our population and the lack of seizure-free "control" for our data. Our population is heterogeneous (e.g., age, sex, anatomical differences, type of brain injury, comorbidities, number and type of antiseizure medication and anesthetics,

inotropic support). For example, anesthetics can influence neuronal metabolism (Hernandez-Meza et al., 2015); however, their influence on NVC and brain perfusion remains unclear (Franceschini et al., 2010; Zeiler et al., 2016).

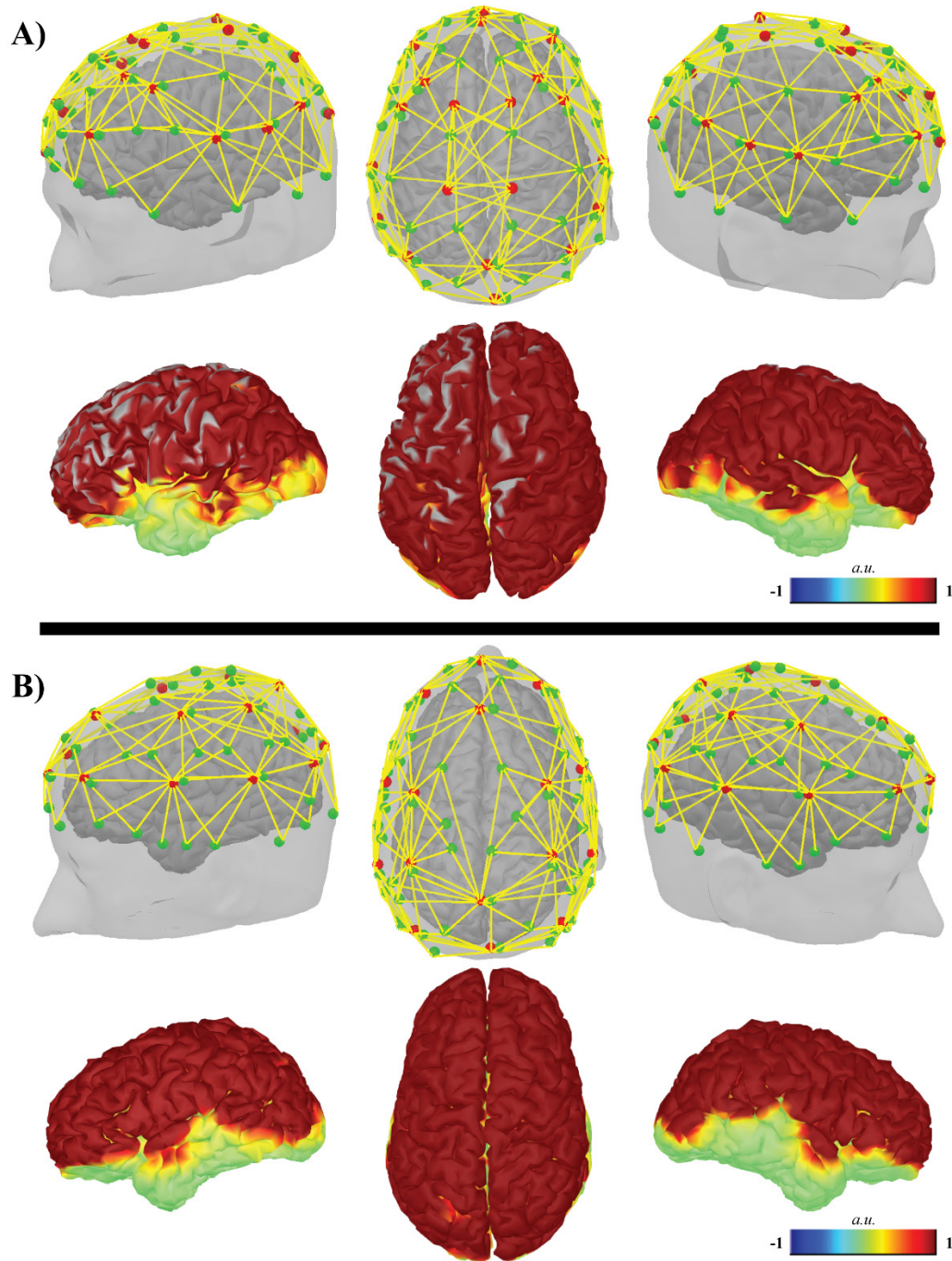
10.6 Conclusions

In conclusion, brain electrophysiology and large-scale cortical hemodynamics were monitored concurrently with systemic cardiovascular physiology during ESE. NVC seemed to be relatively preserved for short-duration recurrent seizures which were associated with increased cortical hemodynamics. In contrast, neurovascular coupling might be disrupted with increased duration of seizures associated with a higher likelihood of inducing insufficient oxygen supply and a hypoxic state. Further studies are required to see if such seizure-induced hypoxic mechanisms play a role in neuronal damage associated with ESE.

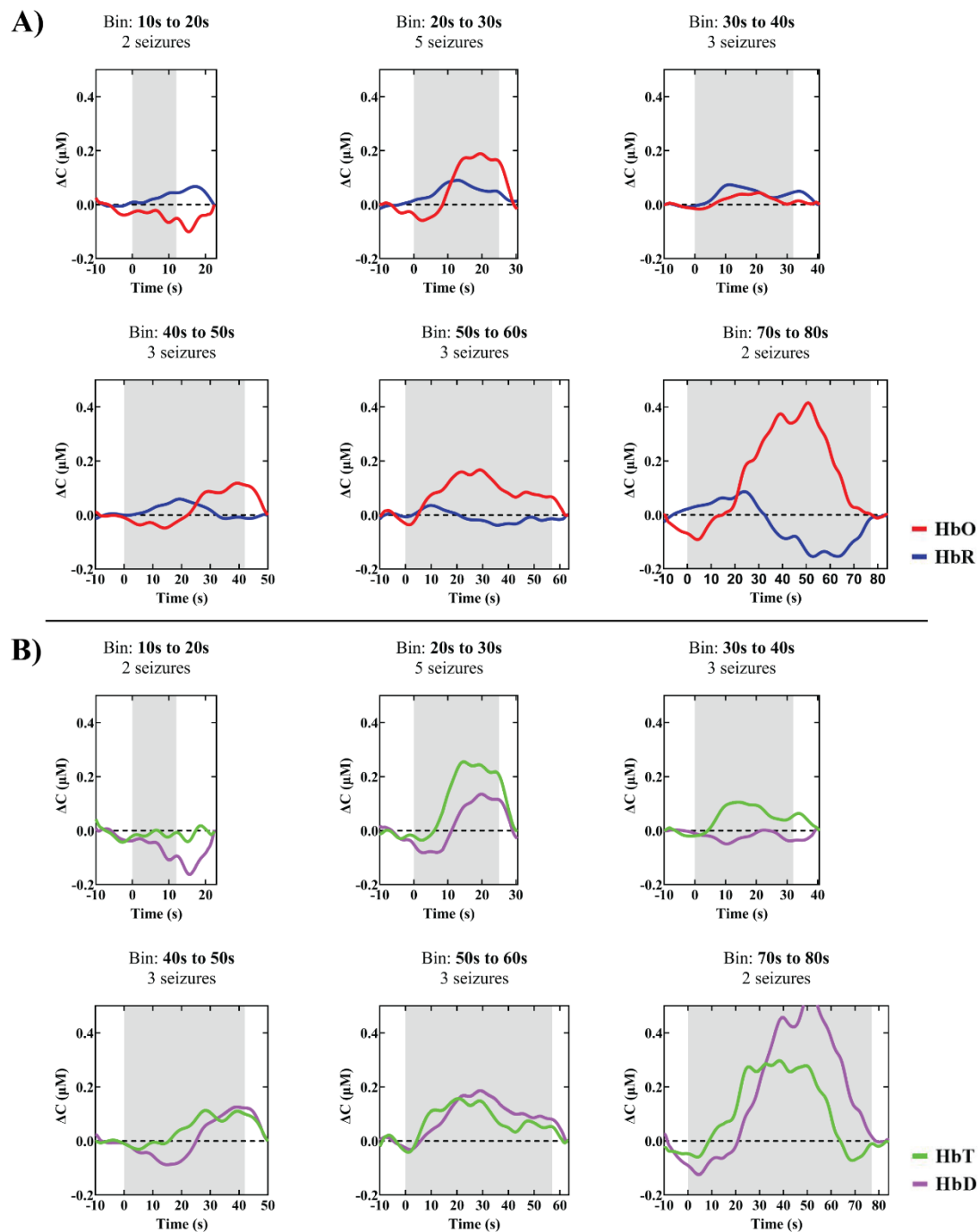
10.7 Acknowledgements

We thank all study subjects and family for their valuable participation. We also thank the ICU nurses and physicians for their support and patience during our study.

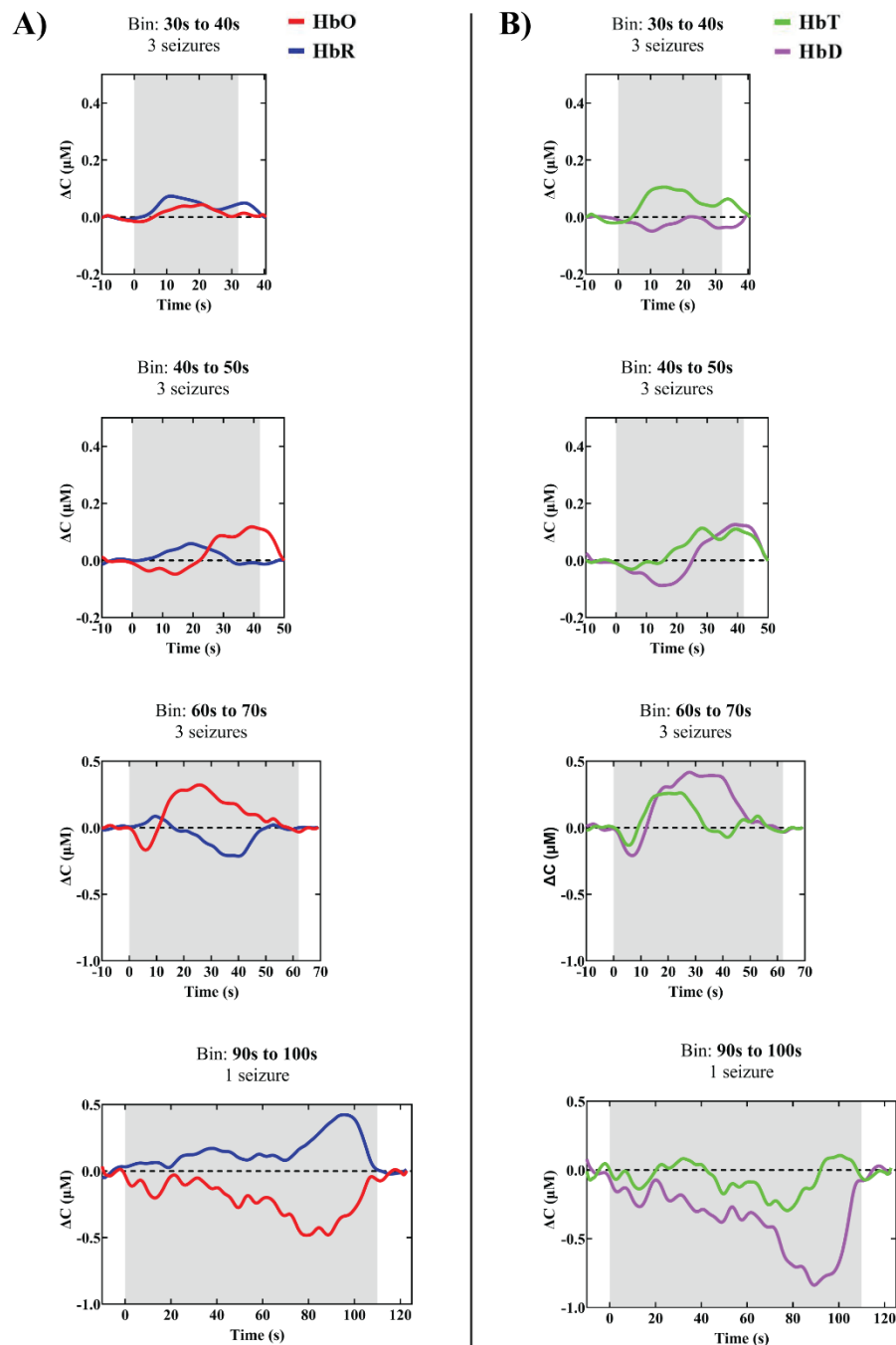
10.8 Appendix



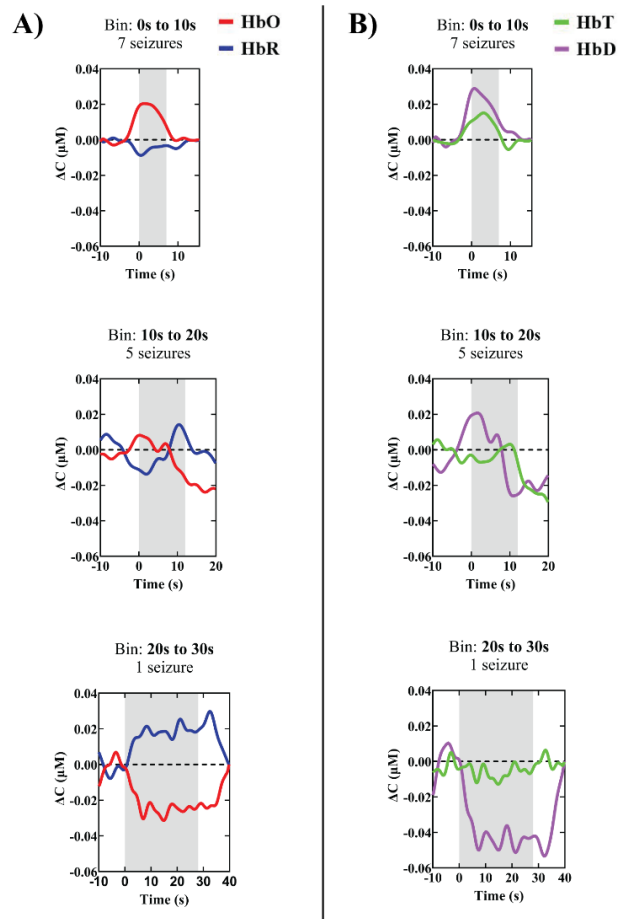
Supplementary Figure 9 – Patient-specific whole-head fNIRS measurement montage and sensitivity profile for patients P01 (A) and P03 (B). The spatial sensitivity profile (i.e., the summation of the sensitivity map of all channels along the cortical surface) was generated using the Brainstorm NIRSTORM plugin (<https://github.com/Nirstorm>) and performed on the patient individual volume space (i.e., patients own MRI). Red and green dots represent sources and detectors. Yellow lines represent channels.



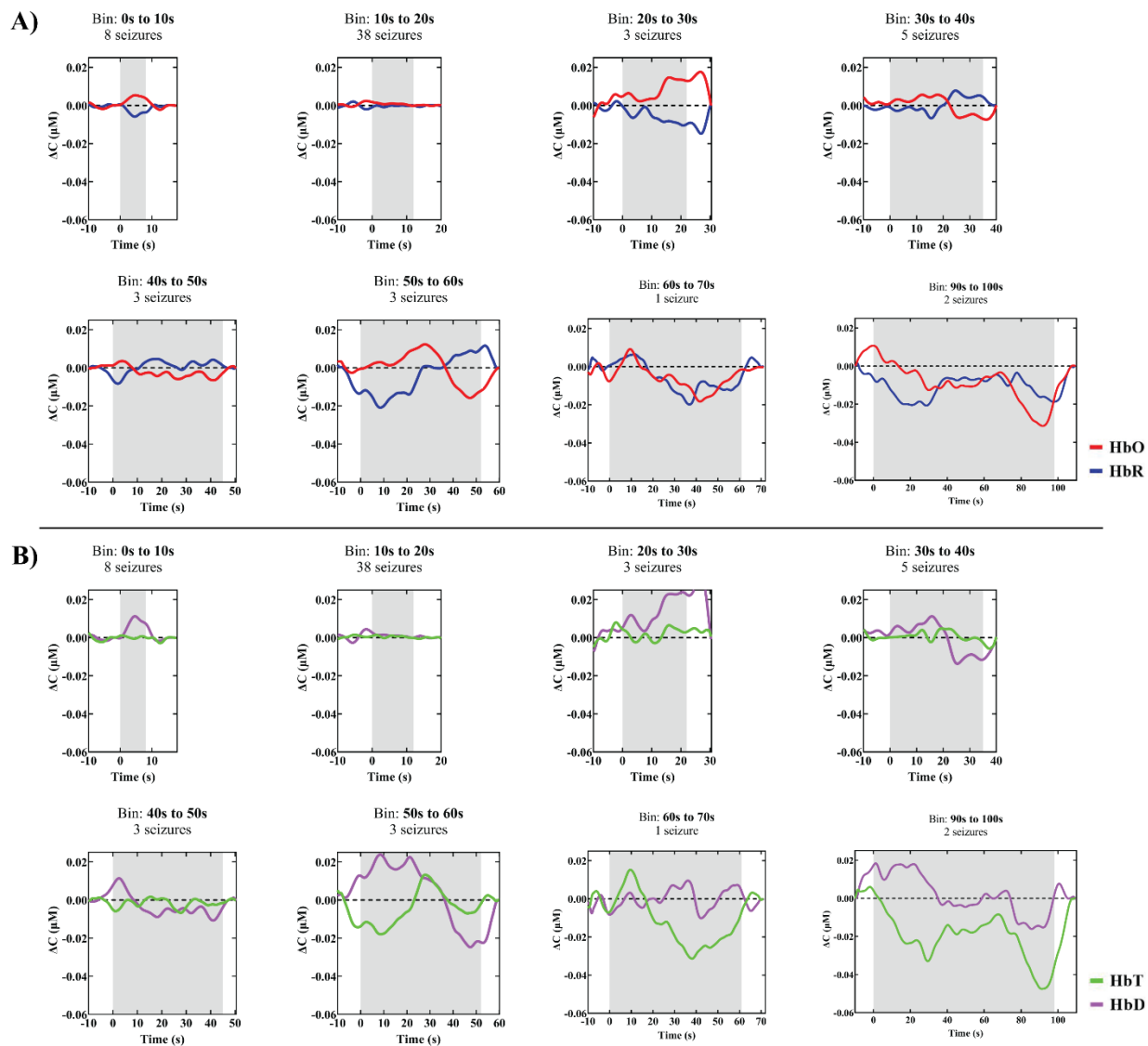
Supplementary Figure 10 – fNIRS results, patient P02: bin analysis of 18 seizures. Each subplot of the figure shows the hemodynamic response functions (HRFs) of oxy- (HbO), deoxy- (HbR) (A), total (HbT) hemoglobin concentration and difference between HbO and HbR (HbD) (B) associated with the seizures. Shaded area indicates the average (mean) length of the seizures within a bin.



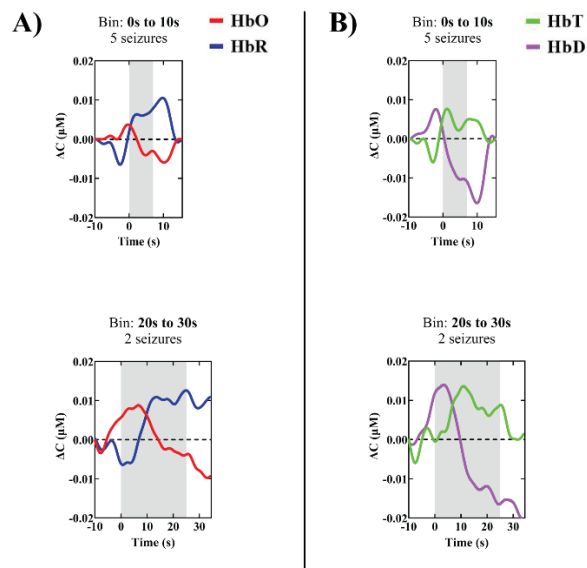
Supplementary Figure 11 – fNIRS results, patient P04: bin analysis of 10 seizures. Each subplot of the figure shows the hemodynamic response functions (HRFs) of oxy- (HbO), deoxy- (HbR) (A), total (HbT) hemoglobin concentration and difference between HbO and HbR (HbD) (B) associated with the seizures. Shaded area indicates the average (mean) length of the seizures within a bin.



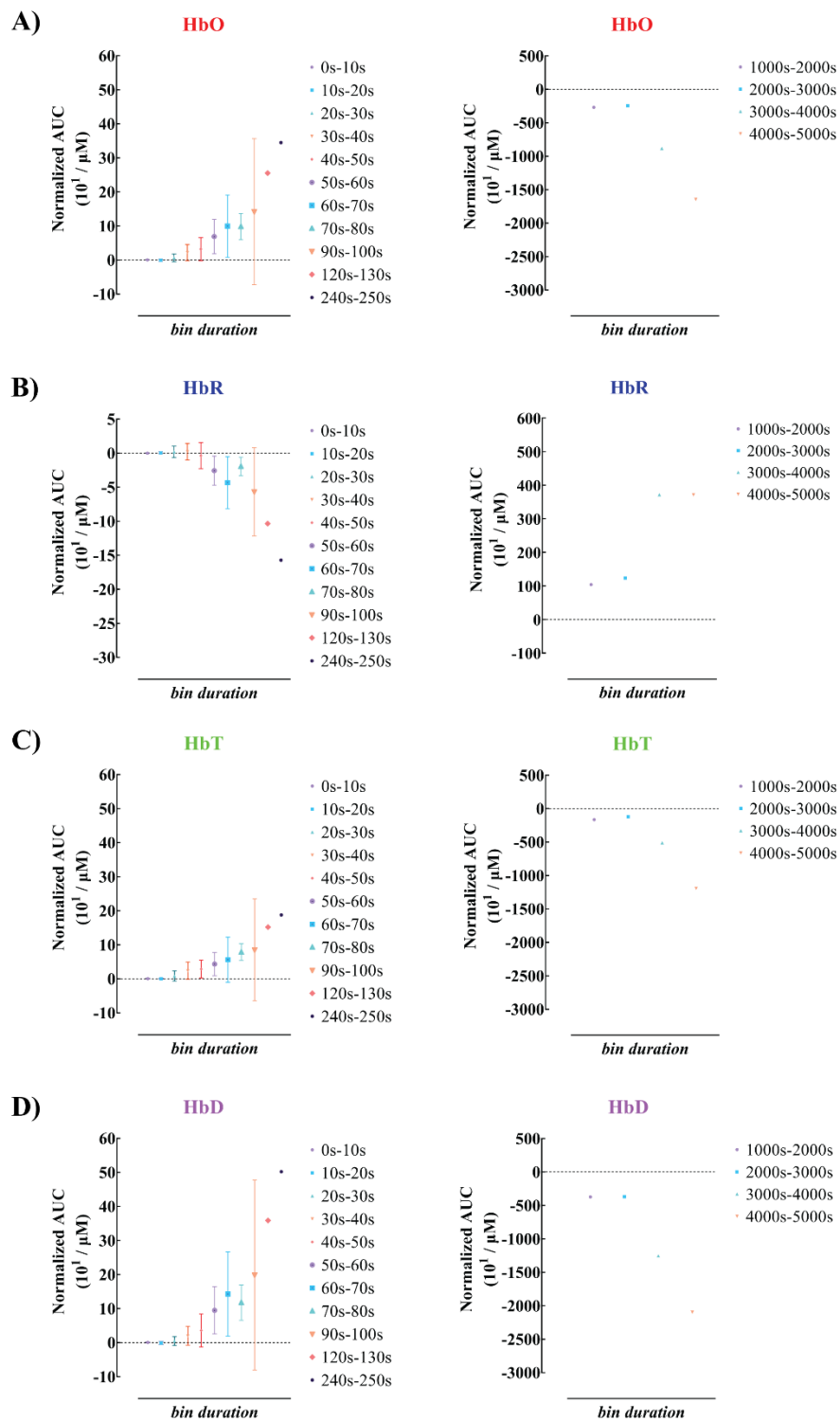
Supplementary Figure 12 – fNIRS results, patient P05: bin analysis of 13 seizures. Each subplot of the figure shows the hemodynamic response functions (HRFs) of oxy- (HbO), deoxy- (HbR) (A), total (HbT) hemoglobin concentration and difference between HbO and HbR (HbD) (B) associated with the seizures. Shaded area indicates the average (mean) length of the seizures within a bin.



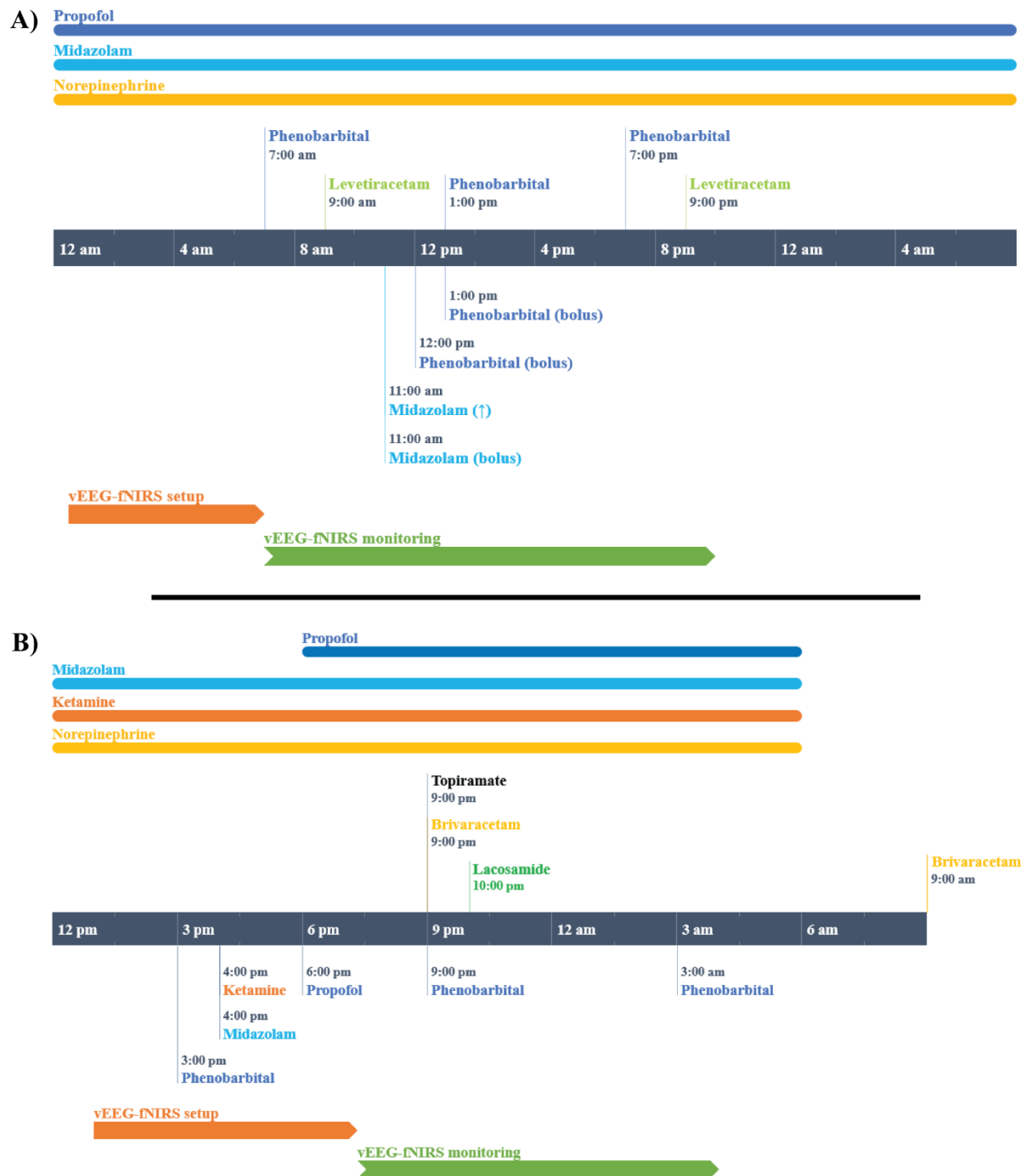
Supplementary Figure 13 – fNIRS results, patient P06: bin analysis of 63 seizures. Each subplot of the figure shows the hemodynamic response functions (HRFs) of oxy- (HbO), deoxy- (HbR) (A), total (HbT) hemoglobin concentration and difference between HbO and HbR (HbD) (B) associated with the seizures. Shaded area indicates the average (mean) length of the seizures within a bin.



Supplementary Figure 14 – fNIRS results, patient P07: bin analysis of 7 seizures. Each subplot of the figure shows the hemodynamic response functions (HRFs) of oxy- (HbO), deoxy- (HbR) (A), total (HbT) hemoglobin concentration and difference between HbO and HbR (HbD) (B) associated with the seizures. Shaded area indicates the average (mean) length of the seizures within a bin.



Supplementary Figure 15 – Group fNIRS bin results. Mean (average) AUC with standard deviation for all HbO (A), HbR (B), HbT (C), and HbD (D) bins.



Supplementary Figure 16 – vEEG-fNIRS monitoring profile and pharmacological management during the first session for patients P01 (A) and P03 (B).

CHAPTER 11 – GENERAL DISCUSSION AND CONCLUSION

11.1 Summary of main contributions

This thesis reports results and progresses in performing long-term whole-head vEEG-fNIRS recordings to assess cerebral hemodynamic responses during seizures and other epileptiform discharges in non-critical and critical care settings.

In this regard, we decided to tackle the considerable challenges imposed by performing such complex monitoring in the clinical setting instead of opting for the habitual experimental set-up and methodology (i.e., short recordings, reduced cortical coverage, recording performed in a laboratory setting). We believe our approach is essential to determine the feasibility of long-term whole-head vEEG-fNIRS monitoring in the adult clinical setting, take full advantage of fNIRS and demonstrate its clinical potential as a neuromonitoring and functional neuroimaging modality, notably in the critically ill. In addition, it allowed us to emphasize some limitations, stressing the need for further technological development.

We achieved our main objective by, first, developing a methodology aiming to capture EEG and fNIRS signals simultaneously over a long period at the patient's bedside. Second, we validated our methodology in neurological and critically ill patients. Finally, we assessed the neurovascular coupling during SE in critically ill comatose patients.

In sum, four papers addressed these challenges and provided significant contributions to their respective field.

11.1.1 Objective 1

The first objective of this thesis was to develop and validate a hybrid multichannel EEG-fNIRS intended for whole-head monitoring of neurological patients at their bedside. This objective was addressed in two chapters (i.e., Chapter 7 and Chapter 8) and motivated by 1) the difficulty of performing simultaneous and long-term vEEG and fNIRS recording at the bedside using commercially available systems and 2) the clinical potential of assessing whole-head hemodynamics in neurologically compromised patients at their bedside.

In Chapter 7, harnessing the advantages of different fNIRS hardware components (i.e., embedded processor, LEDs, APDs), we were able to build a compact (12x9x7 cm³), wearable (< 700 g) and wireless (up to 10 m) multichannel (~128 NIRS channels, 32 EEG channels) EEG-fNIRS system. The wireless option utilized Bluetooth[®] technology with signal loss protection (up to 3s), ensuring data recovery and timing accuracy (msec order).

We also manufactured several personalized EEG-fNIRS caps. These caps were carefully designed for our hybrid system, comfortable enough to be worn over an extended period (>24 h), and stable, allowing a good EEG and fNIRS signal to be captured throughout the monitoring. Even in today's standard, our hybrid system remains relatively unique in small size and whole-scalp coverage (Zhao and Cooper, 2018; Kassab et al., 2018). Similarly, our caps remain distinctive (compared to commercially available caps and with proof-of-concept), enabling comfortable long-term recordings.

After developing our hybrid system and personalized caps, the second important step was validation. As for any neuromonitoring or neuroimaging modality, a qualitative and quantitative evaluation must ensure that the observations (i.e., results) are valid (Lobiondo-Wood and Haber, 2014).

Several strategies can be used to validate a compact hybrid EEG-fNIRS. Most commonly, the use of a phantom (Yurtsever et al., 2003) or a well-established task (e.g., motor task) conducted on one healthy individual (Kiguchi et al., 2012) is employed. These methods have the advantage of being relatively simple to perform, providing quick results. However, the validity and power of

these methods are low as they neither reflect proper hemodynamic changes of a brain (i.e., phantom) nor cannot be generalized to a larger healthy or clinical population (i.e., low number of subjects and all healthy). Therefore, to increase the validity of a neuroimaging system, a particular task, a series of different tasks, or a particular brain event should be evaluated on a more significant number of subjects (or patients). Additionally, these measurements should be compared ideally with a gold standard (often an invasive brain oxygen technique) or, when the context does not permit (such in our case), with commercial systems and additional functional neuroimaging techniques.

When reviewing the literature regarding the methods employed for validating hybrid fNIRS systems, we found that commercial or in-house systems are usually validated using simple methods. However, in our case, we decided to demonstrate a strong validation and precision by evaluating the performance of our system in two groups of subjects during repeated tasks/events. We first asked 12 healthy participants to perform two very different tasks, and we compared the results with two well-established commercial EEG and fNIRS systems. In all participants, constant, repeatable measures (i.e., precision) and firm agreement with commercial devices (i.e., validity and accuracy) were obtained with our hybrid system. As for the performance in a clinical setting, we monitored four patients with diverse neurological conditions and compared our observations with results obtained with different functional neuroimaging techniques, such as single-photon emission computerized tomography, functional MRI, and arterial spin labelling. Similarly, in each patient, our system reported at the bedside the same observations on multiple occasions with respect to the specific conditions and were concordant with other neuroimaging methods (i.e., validity and accuracy).

In addition to contributing significantly to the field of hybrid EEG-fNIRS systems, we were also able to monitor patients at their bedside and obtain relevant hemodynamic changes (i.e., both fundamentally and clinically). As an example, detailed in Chapter 8, the ability to continuously monitor brain hemodynamics during limb-shaking TIA allowed us, for the first time, to shed light on the pathophysiology of this condition by capturing in real-time the full-time course of the decrease in hemodynamics along with associated clinical manifestations. While several functional neuroimaging techniques are usually employed in patients with cerebrovascular disorders and

epilepsy, we demonstrated that fNIRS could be used as a noninvasive and safe method for continuously evaluating whole-brain hemodynamics at the bedside regardless of the setting (e.g., patient seizing, symptoms provoked by a specific maneuver) and aims (e.g., diagnostic, clinical management, neurovascular coupling assessment).

These results suggest that by carefully conceiving a methodology adapted for the clinical setting (i.e., compact and hybrid EEG-fNIRS system with personalized caps), we can enable long-term whole-head vEEG-fNIRS recordings in the clinical setting to capture relatively unique brain hemodynamics changes occurring in neurological patients at their bedside.

11.1.2 Objective 2

Chapter 9 addressed the feasibility of performing long-term vEEG-fNIRS recordings in critically ill adults presenting seizures, periodic discharges, and burst-suppression patterns on the EEG. This objective was mainly motivated by the potential for EEG-"NIRS" in critically ill neonates in 1) assessing the neurovascular coupling during critical care seizures ([Singh et al., 2014](#); [Sokoloff et al., 2015](#); [Mitra et al., 2016](#); [Martini et al., 2019](#)) and burst-suppression ([Chalia et al., 2016](#)), 2) pharmacological management seizures ([Arca Diaz et al., 2006](#)), and 3) the lack of optical imaging studies using "NIRS" beyond a simple cerebral oximeter to assessing the hemodynamic changes during periodic discharges ([Winslow et al., 2021](#)).

The challenges that arose during this study were mainly related to the complex monitoring setting: the ICU. In our previous study, recordings were performed at the patient's bedside in non-critical care environments (i.e., private hospital room, EMU). While recordings in these settings still impose significant challenges for long-term vEEG-fNIRS monitoring, recordings in the ICU come with additional and relatively unique difficulties.

First, particular sources of noise can contaminate the fNIRS signal. Significant motion artifacts can emerge from the specialized pneumatic bed on which they lie and from the constant care provided to the patient. Additional electronic interference/noise can derive from the impressive amount of electronic medical equipment present at the patient's bedside. Therefore, more careful analysis had to be performed to consider these "new" sources of motion and noise. Also, more

attention must be paid to the pressure level used to apply the optodes as the patients are comatose (i.e., no feedback regarding comfort level). The latter is critical to prevent any skin pressure or wound that might potentially arise after several hours or even days of monitoring.

Second, the high-profile optode of our hybrid EEG-fNIRS system was not compatible with occipital monitoring of brain hemodynamics as patients were lying down. In addition, the original concept of our personalized EEG-fNIRS caps, which included an occipital coverage, had to be modified because they reduce cap stability. Since we decided not to assess the occipital portion of the head, we decided to use this portion of the cap as a "stabilizer". Therefore, we developed a new generation of EEG-fNIRS caps that covered > 80% of the head and successfully monitored seven critically ill patients.

Three patients had seizures (two fulfilling the diagnostic criteria of NCSE). For both types of seizures (non-recurrent and recurrent seizures), we observed an increase in brain hemodynamics (i.e., [HbO] and CBV increase, [HbR] decrease), which was in line with the hypermetabolic/hypervascular state in which seizures occur, including SE (Siclari et al., 2013; Lee et al., 2018). More interestingly, we observed a positive correlation between the seizure duration and amplitude of the hemodynamic changes. We discussed in Chapter 3 how hemodynamic response in a "healthy" brain could be modulated by different factors (e.g., stimulus duration, stimulus intensity) reflecting the adaptive mechanism of neurovascular coupling (Devor et al., 2003). Similarly, neurovascular coupling during seizures can adapt, as shown by studies performed in rat models of epilepsy (Kreisman, 1983; Harris et al., 2018) and by our *in vivo* observations in comatose patients.

In four patients, we captured cortical hemodynamic changes associated with burst suppression. Similar to seizures, burst periods were associated with increased brain hemodynamics, which is in line with previous animal studies (Liu et al., 2011, MÄkiranta et al., 2002) and human studies (Chalia et al., 2016). More interestingly, and due to the large cortical sampling in our study, we observed a heterogeneous spatial distribution of the cortical hemodynamic changes, reflecting the asynchronous electrophysiological nature of burst suppression (Lewis et al., 2013). This observation was also reported previously in the study by Chalia and his colleagues during hypoxic-

ischemic brain injury in neonates (Chalia et al., 2016), further supporting the direction and spatial variability associated with burst. In contrast to the study performed by Chalia and his colleagues, we also reported the hemodynamic changes during periods of suppression. A decrease in brain hemodynamics was observed, supporting the hypometabolic state reported in animal models during suppression periods (Sutin et al., 2014).

Periodic discharges remain a clinical challenge as their true nature (ictal events vs. non-ictal events) remains controversial (Claassen, 2009). In our study, three patients presented periodic discharges (one with generalized periodic discharges, and one with lateralized periodic discharges), all with frequencies < 2 Hz. In all patients, an increase in brain hemodynamics was observed potentially suggesting a normal neurovascular coupling process and sufficient compensation of oxygen delivery following the periodic discharges. More recently, preliminary analysis obtained from a larger pool of patients enabled us to capture a slightly different temporal association between the onset of low-frequency (i.e. < 2 Hz) periodic discharge and brain hemodynamics (i.e., increase in HbR, and decrease in HbO, with further increase in the frequency of periodic discharges). Together, these findings are in line with the observation reported by Witsch et al. in 2017 (Witsch et al., 2017). Using invasive monitoring technique (i.e., PbtO₂) to monitor brain oxygenation, periodic discharges with a frequency below 2 Hz was associated with an increase in PbtO₂, while a decrease in PbtO₂ was observed when periodic discharge frequency ≥ 2 Hz (i.e., high-frequency periodic discharges) suggesting metabolic decompensation and more aggressive treatment to be considered (Witsch et al., 2017).

As we can see, vEEG-fNIRS can provide a valuable assessment of the hemodynamic changes in the critically ill with high temporal resolution and over a large cortical area, which are currently not possible via other neuromonitoring techniques currently used in critically ill patients. Invasive monitoring techniques (e.g., PbtO₂, cerebral microdialysis) have a high temporal resolution but can only sample a very limited brain area, carry significant risk, and are currently indicated only in specific conditions (e.g., traumatic brain injury, subarachnoid hemorrhage). In addition, whole-brain neuroimaging techniques (e.g., single-photon emission computerized tomography, arterial spin labelling) require the patient to be transferred outside the critical care setting, which poses a particular risk. Moreover, whole-brain modalities only give a snapshot of hemodynamics that

might not accurately reflect neurovascular coupling, critical care seizures are dynamic and present with accompanying additional and also constantly evolving abnormal EEG events (e.g., periodic discharges). Finally, other techniques such as EEG-fMRI are simply not suitable for critical care settings.

11.1.3 Objective 3

In Chapter 9, we performed for the first time vEEG-fNIRS in critical care adults presenting with seizures. However, we reported hemodynamics changes associated with mostly short duration seizures (i.e. < 25s) in only three patients, as the primary goal of the previous study was not to precisely assess the neurovascular coupling during critical care seizures but to evaluate the feasibility of performing such complex long-term recording in the neuroICU.

The relatively unique observations we obtained in our study motivated us to investigate, more specifically, the neurovascular coupling of seizures in comatose ICU patients. Therefore, achieving this aim would require a larger population of patients and, ideally, a larger number of recorded seizures of both short and long durations. In addition, we wanted to overcome two significant limitations in our previous study: 1) the absence of whole-head coverage and 2) the absence of continuous systemic physiological monitoring. Thus, we upgraded our methodology, employing a commercial EEG and fNIRS system compatible with collodion, and added noninvasive systemic hemodynamic monitoring.

Over a period extending a little more than a year, we successfully monitored 11 patients with NCSE. Preliminary results are promising. For most patients, we observed increases in HbO concentrations and decreases in HbR concentrations. This is consistent with the results obtained from our previous study, showing an adaptive mechanism of the neurovascular coupling within a certain duration range. However, with seizures of longer duration, we observed significant and long-lasting HbO decreases and HbR increases suggesting abnormal neurovascular coupling (its adaptive mechanism) and an underlying hypoxic state.

Altogether, these results support that it is feasible to conduct prolonged vEEG-fNIRS monitoring in critically ill patients with NCSE; that the study of hemodynamic changes may be helpful in

enhancing our understanding of the neurovascular coupling particularly in neurological disorders and critical conditions; and that this method may be useful in the ICU to detect abnormal hemodynamic variations and critical time periods that may be associated with hypoxia and potential brain damage.

11.2 Limitations and future directions

11.2.1 Limitations

The methodology in this thesis has some limitations.

Compact and hybrid EEG-fNIRS system. The use of bulky commercial EEG and fNIRS systems represents a challenge. Developing a compact and hybrid EEG-fNIRS system intended for clinical monitoring offers several advantages when performing simultaneous EEG-fNIRS recordings in the clinical setting. However, we understand that developing such a hybrid system de novo is not always possible. Over the past few years, commercial fNIRS have become less bulky and portable. Examples include the system we have used in this thesis, the Brainsight© NIRS system (Rogue Research®), as well as the OxyMon© NIRS system (Artinis®), and the NIRScout© (NIRx®). We believe that with a few minor adjustments, combining one of those systems with a commercial EEG (e.g., Brainproduct®) can be achieved without too much work and offers the ability to simultaneously capture EEG and fNIRS data, as we have demonstrated with our commercial systems in Chapter 10. For fNIRS studies that require wearability and compactness (i.e., outdoors fNIRS studies), wearable commercial fNIRS systems are also available. However, these systems do not integrate EEG and, therefore, must also be combined with a wearable EEG system, which is also available (Brainproduct®) and has become relatively easy to combine (please visit Brainproduct® website for more details). These solutions have been established to work well for outdoor fNIRS studies but remain demonstrated for clinical purposes.

Personalized caps and collodion. We are aware that the methods used to install the electrodes and optodes require significant time and expertise. By significantly reducing the installation time required to install electrodes and optodes (i.e., ~200%-500%) and increasing long-term comfort, personalized EEG-fNIRS caps can greatly facilitate EEG-fNIRS monitoring of patients. However,

these caps do take a considerable time to manufacture (i.e., days or weeks), as they need to be carefully designed in advance by someone with experience (i.e., proper material, proper head measurements, careful stitching and sewing). On the other hand, collodion adhesive represents the ideal solution for long-term recordings, as it offers excellent stability (i.e., optode positioning), reliability (i.e., signal quality) and comfort. Concerning signal quality, we noticed a decrease in the average number of channels discarded using collodion (i.e., cap ~40% vs. collodion ~20%). However, collodion for whole-head fNIRS coverage takes substantial time (in contrast to a typical EEG collodion installation), which is less practical in the clinical setting. However, currently the use of collodion represents the most suitable approach for long-term EEG-fNIRS monitoring at the clinical bedside. Although less ideal, an alternative could be the development of a large variety of EEG-fNIRS caps in different sizes and shapes. We believe that the time spent at the beginning manufacturing them is time well invested, as once several caps are produced (for different head sizes and shapes), providing researchers with a relatively easy, fast and reusable solution (ecological) for the installation of electrodes and optodes on the head. While we are aware that several commercial EEG-fNIRS caps (Rogue Research[®], Artinis[®], NIRx[®]) are currently available, personalized EEG-fNIRS caps can be more adapted to the study (i.e., environment, condition) in which subjects are being tested, thus providing more comfort and reducing signal artifacts.

Accurate digitization. Anatomic specificity was essential in our studies. Therefore, for each patient, we carefully digitize the optode position. This step significantly increases the setup time (i.e., ~45-60 min for whole head recordings) and requires the usage of a digitization system, which might not always be available. However, except for pure cerebral oximeters used in critical care settings where timely installation is essential and where global cerebral oxygenation is the primary purpose, it is usually recommended that fNIRS studies, which nowadays use multichannel to cover bilateral areas or even whole-head coverage, use some form of localization strategy, the most common and simple one being referencing according to EEG standard such as the 10-20 system (Jurcak et al., 2005). In addition, several commercial caps (e.g., Rogue Research[®], NIRx[®], Artinis[®]) integrate these simple methods and are currently available.

Whole-head sparse montage. A specific goal of this thesis was to assess the hemodynamic changes over the entire head. Therefore, a sparse montage was deemed the most feasible, as whole-

head coverage can already be a challenge, especially in the clinical setting. We are aware that other types of montage have a better spatial resolution (i.e., double density montage, multicentered or rectangular high-density montage). However, these montages are less common in fNIRS studies and, in regards to the work in this thesis, would have been unrealistic considering the long installation time we had to face already. Thus, in our studies, we believe that a sparse montage was a good trade-off between preserving a relatively acceptable spatial resolution (i.e., up to 1 cm) and whole-head coverage.

Analysis. Cardiovascular state (e.g., [hypotension](#), [hypertension](#), [hypoxemia](#)) ([Tachtsidis et al., 2009](#); [Lucas et al., 2010](#); [Lühns and Goebel, 2017](#)) can affect extracerebral and/or cerebral blood flow. For this thesis, systemic physiological confounders were controlled differently between studies. All our studies used short-channel regression except in Chapter 9, where an alternative strategy was applied (i.e., global principal component analysis). This choice had to be made since the short-channel option was no longer available after modifying the personalized caps for the ICU setting. This was no longer an issue in the following study (i.e., Chapter 10) as we used collodion, and all sources were paired with a short-channel. Also, in Chapter 10, we started to measure continuous systemic physiological changes such as MABP, HR, and SpO₂, where very mild to no differences were observed in our population. Although our changes were significantly less than what has been reported during seizures in neonates (range Δ MABP: -3 to 4 mmHg vs. 8-17 mmHg) ([Silas et al., 2012](#)), it should be mentioned that MABP and HR do not necessarily reflect cardiac output, and consequently CBF. Also, SpO₂ values can remain within the normal range despite changes in PaO₂ (i.e., from 100 to 300 mmHg). While it was not the scope of this thesis, the effect of extracerebral (i.e., the amplitude of changes captured by short-distance channels) or systemic physiology (i.e., changes in mean arterial blood pressure) during seizures will be investigated by also integrating additional measurement such as absolute cerebral oximetry.

Another important factor to remember when interpreting our results is the contribution of certain drugs, such as anesthetics and ASMs. Indeed, such drugs have been shown to impact NVC and CBF ([Masamoto and Kanno, 2012](#)). The heterogeneity of our patient population did not allow us to assess the effects of such medication on the cortical hemodynamic response during seizures.

The Bland-Altman method was used in Chapter 7 to measure the limits of agreement between measurements obtained from our prototype (i.e., new system) and those obtained from commercial EEG and fNIRS systems (i.e., clinically valid system and/or gold standard). This method is frequently employed and represents the most appropriate and quickest way to investigate whether measurements obtained from a new method and/or system are reliable (i.e., acceptable) (Doğan NO., 2018).

Lastly, regarding the preference for the GLM model, a Gaussian basis function was selected as it allows more freedom in estimating the hemodynamic response, which is known to vary between, and within-subjects (i.e., different brain regions, different tasks) (Jasdzewski et al., 2003; Yücel et al., 2015), as well as in brain conditions where the neurovascular coupling might be altered (Schroeter et al., 2004; Tak et al., 2014). However, this approach might not be suitable in all cases, especially if the hemodynamic response is asymmetrical. More recently, several studies have used a deconvolution method to estimate the hemodynamic response more accurately. These approaches will be assessed more specifically for the context of seizures in future investigations.

Limited sample size

In addition, as for any clinical (or research) modality, reproducibility and replicability are essential for ensuring that results are clinically accurate and trustworthy. More specifically for fNIRS, reproducibility remains a critical aspect of that technology, as the literature often reports different values obtained by different systems under similar conditions. Hence, a larger sample size for our study would have been preferable, and thus, our results should be considered preliminary, and further studies are essential to ensure reproducibility.

11.2.2 Future directions

In this thesis, we have demonstrated that long-term whole head vEEG-fNIRS monitoring at the patient's bedside can be applied to assess the hemodynamic changes during seizures, periodic discharges, and burst-suppression patterns (i.e., Chapter 10). While we are currently focusing on investigating the neurovascular coupling during NCSE, the neurovascular coupling during periodic discharges and burst-suppression remains poorly understood and requires further study. We are also improving our acquisition and analysis methodology by systematically integrating

physiological changes such as peripheral arterial saturation, heart rate, respiratory rate, and mean arterial blood pressure, non-invasive absolute measurement of cerebral oxygenation, and exploring the possibility of utilizing data obtained from invasive cardiorespiratory monitoring. A better understanding of the impact of periodic discharges will undoubtedly aid clinicians managing these EEG patterns in the critically ill. We hope to monitor a larger number of patients in future studies, which could enable us to characterize neurovascular changes during abnormal epileptiform events better and explore outcomes based on our observations. The neuromonitoring advantage of vEEG-fNIRS might offer a novel and safe strategy for studying and monitoring in the critically ill the impact of other acute events aside from periodic discharges, NCS and SE. Indeed, events such as vasospasm or cardiac embolism leading to regional brain ischemia could potentially be monitored with vEEG-fNIRS.

In parallel to our investigations in the ICU, there is more work to be done in the epilepsy monitoring unit. Over the past few years, we have recorded numerous patients, and preliminary results are engaging. Other avenues worth investigating include the potential of vEEG-fNIRS in monitoring patients in the stroke unit after an acute ischemic stroke or a transient ischemic stroke as they are at high risk of recurrence in the first few days.

Lastly, we have been recently developing a new generation of EEG-fNIRS caps. Compared to our previous caps (i.e., personalized EEG-fNIRS caps), these caps should provide more stability over a long recording period and remain comfortable. In addition, they are easier to assemble and can accommodate several head shapes. We are currently in the process of validating one of those caps.

11.3 Conclusion

In this thesis, we first developed and validated a compact and hybrid EEG-fNIRS system dedicated to long-term whole-head bedside monitoring of neurological patients. The proposed methodology, including the development of “personalized” EEG-fNIRS caps, can potentially be applied to other clinical settings requiring long-term monitoring (e.g., stroke, subarachnoid hemorrhage, traumatic brain injury). We then demonstrated the feasibility of performing such complex recordings in

various clinical settings (i.e., patient room, epilepsy monitoring unit, neuroICU) and illustrated the fundamental and clinical potential of vEEG-fNIRS by providing complementary and often relatively unique assessment of the hemodynamic changes occurring during abnormal brain activity (i.e., limb-shaking transient ischemic attack, non-convulsive seizures, periodic discharges, and burst-suppression). In particular, we were able to capture heterogenous changes in brain hemodynamics during seizures of various duration. While short seizures were usually associated with an increase in brain oxygen concentration, longer seizures exhibited a deoxygenation pattern. With further technological improvements (e.g., wireless collodion compatible optodes, automatic or real-time analysis, standard measurements of hemodynamic and metabolic parameters), larger prospective and comparative studies could be conducted and provide sufficient evidence to adopt vEEG-fNIRS as a clinical neuroimaging technique for bedside monitoring of patients at risk of secondary brain injury.

CHAPTER 12 – PARRALEL AND COLLABORATIVE WORK

In addition to investigating the neurovascular dynamics of seizures, patterns falling in the ictal-interictal continuum, and burst-suppression patterns in the critically ill, I have been actively involved in vEEG-fNIRS recordings of patients admitted to the CHUM epilepsy monitoring unit. The large amount of data collected in this particular setting are in the midst of being analyzed by me and another student. Moreover, other collaborative work during my Ph.D has led to other publications.

Article on assessing the performance of integration multimodal EEG-fNIRS and machine learning for seizure detection, for which I have helped in the preparation, analysis and visualization of EEG-fNIRS results.

- *Sirpal P., **Kassab A.**, Pouliot P., Nguyen DK., Lesage F., fNIRS improves seizure detection in multimodal EEG-fNIRS recordings, J Biomed Opt., Feb;24(5):1-9, 2019*

Article on assessing the effect of exercise on brain hemodynamics in patients with high cardiovascular risk using fNIRS, for which I have helped set up the acquisition environment, collected and visualize the fNIRS data.

- *Mohammadi H., Gagnon C., Vincent T., **Kassab A.**, Fraser S., Nigam A., Lesage F., Bherer L., Longitudinal Impact of Physical Activity on Brain Pulsatility Index and Cognition in Older Adults with Cardiovascular Risk Factors: A NIRS Study, Brain Sci., May 31;11(6):730, 2021*

Article on assessing the relationship between cortical thickness and regional cerebral pulsatility using fNIRS, for which I have helped set up the acquisition environment, collected and visualize the fNIRS data.

- *Mohammadi H., Peng K., **Kassab A.**, Nigam A., Bherer L., Lesage F., Joannette Y., Cortical thinning is associated with brain pulsatility in older adults: An MRI and NIRS study, *Neurobiology of Aging*, Oct;106:103-118, 2021*

Article on assessing the possibility of using combined continuous-wave fNIRS (CW-fNIRS) and time-resolved spectroscopy (TRS) to monitor cortical tissue oxygen saturation variations associated with epileptiform discharges and during language production in epileptic patients and epileptiform discharges on, for which I organized the recording sessions, collected the data, and collaborated in the analysis:

- *Peng, K., **Kassab, A.**, Nguyen, D.K., Auger, H., Dehaes, M., Hoge, R., Lesage F., and Pouliot P., Observing cortical tissue oxygen saturation variations during language production in patients with epilepsy using combined functional near-infrared spectroscopy and time-resolved spectroscopy, in preparation.*

Article on investigating the neurovascular dynamics of patterns falling in the ictal-interictal continuum in the critically ill, for which I organized the recording sessions, collected the data, and collaborated in the analysis:

- *Ke Peng, **Ali Kassab**, Dènahin Hinnoutondji Toffa, Manon Robert, Frédéric Lesage, Dang Khoa Nguyen., Assessing brain hemodynamics associated with ictal-interictal continuum patterns in the critically ill, in preparation.*

REFERENCES

- Reports of Medical Cases, Selected with a View of Illustrating the Symptoms and Cure of Diseases, by a Reference to Morbid Anatomy. (1831). *Med Chir Rev*, 15(30), 289-330.
<https://www.ncbi.nlm.nih.gov/pubmed/29918205>
- A Practical Treatise on the Diseases of the Testis and of the Spermatic Cord and Scrotum. (1866). *Br Foreign Med Chir Rev*, 38(76), 407-417.
<https://www.ncbi.nlm.nih.gov/pubmed/30163227>
- Report of the committee on methods of clinical examination in electroencephalography: 1957. (1958). *Electroencephalography and Clinical Neurophysiology*, 10(2), 370-375.
[https://doi.org/https://doi.org/10.1016/0013-4694\(58\)90053-1](https://doi.org/https://doi.org/10.1016/0013-4694(58)90053-1)
- Heart rate variability: standards of measurement, physiological interpretation and clinical use. Task Force of the European Society of Cardiology and the North American Society of Pacing and Electrophysiology. (1996). *Circulation*, 93(5), 1043-1065.
- An Introduction to Epilepsy. (2006). American Epilepsy Society Copyright © 2006, American Epilepsy Society.
- Measurement of Frontal Lobe Functional Activation and Related Systemic Effects: A Near-Infrared Spectroscopy Investigation. (2008). *Oxygen Transport to Tissue XXIX*, Aasted, C. M., Yücel, M. A., Cooper, R. J., Dubb, J., Tsuzuki, D., Becerra, L., Petkov, M. P., Borsook, D., Dan, I., & Boas, D. A. (2015). Anatomical guidance for functional near-infrared spectroscopy: AtlasViewer tutorial. *Neurophotonics*, 2(2), 020801.
<https://doi.org/10.1117/1.NPh.2.2.020801>
- Abbott, N. J., & Friedman, A. (2012). Overview and introduction: the blood-brain barrier in health and disease. *Epilepsia*, 53 Suppl 6(0 6), 1-6. <https://doi.org/10.1111/j.1528-1167.2012.03696.x>
- Abtahi, M., Cay, G., Saikia, M. J., & Mankodiya, K. (2016). Designing and testing a wearable, wireless fNIRS patch. *Annu Int Conf IEEE Eng Med Biol Soc*, 2016, 6298-6301.
<https://doi.org/10.1109/embc.2016.7592168>
- Acharya, J. N., Hani, A., Cheek, J., Thirumala, P., & Tsuchida, T. N. (2016). American Clinical Neurophysiology Society Guideline 2: Guidelines for Standard Electrode Position Nomenclature. *J Clin Neurophysiol*, 33(4), 308-311.
<https://doi.org/10.1097/wnp.0000000000000316>

- Acharya, M. M., & Katyare, S. S. (2005). Structural and functional alterations in mitochondrial membrane in picrotoxin-induced epileptic rat brain. *Exp Neurol*, 192(1), 79-88.
<https://doi.org/10.1016/j.expneurol.2004.11.004>
- Adams, S. M., & Knowles, P. D. (2007). Evaluation of a first seizure. *Am Fam Physician*, 75(9), 1342-1347. <https://www.ncbi.nlm.nih.gov/pubmed/17508528>
- Adelson, P. D., Nemoto, E., Scheuer, M., Painter, M., Morgan, J., & Yonas, H. (1999). Noninvasive continuous monitoring of cerebral oxygenation periictally using near-infrared spectroscopy: a preliminary report. *Epilepsia*, 40(11), 1484-1489.
<https://doi.org/10.1111/j.1528-1157.1999.tb02030.x>
- Aghakhani, Y., Bagshaw, A. P., Bénar, C. G., Hawco, C., Andermann, F., Dubeau, F., & Gotman, J. (2004). fMRI activation during spike and wave discharges in idiopathic generalized epilepsy. *Brain*, 127(Pt 5), 1127-1144. <https://doi.org/10.1093/brain/awh136>
- Aguirre, G. K., Zarahn, E., & D'Esposito, M. (1998). The variability of human, BOLD hemodynamic responses. *Neuroimage*, 8(4), 360-369.
<https://doi.org/10.1006/nimg.1998.0369>
- Akrawi, W. P., Drummond, J. C., Kalkman, C. J., & Patel, P. M. (1996). A comparison of the electrophysiologic characteristics of EEG burst-suppression as produced by isoflurane, thiopental, etomidate, and propofol. *J Neurosurg Anesthesiol*, 8(1), 40-46.
<https://doi.org/10.1097/00008506-199601000-00010>
- Al Kasab, S., Dawson, R. A., Jaramillo, J. L., & Halford, J. J. (2016). Correlation of seizure frequency and medication down-titration rate during video-EEG monitoring. *Epilepsy Behav*, 64(Pt A), 51-56. <https://doi.org/10.1016/j.yebeh.2016.08.026>
- Alfonso, I., Vasconcellos, E., Shuhaiber, H. H., Yaylali, I., & Papazian, O. (2004). Bilateral decreased oxygenation during focal status epilepticus in a neonate with hemimegalencephaly. *J Child Neurol*, 19(5), 394-396.
<https://doi.org/10.1177/088307380401900516>
- Ali, II, Pirzada, N. A., & Vaughn, B. V. (2001). Periodic lateralized epileptiform discharges after complex partial status epilepticus associated with increased focal cerebral blood flow. *J Clin Neurophysiol*, 18(6), 565-569. <https://doi.org/10.1097/00004691-200111000-00007>
- Ali, M. S., Harmer, M., Vaughan, R. S., Dunne, J. A., & Latto, I. P. (2001). Spatially resolved spectroscopy (NIRO-300) does not agree with jugular bulb oxygen saturation in patients

- undergoing warm bypass surgery. *Can J Anaesth*, 48(5), 497-501.
<https://doi.org/10.1007/bf03028317>
- Ali, S., Khan, M. A., & Khealani, B. (2006). Limb-shaking Transient Ischemic Attacks: case report and review of literature. *BMC Neurol*, 6, 5. <https://doi.org/10.1186/1471-2377-6-5>
- Alkhachroum, A., Kromm, J., & De Georgia, M. A. (2022). Big data and predictive analytics in neurocritical care. *Curr Neurol Neurosci Rep*, 22(1), 19-32.
<https://doi.org/10.1007/s11910-022-01167-w>
- Allen, B., & Vespa, P. M. (2019). Antiseizure medications in critical care: an update. *Curr Opin Crit Care*, 25(2), 117-125. <https://doi.org/10.1097/mcc.0000000000000587>
- Al-Rawi, P. G., & Kirkpatrick, P. J. (2006). Tissue oxygen index: thresholds for cerebral ischemia using near-infrared spectroscopy. *Stroke*, 37(11), 2720-2725.
<https://doi.org/10.1161/01.STR.0000244807.99073.ae>
- Aminoff, M. J., & Simon, R. P. (1980). Status epilepticus. Causes, clinical features and consequences in 98 patients. *Am J Med*, 69(5), 657-666. [https://doi.org/10.1016/0002-9343\(80\)90415-5](https://doi.org/10.1016/0002-9343(80)90415-5)
- Amzica, F. (2009). Basic physiology of burst-suppression. *Epilepsia*, 50(s12), 38-39.
<https://doi.org/https://doi.org/10.1111/j.1528-1167.2009.02345.x>
- Amzica, F. (2015). What does burst suppression really mean? *Epilepsy Behav*, 49, 234-237.
<https://doi.org/10.1016/j.yebeh.2015.06.012>
- Arango-Lievano, M., Boussadia, B., De Terdonck, L. D. T., Gault, C., Fontanaud, P., Lafont, C., Mollard, P., Marchi, N., & Jeanneteau, F. (2018). Topographic Reorganization of Cerebrovascular Mural Cells under Seizure Conditions. *Cell Rep*, 23(4), 1045-1059.
<https://doi.org/10.1016/j.celrep.2018.03.110>
- Arca Diaz, G., Cesaron, E., Alfonso, I., Dunoyer, C., & Yaylali, I. (2006). Near infrared spectroscopy in the management of status epilepticus in a young infant. *Eur J Paediatr Neurol*, 10(1), 19-21. <https://doi.org/10.1016/j.ejpn.2005.11.001>
- Arenth, P. M., Ricker, J. H., & Schultheis, M. T. (2007). Applications of functional near-infrared spectroscopy (fNIRS) to Neurorehabilitation of cognitive disabilities. *Clin Neuropsychol*, 21(1), 38-57. <https://doi.org/10.1080/13854040600878785>
- Arridge, S. R. (1999). Optical tomography in medical imaging. *Inverse Problems*, 15(2), R41.
<https://doi.org/10.1088/0266-5611/15/2/022>

- Arridge, S. R., Schweiger, M., Hiraoka, M., & Delpy, D. T. (1993). A finite element approach for modeling photon transport in tissue. *Med Phys*, 20(2 Pt 1), 299-309.
<https://doi.org/10.1118/1.597069>
- Assal, F., Papazyan, J. P., Slosman, D. O., Jallon, P., & Goerres, G. W. (2001). SPECT in periodic lateralized epileptiform discharges (PLEDs): a form of partial status epilepticus? *Seizure*, 10(4), 260-265. <https://doi.org/10.1053/seiz.2000.0506>
- Atsumori, H., Kiguchi, M., Obata, A., Sato, H., Katura, T., Utsugi, K., Funane, T., & Maki, A. (2007). Development of a multi-channel, portable optical topography system. *Annu Int Conf IEEE Eng Med Biol Soc*, 2007, 3362-3364.
<https://doi.org/10.1109/iembs.2007.4353051>
- Attwell, D., Buchan, A. M., Charpak, S., Lauritzen, M., Macvicar, B. A., & Newman, E. A. (2010). Glial and neuronal control of brain blood flow. *Nature*, 468(7321), 232-243.
<https://doi.org/10.1038/nature09613>
- Avants, B. B., Tustison, N. J., Stauffer, M., Song, G., Wu, B., & Gee, J. C. (2014). The Insight ToolKit image registration framework. *Front Neuroinform*, 8, 44.
<https://doi.org/10.3389/fninf.2014.00044>
- Ayala, G. F., Dichter, M., Gumnit, R. J., Matsumoto, H., & Spencer, W. A. (1973). Genesis of epileptic interictal spikes. New knowledge of cortical feedback systems suggests a neurophysiological explanation of brief paroxysms. *Brain Res*, 52, 1-17.
[https://doi.org/10.1016/0006-8993\(73\)90647-1](https://doi.org/10.1016/0006-8993(73)90647-1)
- Aye, S. M., Lim, K. S., Ramli, N. M., & Tan, C. T. (2013). Periodic lateralized epileptiform discharges (PLEDs) in cerebral lupus correlated with white-matter lesions in brain MRI and reduced cerebral blood flow in SPECT. *Lupus*, 22(5), 510-514.
<https://doi.org/10.1177/0961203312474705>
- Badawy, R. A., Harvey, A. S., & Macdonell, R. A. (2009). Cortical hyperexcitability and epileptogenesis: understanding the mechanisms of epilepsy - part 1. *J Clin Neurosci*, 16(3), 355-365. <https://doi.org/10.1016/j.jocn.2008.08.026>
- Bagshaw, A. P., Aghakhani, Y., Bénar, C. G., Kobayashi, E., Hawco, C., Dubeau, F., Pike, G. B., & Gotman, J. (2004). EEG-fMRI of focal epileptic spikes: analysis with multiple haemodynamic functions and comparison with gadolinium-enhanced MR angiograms. *Hum Brain Mapp*, 22(3), 179-192. <https://doi.org/10.1002/hbm.20024>

- Bagshaw, A. P., Hawco, C., Bénar, C. G., Kobayashi, E., Aghakhani, Y., Dubeau, F., Pike, G. B., & Gotman, J. (2005). Analysis of the EEG-fMRI response to prolonged bursts of interictal epileptiform activity. *Neuroimage*, 24(4), 1099-1112. <https://doi.org/10.1016/j.neuroimage.2004.10.010>
- Bagshaw, A. P., Torab, L., Kobayashi, E., Hawco, C., Dubeau, F., Pike, G. B., & Gotman, J. (2006). EEG-fMRI using z-shimming in patients with temporal lobe epilepsy. *J Magn Reson Imaging*, 24(5), 1025-1032. <https://doi.org/10.1002/jmri.20744>
- Bahar, S., Suh, M., Zhao, M., & Schwartz, T. H. (2006). Intrinsic optical signal imaging of neocortical seizures: the 'epileptic dip'. *Neuroreport*, 17(5), 499-503. <https://doi.org/10.1097/01.wnr.0000209010.78599.f5>
- Balbi, M., Koide, M., Wellman, G. C., & Plesnila, N. (2017). Inversion of neurovascular coupling after subarachnoid hemorrhage in vivo. *J Cereb Blood Flow Metab*, 37(11), 3625-3634. <https://doi.org/10.1177/0271678x16686595>
- Bale, G., Elwell, C. E., & Tachtsidis, I. (2016). From Jöbsis to the present day: a review of clinical near-infrared spectroscopy measurements of cerebral cytochrome-c-oxidase. *J Biomed Opt*, 21(9), 091307. <https://doi.org/10.1117/1.Jbo.21.9.091307>
- Bale, G., Taylor, N., Mitra, S., Sudakou, A., de Roeve, I., Meek, J., Robertson, N., & Tachtsidis, I. (2020). Near-Infrared Spectroscopy Measured Cerebral Blood Flow from Spontaneous Oxygenation Changes in Neonatal Brain Injury. *Adv Exp Med Biol*, 1232, 3-9. https://doi.org/10.1007/978-3-030-34461-0_1
- Bankstahl, M., Breuer, H., Leiter, I., Märkel, M., Bascuñana, P., Michalski, D., Bengel, F. M., Löscher, W., Meier, M., Bankstahl, J. P., & Härtig, W. (2018). Blood-Brain Barrier Leakage during Early Epileptogenesis Is Associated with Rapid Remodeling of the Neurovascular Unit. *eNeuro*, 5(3). <https://doi.org/10.1523/eneuro.0123-18.2018>
- Bansal, L., Miller, I., Hyslop, A., Bhatia, S., Duchowny, M., & Jayakar, P. (2016). PET hypermetabolism in medically resistant childhood epilepsy: Incidence, associations, and surgical outcome. *Epilepsia*, 57(3), 436-444. <https://doi.org/10.1111/epi.13311>
- Barker, J. W., Aarabi, A., & Huppert, T. J. (2013). Autoregressive model based algorithm for correcting motion and serially correlated errors in fNIRS. *Biomed Opt Express*, 4(8), 1366-1379. <https://doi.org/10.1364/boe.4.001366>

- Bar-Klein, G., Lublinsky, S., Kamintsky, L., Noyman, I., Veksler, R., Dalipaj, H., Senatorov, V. V., Jr., Swissa, E., Rosenbach, D., Elazary, N., Milikovsky, D. Z., Milk, N., Kassirer, M., Rosman, Y., Serlin, Y., Eisenkraft, A., Chassidim, Y., Parmet, Y., Kaufer, D., & Friedman, A. (2017). Imaging blood-brain barrier dysfunction as a biomarker for epileptogenesis. *Brain*, 140(6), 1692-1705. <https://doi.org/10.1093/brain/awx073>
- Bar-Klein, G., Lublinsky, S., Kamintsky, L., Noyman, I., Veksler, R., Dalipaj, H., Senatorov, V. V., Jr., Swissa, E., Rosenbach, D., Elazary, N., Milikovsky, D. Z., Milk, N., Kassirer, M., Rosman, Y., Serlin, Y., Eisenkraft, A., Chassidim, Y., Parmet, Y., Kaufer, D., & Friedman, A. (2017). Imaging blood-brain barrier dysfunction as a biomarker for epileptogenesis. *Brain*, 140(6), 1692-1705. <https://doi.org/10.1093/brain/awx073>
- Baruah, J., Vasudevan, A., & Köhling, R. (2019). Vascular Integrity and Signaling Determining Brain Development, Network Excitability, and Epileptogenesis. *Front Physiol*, 10, 1583. <https://doi.org/10.3389/fphys.2019.01583>
- Bauer, G., Trinka, E., & Kaplan, P. W. (2013). EEG patterns in hypoxic encephalopathies (post-cardiac arrest syndrome): fluctuations, transitions, and reactions. *J Clin Neurophysiol*, 30(5), 477-489. <https://doi.org/10.1097/WNP.0b013e3182a73e47>
- Beers, C. A., Williams, R. J., Gaxiola-Valdez, I., Pittman, D. J., Kang, A. T., Aghakhani, Y., Pike, G. B., Goodyear, B. G., & Federico, P. (2015). Patient specific hemodynamic response functions associated with interictal discharges recorded via simultaneous intracranial EEG-fMRI. *Hum Brain Mapp*, 36(12), 5252-5264. <https://doi.org/10.1002/hbm.23008>
- Begley, D. J., & Brightman, M. W. (2003). Structural and functional aspects of the blood-brain barrier. *Prog Drug Res*, 61, 39-78. https://doi.org/10.1007/978-3-0348-8049-7_2
- Bell, A. J., & Sejnowski, T. J. (1995). An information-maximization approach to blind separation and blind deconvolution. *Neural Comput*, 7(6), 1129-1159. <https://doi.org/10.1162/neco.1995.7.6.1129>
- Bénar, C. G., Gross, D. W., Wang, Y., Petre, V., Pike, B., Dubeau, F., & Gotman, J. (2002). The BOLD response to interictal epileptiform discharges. *Neuroimage*, 17(3), 1182-1192. <https://doi.org/10.1006/nimg.2002.1164>
- Berman, M. G., Jonides, J., & Nee, D. E. (2006). Studying mind and brain with fMRI. *Soc Cogn Affect Neurosci*, 1(2), 158-161. <https://doi.org/10.1093/scan/nsi019>

- Berndt, N., Kann, O., & Holzhütter, H. G. (2015). Physiology-based kinetic modeling of neuronal energy metabolism unravels the molecular basis of NAD(P)H fluorescence transients. *J Cereb Blood Flow Metab*, 35(9), 1494-1506.
<https://doi.org/10.1038/jcbfm.2015.70>
- Berndt, N., Kovács, R., Schoknecht, K., Rösner, J., Reiffurth, C., Maechler, M., Holzhütter, H. G., Dreier, J. P., Spies, C., & Liotta, A. (2021). Low neuronal metabolism during isoflurane-induced burst suppression is related to synaptic inhibition while neurovascular coupling and mitochondrial function remain intact. *J Cereb Blood Flow Metab*, 41(10), 2640-2655. <https://doi.org/10.1177/0271678x211010353>
- Berto, P. (2002). Quality of life in patients with epilepsy and impact of treatments. *Pharmacoeconomics*, 20(15), 1039-1059. <https://doi.org/10.2165/00019053-200220150-00002>
- Bewernitz, M., & Derendorf, H. (2012). Electroencephalogram-based pharmacodynamic measures: a review. *Int J Clin Pharmacol Ther*, 50(3), 162-184.
<https://doi.org/10.5414/cp201484>
- Blanco, B., Molnar, M., & Caballero-Gaudes, C. (2018). Effect of prewhitening in resting-state functional near-infrared spectroscopy data. *Neurophotonics*, 5(4), 040401.
<https://doi.org/10.1117/1.NPh.5.4.040401>
- Bland, J. M., & Altman, D. G. (1986). Statistical methods for assessing agreement between two methods of clinical measurement. *Lancet*, 1(8476), 307-310.
- Bland, J. M., & Altman, D. G. (1996). Measurement error. *Bmj*, 312(7047), 1654.
<https://doi.org/10.1136/bmj.312.7047.1654>
- Blasi, A., Phillips, D., Lloyd-Fox, S., Koh, P. H., & Elwell, C. E. (2010). Automatic detection of motion artifacts in infant functional optical topography studies. *Adv Exp Med Biol*, 662, 279-284. https://doi.org/10.1007/978-1-4419-1241-1_40
- Blennow, G., Folbergrova, J., Nilsson, B., & Siesjö, B. K. (1979). Cerebral metabolic and circulatory changes in the rat during sustained seizures induced by DL-homocysteine. *Brain Res*, 179(1), 129-146. [https://doi.org/10.1016/0006-8993\(79\)90497-9](https://doi.org/10.1016/0006-8993(79)90497-9)
- Blount, J. P., Cormier, J., Kim, H., Kankirawatana, P., Riley, K. O., & Knowlton, R. C. (2008). Advances in intracranial monitoring. *Neurosurg Focus*, 25(3), E18.
<https://doi.org/10.3171/foc/2008/25/9/e18>

- Boas, D. A., Culver, J. P., Stott, J. J., & Dunn, A. K. (2002). Three dimensional Monte Carlo code for photon migration through complex heterogeneous media including the adult human head. *Optics Express*, 10(3), 159-170. <https://doi.org/10.1364/OE.10.000159>
- Boas, D. A., Dale, A. M., & Franceschini, M. A. (2004). Diffuse optical imaging of brain activation: approaches to optimizing image sensitivity, resolution, and accuracy. *Neuroimage*, 23 Suppl 1, S275-288. <https://doi.org/10.1016/j.neuroimage.2004.07.011>
- Boas, D. A., Elwell, C. E., Ferrari, M., & Taga, G. (2014). Twenty years of functional near-infrared spectroscopy: introduction for the special issue. *Neuroimage*, 85 Pt 1, 1-5. <https://doi.org/10.1016/j.neuroimage.2013.11.033>
- Boas, D. A., Gaudette, T., Strangman, G., Cheng, X., Marota, J. J., & Mandeville, J. B. (2001). The accuracy of near infrared spectroscopy and imaging during focal changes in cerebral hemodynamics. *Neuroimage*, 13(1), 76-90. <https://doi.org/10.1006/nimg.2000.0674>
- Bourel-Ponchel, E., Mahmoudzadeh, M., Delignières, A., Berquin, P., & Wallois, F. (2017). Non-invasive, multimodal analysis of cortical activity, blood volume and neurovascular coupling in infantile spasms using EEG-fNIRS monitoring. *Neuroimage Clin*, 15, 359-366. <https://doi.org/10.1016/j.nicl.2017.05.004>
- Boushel, R., Langberg, H., Olesen, J., Nowak, M., Simonsen, L., Bülow, J., & Kjaer, M. (2000). Regional blood flow during exercise in humans measured by near-infrared spectroscopy and indocyanine green. *J Appl Physiol* (1985), 89(5), 1868-1878. <https://doi.org/10.1152/jappl.2000.89.5.1868>
- Bozkurt, A., Rosen, A., Rosen, H., & Onaral, B. (2005). A portable near infrared spectroscopy system for bedside monitoring of newborn brain. *Biomed Eng Online*, 4, 29. <https://doi.org/10.1186/1475-925x-4-29>
- Bozkurt, M. F., Saygi, S., & Erbas, B. (2002). SPECT in a patient with postictal PLEDs: is hyperperfusion evidence of electrical seizure? *Clin Electroencephalogr*, 33(4), 171-173. <https://doi.org/10.1177/155005940203300407>
- Brassard, P., Labrecque, L., Smirl, J. D., Tymko, M. M., Caldwell, H. G., Hoiland, R. L., Lucas, S. J. E., Denault, A. Y., Couture, E. J., & Ainslie, P. N. (2021). Losing the dogmatic view of cerebral autoregulation. *Physiol Rep*, 9(15), e14982. <https://doi.org/10.14814/phy2.14982>

- Brazy, J. E., Lewis, D. V., Mitnick, M. H., & Jöbsis vander Vliet, F. F. (1985). Noninvasive monitoring of cerebral oxygenation in preterm infants: preliminary observations. *Pediatrics*, 75(2), 217-225. <https://www.ncbi.nlm.nih.gov/pubmed/2982128>
- Brazy, J. E., Lewis, D. V., Mitnick, M. H., & vander Vliet, F. F. J. b. (1985). Noninvasive Monitoring of Cerebral Oxygenation in Preterm Infants: Preliminary Observations. *Pediatrics*, 75(2), 217-225. <https://doi.org/10.1542/peds.75.2.217>
- Brigadoi, S., Ceccherini, L., Cutini, S., Scarpa, F., Scatturin, P., Selb, J., Gagnon, L., Boas, D. A., & Cooper, R. J. (2014). Motion artifacts in functional near-infrared spectroscopy: a comparison of motion correction techniques applied to real cognitive data. *Neuroimage*, 85 Pt 1(0 1), 181-191. <https://doi.org/10.1016/j.neuroimage.2013.04.082>
- Brigadoi, S., & Cooper, R. J. (2015). How short is short? Optimum source-detector distance for short-separation channels in functional near-infrared spectroscopy. *Neurophotonics*, 2(2), 025005. <https://doi.org/10.1117/1.NPh.2.2.025005>
- Brigadoi, S., Powell, S., Cooper, R. J., Dempsey, L. A., Arridge, S., Everdell, N., Hebden, J., & Gibson, A. P. (2015). Evaluating real-time image reconstruction in diffuse optical tomography using physiologically realistic test data. *Biomed Opt Express*, 6(12), 4719-4737. <https://doi.org/10.1364/boe.6.004719>
- Bright, R. (1831). Reports of Medical Cases, Selected with a View of Illustrating the Symptoms and Cure of Diseases, by a Reference to Morbid Anatomy. *Med Chir Rev*, 15(30), 289-330. <https://www.ncbi.nlm.nih.gov/pubmed/29918205>
- Britton, J. W., Frey, L. C., Hopp, J. L., Korb, P., Koubeissi, M. Z., Lievens, W. E., Pestana-Knight, E. M., & St. Louis, E. K. (2016). In E. K. St. Louis & L. C. Frey (Eds.), *Electroencephalography (EEG): An Introductory Text and Atlas of Normal and Abnormal Findings in Adults, Children, and Infants*. American Epilepsy Society
Copyright ©2016 by American Epilepsy Society.
- Brophy, G. M., Bell, R., Claassen, J., Alldredge, B., Bleck, T. P., Glauser, T., Laroche, S. M., Riviello, J. J., Jr., Shutter, L., Sperling, M. R., Treiman, D. M., & Vespa, P. M. (2012). Guidelines for the evaluation and management of status epilepticus. *Neurocrit Care*, 17(1), 3-23. <https://doi.org/10.1007/s12028-012-9695-z>

- Brown, E. N., Lydic, R., & Schiff, N. D. (2010). General Anesthesia, Sleep, and Coma. *New England Journal of Medicine*, 363(27), 2638-2650.
<https://doi.org/10.1056/NEJMra0808281>
- Buchheim, K., Obrig, H., v Pannwitz, W., Müller, A., Heekeren, H., Villringer, A., & Meierkord, H. (2004). Decrease in haemoglobin oxygenation during absence seizures in adult humans. *Neurosci Lett*, 354(2), 119-122. <https://doi.org/10.1016/j.neulet.2003.10.001>
- Buckley, E. M., Parthasarathy, A. B., Grant, P. E., Yodh, A. G., & Franceschini, M. A. (2014). Diffuse correlation spectroscopy for measurement of cerebral blood flow: future prospects. *Neurophotonics*, 1(1). <https://doi.org/10.1117/1.NPh.1.1.011009>
- Bunce, S. C., Izzetoglu, M., Izzetoglu, K., Onaral, B., & Pourrezaei, K. (2006). Functional near-infrared spectroscopy. *IEEE Eng Med Biol Mag*, 25(4), 54-62.
<https://doi.org/10.1109/memb.2006.1657788>
- Burneo, J. G., Poon, R., Kellett, S., & Snead, O. C. (2015). The Utility of Positron Emission Tomography in Epilepsy. *Can J Neurol Sci*, 42(6), 360-371.
<https://doi.org/10.1017/cjn.2015.279>
- Cai, Z., Machado, A., Chowdhury, R. A., Spilkin, A., Vincent, T., Aydin, Ü., Pellegrino, G., Lina, J. M., & Grova, C. (2022). Diffuse optical reconstructions of functional near infrared spectroscopy data using maximum entropy on the mean. *Sci Rep*, 12(1), 2316.
<https://doi.org/10.1038/s41598-022-06082-1>
- Cai, Z., Machado, A., Chowdhury, R. A., Spilkin, A., Vincent, T., Aydin, Ü., Pellegrino, G., Lina, J.-M., & Grova, C. (2022). Diffuse optical reconstructions of functional near infrared spectroscopy data using maximum entropy on the mean. *Scientific Reports*, 12(1), 2316. <https://doi.org/10.1038/s41598-022-06082-1>
- Cai, Z., Pellegrino, G., Spilkin, A., Delaire, E., Uji, M., Abdallah, C., Lina, J.-M., Fecteau, S., & Grova, C. (2021). Hemodynamic Correlates of Fluctuations in Neuronal Excitability: A Simultaneous Paired Associative Stimulation (PAS) and functional Near Infra-Red Spectroscopy (fNIRS) Study. *bioRxiv*, 2021.2009.2029.462418.
<https://doi.org/10.1101/2021.09.29.462418>
- Cai, Z., Pellegrino, G., Spilkin, A., Delaire, E., Uji, M., Abdallah, C., Lina, J.-M., Fecteau, S., & Grova, C. (2022). Hemodynamic correlates of fluctuations in neuronal excitability: A simultaneous Paired Associative Stimulation (PAS) and functional near infra-red

- spectroscopy (fNIRS) study. *Neuroimage: Reports*, 2(3), 100099.
<https://doi.org/https://doi.org/10.1016/j.ynirp.2022.100099>
- Cai, Z., Uji, M., Aydin, Ü., Pellegrino, G., Spilkin, A., Delaire, É., Abdallah, C., Lina, J. M., & Grova, C. (2021). Evaluation of a personalized functional near infra-red optical tomography workflow using maximum entropy on the mean. *Hum Brain Mapp*, 42(15), 4823-4843. <https://doi.org/10.1002/hbm.25566>
- Caldwell, M., Scholkmann, F., Wolf, U., Wolf, M., Elwell, C., & Tachtsidis, I. (2016). Modelling confounding effects from extracerebral contamination and systemic factors on functional near-infrared spectroscopy. *Neuroimage*, 143, 91-105.
<https://doi.org/10.1016/j.neuroimage.2016.08.058>
- Caliandro, P., Serrao, M., Padua, L., Silvestri, G., Iacovelli, C., Simbolotti, C., Mari, S., Reale, G., Casali, C., & Rossini, P. M. (2015). Prefrontal cortex as a compensatory network in ataxic gait: a correlation study between cortical activity and gait parameters. *Restor Neurol Neurosci*, 33(2), 177-187. <https://doi.org/10.3233/rmn-140449>
- Camello-Almaraz, C., Gomez-Pinilla, P. J., Pozo, M. J., & Camello, P. J. (2006). Mitochondrial reactive oxygen species and Ca²⁺ signaling. *Am J Physiol Cell Physiol*, 291(5), C1082-1088. <https://doi.org/10.1152/ajpcell.00217.2006>
- Carter, L. P. (1996). Thermal diffusion flowmetry. *Neurosurg Clin N Am*, 7(4), 749-754.
<https://www.ncbi.nlm.nih.gov/pubmed/8905786>
- Cascino, G. D., Hulihan, J. F., Sharbrough, F. W., & Kelly, P. J. (1993). Parietal Lobe Lesional Epilepsy: Electroclinical Correlation and Operative Outcome. *Epilepsia*, 34(3), 522-527.
<https://doi.org/https://doi.org/10.1111/j.1528-1157.1993.tb02591.x>
- Cauli, B., & Hamel, E. (2010). Revisiting the role of neurons in neurovascular coupling. *Front Neuroenergetics*, 2, 9. <https://doi.org/10.3389/fnene.2010.00009>
- Cerbo, R. M., Cabano, R., Di Comite, A., Longo, S., Maragliano, R., & Stronati, M. (2012). Cerebral and somatic rSO₂ in sick preterm infants. *J Matern Fetal Neonatal Med*, 25 Suppl 4, 97-100. <https://doi.org/10.3109/14767058.2012.715030>
- Chalia, M., Lee, C. W., Dempsey, L. A., Edwards, A. D., Singh, H., Michell, A. W., Everdell, N. L., Hill, R. W., Hebden, J. C., Austin, T., & Cooper, R. J. (2016). Hemodynamic response to burst-suppressed and discontinuous electroencephalography activity in

- infants with hypoxic ischemic encephalopathy. *Neurophotonics*, 3(3), 031408.
<https://doi.org/10.1117/1.NPh.3.3.031408>
- Chamoun, R., Suki, D., Gopinath, S. P., Goodman, J. C., & Robertson, C. (2010). Role of extracellular glutamate measured by cerebral microdialysis in severe traumatic brain injury. *J Neurosurg*, 113(3), 564-570. <https://doi.org/10.3171/2009.12.Jns09689>
- Chance, B., Dait, M. T., Zhang, C., Hamaoka, T., & Hagerman, F. (1992). Recovery from exercise-induced desaturation in the quadriceps muscles of elite competitive rowers. *Am J Physiol*, 262(3 Pt 1), C766-775. <https://doi.org/10.1152/ajpcell.1992.262.3.C766>
- Ch'ang, J., & Claassen, J. (2017). Seizures in the critically ill. *Handb Clin Neurol*, 141, 507-529. <https://doi.org/10.1016/b978-0-444-63599-0.00028-4>
- Chapman, A. G., Meldrum, B. S., & Siesjö, B. K. (1977). CEREBRAL METABOLIC CHANGES DURING PROLONGED EPILEPTIC SEIZURES IN RATS. *Journal of Neurochemistry*, 28(5), 1025-1035. <https://doi.org/https://doi.org/10.1111/j.1471-4159.1977.tb10665.x>
- Chapman, A. G., Meldrum, B. S., & Siesjö, B. K. (1977). Cerebral metabolic changes during prolonged epileptic seizures in rats. *J Neurochem*, 28(5), 1025-1035. <https://doi.org/10.1111/j.1471-4159.1977.tb10665.x>
- Chaudhary, U. J., Carmichael, D. W., Rodionov, R., Thornton, R. C., Bartlett, P., Vulliemoz, S., Micallef, C., McEvoy, A. W., Diehl, B., Walker, M. C., Duncan, J. S., & Lemieux, L. (2012). Mapping preictal and ictal haemodynamic networks using video-electroencephalography and functional imaging. *Brain*, 135(Pt 12), 3645-3663. <https://doi.org/10.1093/brain/aws302>
- Chen, W. L., Wagner, J., Heugel, N., Sugar, J., Lee, Y. W., Conant, L., Malloy, M., Heffernan, J., Quirk, B., Zinos, A., Beardsley, S. A., Prost, R., & Whelan, H. T. (2020). Functional Near-Infrared Spectroscopy and Its Clinical Application in the Field of Neuroscience: Advances and Future Directions. *Front Neurosci*, 14, 724. <https://doi.org/10.3389/fnins.2020.00724>
- Chen, Z., Brodie, M. J., Liew, D., & Kwan, P. (2018). Treatment Outcomes in Patients With Newly Diagnosed Epilepsy Treated With Established and New Antiepileptic Drugs: A 30-Year Longitudinal Cohort Study. *JAMA Neurol*, 75(3), 279-286. <https://doi.org/10.1001/jamaneurol.2017.3949>

- Chenier, F., & Sawan, M. (2007). A new brain imaging device based on fNIRS. 2007 IEEE Biomedical Circuits and Systems Conference,
- Chiarelli, A. M., Zappasodi, F., Di Pompeo, F., & Merla, A. (2017). Simultaneous functional near-infrared spectroscopy and electroencephalography for monitoring of human brain activity and oxygenation: a review. *Neurophotonics*, 4(4), 041411.
<https://doi.org/10.1117/1.NPh.4.4.041411>
- Chierigato, A., Calzolari, F., Trasforini, G., Targa, L., & Latronico, N. (2003). Normal jugular bulb oxygen saturation. *J Neurol Neurosurg Psychiatry*, 74(6), 784-786.
<https://doi.org/10.1136/jnnp.74.6.784>
- Ching, S., Purdon, P. L., Vijayan, S., Kopell, N. J., & Brown, E. N. (2012). A neurophysiological-metabolic model for burst suppression. *Proc Natl Acad Sci U S A*, 109(8), 3095-3100. <https://doi.org/10.1073/pnas.1121461109>
- Chitnis, D., Airantzis, D., Highton, D., Williams, R., Phan, P., Giagka, V., Powell, S., Cooper, R. J., Tachtsidis, I., Smith, M., Elwell, C. E., Hebden, J. C., & Everdell, N. (2016). Towards a wearable near infrared spectroscopic probe for monitoring concentrations of multiple chromophores in biological tissue in vivo. *Rev Sci Instrum*, 87(6), 065112.
<https://doi.org/10.1063/1.4954722>
- Cho, H., Nemoto, E. M., Sanders, M., Fernandez, K., & Yonas, H. (2000). Comparison of two commercially available near-infrared spectroscopy instruments for cerebral oximetry. Technical note. *J Neurosurg*, 93(2), 351-354. <https://doi.org/10.3171/jns.2000.93.2.0351>
- Chong, D. J., & Hirsch, L. J. (2005). Which EEG patterns warrant treatment in the critically ill? Reviewing the evidence for treatment of periodic epileptiform discharges and related patterns. *J Clin Neurophysiol*, 22(2), 79-91.
<https://doi.org/10.1097/01.wnp.0000158699.78529.af>
- Choy, M., Wells, J. A., Thomas, D. L., Gadian, D. G., Scott, R. C., & Lythgoe, M. F. (2010). Cerebral blood flow changes during pilocarpine-induced status epilepticus activity in the rat hippocampus. *Exp Neurol*, 225(1), 196-201.
<https://doi.org/10.1016/j.expneurol.2010.06.015>
- Ciftçi, K., Sankur, B., Kahya, Y. P., & Akin, A. (2008). Constraining the general linear model for sensible hemodynamic response function waveforms. *Med Biol Eng Comput*, 46(8), 779-787. <https://doi.org/10.1007/s11517-008-0347-6>

- Çiftçi*, K., Sankur, B., Kahya, Y. P., & Akin, A. (2008). Multilevel Statistical Inference From Functional Near-Infrared Spectroscopy Data During Stroop Interference. *IEEE Transactions on Biomedical Engineering*, 55(9), 2212-2220. <https://doi.org/10.1109/TBME.2008.923918> , ISSN= 1558-2531
- Claassen, J. (2009). How I treat patients with EEG patterns on the ictal-interictal continuum in the neuro ICU. *Neurocrit Care*, 11(3), 437-444. <https://doi.org/10.1007/s12028-009-9295-8>
- Claassen, J. (2009). How I Treat Patients with EEG Patterns on the Ictal–Interictal Continuum in the Neuro ICU. *Neurocritical Care*, 11(3), 437. <https://doi.org/10.1007/s12028-009-9295-8>
- Claassen, J., & Goldstein, J. N. (2017). Emergency Neurological Life Support: Status Epilepticus. *Neurocrit Care*, 27(Suppl 1), 152-158. <https://doi.org/10.1007/s12028-017-0460-1>
- Claassen, J., Hirsch, L. J., Frontera, J. A., Fernandez, A., Schmidt, M., Kapinos, G., Wittman, J., Connolly, E. S., Emerson, R. G., & Mayer, S. A. (2006). Prognostic significance of continuous EEG monitoring in patients with poor-grade subarachnoid hemorrhage. *Neurocrit Care*, 4(2), 103-112. <https://doi.org/10.1385/ncc:4:2:103>
- Claassen, J., Hirsch, L. J., Kreiter, K. T., Du, E. Y., Connolly, E. S., Emerson, R. G., & Mayer, S. A. (2004). Quantitative continuous EEG for detecting delayed cerebral ischemia in patients with poor-grade subarachnoid hemorrhage. *Clin Neurophysiol*, 115(12), 2699-2710. <https://doi.org/10.1016/j.clinph.2004.06.017>
- Claassen, J., Jetté, N., Chum, F., Green, R., Schmidt, M., Choi, H., Jirsch, J., Frontera, J. A., Connolly, E. S., Emerson, R. G., Mayer, S. A., & Hirsch, L. J. (2007). Electrographic seizures and periodic discharges after intracerebral hemorrhage. *Neurology*, 69(13), 1356-1365. <https://doi.org/10.1212/01.wnl.0000281664.02615.6c>
- Claassen, J., Mayer, S. A., Kowalski, R. G., Emerson, R. G., & Hirsch, L. J. (2004). Detection of electrographic seizures with continuous EEG monitoring in critically ill patients. *Neurology*, 62(10), 1743-1748. <https://doi.org/10.1212/01.wnl.0000125184.88797.62>
- Claassen, J., Perotte, A., Albers, D., Kleinberg, S., Schmidt, J. M., Tu, B., Badjatia, N., Lantigua, H., Hirsch, L. J., Mayer, S. A., Connolly, E. S., & Hripcsak, G. (2013). Nonconvulsive

- seizures after subarachnoid hemorrhage: Multimodal detection and outcomes. *Ann Neurol*, 74(1), 53-64. <https://doi.org/10.1002/ana.23859>
- Claassen, J., & Vespa, P. (2014). Electrophysiologic monitoring in acute brain injury. *Neurocrit Care*, 21 Suppl 2, S129-147. <https://doi.org/10.1007/s12028-014-0022-8>
- Cloostermans, M. C., van Meulen, F. B., Eertman, C. J., Hom, H. W., & van Putten, M. J. (2012). Continuous electroencephalography monitoring for early prediction of neurological outcome in postanoxic patients after cardiac arrest: a prospective cohort study. *Crit Care Med*, 40(10), 2867-2875. <https://doi.org/10.1097/CCM.0b013e31825b94f0>
- Coan, A. C., Chaudhary, U. J., Grouiller, F., Campos, B. M., Perani, S., De Ciantis, A., Vulliemoz, S., Diehl, B., Beltramini, G. C., Carmichael, D. W., Thornton, R. C., Covolan, R. J., Cendes, F., & Lemieux, L. (2016). EEG-fMRI in the presurgical evaluation of temporal lobe epilepsy. *J Neurol Neurosurg Psychiatry*, 87(6), 642-649. <https://doi.org/10.1136/jnnp-2015-310401>
- Cohen, M. S., & Bookheimer, S. Y. (1994). Localization of brain function using magnetic resonance imaging. *Trends Neurosci*, 17(7), 268-277. [https://doi.org/10.1016/0166-2236\(94\)90055-8](https://doi.org/10.1016/0166-2236(94)90055-8)
- Coles, J. P., Minhas, P. S., Fryer, T. D., Smielewski, P., Aigbirihio, F., Donovan, T., Downey, S. P., Williams, G., Chatfield, D., Matthews, J. C., Gupta, A. K., Carpenter, T. A., Clark, J. C., Pickard, J. D., & Menon, D. K. (2002). Effect of hyperventilation on cerebral blood flow in traumatic head injury: clinical relevance and monitoring correlates. *Crit Care Med*, 30(9), 1950-1959. <https://doi.org/10.1097/00003246-200209000-00002>
- Colier, W. N., van Haaren, N. J., & Oeseburg, B. (1995). A comparative study of two near infrared spectrophotometers for the assessment of cerebral haemodynamics. *Acta Anaesthesiol Scand Suppl*, 107, 101-105. <https://doi.org/10.1111/j.1399-6576.1995.tb04342.x>
- Collaborators, G. E. (2019). Global, regional, and national burden of epilepsy, 1990-2016: a systematic analysis for the Global Burden of Disease Study 2016. *Lancet Neurol*, 18(4), 357-375. [https://doi.org/10.1016/s1474-4422\(18\)30454-x](https://doi.org/10.1016/s1474-4422(18)30454-x)
- Connolly, M., Vespa, P., Pouratian, N., Gonzalez, N. R., & Hu, X. (2015). Characterization of the relationship between intracranial pressure and electroencephalographic monitoring in

- burst-suppressed patients. *Neurocrit Care*, 22(2), 212-220.
<https://doi.org/10.1007/s12028-014-0059-8>
- Cooper, C. E., Elwell, C. E., Meek, J. H., Matcher, S. J., Wyatt, J. S., Cope, M., & Delpy, D. T. (1996). The noninvasive measurement of absolute cerebral deoxyhemoglobin concentration and mean optical path length in the neonatal brain by second derivative near infrared spectroscopy. *Pediatr Res*, 39(1), 32-38. <https://doi.org/10.1203/00006450-199601000-00005>
- Cooper, R. J., Hebden, J. C., O'Reilly, H., Mitra, S., Michell, A. W., Everdell, N. L., Gibson, A. P., & Austin, T. (2011). Transient haemodynamic events in neurologically compromised infants: a simultaneous EEG and diffuse optical imaging study. *Neuroimage*, 55(4), 1610-1616. <https://doi.org/10.1016/j.neuroimage.2011.01.022>
- Cooper, R. J., Selb, J., Gagnon, L., Phillip, D., Schytz, H. W., Iversen, H. K., Ashina, M., & Boas, D. A. (2012). A systematic comparison of motion artifact correction techniques for functional near-infrared spectroscopy. *Front Neurosci*, 6, 147.
<https://doi.org/10.3389/fnins.2012.00147>
- Cope, M. (1991). The development of a near infrared spectroscopy system and its application for non invasive monitoring of cerebral blood and tissue oxygenation in the newborn infants [University of London]. <https://discovery.ucl.ac.uk/id/eprint/1317956>
- Cormier, J., Maciel, C. B., & Gilmore, E. J. (2017). Ictal-Interictal Continuum: When to Worry About the Continuous Electroencephalography Pattern. *Semin Respir Crit Care Med*, 38(6), 793-806. <https://doi.org/10.1055/s-0037-1607987>
- Cormio, M., Valadka, A. B., & Robertson, C. S. (1999). Elevated jugular venous oxygen saturation after severe head injury. *J Neurosurg*, 90(1), 9-15.
<https://doi.org/10.3171/jns.1999.90.1.0009>
- Correia, M. M., Carpenter, T. A., & Williams, G. B. (2009). Looking for the optimal DTI acquisition scheme given a maximum scan time: are more b-values a waste of time? *Magn Reson Imaging*, 27(2), 163-175. <https://doi.org/10.1016/j.mri.2008.06.011>
- Cox, D. R., & Wermuth, N. (2014). *Multivariate dependencies: Models, analysis and interpretation* (Vol. 67). CRC Press.
- Cui, X., Bray, S., & Reiss, A. L. (2010). Functional near infrared spectroscopy (NIRS) signal improvement based on negative correlation between oxygenated and deoxygenated

- hemoglobin dynamics. *Neuroimage*, 49(4), 3039-3046.
<https://doi.org/10.1016/j.neuroimage.2009.11.050>
- Culver, J. P., Siegel, A. M., Stott, J. J., & Boas, D. A. (2003). Volumetric diffuse optical tomography of brain activity. *Optics Letters*, 28(21), 2061-2063.
<https://doi.org/10.1364/OL.28.002061>
- Curling, T. B. (1866). A Practical Treatise on the Diseases of the Testis and of the Spermatic Cord and Scrotum. *Br Foreign Med Chir Rev*, 38(76), 407-417.
<https://www.ncbi.nlm.nih.gov/pubmed/30163227>
- Curtin, A., Tong, S., Sun, J., Wang, J., Onaral, B., & Ayaz, H. (2019). A Systematic Review of Integrated Functional Near-Infrared Spectroscopy (fNIRS) and Transcranial Magnetic Stimulation (TMS) Studies. *Front Neurosci*, 13, 84.
<https://doi.org/10.3389/fnins.2019.00084>
- Custo, A., Boas, D. A., Tsuzuki, D., Dan, I., Mesquita, R., Fischl, B., Grimson, W. E., & Wells, W., 3rd. (2010). Anatomical atlas-guided diffuse optical tomography of brain activation. *Neuroimage*, 49(1), 561-567. <https://doi.org/10.1016/j.neuroimage.2009.07.033>
- CUTLER, M. (1931). TRANSILLUMINATION OF THE BREAST. *Annals of Surgery*, 93(1), 223-234. <https://doi.org/10.1097/00000658-193101000-00032>
- Czosnyka, Z., & Czosnyka, M. (2017). Long-term monitoring of intracranial pressure in normal pressure hydrocephalus and other CSF disorders. *Acta Neurochir (Wien)*, 159(10), 1979-1980. <https://doi.org/10.1007/s00701-017-3282-1>
- Dahnke, R., Yotter, R. A., & Gaser, C. (2013). Cortical thickness and central surface estimation. *Neuroimage*, 65, 336-348. <https://doi.org/10.1016/j.neuroimage.2012.09.050>
- Dale, A. M., & Buckner, R. L. (1997). Selective averaging of rapidly presented individual trials using fMRI. *Hum Brain Mapp*, 5(5), 329-340. [https://doi.org/10.1002/\(sici\)1097-0193\(1997\)5:5<329::Aid-hbm1>3.0.Co;2-5](https://doi.org/10.1002/(sici)1097-0193(1997)5:5<329::Aid-hbm1>3.0.Co;2-5)
- Dalsgaard, M. K., & Secher, N. H. (2007). The brain at work: a cerebral metabolic manifestation of central fatigue? *J Neurosci Res*, 85(15), 3334-3339. <https://doi.org/10.1002/jnr.21274>
- Darbin, O., Risso, J. J., Carre, E., Lonjon, M., & Naritoku, D. K. (2005). Metabolic changes in rat striatum following convulsive seizures. *Brain Res*, 1050(1-2), 124-129.
<https://doi.org/10.1016/j.brainres.2005.05.030>

- Davie, S. N., & Grocott, H. P. (2012). Impact of extracranial contamination on regional cerebral oxygen saturation: a comparison of three cerebral oximetry technologies. *Anesthesiology*, 116(4), 834-840. <https://doi.org/10.1097/ALN.0b013e31824c00d7>
- Davies, D. J., Clancy, M., Lighter, D., Balanos, G. M., Lucas, S. J. E., Dehghani, H., Su, Z., Forcione, M., & Belli, A. (2017). Frequency-domain vs continuous-wave near-infrared spectroscopy devices: a comparison of clinically viable monitors in controlled hypoxia. *J Clin Monit Comput*, 31(5), 967-974. <https://doi.org/10.1007/s10877-016-9942-5>
- Dehghani, H., White, B. R., Zeff, B. W., Tizzard, A., & Culver, J. P. (2009). Depth sensitivity and image reconstruction analysis of dense imaging arrays for mapping brain function with diffuse optical tomography. *Appl Opt*, 48(10), D137-143. <https://doi.org/10.1364/ao.48.00d137>
- DeLorenzo, R. J., Hauser, W. A., Towne, A. R., Boggs, J. G., Pellock, J. M., Penberthy, L., Garnett, L., Fortner, C. A., & Ko, D. (1996). A prospective, population-based epidemiologic study of status epilepticus in Richmond, Virginia. *Neurology*, 46(4), 1029-1035. <https://doi.org/10.1212/wnl.46.4.1029>
- Delpont, E., Dolisi, C., Suisse, G., Bodino, G., & Gastaud, M. (1991). Visual evoked potentials: differences related to physical activity. *Int J Sports Med*, 12(3), 293-298. <https://doi.org/10.1055/s-2007-1024684>
- Delpy, D. T., Cope, M., van der Zee, P., Arridge, S., Wray, S., & Wyatt, J. (1988). Estimation of optical pathlength through tissue from direct time of flight measurement. *Phys Med Biol*, 33(12), 1433-1442. <https://doi.org/10.1088/0031-9155/33/12/008>
- Denault, A., Deschamps, A., & Murkin, J. M. (2007). A proposed algorithm for the intraoperative use of cerebral near-infrared spectroscopy. *Semin Cardiothorac Vasc Anesth*, 11(4), 274-281. <https://doi.org/10.1177/1089253207311685>
- Devor, A., Dunn, A. K., Andermann, M. L., Ulbert, I., Boas, D. A., & Dale, A. M. (2003). Coupling of total hemoglobin concentration, oxygenation, and neural activity in rat somatosensory cortex. *Neuron*, 39(2), 353-359. [https://doi.org/10.1016/s0896-6273\(03\)00403-3](https://doi.org/10.1016/s0896-6273(03)00403-3)
- Devor, A., Hillman, E. M., Tian, P., Waeber, C., Teng, I. C., Ruvinskaya, L., Shalinsky, M. H., Zhu, H., Haslinger, R. H., Narayanan, S. N., Ulbert, I., Dunn, A. K., Lo, E. H., Rosen, B. R., Dale, A. M., Kleinfeld, D., & Boas, D. A. (2008). Stimulus-induced changes in blood

- flow and 2-deoxyglucose uptake dissociate in ipsilateral somatosensory cortex. *J Neurosci*, 28(53), 14347-14357. <https://doi.org/10.1523/jneurosci.4307-08.2008>
- Dham, B. S., Hunter, K., & Rincon, F. (2014). The epidemiology of status epilepticus in the United States. *Neurocrit Care*, 20(3), 476-483. <https://doi.org/10.1007/s12028-013-9935-x>
- Dix, L. M., van Bel, F., Baerts, W., & Lemmers, P. M. (2013). Comparing near-infrared spectroscopy devices and their sensors for monitoring regional cerebral oxygen saturation in the neonate. *Pediatr Res*, 74(5), 557-563. <https://doi.org/10.1038/pr.2013.133>
- Dix, L. M. L., Weeke, L. C., de Vries, L. S., Groenendaal, F., Baerts, W., van Bel, F., & Lemmers, P. M. A. (2017). Carbon Dioxide Fluctuations Are Associated with Changes in Cerebral Oxygenation and Electrical Activity in Infants Born Preterm. *J Pediatr*, 187, 66-72.e61. <https://doi.org/10.1016/j.jpeds.2017.04.043>
- Doerschuk, P. C. (1994). Bayesian reconstruction of signals invariant under a space-group symmetry from Fourier transform magnitudes. *IEEE Trans Image Process*, 3(4), 438-449. <https://doi.org/10.1109/83.298397>
- Doherty, C. P., Cole, A. J., Grant, P. E., Fischman, A., Dooling, E., Hoch, D. B., White, T. H., & Cosgrove, G. R. (2004). Multimodal longitudinal imaging of focal status epilepticus. *Can J Neurol Sci*, 31(2), 276-281. <https://doi.org/10.1017/s031716710005397x>
- Doman, G., & Pelligra, R. (2003). Ictogenesis: the origin of seizures in humans. A new look at an old theory. *Med Hypotheses*, 60(1), 129-132. [https://doi.org/10.1016/s0306-9877\(02\)00348-1](https://doi.org/10.1016/s0306-9877(02)00348-1)
- Doman, G., & Pelligra, R. (2004). A unifying concept of seizure onset and termination. *Med Hypotheses*, 62(5), 740-745. <https://doi.org/10.1016/j.mehy.2003.10.020>
- Doyle, P. W., & Matta, B. F. (1999). Burst suppression or isoelectric encephalogram for cerebral protection: evidence from metabolic suppression studies. *Br J Anaesth*, 83(4), 580-584. <https://doi.org/10.1093/bja/83.4.580>
- Drew, P. J., Shih, A. Y., & Kleinfeld, D. (2011). Fluctuating and sensory-induced vasodynamics in rodent cortex extend arteriole capacity. *Proc Natl Acad Sci U S A*, 108(20), 8473-8478. <https://doi.org/10.1073/pnas.1100428108>

- Duffy, T. E., Howse, D. C., & Plum, F. (1975). Cerebral energy metabolism during experimental status epilepticus. *J Neurochem*, 24(5), 925-934. <https://doi.org/10.1111/j.1471-4159.1975.tb03657.x>
- Duffy, T. E., Howse, D. C., & Plum, F. (1975). CEREBRAL ENERGY METABOLISM DURING EXPERIMENTAL STATUS EPILEPTICUS1. *Journal of Neurochemistry*, 24(5), 925-934. <https://doi.org/https://doi.org/10.1111/j.1471-4159.1975.tb03657.x>
- Dullenkopf, A., Frey, B., Baenziger, O., Gerber, A., & Weiss, M. (2003). Measurement of cerebral oxygenation state in anaesthetized children using the INVOS 5100 cerebral oximeter. *Paediatr Anaesth*, 13(5), 384-391. <https://doi.org/10.1046/j.1460-9592.2003.01111.x>
- Duncan, A., Meek, J. H., Clemence, M., Elwell, C. E., Fallon, P., Tyszczuk, L., Cope, M., & Delpy, D. T. (1996). Measurement of cranial optical path length as a function of age using phase resolved near infrared spectroscopy. *Pediatr Res*, 39(5), 889-894. <https://doi.org/10.1203/00006450-199605000-00025>
- Duncan, A., Meek, J. H., Clemence, M., Elwell, C. E., Tyszczuk, L., Cope, M., & Delpy, D. (1995). Optical pathlength measurements on adult head, calf and forearm and the head of the newborn infant using phase resolved optical spectroscopy. *Physics in Medicine & Biology*, 40(2), 295. <https://doi.org/10.1088/0031-9155/40/2/007>
- Duncan, A., Meek, J. H., Clemence, M., Elwell, C. E., Tyszczuk, L., Cope, M., & Delpy, D. T. (1995). Optical pathlength measurements on adult head, calf and forearm and the head of the newborn infant using phase resolved optical spectroscopy. *Phys Med Biol*, 40(2), 295-304. <https://doi.org/10.1088/0031-9155/40/2/007>
- Duncan, J. S., Winston, G. P., Koepp, M. J., & Ourselin, S. (2016). Brain imaging in the assessment for epilepsy surgery. *Lancet Neurol*, 15(4), 420-433. [https://doi.org/10.1016/s1474-4422\(15\)00383-x](https://doi.org/10.1016/s1474-4422(15)00383-x)
- During, M. J., Fried, I., Leone, P., Katz, A., & Spencer, D. D. (1994). Direct measurement of extracellular lactate in the human hippocampus during spontaneous seizures. *J Neurochem*, 62(6), 2356-2361. <https://doi.org/10.1046/j.1471-4159.1994.62062356.x>
- Edmonds, H. L., Jr., Ganzel, B. L., & Austin, E. H., 3rd. (2004). Cerebral oximetry for cardiac and vascular surgery. *Semin Cardiothorac Vasc Anesth*, 8(2), 147-166. <https://doi.org/10.1177/108925320400800208>

- Eggebrecht, A. T., Ferradal, S. L., Robichaux-Viehoever, A., Hassanpour, M. S., Dehghani, H., Snyder, A. Z., Hershey, T., & Culver, J. P. (2014). Mapping distributed brain function and networks with diffuse optical tomography. *Nat Photonics*, 8(6), 448-454. <https://doi.org/10.1038/nphoton.2014.107>
- Eggebrecht, A. T., White, B. R., Ferradal, S. L., Chen, C., Zhan, Y., Snyder, A. Z., Dehghani, H., & Culver, J. P. (2012). A quantitative spatial comparison of high-density diffuse optical tomography and fMRI cortical mapping. *Neuroimage*, 61(4), 1120-1128. <https://doi.org/10.1016/j.neuroimage.2012.01.124>
- Ehlis, A. C., Schneider, S., Dresler, T., & Fallgatter, A. J. (2014). Application of functional near-infrared spectroscopy in psychiatry. *Neuroimage*, 85 Pt 1, 478-488. <https://doi.org/10.1016/j.neuroimage.2013.03.067>
- Enblad, P., Valtysson, J., Andersson, J., Lilja, A., Valind, S., Antoni, G., Långström, B., Hillered, L., & Persson, L. (1996). Simultaneous intracerebral microdialysis and positron emission tomography in the detection of ischemia in patients with subarachnoid hemorrhage. *J Cereb Blood Flow Metab*, 16(4), 637-644. <https://doi.org/10.1097/00004647-199607000-00014>
- Engel, J., Jr. (1991). PET scanning in partial epilepsy. *Can J Neurol Sci*, 18(4 Suppl), 588-592. <https://doi.org/10.1017/s0317167100032765>
- Engl, E., & Attwell, D. (2015). Non-signalling energy use in the brain. *J Physiol*, 593(16), 3417-3429. <https://doi.org/10.1113/jphysiol.2014.282517>
- Ergün, E. L., Salanci, B. V., Erbaş, B., & Saygi, S. (2006). SPECT in periodic lateralized epileptiform discharges (PLEDs): a case report on PLEDs. *Ann Nucl Med*, 20(3), 227-231. <https://doi.org/10.1007/bf03027435>
- Eriksson, E. A., Barletta, J. F., Figueroa, B. E., Bonnell, B. W., Vanderkolk, W. E., McAllen, K. J., & Ott, M. M. (2012). Cerebral perfusion pressure and intracranial pressure are not surrogates for brain tissue oxygenation in traumatic brain injury. *Clin Neurophysiol*, 123(6), 1255-1260. <https://doi.org/10.1016/j.clinph.2011.08.035>
- Evans, B. M. (1976). Patterns of arousal in comatose patients. *J Neurol Neurosurg Psychiatry*, 39(4), 392-402. <https://doi.org/10.1136/jnnp.39.4.392>
- Fabene, P. F., Merigo, F., Galiè, M., Benati, D., Bernardi, P., Farace, P., Nicolato, E., Marzola, P., & Sbarbati, A. (2007). Pilocarpine-induced status epilepticus in rats involves ischemic

- and excitotoxic mechanisms. *PLoS One*, 2(10), e1105.
<https://doi.org/10.1371/journal.pone.0001105>
- Fang, Q., & Boas, D. A. (2009). Monte Carlo simulation of photon migration in 3D turbid media accelerated by graphics processing units. *Opt Express*, 17(22), 20178-20190.
<https://doi.org/10.1364/oe.17.020178>
- Fang, Q., Moore, R. H., Kopans, D. B., & Boas, D. A. (2010). Compositional-prior-guided image reconstruction algorithm for multi-modality imaging. *Biomedical Optics Express*, 1(1), 223-235. <https://doi.org/10.1364/BOE.1.000223>
- Fantini, S., Frederick, B., & Sassaroli, A. (2018). Perspective: Prospects of non-invasive sensing of the human brain with diffuse optical imaging. *APL Photonics*, 3(11).
<https://doi.org/10.1063/1.5038571>
- Farrell, J. S., Gaxiola-Valdez, I., Wolff, M. D., David, L. S., Dika, H. I., Geeraert, B. L., Rachel Wang, X., Singh, S., Spanswick, S. C., Dunn, J. F., Antle, M. C., Federico, P., & Teskey, G. C. (2016). Postictal behavioural impairments are due to a severe prolonged hypoperfusion/hypoxia event that is COX-2 dependent. *Elife*, 5.
<https://doi.org/10.7554/eLife.19352>
- Farrell, J. S., Greba, Q., Snutch, T. P., Howland, J. G., & Teskey, G. C. (2018). Fast oxygen dynamics as a potential biomarker for epilepsy. *Scientific Reports*, 8(1), 17935.
<https://doi.org/10.1038/s41598-018-36287-2>
- Fedorov, A., Beichel, R., Kalpathy-Cramer, J., Finet, J., Fillion-Robin, J. C., Pujol, S., Bauer, C., Jennings, D., Fennessy, F., Sonka, M., Buatti, J., Aylward, S., Miller, J. V., Pieper, S., & Kikinis, R. (2012). 3D Slicer as an image computing platform for the Quantitative Imaging Network. *Magn Reson Imaging*, 30(9), 1323-1341.
<https://doi.org/10.1016/j.mri.2012.05.001>
- Fellahi, J. L., Butin, G., Fischer, M. O., Zamparini, G., Gérard, J. L., & Hanouz, J. L. (2013). Dynamic evaluation of near-infrared peripheral oximetry in healthy volunteers: a comparison between INVOS and EQUANOX. *J Crit Care*, 28(5), 881.e881-886.
<https://doi.org/10.1016/j.jcrc.2013.05.004>
- Ferlini, L., Su, F., Creteur, J., Taccone, F. S., & Gaspard, N. (2021). Cerebral and systemic hemodynamic effect of recurring seizures. *Sci Rep*, 11(1), 22209.
<https://doi.org/10.1038/s41598-021-01704-6>

- Fernández-Torre, J. L., Hernández-Hernández, M. A., Mato-Mañas, D., Marco de Lucas, E., Gómez-Ruiz, E., & Martín-Láez, R. (2021). Intracortical focal non-convulsive status epilepticus causing cerebral hypoxia and intracranial hypertension. *Epileptic Disord*, 23(6), 911-916. <https://doi.org/10.1684/epd.2021.1348>
- Ferrari, M., De Marchis, C., Giannini, I., Di Nicola, A., Agostino, R., Nodari, S., & Bucci, G. (1986). Cerebral Blood Volume and Hemoglobin Oxygen Saturation Monitoring in Neonatal Brain by near IR Spectroscopy. In I. S. Longmuir (Ed.), *Oxygen Transport to Tissue VIII* (pp. 203-211). Springer US. https://doi.org/10.1007/978-1-4684-5188-7_27
- Ferrari, M., Giannini, I., Sideri, G., & Zanette, E. (1985). Continuous non invasive monitoring of human brain by near infrared spectroscopy. *Adv Exp Med Biol*, 191, 873-882. https://doi.org/10.1007/978-1-4684-3291-6_88
- Ferrari, M., Mottola, L., & Quaresima, V. (2004). Principles, techniques, and limitations of near infrared spectroscopy. *Can J Appl Physiol*, 29(4), 463-487. <https://doi.org/10.1139/h04-031>
- Ferrari, M., Muthalib, M., & Quaresima, V. (2011). The use of near-infrared spectroscopy in understanding skeletal muscle physiology: recent developments. *Philos Trans A Math Phys Eng Sci*, 369(1955), 4577-4590. <https://doi.org/10.1098/rsta.2011.0230>
- Ferrari, M., & Quaresima, V. (2012). A brief review on the history of human functional near-infrared spectroscopy (fNIRS) development and fields of application. *Neuroimage*, 63(2), 921-935. <https://doi.org/10.1016/j.neuroimage.2012.03.049>
- Ferreri, L., Bigand, E., Perrey, S., & Bugańska, A. (2014). The promise of Near-Infrared Spectroscopy (NIRS) for psychological research: A brief review. *L'Année psychologique*, 114(3), 537-569. <https://doi.org/10.3917/anpsy.143.0537>
- Ferron, J. F., Kroeger, D., Chever, O., & Amzica, F. (2009). Cortical inhibition during burst suppression induced with isoflurane anesthesia. *J Neurosci*, 29(31), 9850-9860. <https://doi.org/10.1523/jneurosci.5176-08.2009>
- Fischl, B. (2012). FreeSurfer. *Neuroimage*, 62(2), 774-781. <https://doi.org/10.1016/j.neuroimage.2012.01.021>
- Fishburn, F. A., Ludlum, R. S., Vaidya, C. J., & Medvedev, A. V. (2019). Temporal Derivative Distribution Repair (TDDR): A motion correction method for fNIRS. *Neuroimage*, 184, 171-179. <https://doi.org/10.1016/j.neuroimage.2018.09.025>

- Flexman, M. L., Kim, H. K., Stoll, R., Khalil, M. A., Fong, C. J., & Hielscher, A. H. (2012). A wireless handheld probe with spectrally constrained evolution strategies for diffuse optical imaging of tissue. *Rev Sci Instrum*, 83(3), 033108.
<https://doi.org/10.1063/1.3694494>
- Foiadelli, T., Lagae, L., Goffin, K., Theys, T., De Amici, M., Sacchi, L., Van Loon, J., Savasta, S., & Jansen, K. (2020). Subtraction Ictal SPECT coregistered to MRI (SISCOM) as a guide in localizing childhood epilepsy. *Epilepsia Open*, 5(1), 61-72.
<https://doi.org/10.1002/epi4.12373>
- Folbergrová, J., Jesina, P., Drahotka, Z., Lisý, V., Haugvicová, R., Vojtísková, A., & Houstěk, J. (2007). Mitochondrial complex I inhibition in cerebral cortex of immature rats following homocysteic acid-induced seizures. *Exp Neurol*, 204(2), 597-609.
<https://doi.org/10.1016/j.expneurol.2006.12.010>
- Foldvary, N., Lee, N., Hanson, M. W., Coleman, R. E., Hulette, C. M., Friedman, A. H., Bej, M. D., & Radtke, R. A. (1999). Correlation of hippocampal neuronal density and FDG-PET in mesial temporal lobe epilepsy. *Epilepsia*, 40(1), 26-29. <https://doi.org/10.1111/j.1528-1157.1999.tb01984.x>
- Fornai, F., Bassi, L., Gesi, M., Giorgi, F. S., Guerrini, R., Bonaccorsi, I., & Alessandri, M. G. (2000). Similar increases in extracellular lactic acid in the limbic system during epileptic and/or olfactory stimulation. *Neuroscience*, 97(3), 447-458.
[https://doi.org/10.1016/s0306-4522\(00\)00038-5](https://doi.org/10.1016/s0306-4522(00)00038-5)
- Fortune, J. B., Feustel, P. J., Weigle, C. G., & Popp, A. J. (1994). Continuous measurement of jugular venous oxygen saturation in response to transient elevations of blood pressure in head-injured patients. *J Neurosurg*, 80(3), 461-468.
<https://doi.org/10.3171/jns.1994.80.3.0461>
- Foster, K. A., Beaver, C. J., & Turner, D. A. (2005). Interaction between tissue oxygen tension and NADH imaging during synaptic stimulation and hypoxia in rat hippocampal slices. *Neuroscience*, 132(3), 645-657. <https://doi.org/10.1016/j.neuroscience.2005.01.040>
- Fox, P. T. (2012). The coupling controversy. *Neuroimage*, 62(2), 594-601.
<https://doi.org/10.1016/j.neuroimage.2012.01.103>

- Fox, P. T., & Raichle, M. E. (1986). Focal physiological uncoupling of cerebral blood flow and oxidative metabolism during somatosensory stimulation in human subjects. *Proc Natl Acad Sci U S A*, 83(4), 1140-1144. <https://doi.org/10.1073/pnas.83.4.1140>
- Franceschini, M. A., Joseph, D. K., Huppert, T. J., Diamond, S. G., & Boas, D. A. (2006). Diffuse optical imaging of the whole head. *J Biomed Opt*, 11(5), 054007. <https://doi.org/10.1117/1.2363365>
- Franceschini, M. A., Radhakrishnan, H., Thakur, K., Wu, W., Ruvinskaya, S., Carp, S., & Boas, D. A. (2010). The effect of different anesthetics on neurovascular coupling. *Neuroimage*, 51(4), 1367-1377. <https://doi.org/10.1016/j.neuroimage.2010.03.060>
- Franck, G., Sadzot, B., Salmon, E., Maquet, P., Peter, J. M., Quaglia, L., Delfiore, G., & Lamotte, D. (1986). [Study of cerebral metabolism and blood flow in partial complex epilepsy and status epilepticus in man using positron emission tomography]. *Rev Electroencephalogr Neurophysiol Clin*, 16(3), 199-216. [https://doi.org/10.1016/s0370-4475\(86\)80048-x](https://doi.org/10.1016/s0370-4475(86)80048-x) (Etude chez l'homme, par tomographie à émission de positons, du métabolisme et du débit sanguin cérébral dans les épilepsies partielles complexes et dans différents états de mal.)
- Freeman, R. D., & Li, B. (2016). Neural-metabolic coupling in the central visual pathway. *Philos Trans R Soc Lond B Biol Sci*, 371(1705). <https://doi.org/10.1098/rstb.2015.0357>
- Friedman, D., Claassen, J., & Hirsch, L. J. (2009). Continuous electroencephalogram monitoring in the intensive care unit. *Anesth Analg*, 109(2), 506-523. <https://doi.org/10.1213/ane.0b013e3181a9d8b5>
- Friston, K. J., Fletcher, P., Josephs, O., Holmes, A., Rugg, M. D., & Turner, R. (1998). Event-related fMRI: characterizing differential responses. *Neuroimage*, 7(1), 30-40. <https://doi.org/10.1006/nimg.1997.0306>
- Funane, T., Atsumori, H., Katura, T., Obata, A. N., Sato, H., Tanikawa, Y., Okada, E., & Kiguchi, M. (2014). Quantitative evaluation of deep and shallow tissue layers' contribution to fNIRS signal using multi-distance optodes and independent component analysis. *Neuroimage*, 85 Pt 1, 150-165. <https://doi.org/10.1016/j.neuroimage.2013.02.026>
- Funane, T., Homae, F., Watanabe, H., Kiguchi, M., & Taga, G. (2014). Greater contribution of cerebral than extracerebral hemodynamics to near-infrared spectroscopy signals for

- functional activation and resting-state connectivity in infants. *Neurophotonic*, 1(2), 025003. <https://doi.org/10.1117/1.NPh.1.2.025003>
- Fung, F. W., Fan, J., Vala, L., Jacobwitz, M., Parikh, D. S., Donnelly, M., Topjian, A. A., Xiao, R., & Abend, N. S. (2020). EEG monitoring duration to identify electroencephalographic seizures in critically ill children. *Neurology*, 95(11), e1599-e1608. <https://doi.org/10.1212/wnl.00000000000010421>
- Fushimi, M., Matsubuchi, N., Sekine, A., & Shimizu, T. (2003). Benign bilateral independent periodic lateralized epileptiform discharges. *Acta Neurol Scand*, 108(1), 55-59. <https://doi.org/10.1034/j.1600-0404.2003.00084.x>
- Gagnon, L., Cooper, R. J., Yücel, M. A., Perdue, K. L., Greve, D. N., & Boas, D. A. (2012). Short separation channel location impacts the performance of short channel regression in NIRS. *Neuroimage*, 59(3), 2518-2528. <https://doi.org/10.1016/j.neuroimage.2011.08.095>
- Gagnon, L., Yücel, M. A., Boas, D. A., & Cooper, R. J. (2014). Further improvement in reducing superficial contamination in NIRS using double short separation measurements. *Neuroimage*, 85 Pt 1(0 1), 127-135. <https://doi.org/10.1016/j.neuroimage.2013.01.073>
- Gagnon, L., Yücel, M. A., Dehaes, M., Cooper, R. J., Perdue, K. L., Selb, J., Huppert, T. J., Hoge, R. D., & Boas, D. A. (2012). Quantification of the cortical contribution to the NIRS signal over the motor cortex using concurrent NIRS-fMRI measurements. *Neuroimage*, 59(4), 3933-3940. <https://doi.org/10.1016/j.neuroimage.2011.10.054>
- Gaillard, W. D., Bookheimer, S. Y., & Cohen, M. (2000). The use of fMRI in neocortical epilepsy. *Adv Neurol*, 84, 391-404. <https://www.ncbi.nlm.nih.gov/pubmed/11091882>
- Gallagher, A., Bastien, D., Pelletier, I., Vannasing, P., Legatt, A. D., Moshé, S. L., Jehle, R., Carmant, L., Lepore, F., Béland, R., & Lassonde, M. (2008). A noninvasive, presurgical expressive and receptive language investigation in a 9-year-old epileptic boy using near-infrared spectroscopy. *Epilepsy Behav*, 12(2), 340-346. <https://doi.org/10.1016/j.yebeh.2007.10.008>
- Gallagher, A., Béland, R., & Lassonde, M. (2012). The contribution of functional near-infrared spectroscopy (fNIRS) to the presurgical assessment of language function in children. *Brain Lang*, 121(2), 124-129. <https://doi.org/10.1016/j.bandl.2011.03.006>
- Gallagher, A., Lassonde, M., Bastien, D., Vannasing, P., Lesage, F., Grova, C., Bouthillier, A., Carmant, L., Lepore, F., Béland, R., & Nguyen, D. K. (2008). Non-invasive pre-surgical

- investigation of a 10 year-old epileptic boy using simultaneous EEG-NIRS. *Seizure*, 17(6), 576-582. <https://doi.org/10.1016/j.seizure.2008.01.009>
- Gallagher, A., Thériault, M., Maclin, E., Low, K., Gratton, G., Fabiani, M., Gagnon, L., Valois, K., Rouleau, I., Sauerwein, H. C., Carmant, L., Nguyen, D. K., Lortie, A., Lepore, F., Béland, R., & Lassonde, M. (2007). Near-infrared spectroscopy as an alternative to the Wada test for language mapping in children, adults and special populations. *Epileptic Disord*, 9(3), 241-255. <https://doi.org/10.1684/epd.2007.0118>
- Gavvala, J., Abend, N., LaRoche, S., Hahn, C., Herman, S. T., Claassen, J., Macken, M., Schuele, S., & Gerard, E. (2014). Continuous EEG monitoring: a survey of neurophysiologists and neurointensivists. *Epilepsia*, 55(11), 1864-1871. <https://doi.org/10.1111/epi.12809>
- Giacometti, P., & Diamond, S. G. (2013). Compliant head probe for positioning electroencephalography electrodes and near-infrared spectroscopy optodes. *J Biomed Opt*, 18(2), 27005. <https://doi.org/10.1117/1.Jbo.18.2.027005>
- Gibbs, F. A. (1933). A Thermoelectric Blood Flow Recorder in the Form of a Needle. *Proceedings of the Society for Experimental Biology and Medicine*, 31(1), 141-146. <https://doi.org/10.3181/00379727-31-7031c>
- Gibson, A., & Dehghani, H. (2009). Diffuse optical imaging. *Philos Trans A Math Phys Eng Sci*, 367(1900), 3055-3072. <https://doi.org/10.1098/rsta.2009.0080>
- Gibson, A. P., Hebden, J. C., & Arridge, S. R. (2005). Recent advances in diffuse optical imaging. *Phys Med Biol*, 50(4), R1-43. <https://doi.org/10.1088/0031-9155/50/4/r01>
- Gibson, Q. H. (1999). Kinetics of Oxygen Binding to Hemoglobin A. *Biochemistry*, 38(16), 5191-5199. <https://doi.org/10.1021/bi982970t>
- Gilmour, H., Ramage-Morin, P., & Wong, S. L. (2016). Epilepsy in Canada: Prevalence and impact. *Health Rep*, 27(9), 24-30. <https://www.ncbi.nlm.nih.gov/pubmed/27655169>
- Giorni, C., Di Chiara, L., Cilio, M. R., Ricci, Z., Morelli, S., Garisto, C., & Picardo, S. (2009). The usefulness of near-infrared spectroscopy for detecting and monitoring status epilepticus after pediatric cardiac surgery. *J Cardiothorac Vasc Anesth*, 23(5), 668-671. <https://doi.org/10.1053/j.jvca.2008.12.004>
- Girouard, H., Bonev, A. D., Hannah, R. M., Meredith, A., Aldrich, R. W., & Nelson, M. T. (2010). Astrocytic endfoot Ca²⁺ and BK channels determine both arteriolar dilation and

- constriction. *Proc Natl Acad Sci U S A*, 107(8), 3811-3816.
<https://doi.org/10.1073/pnas.0914722107>
- Girouard, H., & Iadecola, C. (2006). Neurovascular coupling in the normal brain and in hypertension, stroke, and Alzheimer disease. *J Appl Physiol* (1985), 100(1), 328-335.
<https://doi.org/10.1152/japplphysiol.00966.2005>
- Glover, G. H. (1999). Deconvolution of impulse response in event-related BOLD fMRI. *Neuroimage*, 9(4), 416-429. <https://doi.org/10.1006/nimg.1998.0419>
- Goda, K. (2019). Biophotonics and beyond. *APL Photonics*, 4(5), 050401.
<https://doi.org/10.1063/1.5100614>
- Goffin, K., Dedeurwaerdere, S., Van Laere, K., & Van Paesschen, W. (2008). Neuronuclear assessment of patients with epilepsy. *Semin Nucl Med*, 38(4), 227-239.
<https://doi.org/10.1053/j.semnuclmed.2008.02.004>
- Gollwitzer, S., Groemer, T., Rampp, S., Hagge, M., Olmes, D., Huttner, H. B., Schwab, S., Madžar, D., Hopfengaertner, R., & Hamer, H. M. (2015). Early prediction of delayed cerebral ischemia in subarachnoid hemorrhage based on quantitative EEG: A prospective study in adults. *Clin Neurophysiol*, 126(8), 1514-1523.
<https://doi.org/10.1016/j.clinph.2014.10.215>
- Gomersall, C. D., Leung, P. L., Gin, T., Joynt, G. M., Young, R. J., Poon, W. S., & Oh, T. E. (1998). A comparison of the Hamamatsu NIRO 500 and the INVOS 3100 near-infrared spectrophotometers. *Anaesth Intensive Care*, 26(5), 548-557.
<https://doi.org/10.1177/0310057x9802600512>
- Gómez-Gonzalo, M., Losi, G., Brondi, M., Uva, L., Sato, S. S., de Curtis, M., Ratto, G. M., & Carmignoto, G. (2011). Ictal but not interictal epileptic discharges activate astrocyte endfeet and elicit cerebral arteriole responses. *Front Cell Neurosci*, 5, 8.
<https://doi.org/10.3389/fncel.2011.00008>
- Gorelov, V. (2004). Theoretical value of Hüfner's constant. *Anaesthesia*, 59(1), 97-97.
<https://doi.org/https://doi.org/10.1111/j.1365-2044.2004.03598.x>
- Gorter, J. A., van Vliet, E. A., & Aronica, E. (2015). Status epilepticus, blood-brain barrier disruption, inflammation, and epileptogenesis. *Epilepsy Behav*, 49, 13-16.
<https://doi.org/10.1016/j.yebeh.2015.04.047>

- Gotman, J. (2008). Epileptic networks studied with EEG-fMRI. *Epilepsia*, 49 Suppl 3(Suppl 3), 42-51. <https://doi.org/10.1111/j.1528-1167.2008.01509.x>
- Gotman, J., Kobayashi, E., Bagshaw, A. P., Bénar, C. G., & Dubeau, F. (2006). Combining EEG and fMRI: a multimodal tool for epilepsy research. *J Magn Reson Imaging*, 23(6), 906-920. <https://doi.org/10.1002/jmri.20577>
- Green, D. W., & Kunst, G. (2017). Cerebral oximetry and its role in adult cardiac, non-cardiac surgery and resuscitation from cardiac arrest. *Anaesthesia*, 72(S1), 48-57. <https://doi.org/https://doi.org/10.1111/anae.13740>
- Groch, M. W., & Erwin, W. D. (2000). SPECT in the year 2000: basic principles. *J Nucl Med Technol*, 28(4), 233-244. <https://www.ncbi.nlm.nih.gov/pubmed/11142324>
- Grouiller, F., Vercueil, L., Krainik, A., Segebarth, C., Kahane, P., & David, O. (2010). Characterization of the hemodynamic modes associated with interictal epileptic activity using a deformable model-based analysis of combined EEG and functional MRI recordings. *Hum Brain Mapp*, 31(8), 1157-1173. <https://doi.org/10.1002/hbm.20925>
- Grova, C., Daunizeau, J., Lina, J. M., Bénar, C. G., Benali, H., & Gotman, J. (2006). Evaluation of EEG localization methods using realistic simulations of interictal spikes. *Neuroimage*, 29(3), 734-753. <https://doi.org/10.1016/j.neuroimage.2005.08.053>
- Grubhofer, G., Tonninger, W., Keznickl, P., Skyllouriotis, P., Ehrlich, M., Hiesmayr, M., & Lassnigg, A. (1999). A comparison of the monitors INVOS 3100 and NIRO 500 in detecting changes in cerebral oxygenation. *Acta Anaesthesiol Scand*, 43(4), 470-475. <https://doi.org/10.1034/j.1399-6576.1999.430417.x>
- Gu, Y., Han, J., Liang, Z., Yan, J., Li, Z., & Li, X. (2016). Empirical mode decomposition-based motion artifact correction method for functional near-infrared spectroscopy. *J Biomed Opt*, 21(1), 15002. <https://doi.org/10.1117/1.Jbo.21.1.015002>
- Guenette, J. A., Henderson, W. R., Dominelli, P. B., Querido, J. S., Brasher, P. M., Griesdale, D. E., Boushel, R., & Sheel, A. W. (2011). Blood flow index using near-infrared spectroscopy and indocyanine green as a minimally invasive tool to assess respiratory muscle blood flow in humans. *Am J Physiol Regul Integr Comp Physiol*, 300(4), R984-992. <https://doi.org/10.1152/ajpregu.00739.2010>

- Gunadi, S., Leung, T. S., Elwell, C. E., & Tachtsidis, I. (2014). Spatial sensitivity and penetration depth of three cerebral oxygenation monitors. *Biomed Opt Express*, 5(9), 2896-2912. <https://doi.org/10.1364/boe.5.002896>
- Gupta, A. K., Hutchinson, P. J., Al-Rawi, P., Gupta, S., Swart, M., Kirkpatrick, P. J., Menon, D. K., & Datta, A. K. (1999). Measuring brain tissue oxygenation compared with jugular venous oxygen saturation for monitoring cerebral oxygenation after traumatic brain injury. *Anesth Analg*, 88(3), 549-553. <https://doi.org/10.1097/00000539-199903000-00016>
- Haginoya, K., Munakata, M., Kato, R., Yokoyama, H., Ishizuka, M., & Iinuma, K. (2002). Ictal cerebral haemodynamics of childhood epilepsy measured with near-infrared spectrophotometry. *Brain*, 125(Pt 9), 1960-1971. <https://doi.org/10.1093/brain/awf213>
- Haginoya, K., Munakata, M., Kato, R., Yokoyama, H., Ishizuka, M., & Iinuma, K. (2002). Ictal cerebral haemodynamics of childhood epilepsy measured with near-infrared spectrophotometry. *Brain*, 125(9), 1960-1971. <https://doi.org/10.1093/brain/awf213>
- Haider, H. A., Esteller, R., Hahn, C. D., Westover, M. B., Halford, J. J., Lee, J. W., Shafi, M. M., Gaspard, N., Herman, S. T., Gerard, E. E., Hirsch, L. J., Ehrenberg, J. A., & LaRoche, S. M. (2016). Sensitivity of quantitative EEG for seizure identification in the intensive care unit. *Neurology*, 87(9), 935-944. <https://doi.org/10.1212/wnl.0000000000003034>
- Hall, C. N., Reynell, C., Gesslein, B., Hamilton, N. B., Mishra, A., Sutherland, B. A., O'Farrell, F. M., Buchan, A. M., Lauritzen, M., & Attwell, D. (2014). Capillary pericytes regulate cerebral blood flow in health and disease. *Nature*, 508(7494), 55-60. <https://doi.org/10.1038/nature13165>
- Hall, L. T., Beart, G. C. G., Thomas, E. A., Simpson, D. A., McGuinness, L. P., Cole, J. H., Manton, J. H., Scholten, R. E., Jelezko, F., Wrachtrup, J., Petrou, S., & Hollenberg, L. C. L. (2012). High spatial and temporal resolution wide-field imaging of neuron activity using quantum NV-diamond. *Scientific Reports*, 2(1), 401. <https://doi.org/10.1038/srep00401>
- Hämäläinen, M. S., & Ilmoniemi, R. J. (1994). Interpreting magnetic fields of the brain: minimum norm estimates. *Medical & Biological Engineering & Computing*, 32(1), 35-42. <https://doi.org/10.1007/BF02512476>

- Handforth, A., Cheng, J. T., Mandelkern, M. A., & Treiman, D. M. (1994). Markedly increased mesiotemporal lobe metabolism in a case with PLEDs: further evidence that PLEDs are a manifestation of partial status epilepticus. *Epilepsia*, 35(4), 876-881.
<https://doi.org/10.1111/j.1528-1157.1994.tb02526.x>
- Handwerker, D. A., Gonzalez-Castillo, J., D'Esposito, M., & Bandettini, P. A. (2012). The continuing challenge of understanding and modeling hemodynamic variation in fMRI. *Neuroimage*, 62(2), 1017-1023. <https://doi.org/10.1016/j.neuroimage.2012.02.015>
- Hansen, M. L., Hyttel-Sørensen, S., Jakobsen, J. C., Gluud, C., Kooi, E. M. W., Mintzer, J., de Boode, W. P., Fumagalli, M., Alarcon, A., Alderliesten, T., Greisen, G., Austin, T., Bruckner, M., de Boode, W. P., Dempsey, E., Ergenekon, E., Gucuyener, K., Levy, P. T., Liem, K. D., . . . on behalf of the European Society for Paediatric Research Special Interest Group 'NearInfraRed, S. (2022). Cerebral near-infrared spectroscopy monitoring (NIRS) in children and adults: a systematic review with meta-analysis. *Pediatric Research*. <https://doi.org/10.1038/s41390-022-01995-z>
- Harris, S., Boorman, L., Bruyns-Haylett, M., Kennerley, A., Ma, H., Zhao, M., Overton, P. G., Schwartz, T. H., & Berwick, J. (2014). Contralateral dissociation between neural activity and cerebral blood volume during recurrent acute focal neocortical seizures. *Epilepsia*, 55(9), 1423-1430. <https://doi.org/10.1111/epi.12726>
- Harris, S., Ma, H., Zhao, M., Boorman, L., Zheng, Y., Kennerley, A., Bruyns-Haylett, M., Overton, P. G., Berwick, J., & Schwartz, T. H. (2014). Coupling between gamma-band power and cerebral blood volume during recurrent acute neocortical seizures. *Neuroimage*, 97, 62-70. <https://doi.org/10.1016/j.neuroimage.2014.04.014>
- Harris, S. S., Boorman, L. W., Kennerley, A. J., Sharp, P. S., Martin, C., Redgrave, P., Schwartz, T. H., & Berwick, J. (2018). Seizure epicenter depth and translaminar field potential synchrony underlie complex variations in tissue oxygenation during ictal initiation. *Neuroimage*, 171, 165-175. <https://doi.org/10.1016/j.neuroimage.2017.12.088>
- Harsimrat, S., Robert, J. C., Chuen, Laura, D., Andrea, E., Sabrina, B., Dimitrios, A., Nick, E., Andrew, M., David, H., Jeremy, C. H., & Topun, A. (2014). Mapping cortical haemodynamics during neonatal seizures using diffuse optical tomography: A case study. *NeuroImage: Clinical*, 5, 256-265.
<https://doi.org/https://doi.org/10.1016/j.nicl.2014.06.012>

- Hartings, J. A., Watanabe, T., Bullock, M. R., Okonkwo, D. O., Fabricius, M., Woitzik, J., Dreier, J. P., Puccio, A., Shutter, L. A., Pahl, C., & Strong, A. J. (2011). Spreading depolarizations have prolonged direct current shifts and are associated with poor outcome in brain trauma. *Brain*, 134(Pt 5), 1529-1540. <https://doi.org/10.1093/brain/awr048>
- Hauf, M., Slotboom, J., Nirkko, A., von Bredow, F., Ozdoba, C., & Wiest, R. (2009). Cortical regional hyperperfusion in nonconvulsive status epilepticus measured by dynamic brain perfusion CT. *AJNR Am J Neuroradiol*, 30(4), 693-698. <https://doi.org/10.3174/ajnr.A1456>
- Hautala, A. J., Kiviniemi, A. M., & Tulppo, M. P. (2009). Individual responses to aerobic exercise: the role of the autonomic nervous system. *Neurosci Biobehav Rev*, 33(2), 107-115. <https://doi.org/10.1016/j.neubiorev.2008.04.009>
- Hayward, N. M., Ndode-Ekane, X. E., Kutchiashvili, N., Gröhn, O., & Pitkänen, A. (2010). Elevated cerebral blood flow and vascular density in the amygdala after status epilepticus in rats. *Neurosci Lett*, 484(1), 39-42. <https://doi.org/10.1016/j.neulet.2010.08.013>
- Heinemann, U., Kaufer, D., & Friedman, A. (2012). Blood-brain barrier dysfunction, TGFβ signaling, and astrocyte dysfunction in epilepsy. *Glia*, 60(8), 1251-1257. <https://doi.org/10.1002/glia.22311>
- Henson, R. N. A., & Friston, K. J. (2007). Convolution Models for fMRI.
- Herlopian, A., Struck, A. F., Rosenthal, E., & Westover, B. M. (2018). Neuroimaging Correlates of Periodic Discharges. *J Clin Neurophysiol*, 35(4), 279-294. <https://doi.org/10.1097/wnp.0000000000000466>
- Herman, S. T., Abend, N. S., Bleck, T. P., Chapman, K. E., Drislane, F. W., Emerson, R. G., Gerard, E. E., Hahn, C. D., Husain, A. M., Kaplan, P. W., LaRoche, S. M., Nuwer, M. R., Quigg, M., Riviello, J. J., Schmitt, S. E., Simmons, L. A., Tsuchida, T. N., & Hirsch, L. J. (2015). Consensus statement on continuous EEG in critically ill adults and children, part I: indications. *J Clin Neurophysiol*, 32(2), 87-95. <https://doi.org/10.1097/wnp.0000000000000166>
- Herrschaft, H., Hossmann, K. A., Mies, G., & Zülich, K. J. (1977). Relationship between cerebral blood flow and EEG frequency content in patients with acute brain ischemia. *Acta Neurol Scand Suppl*, 64, 414-415. <https://www.ncbi.nlm.nih.gov/pubmed/268855>

- Hessel, T. W., Hyttel-Sorensen, S., & Greisen, G. (2014). Cerebral oxygenation after birth - a comparison of INVOS(®) and FORE-SIGHT™ near-infrared spectroscopy oximeters. *Acta Paediatr*, 103(5), 488-493. <https://doi.org/10.1111/apa.12567>
- Hielscher, A. H., Bluestone, A. Y., Abdoulaev, G. S., Klose, A. D., Lasker, J., Stewart, M., Netz, U., & Beuthan, J. (2002). Near-infrared diffuse optical tomography. *Dis Markers*, 18(5-6), 313-337. <https://doi.org/10.1155/2002/164252>
- Hill, C. E., Blank, L. J., Thibault, D., Davis, K. A., Dahodwala, N., Litt, B., & Willis, A. W. (2019). Continuous EEG is associated with favorable hospitalization outcomes for critically ill patients. *Neurology*, 92(1), e9-e18. <https://doi.org/10.1212/wnl.00000000000006689>
- Hirsch, L. J., Fong, M. W. K., Leitinger, M., LaRoche, S. M., Beniczky, S., Abend, N. S., Lee, J. W., Wusthoff, C. J., Hahn, C. D., Westover, M. B., Gerard, E. E., Herman, S. T., Haider, H. A., Osman, G., Rodriguez-Ruiz, A., Maciel, C. B., Gilmore, E. J., Fernandez, A., Rosenthal, E. S., . . . Gaspard, N. (2021). American Clinical Neurophysiology Society's Standardized Critical Care EEG Terminology: 2021 Version. *Journal of Clinical Neurophysiology*, 38(1), 1-29. <https://doi.org/10.1097/wnp.0000000000000806>
- Hirsch, L. J., LaRoche, S. M., Gaspard, N., Gerard, E., Svoronos, A., Herman, S. T., Mani, R., Arif, H., Jette, N., Minazad, Y., Kerrigan, J. F., Vespa, P., Hantus, S., Claassen, J., Young, G. B., So, E., Kaplan, P. W., Nuwer, M. R., Fountain, N. B., & Drislane, F. W. (2013). American Clinical Neurophysiology Society's Standardized Critical Care EEG Terminology: 2012 version. *J Clin Neurophysiol*, 30(1), 1-27. <https://doi.org/10.1097/WNP.0b013e3182784729>
- Hisada, K., Morioka, T., Nishio, S., Muraishi, M., Yamamoto, T., Yoshida, T., & Fukui, M. (2000). Magnetoencephalographic analysis of periodic lateralized epileptiform discharges (PLEDs). *Clin Neurophysiol*, 111(1), 122-127. [https://doi.org/10.1016/s1388-2457\(99\)00184-4](https://doi.org/10.1016/s1388-2457(99)00184-4)
- Hodgkin, A. L., & Huxley, A. F. (1952). A quantitative description of membrane current and its application to conduction and excitation in nerve. *J Physiol*, 117(4), 500-544. <https://doi.org/10.1113/jphysiol.1952.sp004764>
- Hoffman, G. M., Ghanayem, N. S., Scott, J. P., Tweddell, J. S., Mitchell, M. E., & Mussatto, K. A. (2017). Postoperative Cerebral and Somatic Near-Infrared Spectroscopy Saturations

- and Outcome in Hypoplastic Left Heart Syndrome. *Ann Thorac Surg*, 103(5), 1527-1535.
<https://doi.org/10.1016/j.athoracsur.2016.09.100>
- Hoge, R. D., Atkinson, J., Gill, B., Crelier, G. R., Marrett, S., & Pike, G. B. (1999). Investigation of BOLD signal dependence on cerebral blood flow and oxygen consumption: the deoxyhemoglobin dilution model. *Magn Reson Med*, 42(5), 849-863.
[https://doi.org/10.1002/\(sici\)1522-2594\(199911\)42:5<849::aid-mrm4>3.0.co;2-z](https://doi.org/10.1002/(sici)1522-2594(199911)42:5<849::aid-mrm4>3.0.co;2-z)
- Hoge, R. D., Atkinson, J., Gill, B., Crelier, G. R., Marrett, S., & Pike, G. B. (1999). Linear coupling between cerebral blood flow and oxygen consumption in activated human cortex. *Proc Natl Acad Sci U S A*, 96(16), 9403-9408.
<https://doi.org/10.1073/pnas.96.16.9403>
- Hoge, R. D., Franceschini, M. A., Covolan, R. J., Huppert, T., Mandeville, J. B., & Boas, D. A. (2005). Simultaneous recording of task-induced changes in blood oxygenation, volume, and flow using diffuse optical imaging and arterial spin-labeling MRI. *Neuroimage*, 25(3), 701-707. <https://doi.org/10.1016/j.neuroimage.2004.12.032>
- Holmes, C. J., Hoge, R., Collins, L., Woods, R., Toga, A. W., & Evans, A. C. (1998). Enhancement of MR images using registration for signal averaging. *J Comput Assist Tomogr*, 22(2), 324-333. <https://doi.org/10.1097/00004728-199803000-00032>
- Hosford, P. S., & Gourine, A. V. (2019). What is the key mediator of the neurovascular coupling response? *Neurosci Biobehav Rev*, 96, 174-181.
<https://doi.org/10.1016/j.neubiorev.2018.11.011>
- Hoshi, Y. (2016). Hemodynamic signals in fNIRS. *Prog Brain Res*, 225, 153-179.
<https://doi.org/10.1016/bs.pbr.2016.03.004>
- Hoshi, Y., & Tamura, M. (1993). Dynamic multichannel near-infrared optical imaging of human brain activity. *J Appl Physiol* (1985), 75(4), 1842-1846.
<https://doi.org/10.1152/jappl.1993.75.4.1842>
- Hu, X. S., Hong, K. S., & Ge, S. S. (2011). Recognition of stimulus-evoked neuronal optical response by identifying chaos levels of near-infrared spectroscopy time series. *Neurosci Lett*, 504(2), 115-120. <https://doi.org/10.1016/j.neulet.2011.09.011>
- Hunter, G., & Young, G. B. (2012). Status epilepticus: a review, with emphasis on refractory cases. *Can J Neurol Sci*, 39(2), 157-169. <https://doi.org/10.1017/s0317167100013160>

- Huppert, T., Barker, J., Schmidt, B., Walls, S., & Ghuman, A. (2017). Comparison of group-level, source localized activity for simultaneous functional near-infrared spectroscopy-magnetoencephalography and simultaneous fNIRS-fMRI during parametric median nerve stimulation. *Neurophotonics*, 4(1), 015001. <https://doi.org/10.1117/1.NPh.4.1.015001>
- Huppert, T. J. (2016). Commentary on the statistical properties of noise and its implication on general linear models in functional near-infrared spectroscopy. *Neurophotonics*, 3(1), 010401. <https://doi.org/10.1117/1.NPh.3.1.010401>
- Huppert, T. J., Diamond, S. G., Franceschini, M. A., & Boas, D. A. (2009). HomER: a review of time-series analysis methods for near-infrared spectroscopy of the brain. *Appl Opt*, 48(10), D280-298. <https://doi.org/10.1364/ao.48.00d280>
- Huppert, T. J., Hoge, R. D., Diamond, S. G., Franceschini, M. A., & Boas, D. A. (2006). A temporal comparison of BOLD, ASL, and NIRS hemodynamic responses to motor stimuli in adult humans. *Neuroimage*, 29(2), 368-382. <https://doi.org/10.1016/j.neuroimage.2005.08.065>
- Hurth, H., Schlak, D., & Ebner, F. H. (2020). Microdialysis Findings in a Patient with New Onset Refractory Non-convulsive Status Epilepticus. *Neurocrit Care*, 32(3), 889-893. <https://doi.org/10.1007/s12028-019-00848-8>
- Hutchinson, P. J., O'Connell, M. T., Al-Rawi, P. G., Maskell, L. B., Kett-White, R., Gupta, A. K., Richards, H. K., Hutchinson, D. B., Kirkpatrick, P. J., & Pickard, J. D. (2000). Clinical cerebral microdialysis: a methodological study. *J Neurosurg*, 93(1), 37-43. <https://doi.org/10.3171/jns.2000.93.1.0037>
- Hwang, W. S., Gwak, H. M., & Seo, D. W. (2013). Propofol infusion syndrome in refractory status epilepticus. *J Epilepsy Res*, 3(1), 21-27. <https://doi.org/10.14581/jer.13004>
- Hyttel-Sorensen, S., Pellicer, A., Alderliesten, T., Austin, T., van Bel, F., Benders, M., Claris, O., Dempsey, E., Franz, A. R., Fumagalli, M., Glud, C., Grevstad, B., Hagmann, C., Lemmers, P., van Oeveren, W., Pichler, G., Plomgaard, A. M., Riera, J., Sanchez, L., . . . Greisen, G. (2015). Cerebral near infrared spectroscopy oximetry in extremely preterm infants: phase II randomised clinical trial. *Bmj*, 350, g7635. <https://doi.org/10.1136/bmj.g7635>
- Hyttel-Sorensen, S., Sorensen, L. C., Riera, J., & Greisen, G. (2011). Tissue oximetry: a comparison of mean values of regional tissue saturation, reproducibility and dynamic

- range of four NIRS-instruments on the human forearm. *Biomed Opt Express*, 2(11), 3047-3057. <https://doi.org/10.1364/boe.2.003047>
- Iadecola, C. (2017). The Neurovascular Unit Coming of Age: A Journey through Neurovascular Coupling in Health and Disease. *Neuron*, 96(1), 17-42. <https://doi.org/10.1016/j.neuron.2017.07.030>
- Idelson, C. R., Vogt, W. C., King-Casas, B., LaConte, S. M., & Rylander, C. G. (2015). Effect of mechanical optical clearing on near-infrared spectroscopy. *Lasers Surg Med*, 47(6), 495-502. <https://doi.org/10.1002/lsm.22373>
- Ingvar, M. (1986). Cerebral blood flow and metabolic rate during seizures. Relationship to epileptic brain damage. *Ann N Y Acad Sci*, 462, 194-206. <https://doi.org/10.1111/j.1749-6632.1986.tb51254.x>
- Ingvar, M., & Siesjö, B. K. (1983). Local blood flow and glucose consumption in the rat brain during sustained bicuculline-induced seizures. *Acta Neurologica Scandinavica*, 68(3), 129-144. <https://doi.org/https://doi.org/10.1111/j.1600-0404.1983.tb05339.x>
- Ivanov, A. I., Bernard, C., & Turner, D. A. (2015). Metabolic responses differentiate between interictal, ictal and persistent epileptiform activity in intact, immature hippocampus in vitro. *Neurobiol Dis*, 75, 1-14. <https://doi.org/10.1016/j.nbd.2014.12.013>
- Izzetoglu, M., Chitrapu, P., Bunce, S., & Onaral, B. (2010). Motion artifact cancellation in NIR spectroscopy using discrete Kalman filtering. *Biomed Eng Online*, 9, 16. <https://doi.org/10.1186/1475-925x-9-16>
- Izzetoglu, M., Devaraj, A., Bunce, S., & Onaral, B. (2005). Motion artifact cancellation in NIR spectroscopy using Wiener filtering. *IEEE Trans Biomed Eng*, 52(5), 934-938. <https://doi.org/10.1109/tbme.2005.845243>
- Jacobs, J., Menzel, A., Ramantani, G., Körbl, K., Assländer, J., Schulze-Bonhage, A., Hennig, J., & LeVan, P. (2014). Negative BOLD in default-mode structures measured with EEG-MREG is larger in temporal than extra-temporal epileptic spikes [Original Research]. *Frontiers in Neuroscience*, 8. <https://doi.org/10.3389/fnins.2014.00335>
- Jaeger, M., Schuhmann, M. U., Soehle, M., Nagel, C., & Meixensberger, J. (2007). Continuous monitoring of cerebrovascular autoregulation after subarachnoid hemorrhage by brain tissue oxygen pressure reactivity and its relation to delayed cerebral infarction. *Stroke*, 38(3), 981-986. <https://doi.org/10.1161/01.Str.0000257964.65743.99>

- Jahani, S., Setarehdan, S. K., Boas, D. A., & Yücel, M. A. (2018). Motion artifact detection and correction in functional near-infrared spectroscopy: a new hybrid method based on spline interpolation method and Savitzky-Golay filtering. *Neurophotonics*, 5(1), 015003. <https://doi.org/10.1117/1.NPh.5.1.015003>
- Janani, A., & Sasikala, M. (2017). Investigation of different approaches for noise reduction in functional near-infrared spectroscopy signals for brain-computer interface applications. *Neural Computing and Applications*, 28(10), 2889-2903. <https://doi.org/10.1007/s00521-017-2961-4>
- Jarry, S., Couture, E. J., Falih, J., Lebon, J. S., Ayoub, C., Rochon, A., Rousseau-Saine, N., & Denault, A. (2023). New Development in Brain Monitoring for Cardiac Surgery. *Can J Cardiol*, 39(2), 229-232. <https://doi.org/10.1016/j.cjca.2022.11.006>
- Jasper, H. H. (1958). Report of the committee on methods of clinical examination in electroencephalography: 1957. *Electroencephalography and Clinical Neurophysiology*, 10(2), 370-375. [https://doi.org/https://doi.org/10.1016/0013-4694\(58\)90053-1](https://doi.org/https://doi.org/10.1016/0013-4694(58)90053-1)
- Jefferys, J. G. R., Ashby-Lumsden, A., & Lovick, T. A. (2020). Cardiac effects of repeated focal seizures in rats induced by intrahippocampal tetanus toxin: Bradyarrhythmias, tachycardias, and prolonged interictal QT interval. *Epilepsia*, 61(4), 798-809. <https://doi.org/10.1111/epi.16479>
- Jöbsis, F. F. (1977). Noninvasive, infrared monitoring of cerebral and myocardial oxygen sufficiency and circulatory parameters. *Science*, 198(4323), 1264-1267. <https://doi.org/10.1126/science.929199>
- Jöbsis, F. F., Keizer, J. H., LaManna, J. C., & Rosenthal, M. (1977). Reflectance spectrophotometry of cytochrome aa3 in vivo. *J Appl Physiol Respir Environ Exerc Physiol*, 43(5), 858-872. <https://doi.org/10.1152/jappl.1977.43.5.858>
- Jordan, K. G. (1999). Continuous EEG monitoring in the neuroscience intensive care unit and emergency department. *J Clin Neurophysiol*, 16(1), 14-39. <https://doi.org/10.1097/00004691-199901000-00002>
- Jordan, K. G. (2004). Emergency EEG and continuous EEG monitoring in acute ischemic stroke. *J Clin Neurophysiol*, 21(5), 341-352. <https://www.ncbi.nlm.nih.gov/pubmed/15592008>

- Jordan, K. G., & Hirsch, L. J. (2006). In nonconvulsive status epilepticus (NCSE), treat to burst-suppression: pro and con. *Epilepsia*, 47 Suppl 1, 41-45. <https://doi.org/10.1111/j.1528-1167.2006.00659.x>
- Kaiser, V., Bauernfeind, G., Kreilinger, A., Kaufmann, T., Kübler, A., Neuper, C., & Müller-Putz, G. R. (2014). Cortical effects of user training in a motor imagery based brain-computer interface measured by fNIRS and EEG. *Neuroimage*, 85 Pt 1, 432-444. <https://doi.org/10.1016/j.neuroimage.2013.04.097>
- Kälviäinen, R. (2007). Status epilepticus treatment guidelines. *Epilepsia*, 48(s8), 99-102. <https://doi.org/https://doi.org/10.1111/j.1528-1167.2007.01364.x>
- Kan, R., Takahashi, Y., Sato, K., Watabe, M., Tago, H., Yashima, Y., & Kumashiro, H. (1992). Serial changes of SPECT in periodic synchronous discharges in a case with Creutzfeldt-Jakob disease. *Jpn J Psychiatry Neurol*, 46(1), 175-179. <https://doi.org/10.1111/j.1440-1819.1992.tb00831.x>
- Kanayama, N., & Niwayama, M. (2014). Examiner's finger-mounted fetal tissue oximetry. *J Biomed Opt*, 19(6), 067008. <https://doi.org/10.1117/1.Jbo.19.6.067008>
- Kassab, A., Hinnoutondji Toffa, D., Robert, M., Lesage, F., Peng, K., & Khoa Nguyen, D. (2021). Hemodynamic changes associated with common EEG patterns in critically ill patients: Pilot results from continuous EEG-fNIRS study. *Neuroimage Clin*, 32, 102880. <https://doi.org/10.1016/j.nicl.2021.102880>
- Kassab, A., Lan, J. L., Vannasing, P., & Sawan, M. (2015). Functional near-infrared spectroscopy caps for brain activity monitoring: a review. *Applied Optics*, 54(3), 576-586. <https://doi.org/10.1364/AO.54.000576>
- Kassab, A., Le Lan, J., Tremblay, J., Vannasing, P., Dehbozorgi, M., Pouliot, P., Gallagher, A., Lesage, F., Sawan, M., & Nguyen, D. K. (2018). Multichannel wearable fNIRS-EEG system for long-term clinical monitoring. *Hum Brain Mapp*, 39(1), 7-23. <https://doi.org/10.1002/hbm.23849>
- Kassab, A., Tremblay, J., Poppe, A. Y., Létourneau-Guillon, L., Gallagher, A., & Nguyen, D. K. (2016). Cerebral hemodynamic changes during limb-shaking TIA: A near-infrared spectroscopy study. *Neurology*, 86(12), 1166-1168. <https://doi.org/10.1212/wnl.0000000000002505>

- Kato, S., Yoshitani, K., & Ohnishi, Y. (2016). Cerebral Blood Flow Measurement by Near-Infrared Spectroscopy During Carotid Endarterectomy. *J Neurosurg Anesthesiol*, 28(4), 291-295. <https://doi.org/10.1097/ana.0000000000000223>
- Kato, T., Kamei, A., Takashima, S., & Ozaki, T. (1993). Human visual cortical function during photic stimulation monitoring by means of near-infrared spectroscopy. *J Cereb Blood Flow Metab*, 13(3), 516-520. <https://doi.org/10.1038/jcbfm.1993.66>
- Katyal, N., Singh, I., Narula, N., Idiculla, P. S., Premkumar, K., Beary, J. M., Nattanmai, P., & Newey, C. R. (2020). Continuous Electroencephalography (CEEG) in Neurological Critical Care Units (NCCU): A Review. *Clin Neurol Neurosurg*, 198, 106145. <https://doi.org/10.1016/j.clineuro.2020.106145>
- Keller, E., Froehlich, J., Baumann, D., Böcklin, C., Sikorski, C., Oberle, M., & Muser, M. (2015). Detection of delayed cerebral ischemia (DCI) in subarachnoid haemorrhage applying near-infrared spectroscopy: elimination of the extracerebral signal by transcutaneous and intraparenchymatous measurements in parallel. *Acta Neurochir Suppl*, 120, 243-247. https://doi.org/10.1007/978-3-319-04981-6_41
- Kett-White, R., Hutchinson, P. J., Al-Rawi, P. G., Czosnyka, M., Gupta, A. K., Pickard, J. D., & Kirkpatrick, P. J. (2002). Cerebral oxygen and microdialysis monitoring during aneurysm surgery: effects of blood pressure, cerebrospinal fluid drainage, and temporary clipping on infarction. *J Neurosurg*, 96(6), 1013-1019. <https://doi.org/10.3171/jns.2002.96.6.1013>
- Kett-White, R., Hutchinson, P. J., Czosnyka, M., Boniface, S., Pickard, J. D., & Kirkpatrick, P. J. (2002). Multi-modal monitoring of acute brain injury. *Adv Tech Stand Neurosurg*, 27, 87-134. https://doi.org/10.1007/978-3-7091-6174-6_3
- Khan, B., Hodics, T., Hervey, N., Kondraske, G., Stowe, A. M., & Alexandrakis, G. (2013). Functional near-infrared spectroscopy maps cortical plasticity underlying altered motor performance induced by transcranial direct current stimulation. *J Biomed Opt*, 18(11), 116003. <https://doi.org/10.1117/1.Jbo.18.11.116003>
- Khan, M. J., & Hong, K. S. (2017). Hybrid EEG-fNIRS-Based Eight-Command Decoding for BCI: Application to Quadcopter Control. *Front Neurobot*, 11, 6. <https://doi.org/10.3389/fnbot.2017.00006>

- Kiguchi, M., Atsumori, H., Fukasaku, I., Kumagai, Y., Funane, T., Maki, A., Kasai, Y., & Ninomiya, A. (2012). Note: wearable near-infrared spectroscopy imager for haired region. *Rev Sci Instrum*, 83(5), 056101. <https://doi.org/10.1063/1.4704456>
- Kim, H. Y., Kim, J. Y., Kim, G. U., Han, H. J., & Shin, D. I. (2012). Alien hand syndrome after epilepsy partialis continua: FDG PET and MRI studies. *Epilepsy Behav*, 23(1), 71-73. <https://doi.org/10.1016/j.yebeh.2011.08.043>
- Kim, S., & Mountz, J. M. (2011). SPECT Imaging of Epilepsy: An Overview and Comparison with F-18 FDG PET. *Int J Mol Imaging*, 2011, 813028. <https://doi.org/10.1155/2011/813028>
- Kim, S. J., Kim, B. H., Jeon, Y. K., Kim, S. S., & Kim, I. J. (2011). Limited diagnostic and predictive values of dual-time-point 18F FDG PET/CT for differentiation of incidentally detected thyroid nodules. *Ann Nucl Med*, 25(5), 347-353. <https://doi.org/10.1007/s12149-011-0468-0>
- Kirilina, E., Jelzow, A., Heine, A., Niessing, M., Wabnitz, H., Brühl, R., Ittermann, B., Jacobs, A. M., & Tachtsidis, I. (2012). The physiological origin of task-evoked systemic artefacts in functional near infrared spectroscopy. *Neuroimage*, 61(1), 70-81. <https://doi.org/10.1016/j.neuroimage.2012.02.074>
- Kirilina, E., Yu, N., Jelzow, A., Wabnitz, H., Jacobs, A. M., & Tachtsidis, I. (2013). Identifying and quantifying main components of physiological noise in functional near infrared spectroscopy on the prefrontal cortex. *Front Hum Neurosci*, 7, 864. <https://doi.org/10.3389/fnhum.2013.00864>
- Kleinschmidt, A., Obrig, H., Requardt, M., Merboldt, K. D., Dirnagl, U., Villringer, A., & Frahm, J. (1996). Simultaneous recording of cerebral blood oxygenation changes during human brain activation by magnetic resonance imaging and near-infrared spectroscopy. *J Cereb Blood Flow Metab*, 16(5), 817-826. <https://doi.org/10.1097/00004647-199609000-00006>
- Kleiser, S., Ostojic, D., Nasser, N., Isler, H., Bucher, H. U., Bassler, D., Wolf, M., Scholkmann, F., & Karen, T. (2018). In vivo precision assessment of a near-infrared spectroscopy-based tissue oximeter (OxyPrem v1.3) in neonates considering systemic hemodynamic fluctuations. *J Biomed Opt*, 23(6), 1-10. <https://doi.org/10.1117/1.Jbo.23.6.067003>

- Klem, G. H., Lüders, H. O., Jasper, H. H., & Elger, C. (1999). The ten-twenty electrode system of the International Federation. *The International Federation of Clinical Neurophysiology. Electroencephalogr Clin Neurophysiol Suppl*, 52, 3-6.
<https://www.ncbi.nlm.nih.gov/pubmed/10590970>
- Knake, S., Hamer, H. M., & Rosenow, F. (2009). Status epilepticus: a critical review. *Epilepsy Behav*, 15(1), 10-14. <https://doi.org/10.1016/j.yebeh.2009.02.027>
- Knecht, S., Jansen, A., Frank, A., van Randenborgh, J., Sommer, J., Kanowski, M., & Heinze, H. J. (2003). How atypical is atypical language dominance? *Neuroimage*, 18(4), 917-927.
[https://doi.org/10.1016/s1053-8119\(03\)00039-9](https://doi.org/10.1016/s1053-8119(03)00039-9)
- Ko, S. B., Ortega-Gutierrez, S., Choi, H. A., Claassen, J., Presciutti, M., Schmidt, J. M., Badjatia, N., Lee, K., & Mayer, S. A. (2011). Status epilepticus-induced hyperemia and brain tissue hypoxia after cardiac arrest. *Arch Neurol*, 68(10), 1323-1326.
<https://doi.org/10.1001/archneurol.2011.240>
- Kobayashi, E., Grova, C., Tyvaert, L., Dubeau, F., & Gotman, J. (2009). Structures involved at the time of temporal lobe spikes revealed by interindividual group analysis of EEG/fMRI data. *Epilepsia*, 50(12), 2549-2556. <https://doi.org/10.1111/j.1528-1167.2009.02180.x>
- Kocsis, L., Herman, P., & Eke, A. (2006). The modified Beer-Lambert law revisited. *Phys Med Biol*, 51(5), N91-98. <https://doi.org/10.1088/0031-9155/51/5/n02>
- Kohno, S., Miyai, I., Seiyama, A., Oda, I., Ishikawa, A., Tsuneishi, S., Amita, T., & Shimizu, K. (2007). Removal of the skin blood flow artifact in functional near-infrared spectroscopic imaging data through independent component analysis. *J Biomed Opt*, 12(6), 062111.
<https://doi.org/10.1117/1.2814249>
- Kohri, S., Hoshi, Y., Tamura, M., Kato, C., Kuge, Y., & Tamaki, N. (2002). Quantitative evaluation of the relative contribution ratio of cerebral tissue to near-infrared signals in the adult human head: a preliminary study. *Physiol Meas*, 23(2), 301-312.
<https://doi.org/10.1088/0967-3334/23/2/306>
- Koizumi, H., Yamashita, Y., Maki, A., Yamamoto, T., Ito, Y., Itagaki, H., & Kennan, R. (1999). Higher-order brain function analysis by trans-cranial dynamic near-infrared spectroscopy imaging. *J Biomed Opt*, 4(4), 403-413. <https://doi.org/10.1117/1.429959>
- Kono, T., Matsuo, K., Tsunashima, K., Kasai, K., Takizawa, R., Rogers, M. A., Yamasue, H., Yano, T., Taketani, Y., & Kato, N. (2007). Multiple-time replicability of near-infrared

- spectroscopy recording during prefrontal activation task in healthy men. *Neuroscience Research*, 57(4), 504-512. <https://doi.org/https://doi.org/10.1016/j.neures.2006.12.007>
- Kopton, I. M., & Kenning, P. (2014). Near-infrared spectroscopy (NIRS) as a new tool for neuroeconomic research. *Front Hum Neurosci*, 8, 549. <https://doi.org/10.3389/fnhum.2014.00549>
- Korbakis, G., & Vespa, P. M. (2017). Multimodal neurologic monitoring. *Handb Clin Neurol*, 140, 91-105. <https://doi.org/10.1016/b978-0-444-63600-3.00006-4>
- Koutroumanidis, M., Hennessy, M. J., Seed, P. T., Elwes, R. D., Jarosz, J., Morris, R. G., Maisey, M. N., Binnie, C. D., & Polkey, C. E. (2000). Significance of interictal bilateral temporal hypometabolism in temporal lobe epilepsy. *Neurology*, 54(9), 1811-1821. <https://doi.org/10.1212/wnl.54.9.1811>
- Kovács, R., Gerevich, Z., Friedman, A., Otáhal, J., Prager, O., Gabriel, S., & Berndt, N. (2018). Bioenergetic Mechanisms of Seizure Control. *Front Cell Neurosci*, 12, 335. <https://doi.org/10.3389/fncel.2018.00335>
- Kovács, R., Rabanus, A., Otáhal, J., Patzak, A., Kardos, J., Albus, K., Heinemann, U., & Kann, O. (2009). Endogenous nitric oxide is a key promoting factor for initiation of seizure-like events in hippocampal and entorhinal cortex slices. *J Neurosci*, 29(26), 8565-8577. <https://doi.org/10.1523/jneurosci.5698-08.2009>
- Kovács, R., Schuchmann, S., Gabriel, S., Kann, O., Kardos, J., & Heinemann, U. (2002). Free radical-mediated cell damage after experimental status epilepticus in hippocampal slice cultures. *J Neurophysiol*, 88(6), 2909-2918. <https://doi.org/10.1152/jn.00149.2002>
- Kovacsova, Z., Bale, G., Mitra, S., Lange, F., & Tachtsidis, I. (2021). Absolute quantification of cerebral tissue oxygen saturation with multidistance broadband NIRS in newborn brain. *Biomed Opt Express*, 12(2), 907-925. <https://doi.org/10.1364/boe.412088>
- Kramer, K. (1934). Bestimmung des 'Sauerstoffgehaltes und der F~ moglobinkonzentration in Hlmoglobinliisungen und hiimolysiertem Blut auf lickte! ektrischem Wege, *Zeitschr. f. Biol*, 95, 126.
- Kreisman, N. R., Lamanna, J. C., Rosenthal, M., & Sick, T. J. (1981). Oxidative metabolic responses with recurrent seizures in rat cerebral cortex: role of systemic factors. *Brain Res*, 218(1-2), 175-188. [https://doi.org/10.1016/0006-8993\(81\)91299-3](https://doi.org/10.1016/0006-8993(81)91299-3)

- Kreisman, N. R., Magee, J. C., & Brizzee, B. L. (1991). Relative hypoperfusion in rat cerebral cortex during recurrent seizures. *J Cereb Blood Flow Metab*, 11(1), 77-87.
<https://doi.org/10.1038/jcbfm.1991.9>
- Kreisman, N. R., Sick, T. J., & Rosenthal, M. (1983). Importance of vascular responses in determining cortical oxygenation during recurrent paroxysmal events of varying duration and frequency of repetition. *J Cereb Blood Flow Metab*, 3(3), 330-338.
<https://doi.org/10.1038/jcbfm.1983.48>
- Kreisman, N. R., Sick, T. J., & Rosenthal, M. (1984). Concepts of brain oxygen sufficiency during seizures. *Adv Exp Med Biol*, 180, 381-392. https://doi.org/10.1007/978-1-4684-4895-5_36
- Kubota, H., & Awaya, Y. (2010). Assessment of health-related quality of life and influencing factors using QOLIE-31 in Japanese patients with epilepsy. *Epilepsy & Behavior*, 18(4), 381-387. <https://doi.org/10.1016/j.yebeh.2010.04.045>
- Kuhr, W. G., & Korf, J. (1988). Extracellular lactic acid as an indicator of brain metabolism: continuous on-line measurement in conscious, freely moving rats with intrastriatal dialysis. *J Cereb Blood Flow Metab*, 8(1), 130-137.
<https://doi.org/10.1038/jcbfm.1988.17>
- Kuhr, W. G., & Korf, J. (1988). N-methyl-D-aspartate receptor involvement in lactate production following ischemia or convulsion in rats. *Eur J Pharmacol*, 155(1-2), 145-149.
[https://doi.org/10.1016/0014-2999\(88\)90412-8](https://doi.org/10.1016/0014-2999(88)90412-8)
- Kutluay, E., Beattie, J., Passaro, E. A., Edwards, J. C., Minecan, D., Milling, C., Selwa, L., & Beydoun, A. (2005). Diagnostic and localizing value of ictal SPECT in patients with nonconvulsive status epilepticus. *Epilepsy Behav*, 6(2), 212-217.
<https://doi.org/10.1016/j.yebeh.2004.12.001>
- Kwan, P., & Brodie, M. J. (2000). Early Identification of Refractory Epilepsy. *New England Journal of Medicine*, 342(5), 314-319. <https://doi.org/10.1056/nejm200002033420503>
- Kwan, P., & Brodie, M. J. (2001). Effectiveness of First Antiepileptic Drug. *Epilepsia*, 42(10), 1255-1260. <https://doi.org/https://doi.org/10.1046/j.1528-1157.2001.04501.x>
- la Fougère, C., Rominger, A., Förster, S., Geisler, J., & Bartenstein, P. (2009). PET and SPECT in epilepsy: a critical review. *Epilepsy Behav*, 15(1), 50-55.
<https://doi.org/10.1016/j.yebeh.2009.02.025>

- Laman, D. M., van der Reijden, C. S., Wieneke, G. H., van Duijn, H., & van Huffelen, A. C. (2001). EEG evidence for shunt requirement during carotid endarterectomy: optimal EEG derivations with respect to frequency bands and anesthetic regimen. *J Clin Neurophysiol*, 18(4), 353-363. <https://doi.org/10.1097/00004691-200107000-00007>
- Lamblin, M. D., Walls Esquivel, E., & André, M. (2013). The electroencephalogram of the full-term newborn: review of normal features and hypoxic-ischemic encephalopathy patterns. *Neurophysiol Clin*, 43(5-6), 267-287. <https://doi.org/10.1016/j.neucli.2013.07.001>
- Lamusuo, S., Jutila, L., Ylinen, A., Kälviäinen, R., Mervaala, E., Haaparanta, M., Jääskeläinen, S., Partanen, K., Vapalahti, M., & Rinne, J. (2001). [18F]FDG-PET reveals temporal hypometabolism in patients with temporal lobe epilepsy even when quantitative MRI and histopathological analysis show only mild hippocampal damage. *Arch Neurol*, 58(6), 933-939. <https://doi.org/10.1001/archneur.58.6.933>
- Lange, F., Bale, G., Kaynezhad, P., Pollock, R. D., Stevenson, A., & Tachtsidis, I. (2020). Broadband NIRS Cerebral Evaluation of the Hemodynamic and Oxidative State of Cytochrome-c-Oxidase Responses to +Gz Acceleration in Healthy Volunteers. *Adv Exp Med Biol*, 1232, 339-345. https://doi.org/10.1007/978-3-030-34461-0_43
- Lange, F., Dunne, L., Hale, L., & Tachtsidis, I. (2019). MAESTROS: A Multiwavelength Time-Domain NIRS System to Monitor Changes in Oxygenation and Oxidation State of Cytochrome-C-Oxidase. *IEEE J Sel Top Quantum Electron*, 25(1), 7100312. <https://doi.org/10.1109/jstqe.2018.2833205>
- Lange, F., & Tachtsidis, I. (2019). Clinical Brain Monitoring with Time Domain NIRS: A Review and Future Perspectives. *Applied Sciences*, 9(8), 1612. <https://www.mdpi.com/2076-3417/9/8/1612>
- Lareau, E., Lesage, F., Pouliot, P., Nguyen, D., Le Lan, J., & Sawan, M. (2011). Multichannel wearable system dedicated for simultaneous electroencephalography/near-infrared spectroscopy real-time data acquisitions. *J Biomed Opt*, 16(9), 096014. <https://doi.org/10.1117/1.3625575>
- Lareau, E., Simard, G., Lesage, F., Nguyen, D., & Sawan, M. (2011). Near infrared spectrometer combined with multichannel EEG for functional brain imaging 5th International Symposium on Medical Information and Communication Technology (ISMICT 2011), Montreux, Switzerland. <https://doi.org/10.1109/ismict.2011.5759810>

- Lazeyras, F., Blanke, O., Perrig, S., Zimine, I., Golay, X., Delavelle, J., Michel, C. M., de Tribolet, N., Villemure, J. G., & Seeck, M. (2000). EEG-triggered functional MRI in patients with pharmaco-resistant epilepsy. *J Magn Reson Imaging*, 12(1), 177-185. [https://doi.org/10.1002/1522-2586\(200007\)12:1<177::aid-jmri20>3.0.co;2-3](https://doi.org/10.1002/1522-2586(200007)12:1<177::aid-jmri20>3.0.co;2-3)
- Le Roux, P., Menon, D. K., Citerio, G., Vespa, P., Bader, M. K., Brophy, G. M., Diringer, M. N., Stocchetti, N., Videtta, W., Armonda, R., Badjatia, N., Böesel, J., Chesnut, R., Chou, S., Claassen, J., Czosnyka, M., De Georgia, M., Figaji, A., Fugate, J., . . . Taccone, F. (2014). Consensus summary statement of the International Multidisciplinary Consensus Conference on Multimodality Monitoring in Neurocritical Care : a statement for healthcare professionals from the Neurocritical Care Society and the European Society of Intensive Care Medicine. *Intensive Care Med*, 40(9), 1189-1209. <https://doi.org/10.1007/s00134-014-3369-6>
- Leal-Campanario, R., Alarcon-Martinez, L., Rieiro, H., Martinez-Conde, S., Alarcon-Martinez, T., Zhao, X., LaMee, J., Popp, P. J., Calhoun, M. E., Arribas, J. I., Schlegel, A. A., Stasi, L. L., Rho, J. M., Inge, L., Otero-Millan, J., Treiman, D. M., & Macknik, S. L. (2017). Abnormal Capillary Vasodynamics Contribute to Ictal Neurodegeneration in Epilepsy. *Sci Rep*, 7, 43276. <https://doi.org/10.1038/srep43276>
- Leamy, D. J., Collins, R., & Ward, T. E. (2011). Combining fNIRS and EEG to improve motor cortex activity classification during an imagined movement-based task. In FAC'11 Proceedings of the 6th international conference on Foundations of augmented cognition: directing the future of adaptive systems (pp. 177-185). Springer-Verlag Berlin. <https://mural.maynoothuniversity.ie/4365/>
- Leblanc, R. (2019). Wilder Penfield and the vascular hypothesis of focal epilepsy. *J Neurosurg*, 131(6), 1947-1953. <https://doi.org/10.3171/2018.8.Jns181990>
- Lecrux, C., Bourourou, M., & Hamel, E. (2019). How reliable is cerebral blood flow to map changes in neuronal activity? *Auton Neurosci*, 217, 71-79. <https://doi.org/10.1016/j.autneu.2019.01.005>
- Lecrux, C., & Hamel, E. (2016). Neuronal networks and mediators of cortical neurovascular coupling responses in normal and altered brain states. *Philos Trans R Soc Lond B Biol Sci*, 371(1705). <https://doi.org/10.1098/rstb.2015.0350>

- Lee, B. I., Markand, O. N., Wellman, H. N., Siddiqui, A. R., Park, H. M., Mock, B., Worth, R. M., Edwards, M. K., & Krepshaw, J. (1988). HIPDM-SPECT in patients with medically intractable complex partial seizures. Ictal study. *Arch Neurol*, 45(4), 397-402.
<https://doi.org/10.1001/archneur.1988.00520280043014>
- Lee, D. S., Lee, S. K., & Lee, M. C. (2001). Functional neuroimaging in epilepsy: FDG PET and ictal SPECT. *J Korean Med Sci*, 16(6), 689-696.
<https://doi.org/10.3346/jkms.2001.16.6.689>
- Lee, J., Mukae, N., Arata, J., Iwata, H., Iramina, K., Iihara, K., & Hashizume, M. (2017). A multichannel-near-infrared-spectroscopy-triggered robotic hand rehabilitation system for stroke patients. *IEEE Int Conf Rehabil Robot*, 2017, 158-163.
<https://doi.org/10.1109/icorr.2017.8009239>
- Lee, K., Bohnert, S., Wu, Y., Vair, C., Mikler, J., Campbell Teskey, G., & Dunn, J. F. (2018). Assessment of brain oxygenation imbalance following soman exposure in rats. *Neurotoxicology*, 65, 28-37. <https://doi.org/10.1016/j.neuro.2018.01.007>
- Lee, S., Shin, Y., Kumar, A., Kim, M., & Lee, H. N. (2019). Dry Electrode-Based Fully Isolated EEG/fNIRS Hybrid Brain-Monitoring System. *IEEE Trans Biomed Eng*, 66(4), 1055-1068. <https://doi.org/10.1109/tbme.2018.2866550>
- Leff, D. R., Orihuela-Espina, F., Elwell, C. E., Athanasiou, T., Delpy, D. T., Darzi, A. W., & Yang, G. Z. (2011). Assessment of the cerebral cortex during motor task behaviours in adults: a systematic review of functional near infrared spectroscopy (fNIRS) studies. *Neuroimage*, 54(4), 2922-2936. <https://doi.org/10.1016/j.neuroimage.2010.10.058>
- Leite, M., Leal, A., & Figueiredo, P. (2013). Transfer Function between EEG and BOLD Signals of Epileptic Activity. *Front Neurol*, 4, 1. <https://doi.org/10.3389/fneur.2013.00001>
- Leitinger, M., Trinka, E., Zimmermann, G., & Beniczky, S. (2019). Salzburg criteria for nonconvulsive status epilepticus: Details matter. *Epilepsia*, 60(11), 2334-2336.
<https://doi.org/https://doi.org/10.1111/epi.16361>
- Lemieux, L., Salek-Haddadi, A., Lund, T. E., Laufs, H., & Carmichael, D. (2007). Modelling large motion events in fMRI studies of patients with epilepsy. *Magn Reson Imaging*, 25(6), 894-901. <https://doi.org/10.1016/j.mri.2007.03.009>
- Leonardi, M., & Ustun, T. B. (2002). The global burden of epilepsy. *Epilepsia*, 43 Suppl 6, 21-25. <https://doi.org/10.1046/j.1528-1157.43.s.6.11.x>

- Leung, T. S., Elwell, C. E., & Delpy, D. T. (2005). Estimation of cerebral oxy- and deoxy-haemoglobin concentration changes in a layered adult head model using near-infrared spectroscopy and multivariate statistical analysis. *Phys Med Biol*, 50(24), 5783-5798. <https://doi.org/10.1088/0031-9155/50/24/002>
- Lewis, D. V., O'Connor, M. J., & Schuette, W. H. (1974). Oxidative metabolism during recurrent seizures in the penicillin treated hippocampus. *Electroencephalogr Clin Neurophysiol*, 36(4), 347-356. [https://doi.org/10.1016/0013-4694\(74\)90184-9](https://doi.org/10.1016/0013-4694(74)90184-9)
- Lewis, D. V., & Schuette, W. H. (1975). NADH fluorescence and $[K^+]_o$ changes during hippocampal electrical stimulation. *J Neurophysiol*, 38(2), 405-417. <https://doi.org/10.1152/jn.1975.38.2.405>
- Lewis, L. D., Ching, S., Weiner, V. S., Peterfreund, R. A., Eskandar, E. N., Cash, S. S., Brown, E. N., & Purdon, P. L. (2013). Local cortical dynamics of burst suppression in the anaesthetized brain. *Brain*, 136(Pt 9), 2727-2737. <https://doi.org/10.1093/brain/awt174>
- Li, B., & Freeman, R. D. (2015). Neurometabolic coupling between neural activity, glucose, and lactate in activated visual cortex. *J Neurochem*, 135(4), 742-754. <https://doi.org/10.1111/jnc.13143>
- Liley, D., & Walsh, M. (2013). The Mesoscopic Modeling of Burst Suppression during Anesthesia [Hypothesis and Theory]. *Frontiers in Computational Neuroscience*, 7, 46. <https://doi.org/10.3389/fncom.2013.00046>
- Lindauer, U., Dirnagl, U., Füchtmeier, M., Böttiger, C., Offenhauser, N., Leithner, C., & Royl, G. (2010). Pathophysiological interference with neurovascular coupling - when imaging based on hemoglobin might go blind. *Front Neuroenergetics*, 2. <https://doi.org/10.3389/fnene.2010.00025>
- Liu, N., Cui, X., Bryant, D. M., Glover, G. H., & Reiss, A. L. (2015). Inferring deep-brain activity from cortical activity using functional near-infrared spectroscopy. *Biomed Opt Express*, 6(3), 1074-1089. <https://doi.org/10.1364/boe.6.001074>
- Liu, X., Zhu, X. H., Zhang, Y., & Chen, W. (2011). Neural origin of spontaneous hemodynamic fluctuations in rats under burst-suppression anesthesia condition. *Cereb Cortex*, 21(2), 374-384. <https://doi.org/10.1093/cercor/bhq105>

- Lloyd-Fox, S., Blasi, A., & Elwell, C. E. (2010). Illuminating the developing brain: the past, present and future of functional near infrared spectroscopy. *Neurosci Biobehav Rev*, 34(3), 269-284. <https://doi.org/10.1016/j.neubiorev.2009.07.008>
- Logothetis, N. K., Pauls, J., Augath, M., Trinath, T., & Oeltermann, A. (2001). Neurophysiological investigation of the basis of the fMRI signal. *Nature*, 412(6843), 150-157. <https://doi.org/10.1038/35084005>
- Logroscino, G., & Hesdorffer, D. C. (2005). Methodologic Issues in Studies of Mortality Following Epilepsy: Measures, Types of Studies, Sources of Cases, Cohort Effects, and Competing Risks. *Epilepsia*, 46(s11), 3-7. <https://doi.org/https://doi.org/10.1111/j.1528-1167.2005.00399.x>
- Logroscino, G., Hesdorffer, D. C., Cascino, G., & Hauser, W. A. (2008). Status Epilepticus Without an Underlying Cause and Risk of Death: A Population-Based Study. *Archives of Neurology*, 65(2), 221-224. <https://doi.org/10.1001/archneurol.2007.43>
- Lothman, E. (1990). The biochemical basis and pathophysiology of status epilepticus. *Neurology*, 40(5 Suppl 2), 13-23. <https://www.ncbi.nlm.nih.gov/pubmed/2185436>
- Lothman, E., Lamanna, J., Cordingley, G., Rosenthal, M., & Somjen, G. (1975). Responses of electrical potential, potassium levels, and oxidative metabolic activity of the cerebral neocortex of cats. *Brain Res*, 88(1), 15-36. [https://doi.org/10.1016/0006-8993\(75\)90943-9](https://doi.org/10.1016/0006-8993(75)90943-9)
- Lowenstein, D. H., & Alldredge, B. K. (1998). Status epilepticus. *N Engl J Med*, 338(14), 970-976. <https://doi.org/10.1056/nejm199804023381407>
- Lucas, S. J., Tzeng, Y. C., Galvin, S. D., Thomas, K. N., Ogoh, S., & Ainslie, P. N. (2010). Influence of changes in blood pressure on cerebral perfusion and oxygenation. *Hypertension*, 55(3), 698-705. <https://doi.org/10.1161/hypertensionaha.109.146290>
- Luengo, C., Resche-Rigon, M., Damoiseil, C., Kerever, S., Creteur, J., & Payen, D. (2013). Comparison of two different generations of "NIRS" devices and transducers in healthy volunteers and ICU patients. *J Clin Monit Comput*, 27(1), 71-79. <https://doi.org/10.1007/s10877-012-9400-y>
- Lühns, M., & Goebel, R. (2017). Turbo-Satori: a neurofeedback and brain-computer interface toolbox for real-time functional near-infrared spectroscopy. *Neurophotonics*, 4(4), 041504. <https://doi.org/10.1117/1.NPh.4.4.041504>

- Ma, H., Zhao, M., & Schwartz, T. H. (2013). Dynamic neurovascular coupling and uncoupling during ictal onset, propagation, and termination revealed by simultaneous in vivo optical imaging of neural activity and local blood volume. *Cereb Cortex*, 23(4), 885-899.
<https://doi.org/10.1093/cercor/bhs079>
- Ma, K., & Bebawy, J. F. (2022). Electroencephalographic Burst-Suppression, Perioperative Neuroprotection, Postoperative Cognitive Function, and Mortality: A Focused Narrative Review of the Literature. *Anesthesia & Analgesia*, 135(1), 79-90.
<https://doi.org/10.1213/ane.0000000000005806>
- Machado, A., Cai, Z., Pellegrino, G., Marcotte, O., Vincent, T., Lina, J. M., Kobayashi, E., & Grova, C. (2018). Optimal positioning of optodes on the scalp for personalized functional near-infrared spectroscopy investigations. *J Neurosci Methods*, 309, 91-108.
<https://doi.org/10.1016/j.jneumeth.2018.08.006>
- Machado, A., Cai, Z., Vincent, T., Pellegrino, G., Lina, J. M., Kobayashi, E., & Grova, C. (2021). Deconvolution of hemodynamic responses along the cortical surface using personalized functional near infrared spectroscopy. *Scientific Reports*, 11(1), 5964.
<https://doi.org/10.1038/s41598-021-85386-0>
- Machado, A., Lina, J. M., Tremblay, J., Lassonde, M., Nguyen, D. K., Lesage, F., & Grova, C. (2011). Detection of hemodynamic responses to epileptic activity using simultaneous Electro-EncephaloGraphy (EEG)/Near Infra Red Spectroscopy (NIRS) acquisitions. *Neuroimage*, 56(1), 114-125. <https://doi.org/10.1016/j.neuroimage.2010.12.026>
- Maciel, C. B., & Hirsch, L. J. (2018). Changing Cardiopulmonary Resuscitation to Cardiocerebral Resuscitation: The Reason We Push Hard and Fast. *Crit Care Med*, 46(5), 823-825. <https://doi.org/10.1097/ccm.0000000000003046>
- Madsen, P. L., & Secher, N. H. (1999). Near-infrared oximetry of the brain. *Prog Neurobiol*, 58(6), 541-560. [https://doi.org/10.1016/s0301-0082\(98\)00093-8](https://doi.org/10.1016/s0301-0082(98)00093-8)
- Madsen, P. L., Skak, C., Rasmussen, A., & Secher, N. H. (2000). Interference of cerebral near-infrared oximetry in patients with icterus. *Anesth Analg*, 90(2), 489-493.
<https://doi.org/10.1097/00000539-200002000-00046>
- Magistretti, P. J., & Allaman, I. (2015). A cellular perspective on brain energy metabolism and functional imaging. *Neuron*, 86(4), 883-901.
<https://doi.org/10.1016/j.neuron.2015.03.035>

- Makeig, S., Bell, A., Jung, T.-P., & Sejnowski, T. J. (1995). Independent Component Analysis of Electroencephalographic Data
<https://proceedings.neurips.cc/paper/1995/file/754dda4b1ba34c6fa89716b85d68532b-Paper.pdf>
- Mäkiranta, M. J., Jauhiainen, J. P., Oikarinen, J. T., Suominen, K., Tervonen, O., Alahuhta, S., & Jääntti, V. (2002). Functional magnetic resonance imaging of swine brain during change in thiopental anesthesia into EEG burst-suppression level--a preliminary study. *Magma*, 15(1-3), 27-35. <https://doi.org/10.1007/bf02693841>
- Maldonado, Y., Singh, S., & Taylor, M. A. (2014). Cerebral near-infrared spectroscopy in perioperative management of left ventricular assist device and extracorporeal membrane oxygenation patients. *Curr Opin Anaesthesiol*, 27(1), 81-88.
<https://doi.org/10.1097/aco.0000000000000035>
- Malinska, D., Kulawiak, B., Kudin, A. P., Kovacs, R., Huchzermeyer, C., Kann, O., Szewczyk, A., & Kunz, W. S. (2010). Complex III-dependent superoxide production of brain mitochondria contributes to seizure-related ROS formation. *Biochim Biophys Acta*, 1797(6-7), 1163-1170. <https://doi.org/10.1016/j.bbabbio.2010.03.001>
- Marion, D. W. (1997). Therapeutic Moderate Hypothermia for Severe Traumatic Brain Injury. *Journal of Intensive Care Medicine*, 12(5), 239-248.
<https://doi.org/https://doi.org/10.1111/j.1525-1489.1997.00239.pp.x>
- Marshall, G. T., James, R. F., Landman, M. P., O'Neill, P. J., Cotton, B. A., Hansen, E. N., Morris, J. A., Jr., & May, A. K. (2010). Pentobarbital coma for refractory intra-cranial hypertension after severe traumatic brain injury: mortality predictions and one-year outcomes in 55 patients. *J Trauma*, 69(2), 275-283.
<https://doi.org/10.1097/TA.0b013e3181de74c7>
- Martini, S., Paoletti, V., Faldella, G., & Corvaglia, L. (2019). Cerebral Oxygenation Patterns during Electroclinical Neonatal Seizures. *Neuropediatrics*, 50(6), 408-409.
<https://doi.org/10.1055/s-0039-1693058>
- Masterton, R. A., Harvey, A. S., Archer, J. S., Lillywhite, L. M., Abbott, D. F., Scheffer, I. E., & Jackson, G. D. (2010). Focal epileptiform spikes do not show a canonical BOLD response in patients with benign rolandic epilepsy (BECTS). *Neuroimage*, 51(1), 252-260. <https://doi.org/10.1016/j.neuroimage.2010.01.109>

- Matcher, S., Kirkpatrick, P., Nahid, K., Cope, M., & Delpy, D. (1995). Absolute quantification methods in tissue near-infrared spectroscopy (Vol. 2389). SPIE.
<https://doi.org/10.1117/12.209997>
- Matcher, S. J., & Cooper, C. E. (1994). Absolute quantification of deoxyhaemoglobin concentration in tissue near infrared spectroscopy. *Phys Med Biol*, 39(8), 1295-1312.
<https://doi.org/10.1088/0031-9155/39/8/008>
- Matthes, K. (1935). Untersuchungen über die Sauerstoffsättigung des menschlichen Arterienblutes. *Naunyn-Schmiedebergs Archiv für experimentelle Pathologie und Pharmakologie*, 179(6), 698-711.
- Matthes, K., & Groß, F. (1938). Fortlaufende Registrierung der Lichtabsorption des Blutes in zwei verschiedenen Spektralbezirken. *Naunyn-Schmiedebergs Archiv für experimentelle Pathologie und Pharmakologie*, 191(2), 381-390.
- Matthes, K., & Gross, F. (1938). Untersuchungen über die Absorption von rotem und ultrarotem Licht durch kohlenoxydgesättigtes, sauerstoffgesättigtes und reduziertes Blut. *Naunyn-Schmiedebergs Archiv für experimentelle Pathologie und Pharmakologie*, 191(2), 369-380.
- Matthes, K., & Gross, F. (1938). Zur Methode der fortlaufenden Registrierung der Farbe des menschlichen Blutes. *Naunyn-Schmiedebergs Archiv für experimentelle Pathologie und Pharmakologie*, 191(2), 523-528.
- Mauritzon, S., Ginstman, F., Hillman, J., & Wårdell, K. (2022). Analysis of laser Doppler flowmetry long-term recordings for investigation of cerebral microcirculation during neurointensive care [Original Research]. *Frontiers in Neuroscience*, 16, 1030805.
<https://doi.org/10.3389/fnins.2022.1030805>
- McKeating, E. G., Monjardino, J. R., Signorini, D. F., Souter, M. J., & Andrews, P. J. (1997). A comparison of the Invos 3100 and the Critikon 2020 near-infrared spectrophotometers as monitors of cerebral oxygenation. *Anaesthesia*, 52(2), 136-140.
<https://doi.org/10.1111/j.1365-2044.1997.18-az015.x>
- Mecarelli, O., Piacenti, A., Pulitano, P., Vicenzini, E., Rizzo, C., Rinalduzzi, S., de Feo, M. R., & Accornero, N. (2001). Clinical and electroencephalographic effects of topiramate in patients with epilepsy and healthy volunteers. *Clin Neuropharmacol*, 24(5), 284-289.
<https://doi.org/10.1097/00002826-200109000-00005>

- Meester, D., Al-Yahya, E., Dawes, H., Martin-Fagg, P., & Piñon, C. (2014). Associations between prefrontal cortex activation and H-reflex modulation during dual task gait. *Front Hum Neurosci*, 8, 78. <https://doi.org/10.3389/fnhum.2014.00078>
- Meldrum, B. S., & Brierley, J. B. (1973). Prolonged epileptic seizures in primates. Ischemic cell change and its relation to ictal physiological events. *Arch Neurol*, 28(1), 10-17. <https://doi.org/10.1001/archneur.1973.00490190028002>
- Meldrum, B. S., & Horton, R. W. (1973). Physiology of status epilepticus in primates. *Arch Neurol*, 28(1), 1-9. <https://doi.org/10.1001/archneur.1973.00490190019001>
- Meldrum, B. S., & Nilsson, B. (1976). Cerebral blood flow and metabolic rate early and late in prolonged epileptic seizures induced in rats by bicuculline. *Brain*, 99(3), 523-542. <https://doi.org/10.1093/brain/99.3.523>
- Meldrum, B. S., Vigouroux, R. A., & Brierley, J. B. (1973). Systemic factors and epileptic brain damage. Prolonged seizures in paralyzed, artificially ventilated baboons. *Arch Neurol*, 29(2), 82-87. <https://doi.org/10.1001/archneur.1973.00490260026003>
- Meldrum, B. S., Vigouroux, R. A., Rage, P., & Brierley, J. B. (1973). Hippocampal lesions produced by prolonged seizures in paralyzed artificially ventilated baboons. *Experientia*, 29(5), 561-563. <https://doi.org/10.1007/bf01926665>
- Meyer, N., Voysey, M., Holmes, J., Casey, D., & Hawton, K. (2014). Self-harm in people with epilepsy: a retrospective cohort study. *Epilepsia*, 55(9), 1355-1365. <https://doi.org/10.1111/epi.12723>
- Mihara, M., & Miyai, I. (2016). Review of functional near-infrared spectroscopy in neurorehabilitation. *Neurophotronics*, 3(3), 031414. <https://doi.org/10.1117/1.NPh.3.3.031414>
- Mihara, M., Miyai, I., Hatakenaka, M., Kubota, K., & Sakoda, S. (2007). Sustained prefrontal activation during ataxic gait: a compensatory mechanism for ataxic stroke? *Neuroimage*, 37(4), 1338-1345. <https://doi.org/10.1016/j.neuroimage.2007.06.014>
- Mihara, M., Yagura, H., Hatakenaka, M., Hattori, N., & Miyai, I. (2010). [Clinical application of functional near-infrared spectroscopy in rehabilitation medicine]. *Brain Nerve*, 62(2), 125-132.
- Milesi, S., Boussadia, B., Plaud, C., Catteau, M., Rousset, M. C., De Bock, F., Schaeffer, M., Lerner-Natoli, M., Rigau, V., & Marchi, N. (2014). Redistribution of PDGFR β cells and

- NG2DsRed pericytes at the cerebrovasculature after status epilepticus. *Neurobiol Dis*, 71, 151-158. <https://doi.org/10.1016/j.nbd.2014.07.010>
- Millikan, G., Pappenheimer, J., Rawson, A., & Hervey, J. (1941). Continuous measurement of oxygen saturation in man. *Am J Physiol*, 133, 390.
- Minati, L., Jones, C. L., Gray, M. A., Medford, N., Harrison, N. A., & Critchley, H. D. (2009). Emotional modulation of visual cortex activity: a functional near-infrared spectroscopy study. *Neuroreport*, 20(15), 1344-1350. <https://doi.org/10.1097/WNR.0b013e328330c751>
- Mirski, M. A., & Varelas, P. N. (2008). Seizures and status epilepticus in the critically ill. *Crit Care Clin*, 24(1), 115-147, ix. <https://doi.org/10.1016/j.ccc.2007.11.005>
- Mitra, S., Bale, G., Mathieson, S., Uria-Avellanal, C., Meek, J., Tachtsidis, I., & Robertson, N. J. (2016). Changes in Cerebral Oxidative Metabolism during Neonatal Seizures Following Hypoxic-Ischemic Brain Injury. *Front Pediatr*, 4, 83. <https://doi.org/10.3389/fped.2016.00083>
- Mitra, S., Bale, G., Meek, J., Mathieson, S., Uria, C., Kendall, G., Robertson, N. J., & Tachtsidis, I. (2016). In Vivo Measurement of Cerebral Mitochondrial Metabolism Using Broadband Near Infrared Spectroscopy Following Neonatal Stroke. *Adv Exp Med Biol*, 876, 493-500. https://doi.org/10.1007/978-1-4939-3023-4_62
- Mitra, S., Bale, G., Meek, J., Tachtsidis, I., & Robertson, N. J. (2020). Cerebral Near Infrared Spectroscopy Monitoring in Term Infants With Hypoxic Ischemic Encephalopathy-A Systematic Review. *Front Neurol*, 11, 393. <https://doi.org/10.3389/fneur.2020.00393>
- Miyai, I., Tanabe, H. C., Sase, I., Eda, H., Oda, I., Konishi, I., Tsunazawa, Y., Suzuki, T., Yanagida, T., & Kubota, K. (2001). Cortical mapping of gait in humans: a near-infrared spectroscopic topography study. *Neuroimage*, 14(5), 1186-1192. <https://doi.org/10.1006/nimg.2001.0905>
- Miyasaka, K., Shelley, K., Takahashi, S., Kubota, H., Ito, K., Yoshiya, I., Yamanishi, A., Cooper, J. B., Steward, D. J., Nishida, H., Kiani, J., Ogino, H., Sata, Y., Kopotic, R. J., Jenkin, K., Hannenberg, A., & Gawande, A. (2021). Tribute to Dr. Takuo Aoyagi, inventor of pulse oximetry. *J Anesth*, 35(5), 671-709. <https://doi.org/10.1007/s00540-021-02967-z>
- Moeller, F., Siebner, H. R., Ahlgrimm, N., Wolff, S., Muhle, H., Granert, O., Boor, R., Jansen, O., Gotman, J., Stephani, U., & Siniatchkin, M. (2009). fMRI activation during spike and

- wave discharges evoked by photic stimulation. *Neuroimage*, 48(4), 682-695.
<https://doi.org/10.1016/j.neuroimage.2009.07.019>
- Moeller, F., Siebner, H. R., Wolff, S., Muhle, H., Granert, O., Jansen, O., Stephani, U., & Siniatchkin, M. (2009). Mapping brain activity on the verge of a photically induced generalized tonic-clonic seizure. *Epilepsia*, 50(6), 1632-1637.
<https://doi.org/10.1111/j.1528-1167.2009.02011.x>
- Mohammadi, H., Vincent, T., Peng, K., Nigam, A., Gayda, M., Fraser, S., Joannette, Y., Lesage, F., & Bherer, L. (2021). Coronary artery disease and its impact on the pulsatile brain: A functional NIRS study. *Human Brain Mapping*, 42(12), 3760-3776.
<https://doi.org/https://doi.org/10.1002/hbm.25463>
- Moir, M. E., & Vermeulen, T. D. (2021). Advancing our k'NO'wledge for neurovascular coupling of brain blood flow in humans. *J Physiol*, 599(4), 1033-1034.
<https://doi.org/10.1113/jp280688>
- Molavi, B., & Dumont, G. A. (2012). Wavelet-based motion artifact removal for functional near-infrared spectroscopy. *Physiol Meas*, 33(2), 259-270. <https://doi.org/10.1088/0967-3334/33/2/259>
- Monrad, P., Sannagowdara, K., Bozarth, X., Bhosrekar, S., Hecox, K., Nwosu, M., Schwabe, M., Meyer, M., Szabo, A., Prigge, J., Lemke, R., Horn, B., & Whelan, H. T. (2015). Haemodynamic response associated with both ictal and interictal epileptiform activity using simultaneous video electroencephalography/near infrared spectroscopy in a within-subject study. *J Near Infrared Spectrosc*, 23(4), 209-218.
<https://doi.org/10.1255/jnirs.1170>
- Monti, M. M. (2011). Statistical analysis of fMRI time-series: A critical review of the GLM approach. *Frontiers in Human Neuroscience*, 5, 28.
<https://doi.org/10.3389/fnhum.2011.00028>
- Morin-Brureau, M., Lebrun, A., Rousset, M. C., Fagni, L., Bockaert, J., de Bock, F., & Lerner-Natoli, M. (2011). Epileptiform activity induces vascular remodeling and zonula occludens 1 downregulation in organotypic hippocampal cultures: role of VEGF signaling pathways. *J Neurosci*, 31(29), 10677-10688.
<https://doi.org/10.1523/jneurosci.5692-10.2011>

- Morris, S. J., Shore, A. C., & Tooke, J. E. (1995). Responses of the skin microcirculation to acetylcholine and sodium nitroprusside in patients with NIDDM. *Diabetologia*, 38(11), 1337-1344. <https://doi.org/10.1007/bf00401767>
- Murkin, J. M., & Arango, M. (2009). Near-infrared spectroscopy as an index of brain and tissue oxygenation. *Br J Anaesth*, 103 Suppl 1, i3-13. <https://doi.org/10.1093/bja/aep299>
- Myers, K. A., Sivathamboo, S., & Perucca, P. (2018). Heart rate variability measurement in epilepsy: How can we move from research to clinical practice? *Epilepsia*, 59(12), 2169-2178. <https://doi.org/10.1111/epi.14587>
- Nagata, K., Tagawa, K., Hiroi, S., Shishido, F., & Uemura, K. (1989). Electroencephalographic correlates of blood flow and oxygen metabolism provided by positron emission tomography in patients with cerebral infarction. *Electroencephalogr Clin Neurophysiol*, 72(1), 16-30. [https://doi.org/10.1016/0013-4694\(89\)90027-8](https://doi.org/10.1016/0013-4694(89)90027-8)
- Naqvi, J., Yap, K. H., Ahmad, G., & Ghosh, J. (2013). Transcranial Doppler ultrasound: a review of the physical principles and major applications in critical care. *Int J Vasc Med*, 2013, 629378. <https://doi.org/10.1155/2013/629378>
- Narotam, P. K., Morrison, J. F., & Nathoo, N. (2009). Brain tissue oxygen monitoring in traumatic brain injury and major trauma: outcome analysis of a brain tissue oxygen-directed therapy. *J Neurosurg*, 111(4), 672-682. <https://doi.org/10.3171/2009.4.Jns081150>
- Nass, R. D., Hampel, K. G., Elger, C. E., & Surges, R. (2019). Blood Pressure in Seizures and Epilepsy. *Front Neurol*, 10, 501. <https://doi.org/10.3389/fneur.2019.00501>
- Neppl, R., Nguyen, C. M., Bowen, W., Al-Saadi, T., Pallagi, J., Morris, G., Mueller, W., Johnson, R., Prost, R., & Rand, S. D. (2001). In vivo detection of postictal perturbations of cerebral metabolism by use of proton MR spectroscopy: preliminary results in a canine model of prolonged generalized seizures. *AJNR Am J Neuroradiol*, 22(10), 1933-1943. <https://www.ncbi.nlm.nih.gov/pubmed/11733328>
- Ngai, A. C., Ko, K. R., Morii, S., & Winn, H. R. (1988). Effect of sciatic nerve stimulation on pial arterioles in rats. *Am J Physiol*, 254(1 Pt 2), H133-139. <https://doi.org/10.1152/ajpheart.1988.254.1.H133>
- Nguyen, D. K., Tremblay, J., Pouliot, P., Vannasing, P., Florea, O., Carmant, L., Lepore, F., Sawan, M., Lesage, F., & Lassonde, M. (2012). Non-invasive continuous EEG-fNIRS

- recording of temporal lobe seizures. *Epilepsy Res*, 99(1-2), 112-126.
<https://doi.org/10.1016/j.eplepsyres.2011.10.035>
- Nguyen, D. K., Tremblay, J., Pouliot, P., Vannasing, P., Florea, O., Carmant, L., Lepore, F., Sawan, M., Lesage, F., & Lassonde, M. (2013). Noninvasive continuous functional near-infrared spectroscopy combined with electroencephalography recording of frontal lobe seizures. *Epilepsia*, 54(2), 331-340. <https://doi.org/10.1111/epi.12011>
- Nguyen, H. D., Hong, K. S., & Shin, Y. I. (2016). Bundled-Optode Method in Functional Near-Infrared Spectroscopy. *PLoS One*, 11(10), e0165146.
<https://doi.org/10.1371/journal.pone.0165146>
- Nguyen, N., Milanfar, P., & Golub, G. (2001). A computationally efficient superresolution image reconstruction algorithm. *IEEE Trans Image Process*, 10(4), 573-583.
<https://doi.org/10.1109/83.913592>
- Nicolai, L. (1932). Über Sichtbarmachung, Verlauf und chemische Kinetik der Oxyhämoglobinreduktion im lebenden Gewebe, besonders in der menschlichen Haut. *Pflüger's Archiv für die gesamte Physiologie des Menschen und der Tiere*, 229(1), 372-384.
- Nikaina, I., Paterakis, K., Paraforos, G., Dardiotis, E., Chovas, A., Papadopoulos, D., Brotis, A., & Komnos, A. (2012). Cerebral perfusion pressure, microdialysis biochemistry, and clinical outcome in patients with spontaneous intracerebral hematomas. *J Crit Care*, 27(1), 83-88. <https://doi.org/10.1016/j.jcrc.2011.04.004>
- Nilsson, O. G., Brandt, L., Ungerstedt, U., & Säveland, H. (1999). Bedside detection of brain ischemia using intracerebral microdialysis: subarachnoid hemorrhage and delayed ischemic deterioration. *Neurosurgery*, 45(5), 1176-1184; discussion 1184-1175.
<https://doi.org/10.1097/00006123-199911000-00032>
- Novi, S. L., Forero, E. J., Rubianes Silva, J. A. I., de Souza, N., Martins, G. G., Quiroga, A., Wu, S. T., & Mesquita, R. C. (2020). Integration of Spatial Information Increases Reproducibility in Functional Near-Infrared Spectroscopy. *Front Neurosci*, 14, 746.
<https://doi.org/10.3389/fnins.2020.00746>
- Obrig, H. (2014). NIRS in clinical neurology - a 'promising' tool? *Neuroimage*, 85 Pt 1, 535-546.
<https://doi.org/10.1016/j.neuroimage.2013.03.045>

- Obrig, H., Neufang, M., Wenzel, R., Kohl, M., Steinbrink, J., Einhüpl, K., & Villringer, A. (2000). Spontaneous low frequency oscillations of cerebral hemodynamics and metabolism in human adults. *Neuroimage*, 12(6), 623-639.
<https://doi.org/10.1006/nimg.2000.0657>
- Oddo, M., & Bösel, J. (2014). Monitoring of brain and systemic oxygenation in neurocritical care patients. *Neurocrit Care*, 21 Suppl 2, S103-120. <https://doi.org/10.1007/s12028-014-0024-6>
- Oddo, M., Carrera, E., Claassen, J., Mayer, S. A., & Hirsch, L. J. (2009). Continuous electroencephalography in the medical intensive care unit. *Crit Care Med*, 37(6), 2051-2056. <https://doi.org/10.1097/CCM.0b013e3181a00604>
- Oddo, M., & Hutchinson, P. J. (2018). Understanding and monitoring brain injury: the role of cerebral microdialysis. *Intensive Care Med*, 44(11), 1945-1948.
<https://doi.org/10.1007/s00134-017-5031-6>
- Oddo, M., Levine, J. M., Kumar, M., Iglesias, K., Frangos, S., Maloney-Wilensky, E., & Le Roux, P. D. (2012). Anemia and brain oxygen after severe traumatic brain injury. *Intensive Care Med*, 38(9), 1497-1504. <https://doi.org/10.1007/s00134-012-2593-1>
- Oddo, M., Schmidt, J. M., Carrera, E., Badjatia, N., Connolly, E. S., Presciutti, M., Ostapkovich, N. D., Levine, J. M., Le Roux, P., & Mayer, S. A. (2008). Impact of tight glycemic control on cerebral glucose metabolism after severe brain injury: a microdialysis study. *Crit Care Med*, 36(12), 3233-3238. <https://doi.org/10.1097/CCM.0b013e31818f4026>
- Oddo, M., Villa, F., & Citerio, G. (2012). Brain multimodality monitoring: an update. *Curr Opin Crit Care*, 18(2), 111-118. <https://doi.org/10.1097/MCC.0b013e32835132a5>
- Olson, D. M., Stutzman, S., Saju, C., Wilson, M., Zhao, W., & Aiyagari, V. (2016). Interrater Reliability of Pupillary Assessments. *Neurocritical Care*, 24(2), 251-257.
<https://doi.org/10.1007/s12028-015-0182-1>
- Ortega-Martinez, A., Rogers, D. J., Anderson, J., Farzam, P., Gao, Y., Zimmermann, B., Yücel, M., & Boas, D. (2022). How much do time-domain functional near-infrared spectroscopy (fNIRS) moments improve estimation of brain activity over traditional fNIRS? *Neurophotonics*, 10(1), 013504. <https://doi.org/10.1117/1.NPh.10.1.013504>

- Owen-Reece, H., Elwell, C. E., Fallon, P., Goldstone, J., & Smith, M. (1994). Near infrared oximetry and near infrared spectroscopy. *Anaesthesia*, 49(12), 1102-1103. <https://doi.org/10.1111/j.1365-2044.1994.tb04380.x>
- Owen-Reece, H., Smith, M., Elwell, C. E., & Goldstone, J. C. (1999). Near infrared spectroscopy. *Br J Anaesth*, 82(3), 418-426. <https://doi.org/10.1093/bja/82.3.418>
- Özbay, P. S., Chang, C., Picchioni, D., Mandelkow, H., Chappel-Farley, M. G., van Gelderen, P., de Zwart, J. A., & Duyn, J. (2019). Sympathetic activity contributes to the fMRI signal. *Communications Biology*, 2(1), 421. <https://doi.org/10.1038/s42003-019-0659-0>
- Pacella, M., Ghosh, S., Middlebrook, E., Bennett, J., Bliznyuk, N., Huene, M., Copenhaver, N., Sura, L., & Weiss, M. D. (2020). Combined vEEG and Cerebral Oximetry Results to Determine the Severity of Hypoxic–Ischemic Encephalopathy. *Journal of Pediatric Neurology*, 18(02), 079-087. <https://doi.org/10.1055/s-0039-1687883>
- Papangelou, A., Zink, E. K., Chang, W.-T. W., Frattalone, A., Gergen, D., Gottschalk, A., & Geocadin, R. G. (2018). Automated Pupillometry and Detection of Clinical Transtentorial Brain Herniation: A Case Series. *Military Medicine*, 183(1-2), e113-e121. <https://doi.org/10.1093/milmed/usx018>
- Paraforou, T., Paterakis, K., Fountas, K., Paraforos, G., Chovas, A., Tasiou, A., Mpakopoulou, M., Papadopoulos, D., Karavellis, A., & Komnos, A. (2011). Cerebral perfusion pressure, microdialysis biochemistry and clinical outcome in patients with traumatic brain injury. *BMC Res Notes*, 4, 540. <https://doi.org/10.1186/1756-0500-4-540>
- Parvizi, J., & Kastner, S. (2018). Promises and limitations of human intracranial electroencephalography. *Nat Neurosci*, 21(4), 474-483. <https://doi.org/10.1038/s41593-018-0108-2>
- Patel, K. S., Zhao, M., Ma, H., & Schwartz, T. H. (2013). Imaging preictal hemodynamic changes in neocortical epilepsy. *Neurosurg Focus*, 34(4), E10. <https://doi.org/10.3171/2013.1.Focus12408>
- Paulson, O. B., Strandgaard, S., & Edvinsson, L. (1990). Cerebral autoregulation. *Cerebrovasc Brain Metab Rev*, 2(2), 161-192. <https://www.ncbi.nlm.nih.gov/pubmed/2201348>
- Peacock, S. H., & Tomlinson, A. D. (2018). Multimodal Neuromonitoring in Neurocritical Care. *AACN Adv Crit Care*, 29(2), 183-194. <https://doi.org/10.4037/aacnacc2018632>

- Pellegrino, G., Machado, A., von Ellenrieder, N., Watanabe, S., Hall, J. A., Lina, J. M., Kobayashi, E., & Grova, C. (2016). Hemodynamic Response to Interictal Epileptiform Discharges Addressed by Personalized EEG-fNIRS Recordings. *Front Neurosci*, 10, 102. <https://doi.org/10.3389/fnins.2016.00102>
- Pellerin, L., Bouzier-Sore, A. K., Aubert, A., Serres, S., Merle, M., Costalat, R., & Magistretti, P. J. (2007). Activity-dependent regulation of energy metabolism by astrocytes: an update. *Glia*, 55(12), 1251-1262. <https://doi.org/10.1002/glia.20528>
- Penfield, W. (1933). THE EVIDENCE FOR A CEREBRAL VASCULAR MECHANISM IN EPILEPSY. *Annals of Internal Medicine*, 7(3), 303-310. <https://doi.org/10.7326/0003-4819-7-3-303>
- Penfield, W., von S'ntha, K. I. n., & Cipriani, A. (1939). Cerebral Blood Flow during Induced Epileptiform Seizures in Animals and Man. *Journal of Neurophysiology*, 2(4), 257-267. <https://doi.org/10.1152/jn.1939.2.4.257>
- Peng, K., Nguyen, D. K., Tayah, T., Vannasing, P., Tremblay, J., Sawan, M., Lassonde, M., Lesage, F., & Pouliot, P. (2014). fNIRS-EEG study of focal interictal epileptiform discharges. *Epilepsy Res*, 108(3), 491-505. <https://doi.org/10.1016/j.eplepsyres.2013.12.011>
- Peng, K., Nguyen, D. K., Vannasing, P., Tremblay, J., Lesage, F., & Pouliot, P. (2016). Using patient-specific hemodynamic response function in epileptic spike analysis of human epilepsy: a study based on EEG-fNIRS. *Neuroimage*, 126, 239-255. <https://doi.org/10.1016/j.neuroimage.2015.11.045>
- Peng, K., Pouliot, P., Lesage, F., & Nguyen, D. K. (2016). Multichannel continuous electroencephalography-functional near-infrared spectroscopy recording of focal seizures and interictal epileptiform discharges in human epilepsy: a review. *Neurophotonics*, 3(3), 031402. <https://doi.org/10.1117/1.NPh.3.3.031402>
- Pereira de Vasconcelos, A., Ferrandon, A., & Nehlig, A. (2002). Local cerebral blood flow during lithium-pilocarpine seizures in the developing and adult rat: role of coupling between blood flow and metabolism in the genesis of neuronal damage. *J Cereb Blood Flow Metab*, 22(2), 196-205. <https://doi.org/10.1097/00004647-200202000-00007>
- Perera, K., Khan, S., Singh, S., Kromm, J., Wang, M., Sajobi, T., Jetté, N., Wiebe, S., & Josephson, C. B. (2022). EEG Patterns and Outcomes After Hypoxic Brain Injury: A

- Systematic Review and Meta-analysis. *Neurocrit Care*, 36(1), 292-301.
<https://doi.org/10.1007/s12028-021-01322-0>
- Perks, A., Cheema, S., & Mohanraj, R. (2012). Anaesthesia and epilepsy. *BJA: British Journal of Anaesthesia*, 108(4), 562-571. <https://doi.org/10.1093/bja/aes027>
- Persoon, S., Kappelle, L. J., & Klijn, C. J. (2010). Limb-shaking transient ischaemic attacks in patients with internal carotid artery occlusion: a case-control study. *Brain*, 133(Pt 3), 915-922. <https://doi.org/10.1093/brain/awq009>
- Perutz, M. (1995). Hoppe-Seyler, Stokes and haemoglobin. *Biol Chem Hoppe Seyler*, 376(8), 449-450. <https://doi.org/10.1515/bchm3.1995.376.8.449>
- Perutz, M. F. (1979). Regulation of Oxygen Affinity of Hemoglobin: Influence of Structure of the Globin on the Heme Iron. *Annual Review of Biochemistry*, 48(1), 327-386.
<https://doi.org/10.1146/annurev.bi.48.070179.001551>
- Perutz, M. F. (1980). Review Lecture: Stereochemical Mechanism of Oxygen Transport by Haemoglobin. *Proceedings of the Royal Society of London. Series B, Biological Sciences*, 208(1171), 135-162. <http://www.jstor.org/stable/35437>
- Pfeifer, M. D., Scholkmann, F., & Labruyère, R. (2018). Signal Processing in Functional Near-Infrared Spectroscopy (fNIRS): Methodological Differences Lead to Different Statistical Results [Original Research]. *Frontiers in Human Neuroscience*, 11, 641.
<https://doi.org/10.3389/fnhum.2017.00641>
- Phabphal, K., Chisurajinda, S., Somboon, T., Unwongse, K., & Geater, A. (2018). Does burst-suppression achieve seizure control in refractory status epilepticus? *BMC Neurol*, 18(1), 46. <https://doi.org/10.1186/s12883-018-1050-3>
- Pham, T., Tgavalekos, K., Sassaroli, A., Blaney, G., & Fantini, S. (2019). Quantitative measurements of cerebral blood flow with near-infrared spectroscopy. *Biomed Opt Express*, 10(4), 2117-2134. <https://doi.org/10.1364/boe.10.002117>
- Phillips, A. A., Chan, F. H., Zheng, M. M., Krassioukov, A. V., & Ainslie, P. N. (2016). Neurovascular coupling in humans: Physiology, methodological advances and clinical implications. *J Cereb Blood Flow Metab*, 36(4), 647-664.
<https://doi.org/10.1177/0271678x15617954>
- Piantadosi, C. A. (2007). Early development of near-infrared spectroscopy at Duke University. *J Biomed Opt*, 12(6), 062102. <https://doi.org/10.1117/1.2804925>

- Pillai, J., & Sperling, M. R. (2006). Interictal EEG and the diagnosis of epilepsy. *Epilepsia*, 47 Suppl 1, 14-22. <https://doi.org/10.1111/j.1528-1167.2006.00654.x>
- Pinti, P., Scholkmann, F., Hamilton, A., Burgess, P., & Tachtsidis, I. (2018). Current Status and Issues Regarding Pre-processing of fNIRS Neuroimaging Data: An Investigation of Diverse Signal Filtering Methods Within a General Linear Model Framework. *Front Hum Neurosci*, 12, 505. <https://doi.org/10.3389/fnhum.2018.00505>
- Piper, S. K., Krueger, A., Koch, S. P., Mehnert, J., Habermehl, C., Steinbrink, J., Obrig, H., & Schmitz, C. H. (2014). A wearable multi-channel fNIRS system for brain imaging in freely moving subjects. *Neuroimage*, 85 Pt 1(0 1), 64-71. <https://doi.org/10.1016/j.neuroimage.2013.06.062>
- Pittau, F., Dubeau, F., & Gotman, J. (2012). Contribution of EEG/fMRI to the definition of the epileptic focus. *Neurology*, 78(19), 1479-1487. <https://doi.org/10.1212/WNL.0b013e3182553bf7>
- Pittau, F., Fahoum, F., Zelmann, R., Dubeau, F., & Gotman, J. (2013). Negative BOLD response to interictal epileptic discharges in focal epilepsy. *Brain Topogr*, 26(4), 627-640. <https://doi.org/10.1007/s10548-013-0302-1>
- Pivovarov, A. S., Calahorra, F., & Walker, R. J. (2018). Na(+)/K(+)-pump and neurotransmitter membrane receptors. *Invert Neurosci*, 19(1), 1. <https://doi.org/10.1007/s10158-018-0221-7>
- Plichta, M. M., Herrmann, M. J., Baehne, C. G., Ehlis, A. C., Richter, M. M., Pauli, P., & Fallgatter, A. J. (2006). Event-related functional near-infrared spectroscopy (fNIRS): are the measurements reliable? *Neuroimage*, 31(1), 116-124. <https://doi.org/10.1016/j.neuroimage.2005.12.008>
- Plum, F., Howse, D. C., & Duffy, T. E. (1974). Metabolic effects of seizures. *Res Publ Assoc Res Nerv Ment Dis*, 53, 141-157. <https://www.ncbi.nlm.nih.gov/pubmed/4373805>
- Pohlmann-Eden, B., Hoch, D. B., Cochius, J. I., & Chiappa, K. H. (1996). Periodic lateralized epileptiform discharges--a critical review. *J Clin Neurophysiol*, 13(6), 519-530. <https://doi.org/10.1097/00004691-199611000-00007>
- Ponce, L. L., Pillai, S., Cruz, J., Li, X., Julia, H., Gopinath, S., & Robertson, C. S. (2012). Position of probe determines prognostic information of brain tissue PO2 in severe

- traumatic brain injury. *Neurosurgery*, 70(6), 1492-1502; discussion 1502-1493.
<https://doi.org/10.1227/NEU.0b013e31824ce933>
- Popp, J. (2011). Journal of Biophotonics is growing up. *J Biophotonics*, 4(1-2), 8.
<https://doi.org/10.1002/jbio.201000525>
- Pouliot, P., Tran, T. P., Birca, V., Vannasing, P., Tremblay, J., Lassonde, M., & Nguyen, D. K. (2014). Hemodynamic changes during posterior epilepsies: an EEG-fNIRS study. *Epilepsy Res*, 108(5), 883-890. <https://doi.org/10.1016/j.eplespsyres.2014.03.007>
- Pouliot, P., Tremblay, J., Robert, M., Vannasing, P., Lepore, F., Lassonde, M., Sawan, M., Nguyen, D. K., & Lesage, F. (2012). Nonlinear hemodynamic responses in human epilepsy: a multimodal analysis with fNIRS-EEG and fMRI-EEG. *J Neurosci Methods*, 204(2), 326-340. <https://doi.org/10.1016/j.jneumeth.2011.11.016>
- Powers, S. K., Dodd, S., Criswell, D. D., Lawler, J., Martin, D., & Grinton, S. (1991). Evidence for an alveolar-arterial PO₂ gradient threshold during incremental exercise. *Int J Sports Med*, 12(3), 313-318. <https://doi.org/10.1055/s-2007-1024688>
- Powers, W. J., Hirsch, I. B., & Cryer, P. E. (1996). Effect of stepped hypoglycemia on regional cerebral blood flow response to physiological brain activation. *Am J Physiol*, 270(2 Pt 2), H554-559. <https://doi.org/10.1152/ajpheart.1996.270.2.H554>
- Prager, O., Kamintsky, L., Hasam-Henderson, L. A., Schoknecht, K., Wuntke, V., Papageorgiou, I., Swolinsky, J., Muoio, V., Bar-Klein, G., Vazana, U., Heinemann, U., Friedman, A., & Kovács, R. (2019). Seizure-induced microvascular injury is associated with impaired neurovascular coupling and blood–brain barrier dysfunction. *Epilepsia*, 60(2), 322-336. <https://doi.org/https://doi.org/10.1111/epi.14631>
- Pujol, J., Deus, J., Losilla, J. M., & Capdevila, A. (1999). Cerebral lateralization of language in normal left-handed people studied by functional MRI. *Neurology*, 52(5), 1038-1043. <https://doi.org/10.1212/wnl.52.5.1038>
- Putze, F., Hesslinger, S., Tse, C. Y., Huang, Y., Herff, C., Guan, C., & Schultz, T. (2014). Hybrid fNIRS-EEG based classification of auditory and visual perception processes. *Front Neurosci*, 8, 373. <https://doi.org/10.3389/fnins.2014.00373>
- Quaresima, V., & Ferrari, M. (2019). A Mini-Review on Functional Near-Infrared Spectroscopy (fNIRS): Where Do We Stand, and Where Should We Go? *Photonics*, 6(3), 87. <https://www.mdpi.com/2304-6732/6/3/87>

- Rabinowicz, A. L., Correale, J. D., Bracht, K. A., Smith, T. D., & DeGiorgio, C. M. (1995). Neuron-Specific Enolase Is Increased After Nonconvulsive Status Epilepticus. *Epilepsia*, 36(5), 475-479. <https://doi.org/10.1111/j.1528-1157.1995.tb00489.x>
- Raichle, M. E., MacLeod, A. M., Snyder, A. Z., Powers, W. J., Gusnard, D. A., & Shulman, G. L. (2001). A default mode of brain function. *Proc Natl Acad Sci U S A*, 98(2), 676-682. <https://doi.org/10.1073/pnas.98.2.676>
- Ramakrishna, R., Stiefel, M., Udoetuk, J., Spiotta, A., Levine, J. M., Kofke, W. A., Zager, E., Yang, W., & Leroux, P. (2008). Brain oxygen tension and outcome in patients with aneurysmal subarachnoid hemorrhage. *J Neurosurg*, 109(6), 1075-1082. <https://doi.org/10.3171/jns.2008.109.12.1075>
- Rathore, C., & Radhakrishnan, K. (2015). Concept of epilepsy surgery and presurgical evaluation. *Epileptic Disord*, 17(1), 19-31; quiz 31. <https://doi.org/10.1684/epd.2014.0720>
- Ravussin, P., & de Tribolet, N. (1993). Total intravenous anesthesia with propofol for burst suppression in cerebral aneurysm surgery: preliminary report of 42 patients. *Neurosurgery*, 32(2), 236-240 discussion 240. <https://doi.org/10.1227/00006123-199302000-00013>
- Reagan, E. M., Nguyen, R. T., Ravishankar, S. T., Chabra, V., Fuentes, B., Spiegel, R., & Parnia, S. (2018). Monitoring the Relationship Between Changes in Cerebral Oxygenation and Electroencephalography Patterns During Cardiopulmonary Resuscitation: A Feasibility Study. *Crit Care Med*, 46(5), 757-763. <https://doi.org/10.1097/ccm.0000000000003014>
- Robba, C., Goffi, A., Geeraerts, T., Cardim, D., Via, G., Czosnyka, M., Park, S., Sarwal, A., Padayachy, L., Rasulo, F., & Citerio, G. (2019). Brain ultrasonography: methodology, basic and advanced principles and clinical applications. A narrative review. *Intensive Care Med*, 45(7), 913-927. <https://doi.org/10.1007/s00134-019-05610-4>
- Robertson, F. C., Douglas, T. S., & Meintjes, E. M. (2010). Motion artifact removal for functional near infrared spectroscopy: a comparison of methods. *IEEE Trans Biomed Eng*, 57(6), 1377-1387. <https://doi.org/10.1109/tbme.2009.2038667>
- Roche-Labarbe, N., Wallois, F., Ponchel, E., Kongolo, G., & Grebe, R. (2007). Coupled oxygenation oscillation measured by NIRS and intermittent cerebral activation on EEG in

- premature infants. *Neuroimage*, 36(3), 718-727.
<https://doi.org/10.1016/j.neuroimage.2007.04.002>
- Roche-Labarbe, N., Zaaïmi, B., Berquin, P., Nehlig, A., Grebe, R., & Wallois, F. (2008). NIRS-measured oxy- and deoxyhemoglobin changes associated with EEG spike-and-wave discharges in children. *Epilepsia*, 49(11), 1871-1880. <https://doi.org/10.1111/j.1528-1167.2008.01711.x>
- Rossetti, A. O. (2017). Clinical neurophysiology for neurological prognostication of comatose patients after cardiac arrest. *Clin Neurophysiol Pract*, 2, 76-80.
<https://doi.org/10.1016/j.cnp.2017.03.001>
- Rossetti, A. O., Logroscino, G., & Bromfield, E. B. (2005). Refractory status epilepticus: effect of treatment aggressiveness on prognosis. *Arch Neurol*, 62(11), 1698-1702.
<https://doi.org/10.1001/archneur.62.11.1698>
- Rossetti, A. O., Oddo, M., Logroscino, G., & Kaplan, P. W. (2010). Prognostication after cardiac arrest and hypothermia: a prospective study. *Ann Neurol*, 67(3), 301-307.
<https://doi.org/10.1002/ana.21984>
- Rossetti, A. O., Schindler, K., Sutter, R., Rüegg, S., Zubler, F., Novy, J., Oddo, M., Warpelin-Decrausaz, L., & Alvarez, V. (2020). Continuous vs Routine Electroencephalogram in Critically Ill Adults With Altered Consciousness and No Recent Seizure: A Multicenter Randomized Clinical Trial. *JAMA Neurol*, 77(10), 1225-1232.
<https://doi.org/10.1001/jamaneurol.2020.2264>
- Rossetti, A. O., Urbano, L. A., Delodder, F., Kaplan, P. W., & Oddo, M. (2010). Prognostic value of continuous EEG monitoring during therapeutic hypothermia after cardiac arrest. *Crit Care*, 14(5), R173. <https://doi.org/10.1186/cc9276>
- Rostrup, E., Law, I., Pott, F., Ide, K., & Knudsen, G. M. (2002). Cerebral hemodynamics measured with simultaneous PET and near-infrared spectroscopy in humans. *Brain Res*, 954(2), 183-193. [https://doi.org/10.1016/s0006-8993\(02\)03246-8](https://doi.org/10.1016/s0006-8993(02)03246-8)
- Rouach, N., Koulakoff, A., Abudara, V., Willecke, K., & Giaume, C. (2008). Astroglial metabolic networks sustain hippocampal synaptic transmission. *Science*, 322(5907), 1551-1555. <https://doi.org/10.1126/science.1164022>

- Saager, R. B., & Berger, A. J. (2005). Direct characterization and removal of interfering absorption trends in two-layer turbid media. *J Opt Soc Am A Opt Image Sci Vis*, 22(9), 1874-1882. <https://doi.org/10.1364/josaa.22.001874>
- Saager, R. B., Telleri, N. L., & Berger, A. J. (2011). Two-detector Corrected Near Infrared Spectroscopy (C-NIRS) detects hemodynamic activation responses more robustly than single-detector NIRS. *Neuroimage*, 55(4), 1679-1685. <https://doi.org/10.1016/j.neuroimage.2011.01.043>
- Sacktor, B., Wilson, J. E., & Tiekert, C. G. (1966). Regulation of glycolysis in brain, in situ, during convulsions. *J Biol Chem*, 241(21), 5071-5075. <https://www.ncbi.nlm.nih.gov/pubmed/4380842>
- Safaie, J., Grebe, R., Abrishami Moghaddam, H., & Wallois, F. (2013). Toward a fully integrated wireless wearable EEG-NIRS bimodal acquisition system. *J Neural Eng*, 10(5), 056001. <https://doi.org/10.1088/1741-2560/10/5/056001>
- Sager, S., Ergül, N., Ciftci, H., Cetin, G., Güner, S. I., & Cermik, T. F. (2011). The value of FDG PET/CT in the initial staging and bone marrow involvement of patients with multiple myeloma. *Skeletal Radiol*, 40(7), 843-847. <https://doi.org/10.1007/s00256-010-1088-9>
- Saito, S., Yoshikawa, D., Nishihara, F., Morita, T., Kitani, Y., Amaya, T., & Fujita, T. (1995). The cerebral hemodynamic response to electrically induced seizures in man. *Brain Res*, 673(1), 93-100. [https://doi.org/10.1016/0006-8993\(94\)01408-a](https://doi.org/10.1016/0006-8993(94)01408-a)
- Sakakibara, E., Takahashi, Y., Murata, Y., Taniguchi, G., Sone, D., & Watanabe, M. (2014). Chronic periodic lateralised epileptic discharges and anti-N-methyl-D-aspartate receptor antibodies. *Epileptic Disord*, 16(2), 218-222. <https://doi.org/10.1684/epd.2014.0655>
- Salek-Haddadi, A., Diehl, B., Hamandi, K., Merschhemke, M., Liston, A., Friston, K., Duncan, J. S., Fish, D. R., & Lemieux, L. (2006). Hemodynamic correlates of epileptiform discharges: an EEG-fMRI study of 63 patients with focal epilepsy. *Brain Res*, 1088(1), 148-166. <https://doi.org/10.1016/j.brainres.2006.02.098>
- Salek-Haddadi, A., Merschhemke, M., Lemieux, L., & Fish, D. R. (2002). Simultaneous EEG-Correlated Ictal fMRI. *Neuroimage*, 16(1), 32-40. <https://doi.org/10.1006/nimg.2002.1073>

- Salinet, A. S., Robinson, T. G., & Panerai, R. B. (2013). Cerebral blood flow response to neural activation after acute ischemic stroke: a failure of myogenic regulation? *J Neurol*, 260(10), 2588-2595. <https://doi.org/10.1007/s00415-013-7022-z>
- Samraj, R. S., & Nicolas, L. (2015). Near infrared spectroscopy (NIRS) derived tissue oxygenation in critical illness. *Clin Invest Med*, 38(5), E285-295. <https://doi.org/10.25011/cim.v38i5.25685>
- Sánchez Fernández, I., Goodkin, H. P., & Scott, R. C. (2019). Pathophysiology of convulsive status epilepticus. *Seizure*, 68, 16-21. <https://doi.org/10.1016/j.seizure.2018.08.002>
- Sandroni, C., Citerio, G., & Taccone, F. S. (2022). Automated pupillometry in intensive care. *Intensive Care Med*, 48(10), 1467-1470. <https://doi.org/10.1007/s00134-022-06772-4>
- Sandroni, C., Cronberg, T., & Sekhon, M. (2021). Brain injury after cardiac arrest: pathophysiology, treatment, and prognosis. *Intensive Care Medicine*, 47(12), 1393-1414. <https://doi.org/10.1007/s00134-021-06548-2>
- Santosa, H., Fishburn, F., Zhai, X., & Huppert, T. J. (2019). Investigation of the sensitivity-specificity of canonical- and deconvolution-based linear models in evoked functional near-infrared spectroscopy. *Neurophotonics*, 6(2), 025009. <https://doi.org/10.1117/1.NPh.6.2.025009>
- Santosa, H., Hong, M. J., Kim, S. P., & Hong, K. S. (2013). Noise reduction in functional near-infrared spectroscopy signals by independent component analysis. *Rev Sci Instrum*, 84(7), 073106. <https://doi.org/10.1063/1.4812785>
- Sappia, M. S., Hakimi, N., Colier, W., & Horschig, J. M. (2020). Signal quality index: an algorithm for quantitative assessment of functional near infrared spectroscopy signal quality. *Biomed Opt Express*, 11(11), 6732-6754. <https://doi.org/10.1364/boe.409317>
- Sato, H., Kiguchi, M., Kawaguchi, F., & Maki, A. (2004). Practicality of wavelength selection to improve signal-to-noise ratio in near-infrared spectroscopy. *Neuroimage*, 21(4), 1554-1562. <https://doi.org/10.1016/j.neuroimage.2003.12.017>
- Sato, Y., Uzuka, T., Aoki, H., Natsumeda, M., Oishi, M., Fukuda, M., & Fujii, Y. (2012). Near-infrared spectroscopic study and the Wada test for presurgical evaluation of expressive and receptive language functions in glioma patients: with a case report of dissociated language functions. *Neurosci Lett*, 510(2), 104-109. <https://doi.org/10.1016/j.neulet.2012.01.011>

- Savic, I., Altshuler, L., Baxter, L., & Engel, J., Jr. (1997). Pattern of interictal hypometabolism in PET scans with fludeoxyglucose F 18 reflects prior seizure types in patients with mesial temporal lobe seizures. *Arch Neurol*, 54(2), 129-136.
<https://doi.org/10.1001/archneur.1997.00550140011006>
- Sawan, M., Salam, M. T., Le Lan, J., Kassab, A., Gelinas, S., Vannasing, P., Lesage, F., Lassonde, M., & Nguyen, D. K. (2013). Wireless recording systems: from noninvasive EEG-NIRS to invasive EEG devices. *IEEE Trans Biomed Circuits Syst*, 7(2), 186-195.
<https://doi.org/10.1109/tbcas.2013.2255595>
- Scarapicchia, V., Brown, C., Mayo, C., & Gawryluk, J. R. (2017). Functional Magnetic Resonance Imaging and Functional Near-Infrared Spectroscopy: Insights from Combined Recording Studies [Review]. *Frontiers in Human Neuroscience*, 11, 419.
<https://doi.org/10.3389/fnhum.2017.00419>
- Schecklmann, M., Mann, A., Langguth, B., Ehlis, A. C., Fallgatter, A. J., & Haeussinger, F. B. (2017). The Temporal Muscle of the Head Can Cause Artifacts in Optical Imaging Studies with Functional Near-Infrared Spectroscopy. *Front Hum Neurosci*, 11, 456.
<https://doi.org/10.3389/fnhum.2017.00456>
- Scher, M. (2001). Perinatal asphyxia: Timing and mechanisms of injury in neonatal encephalopathy. *Current Neurology and Neuroscience Reports*, 1(2), 175-184.
<https://doi.org/10.1007/s11910-001-0014-x>
- Schoknecht, K., Berndt, N., Rösner, J., Heinemann, U., Dreier, J. P., Kovács, R., Friedman, A., & Liotta, A. (2017). Event-Associated Oxygen Consumption Rate Increases ca. Five-Fold When Interictal Activity Transforms into Seizure-Like Events In Vitro. *Int J Mol Sci*, 18(9). <https://doi.org/10.3390/ijms18091925>
- Scholkmann, F., Gerber, U., Wolf, M., & Wolf, U. (2013). End-tidal CO₂: an important parameter for a correct interpretation in functional brain studies using speech tasks. *Neuroimage*, 66, 71-79. <https://doi.org/10.1016/j.neuroimage.2012.10.025>
- Scholkmann, F., Kleiser, S., Metz, A. J., Zimmermann, R., Mata Pavia, J., Wolf, U., & Wolf, M. (2014). A review on continuous wave functional near-infrared spectroscopy and imaging instrumentation and methodology. *Neuroimage*, 85 Pt 1, 6-27.
<https://doi.org/10.1016/j.neuroimage.2013.05.004>

- Scholkmann, F., Metz, A. J., & Wolf, M. (2014). Measuring tissue hemodynamics and oxygenation by continuous-wave functional near-infrared spectroscopy--how robust are the different calculation methods against movement artifacts? *Physiol Meas*, 35(4), 717-734. <https://doi.org/10.1088/0967-3334/35/4/717>
- Scholkmann, F., Spichtig, S., Muehlemann, T., & Wolf, M. (2010). How to detect and reduce movement artifacts in near-infrared imaging using moving standard deviation and spline interpolation. *Physiol Meas*, 31(5), 649-662. <https://doi.org/10.1088/0967-3334/31/5/004>
- Scholkmann, F., Tachtsidis, I., Wolf, M., & Wolf, U. (2022). Systemic physiology augmented functional near-infrared spectroscopy: a powerful approach to study the embodied human brain. *Neurophotonics*, 9(3), 030801. <https://doi.org/10.1117/1.NPh.9.3.030801>
- Scholkmann, F., & Wolf, M. (2013). General equation for the differential pathlength factor of the frontal human head depending on wavelength and age. *J Biomed Opt*, 18(10), 105004. <https://doi.org/10.1117/1.Jbo.18.10.105004>
- Scholkmann, F., Wolf, M., & Wolf, U. (2013). The effect of inner speech on arterial CO₂ and cerebral hemodynamics and oxygenation: a functional NIRS study. *Adv Exp Med Biol*, 789, 81-87. https://doi.org/10.1007/978-1-4614-7411-1_12
- Schomer, D. L., & Lopes da Silva, F. H. (2017). *Niedermeyer's Electroencephalography: Basic Principles, Clinical Applications, and Related Fields*. Oxford University Press. <https://doi.org/10.1093/med/9780190228484.001.0001>
- Schur, S., Allen, V., White, A., Mirsky, D., Stence, N., O'Neill, B., Handler, M., Dudley, R., & Laoprasert, P. (2018). Significance of FDG-PET Hypermetabolism in Children with Intractable Focal Epilepsy. *Pediatr Neurosurg*, 53(3), 153-162. <https://doi.org/10.1159/000487088>
- Schurr, A., Miller, J. J., Payne, R. S., & Rigor, B. M. (1999). An increase in lactate output by brain tissue serves to meet the energy needs of glutamate-activated neurons. *J Neurosci*, 19(1), 34-39. <https://doi.org/10.1523/jneurosci.19-01-00034.1999>
- Schurr, A., Payne, R. S., Miller, J. J., & Rigor, B. M. (1997). Brain lactate, not glucose, fuels the recovery of synaptic function from hypoxia upon reoxygenation: an in vitro study. *Brain Res*, 744(1), 105-111. [https://doi.org/10.1016/s0006-8993\(96\)01106-7](https://doi.org/10.1016/s0006-8993(96)01106-7)

- Schurr, A., West, C. A., & Rigor, B. M. (1988). Lactate-supported synaptic function in the rat hippocampal slice preparation. *Science*, 240(4857), 1326-1328.
<https://doi.org/10.1126/science.3375817>
- Schwartz, A. E., Tuttle, R. H., & Poppers, P. J. (1989). Electroencephalographic Burst Suppression in Elderly and Young Patients Anesthetized with Isoflurane. *Anesthesia & Analgesia*, 68(1), 9-12. https://journals.lww.com/anesthesia-analgesia/Fulltext/1989/01000/Electroencephalographic_Burst_Suppression_in.3.aspx
- Schwartz, T. H. (2007). Neurovascular coupling and epilepsy: hemodynamic markers for localizing and predicting seizure onset. *Epilepsy Curr*, 7(4), 91-94.
<https://doi.org/10.1111/j.1535-7511.2007.00183.x>
- Schweiger, M., & Arridge, S. (2003). Image reconstruction in optical tomography using local basis functions. *Journal of Electronic Imaging*, 12(4). <https://doi.org/10.1117/1.1586919>
- Seghier, M. L. (2008). Laterality index in functional MRI: methodological issues. *Magn Reson Imaging*, 26(5), 594-601. <https://doi.org/10.1016/j.mri.2007.10.010>
- Sekar, K., Schiff, N. D., Labar, D., & Forgacs, P. B. (2019). Spectral Content of Electroencephalographic Burst-Suppression Patterns May Reflect Neuronal Recovery in Comatose Post-Cardiac Arrest Patients. *J Clin Neurophysiol*, 36(2), 119-126.
<https://doi.org/10.1097/wnp.0000000000000536>
- Selb, J., Wu, K. C., Sutin, J., Lin, P. I., Farzam, P., Bechek, S., Shenoy, A., Patel, A. B., Boas, D. A., Franceschini, M. A., & Rosenthal, E. S. (2018). Prolonged monitoring of cerebral blood flow and autoregulation with diffuse correlation spectroscopy in neurocritical care patients. *Neurophotonics*, 5(4), 045005. <https://doi.org/10.1117/1.NPh.5.4.045005>
- Seule, M., Keller, E., Unterberg, A., & Sakowitz, O. (2015). The Hemodynamic Response of Spreading Depolarization Observed by Near Infrared Spectroscopy After Aneurysmal Subarachnoid Hemorrhage. *Neurocrit Care*, 23(1), 108-112.
<https://doi.org/10.1007/s12028-015-0111-3>
- Severinghaus, J. W. (2007). Takuo Aoyagi: discovery of pulse oximetry. *Anesth Analg*, 105(6 Suppl), S1-s4. <https://doi.org/10.1213/01.ane.0000269514.31660.09>
- Severinghaus, J. W., & Astrup, P. B. (1986). History of blood gas analysis. VI. Oximetry. *Journal of Clinical Monitoring*, 2(4), 270-288. <https://doi.org/10.1007/BF02851177>

- Shanker, A., Abel, J. H., Schamberg, G., & Brown, E. N. (2021). Etiology of Burst Suppression EEG Patterns [Perspective]. *Frontiers in Psychology*, 12, 673529. <https://doi.org/10.3389/fpsyg.2021.673529>
- Sharbrough, F. W., Messick, J. M., Jr., & Sundt, T. M., Jr. (1973). Correlation of continuous electroencephalograms with cerebral blood flow measurements during carotid endarterectomy. *Stroke*, 4(4), 674-683. <https://doi.org/10.1161/01.str.4.4.674>
- Shimogawa, T., Morioka, T., Sayama, T., Haga, S., Kanazawa, Y., Murao, K., Arakawa, S., Sakata, A., & Iihara, K. (2017). The initial use of arterial spin labeling perfusion and diffusion-weighted magnetic resonance images in the diagnosis of nonconvulsive partial status epileptics. *Epilepsy Res*, 129, 162-173. <https://doi.org/10.1016/j.eplepsyres.2016.12.008>
- Shinohara, Y., Minematsu, K., Amano, T., & Ohashi, Y. (2006). Modified Rankin scale with expanded guidance scheme and interview questionnaire: interrater agreement and reproducibility of assessment. *Cerebrovasc Dis*, 21(4), 271-278. <https://doi.org/10.1159/000091226>
- Shorvon, S. D. (2011). The etiologic classification of epilepsy. *Epilepsia*, 52(6), 1052-1057. <https://doi.org/10.1111/j.1528-1167.2011.03041.x>
- Siclari, F., Prior, J. O., & Rossetti, A. O. (2013). Ictal cerebral positron emission tomography (PET) in focal status epilepticus. *Epilepsy Res*, 105(3), 356-361. <https://doi.org/10.1016/j.eplepsyres.2013.03.006>
- Siesjö, B. K. (1978). *Brain energy metabolism*. John Wiley & Sons.
- Silas, R., Sehgal, A., Walker, A. M., & Wong, F. Y. (2012). Cerebral oxygenation during subclinical seizures in neonatal hypoxic-ischaemic encephalopathy. *Eur J Paediatr Neurol*, 16(3), 304-307. <https://doi.org/10.1016/j.ejpn.2011.09.003>
- Silverman, D. G., Jotkowitz, A. B., Freemer, M., Gutter, V., O'Connor, T. Z., & Braverman, I. M. (1994). Peripheral assessment of phenylephrine-induced vasoconstriction by laser Doppler flowmetry and its potential relevance to homeostatic mechanisms. *Circulation*, 90(1), 23-26. <https://doi.org/10.1161/01.cir.90.1.23>
- Simon, R. P., Aminoff, M. J., & Benowitz, N. L. (1984). Changes in plasma catecholamines after tonic-clonic seizures. *Neurology*, 34(2), 255-257. <https://doi.org/10.1212/wnl.34.2.255>

- Singh, A. K., & Dan, I. (2006). Exploring the false discovery rate in multichannel NIRS. *Neuroimage*, 33(2), 542-549. <https://doi.org/10.1016/j.neuroimage.2006.06.047>
- Singh, H., Cooper, R., Lee, C. W., Dempsey, L., Brigadoi, S., Edwards, A., Airantzis, D., Everdell, N., Michell, A., Holder, D., Austin, T., & Hebden, J. (2016). Neurovascular Interactions in the Neurologically Compromised Neonatal Brain. *Adv Exp Med Biol*, 876, 485-492. https://doi.org/10.1007/978-1-4939-3023-4_61
- Sirpal, P., Damseh, R., Peng, K., Nguyen, D. K., & Lesage, F. (2022). Multimodal Autoencoder Predicts fNIRS Resting State From EEG Signals. *Neuroinformatics*, 20(3), 537-558. <https://doi.org/10.1007/s12021-021-09538-3>
- Sirpal, P., Kassab, A., Pouliot, P., Nguyen, D. K., & Lesage, F. (2019). fNIRS improves seizure detection in multimodal EEG-fNIRS recordings. *J Biomed Opt*, 24(5), 1-9. <https://doi.org/10.1117/1.Jbo.24.5.051408>
- Sokol, D. K., Markand, O. N., Daly, E. C., Luerssen, T. G., & Malkoff, M. D. (2000). Near infrared spectroscopy (NIRS) distinguishes seizure types. *Seizure*, 9(5), 323-327. <https://doi.org/10.1053/seiz.2000.0406>
- Sokoloff, M. D., Plegue, M. A., Chervin, R. D., Barks, J. D., & Shellhaas, R. A. (2015). Phenobarbital and neonatal seizures affect cerebral oxygen metabolism: a near-infrared spectroscopy study. *Pediatr Res*, 78(1), 91-96. <https://doi.org/10.1038/pr.2015.64>
- Solaini, G., Baracca, A., Lenaz, G., & Sgarbi, G. (2010). Hypoxia and mitochondrial oxidative metabolism. *Biochimica et Biophysica Acta (BBA) - Bioenergetics*, 1797(6), 1171-1177. <https://doi.org/https://doi.org/10.1016/j.bbabi.2010.02.011>
- Sorensen, L. C., & Greisen, G. (2006). Precision of measurement of cerebral tissue oxygenation index using near-infrared spectroscopy in preterm neonates. *J Biomed Opt*, 11(5), 054005. <https://doi.org/10.1117/1.2357730>
- Soul, J. S., Taylor, G. A., Wypij, D., Duplessis, A. J., & Volpe, J. J. (2000). Noninvasive detection of changes in cerebral blood flow by near-infrared spectroscopy in a piglet model of hydrocephalus. *Pediatr Res*, 48(4), 445-449. <https://doi.org/10.1203/00006450-200010000-00005>
- Spiotta, A. M., Stiefel, M. F., Gracias, V. H., Garuffe, A. M., Kofke, W. A., Maloney-Wilensky, E., Troxel, A. B., Levine, J. M., & Le Roux, P. D. (2010). Brain tissue oxygen-directed

- management and outcome in patients with severe traumatic brain injury. *J Neurosurg*, 113(3), 571-580. <https://doi.org/10.3171/2010.1.Jns09506>
- Springer, J. A., Binder, J. R., Hammeke, T. A., Swanson, S. J., Frost, J. A., Bellgowan, P. S., Brewer, C. C., Perry, H. M., Morris, G. L., & Mueller, W. M. (1999). Language dominance in neurologically normal and epilepsy subjects: a functional MRI study. *Brain*, 122 (Pt 11), 2033-2046. <https://doi.org/10.1093/brain/122.11.2033>
- Squire, J. (1940). Instrument for measuring quantity of blood and its degree of oxygenation in web of the hand. *Clin Sci*, 4, 331-339.
- Stafstrom, C. E., & Carmant, L. (2015). Seizures and epilepsy: an overview for neuroscientists. *Cold Spring Harb Perspect Med*, 5(6). <https://doi.org/10.1101/cshperspect.a022426>
- Stecker, M. M., Cheung, A. T., Pochettino, A., Kent, G. P., Patterson, T., Weiss, S. J., & Bavaria, J. E. (2001). Deep hypothermic circulatory arrest: I. Effects of cooling on electroencephalogram and evoked potentials. *Ann Thorac Surg*, 71(1), 14-21. [https://doi.org/10.1016/s0003-4975\(00\)01592-7](https://doi.org/10.1016/s0003-4975(00)01592-7)
- Stefanovic, B., Warnking, J. M., & Pike, G. B. (2004). Hemodynamic and metabolic responses to neuronal inhibition. *Neuroimage*, 22(2), 771-778. <https://doi.org/10.1016/j.neuroimage.2004.01.036>
- Steinhoff, B. J., Herrendorf, G., & Kurth, C. (1996). Ictal near infrared spectroscopy in temporal lobe epilepsy: a pilot study. *Seizure*, 5(2), 97-101. <https://www.ncbi.nlm.nih.gov/pubmed/8795123>
- Stockard, J. J., Bickford, R. G., & Aung, M. (1975). The electroencephalogram in traumatic brain injury. *Handbook of clinical neurology*, 23(part I), 217-367.
- Strangman, G., Boas, D. A., & Sutton, J. P. (2002). Non-invasive neuroimaging using near-infrared light. *Biol Psychiatry*, 52(7), 679-693. [https://doi.org/10.1016/s0006-3223\(02\)01550-0](https://doi.org/10.1016/s0006-3223(02)01550-0)
- Strangman, G., Franceschini, M. A., & Boas, D. A. (2003). Factors affecting the accuracy of near-infrared spectroscopy concentration calculations for focal changes in oxygenation parameters. *Neuroimage*, 18(4), 865-879. [https://doi.org/10.1016/s1053-8119\(03\)00021-1](https://doi.org/10.1016/s1053-8119(03)00021-1)
- Strangman, G., Goldstein, R., Rauch, S. L., & Stein, J. (2006). Near-infrared spectroscopy and imaging for investigating stroke rehabilitation: test-retest reliability and review of the

- literature. *Arch Phys Med Rehabil*, 87(12 Suppl 2), S12-19.
<https://doi.org/10.1016/j.apmr.2006.07.269>
- Strangman, G. E., Li, Z., & Zhang, Q. (2013). Depth sensitivity and source-detector separations for near infrared spectroscopy based on the Colin27 brain template. *PLoS One*, 8(8), e66319. <https://doi.org/10.1371/journal.pone.0066319>
- Strangman, G. E., Zhang, Q., & Li, Z. (2014). Scalp and skull influence on near infrared photon propagation in the Colin27 brain template. *Neuroimage*, 85 Pt 1, 136-149.
<https://doi.org/10.1016/j.neuroimage.2013.04.090>
- Strohm, T., Steriade, C., Wu, G., Hantus, S., Rae-Grant, A., & Larvie, M. (2019). FDG-PET and MRI in the Evolution of New-Onset Refractory Status Epilepticus. *AJNR Am J Neuroradiol*, 40(2), 238-244. <https://doi.org/10.3174/ajnr.A5929>
- Struck, A. F., Westover, M. B., Hall, L. T., Deck, G. M., Cole, A. J., & Rosenthal, E. S. (2016). Metabolic Correlates of the Ictal-Interictal Continuum: FDG-PET During Continuous EEG. *Neurocrit Care*, 24(3), 324-331. <https://doi.org/10.1007/s12028-016-0245-y>
- Sudakou, A., Lange, F., Isler, H., Lanka, P., Wojtkiewicz, S., Sawosz, P., Ostojic, D., Wolf, M., Pifferi, A., Tachtsidis, I., Liebert, A., & Gerega, A. (2021). Time-domain NIRS system based on supercontinuum light source and multi-wavelength detection: validation for tissue oxygenation studies. *Biomed Opt Express*, 12(10), 6629-6650.
<https://doi.org/10.1364/boe.431301>
- Sutin, J., Chang, C., Boas, D., Brown, E., & Franceschini, M. A. (2014, 2014/04/26). Diffuse Optical Spectroscopy Measurement Of Cerebral Hemodynamics And Oxygen Metabolism During Anesthesia-Induced Burst Suppression In Rats. OSA Technical Digest (online) Biomedical Optics 2014, Miami, Florida.
- Tachtsidis, I., Leung, T. S., Chopra, A., Koh, P. H., Reid, C. B., & Elwell, C. E. (2009). False positives in functional near-infrared topography. *Adv Exp Med Biol*, 645, 307-314.
https://doi.org/10.1007/978-0-387-85998-9_46
- Tachtsidis, I., & Scholkmann, F. (2016). False positives and false negatives in functional near-infrared spectroscopy: issues, challenges, and the way forward. *Neurophotonics*, 3(3), 031405. <https://doi.org/10.1117/1.NPh.3.3.031405>
- Tachtsidis, I., Tisdall, M., Delpy, D. T., Smith, M., & Elwell, C. E. (2008). Measurement of cerebral tissue oxygenation in young healthy volunteers during acetazolamide

- provocation: a transcranial Doppler and near-infrared spectroscopy investigation. *Adv Exp Med Biol*, 614, 389-396. https://doi.org/10.1007/978-0-387-74911-2_43
- Tadel, F., Baillet, S., Mosher, J. C., Pantazis, D., & Leahy, R. M. (2011). Brainstorm: a user-friendly application for MEG/EEG analysis. *Comput Intell Neurosci*, 2011, 879716. <https://doi.org/10.1155/2011/879716>
- Tak, S., Uga, M., Flandin, G., Dan, I., & Penny, W. D. (2016). Sensor space group analysis for fNIRS data. *J Neurosci Methods*, 264, 103-112. <https://doi.org/10.1016/j.jneumeth.2016.03.003>
- Tak, S., & Ye, J. C. (2014). Statistical analysis of fNIRS data: a comprehensive review. *Neuroimage*, 85 Pt 1, 72-91. <https://doi.org/10.1016/j.neuroimage.2013.06.016>
- Tanaka, Y., Ebihara, A., Ikota, M., Yamaguro, T., Kamochi, H., Kusaka, G., Ishikawa, M., Konno, T., Mashiko, T., & Watanabe, E. (2015). Early diagnosis of cerebral ischemia in cerebral vasospasm by oxygen-pulse near-infrared optical topography. *Acta Neurochir Suppl*, 120, 269-274. https://doi.org/10.1007/978-3-319-04981-6_45
- Tatemichi, T. K., Young, W. L., Prohovnik, I., Gitelman, D. R., Correll, J. W., & Mohr, J. P. (1990). Perfusion insufficiency in limb-shaking transient ischemic attacks. *Stroke*, 21(2), 341-347. <https://doi.org/10.1161/01.str.21.2.341>
- Tatum, W. O., Rubboli, G., Kaplan, P. W., Mirsatari, S. M., Radhakrishnan, K., Gloss, D., Caboclo, L. O., Drislane, F. W., Koutroumanidis, M., Schomer, D. L., Kasteleijn-Nolst Trenite, D., Cook, M., & Beniczky, S. (2018). Clinical utility of EEG in diagnosing and monitoring epilepsy in adults. *Clin Neurophysiol*, 129(5), 1056-1082. <https://doi.org/10.1016/j.clinph.2018.01.019>
- Terraneo, L., Paroni, R., Bianciardi, P., Giallongo, T., Carelli, S., Gorio, A., & Samaja, M. (2017). Brain adaptation to hypoxia and hyperoxia in mice. *Redox Biol*, 11, 12-20. <https://doi.org/10.1016/j.redox.2016.10.018>
- Thavasoathy, M., Broadhead, M., Elwell, C., Peters, M., & Smith, M. (2002). A comparison of cerebral oxygenation as measured by the NIRO 300 and the INVOS 5100 Near-Infrared Spectrophotometers. *Anaesthesia*, 57(10), 999-1006. <https://doi.org/10.1046/j.1365-2044.2002.02826.x>
- Thornton, R., Laufs, H., Rodionov, R., Cannadathu, S., Carmichael, D. W., Vulliemoz, S., Salek-Haddadi, A., McEvoy, A. W., Smith, S. M., Lhatoo, S., Elwes, R. D., Guye, M., Walker,

- M. C., Lemieux, L., & Duncan, J. S. (2010). EEG correlated functional MRI and postoperative outcome in focal epilepsy. *J Neurol Neurosurg Psychiatry*, 81(8), 922-927. <https://doi.org/10.1136/jnnp.2009.196253>
- Thornton, R. C., Rodionov, R., Laufs, H., Vulliemoz, S., Vaudano, A., Carmichael, D., Cannadathu, S., Guye, M., McEvoy, A., Lhatoo, S., Bartolomei, F., Chauvel, P., Diehl, B., De Martino, F., Elwes, R. D., Walker, M. C., Duncan, J. S., & Lemieux, L. (2010). Imaging haemodynamic changes related to seizures: comparison of EEG-based general linear model, independent component analysis of fMRI and intracranial EEG. *Neuroimage*, 53(1), 196-205. <https://doi.org/10.1016/j.neuroimage.2010.05.064>
- Timofeev, I., Carpenter, K. L., Nortje, J., Al-Rawi, P. G., O'Connell, M. T., Czosnyka, M., Smielewski, P., Pickard, J. D., Menon, D. K., Kirkpatrick, P. J., Gupta, A. K., & Hutchinson, P. J. (2011). Cerebral extracellular chemistry and outcome following traumatic brain injury: a microdialysis study of 223 patients. *Brain*, 134(Pt 2), 484-494. <https://doi.org/10.1093/brain/awq353>
- Tisdall, M. M., & Smith, M. (2006). Cerebral microdialysis: research technique or clinical tool. *Br J Anaesth*, 97(1), 18-25. <https://doi.org/10.1093/bja/ae1109>
- Torricelli, A., Contini, D., Pifferi, A., Caffini, M., Re, R., Zucchelli, L., & Spinelli, L. (2014). Time domain functional NIRS imaging for human brain mapping. *Neuroimage*, 85 Pt 1, 28-50. <https://doi.org/10.1016/j.neuroimage.2013.05.106>
- Tosh, W., & Patteril, M. (2016). Cerebral oximetry. *BJA Education*, 16(12), 417-421. <https://doi.org/10.1093/bjaed/mkw024>
- Toth, P., Szarka, N., Farkas, E., Ezer, E., Czeiter, E., Amrein, K., Ungvari, Z., Hartings, J. A., Buki, A., & Koller, A. (2016). Traumatic brain injury-induced autoregulatory dysfunction and spreading depression-related neurovascular uncoupling: Pathomechanisms, perspectives, and therapeutic implications. *Am J Physiol Heart Circ Physiol*, 311(5), H1118-h1131. <https://doi.org/10.1152/ajpheart.00267.2016>
- Towne, A. R., Waterhouse, E. J., Boggs, J. G., Garnett, L. K., Brown, A. J., Smith, J. R., Jr., & DeLorenzo, R. J. (2000). Prevalence of nonconvulsive status epilepticus in comatose patients. *Neurology*, 54(2), 340-345. <https://doi.org/10.1212/wnl.54.2.340>
- Treiman, D. M., & Delgado-Escueta, A. V. (1983). Complex partial status epilepticus. *Adv Neurol*, 34, 69-81. <https://www.ncbi.nlm.nih.gov/pubmed/6829362>

- Treiman, D. M., Meyers, P. D., Walton, N. Y., Collins, J. F., Colling, C., Rowan, A. J., Handforth, A., Faught, E., Calabrese, V. P., Uthman, B. M., Ramsay, R. E., & Mamdani, M. B. (1998). A comparison of four treatments for generalized convulsive status epilepticus. Veterans Affairs Status Epilepticus Cooperative Study Group. *N Engl J Med*, 339(12), 792-798. <https://doi.org/10.1056/nejm199809173391202>
- Treiman, D. M., & Walker, M. C. (2006). Treatment of seizure emergencies: convulsive and non-convulsive status epilepticus. *Epilepsy Res*, 68 Suppl 1, S77-82. <https://doi.org/10.1016/j.eplepsyres.2005.07.020>
- Treiman, D. M., Walton, N. Y., & Kendrick, C. (1990). A progressive sequence of electroencephalographic changes during generalized convulsive status epilepticus. *Epilepsy Res*, 5(1), 49-60. [https://doi.org/10.1016/0920-1211\(90\)90065-4](https://doi.org/10.1016/0920-1211(90)90065-4)
- Trinka, E., Cock, H., Hesdorffer, D., Rossetti, A. O., Scheffer, I. E., Shinnar, S., Shorvon, S., & Lowenstein, D. H. (2015). A definition and classification of status epilepticus--Report of the ILAE Task Force on Classification of Status Epilepticus. *Epilepsia*, 56(10), 1515-1523. <https://doi.org/10.1111/epi.13121>
- Trinka, E., & Leitinger, M. (2022). Management of Status Epilepticus, Refractory Status Epilepticus, and Super-refractory Status Epilepticus. *Continuum (Minneapolis, Minn)*, 28(2), 559-602. <https://doi.org/10.1212/con.0000000000001103>
- Tsuji, M., duPlessis, A., Taylor, G., Crocker, R., & Volpe, J. J. (1998). Near infrared spectroscopy detects cerebral ischemia during hypotension in piglets. *Pediatr Res*, 44(4), 591-595. <https://doi.org/10.1203/00006450-199810000-00020>
- Tyvaert, L., LeVan, P., Dubeau, F., & Gotman, J. (2009). Noninvasive dynamic imaging of seizures in epileptic patients. *Hum Brain Mapp*, 30(12), 3993-4011. <https://doi.org/10.1002/hbm.20824>
- Tzvetanov, P., Rousseff, R. T., & Atanassova, P. (2005). Prognostic value of median and tibial somatosensory evoked potentials in acute stroke. *Neurosci Lett*, 380(1-2), 99-104. <https://doi.org/10.1016/j.neulet.2005.01.023>
- Udina, C., Avtzi, S., Durduran, T., Holtzer, R., Rosso, A. L., Castellano-Tejedor, C., Perez, L. M., Soto-Bagaria, L., & Inzitari, M. (2019). Functional Near-Infrared Spectroscopy to Study Cerebral Hemodynamics in Older Adults During Cognitive and Motor Tasks: A Review. *Front Aging Neurosci*, 11, 367. <https://doi.org/10.3389/fnagi.2019.00367>

- Uga, M., Dan, I., Dan, H., Kyutoku, Y., Taguchi, Y. H., & Watanabe, E. (2015). Exploring effective multiplicity in multichannel functional near-infrared spectroscopy using eigenvalues of correlation matrices. *Neurophotonics*, 2(1), 015002. <https://doi.org/10.1117/1.NPh.2.1.015002>
- Uhlirova, H., Kılıç, K., Tian, P., Thunemann, M., Desjardins, M., Saisan, P. A., Sakadžić, S., Ness, T. V., Mateo, C., Cheng, Q., Weldy, K. L., Razoux, F., Vandenberghe, M., Cremonesi, J. A., Ferri, C. G., Nizar, K., Sridhar, V. B., Steed, T. C., Abashin, M., . . . Devor, A. (2016). Cell type specificity of neurovascular coupling in cerebral cortex. *Elife*, 5. <https://doi.org/10.7554/eLife.14315>
- Uludağ, K., Steinbrink, J., Villringer, A., & Obrig, H. (2004). Separability and cross talk: optimizing dual wavelength combinations for near-infrared spectroscopy of the adult head. *Neuroimage*, 22(2), 583-589. <https://doi.org/10.1016/j.neuroimage.2004.02.023>
- Upham, F. (2012). Limits on the Application of Statistical Correlations to Continuous Response Data. 12th International Conference on Music Perception and Cognition (ICMPC) and the 8th Triennial Conference of the European Society for the Cognitive Sciences of Music (ESCOM), 1037-1041. http://icmpc-escom2012.web.auth.gr/files/papers/1037_Proc.pdf
- Valipour, A., McGown, A. D., Makker, H., O'Sullivan, C., & Spiro, S. G. (2002). Some factors affecting cerebral tissue saturation during obstructive sleep apnoea. *Eur Respir J*, 20(2), 444-450. <https://doi.org/10.1183/09031936.02.00265702>
- van Houdt, P. J., de Munck, J. C., Leijten, F. S. S., Huiskamp, G. J. M., Colon, A. J., Boon, P., & Ossenblok, P. P. W. (2013). EEG-fMRI correlation patterns in the presurgical evaluation of focal epilepsy: a comparison with electrocorticographic data and surgical outcome measures. *Neuroimage*, 75, 238-248. <https://doi.org/10.1016/j.neuroimage.2013.02.033>
- Van Ness, P. C. (1990). Pentobarbital and EEG burst suppression in treatment of status epilepticus refractory to benzodiazepines and phenytoin. *Epilepsia*, 31(1), 61-67. <https://doi.org/10.1111/j.1528-1157.1990.tb05361.x>
- Van Paesschen, W. (2004). Ictal SPECT. *Epilepsia*, 45 Suppl 4, 35-40. <https://doi.org/10.1111/j.0013-9580.2004.04008.x>

- Van Paesschen, W., Dupont, P., Sunaert, S., Goffin, K., & Van Laere, K. (2007). The use of SPECT and PET in routine clinical practice in epilepsy. *Curr Opin Neurol*, 20(2), 194-202. <https://doi.org/10.1097/WCO.0b013e328042baf6>
- van Putten, M. J., Peters, J. M., Mulder, S. M., de Haas, J. A., Bruijninx, C. M., & Tavy, D. L. (2004). A brain symmetry index (BSI) for online EEG monitoring in carotid endarterectomy. *Clin Neurophysiol*, 115(5), 1189-1194. <https://doi.org/10.1016/j.clinph.2003.12.002>
- van Putten, M. J., & Tavy, D. L. (2004). Continuous quantitative EEG monitoring in hemispheric stroke patients using the brain symmetry index. *Stroke*, 35(11), 2489-2492. <https://doi.org/10.1161/01.STR.0000144649.49861.1d>
- Vespa, P. (2005). Continuous EEG monitoring for the detection of seizures in traumatic brain injury, infarction, and intracerebral hemorrhage: "to detect and protect". *J Clin Neurophysiol*, 22(2), 99-106. <https://doi.org/10.1097/01.wnp.0000154919.54202.e0>
- Vespa, P., Tubi, M., Claassen, J., Buitrago-Blanco, M., McArthur, D., Velazquez, A. G., Tu, B., Prins, M., & Nuwer, M. (2016). Metabolic crisis occurs with seizures and periodic discharges after brain trauma. *Ann Neurol*, 79(4), 579-590. <https://doi.org/10.1002/ana.24606>
- Vespa, P. M., McArthur, D. L., Xu, Y., Eliseo, M., Etchepare, M., Dinov, I., Alger, J., Glenn, T. P., & Hovda, D. (2010). Nonconvulsive seizures after traumatic brain injury are associated with hippocampal atrophy. *Neurology*, 75(9), 792-798. <https://doi.org/10.1212/WNL.0b013e3181f07334>
- Vespa, P. M., Miller, C., McArthur, D., Eliseo, M., Etchepare, M., Hirt, D., Glenn, T. C., Martin, N., & Hovda, D. (2007). Nonconvulsive electrographic seizures after traumatic brain injury result in a delayed, prolonged increase in intracranial pressure and metabolic crisis. *Crit Care Med*, 35(12), 2830-2836. <https://www.ncbi.nlm.nih.gov/pubmed/18074483>
- Vespa, P. M., Nenov, V., & Nuwer, M. R. (1999). Continuous EEG monitoring in the intensive care unit: early findings and clinical efficacy. *J Clin Neurophysiol*, 16(1), 1-13. <https://doi.org/10.1097/00004691-199901000-00001>
- Vespa, P. M., Nuwer, M. R., Juhász, C., Alexander, M., Nenov, V., Martin, N., & Becker, D. P. (1997). Early detection of vasospasm after acute subarachnoid hemorrhage using

- continuous EEG ICU monitoring. *Electroencephalogr Clin Neurophysiol*, 103(6), 607-615. [https://doi.org/10.1016/s0013-4694\(97\)00071-0](https://doi.org/10.1016/s0013-4694(97)00071-0)
- Vierordt, K. (1876). *Die quantitative Spectralanalyse in ihrer Anwendung auf Physiologie, Physik, Chemie und Technologie*. Laupp.
- Villringer, A., & Chance, B. (1997). Non-invasive optical spectroscopy and imaging of human brain function. *Trends Neurosci*, 20(10), 435-442. [https://doi.org/10.1016/s0166-2236\(97\)01132-6](https://doi.org/10.1016/s0166-2236(97)01132-6)
- Villringer, A., Planck, J., Hock, C., Schleinkofer, L., & Dirnagl, U. (1993). Near infrared spectroscopy (NIRS): a new tool to study hemodynamic changes during activation of brain function in human adults. *Neurosci Lett*, 154(1-2), 101-104. [https://doi.org/10.1016/0304-3940\(93\)90181-j](https://doi.org/10.1016/0304-3940(93)90181-j)
- Vinette, S. A., Dunn, J. F., Slone, E., & Federico, P. (2015). Artifact reduction in long-term monitoring of cerebral hemodynamics using near-infrared spectroscopy. *Neurophotonics*, 2(2), 025004. <https://doi.org/10.1117/1.NPh.2.2.025004>
- Virtanen, J., Noponen, T., Kotilahti, K., Virtanen, J., & Ilmoniemi, R. J. (2011). Accelerometer-based method for correcting signal baseline changes caused by motion artifacts in medical near-infrared spectroscopy. *J Biomed Opt*, 16(8), 087005. <https://doi.org/10.1117/1.3606576>
- Virtanen, J., Noponen, T., & Meriläinen, P. (2009). Comparison of principal and independent component analysis in removing extracerebral interference from near-infrared spectroscopy signals. *J Biomed Opt*, 14(5), 054032. <https://doi.org/10.1117/1.3253323>
- von Lüthmann, A., Herff, C., Heger, D., & Schultz, T. (2015). Toward a Wireless Open Source Instrument: Functional Near-infrared Spectroscopy in Mobile Neuroergonomics and BCI Applications [Methods]. *Frontiers in Human Neuroscience*, 9, 617. <https://doi.org/10.3389/fnhum.2015.00617>
- von Lüthmann, A., Li, X., Müller, K. R., Boas, D. A., & Yücel, M. A. (2020). Improved physiological noise regression in fNIRS: A multimodal extension of the General Linear Model using temporally embedded Canonical Correlation Analysis. *Neuroimage*, 208, 116472. <https://doi.org/10.1016/j.neuroimage.2019.116472>

- von Lüthmann, A., Ortega-Martinez, A., Boas, D. A., & Yücel, M. A. (2020). Using the General Linear Model to Improve Performance in fNIRS Single Trial Analysis and Classification: A Perspective. *Front Hum Neurosci*, 14, 30. <https://doi.org/10.3389/fnhum.2020.00030>
- von Luhmann, A., Wabnitz, H., Sander, T., & Muller, K. R. (2017). M3BA: A Mobile, Modular, Multimodal Biosignal Acquisition Architecture for Miniaturized EEG-NIRS-Based Hybrid BCI and Monitoring. *IEEE Trans Biomed Eng*, 64(6), 1199-1210. <https://doi.org/10.1109/tbme.2016.2594127>
- Vulliemoz, S., Carmichael, D. W., Rosenkranz, K., Diehl, B., Rodionov, R., Walker, M. C., McEvoy, A. W., & Lemieux, L. (2011). Simultaneous intracranial EEG and fMRI of interictal epileptic discharges in humans. *Neuroimage*, 54(1), 182-190. <https://doi.org/10.1016/j.neuroimage.2010.08.004>
- Wabnitz, H., Moeller, M., Liebert, A., Obrig, H., Steinbrink, J., & Macdonald, R. (2010). Time-resolved near-infrared spectroscopy and imaging of the adult human brain. *Adv Exp Med Biol*, 662, 143-148. https://doi.org/10.1007/978-1-4419-1241-1_20
- Wahr, J. A., Tremper, K. K., Samra, S., & Delpy, D. T. (1996). Near-infrared spectroscopy: theory and applications. *J Cardiothorac Vasc Anesth*, 10(3), 406-418. [https://doi.org/10.1016/s1053-0770\(96\)80107-8](https://doi.org/10.1016/s1053-0770(96)80107-8)
- Walker, M. C. (2018). Pathophysiology of status epilepticus. *Neurosci Lett*, 667, 84-91. <https://doi.org/10.1016/j.neulet.2016.12.044>
- Wallois, F., Patil, A., Kongolo, G., Goudjil, S., & Grebe, R. (2009). Haemodynamic changes during seizure-like activity in a neonate: a simultaneous AC EEG-SPIR and high-resolution DC EEG recording. *Neurophysiol Clin*, 39(4-5), 217-227. <https://doi.org/10.1016/j.neucli.2009.08.001>
- Wasterlain, C. G., Fujikawa, D. G., Penix, L., & Sankar, R. (1993). Pathophysiological Mechanisms of Brain Damage from Status Epilepticus. *Epilepsia*, 34(s1), S37-S53. <https://doi.org/https://doi.org/10.1111/j.1528-1157.1993.tb05905.x>
- Watanabe, E., Maki, A., Kawaguchi, F., Takashiro, K., Yamashita, Y., Koizumi, H., & Mayanagi, Y. (1998). Non-invasive assessment of language dominance with near-infrared spectroscopic mapping. *Neurosci Lett*, 256(1), 49-52. [https://doi.org/10.1016/s0304-3940\(98\)00754-x](https://doi.org/10.1016/s0304-3940(98)00754-x)

- Watanabe, E., Maki, A., Kawaguchi, F., Yamashita, Y., Koizumi, H., & Mayanagi, Y. (2000). Noninvasive cerebral blood volume measurement during seizures using multichannel near infrared spectroscopic topography. *J Biomed Opt*, 5(3), 287-290.
<https://doi.org/10.1117/1.429998>
- Watanabe, E., Nagahori, Y., & Mayanagi, Y. (2002). Focus diagnosis of epilepsy using near-infrared spectroscopy. *Epilepsia*, 43 Suppl 9, 50-55. <https://doi.org/10.1046/j.1528-1157.43.s.9.12.x>
- Watanabe, E., Yamashita, Y., Maki, A., Ito, Y., & Koizumi, H. (1996). Non-invasive functional mapping with multi-channel near infra-red spectroscopic topography in humans. *Neurosci Lett*, 205(1), 41-44. [https://doi.org/10.1016/0304-3940\(96\)12376-4](https://doi.org/10.1016/0304-3940(96)12376-4)
- Watanabe, T., Sekine, R., Mizuno, T., & Miwa, M. (2016). Development of Portable, Wireless and Smartphone Controllable Near-Infrared Spectroscopy System. *Adv Exp Med Biol*, 923, 385-392. https://doi.org/10.1007/978-3-319-38810-6_50
- Watson, N. F., Dodrill, C., Farrell, D., Holmes, M. D., & Miller, J. W. (2004). Determination of language dominance with near-infrared spectroscopy: comparison with the intracarotid amobarbital procedure. *Seizure*, 13(6), 399-402.
<https://doi.org/10.1016/j.seizure.2003.09.008>
- Waziri, A., Claassen, J., Stuart, R. M., Arif, H., Schmidt, J. M., Mayer, S. A., Badjatia, N., Kull, L. L., Connolly, E. S., Emerson, R. G., & Hirsch, L. J. (2009). Intracortical electroencephalography in acute brain injury. *Ann Neurol*, 66(3), 366-377.
<https://doi.org/10.1002/ana.21721>
- Wei, L., Otsuka, T., Acuff, V., Bereczki, D., Pettigrew, K., Patlak, C., & Fenstermacher, J. (1993). The velocities of red cell and plasma flows through parenchymal microvessels of rat brain are decreased by pentobarbital. *J Cereb Blood Flow Metab*, 13(3), 487-497.
<https://doi.org/10.1038/jcbfm.1993.63>
- Westover, M. B., Ching, S., Kumaraswamy, V. M., Akeju, S. O., Pierce, E., Cash, S. S., Kilbride, R., Brown, E. N., & Purdon, P. L. (2015). The human burst suppression electroencephalogram of deep hypothermia. *Clin Neurophysiol*, 126(10), 1901-1914.
<https://doi.org/10.1016/j.clinph.2014.12.022>

- White, B. R., & Culver, J. P. (2010). Quantitative evaluation of high-density diffuse optical tomography: in vivo resolution and mapping performance. *J Biomed Opt*, 15(2), 026006. <https://doi.org/10.1117/1.3368999>
- White, P. T., Grant, P., Mosier, J., & Craig, A. (1961). Changes in cerebral dynamics associated with seizures. *Neurology*, 11(4)Pt 1, 354-361. <https://doi.org/10.1212/wnl.11.4.354>
- Winslow, N., George, M., Michalos, A., Wang, H., Ergene, E., & Xu, M. (2021). Hemodynamic Changes Associated with Lateralized Periodic Discharges: A Near-Infrared Spectroscopy and Continuous EEG Study. *Neurocrit Care*, 35(1), 153-161. <https://doi.org/10.1007/s12028-020-01154-4>
- Witsch, J., Frey, H. P., Schmidt, J. M., Velazquez, A., Falo, C. M., Reznik, M., Roh, D., Agarwal, S., Park, S., Connolly, E. S., & Claassen, J. (2017). Electroencephalographic Periodic Discharges and Frequency-Dependent Brain Tissue Hypoxia in Acute Brain Injury. *JAMA Neurol*, 74(3), 301-309. <https://doi.org/10.1001/jamaneurol.2016.5325>
- Wolf, M., Ferrari, M., & Quaresima, V. (2007). Progress of near-infrared spectroscopy and topography for brain and muscle clinical applications. *J Biomed Opt*, 12(6), 062104. <https://doi.org/10.1117/1.2804899>
- Wolff, M. D., Farrell, J. S., Scantlebury, M. H., & Teskey, G. C. (2020). Dynamic oxygen changes during status epilepticus and subsequent endogenous kindling. *Epilepsia*, 61(7), 1515-1527. <https://doi.org/10.1111/epi.16554>
- Wood, E. H., & Geraci, J. (1949). Photoelectric determination of arterial oxygen saturation in man. *The Journal of laboratory and clinical medicine*, 34(3), 387-401. <https://www.ncbi.nlm.nih.gov/pubmed/18113925>
- Wray, S., Cope, M., Delpy, D. T., Wyatt, J. S., & Reynolds, E. O. (1988). Characterization of the near infrared absorption spectra of cytochrome aa3 and haemoglobin for the non-invasive monitoring of cerebral oxygenation. *Biochim Biophys Acta*, 933(1), 184-192. [https://doi.org/10.1016/0005-2728\(88\)90069-2](https://doi.org/10.1016/0005-2728(88)90069-2)
- Wyatt, J. S., Cope, M., Delpy, D. T., Richardson, C. E., Edwards, A. D., Wray, S., & Reynolds, E. O. (1990). Quantitation of cerebral blood volume in human infants by near-infrared spectroscopy. *J Appl Physiol* (1985), 68(3), 1086-1091. <https://doi.org/10.1152/jappl.1990.68.3.1086>

- Wyatt, J. S., Cope, M., Delpy, D. T., van der Zee, P., Arridge, S., Edwards, A. D., & Reynolds, E. O. (1990). Measurement of optical path length for cerebral near-infrared spectroscopy in newborn infants. *Dev Neurosci*, 12(2), 140-144. <https://doi.org/10.1159/000111843>
- Wyatt, J. S., Cope, M., Delpy, D. T., Wray, S., & Reynolds, E. O. (1986). Quantification of cerebral oxygenation and haemodynamics in sick newborn infants by near infrared spectrophotometry. *Lancet*, 2(8515), 1063-1066. [https://doi.org/10.1016/s0140-6736\(86\)90467-8](https://doi.org/10.1016/s0140-6736(86)90467-8)
- Yamada, Y., Suzuki, H., & Yamashita, Y. (2019). Time-Domain Near-Infrared Spectroscopy and Imaging: A Review. *Applied Sciences*, 9(6), 1127. <https://www.mdpi.com/2076-3417/9/6/1127>
- Yang, F., Li, J., Song, Y., Zhao, M., Niemeyer, J. E., Luo, P., Li, D., Lin, W., Ma, H., & Schwartz, T. H. (2021). Mesoscopic Mapping of Ictal Neurovascular Coupling in Awake Behaving Mice Using Optical Spectroscopy and Genetically Encoded Calcium Indicators [Original Research]. *Frontiers in Neuroscience*, 15, 704834. <https://doi.org/10.3389/fnins.2021.704834>
- Yang, H., Wu, J., Guo, R., Peng, Y., Zheng, W., Liu, D., & Song, Z. (2013). Glycolysis in energy metabolism during seizures. *Neural Regen Res*, 8(14), 1316-1326. <https://doi.org/10.3969/j.issn.1673-5374.2013.14.008>
- Yang, M. T. (2020). Multimodal neurocritical monitoring. *Biomed J*, 43(3), 226-230. <https://doi.org/10.1016/j.bj.2020.05.005>
- Yemisci, M., Gursoy-Ozdemir, Y., Vural, A., Can, A., Topalkara, K., & Dalkara, T. (2009). Pericyte contraction induced by oxidative-nitrative stress impairs capillary reflow despite successful opening of an occluded cerebral artery. *Nat Med*, 15(9), 1031-1037. <https://doi.org/10.1038/nm.2022>
- Yokose, N., Sakatani, K., Murata, Y., Awano, T., Igarashi, T., Nakamura, S., Hoshino, T., & Katayama, Y. (2010). Bedside monitoring of cerebral blood oxygenation and hemodynamics after aneurysmal subarachnoid hemorrhage by quantitative time-resolved near-infrared spectroscopy. *World Neurosurg*, 73(5), 508-513. <https://doi.org/10.1016/j.wneu.2010.02.061>
- Yoo, T. S., Ackerman, M. J., Lorensen, W. E., Schroeder, W., Chalana, V., Aylward, S., Metaxas, D., & Whitaker, R. (2002). Engineering and algorithm design for an image

- processing Api: a technical report on ITK--the Insight Toolkit. *Stud Health Technol Inform*, 85, 586-592. <https://www.ncbi.nlm.nih.gov/pubmed/15458157>
- Yoshino, K., Oka, N., Yamamoto, K., Takahashi, H., & Kato, T. (2013). Functional brain imaging using near-infrared spectroscopy during actual driving on an expressway. *Front Hum Neurosci*, 7, 882. <https://doi.org/10.3389/fnhum.2013.00882>
- Yoshitani, K., Kawaguchi, M., Ishida, K., Maekawa, K., Miyawaki, H., Tanaka, S., Uchino, H., Kakinohana, M., Koide, Y., Yokota, M., Okamoto, H., & Nomura, M. (2019). Guidelines for the use of cerebral oximetry by near-infrared spectroscopy in cardiovascular anesthesia: a report by the cerebrospinal Division of the Academic Committee of the Japanese Society of Cardiovascular Anesthesiologists (JSCVA). *J Anesth*, 33(2), 167-196. <https://doi.org/10.1007/s00540-019-02610-y>
- Yoshitani, K., Kawaguchi, M., Tatsumi, K., Kitaguchi, K., & Furuya, H. (2002). A comparison of the INVOS 4100 and the NIRO 300 near-infrared spectrophotometers. *Anesth Analg*, 94(3), 586-590; table of contents. <https://doi.org/10.1097/00000539-200203000-00020>
- Young, G. B. (2000). The EEG in coma. *J Clin Neurophysiol*, 17(5), 473-485. <https://doi.org/10.1097/00004691-200009000-00006>
- Young, G. B., Bolton, C. F., Archibald, Y. M., Austin, T. W., & Wells, G. A. (1992). The electroencephalogram in sepsis-associated encephalopathy. *J Clin Neurophysiol*, 9(1), 145-152. <https://doi.org/10.1097/00004691-199201000-00016>
- Young, G. B., & Jordan, K. G. (1998). Do nonconvulsive seizures damage the brain?--Yes. *Arch Neurol*, 55(1), 117-119. <https://doi.org/10.1001/archneur.55.1.117>
- Young, G. B., & Mantia, J. (2017). Continuous EEG monitoring in the intensive care unit. *Handb Clin Neurol*, 140, 107-116. <https://doi.org/10.1016/b978-0-444-63600-3.00007-6>
- Young, G. B., Sharpe, M. D., Savard, M., Al Thenayan, E., Norton, L., & Davies-Schinkel, C. (2009). Seizure detection with a commercially available bedside EEG monitor and the subhairline montage. *Neurocrit Care*, 11(3), 411-416. <https://doi.org/10.1007/s12028-009-9248-2>
- Young, M. (1992). Rapid readout biological monitoring system. *J Healthc Mater Manage*, 10(6), 74-75. <https://www.ncbi.nlm.nih.gov/pubmed/10119235>

- Yu, L., Nina-Paravecino, F., Kaeli, D., & Fang, Q. (2018). Scalable and massively parallel Monte Carlo photon transport simulations for heterogeneous computing platforms. *Journal of Biomedical Optics*, 23(1), 010504. <https://doi.org/10.1117/1.JBO.23.1.010504>
- Yücel, M. A., Lühmann, A. V., Scholkmann, F., Gervain, J., Dan, I., Ayaz, H., Boas, D., Cooper, R. J., Culver, J., Elwell, C. E., Eggebrecht, A., Franceschini, M. A., Grova, C., Homae, F., Lesage, F., Obrig, H., Tachtsidis, I., Tak, S., Tong, Y., . . . Wolf, M. (2021). Best practices for fNIRS publications. *Neurophotonics*, 8(1), 012101. <https://doi.org/10.1117/1.NPh.8.1.012101>
- Yücel, M. A., Selb, J., Aasted, C. M., Lin, P. Y., Borsook, D., Becerra, L., & Boas, D. A. (2016). Mayer waves reduce the accuracy of estimated hemodynamic response functions in functional near-infrared spectroscopy. *Biomed Opt Express*, 7(8), 3078-3088. <https://doi.org/10.1364/boe.7.003078>
- Yücel, M. A., Selb, J., Boas, D. A., Cash, S. S., & Cooper, R. J. (2014). Reducing motion artifacts for long-term clinical NIRS monitoring using collodion-fixed prism-based optical fibers. *Neuroimage*, 85 Pt 1(0 1), 192-201. <https://doi.org/10.1016/j.neuroimage.2013.06.054>
- Yücel, M. A., Selb, J., Cooper, R. J., & Boas, D. A. (2014). TARGETED PRINCIPLE COMPONENT ANALYSIS: A NEW MOTION ARTIFACT CORRECTION APPROACH FOR NEAR-INFRARED SPECTROSCOPY. *J Innov Opt Health Sci*, 7(2). <https://doi.org/10.1142/s1793545813500661>
- Zack, M. M., & Kobau, R. (2017). National and State Estimates of the Numbers of Adults and Children with Active Epilepsy - United States, 2015. *MMWR Morb Mortal Wkly Rep*, 66(31), 821-825. <https://doi.org/10.15585/mmwr.mm6631a1>
- Zaidat, O. O., Werz, M. A., Landis, D. M., & Selman, W. (1999). Orthostatic limb shaking from carotid hypoperfusion. *Neurology*, 53(3), 650-651. <https://doi.org/10.1212/wnl.53.3.650>
- Zandbergen, E. G., Hijdra, A., Koelman, J. H., Hart, A. A., Vos, P. E., Verbeek, M. M., & de Haan, R. J. (2006). Prediction of poor outcome within the first 3 days of postanoxic coma. *Neurology*, 66(1), 62-68. <https://doi.org/10.1212/01.wnl.0000191308.22233.88>
- Zeff, B. W., White, B. R., Dehghani, H., Schlaggar, B. L., & Culver, J. P. (2007). Retinotopic mapping of adult human visual cortex with high-density diffuse optical tomography. *Proc Natl Acad Sci U S A*, 104(29), 12169-12174. <https://doi.org/10.1073/pnas.0611266104>

- Zeiler, F. A., Thelin, E. P., Helmy, A., Czosnyka, M., Hutchinson, P. J. A., & Menon, D. K. (2017). A systematic review of cerebral microdialysis and outcomes in TBI: relationships to patient functional outcome, neurophysiologic measures, and tissue outcome. *Acta Neurochir (Wien)*, 159(12), 2245-2273. <https://doi.org/10.1007/s00701-017-3338-2>
- Zeiler, S. R., Hubbard, R., Gibson, E. M., Zheng, T., Ng, K., O'Brien, R., & Krakauer, J. W. (2016). Paradoxical Motor Recovery From a First Stroke After Induction of a Second Stroke: Reopening a Postischemic Sensitive Period. *Neurorehabil Neural Repair*, 30(8), 794-800. <https://doi.org/10.1177/1545968315624783>
- Zeiler, S. R., Turtzo, L. C., & Kaplan, P. W. (2011). SPECT-negative SIRPIDs argues against treatment as seizures. *J Clin Neurophysiol*, 28(5), 493-496. <https://doi.org/10.1097/WNP.0b013e318231c00a>
- Zhang, C., Tabatabaei, M., Bélanger, S., Girouard, H., Moeini, M., Lu, X., & Lesage, F. (2019). Astrocytic endfoot Ca(2+) correlates with parenchymal vessel responses during 4-AP induced epilepsy: An in vivo two-photon lifetime microscopy study. *J Cereb Blood Flow Metab*, 39(2), 260-271. <https://doi.org/10.1177/0271678x17725417>
- Zhang, F., Cheong, D., Khan, A. F., Chen, Y., Ding, L., & Yuan, H. (2021). Correcting physiological noise in whole-head functional near-infrared spectroscopy. *J Neurosci Methods*, 360, 109262. <https://doi.org/10.1016/j.jneumeth.2021.109262>
- Zhang, Q., Brown, E. N., & Strangman, G. E. (2007). Adaptive filtering for global interference cancellation and real-time recovery of evoked brain activity: a Monte Carlo simulation study. *J Biomed Opt*, 12(4), 044014. <https://doi.org/10.1117/1.2754714>
- Zhang, Q., Ivkovic, V., Hu, G., & Strangman, G. E. (2014). Twenty-four-hour ambulatory recording of cerebral hemodynamics, systemic hemodynamics, electrocardiography, and actigraphy during people's daily activities. *J Biomed Opt*, 19(4), 47003. <https://doi.org/10.1117/1.Jbo.19.4.047003>
- Zhang, Q., Yan, X., & Strangman, G. E. (2011). Development of motion resistant instrumentation for ambulatory near-infrared spectroscopy. *J Biomed Opt*, 16(8), 087008. <https://doi.org/10.1117/1.3615248>
- Zhang, X., Noah, J. A., & Hirsch, J. (2016). Separation of the global and local components in functional near-infrared spectroscopy signals using principal component spatial filtering. *Neurophotonics*, 3(1), 015004. <https://doi.org/10.1117/1.NPh.3.1.015004>

- Zhang, Y., Brooks, D. H., Franceschini, M. A., & Boas, D. A. (2005). Eigenvector-based spatial filtering for reduction of physiological interference in diffuse optical imaging. *J Biomed Opt*, 10(1), 11014. <https://doi.org/10.1117/1.1852552>
- Zhang, Y., Tan, F., Xu, X., Duan, L., Liu, H., Tian, F., & Zhu, C. Z. (2015). Multiregional functional near-infrared spectroscopy reveals globally symmetrical and frequency-specific patterns of superficial interference. *Biomed Opt Express*, 6(8), 2786-2802. <https://doi.org/10.1364/boe.6.002786>
- Zhang, Z., & Yi, Z. (2005). An Efficient Independent Component Analysis Algorithm for Sub-Gaussian Sources. In J. Wang, X. Liao, & Z. Yi, *Advances in Neural Networks – ISNN 2005 Berlin, Heidelberg*.
- Zhao, H., Frijia, E. M., Vidal Rosas, E., Collins-Jones, L., Smith, G., Nixon-Hill, R., Powell, S., Everdell, N. L., & Cooper, R. J. (2021). Design and validation of a mechanically flexible and ultra-lightweight high-density diffuse optical tomography system for functional neuroimaging of newborns. *Neurophotonics*, 8(1), 015011. <https://doi.org/10.1117/1.NPh.8.1.015011>
- Zhao, J., Ding, H. S., Hou, X. L., Zhou, C. L., & Chance, B. (2005). In vivo determination of the optical properties of infant brain using frequency-domain near-infrared spectroscopy. *J Biomed Opt*, 10(2), 024028. <https://doi.org/10.1117/1.1891345>
- Zhao, J., Pang, S., & Che, G. (2009). Specificity and sensitivity of visual evoked potentials P100 latency to different events exercise. *Health*, 1(1), 47-50.
- Zhao, M., Ma, H., Suh, M., & Schwartz, T. H. (2009). Spatiotemporal Dynamics of Perfusion and Oximetry during Ictal Discharges in the Rat Neocortex. *The Journal of Neuroscience*, 29(9), 2814-2823. <https://doi.org/10.1523/jneurosci.4667-08.2009>
- Zhao, M., Nguyen, J., Ma, H., Nishimura, N., Schaffer, C. B., & Schwartz, T. H. (2011). Preictal and ictal neurovascular and metabolic coupling surrounding a seizure focus. *J Neurosci*, 31(37), 13292-13300. <https://doi.org/10.1523/jneurosci.2597-11.2011>
- Zijdenbos, A. P., Dawant, B. M., Margolin, R. A., & Palmer, A. C. (1994). Morphometric analysis of white matter lesions in MR images: method and validation. *IEEE Trans Med Imaging*, 13(4), 716-724. <https://doi.org/10.1109/42.363096>
- Zijlstra, W. G. (1951). *Fundamentals and applications of clinical oximetry*. van Gorcum Assen.

Zlokovic, B. V. (2005). Neurovascular mechanisms of Alzheimer's neurodegeneration. *Trends Neurosci*, 28(4), 202-208. <https://doi.org/10.1016/j.tins.2005.02.001>

Zsurka, G., & Kunz, W. S. (2015). Mitochondrial dysfunction and seizures: the neuronal energy crisis. *Lancet Neurol*, 14(9), 956-966. [https://doi.org/10.1016/s1474-4422\(15\)00148-9](https://doi.org/10.1016/s1474-4422(15)00148-9)

Zubler, F., Steimer, A., Gast, H., & Schindler, K. A. (2014). Seizure termination. *Int Rev Neurobiol*, 114, 187-207. <https://doi.org/10.1016/b978-0-12-418693-4.00008-x>